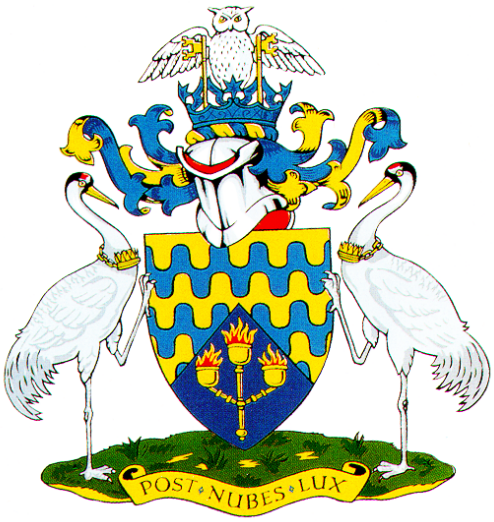

CRANFIELD UNIVERSITY

SCHOOL OF MECHANICAL ENGINEERING

DEPARTMENT OF POWER AND PROPULSION

PhD Thesis

Academic Year 2005-2006

R. SPENCE

CFD Analyses of Centrifugal Pumps with Emphasis on Factors Affecting Internal Pressure Pulsations

Supervisor:

Dr J. Amaral-Teixeira

October 2006

Abstract

The operation of centrifugal pumps can generate instabilities and pressure pulsations that may be detrimental to the integrity and performance of the pump. Until recently these pressure pulsations could only be determined experimentally which resulted in a limited understanding of pressure pulsations around the pump. Industrial pump guarantees are limited to pulsation levels measured at the discharge. However, numerical analysis techniques have advanced to such a stage that they can now be used to explore these effects.

The multi-block, structured grid CFD code TASCflow was used to investigate the time variation of pressure within a complete centrifugal pump. A parametric study covered four geometric parameters, namely the cutwater gap, vane arrangement, snubber gap and the sidewall clearance. Taguchi methods allowed the number of transient analyses to be limited to a total of twenty seven. Three flow rates were investigated and the pulsations were extracted at fifteen different locations covering important pump regions.

The velocity flow patterns from the transient analyses exhibited important features that were in agreement with two independent sources. The transient flow results compared reasonably with the Weir experimental tests and clearly indicated the pump locations experiencing the largest pulsation levels. It was also noted that monitoring pulsations at the top dead centre of the pump volute casing would provide a better indication of internal pump pulsations than monitoring at the discharge. Taguchi post-processing analysis tools were used to rank the relative importance of the four geometric parameters at each location for each flow rate. The cutwater gap and vane arrangement were found to exert the greatest influence across the various monitored locations and the flow range. However the snubber gap had a dominant influence on the pressure differential across the impeller shroud and pulses in the pressure differential were evident at reduced flows. Through a rationalisation process reductions in pressure pulsations aimed at increased component life and reduced noise/vibration have resulted in a single recommended geometric arrangement. Further analyses confirmed that the new arrangement did indeed produce lesser pulsations levels.

Multiple steady state simulations were analysed to determine if they were a viable substitute for the transient analyses. However it was demonstrated that the steady state pulsations did not adequately capture the magnitude and phase of the pulsations shown by the transient results. Likewise the steady state analyses were unable to predict trends for two differing pump geometries.

In order to identify the implications of the CFD data for mechanical integrity, the pressure differential predicted by the transient analyses was compared with the pressure loadings currently utilised in Weir design guidelines; this resulted in a new recommendation for use in future designs. Also finite element analyses were conducted using four pressure loadings taken from the numerical results and a centrifugal loading. These supported the recommendation for an increased loading to be used in the design guidelines. The stress levels at the impeller outlet were found to be extremely sensitive to the snubber gap. The completion of this project has allowed a useful set of recommendations to be made regarding the design of high head double entry pumps.

Acknowledgements

The author wishes to thank his supervisors, Dr. A Tourlidakis, Prof. P. Ivey and Dr J. Amaral-Teixiera for their advice and guidance throughout the time of this project. Dr L. Oswald's assistance regarding the usage and remote access of the Cranfield University facilities is also greatly appreciated.

The author is grateful to the engineering management at Weir Pumps Limited for numerous acts; to David France for the opportunity and arranging the funding for the work, to Peter Smith for his support in the initial stages and to Robert Brown for overseeing its completion. The advice and support of the authors' colleagues has been greatly appreciated on many occasions. Particular thanks go to Tom Purdom for his continuing interest in discussing CFD matters and for his assistance in conducting the stress analyses in the latter stages of this project. Assistance was also received from the Noise and Vibration and the Research and Development departments.

Many thanks are due to the author's friends and family for their kindness and support throughout the study. Special thanks are due to my wife, Pamela, for her unfailing support and efforts to keep the project moving in difficult times. Special thanks are also due to my parents for their encouragement over many years, particularly to my father for the numerous discussions and his ever constructive advice.

Table of Contents

List of Tables

List of Figures

Nomenclature

R_i	Radius at location
D_i	Diameter at location
b_2	Impeller Outlet Width
z	Blade number (per side)
θ	Total Wrap Angle
t_B	Blade Thickness
R_L	Leading Edge Radius
D_s	Suction Branch Diameter
D_d	Discharge Branch Diameter
B_3	Volute Width
R_3	Cutwater Radius
Q_n	Nominal (Best Efficiency Point) Flow Rate
U_i	absolute velocity at location
u_i	component velocity in x direction at location
v_i	component velocity in y direction at location
w_i	component velocity in z direction at location
C_{ti}	tangential component of the absolute velocity at location
C_{ri}	radial component of the absolute velocity at location
u*	alternative velocity scale used in place of u+
u+	near wall tangential velocity
p	pressure
P_{ti}	Mass averaged total pressure at location
Δp	pressure pulsation
Δp*	normalised pressure pulsation
Δp_{p-p}	peak-to-peak pressure pulsation
Δp_a	pressure pulsation amplitude
Δp_{RMS}	RMS pressure pulsation
$\dot{\phi}$	rate of volumetric heat addition per unit mass
k	thermal conductivity
g	gravitational acceleration
$\dot{m}$	mass flow through the pump
T	temperature
R	real gas constant
M	torque
H	is the pump generated head
H_e	is the Euler predicted head
N	is the pump speed (RPM)
f	Frequency (Hz)
L	Path distance (quarter wavelength) (m)
r	Number of repetitions
n	Number of arrangements/trials
n_{pj}	Number of level factor arrangements/trials
k_j	Number of data items for a level
f_d	Degrees of freedom

f_{TOT}	total degrees of freedom
f_P	Factor Degrees of Freedom
R_{TOT}	Total of Results
CF	Correction Factor
S_{TOT}	Total Variation
P_p	Factor Totals
S_P	Factor Total Variance
V_P	Variance
P_P	Percentage Contribution per factor
y_P	the predicted response
y_{GM}	the grand mean (average of all response values)
$(\Delta_A/2)$	half effect for factor A
$(\Delta_B/2)$	half effect for factor B
$(\Delta_{AB}/2)$	half effect for interaction AB

σ_{cs}	centrifugal stress
σ_{bs}	bending stress
σ_y	material yield stress
σ_m	material un-notched endurance limit
ρ_m	density of the material
K	constant, which is a function of the radius ration of the rotating disc
K’	impeller theoretical geometric stress concentration factor
K_t	impeller shroud to blade fatigue stress concentration factor

Greek Symbols

B_k	Average Blade Angle at location (^{o})
υ	Speed of sound in water (m/s)
δ	density of the fluid
ρ	density of the fluid
μ	molecular viscosity
λ	the second viscosity coefficient
ν	kinematic viscosity of the fluid
ω	rotational velocity
ν^*	Poisson’s ratio

suffixes

i	1 denotes inlet 2 denotes outlet 3 denotes cutwater 4 denotes outer snubber gap position wr denotes wear ring
j	level of Taguchi factor (-1: low, 0: mid, +1: high)
k	blade position L: impeller leading edge T: impeller trailing edge

P	denotes geometric factors A: cutwater gap B: snubber gap C: sidewall clearance D: vane arrangement
TOT	total
t	tangential
r	radial

Note: SI units are used for physical quantities, except where noted.

Chapter 1

Introduction and Statement of Problem for Study

1.1 General Overview

1.2 Objectives of the present Study

1.3 Structure of Thesis

1 Introduction and Statement of Problem for Study

1.1 General Overview

From the earliest of times it has been necessary to move water from one location to another and this requirement remains important to the present day. The mechanical pump is widely reported to be the second most common machine, the first being the electric motor. History records that a great number of devices have been created to transport fluids, from the Egyptian shaduf, to the Archimedean screw pump (1) including reciprocating pumps developed in Roman times. The origin of the centrifugal pump dates back to the seventeenth century and is generally credited to Denis Papin (2), although it is recorded that others had considered using centrifugal force to lift fluid prior to Papin. His concept was important as it involved the creation of a forced vortex within a circular or spiral casing by means of blades.

While major developments were made in the design of the centrifugal pump following Papin, it was the advent of the electric motor that allowed significant advancements to become possible. The capability to supply sufficient speed and power allowed higher efficiencies to be achieved although it wasn't until the latter years of the nineteenth century that widespread manufacturing of centrifugal pumps was established. Elms provides a brief summary of historical pump innovators in his online document (3). Today centrifugal pumps are available in a tremendous array of sizes, from those that can literally be held in one hand, to others that can comfortably accommodate a person standing in the suction inlet. Pumps are available in single or double entry arrangements, with multiple rotor stages and with a variety of diffusing options from vaned diffusers to scroll volutes. Efficiencies of over ninety percent are now a practical possibility although the ability to reach such high values is often dependent on the

application. Centrifugal pumps are used in a wide range of applications and they can handle a variety of liquids and gases at relatively high pressures and/or temperatures.

A basic centrifugal pump consists of two main components, a rotor that imparts energy to the fluid (often called the impeller) and a component that diffuses the flow as it moves around it (generally termed the volute). However, this simple arrangement creates extremely complex fluid conditions. In general, flows are three dimensional, turbulent in nature and unsteady. Within centrifugal pumps, it is important to transfer energy from the impeller to the fluid in an efficient manner. High efficiency is achieved through the design of the impeller shape, but the complexity of a well designed impeller contributes to the three dimensionality of the flow. Gülich (4) suggests that in the impeller alone there are four main secondary flow mechanisms (i.e. velocity components normal to the direction of the main flow) arising because of the meridional curvature, rotational effects, blade forces and axial flow. The specific flow structure will obviously depend on individual pump geometry, although the same fluid dynamics phenomena will exist to some degree. Flow in rotodynamic water pumps, generally has a high Reynolds number and thus it is considered turbulent. This gives rise to turbulent mixing losses and consideration of turbulent boundary layers is required. At part flow conditions features such as recirculation and separation can occur; additionally under certain conditions, vapour bubbles can form leading to the development of cavitation. All flow in hydraulic machines is inherently unsteady, due to the relative motion between rotating and stationary components. In centrifugal pumps, the unsteadiness arises primarily due to the rotating impeller blade passing the stationary volute cutwater, or diffuser blade. Unsteady effects are particularly prominent at off design conditions and influence the variation of mass flow through the pump with respect to time. The pulsation in the mass flow creates unsteady pressure forces, which may lead to excessive loading of mechanical components. In turn this may lead to high cycle fatigue and can result in impeller blade failure.

In practice the design of both the impeller and volute are complex, with numerous geometrical parameters being required to identify a design that will form a hydraulically efficient pump. In order for an impeller to impart energy efficiently to the fluid,

features such as the number of blades, inlet and outlet blade angles, blade sweep, meridional profile, leading and trailing edge, blade thickness and eye diameter have to be carefully considered and specified. The volute can be of a circular or spiral design, with the cross-sectional area being based on circular, rectangular or trapezoidal shapes. Additional information must be specified including, for example, cutwater diameter, inclusion of a splitter and if necessary the requirement for an inline (with the pump) centreline discharge. These geometrical details are often generated from empirical data, from experience, because of manufacturing methods or a combination of all three.

The designer needs to understand the effect of these geometrical parameters in order to arrive at an optimum design for a specified application. However, most importantly, from an industrial viewpoint, the pump design must be market orientated and fulfil the needs of the client. A recent study commissioned by the German Association of Pump manufacturers, reported by P. Hergt (5), produced a "top ten" list of desired pump features (in no specific order),

Reduced Energy consumption	Improved Suction behaviour
Increased Reliability, Availability	Zero Leakage
Increased Control Range	Reduced Sound Emission
Reduced Price	Reduced Pulsations
Increased Recyclability	Super Synchronous Speeds

Many of these features are interlinked but the relationship between them and the pump geometric parameters is not always obvious. For example, higher efficiencies that reduce energy consumption might be achieved through a reduction in flow leakage paths, but this in turn may lead to mechanical problems. Hergt concluded that pump manufacturers must think in terms of "providing solutions" rather than "selling products".

Regardless of the design process used, the final decision regarding the suitability of any new pump design is usually made following physical testing. These tests are often expensive in terms of time and resources, for example, due to the manufacturing of

pattern equipment and the pump itself as well as the assembly and the use of test facilities. The associated costs can limit the scope of a designer, either by preventing an in-depth examination of the effect of a particular design parameter or preventing the investigation of new innovative ideas in favour of more conservative, reliable designs. Gradually, pump manufacturers are turning to computational techniques to study design features with a view to reducing, or eliminating the number of tests conducted and to highlight any undesirable design characteristics at an early stage.

Computational analysis techniques, when applied to fluid flow, are commonly referred to as Computational Fluid Dynamics (CFD) and involve the solution of "simplified" Navier Stokes equations. Simplifications are necessary in the modelling of viscous effects, discretisation and averaging unsteady terms. However, as more and more refinements become available they require a skilled user to understand the flow effects to be modelled and to select the most appropriate refinement for a particular application. Despite these refinements, any result produced using computational means can only approximate the "real" flow. Nevertheless, the improvement of designs can be achieved by analysing multiple geometric arrangements using an identical set of simplifications. With the mathematical and computational error between two analyses being identical (or more realistically as similar as can be achieved), it is possible to predict an arrangement that produces a better performance. With technological advancements allowing increasingly powerful and affordable computing facilities, users can utilise these resources in different ways, for example, improving accuracy by using larger numbers of elements, analysing more components to investigate component interactions or producing results in a shorter time period.

1.2 Objectives of the Present Study

As has been mentioned briefly in Section 1.1, the operation of rotodynamic pumps can result in the generation of instabilities and pressure pulsations, which can affect the mechanical integrity of the pump, resulting in component fatigue, excessive vibration and/or noise. Currently, accurate predictions of the magnitude of pressure pulsations

are not easily achievable even by numerical means and experimental/empirical results are often still used in the evaluation of new designs. Recent progress in the ability to predict 3D complex viscous flows numerically suggests a possible alternative method to predict pump generated pulsations. In order to better understand the complex internal pump flows, especially at part load conditions, CFD models have been developed in this thesis to analyse the complete pump design. The relationship between the pressure pulsations and pressure differentials produced under these conditions and the effect on the mechanical integrity of the pump is also considered.

The work presented in this thesis aims to provide a contribution in the following areas:

1. **A Complete Pump Model**: Current commercial CFD packages have been used to predict time dependent pressure pulsations but computational facilities seem to have limited that work to simulating the volute and impeller interactions only, without the suction inlet branch and leakage flow paths being considered, González et al (6). The current work aims to improve the quality and scope of previous work related to pressure pulsations by performing simulations involving the complete hydraulic pump geometry. The numerical model incorporates all of the major flow paths in a pump encompassing the suction inlet, impeller, leakage pathways and the volute casing. Modelling the interaction of these components enables a more complete investigation of the pressure pulsations and a better understanding of how they are generated. This involves deriving the flow patterns within the pump at distinct moments in time and the change in these flow patterns as the impeller rotates. The work focuses on a reduced scale version of a high energy impeller in a double entry, single stage pump arrangement and the analyses will concentrate on the lower end of a typical continuous operating flow range.

2. **Pressure Pulsations:** The understanding of pressure pulsations by pump manufacturers is surprisingly limited. No official standards exist for safe levels of pressure pulsations in pumps; the only industry adopted guideline is a guarantee of less than 3% variation in the pump outlet pressure. Yet, it is

unknown whether a limitation of 3% variation in the discharge corresponds to a safe limit at other locations within a pump. Therefore a detailed assessment of pressure pulsations in both the impeller and volute will be performed to gauge whether the 3% adopted limit at the discharge actually provides any guarantee for other critical parts of the pump. This work will be conducted at three flow rates over a flow range extending from the pump duty condition to a common pump minimum operating point of twenty five percent of the duty condition.

3. **Effect of Geometric Variations:** In conjunction with the above, a parametric study investigating the effect of various pump geometry features on the pressure pulsation is of interest. For example, it is important to know if a specific pump geometric design amplifies or attenuates the pulsations. A survey of literature and industrial experience provided a shortlist of key parameters that can be controlled in the design process and that are likely to have an effect on the pressure variation in the pump. These key areas are listed below

    - Cutwater Clearance Gap: radial distance between impeller blade tip and the volute cutwater.
    - Snubber Clearance Gap: radial distance between the shroud outer diameter and the volute casing.
    - Sidewall Clearance: minimum axial distance between the impeller shroud and the volute casing.
    - Blade Clocking or Stagger: on a double entry impeller this is the practice of offsetting the arrangement of blades on one side of the impeller so that they do not coincide with the blades on the opposite side.

    Figures 4.6 and 4.7 provide the relative location of these areas within the pump The parametric study utilises a Taguchi array to reduce the number of analyses required at each flow rate. The array provides a framework for the post processing of the results and allows the reduction of the pressure pulsations in conjunction with the adjustment of the above variables. This is a rationalisation process that does not solely focus on reducing the pressure pulsation since other

critical factors, such as the pump generated head, are also considered. Broadly, the objective of this work is to assist the development of pump designs, which will achieve reduced levels of pulsations without significant loss in performance.

4. **Approximation to Transient Pressure Pulsations via Steady State Analyses:** The complete pump transient analyses described above are exceedingly expensive in terms of computational time. Thus the work also attempts to assess a possible methodology for estimating transient pressure pulsations in a shorter timeframe (steady state analyses) and its possible application to the pump type considered. Such a method, if successful, would be beneficial, as it would assist in gaining an estimate of pressure pulsations for designs that are utilised in situations not covered by the design guidelines. Additionally it would enable the designer to perform a quick final check on his design to ascertain whether the pressure pulsations are of the order of magnitude that is predicted by the guidelines.

5. **Development of Design Recommendations:** In order to extend the application of the CFD analyses beyond the parametric study and be of benefit in a design process, a set of design guidelines are examined and refined. These revised guidelines will provide pump designers with a better understanding of how to control pressure pulsations within the various sections of the pump that are susceptible to high pressure pulsations, while at the same time understanding the effects of any design decisions on the expected performance of the pump. Additionally a process that could be used to transfer the pressure data from the CFD analyses for inclusion in a finite element stress analysis is presented and the results discussed.

In order to successfully complete the above programme two key steps must first be achieved.

- The generation of a complete pump numerical model. This is constructed in such a way as to allow the easy modification of the various geometric parts to facilitate the modelling of variant design arrangements.

- The completion of a reasonable number of analyses covering the above variables in order to allow rationalisation studies. These are carried out using a Taguchi L_9 orthogonal array. Without this approach a very large number of analyses would be required. Even utilising such an efficient arrangement a minimum of twenty-seven transient analyses must be conducted to cover the effect of the geometry variations on the pressure pulsations over the three flow rates.

It is acknowledged that not all pressure pulsations occurring in a pumping system necessarily arise from within pumps, as there will always be a transient element to any flow prior to the flow entering the pump. The transient flow elements have not been considered as part of this study for two main reasons. Firstly, although a designer does take some elements of the hydraulic conditions at the pump inlet into account when designing a pump, external effects are not normally included. Secondly it is reasoned that a pump that generates large pressure pulsations due to its design is unlikely to cope well with external pulsations and vice versa, i.e. a pump's capability to deal with pulsations is dependent on its internal geometry regardless whether the source of the pulsations is internal or external to the pump.

The parametric study has been limited to three flow rates as each additional flow rate increases the timeframe for the analyses significantly. A set of analyses at the duty flow rate would be the minimum requirement for the process. As the avoidance of fatigue failure is one of the motivational factors behind the work and as experience has indicated that this failure mode is often associated with continual running at low flow conditions, two lower flow conditions were also selected for analysis (25% and 50% of the duty flow condition).

The present contribution is rooted in the application of CFD as a useful tool in the practical design of pumps for operation in industry and the final outcome of the work is the provision of improved guidelines for designers. However, this work also analyses the fluid physics involved in complicated flow patterns that arise due to the interaction of rotation and stationary components in tight clearances. It is anticipated that the

outcome of this project will provide both a better understanding of the pressure pulsations in centrifugal pumps, and provide designers with an effective tool to minimise pulsations within their designs.

While there have been many individual contributions to turbomachinery using CFD, there is little previous published information on a complete pump geometry or on a systematic examination of the geometric variables that affect pulsations and performance. The present work seeks to rectify this position and should allow tangible design improvements to be realised.

1.3 Structure of Thesis

Following this initial chapter, which has introduced centrifugal pumps and the project objectives, Chapter 2 presents a review of relevant published literature. The review briefly discusses the origins of CFD and the history of its use related to pumps. It is noted that the work published to date on pressure pulsations has been mainly experimental in nature. The chapter will include a summary of literature where the effect of design modifications on pump behaviour has been investigated.

Chapter 3 reports some preliminary work conducted by the author on multistage and double entry pump designs including fatigue effects. This work was important in that lessons were learned and it highlighted a number of issues that merited further attention before the main body of work could proceed. Chapter 4 details some (limited) industrial based experimental work conducted prior to the project that has been used for comparison with the computational model. However, the author encountered a number of difficulties regarding the experimental work. Only the raw experimental data was available for use, since a proper report was not written on the test work and the original experimentalists were not available for discussion on the experimental work. The author has therefore analysed and interpreted the data to provide it in a suitable form for comparison with the analyses. The chapter includes descriptions of the test rig set up,

the test procedure and the programme of tests performed as well as a discussion of the results.

In Chapter 5 the methodology adopted in generating a three dimensional numerical model of a scaled high energy centrifugal pump is presented. The chapter describes the procedure used to obtain a high quality grid throughout the computational model, including the grid independence check made on the impeller and the process used to assemble the model in separate steps. Multiple CFD analysis models are created, with each encompassing a complete pump of a different internal geometry and include suction inlet, double entry impeller, leakage flow paths and the double volute. The chapter details the measures incorporated into the modelling of the geometry to simplify the analysis of different geometrical arrangements. Information on the selection of a turbulence model and the boundary conditions chosen is also provided alongside the numerical controls used for the analyses.

Chapter 6 provides an initial examination of a selection of the results. Some general investigations are conducted relating to the pressure distribution and velocity field local to the impeller. The flow features identified above are compared with two independent, external experimental tests to determine if they are comparable. There is particular focus on pressure pulsations in the pump, with the pulsations being monitored at fifteen locations around the pump. The RMS pulsations predicted by the CFD analyses are compared with the experimental data discussed in Chapter 4. The comparison is conducted for two similar arrangements of pump and for three flow conditions.

Chapter 7 presents a full set of results detailing the pulsations at all flow rates for all arrangements. Taguchi post-processing techniques are used to provide a structure for the interpretation of the results. These techniques identify the relative influence of the four geometric parameters on the pressure pulsations at each location monitored at each of the flow rates analysed. Thus an understanding of the pulsation and its distribution in the pump can be gained. This aspect is also extended to include performance characteristics and the pressure differential across the shroud at the impeller outlet. A new pump arrangement is derived through a rationalisation process with a view to

reducing the pressure pulsation levels within the pump, without a significant loss of performance. Details are provided concerning the steady state analysis results and comparisons made with the transient analyses for three different flow rates and between two different geometrical arrangements. This seeks to determine whether a relationship exists between the pressure pulsations obtained by the two analysis methods. The relevance of the CFD pressure data to the mechanical impeller design is investigated using two methods. The first compares the CFD predicted pressure differential across the impeller shroud with assumed pressure differentials in Weir Pumps design guidelines. Recommendations are given to refine the design guidelines in light of the CFD data. The second method demonstrates a method for transferring CFD pressure data for use in finite element stress analyses. The resulting stress levels are compared with theoretically predicted results. The chapter concludes with a summary of the various recommendations made regarding the design of pumps with lower pressure pulsations. Finally, general conclusions and comments regarding aspects of work that require further attention are provided in Chapter 8.

Chapter 2

Literature Review Concerning Methods of Characterisation of Internal Flow in Centrifugal Pumps

2.1 Experimental Investigations on Stationary and Periodic Unsteadiness

2.2 Computational Methods

2.3 Pressure Variations Due to Pump Modifications

2.4 Chapter Summary

2 Literature Review Concerning Methods of Characterisation of Internal Flow in Centrifugal Pumps

The search for a greater understanding of the fluid flow within turbomachinery has spanned more than two centuries. For example, the first major contribution was made by Euler who provided the first theoretical analysis in 1750 (7) and indeed his work is still in use in some respects today. Although, theoretical methods usually provide better approximations to actual flows and help to generate improved designs, yet, strangely in Euler's case his theories did not lead directly to improvements until almost a century later. This present review presents a summary of the significant published events charting the development of the understanding of fluid flows within turbomachinery and centrifugal pumps with a special focus on unsteady flows.

The review is presented in three main sections.

- The first introduces literature that describes experimental work carried out to investigate fluid flow in turbomachinery. This first section is split into two subsections; it initially centres on work detailing "unsteady stationary" flows and progresses to literature investigating flows of an "unsteady periodic" nature. These terms are conveniently defined by Abramin and Howard (8) as,

  Stationary Unsteadiness: "*the flow separation and wakes associated with the passage pressure gradients, secondary flows and boundary layer stability*." For example, the flow past a stationary body such as an aerofoil gives rise to such unsteadiness that exhibits itself as vortex shedding at the trailing edge.

  Periodic Unsteadiness: "*the rotating stall and cyclic flow phenomena induced by the volute/casing.*" For example, this is characterized by the disturbance in the flow due to the rotating impeller blade passing the stationary volute cutwater.

Although the main focus of this review is periodic unsteadiness, both of the unsteady flow features coexist within centrifugal pump flow and so both are of significance.

- The second section discusses literature detailing computation simulation of fluid flow within turbomachinery. Although the main interest in this review is centrifugal pumps, computational analyses of other turbomachinery devices are included where appropriate.

- The final section provides a brief overview of published work that has examined the effect of geometrical modifications in relation to both pressure pulsations and turbomachinery performance.

2.1 Experimental Investigations on Stationary and Periodic Unsteadiness

With research into pumps taking place as early as the eighteenth century and computational fluid dynamics only being present in some shape or form for the last fifty years, it is important to consider experimental investigations involving pumps in addition to numerical studies. In a recent paper (9), Ohashi and Tsujimoto review CFD papers published in the Transactions of the Japan Society of Mechanical Engineers and also identify the number of pump related papers. In a figure, reproduced here as Figure 2.1, the authors identify that the volume of CFD papers has increased dramatically in the last twenty to twenty five years, but also point out that the volume of pump related papers including experimental papers peaked during the eighties. It is noted that in Japan in the fifties and early sixties, nearly twenty percent of fluids engineering research was pump related. This simply highlights the wealth of experimental pump research conducted prior to the emergence of CFD.

It is also important to recognise that experimental techniques have changed enormously and that published work can only take advantage of the most advanced measurement

techniques at a specific period in time. The majority of the published literature identifies the instrumentation techniques adopted during tests and Durst (10) provides a useful overview of developments made in measurement techniques related to fluid mechanics. His review includes a summary of techniques such as laser-doppler anemometry, flow visualisation techniques and particle image velocimetry.

The unsteady stationary section that follows relates mainly to general flow in pumps, while the periodic unsteady section includes more information on pressure distributions and resultant effects. Pressure variations and pulsations will be considered specifically in Section 2.3.

2.1.1 Unsteady Stationary Investigations

One of the earliest, accessible investigations was conducted by Fischer and Thoma (11), who compared two-dimensional predicted flow with actual flow behaviour inside an impeller. The comparison was achieved using early flow visualisation techniques involving a rotating prism. Fischer and Thoma concluded that the theoretical predictions for an ideal frictionless fluid were fundamentally different from the flows predicted using their apparatus. The experimental results identified a region of flow separation occurring at the suction side of the impeller that was present during most part-load flow conditions but was not predicted by their theoretical work. Importantly this zone of separation was observed to increase as the flow rate decreased.

By the mid fifties, there were two basic methods of observing velocities within the impeller namely, hot wire anemometry and the use of photography to monitor tracers in the flow. Work using these methods added weight to the observations made by Fischer and Thoma. Lennemann and Howard (12) used a photographic technique to identify that the reverse flow in the blade passage was due to a boundary separation problem, which was strongly influenced by the secondary flow pattern in the impeller. These experiments were conducted both at part load and very low (zero) flow conditions.

In the mid-seventies, Laser Doppler Anemometry (LDA) emerged as a promising tool for velocity measurements inside turbomachinery impellers. Eckardt (13) used this method to examine the flow in the radial-exit impeller and discovered that a jet wake flow is present as a result of separation-like phenomenon combined with secondary flows. Using these results to compare the flow in a closed, backswept, centrifugal impeller of the radial exit type, Adler and Levy (14) conducted LDA measurements in a shrouded impeller. Adler and Levy reported that the flow at the design condition was stable, even with undesirable flow distortion at the inlet. The reason for this stability was suggested to be associated with the backward swept blades.

Eckardt's discovery of the presence of a jet wake flow in the blade passage was of interest to Krain (15), who investigated the effect of a vaneless and vaned diffuser on this flow pattern. Krain showed that the difference between vaned and vaneless diffusers is small, only exhibiting a weak effect on the impeller flow. Krain surmised that this weak effect was due to the low diffuser leading edge Mach number and the special vaned diffuser design (high diffuser leading edge radius to impeller exit radius ratio, i.e. essentially a measure of the gap between impeller and diffuser blades) used in the experiments.

Work on unsteady stationary flows continued into the late eighties, with Rose (16) performing work based on Eckardt's research as well as that of Adler and Levy. Rose highlighted that the impeller blades used in both of the previous experiments were of a two-dimensional type that had been rejected by industry as being inefficient. Applying LDA and surface static measurements, Rose investigated the flow through an impeller design that employed impeller vanes that twist in three dimensions. Results indicated that the flow field within the pump impeller was unlike those found in other turbomachines. The flow was very "mixed out" due to the strong secondary flows caused by the "centrifuging" of high-energy boundary layers.

2.1.2 Unsteady Periodic Investigations

Using a single pump arrangement Binder and Knapp (17) investigated the pressure distribution in the volute at low flow rates. The investigation concluded that the radial force is related to the volute pressure distribution, together with the non-uniform momentum-rate distribution of the flow discharging around the periphery. Iverson et al (18) reported similar pressure distributions in the volute, i.e. increasing from the cutwater through to the discharge, with a rapid pressure drop at the cutwater.

In the early sixties, Csanady (19) suggested replacing the volute casing with an "equivalent" logarithmic scroll, generated using the assumption that at the design flow there is no radial force exerted by the impeller. The pressure distribution was established by mapping the spiral on to a flat plate and utilising velocity triangles for the impeller outlet. From the resulting data some qualitative features of the behaviour of radial forces on the impeller were deduced. The results of the calculations were found to be in good agreement with the work performed by Iverson (18).

Almost twenty years after the publication of Csanady's theoretical model, Colding-Jorgenson (20) utilised the model to introduce the concept of hydrodynamic stiffness matrices. Stiffness matrices employed a two dimensional method to identify the connection between radial forces and the position of the impeller. The matrices included the effect of the impeller rotating within the volute and introduced hydraulic forces exerted on the impeller due to the impeller being offset from the centre of the volute at the design flow condition. Chamieh et al (21) conducted experiments measuring the hydrodynamic force acting on a centrifugal impeller as a function of the impeller position within two geometrically different volutes. The hydrodynamic matrices formulated from their tests were found to be of a form that would indicate that there would be excitation of whirl motion of the impeller

The idea of a whirling impeller and its effects was investigated by Adkins and Brennen (22). The investigation conducted experiments aimed at providing a better understanding of the destabilising force observed by Chamieh. A theoretical model, generated from the experiments, included a quasi one-dimensional treatment of the flow

in the volute. The theoretical model considered off flow streamlines that deviated from the ideal condition and was used to obtain pulsations of force acting in the volute due to the eccentric whirling motion of the impeller.

Baun et al (23) also considered the implications of an impeller located at a differing centreline to the volute. The tests involved measuring the characteristics such as the hydraulic performance and radial hydraulic force against the impellers relative position within the volute. Multiple flow rates were examined including both design and part load flows, within circular and spiral volutes. Baun et al observed that the results indicated an optimum volute to impeller offset distance that provided the required performance characteristics and reduced the radial force. The authors observed that the tests were only conducted for a single specific speed impeller and therefore further testing would be required to determine if the observed optimum location was consistent for various impeller shapes.

Miner et al (24), identified that the majority of the work conducted on centrifugal pumps up until the end of the eighties had focused on the impeller or the volute separately. Miner's work sought to bridge the gap by providing measurements in both impeller and volute for the same operating conditions. Some conclusions of importance were that even at design flow, flow within the impeller is not axisymmetric due to interaction between impeller and volute. Evidence for recirculating flow within the impeller blade passages was found at the 40% flow condition. The influence of the blade effect was rapidly damped out within the volute.

That same year Arndt et al (25) presented a paper containing both unsteady impeller blade and unsteady diffuser vane pressure measurements in a diffuser pump. The authors noted that pressure fluctuations were larger on the suction side than on the pressure side and that increasing the radial gap between impeller and diffuser blades resulted in a significant decrease in the large pressure fluctuations.

Dong et al (26, 27) introduced a technique and a procedure that could be used for quantative flow visualisation. This was utilised to provide detailed information in the

form of circumferential, radial and axial variation in the velocity distribution within the volute. The authors noted that Miner et al had previously reported the majority of the blade effects observed; however they added that these effects were not damped out rapidly but that the flow in the entire volute was pulsating. This work was followed up by two papers by Chu et al (28, 29) explaining the use of velocity to compute the pressure field within the volute of a centrifugal pump. The first showed that the effect of vorticity couldn't be ignored, which led to the conclusion that a potential flow model cannot describe the flow adequately. The second paper (29) focused on the relationship between pressure pulsation and noise. Chu et al conclude that the pressure in the volute was dependent on the relative location of the impeller to the cutwater. It was also shown that the noise emitted by the pump was related to the changing pressure distribution caused by impeller/cutwater interaction. This investigation was only performed at a run out condition (at a flow 35% above the duty condition). A possible, logical, extension of this work would be to attempt to relate the pressure pulsation to the noise generated to identify any reduction gained from modifying the impeller/cutwater clearance.

Abramin and Howard (30) published details of their rotating laser-Doppler anemometry system that allowed direct measurement of relative flow and has application in non-periodic flows. A related second paper (8) used the method to investigate the unsteady behaviour in a low specific speed pump impeller. Stationary unsteady flow was found in the rotor, initiated at the inlet and combined with a potential vortex that dominated the exit; this resulted in separation on the pressure face of the impeller at low flow operating conditions. Periodic unsteadiness was also found due to the interaction of the impeller and the volute. Unfortunately, the method described by Abramin and Howard to generate their results is limited in that it is only applicable for low speed machines.

Wo and Bon (31) investigated the flow within the volute of a centrifugal pump with a view to identifying physical reasons for instability of the flow characteristic. Wo and Bon identified that adverse flow in the cutwater region was one of the important features contributing to instability in the pump's characteristic.

Kaupert and Staubli, conducted an investigation of the unsteady flow within a centrifugal pump with a high specific speed impeller. An impressive 32 pressure taps were located in the volute in addition to 25 piezoresistive pressure transducers in a single blade passage. Their work is presented in two papers (32) (33). The first paper (32) details a circumferential pressure distribution within the volute, as had been identified by many authors before them. It is noted that the further away from the duty condition, the greater the magnitude of the fluctuation of the unsteadiness, however the author concedes that this has also been identified in prior publications. The authors quantify their discovery by noting that at some low flow conditions the fluctuations were as high as 35% of the pump head. Kaupert and Staubli also used their experimentation to further the work conducted by Wo and Bon, regarding instabilities in pump characteristics. The authors observe that the inlet and outlet recirculation zones are considered as a singular recirculation zone that is connected transiently through the impeller. It is noted that the outlet recirculation zone was influenced by the volute arrangement. The second paper (33) deals with the transient hysteresis in the performance characteristic and is not considered further here.

The advent of numerical modelling methods has gradually reduced the number of published experimental programmes in centrifugal pumps. In fact it is not uncommon for the experimental test to be performed primarily with the intention of providing validation for a numerical analysis. A recent example of this is displayed in work conducted at the University of Oviedo that has been presented by Parrondo-Gayo et al (34)(35)(36) where an initial experimental investigation is covered briefly and is then referred to in various, subsequent numerical papers Blanco-Marigorta et al (37) (39) and González et al (38). The experimental work presented by Parrondo-Gayo et al, is still significant in that it provides excellent data concerning the impeller/cutwater interaction, in addition to a rough estimate of the effect of cutwater clearances on the pressure pulsation. It is also worthwhile to note that the authors identify that the pressure fluctuations at any point in the volute are caused by: i) the passage of any impeller blade relative to that point; and ii) the passage of the each blade relative to the volute cutwater. The authors also consider the impeller blade/cutwater interaction to be responsible for noise generation.

The idea of attempting to relate flow behaviour to noise is not new. In the late seventies Everett (40) produced a short but interesting paper on the relation of hydraulic loss to pump noise where he referred to works ten to fifteen years earlier. Little else is in evidence until more recently, except Marshcher's (41) study of the effects of steady and fluctuating fluid force on the shaft. Corley (42) and Jones and Burley (43) have performed work relating fluid flow to noise; however neither of these holds particular relevance to a pump review, although some of the general principles involved are of note, for instance the latter focuses on the effect of blade shape on rotor noise.

2.2 Computational Methods

For the purposes of this review, it is not necessary to enquire into the past origins of numerical modelling or to detail its development. McNally and Sockol have provided an excellent history of the development of CFD codes for turbomachinery (44) and Denton and Dawes (45) also provide a good introduction to CFD methods and the numerical prediction of flows in general. John Anderson's book, "Computational Fluid Dynamics – the basics with applications" (46), is one of many books that provide a good introduction to the elementary concepts of CFD.

In short, CFD is concerned with solving the Euler and Navier-Stokes equations governing the flow field in external and internal flows. Areas of importance in the development of the solution of these equations are grid generation, turbulence modelling, application of boundary conditions, data processing and efficient use of the computational power available.

It wasn't until the eighties that CFD began to attract more attention**;** Barber's preface (47) to an issue of the Journal of Propulsion and Power provides a brief overview of past development in addition to broadly specifying the requirements of CFD codes at that time.

As evidence of the growing capability of numerical prediction methods, Lorett and Gopalakrishnan (48) investigated the flow behaviour involved in a complete flow reversal occurring over part of the impeller periphery near the volute cutwater. Due to difficulties in obtaining an analytical solution, a step-by-step computation was used and the results compared favourably with available test data. The method illustrated that the velocity in the flow channel varies as it rotates, contradicting the classical assumption that the relative flow in the impeller is steady. It was also found that the reverse flow condition occurred at below 40% of the rated flow. Blade/vane, rotor/stator interactions were of particular interest around the late eighties/early nineties, with Giles (49), Weber et al (50) and Rai and Madavan (51) all investigating different aspects of the interactions, the latter two using different gridding methods (C-type and O-type respectively) to investigate the interactions.

At that time little confidence was placed in the results of CFD analyses and experimental testing of the design was usually performed in addition, in order to validate the CFD code and the CFD model. Ingersoll-Rand presented one of the early industrial CFD analysis papers in 1990 related to centrifugal pumps (52) using CFX-TASCflow (a commercial Navier Stokes code). In this work, Graf et al performed a 3-D computational analysis of a pump crossover diffuser and discovered some flow patterns that were not immediately intuitive. This paper provided a number of interesting points for the pump industry; these included, identifying that CFD codes had reached the stage where they could be used cost effectively to analyse pumps, that their use could increase understanding of flow phenomena and thirdly that flow patterns may not conform to the designer's initial thoughts. The paper also notes that commercial Navier Stokes solvers raise a host of issues including certification of a code's accuracy, integrity and applicability to a problem. Cooper et al (53) from Ingersoll-Dresser published a paper, using CFX-TASCflow, to analyse the flow in a single blade impeller passage and stationary crossover separately. The paper provided typical solution times related to grid size, noted the importance of including all regions that may affect flow in the model and generally illustrated CFD's use as a tool to improve existing pumps or existing designs.

Computational methods were themselves also being developed. Rai's (54) paper on solving rotor/stator interactive effects using patched and overlaid grids detailed a number of computational improvements and also highlighted problem areas to be addressed. Denton (55) detailed the extension of established three-dimensional flow calculation methods to calculate flow through multiple blade rows. This avoided calculating unsteady flow and used a mixing process between adjacent blade rows. Tsung et al (56) produced a finite volume method to analyse the unsteady, unstructured, three-dimensional Navier-Stokes equations. The finite volume method, although found to be generally acceptable, required considerable work to resolve issues found in the examples used. Shortly afterwards Hah et al (57) reported an interesting comparison of numerical results of two three-dimensional Navier-Stokes codes, one structured, the other unstructured, for both steady and unsteady applications. Both solvers are shown to be capable of resolving the essential flow features when compared to experimental data; however the unstructured solver does not manage to obtain as high a quality resolution as the structured solver.

Chen and Liaw (58) conducted a study aimed at understanding the effect of the volute on the performance of the impeller and any associated unsteady effects at the design flow rate. The analysis was split into two sections with the first analysing a single blade passage and the second a four bladed impeller within a volute. This second model utilised a frozen-rotor interface between impeller and volute and was far more complex that the first. It is perhaps worth noting that a common physical analogy used in describing the frozen rotor interface is to imagine observing the flow crossing between components in the rotational and stationary frames under stroboscopic lighting. The various interfaces that can be used in multiple frame of reference analyses will be considered in more detail in Chapter 5. In an attempt to reduce the effect of the additional complexity on analysis time scales, flow results were only taken at 18 degree intervals in blade position, however the second analysis was still eight times that of the initial problem. It is of importance that the second method of analysis provided a better performance prediction and a more detailed explanation of the behaviour of the flow. Interestingly, Chen and Liaw commented that the predicted radial force associated with the flow field is believed valuable for rotor-dynamic and pump vibration studies. Badie

et al (59) conducted a similar analysis but developed their own algorithm, with an aim to model two-dimensional flow through a centrifugal pump with particular focus on the volute cutwater area. They predicted the velocity and pressure variation in the volute to their satisfaction, with the largest discrepancies being found at low flows. They suggested that it was possible to optimise the shape of a volute for a given impeller using potential flow methods. This conclusion seems to conflict with the conclusions reached by Chu et al (28) as a result of their experimental testing two years earlier. This difference of opinion may have arisen due to the different level of accuracy that each team of researchers deemed acceptable in their results. It is worth noting that while Chu, Dong and Katz provide an estimate of the level of error in their experimentation, they do not quantify the effect of the non-potential flow aspect of the fluid observed. Badie et al (59) seem to indicate that the potential flow model produces results that are within 3%-10% of experimental results depending on the flow rate.

Tsukamoto and Shi (60) highlight that although rotor/stator interactions have been examined extensively in axial gas turbines, there are very few similar studies covering the interaction in centrifugal pumps. The pump they analysed is of a diffuser volute type and so involves important interactions between impeller blades and diffuser vanes rather than between the impeller blades and volute. The paper documents the arrangement of the transient analysis in some detail and performs both two-dimensional and three-dimensional simulations. The simulations are used to analyse both the potential and wake effects along with their downstream effects. The analyses seem only to have been performed at the duty flow rate, although low flow analyses are mentioned as part of future work considerations.

As mentioned in Section 2.1.2, the University of Oviedo in Spain has published a number of papers, Parrondo-Gayo et al (35, 36), detailing investigations concerning pressure fluctuations within a centrifugal pump. Following this experimental investigation and some preliminary 2D validation work (37), Blanco-Marigorta et al (39) published detailed information concerning a 3D numerical model focusing on the pressure fluctuations at the blade passing frequency. The authors state that it is possible to obtain improved results by specifying and controlling flow using a total pressure inlet

condition. However, this also results in poor convergence at lower flow rates, increased analysis time and less stability during the analysis. Unsurprisingly the authors list the impeller volute interaction as playing a lead role in the generation of these pulsations. A point of interest is that the location of the pulsations relative to the position of the impeller blade from the volute tongue is found to be dependent on the flow rate. This work has progressed with a further two papers being published involving three-dimensional transient analyses of the pump, ((Gonzalez et al (38) and (39)). The numerical model although larger that that detailed by Blanco-Marigorta, is still relatively coarse, containing only 330000 cells for the pump and volute. The numerical model seems to successfully capture the amplitude of the fluctuations, but the analyses are only conducted at 60% flow and higher. It is presumed that this is due to the instability and convergence problems originally noted by Blanco-Marigorta. To date all of the numerical models have only modelled the impeller and volute, the influence of leakage flow paths on the pressure fluctuations has not been considered.

Interest in CFD continued to increase, although some areas of industry tended to remain sceptical as to its serious application without further validation. To this end, Burt et al (61), conducted a detailed analysis of a mixed flow bowl analysis in the late nineties and compared the results to extensive LDA work, which was provided by Weir Pumps. The CFD predicted pump performance (head, flow, power and efficiency) was found to compare favourably with the LDA measurements for a wide range of flows (from approximately closed valve to 150% BEP). Importantly CFD also correctly predicted instability in the pump characteristic.

Gradually typical CFD analysis became more complex and time consuming as more and more complicated situations were investigated. In 2000, Miller (62) took analyses in a different direction when, instead of refining grids, he conducted a study using coarse grids to analyse flow in axial pump impellers. The coarse CFD grids produced good agreement with experimental results within a short analysis time, the largest errors being found to be in the tangential velocity component. This demonstrated that, in certain applications, CFD analyses could be conducted in a relatively short period of time and still produce results with a reasonable level of accuracy.

Interest has been expressed by industry concerning how CFD will fit into the design process in a practical sense. Gülich (4) of Sulzer Pumps provided a good practical explanation about the use of CFD with regard to creating a new pump design, covering such areas as preliminary design and CFD data interpretation. The paper described the impact of various geometric parameters and flow features along with their effect on the pump performance across a variety of flow conditions. Williams et al (63) illustrated how CFD can be being used practically and cites benefits over conventional model testing. The authors conducted CFD analyses with a view to designing a two-stage unshrouded fuel pump that will match the performance criteria of a three-stage shrouded pump. The team were able to analyse a variety of designs, select the one that best fulfilled their requirements and then analyse variations on this design to arrive at an optimum design for the application. Dyson (64) also provides some recommendations for designers in conducting CFD pump impeller and diffuser simulations.

Mirroring the experimental interest in relating hydrodynamic characteristics to mechanical problems, recent papers have used CFD to improve not only flow characteristics but also acoustic characteristics of turbomachinery. Pembroke (65) conducted a CFD analysis using a model of the suction portion of the casing and the impeller. The CFD analysis highlighted a poor area of design that caused a vortex to develop in the casing and a modification was made to minimise this disturbance in the flow. Conventional pump tests were performed for both designs and it was found that the noise had dropped 3dBA from a noise level of 96dBA. This paper does not relate the hydrodynamic behaviour to noise, but provides an example of how benefits from CFD can extend further than just providing a better understanding of flow behaviour. More recently most research in the area of noise has concentrated on fan behaviour as shown by Cailleau et al (66) and Biedron et al (67) who both use numerical techniques to predict unsteady rotor/stator interactions and relate these to acoustics. The latter paper provided an in-depth look at the feasibility of using Navier Stokes to directly capture the sound generation mechanisms of rotor-stator interaction. However, computed values were found to be considerably different from measured results, illustrating that further work was required.

"Optimised design" is often regarded as the ultimate goal of CFD, however this is still some distance away. At a recent conference at Institution of Mechanical Engineers, London, entitled "Advances of CFD in Fluid Machinery Design" one presentation by Scheuerer (68), discussed the "Coupling of CFD and Optimisation Methods for Turbomachinery Applications". Another method of connecting CFD to the automated design of turbomachinery is the inverse design method, Zangeneh et al (69, 70, 71, 72) which utilises a series of parameters, including, ideal blade loadings, to generate the blade shape. This method, although being offered as the software programme Turbodesign-1, is still regarded with a great deal of uncertainty within certain areas of industry. Several typical questions that arise concerning such optimisers include the understanding and derivation of ideal blade loadings, the marrying together of the optimised design with available economic manufacturing processes and the interaction of an optimised impeller with other components such as the volute. However, such programs are under continual development and further advances in methodologies are expected.

2.3 Pressure Variations Due to Pump Modifications

2.3.1 Hydraulic Thrust Investigations

Traditionally more interest has been shown in the effect of hydraulic pump forces as opposed to actual measured pressure pulsations, although there is an undeniable connection between the two. Uchida et al (73) performed tests that involved monitoring the radial force and pump performance for different volute cutwater gaps and cutwater shapes. The authors noted that when varying the cutwater gap, while keeping the impeller outer diameter constant, the best efficiency point did not change when the gap was modified. Other cutwater designs were considered and these were found to have an effect on the best efficiency point. It was also noted that certain cutwater shapes performed better at different flow conditions.

In 1986, the Fluid Machinery Committee of the Power Industries Division of the Institution of Mechanical Engineers, held a seminar titled “Radial loads and axial thrusts on centrifugal pumps”. Several papers presented at this seminar contain information of relevance to this thesis. Milne (74) provided a report of some tests that showed that an approximately linear relationship existed between a volute differential static pressure and pump flowrate. This in turn suggested that there was also a relationship between the volute differential static pressure and the radial load. Guelich et al of Sulzer (75) presented detailed information regarding the radial and hydraulic loadings for a variety of pump volutes. This work included an excellent discussion on radial thrust that covered a broad range of items relating to radial thrust such as, advantages and disadvantages of different measurement techniques, design data for various volute types and the influence of geometric parameters on the radial thrust. It is worth noting that, although axial thrust was considered it did not receive the same level of detail as the radial thrust. Konno & Ohno (76), in a brief paper, demonstrated through experimentation that an increase in the specific speed of a pump increases the fluctuating axial thrust. In a direct attempt to reduce pressure pulsations Konno & Ohno also examined the influence of a skewed cutwater shape in the volute. It was reported that the skewed cutwater shapes corresponded with an increase in the fluctuating axial thrust, which was considered to be due to the non-symmetrical cutwater geometry generating non-symmetrical pressure distributions within the volute. Goulas & Truscott (77) reported on work that studied the radial and axial forces as a function of the flow rate, cutwater clearance and angular distance of the blade tip from the cutwater. While the study revisited work performed by Uchida et al (73) to some degree, it provided a clear set of data illustrating the relationship between the above variations and the radial load. Unfortunately, due to the nature of the instrumentation there is no understanding of the flow patterns that result in the change in radial force. It is of interest that Uchida’s work discovered that the best efficiency point (BEP) does not change when the cutwater gap changes. On the other hand Goulas & Trustcott’s results, shown in Figure 2.2, indicate that the BEP does indeed change. It is important to note that Uchida et al varied the cutwater gap using different cutwater arrangements, whereas Goulas & Trustcott varied the same gap by using different impeller diameters.

Therefore, it seems likely that the change in the efficiency point is due to the reduction in the impeller diameter rather than as a result of the increased cutwater gap.

Two years later, a further conference was held at the Institute of Mechanical Engineers this time with the title "Part-Load Pumping Operation, Control & Behaviour". Stanmore of Wilson-Snyder Pumps presented a paper (78) concerning operational problems with a centrifugal pump at part load flow conditions. It was identified that at certain flow conditions pressure pulsations could reach a value of approximately 20% of the discharge pressure due to recirculation at the impeller inlet. It was noted that the cutwater gap as a percentage of the impeller radius was small, less than 1%. The author then implemented a number of geometrical modifications that were greatly influenced by work published by Makay (Makay's work is reviewed below). A significant number of modifications were made; however the two relevant to this review were increasing the cutwater clearance from 1% of the impeller radii to 9% and reducing the snubber clearance. Stanmore reports an immediate audible reduction in the noise level of the operating pump and these casual observations were corroborated by the experimental results. The author notes that the modified pump suffered an impeller failure after approximately six months, however this was considered to be due to the pump operating at and below the minimum recommended flow rate for prolonged periods. Stanmore concluded that the minimum safe operating flow for that specific pump design was 45% of BEP.

In recent years work relating to the hydraulic forces within centrifugal pumps has been limited. Hsu and Brennan (79) published a study investigating forces caused by swirl due to front shroud leakage flow. This work concentrates on the swirling flow and the discussion is exceptionally brief, which limits its interest for the current project. Baun and Flack have recently published a number of papers on the subject, however their most recent work (80) simply utilises modern measurement techniques to monitor the effects studied previously others. For example, the work conducted by Guelich et al (75) included a study of the influence of different volute types that was repeated by Baun and Flack.

2.3.2 Direct Measurement of Pressure Pulsations

Early work was performed in the fifties under the guidance of the British Hydromechanics Research Association (BHRA) that investigated the effect of various geometrical changes on a pump. This covered a wide range of pump geometrical influences; for example two such early papers by R. Worster examined the effect of vanes in the volute and the effect of the impeller outlet width (81), (82). Unfortunately these studies stop short of a thorough investigation and so any conclusions must be tempered with an element of uncertainty. BHRA also kept up to date with developments in other countries, a good example being the translation of a German paper by Rasheed that examined the pressure pulsations in a centrifugal pump (83). Rasheed performed numerous experiments, monitoring the pressure at various locations in the pump volute while varying the pump rotational speed. It is reported that the maximum pulsations were found between 50% and 65% of duty flow, with the largest pulsations occurring near the volute cutwater. The summary mentions other work involving the effect of the number of vanes and the pump delivery on the pressure developed. It is assumed that this further work is in part 1 of the German report. Unfortunately only the second part of the report was translated by BHRA and the original part 1 is not referenced in part 2. Attempts to locate a translation of part 1 have been unsuccessful.

Through the seventies and into the early eighties Makay published a significant amount of data concerning pump operation and provided specific recommendations to achieve a reduction in pressure pulsations. In an article in the “Power” magazine Makay and Nass (84) emphasises that pressure pulsations are one of a number of phenomena that “tax safe pump operation”. He notes that such pulsations have been magnified in high-output, high-speed pumps and frequently result in fatigue failure of the impeller. This article contains a simple, yet important definition concerning pressure pulsations namely, that pressure pulsations are “low- and high- frequency response of fluid particles to complex nonlinear forces.”

Research into the major causes of pump failure was reported by Makay and Szamody in 1978 (85). The study involved gathering operational information from 138 utilities in

America, paying particular attention to design features present and relating these to specific failure conditions. In general, the work noted that emphasis on gaining high efficiencies at design conditions led to undesirable flow features at part load operation and provided a thorough examination of pumps and pump design relating to performance difficulties. Throughout the report Makay and Szamody provided small items of information that were of interest to designers working with such pumps. One example would be the author's observation that pump reliability suffers when the delivered head per stage exceeds 2200 feet and this could be used to provide a warning sign for a designer on particular pump types. Emphasis is placed on internal pump clearances, especially those between rotating and stationary parts where high differentials exist such as the gap between impeller periphery and the volute cutwater. This work increases Makay's previously published recommendation, (86), regarding the minimum gap between impeller blades and volute cutwater, from five percent to six percent of the impeller diameter. During the survey it was observed that the majority of the impeller breakages reported occurred in pumps with unusually close clearances. This work while being of some value to a designer of high-energy centrifugal pumps often provides recommendations with little actual data to back up these claims. Makay and Szamody provide a graph plotting the peak-to-peak pressure pulsations against the impeller-volute (cutwater) gap (reproduced in Figure 2.3). This illustrates that the relationship between the pressure pulsations and a reduction in the cutwater gap is exponential, however the pulsation axis has no scale and no information is provided to support this claim. It can perhaps be assumed that this information is compiled from the data gained from the pump utility companies, but such information would not have been gained under controlled test conditions. Additionally, from the work performed by Uchida et al (73) and Goulas & Truscott (77), discussed in Section 2.3.1, it is important to identify the method used to vary the radial gap when considering the results, i.e. is the impeller diameter constant or is it varied.

Makay and Szamody also produced a second report two years later (87). A significant amount of this report covered the same ground as their previous publication, but additional relevant information is included. In this work Makay notes that no official pressure pulsation standards exist and that typically manufacturers quote a 3 percent

maximum of the pump generated head (measured at the discharge). It is interesting to note that Makay recommends that any pump that has a safe minimum flow rate of around 45 percent of design flow is not acceptable and that the pump design should be "examined and improved". This implies that some of the problems reported by Stanmore (78) in Section 2.3.1 were likely to be due to the actual impeller design and that this design should have been reviewed. In their earlier work (85), Makay and Szamody suggested that a low flow limit of 45 percent often indicates previous low flow operating difficulties with the design and in such a case the pump's failure history should be reviewed. It is also recommended that the safe minimum flow for a large feed pump should be 25% of the design flow condition. Other recommendations regarding the geometrical design of the pump are that on double-entry impellers the impeller blade should be staggered (or clocked) to minimise hydraulic forces. They also recommend that for double entry impellers the central shroud should be extended to the impeller outer diameter. As with their previous publication these recommendations are not presented with any back up information, for example, there is no discussion of the possible performance changes in the pump due to either design modification. Extending the central shroud effectively reduces the flow area at the impeller outlet, and from Worster's (82) investigation it appears that this will certainly affect the performance.

The subject of stagger vanes or clocked vanes, mentioned briefly by Makay above, is one that has received little to no attention in published literature with reference to centrifugal pumps. However, Sudo et al (88) provide brief information concerning the variation in pressure pulsations at the pump discharge due to the cutwater gap, skew of the cutwater tongue and the clocking of the impeller. Details are limited and the information relating to the skewed tongue is hard to separate from the cutwater gap variation data. Sudo et al report that the staggered impeller vanes produce pulsation amplitudes of around a quarter of those present for an inline impeller arrangement. It is worth noting that clocking has been used in turbines and a number of papers have been published regarding the approach. One recent paper by Haldeman et al (89) identifies clocking in turbines as being the "technique of locating a downstream vane row in different circumferential positions relative to an upstream blade row". This is obviously

significantly different from clocking in centrifugal pumps, but Haldeman et al does report an improvement in performance due to the clocked vanes.

Guelich and Bolleter wrote one of the most definitive pieces of published literature relating to pressure pulsations in centrifugal pumps (90). The work comprised the results of 36 different tests, which examined the physical mechanisms causing pressure pulsations and the effect of design parameters on the pulsations. The authors provide an excellent comparison, summarising current work in a tabulated form for important design features, such as the size of the cutwater gap and its effect on pressure pulsations. The work suggests using a dimensionless pressure pulsation parameter by assuming a square law relationship between the pressure pulsations and the circumferential impeller velocity. This dimensionless term has been adopted in a number of published works including that of González et al (38) when describing measured pressure pulsations. Guelich and Bolleter acknowledge that significant deviations from this scaling law can occur, however no general, easily applied procedures exist to provide a better estimate. The authors share the concerns highlighted by Makay & Szamody (87) concerning the lack of standards relating to allowable pressure pulsations and provide statistical data for reference in the absence of other standard data. The information presented in this paper, while highly valuable, does not provide any detailed understanding of the variation of pressure (or pressure pulsations) at varying locations within the pump. The data provided in the paper appears to be limited to the suction and delivery branches, as opposed to known regions of high pulsation such as the volute cutwater area. Therefore while their statistical data does provide a standard for comparison it does not provide any assurances relating to pressure pulsations away from the measured discharge or suction locations.

2.4 Chapter Summary

As can be seen from the literature review, pump manufacturers have been interested in identifying and understanding pressure pulsations or the effect of the pulsations within their product for a considerable period of time. Yet, there are numerous difficulties in obtaining pressure pulsations utilising experimental methods, which leads any investigation relating to pressure pulsations to consider utilising CFD techniques. One significant drawback of experimental testing is that results are only obtained for the specific locations measured. As has been shown by Parrondo-Gayo et al (35) the pressure pulsations vary significantly depending on the location measured, however at the same time it is only feasible to measure a finite number of locations. CFD provides the benefit that a pressure value is calculated for each grid element within the model and so provides a far greater wealth of information; however identifying the relevant portions of this information is a separate problem.

Conducting investigations involving pump impellers that have experienced operational problems is often unhelpful in terms of the timescales involved and the financial resources required, especially when such efforts are usually only concerned with analysing the problem rather than achieving a better design. CFD allows such an investigation to be conducted in a more effective manner, as the original design can be analysed as well as possible improvements. The CFD investigation can also provide input for stress analysis packages to better identify the physical effect of the pulsations on the mechanical components.

2.5 Figures

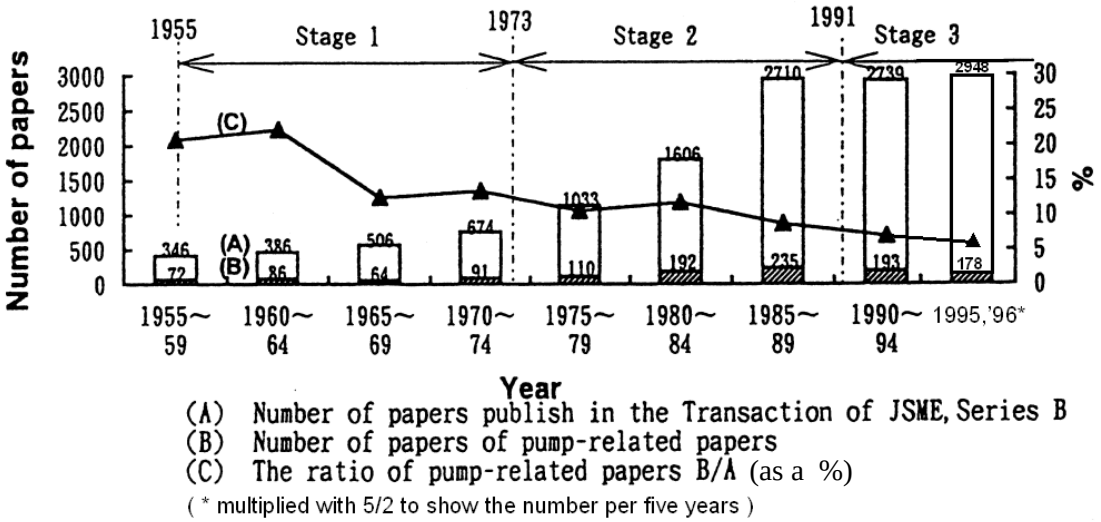

Figure 2.1: Number of papers published in the transactions of the Japan Society of Mechanical Engineers (JSME), series B (reproduced from Ohashi and Tsujimoto (9))

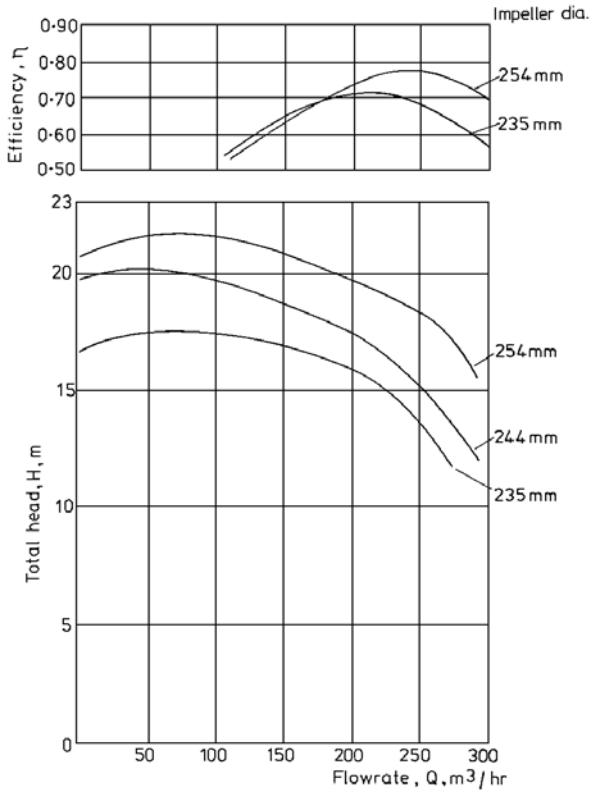

Figure 2.2: Pump related Performance at differing impeller diameters

(reproduced from Goulas and Truscott (77))

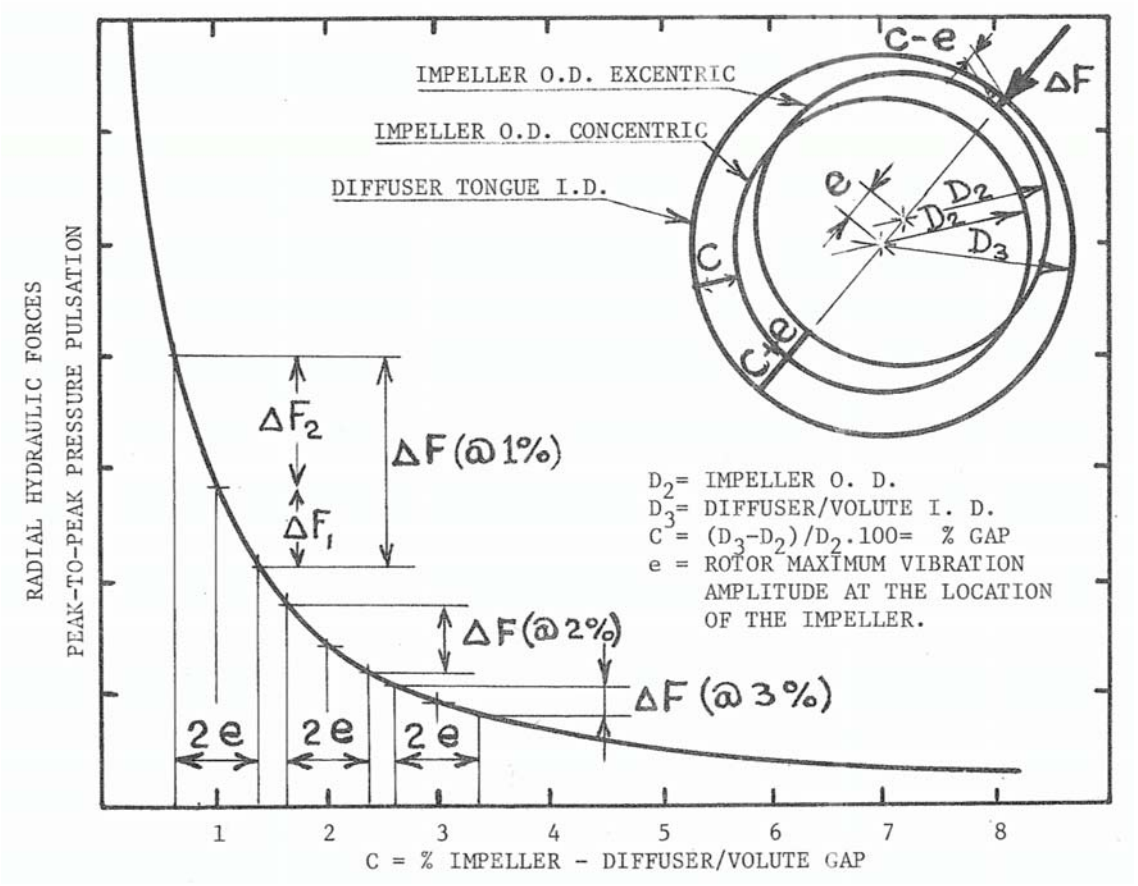

Figure: 2.3 Influence of impeller-to-diffuser/volute radial gap on pressure pulsation and radial dynamic forces (reproduced from Makay and Szamody (87)).

Chapter 3

Preliminary CFD Work Arising From Impeller Fatigue Failure in Pumps

3.1 Single Stage High Energy Impeller Fatigue Investigation

3.1.1 Set Up

3.1.2 Results & Discussion

3.1.3 Conclusions & Relevance to Thesis

3.2 Multistage Impeller Investigation

3.2.1 Set Up

3.2.2 Results & Discussion

3.2.3 Conclusions & Relevance to Thesis

3.3 Chapter Summary

3.4 Figures

3 Preliminary CFD Work Arising From Impeller Fatigue Failure in Pumps

Chapter 2 has indicated that opportunities exist in industrial applications for CFD to be utilised effectively when dealing with the deleterious effect of pressure pulsations within pumps. Ideally CFD would be used to provide an in-depth analysis in order to aid the understanding of the source of the pulsations and how to reduce them during continuous pump operation. However, timescales involved in such an investigations are often prohibitive, as customers require a quick and effective solution to any problem. Therefore it is often expedient to investigate the immediate problem and affect a specific solution. Nevertheless, the knowledge gained from the initial problem can help provide useful background for the application of CFD in analysing the more fundamental issues involved in understanding the generation of pressure pulsations in pumps.

In relation to this project and its aim to both identify pressure pulsations and provide guidelines of how best to reduce these pulsations, two such preliminary analyses on actual pump configurations were conducted. Both analyses incorporated the transient effects of the impeller rotation within a stationary casing, albeit for different applications. The first analysis investigated the fatigue failure of a single stage high-energy pump, with a focus on the effect of low flow condition on the pressure variations. The second involved a more general investigation to identify why the last stage impeller in a multistage pump is more likely to suffer from fatigue failure even though the impeller design is identical to those used on earlier stages in the same pump.

An overview of these analyses is provided here, although further information can be found in the published works Spence and Purdom (91) and (92). The work performed in both of these sets of analyses was conducted using the CFX-TASCflow program; the features of this program will be described in more detail in Chapter 5.

3.1 Single Stage High Energy Impeller Fatigue Investigation

Today's marketplace demands that a single pump should be capable of operating under an ever-widening range of conditions due to economic demands. As pump designs only have a single optimised operational point, a pump often operates outside of its ideal environment for considerable periods of time. This subjects the pump to unbalanced loadings that increase proportionally with the distance between the operational point and the optimised flow condition. In extreme conditions this can lead to the fatigue failure of the pump impeller

Typical impeller failures often start close to the trailing edge of the blade at the impeller outlet due to the stress concentration arising from the blade meeting the shroud. A crack is then formed that propagates across the blade passage meeting the pressure face of the subsequent blade some distance back from the trailing edge. The crack then continues to propagate down the length of the blade towards the impeller outlet until a section of the shroud is broken off. A diagram of the typical failure is shown in Figure 3.1.

In the case of impeller failure, there has been some difficulty in adequately predicting stress levels and patterns using finite element techniques due to uncertainty concerning loadings acting on the impeller. In practice, numerous load distributions are usually guesstimated, covering steady as well as pulse loads due to the blade tip passing the cutwater. However such analyses resulted in stress and fatigue levels that were usually significantly lower than would be expected for failure to occur.

3.1.1 Set Up

The computational model comprised half the actual pump using a symmetry boundary in the casing portion of the model to simulate the double entry interaction. With the impeller blade/volute cutwater interaction being highlighted as the central feature of the model, all six impeller blade passages were modelled. A decision was taken that in

order to keep the model as simple as possible, items such as the suction inlet and leakage flow path would not be included in the analysis.

Transient analyses were conducted at the design point (100% flow) and at the extremes of pump operation (25% flow and 130% flow). The transient analysis produced results that were dependent on the position of the impeller blade within the volute. Summarised details of the analysis set up are shown below.

Half Double Entry Impeller Model (6 passages):	45,000 elements
Half Double Volute Model	100,000 elements
Turbulence Model	k-e model
Wall Boundary	scalable wall function
Inlet Boundary Condition	mass flow
Outlet Boundary Condition	pressure

3.1.2 Results & Discussion

Results were produced for six-degree increments of the impeller, with the pump hydraulic performance characteristics of head, power and efficiency being calculated for each result. The head and power parameter variations for all three flow conditions were plotted against the blade position within the volute and are shown in Figures 3.3 and 3.4.

At the design operating point the analysis shows little fluctuation in the head and power values as the blade rotates. When running at an off-peak flow condition, a significant change is found as fluctuations of up to 10% of the pump generated head are predicted, with the power characteristic fluctuations reaching closer to 20% of an average power value. It is noted that the largest fluctuations were produced at the low flow condition.

The pressure distribution in each of the pump impeller passageways was compared. For results taken at the 100% flow condition, smooth pressure contours were found in the

impeller, with localised variations near the two volute cutwaters. Viewing the contours at different blade positions produced little change in the plots. At the low flow condition an entirely different relationship was discovered. Figures 3.5 and 3.6 show two pressure contour plots taken at the two extremes of the cyclic loading, namely when the mid blade passage is opposite the cutwater and when the impeller blade tip is opposite the cutwater. The detailed scales are in N/m2 and are identical for both figures; at this stage the numerical scales are not important but it should be noted that red represents high pressure and blue, low pressure. When the mid point of the blade passage is opposite the cutwater the pressure contours are still reasonably consistent throughout the impeller (Figure 3.5) and the blade approaching the cutwater has only a small pressure differential across it. When the blade is opposite the cutwater, a considerable variation can be seen in the profile around the impeller (Figure 3.6). A position of great interest is when the blade tip is opposite the cutwater, where it can be identified that the pressure face of the blade is actually experiencing a lower pressure than the suction face. This is the opposite of the pattern on the other five blades in the pump and contrary to expectations. This reversal of the blade loading only occurs for a short period of time, yet its regularity confirms that the trailing edge of the impeller blade is a likely location for fatigue failure.

As the CFD results were predicting a rapid change in pressure loadings on the impeller blade, the pressure values on the hub, shroud and blade were transferred over to a stress analysis package, for the two blade positions identified above. The Principal Engineer for Stress/FEA conducted the stress analysis, which identified that the two sets of pressure data tended to produce a similar stress pattern. However, closer examination identified that in small regions at the blade tip close to stress concentrations the large pressure differential found between the two sets of data corresponded to a significant cyclic stress. In order to present the information clearly the cyclic stresses were plotted on a Goodman diagram using the impeller design thickness to identify the likelihood of failure, see Figure 3.7. Note an additional point has been plotted to indicate results achieved from postulated loadings (■) prior to those predicted by CFD. The fact that the stress analysis results using the CFD data lie under the line indicates that the design should not fail at that design thickness or material type. With Goodman diagrams the

distance from the plotted point to the line can be viewed as an indication of the factor of safety in the design. Due to the close proximity of our result to the line this may not be satisfactory as a moderate reduction in the local thickness of the impeller would lead to increased stresses which could move the design above the failure line. In this case about ten percent reduction in shroud thickness would be sufficient to move the result to the Goodman line.

3.1.3 Conclusions & Relevance to Thesis

The analysis identified clearly that the operational flow condition of the pump had a significant effect on the generated pressure pulsations. The results illustrated an increase of pressure pulsations at off design conditions, with the largest increase occurring at the lowest flow condition. At the lowest flow condition a reversal in the expected pressure pattern was identified at the blade tip outlet region, which produced a high cyclic loading at this location.

The work was limited in a number of ways. Firstly the analysis model only included half of the impeller and casing, and did not include the suction inlet or leakage flow paths. Both of these components are important as,

(i) the suction inlet guides the flow into the impeller, if this is not done effectively (which is likely at off design flow conditions), this could result in a flow imbalance in the impeller passages which could create greater pressure variations in blade passages.

(ii) the leakage flow path is usually bounded by tight clearances (maintained via wear rings). Tight clearances between rotating and stationary components, especially when in close proximity to the blade tip/ cutwater region could have an effect on the generated pressure pulsations.

Secondly the objective of the analysis was limited as the work only involved identifying the magnitude of the pressure variations in the impeller and did not attempt to identify the cause of the variations or explore how to reduce them in anyway.

3.2 Multistage Impeller Investigation

Multistage pumps are most commonly used for high pressure or boiler pump applications. As shown in Figure 3.8, a series of impellers are mounted on the shaft with each having a diffuser and return guide vane to guide the fluid into the suction inlet of the following impeller. There are three main stages that make up a multistage pump, the suction inlet, at least one but likely multiple interstage sections and the final delivery stage. The impeller design for each stage is identical, with the possible exception of the first stage, which may have a special design to improve the suction performance of the pump. The diffuser and return vane arrangement are also identical for each stage, with the exception of the final stage, which has a different design of diffuser that leads into the delivery chamber rather than a return guide vane.

Pump manufacturers always maintain a record of facilities where their pumps are in operation. This data is useful as prospective customers often request an installation list for a pump and it also allows the manufacturer to track the pumps operation over a long period of time. Using these records, it was observed that for a wide variety of multistage pumps a simple impeller failure trend could be established. Of the three main stages listed above, it was noticed that failures were most common in the delivery stage, with the suction impeller being next and failure in the intermediate impellers being extremely rare in comparison.

While it had been long understood that the most common cause of these failures was fatigue, a detailed examination of the stress levels in the various stages had never been conducted. It was considered that CFD could be utilised to compare the flow through the stages of the same pump, the results then being used directly to investigate the pressure pulsations and reaction forces from each impeller; thereafter the resulting loadings would be applied to a finite element model to investigate the cyclic stress loadings on the impellers

3.2.1 Set Up

Due to time constraints a decision was made to only analyse the delivery and intermediate stages, as experience indicated that these were the worst and best case locations for fatigue failure.

The delivery stage model, Figure 3.9, was constructed using the return vane passage from the previous stage, the impeller, delivery diffuser and the delivery itself. The leakage flow was modelled with the shroud side leakage returning to the impeller inlet, and the hub side forming part of the balance drum arrangement with the pressure being reduced to the suction inlet pressure for the pump. An axial slice through the delivery model is shown as an insert in Figure 3.9. The interstage model, Figure 3.10, includes the return vane passage from the previous stage, impeller, diffuser and return guide vane. The leakage flow in this case was modelled with the shroud side leakage returning to the inlet of the impeller and the hub side leakage flowing to the outlet region of the return vane. The corresponding axial slice view is shown as an insert in Figure 3.10. In both delivery and interstage designs the fluid enters the stage through a return vane passage. Grid limitations did not allow this to be modelled in detail therefore a basic inlet grid was utilised that modelled the meridional shape of the passage but did not contain the detail of the return vanes.

Considering the two geometries it can be observed that the obvious difference is the presence of the delivery passage in the final stage. In order to fully capture the effect of the outlet on the impeller a full 360 degree model had to be created.

The transient analysis of the delivery stage was performed initially and results were obtained dependent on the position of the impeller relative to the diffuser and delivery chamber. This unsteady analysis took more than three months to complete, which was considered an unacceptable length of time for the analysis considering that the interstage model transient analysis had still to be conducted. It was decided that the analysis for the interstage model should utilise a quicker method that involved conducting multiple steady state analyses at differing impeller positions relative to the diffuser. This method allowed the interstage analysis to be completed in less than two

weeks. In order to facilitate a comparison between the two analysis methods (transient and multiple steady analyses), the multiple steady state approach was also performed for the delivery model. All analyses were conducted for the duty (100%) flow condition. A brief summary of the analysis details, providing a comparison between the steady state and transient analysis is given below

Interstage Analysis Model

Impeller Model (6 passages):	166,440 elements
Diffuser/Return Guide Model (9 vanes)	301,404 elements
Leakage Flow Paths + Inlet/Outlet:	148,844 elements
Total Model:	616,688 elements

The turbulence model selected for use was the k-epsilon model, with a scalable wall function at the walls. The inlet boundary condition was a duty point mass flow condition, with the outlet being set as a static pressure condition. The outlet pressure level was set as the pump discharge pressure to allow a direct comparison of the pressure levels between interstage and diffuser models. Frozen rotor interfaces were used between the inlet/impeller and impeller/diffuser grids.

Diffuser Analysis Model

Impeller Mode (6 passages):	166,440 elements
Diffuser (9 vanes)	193,266 elements
Leakage Path + Balance Drum Device	465,744 elements
Discharge	42,324 elements
Total Model:	867,774 elements

The boundary conditions used for this model were identical to the interstage model with slight differences. The main difference was that an opening boundary condition was used at the exit of the balance drum, with the pressure level set to atmospheric pressure. Rotor/stator interfaces were used between the inlet/impeller and impeller/diffuser grids

for the transient analysis. Frozen rotor interfaces were substituted for the rotor/stator interfaces for the steady state analyses.

3.2.2 Results & Discussion

Interstage Model

The pressure distribution within the interstage model is shown in Figure 3.11. The pressure pattern around the impeller is consistent throughout each passageway. Local variations in the pressure can be seen close to the outlet of the impeller and extend into the diffuser covering the leading edge of the diffuser vane. The localised pressure drop immediately following the diffuser leading edge is due to a separation in the flow caused by the variation in flow inlet angle as the impeller blade passes the diffuser vane. These localised effects repeat at 120 degree spacing around the model due to the 6:9 ratio of impeller blades to diffuser vanes.

A graph plotting the pressure around the full 360° of the impeller shroud at a number of different radii is shown in Figure 3.12 (Note: Blade notations indicates the position of a blade aligned with a diffuser blade, the larger spikes indicate an impeller blade aligned with diffuser vane C; the location of diffuser vane C is shown in Figure 3.13). This once again highlights the consistent build up of pressure through the impeller. At small radii, only minimal fluctuations can be seen and the pressure is not skewed in any passageway. Progressing out to the tip of the impeller the fluctuations in the pressure increase, with the largest pulsations appearing at the maximum impeller diameter, on the inside of the shroud. Interestingly, although the average pressure in the leakage flow path (labelled R172O) remains consistent with that present at the impeller tip (labelled R172I), the fluctuations are significantly less.

Delivery Model

Using identical plots to those presented for the interstage model, the pressure distribution for the delivery model is shown in Figure 3.13. It can be seen that the pattern of pressure in each of the impeller passageways is considerably different

depending on its position within the diffuser. No 120 degree repetition is in evidence, this is because the pressure variation is also dependent on the position of the impeller relative to the delivery outlet. Figure 3.13 plots the condition where the impeller blade is in-line with the leading edge of diffuser blade C. This produces a pressure pattern where the impeller blade pressure face is at a lower pressure than the suction face. This phenomenon was discovered to be present on the double entry radial flow pump discussed in Section 3.1, however in that case the flow pattern only appeared at low flow conditions. Advancing the impeller blade twenty degrees, shown in Figure 3.14, placing it midway between diffuser blades C and D, it can be seen that the pressure experienced by the blade changes significantly causing a large pressure fluctuation in a very short period.

This effect is due to the flow moving in a clockwise direction in the delivery chamber and entering the pump outlet from the left, Figure 3.15. This introduces a stagnant flow region over approximately thirty-degree section of the delivery chamber, which in turn produces stagnation in the local diffuser passages. The region of stagnation is consistent regardless of the position of the impeller relative to the diffuser or delivery chamber.

Plotting the pressure along the radii for the delivery impeller, Figure 3.16, produces a radically different graph to that plotted for the interstage model. The pressure on the shroud surface is higher throughout the impeller even at the lower radii, however the average pressure at the impeller tip is not significantly different from that plotted for the interstage model, Figure 3.12. The pressure at all radii is skewed towards a particular passageway and exhibit larger fluctuations than the interstage model. However, at the impeller tip the amplitude of the pulsations is approximately three and a half times that present in the interstage. Again, the pressure pulsations on the outside of the impeller tip are found to be less than those present on the inside of the shroud.

Using a similar method to that employed for the radial flow pump in Section 3.1, the results for the two CFD models at a single moment in time when the impeller blade to diffuser vane position is similar were transferred to a finite element stress model. Although the delivery model is not at the peak of its pressure variation it is considered

close enough that the result will be representative. It is noted that while the mean stresses for both interstage and delivery models are similar, the amplitude of the stress calculated from the delivery model's pressure values is three times that of the interstage.

3.2.3 Conclusions & Relevance to Thesis

The analysis of two stages within the same pump illustrated that the pressure pulsations generated by the same impeller in two different arrangements could be significantly different. The results indicated that modifying the ratio of six impeller blades to nine diffuser blades by adding in a single delivery chamber of constant area increased the fluctuating stress on the impeller by more than a factor of three. This analysis was also the first transient analysis that incorporated the leakage flow path in its entirety and the experience gained furthered the author's knowledge and understanding of how to best include this feature in further models.

Comparing the steady state analyses with the transient analyses found a mixed level of success. The delivery model steady state results produced generated head values of the same order as those gained from the transient. The variation of the head (i.e. the pressure variation) across the stage was significantly different. The transient analysis predicted six main peaks corresponding to the impeller blade number, however the steady state did not predict any regular pattern of peaks and the peaks that were observed were off set from those observed from the transient data.

The interstage steady state results bore more of a resemblance to the transient results than was found for the delivery model. The steady state results showed a definite regular fluctuation in the generated head values as the impeller rotated and were found to be similar to those present in the transient simulation. The average head generated was found to be within 2% of that calculated for the transient results. The steady state peaks were found to have amplitude of just under a third of the transient results and had a lag of around 1.5degrees, in the 60 degree repeating cycle. This indicates that it is possible to gain some understanding of the transient pulsations occurring within a pump using several steady state analyses. However, there are situations where the inherent

unsteadiness of the flow does not suit the use of steady state analyses. Therefore further work would be required to examine applications where the steady state method could be utilised and to investigate whether this technique of identifying pressure pulsations can be employed away from the duty flow rate.

It is worth considering the limitations of this work. Firstly all analyses were only conducted for the duty condition. The fact that such a change in the pressure and stress fluctuations could take place between different stages at the duty condition is considered quite alarming. There was some concern relating to the reversal of the pressure differential across the impeller blade tip. When this was observed during the single stage impeller analysis (Section 3.1) it was considered to be due to the extremely low flow rate. As a pump would not normally be operating at this low flow for any considerable period during typical operation it was not initially considered to be important. To identify this same pressure reversal, but at the duty flow condition highlights it as a feature that suggests fatigue may be a problem in certain specific pump cases.

This work was limited due to the timescales involved. Because of the length of time taken for the analyses it was not possible to investigate possible modifications to alleviate the stagnant flow in the discharge chamber. However it was postulated that a volute or spiral arrangement rather than a constant annulus leading to the pump discharge would reduce the stagnant flow region significantly.

3.3 Chapter Summary

In summary, a list of the important learning points gained from the preliminary work that are of direct relevance to the thesis are as follows

- Information was gained on the change in pressure variations within the impeller and volute due to a rotating impeller.

- An understanding was developed of the effect of the flowrate on the pressure variations in the pump.
- The way pressure variations at stress concentrations can lead to high cyclic stresses was identified.
- The important phenomenon of the reversal of pressure loading on the impeller blade as it passes the cutwater was discovered.
- Fatigue failure caused by pressure pulsations is a problem related to more than one pump type and may be for quite different reasons.
- Steady state analyses can be used to identify certain transient flow features.
- Experience was gained in the modelling of the leakage flow path in combination with impeller and volute for use in a transient analysis.
- An appreciation as to why the final stage of a multistage pump is more susceptible to fatigue failure than intermediate stages was developed.

3.4 Figures

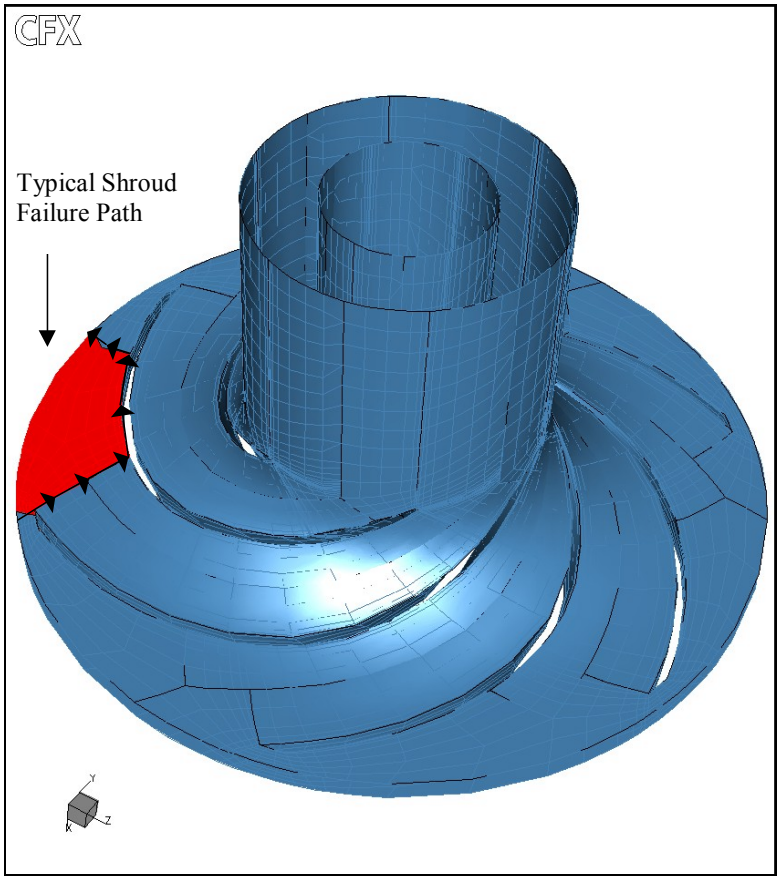

Figure 3.1: Typical shroud failure path

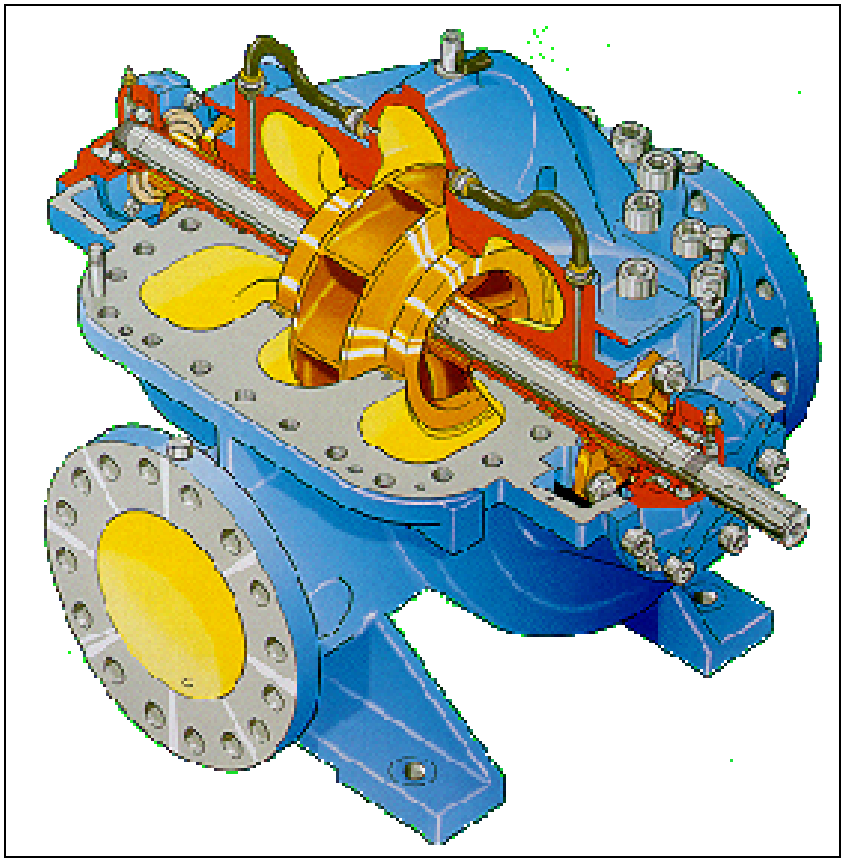

Figure 3.2: Cut away section of a double entry single stage pump

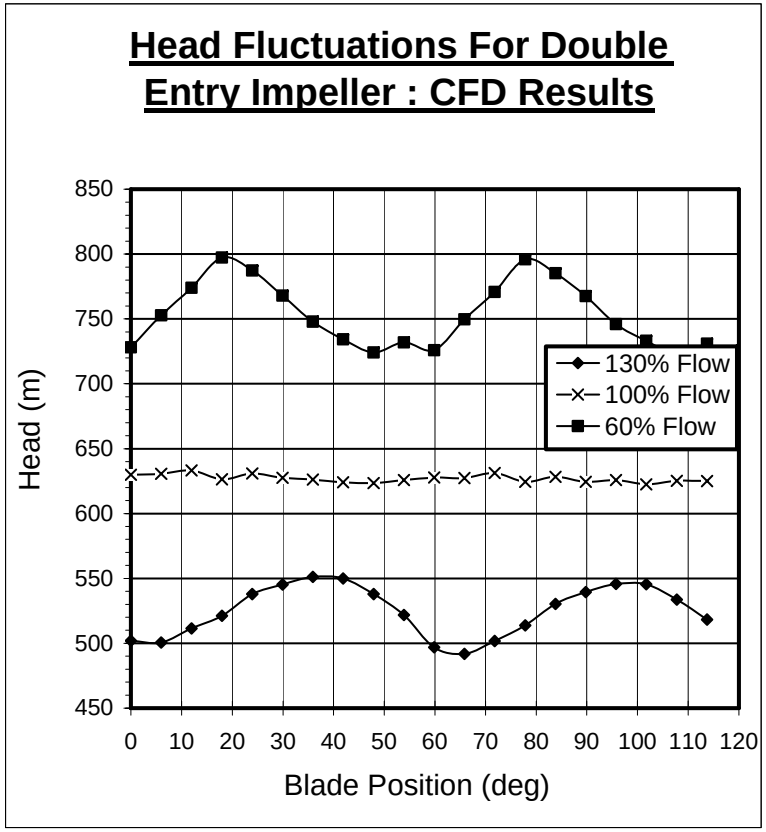

Figure 3.3: Graph of head fluctuations against blade position

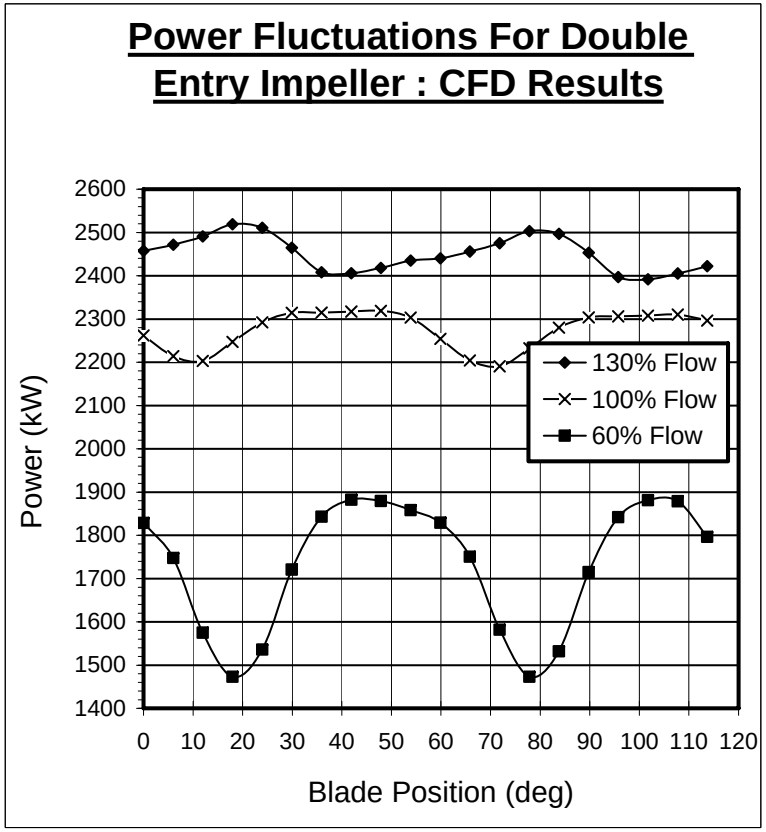

Figure 3.4: Graph of power fluctuations against blade position

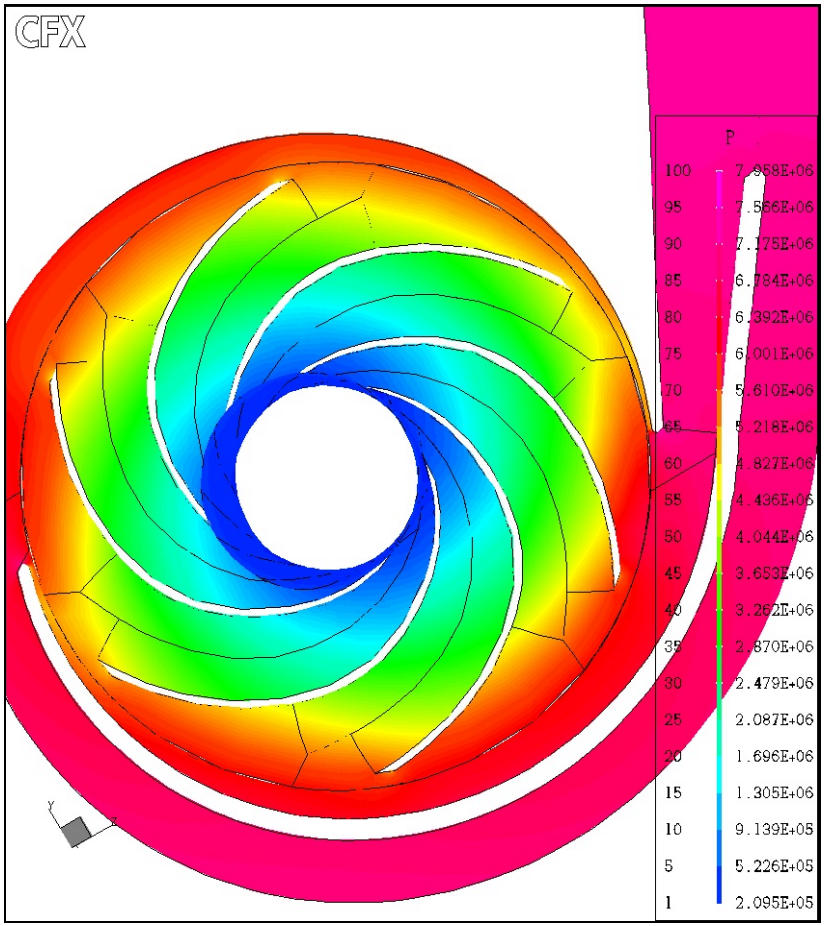

Figure 3.5: Pressure plot within the impeller when the blade is mid way past the cutwater (N/m^2)

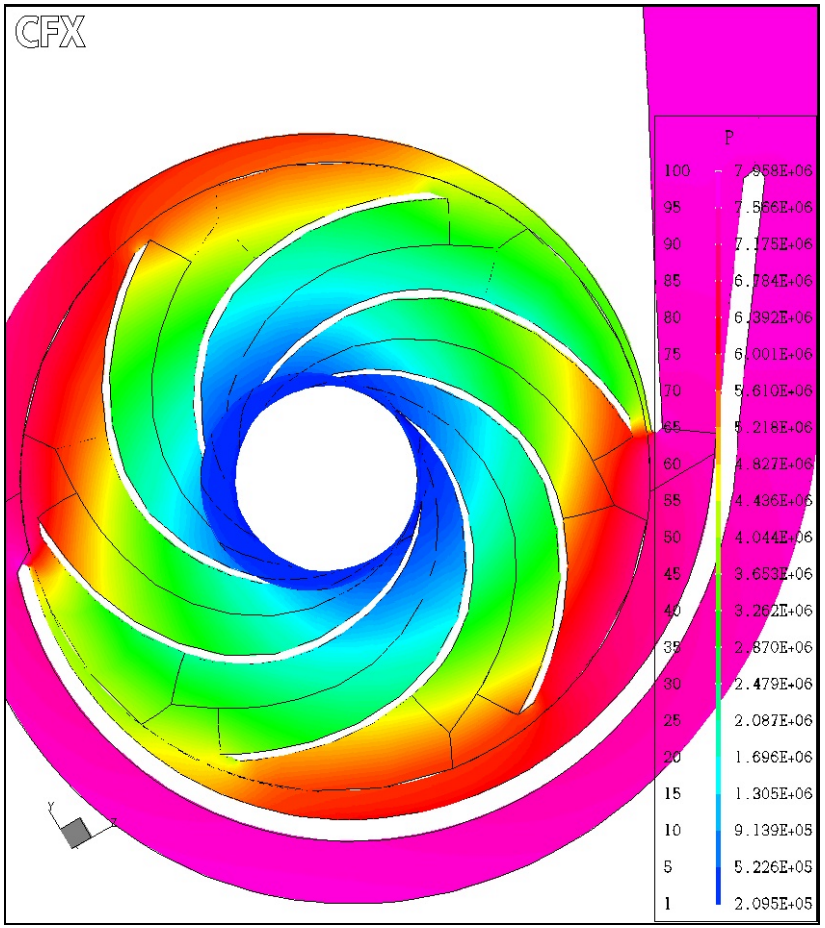

Figure 3.6: Pressure plot within the impeller when the blade is opposite the cutwater (N/m^2)

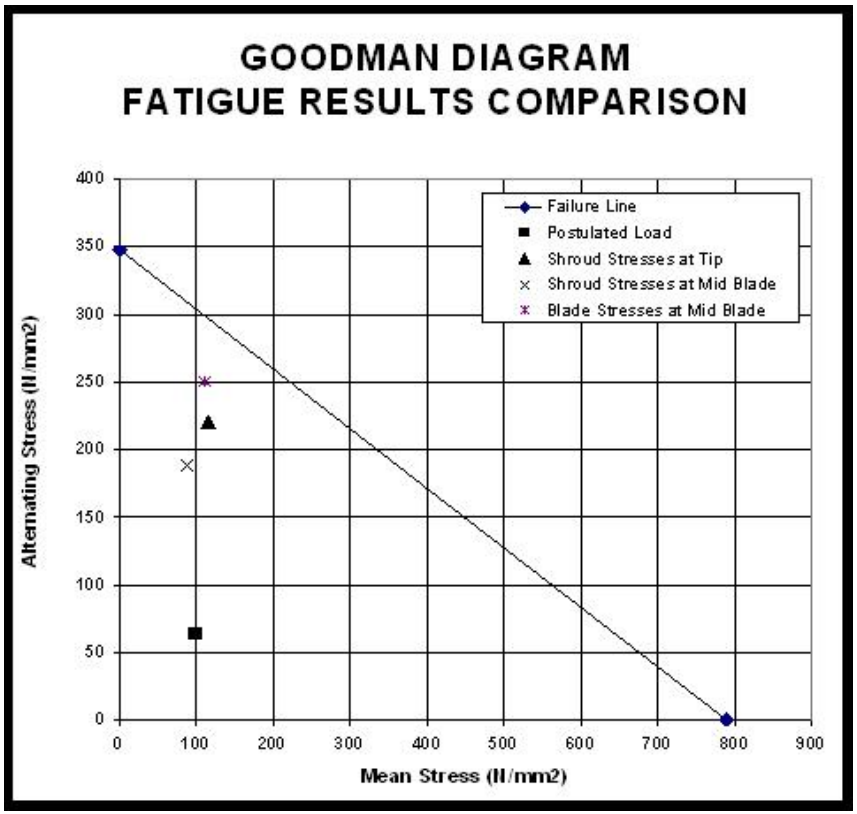

Figure 3.7: Goodman Diagram Fatigue Results Comparison.

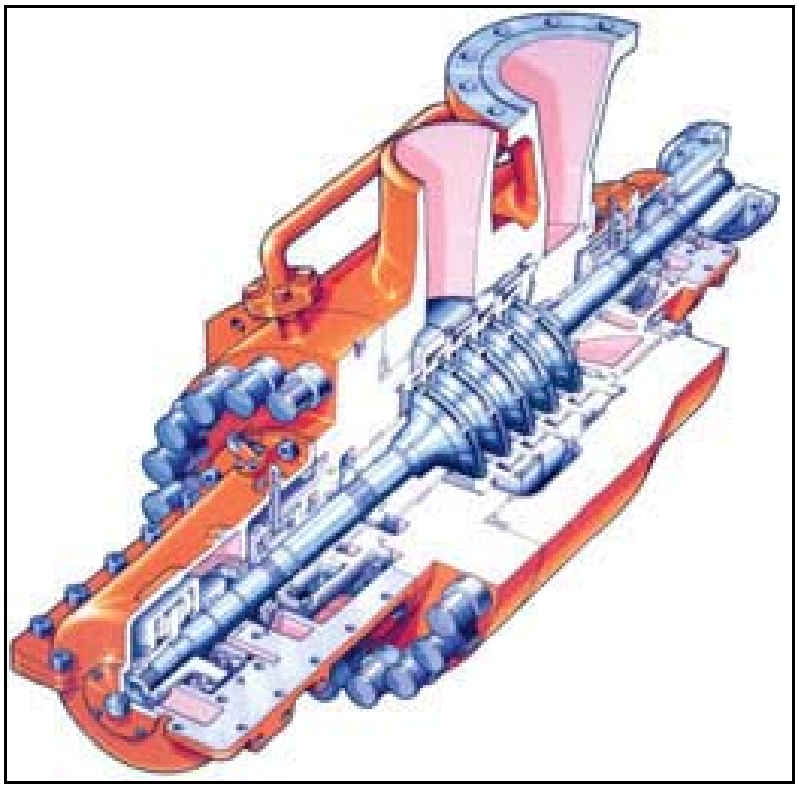

Figure 3.8: Cut away multistage pump

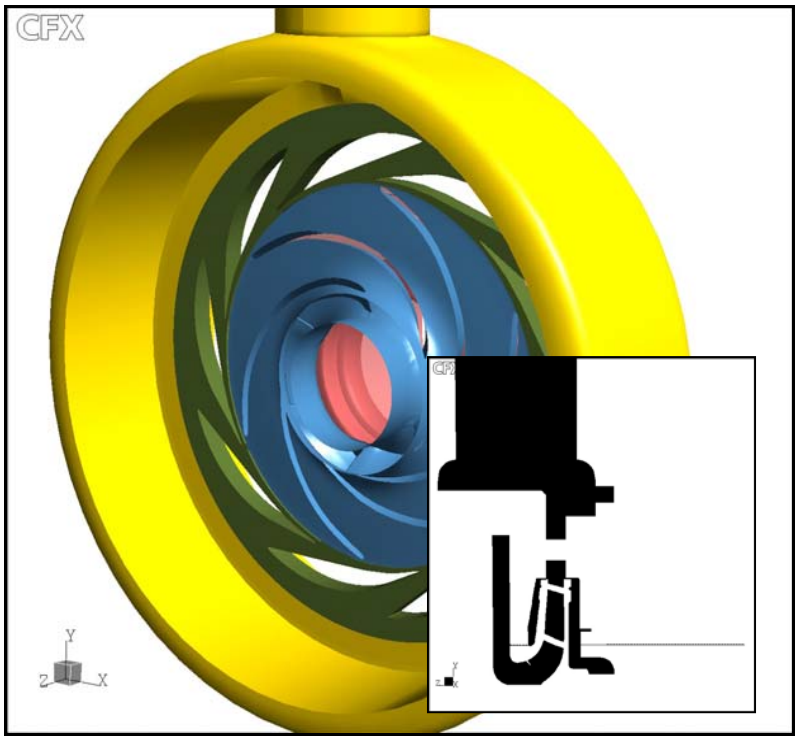

Figure 3.9: Delivery CFD Model (incl. silhouette insert)

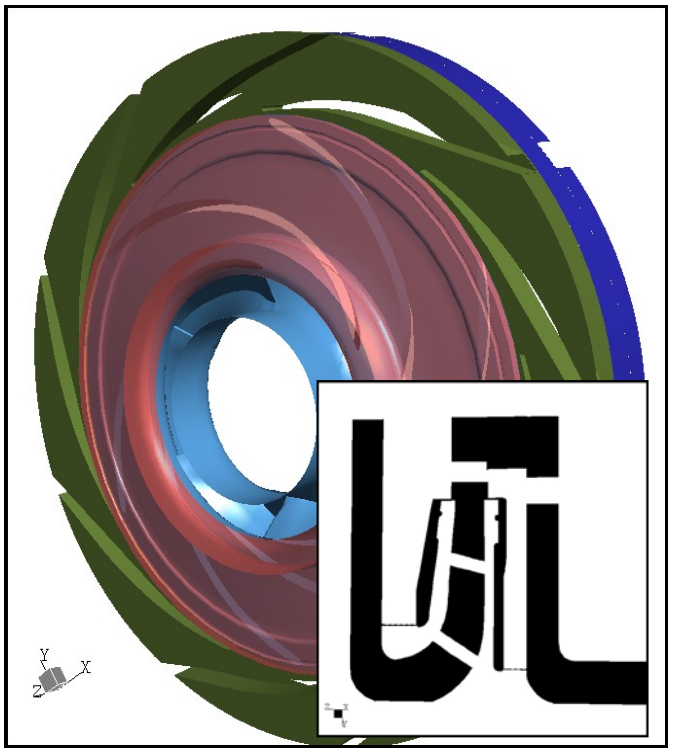

Figure 3.10: Interstage CFD model (incl. silhouette insert)

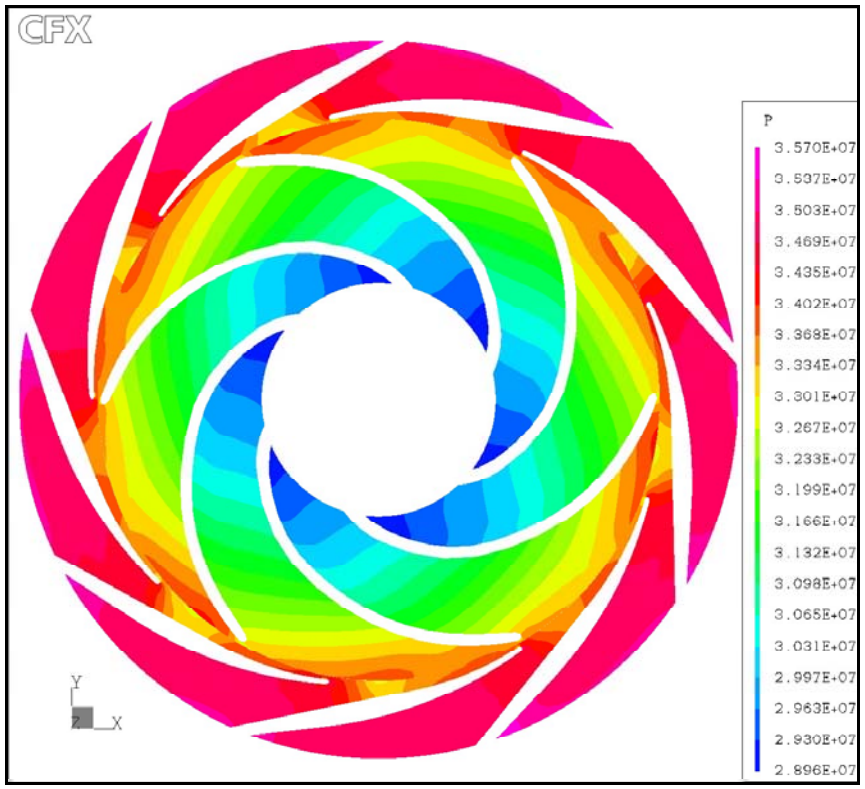

Figure 3.11: Interstage pressure plot (N/m^2)

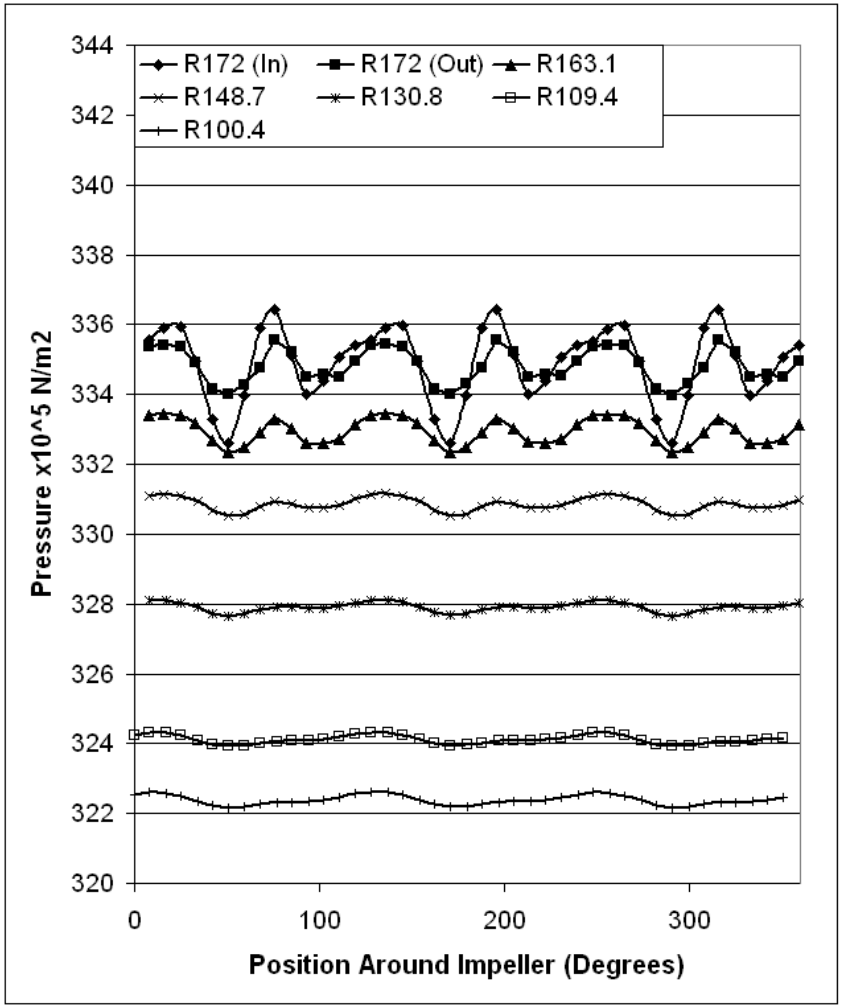

Figure 3.12: Interstage model pressure values within the impeller at different radii

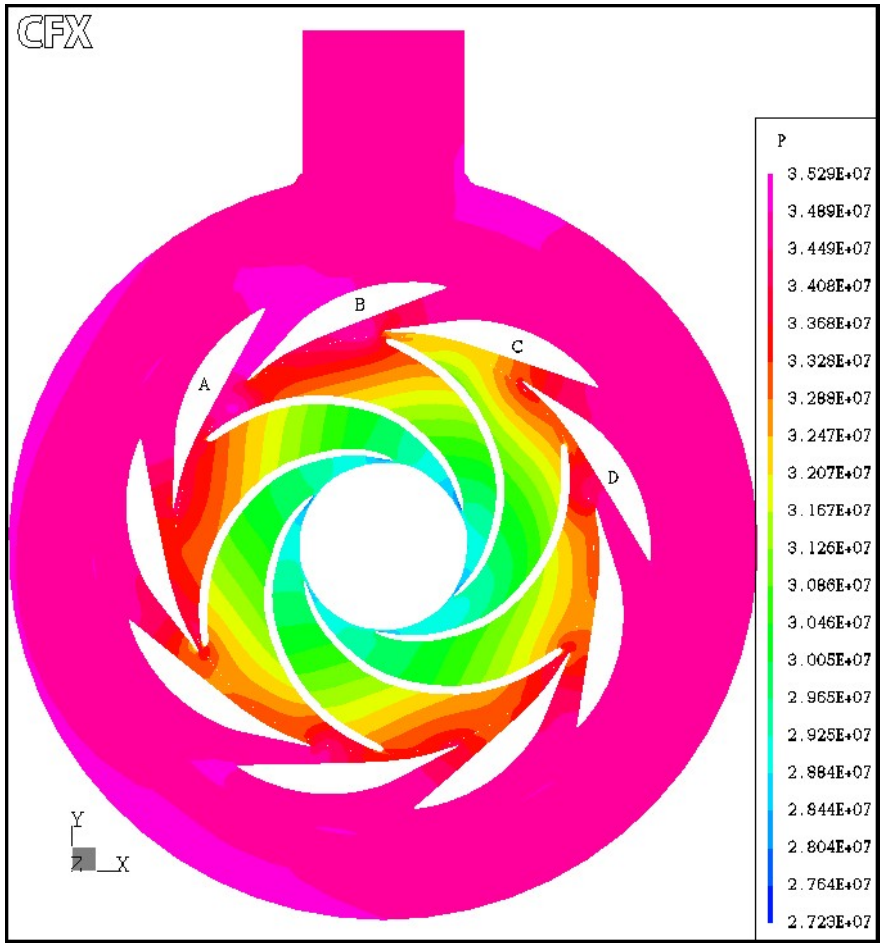

Figure 3.13: Delivery model pressure plot - impeller blade aligned with diffuser C (N/m^2)

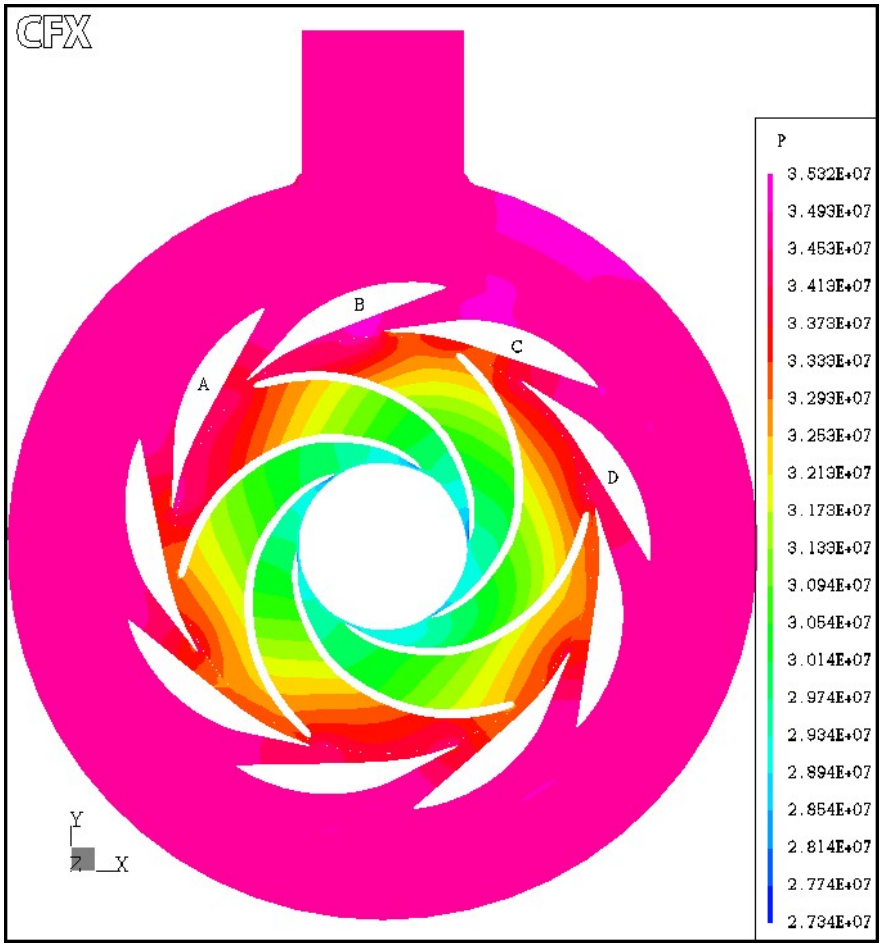

Figure 3.14: Delivery model pressure plot, impeller is advanced 20degrees clockwise (N/m^2)

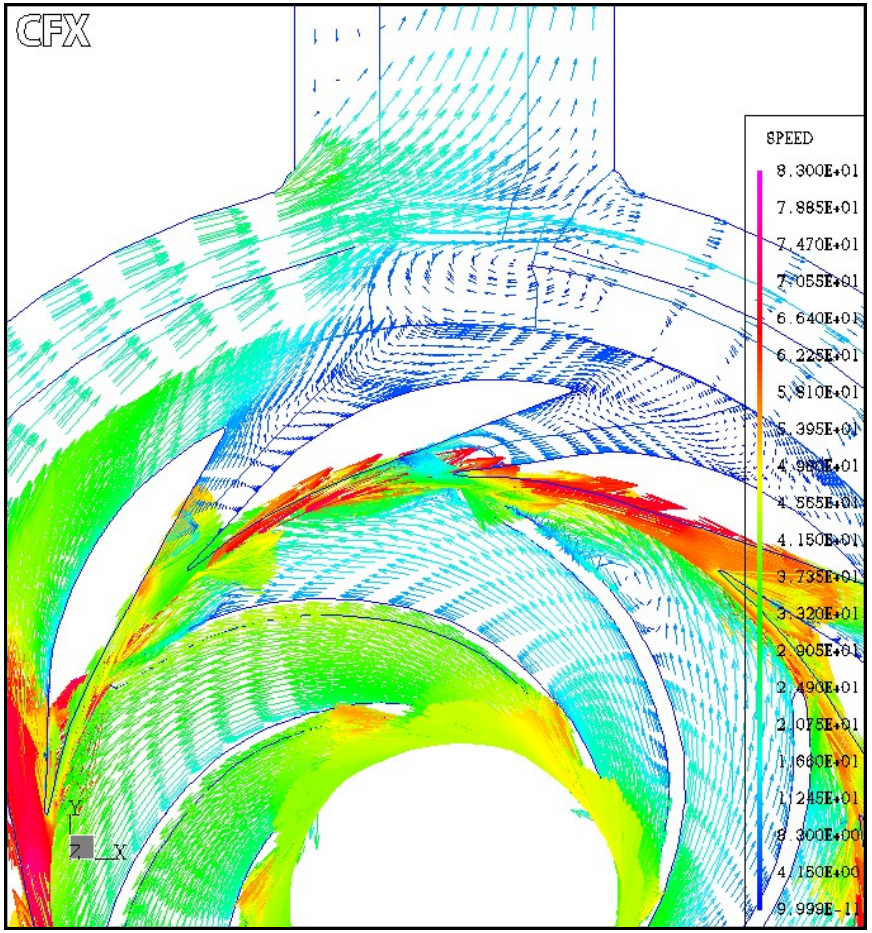

Figure 3.15: Delivery model vector plot (m/s)

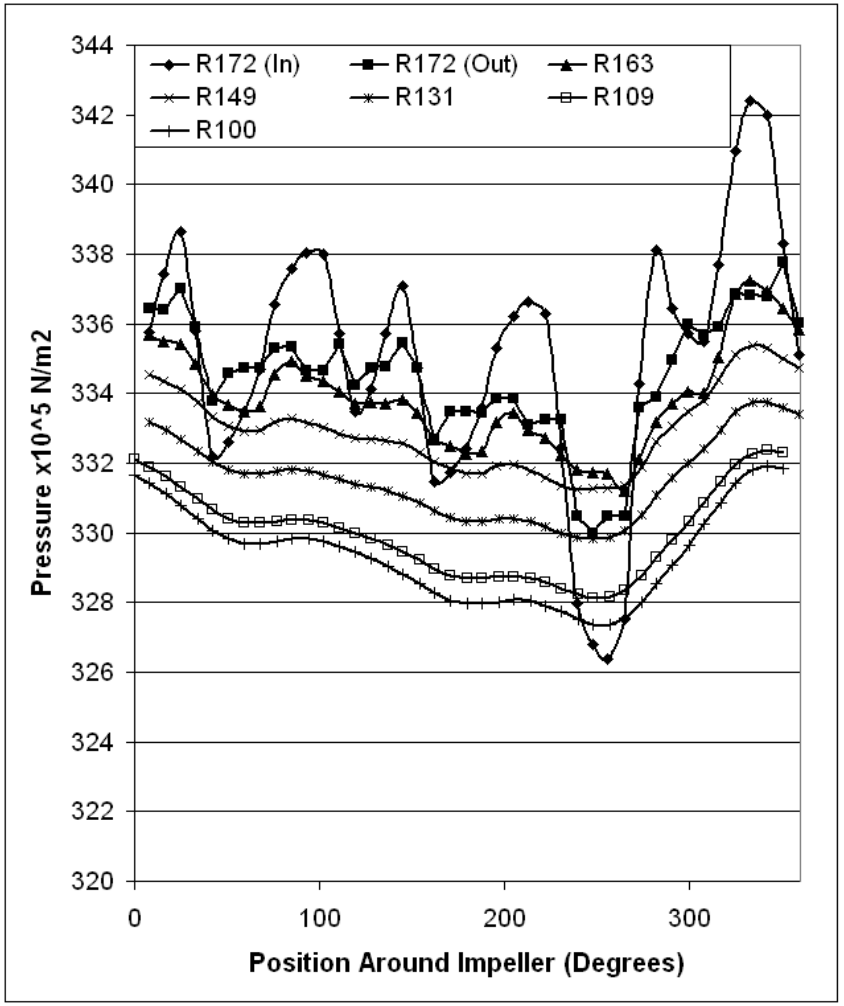

Figure 3.16: Delivery model pressure values within the impeller at different radii

Chapter 4

Experimental Work on a Single Stage High Energy Pump

4.1 General Arrangement of the Test Rig

4.1.1 Test Pump

4.1.2 Test Impeller

4.1.3 Test Casing

4.1.3.1 Cutwater Clearance

4.1.3.2 Snubber Ring Clearance

4.1.3.3 Sidewall Passage Clearance

4.1.3.4 Impeller Vane Arrangement

4.2 Experimental Technique

4.2.1 Equipment

4.2.1.1 Pressure Tappings

4.2.1.2 Pressure Transducers

4.2.2 Test Method

4.2.3 Test Programme

4.3 Results

4.3.1 Interpretation

4.3.1.1 Spectra

4.3.1.2 Pressure Scaling Law

4.3.1.3 Power Law Relationship

4.3.2 Presentation of Results and Discussion

4.3.2.1 General Observations

4.3.2.2 Cutwater Clearance

4.3.2.3 Snubber Gap Clearance

4.3.2.4 Sidewall Passage Clearance

4.3.2.5 Vane Configuration

4.4 Critical Review of Experimental Work

4.5 Chapter Summary

4.6 Tables

4.7 Figures

4 Experimental Work on a Single Stage High Energy Pump

It is recognised that when undertaking CFD analysis work it is important to be able to establish that the results produced are grounded in reality. Some relevant experimental work had been conducted at the Weir Pumps facility in Alloa, approximately six years prior to the instigation of this study (1994). The experimental test rig was assembled to investigate the fatigue failure of a booster pump impeller where it was postulated that the crack initiation was caused by hydraulic pressure pulsations arising from the impeller/volute cutwater gap. A test programme was prepared to investigate the pressure pulsations within a single stage double entry pump and to observe how the pulsations change in relation to flow conditions and modifications made to the pump geometry. Due to tight time constraints involved in contract related issues, the test programme was halted once enough information had been gained relating to the specific contract issue. This abrupt cessation of the tests also meant that the experimental test data has never been properly reported and the data was available to the author only in the raw recorded form. This chapter will present what information is available concerning the experiments, but will also detail the work conducted by the author in collating the results and interpreting them in a manner such that they can be used for comparison with the computational analyses.

4.1 General Arrangement of the Test Rig

The experiments were performed in the test rig shown in Figure 4.1. The closed loop test facility was initially designed for monitoring impeller forces within the tested pump. Adapting the pump to monitor the pressure pulsations at various points within the pump was a relatively straightforward procedure.

As can be seen from the diagram the pump was drawing fluid from the closed system. The loop in which the pump was situated had a bend 3.5 diameters upstream and a

second bend 4 diameters downstream. Directly following the upsteam bend, flow-straighteners were fitted in order to reduce the flow effects caused by the bend on the inflow to the pump. Gülich and Bolleter (90) identify the system pipework as being a possible cause of pressure pulsations. Although this could be the case here, the pipework bends and distances involved are consistent through the entire experimental programme, hence the system pipework can be eliminated as a contributor to the change in pulsations within the pump.

Kistler pressure tappings were located within the volute of the pump and two Entran miniature pressure transducers were mounted on the impeller, Figure 4.2 provides illustrations of the two pressure transducer types. Strain gauge groups were also mounted on the impeller and the vibration of the volute casing was monitored but these results are not of direct relevance and are not discussed further here.

4.1.1 Test Pump

In order to minimise any delay in assembling the test rig, a decision was made to utilise a pump that had been involved in an earlier study examining two different pump design methods used in Weir Pumps Limited. A pump had been manufactured for each of the design methods and both were of the type to be examined in the pressure pulsation test. One of these pumps was selected and modified to incorporate all of the required monitoring equipment. The pump design selected was not identified clearly and so when examining the test data for this project the author had to compare hydraulic layout drawings for the two designs and for the pulsation test rig to identify which pump design was utilised. An additional benefit of utilising the existing pump was that pattern equipment was available allowing variations in impeller arrangements to be considered, such as blade stagger, without the time delay and expense associated with the creation of a new pattern. Although the selected pump was smaller than the failed booster pump (test impeller D_2 was 0.41 times the contract pump), careful arrangement of test pump's internal geometry would render it to be a scale of the pump on site. Thus the results gained for the test could be scaled for the on site booster pump. These modifications involved utilising an oversized impeller and modifying the cutwater and

splitter volute regions to accommodate it. Figure 4.3 shows a photograph of the tested pump, with the upper half of the pump casing removed.

4.1.2 Test Impeller

The pressure pulsation measurement tests were conducted using a six-bladed, shrouded double entry production design impeller. The impeller was originally designed using the step generation method (93) and included a swept angle of 102 degrees. The blade shape was designed on the pressure face with 7 mm thickness being added normal to the face along its length. The blade was tapered from the full thickness down to 4mm at the leading edge over approximately 30mm. A bullnose of 2mm radius formed the leading edge. The trailing edge of the blade was of the cut-off design. In order to ensure that the test dimensions were a scale of those used in the failed booster pump, the impeller used was actually oversized. Therefore the largest impeller diameter used (366mm diameter) was bigger than the maximum impeller diameter recommended for that impeller design (345mm diameter). This increased diameter was subsequently modified to allow further diameters, namely 358.5mm and 352mm, to be tested. A summary of the impeller details is provided in Table 4.1, with an annotated diagram (Figure 4.4) showing some dimensions.

The initial impeller design is termed a “straight” or “inline” impeller as the blades from both sides of the impeller terminate at the same point on the outer diameter of the impeller. As the blades are in line with one another, the central hub is terminated approximately 45mm from the outlet of the impeller, allowing the fluid from one side of the impeller to interact with fluid from the opposite side before exiting the impeller.

In later tests, a “staggered” impeller was used. The term “staggered” is used to denote that the blades on one side of the impeller are offset 30 degrees from the other. In the staggered impeller a central diaphragm is required to maintain structural integrity of the impeller and therefore the hub is extended to the impeller outlet, preventing any mixture of fluids within the impeller. Figure 4.5 provides photographic comparisons of the straight and staggered impeller arrangements.

4.1.3 Test Casing

A double volute casing was used for all experiments. The cutwater/splitter clearance diameter was 190mm, with the cutwater and splitter being offset by an angle of 181 degrees. The volute design was of a trapezoidal shape at the cutwater region with the shape developing into a conventional circular form as the scroll progresses. The flat-sided trapezoidal shape is usually indicative of a high pressure design casing. Due to the oversized impeller the cutwater had to be machined back to preserve the cutwater gap clearance and to make this a scale of the contract dimensions.

4.1.4 Geometric Modifications

The experimental set up allowed the investigation of four geometric parameters, namely the cutwater gap, snubber gap, sidewall clearance and vane arrangement. Figure 4.6 identifies the locations of the parameters within the pump, with Table 4.2 providing a summary of the levels of the geometric parameters tested.

4.1.4.1 Cutwater Clearance

The radial gap between the impeller vanes and outlet cutwater(s) is widely recognised by both pump designers and users to be one of the most important parameters that affects the magnitude of the pressure pulsations. The cutwater gap is usually represented as a percentage of the impeller diameter as shown in equation 4.1

$$CutwaterGap = \frac{(D_3 - D_2)}{D_2} x100\% \qquad \text{Equation 4.1}$$

where D_3 is the cutwater diameter

D_2 is the impeller outlet diameter

The experimental work conducted investigated a range of flow rates through the diametrical clearance gap between the impeller blade and cutwater of 3.93%, 6.0% and 7.95% of the impeller blade diameter. The shroud to cutwater gap was kept at 3.93% of the initial impeller diameter (to maintain the snubber gap); however, additional work was also carried out to identify whether increasing the blade and shroud diametrical clearance gap to 7.95% would have a greater effect than just increasing the blade clearance alone.

4.1.4.2 Snubber Gap Clearance

Snubber rings create a tight annular clearance at the impeller shroud as detailed in Figure 4.7. The concept of snubber rings was conceived by Makay (94) in relation to the control of rotor axial stability of single stage double entry impeller pumps, particularly at low flow. It is claimed that snubber rings work on the principle that unsteady components of pressure (generally low frequency <10 Hz) are attenuated in the gaps between the impeller shrouds and pump casing thus stabilising the hydraulic axial thrust. To date there has been no published data regarding the effect of such devices on the generation of higher frequency pressure pulsations. Such pulsations are important as they have an impact on the impeller service loading and the consequential integrity of the vanes and shrouds. Again the diametral gap is represented as a percentage of the impeller diameter using equation 4.2.

$$SnubberGap = \frac{D_4 - D_2}{D_2} x100\% \qquad \text{Equation 4.2}$$

where D_4 is the outer diameter of the snubber gap

Pressure pulsation measurements were taken over a range of flowrates with snubber ring clearances of 0.27%, 1.1%, 1.64% and 6.38% of the impeller diameter, at a cutwater to impeller blade gap of 3.83% (also of the impeller diameter). Snubber ring gaps of 0.27% and 1.64% at a cutwater to impeller blade gap of 7.95% (all of the impeller diameter) were also investigated.

4.1.4.3 Sidewall Passage Clearance

In principle, the clearance in the sidewall passage could have the effect of accentuating pressure pulsations generated by other component interactions. However, it is not known how significant this clearance is when snubber ring components are part of the assembly.

The sidewall clearance is taken as the distance between the outer shroud face and the pump casing at a section near the impeller outlet. Sidewall clearances of 12mm and 3mm axial gaps respectively, were investigated with the pressure pulsations being measured over a range of flow rates using the 3.83% cutwater gap arrangement only. For convenience, these are termed 100% and 25% sidewall gaps respectively.

4.1.4.4 Impeller Vane Configuration

As already discussed, the radial gap between the impeller blades and the casing cutwater is of importance. A typical impeller design utilises the "straight" vane arrangement as described in section 4.1.2, although this arrangement maximises the pulsation effect as both vanes pass the cutwater at the same instant in time. It is thought that a staggered vane arrangement could even out the pulsations reducing their magnitude while having a minimal effect on the pump performance.

Only a single staggered vane arrangement was investigated. This used an offset of 30 degrees between the blades on one side of the impeller to the other, corresponding to a mid-position between blades on the opposite side of the impeller. Only the 3.83% cutwater gap arrangement along with a sidewall gap of 100% was used during this investigation.

4.2 Experimental Technique

Since the writer was not directly involved in the original test work, it was important to obtain as much information as possible concerning the equipment utilised in the test and the manner in which the test was conducted. The report of the experiments was rather sparse, but fortunately, the writer has been able to gleam information from various sources, which has given a reasonably good understanding of the testing and thus aids the interpretation of the results.

4.2.1 Equipment

Two varieties of pressure measuring devices were used in the pump rig. Both pressure transducers and pressure tappings are described and the position of the devices in the test rig is also specified.

4.2.1.1 Pressure Tappings

Ten Z type Kistler pressure tappings were mounted on the pump. Pressure tappings were used to collect data at various stationary locations around the pump. Holes were drilled at specific locations around the pump and tubes were used to connect the pressure transducers to each location. Due to the complexity of the set up there could be some distance between the location investigated and the pressure transducer, although this distance is normally kept as short as possible. A list of the various positions of the pressure tappings is given below, and diagrammatical representations of the positions are shown in Figures 4.8 and 4.9:

Sidewall tappings (Figure 4.8)
C1 – On the right hand wall, 60mm ahead of the leading edge cutwater
C2 – On the right hand wall 30mm ahead of the leading edge cutwater
C3 – On the right hand wall at the leading edge cutwater
C4 – On the right hand wall 30mm past the leading edge cutwater

Cutwater inner face tappings (Figure 4.9)

C5 – Inner face of the leading edge cutwater 5mm back from the leading edge

C6 – Inner face of the leading edge cutwater 15mm back from the leading edge

C7 – Inner face of the leading edge cutwater 30mm back from the leading edge

C8 – Inner face of the leading edge cutwater 50mm back from the leading edge

C9 – Situated in the discharge volute

C10 – On the left hand wall, 60mm ahead of the leading edge cutwater

When using pressure tappings, care has to be taken in order to obtain quality data. As mentioned above, due to the complex arrangement of pump internals, the pressure transducer may have to be a short distance from the pressure tapping location and connected via a length of tube. Where significant lengths exist between pressure tapping locations and the transducer, normal test practice is to construct the rig to allow any air pockets to be drained from the tubes. Otherwise, these air pockets can produce a resonant frequency on the spectra, with the frequency relating to the path distance between the tapping point and the transducer. For a tapping that is open at one end and closed at the other, a quarter wavelength is generally taken when attempting to identify the frequency related to the path distance. The standard relationship to determine the frequency from the path distance is shown in Equation 4.3,

$$f = \frac{\nu}{4L} \qquad \text{Equation 4.3}$$

where f is the frequency of the resonance (Hz)

ν is the speed of sound in water (m/s)

L is the path distance (quarter wavelength) (m).

4.2.1.2 Pressure Transducers

Two Z type Entran pressure transducers were utilised in the experiment. Entran transducers consist of a small strain gauge bridge, and the transducers were located as

shown in Figure 4.10. The actual transducer is only 10-15mm from the point of interest. This short distance ensures that any expected resonant frequencies caused by the gap are above the measured range. In fact, the blade transducer failed in the second test, as the pressure pulsations were considerably larger than expected. The electrical signals from the transducers were transferred from the rotating element to the stationary data recorder via a slip ring arrangement at the non-drive-end of the pump.

S1 – Transducer mounted in the right hand impeller shroud adjacent to peripheral or sidewall tapping
B1 – Transducer mounted in impeller blade adjacent to right hand shroud, peripheral tapping.

4.2.2 Test Method

The test rig was run at an initial speed of 1400RPM over the flow range 25% to 125% of duty with 5-minute tape recordings of the transducers being taken at each 25% flow increment. The flow rate change was achieved by adjusting a flow valve as slowly and smoothly as possible while continuing the tape recording so that no data was missed. The intermediate data between flow rates has not been used.

In addition to the tape recording, on the spot readings were taken using digital meters for the following parameters

Suction, discharge pressure and flow
Steady and fluctuating strain
Vibration
Dynamic pressure

These readings were used only for spot monitoring, but were taken both at the assigned measurement point and between flow changes.

4.2.3 Test Programme

The original test programme anticipated thirty-three pump configurations. However, the test programme was halted after only seventeen had been completed, with two re-tests being conducted, bringing the total number of tests performed to nineteen. Table 4.3 provides details of the configuration used in each test. The original test numbers have been preserved for convenience.

It should be noted that tests two and three were planned to be identical; but test three was not in fact performed. Tests 19 and 20 were not performed.

Following the initial seventeen tests it was observed by the test engineers that results for tests one and two contained some irregularities. Some of the pressure tappings, particularly at the sidewall locations did not seem to be functioning correctly; there were also irregularities for some results at the 75% flow condition. The pressure pulsations obtained for these tests were of an order of magnitude different than that recorded during any other test. A further two tests were performed (test 21 and 22) and the test results are labelled in such a manner that indicates that that they repeat tests 1 and 2. However late in this project the author observed that the time history data (see Section 4.3.1.1 for discussion of the various spectra produced by the experimental tests) for tests 21 and 22 were significantly different in form from those measured in tests 1 and 2. Closer inspection of the pulsation waveforms indicated that the blade arrangement used in tests 21 and 22 was actually staggered and not straight (as is written on the test results). Some handwritten notes taken at the time of the test confirmed that the impeller for tests 21 and 22 were of a staggered arrangement, however the blade arrangement has been misrepresented in every other item of documentation relating to the tests. Unfortunately this erroneous documentation had consequences relating to the comparison of the experimental data with the CFD results.

4.3 Results

The following section will detail the work conducted by the author in collating the results and interpreting them in a manner such that they can be used for validation by the computational analysis. Firstly, the raw data obtained will be shown and the method of interpretation discussed. Then the results will be presented and, where applicable, a relationship between the geometrical modification and the pressure pulsation experienced will be established.

4.3.1 Interpretation

4.3.1.1 Spectra

The results are available in the form shown in Figure 4.11. This represents a time history for each of the locations at which the pressure was measured. Fourier analysis allows an investigation of the individual frequencies that comprise these histories to be analysed. An example of a frequency spectrum is shown in Figure 4.12. With ten measurements and five flow rates there are 50 such spectra to be considered for each test. The area under the spectra is effectively the energy associated with the pressure pulsation; however the root mean square (RMS) format is used to output information concerning the measured pressure pulsation. The various formats that can be used to display pressure pulsation information is discussed later in Section 6.1.1.

In order to use these results the various spectra need to be analysed and their results converted to a format that facilitates a comparison with the numerical data. This work consisted of examining the fifty frequency spectra for each experimental test case and trying to identify the likely source of the dominant frequencies. Unsurprisingly the majority of the frequencies attributed to the pressure pulsations relate to the rotational component of the pump. This produces frequencies relating to the running speed of 1400RPM resulting in frequencies that occur at multiples of 23.3Hz. The cutwater/ impeller tip interaction effect is related to the running speed and is often termed the blade passing frequency. This interaction effect occurs at a rate equal to the blade

number times the running speed, giving a frequency of 139.8Hz. This frequency (and multiples of it) proves dominant in a large number of the spectra, especially in the measurements taken near the casing cutwater. Another common frequency present in a number of the spectra is that of electrical interference. The source of this signal is most likely from the motor, being 50Hz, and has been ignored.

General features of the spectra can also be identified. Figure 4.13, identifies the frequency spectrum relating to the pressure tapping at location C1 in the pump. It can be seen that in addition to the sharp peaks identifying frequencies contributing to the pressure pulsation there is a gradual rise in the base line signal during a frequency range of 700Hz to 850Hz. This arises due to the distance of the transducer from the point of interest. According to Equation 4.1, a resonant frequency peaking at 775Hz corresponds to a path length of approximately 0.47m between the pressure tapping and the transducer. It is a common test practice to mount the Kistler pressure transducers in the outer casing and use a flexible tube to connect to the region being monitored. The length calculated appears rather large for the dimensions of the pump being tested, as a value of around 0.1m would have been more appropriate, however the actual path distance between the transducer and tapping point have not been recorded. It should also be noted that any results at frequencies higher than the resonant frequency are ignored as they may be unreliable.

Cavitation can also generate random high frequency broadband energy signals, however the cavitation is generally only present at the extreme off flow conditions. There was no recorded occurrence of cavitation during the tests even at the lowest flow condition (25%).

4.3.1.2 Pressure Scaling Law

When results are reported it is common to present the pressure pulsations in normalised form. This form was introduced by Guelich and Bolleter (90) to allow the scaling of pressure pulsation test data with respect to size and speed. In their paper they

recommend that for general spectrum of pressure pulsations for a given pump a square law relationship be used, shown in Equation 4.4.

$$\Delta p^* = \frac{\Delta p}{\rho \frac{u_2^2}{2}} \qquad \text{Equation 4.4}$$

where Δp^* is the normalised pressure pulsation

Δp is the pressure pulsation

ρ is the density of the fluid

u_2 is the circumferential speed at the impeller outlet

This format has been adopted for both the reporting of the experimental data here and the CFD results in Chapters 6 and 7.

4.3.1.3 Power Law Relationship

A power relationship is sometimes used to relate geometric modifications and the corresponding pressure pulsation changes. The general format of the relationship is shown in Equation 4.5,

$$y = x^z \qquad \text{Equation 4.5}$$

Where y is the pressure pulsation, x is the geometric modification and z is the power law index. Thus if z is a positive value the geometric change has an amplification effect on the pressure pulsations; if z is negative it will have a dampening effect.

The use of a power relationship is a common approach to presenting such data clearly in a summarised form. Presenting the complex pressure relationship in such a simple form obviously introduces inaccuracies that are difficult to quantify. In order to use the power law relationship for this project a full factorial set of analyses would be required, this would lead to the geometric parameter set being reduced significantly. The

approach taken in this project to use the Taguchi method does not lend itself to deriving power laws; thus power law relationships will not be presented here.

4.3.2 Presentation of Results and Discussion

The results have been processed to provide the RMS value of the pressure pulsation over the frequency range of 10Hz-1kHz. Firstly, general comments are made providing an overview of the results. Then the results are discussed for each of the geometrical variations in turn and their effect on the pulsations generated at various locations in the pump. This discussion presents results for selected monitoring points in four main locations, the sidewall passageway (Channel 4), local to the cutwater (Channel 7), towards the discharge (Channel 9) and at the trailing edge of the impeller (Shroud).

4.3.2.1 General Observations

A number of general observations can be made regarding the results gained from the majority of the tests and test locations, typical (normalised) results for test number 5 are shown in Figure 4.14. It can be observed that as the flowrate decreases the pressure pulsations increase, however the rate of increase and the magnitude of the pulsation is highly dependant on the location in the pump. It is noted that pressure pulsations are often at a minimum at flows higher than the duty flow condition, this is unusual as Guelich and Bolleter (90) and Parrondo (35) both identify the pressure pulsations as increasing at flows greater than 100%. It is uncertain if this trend is due to some feature of the tests or if it is a function of the oversize impeller used. The scaling laws relating to changes in performance due to changes in impeller diameter are discussed in section 4.3.3 below, however in short when the impeller diameter is increased the duty flow rate will also increase. Thus the "true" best efficiency point, and thus point of lowest pulsation, will lie between the tested 100% and 125% flowrates. It is noted that the 100% flow used for the tests is as calculated for the original impeller diameter and has not been modified for the oversized impeller.

More importantly, pressure pulsations at the lower flow conditions are approximately two to three times those experienced at the higher flow conditions.

As expected the pulsations generated vary widely depending on the location at which they are measured.

In the leakage flow path, Figure 4.14a Channels 1,2 and 10 are circumferentially positioned before the cutwater, whereas Channels 3 and 4 are after the cutwater. Hence the pulsations at Channels 3 and 4 are larger due to the interaction of the impeller and cutwater, with these pulsations increasing as the flow rate decreases.

In the volute, Figure 4.14b, the pulsations measured are approximately double those measured in the leakage flow path, especially at the lower flows. It can be observed that Channels 6 through to 8 provide similar trends in results, however channel 5 shows a significantly different pattern. In general Channel 5 provides results that are not consistent with those taken at other cutwater locations and contradict published data (i.e. overall the tests the results from Channel 5 predict that the pressure pulsations are independent of the cutwater gap, which contradicts the findings of Ardnt et al (25).) Additionally, the largest rate of increase of pulsations is between 100% and 50% flow, with there often being a reduction in this rate of increase or even a reduction in the level of pulsation at 25% flow. Figure 4.14c illustrates the pulsations in the volute away from the cutwater. No pressure measurements were taken in the discharge of the pump and thus the C9 position is the closest indicator to the change in the pulsation as the flow moves towards the pump discharge. It is immediately apparent that the pulsation at C9 is significantly lower than at the cutwater, being closer in magnitude to the pulsations in the leakage region. The increase in pulsation as the flow rate decreases is small, but a larger increase is evident at the higher flow values, with 75% flow appearing the minimum pulsation location.

In the impeller, Figure 4.14d the pulsation at the shroud is found to be similar in magnitude to that found at the cutwater, with it also having a similar trend as the flow rate decreases. Unfortunately no data exists for the impeller blade as the blade

transducer failed on the first experimental test and was not replaced due to time constraints.

4.3.2.2 Cutwater Clearance

In order to compare the effect of the cutwater on the pulsation, Figure 4.15 contains results taken from Experimental Tests 5, 10 and 13. These tests were all conducted using the same sidewall clearance, snubber gap and impeller vane arrangement; hence the only geometrical variable is the impeller outer diameter. At the leakage flow region, Figure 4.15(a) there is a small reduction in pulsation for the reduction in cutwater gap, however this reduction increases slightly at the lowest flow condition. At the cutwater, Figure 4.15(b) the reduction in pulsation is larger from 3.83% to 6.00%, than it is from 6.00% to 7.95%, indicating a non-linear trend between the cutwater gap and the pulsation at this location. At the lowest flow the pulsations tail off as the cutwater gap is increased. Towards the discharge, Figure 4.15(c), the trend is largely unpredictable. Each cutwater gap plot has a slightly different trend, thus it is impossible to reach any definite conclusion. At the impeller, Figure 4.15(d), there is only a slight reduction in the pressure pulsation for the reduction in cutwater gap, with the reduction not changing significantly over the flow range.

In summary the cutwater clearance does affect pressure pulsations across the whole pump, however the significant effects appear to be local to the cutwater or at lower flow rates.

4.3.2.3 Snubber Gap Clearance

The effect of the different snubber ring clearances is shown in Figure 4.16, which contains results taken from Experimental Tests 8, 9 and 10. As before, the tests were conducted with identical geometrical arrangements, except for the snubber gap. At the leakage flow region, Figure 4.16(a) the pulsation increases slightly at duty as the clearance is increased, with this pulsation increasing by progressively larger amounts as the flow rate decreases. At the cutwater region, Figure 4.16(b), there is minimal

pulsation reduction at higher flows, but the reduction increases as the flow rate decreases. Towards the outlet of the volute, Figure 4.16(c), there is no appreciable difference in pulsation at the higher flows, but with some reduction at the lowest flow rate. Finally at the impeller shroud, Figure 4.16(d), there is a reduction in pulsation at all flow rates as the snubber gap is increased.

Indications are that the snubber gap controls the amplitude of the pulsation in the leakage flow area, however a tight snubber gap may have consequences for pulsations in other regions of the pump.

4.3.2.4 Sidewall Passage Clearance

The effect of changing the sidewall clearance is shown in Figure 4.17 at each of the four locations specified. The data used to construct these plots is taken from experimental tests 1 and 7, unfortunately difficulties were experienced on test 1 at the 75% flow condition for Channel 9 and so this data is not available.

At the leakage flow region, Figure 4.17(a), the pulsations follow the typical trend in that the pulsations decrease as the sidewall gap increases and the decrease is larger at lower flows. At the cutwater region, Figure 4.17(b), the pulsation decrease is relatively consistent across the flow rates, however when using the larger gap the pulsation decreases from 50% to 25%, whereas it increases for the smaller gap. Towards the discharge, Figure 4.17(c), the pulsations remain low and there is little to differentiate any variation due to the sidewall gap. At the impeller, Figure 4.17(d), the larger sidewall gap produces a slightly lower pulsation at the shroud. The result at 75% flow rate is markedly different from the trend established at the other flows and so this result may have been affected by the problems that were experienced during this test.

4.3.2.5 Vane Configuration

Two vane arrangements were tested over a range of flowrates at a single cutwater clearance and for four snubber configurations. Typical results illustrating the effect that

the vane configurations have at a single set of snubber clearances has on the pressure pulsations are shown in Figure 4.18.

Again, the results conform to the general trend of higher pulsations at lower flows. It is important to note that the results predict consistently that the staggered impeller will reduce the pressure pulsations in the cutwater region and leakage region by as much as a quarter or a third at the lowest flow condition, Figure 4.18(a)(b). This, however, does not correspond to a similar magnitude of reduction in the discharge or impeller, Figure 4.18(d)(c).

Thus, the staggered impeller configuration has a marked effect on reducing the pressure pulsations at the cutwater and leakage flow path, but appears to have a significantly lesser effect at the impeller outlet.

4.3.3 Performance Data

Although not a requirement of the test program, some performance data was recorded during selected tests. This data consisted of head/flow data taken across the flow range being examined. Using this data it is possible to note briefly the effect the various geometrical modifications will have on the performance of the pump. Figure 4.19 illustrates a broad comparison of the head/flow data for each of the geometrical modifications.

Cutwater Modification (Figure 4.19(a)): The act of cutting an impeller diameter to achieve a particular duty flow condition is common in the pump industry; in-house selection curves typically show the predicted performance of pumps with different impeller diameters. This is effectively the process utilised to vary the cutwater to blade clearance, although in industry both impeller blade and shroud are usually cut. A general understanding of the relationship between the head and impeller diameter can be determined from the scaling laws, which predicts,

$$\text{Constant} = \frac{H}{N^2 D_2^2} \qquad \text{Equation 4.6}$$

where H is the head (m)

N is the pump speed (RPM)

D_2 is the impeller outlet diameter (m).

The above scaling law is derived from a simplified Euler equation for a radial impeller

$$H_e = \frac{u_2^2}{g} \qquad \text{Equation 4.7}$$

where H_e is the Euler predicted head (m)

u_2 is the velocity at the impeller outlet (m/s)

g is the gravitational acceleration (m/s^2)

The full Euler's equation, for an impeller where the flow approaching the impeller eye is not radial (or pre-rotation is allowed), is shown in Equation 4.8. This includes a second subtractive term that is omitted in the simplified equation.

$$H_e = \frac{u_2 c_{u2}}{g} - \frac{u_1 c_{u1}}{g} \qquad \text{Equation 4.8}$$

where c_{u2} is the tangential component of the absolute velocity at outlet

u_1 is the velocity at inlet

c_{u1} is the tangential component of the absolute velocity at inlet

Standard textbooks containing pump theory, such as Stepanoff (95), include more detail concerning basic pump theory and the manipulation of Euler's equation for the theoretical prediction of head.

It is therefore unsurprising that the change in generated head due to modifying the cutwater gap from 3.83% to 7.95% is consistently large across the flow range,

approximately 10% at the BEP. The data set used for the comparison uses a snubber gap of 1.64%, sidewall clearance of 100% and an inline vane arrangement.

Snubber Diameter (Figure 4.19(b)): Performance data suggests that the act of decreasing the snubber clearance gap from 1.64% to 0.27% will have a negligible effect on the head generated by the pump. Any loss in head is most likely to occur at either high or low flows, but even at these extremes of the flow range the loss remains small (around 1%). The data set used for the comparison uses a cutwater gap of 6.00%, sidewall clearance of 100% and an inline vane arrangement.

Sidewall Clearance (Figure 4.19(c): Head/flow data taken for the same cutwater clearance and snubber gap predicts that by reducing the sidewall clearance by a factor of four will correspond to a negligible change in head that is consistent over the flow range. Any difference between the two sets of results is less than 1%. The data set used for the comparison uses a cutwater gap of 3.83%, a snubber gap of 6.38% and an inline vane arrangement.

Vane Configuration (Figure 4.19(d)): A comparison of the performance data indicates that the staggered vane corresponds to a drop in head of around 3.5% to 6.5% depending on the flow in comparison with the straight vane impeller. The loss in the generated head is relatively consistent across the flow range and is approximately half that experienced due to varying the cutwater gap. The data set used for the comparison uses a cutwater gap of 3.83%, a snubber gap of 1.64% and a sidewall clearance of 100%.

4.4 Critical Review of Experimental Work

The experimental test programme that was undertaken contains a substantial amount of information relating to pressure pulsations and how they are affected by pump geometrical selections. However, it is important to highlight the limitations of this work and to appreciate the uncertainties this causes.

Documentation: The lack of documentation providing clear and specific detail relating to the experimental tests causes significant difficulty. In many cases the information is present in an alternative form, but the process of identifying relevant data and assembling the data in a meaningful form can be lengthy and tedious. The absence of a test report or interpreted data, while being a hindrance to the rapid processing of the data, has caused the author to examine the test procedure in more detail than would otherwise be necessary. This has resulted in a greater understanding of the test process and the manipulation of the raw experimental data.

Test Programme: The test programme does not provide a complete range of tests for the relationship between pressure pulsations and the various geometrical modifications being considered. Thus, while the results indicate that a staggered impeller produces a large reduction in pressure pulsations in the volute, it is uncertain whether this will continue to be true when the cutwater gap is greater than 3.83%. This situation is exacerbated by the abrupt halt in the test programme once the contract related test arrangements had been conducted. Although detailed information is available for pressure pulsation variations due to the cutwater gap, limited information is available for the vane configurations, snubber gap and the sidewall clearances. Unfortunately the test results make no mention of any assessment of possible measurement errors or the level of uncertainty in the results. It has been assumed that the test work was conducted in accordance with normal industrial practice.

When faced with utilising this work for comparison with CFD analyses it is therefore prudent to perform the comparison not only with the present experimental data but also with pressure pulsation trends identified in published literature.

4.5 Chapter Summary

The results of the investigations into the effect that geometrical modifications have on the pressure pulsations at different flow conditions in a centrifugal pump, may be summarised as follows:

- The highest pressure fluctuations occur at off design conditions, with the highest occurring most frequently at the 25% flow condition.
- The highest fluctuations are at the volute cutwater and at the impeller outlet.
- Increasing the cutwater clearance gap between the impeller blade and the volute cutwater decreases the pressure pulsations.
- Increasing the snubber clearance decreases the pressure pulsations (excepting in the leakage flow path where it increases them), but to a lesser degree than the cutwater clearance.
- Increasing the sidewall clearance has a similar effect to increasing the snubber clearance in the sidewall area only and its effect is dependant on the level of snubber clearance being used.
- Offsetting the vanes by 50% reduces the pressure pulsations in the pump significantly, with a larger reduction being gained local to the impeller outlet and casing volute than in other locations.

4.6 Tables

Location	Description	Parameter	Value
Double Entry Impeller	Inlet Eye Diameter (m)	D_1	0.177
	Average Leading Edge Blade Angle (^{o})	β_L	26
	Impeller Outlet Diameter (m)	D_2	0.366
	Average Trailing Edge Blade Angle (^{o})	β_T	22.5
	Impeller Outlet Width (m)	b_2	0.061
	Blade number (per side)	z	6
	Total Blade Wrap Angle (^{o})	θ	102
	Blade Thickness (m)	t_B	0.007
	Leading Edge Blade Radius (m)	R_L	0.002
Double Volute	Suction Branch Diameter (m)	D_s	0.400
	Discharge Branch Diameter (m)	D_d	0.300
	Volute Width (m)	B_3	0.105
	Radius to Cutwater (m)	R_3	0.190

Table 4.1: Geometric pump data

Geometry Parameter	Variation			
	1	2	3	4
Cutwater Gap	3.83%	6.00%	7.95%	-
Snubber Gap	6.38%	1.64%	1.10%	0.27%
Sidewall Clearance	100%	25%	-	-
Vane Arrangement	Inline	Mid Position Stagger	-	-

Table 4.2: Variations in the geometric parameters tested

Test No.	Impeller Vane Type	Cutwater/Vane Clearance	Cutwater/Shroud Clearance	Snubber Clearance	Sidewall Clearance
1	Straight	3.83%	3.83%	6.38%	100%
2	Straight	3.83%	3.83%	0.27%	100%
4	Straight	3.83%	3.83%	1.10%	100%
5	Straight	3.83%	3.83%	1.64%	100%
6	Straight	3.83%	3.83%	0.27%	25%
7	Straight	3.83%	3.83%	6.38%	25%
8	Straight	6.00%	3.83%	6.38%	100%
9	Straight	6.00%	3.83%	0.27%	100%
10	Straight	6.00%	3.83%	1.64%	100%
11	Straight	7.95%	3.83%	6.38%	100%
12	Straight	7.95%	3.83%	0.27%	100%
13	Straight	7.95%	3.83%	1.64%	100%
14	Straight	7.95%	3.98%	0.27%	100%
15	Staggered	3.83%	3.83%	6.38%	100%
16	Staggered	3.83%	3.83%	0.27%	100%
17	Staggered	3.83%	3.83%	1.10%	100%
18	Staggered	3.83%	3.83%	1.64%	100%
21	Staggered	3.83%	3.83%	6.38%	100%
22	Staggered	3.83%	3.83%	0.27%	100%

Table 4.3: Experimental test programme

4.7 Figures

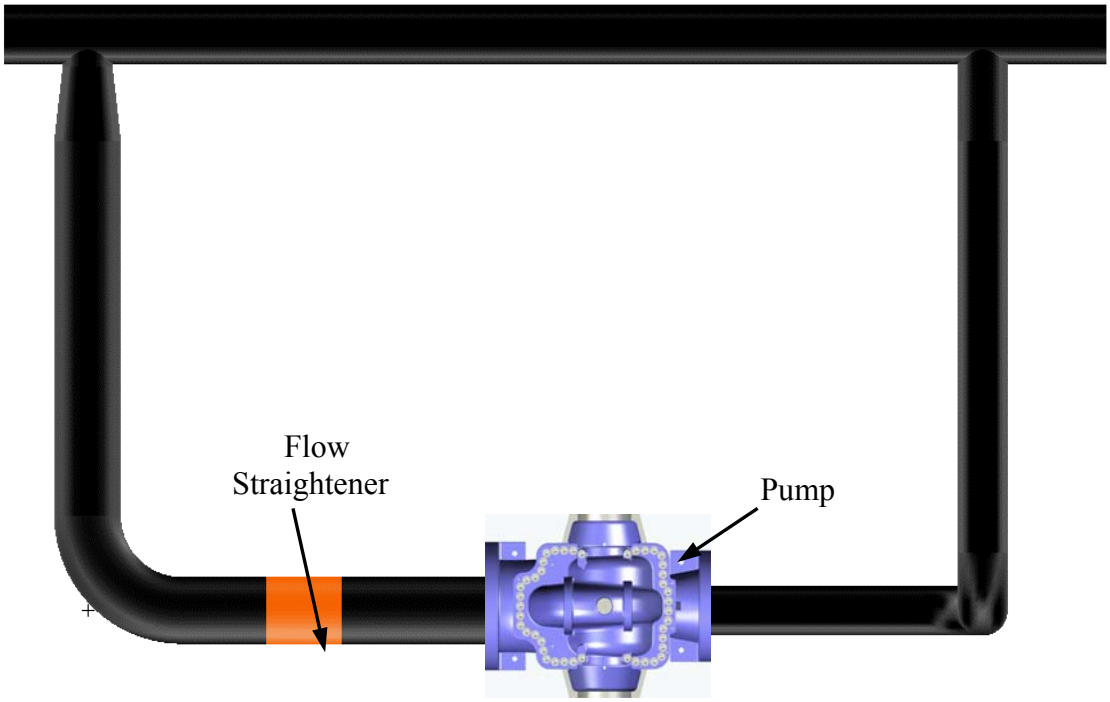

Figure 4.1: Closed loop test rig

(a) Kistler (b) Entran

Figure 4.2: Pressure transducer types (not to scale)

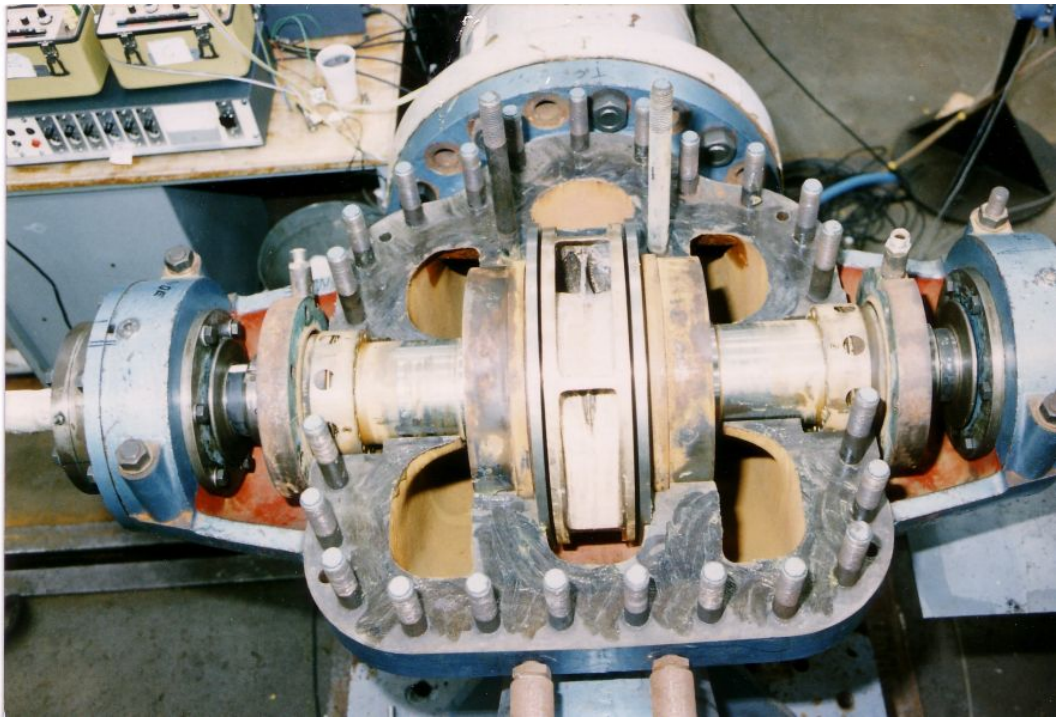

Figure 4.3: Photograph of test pump with top half casing removed

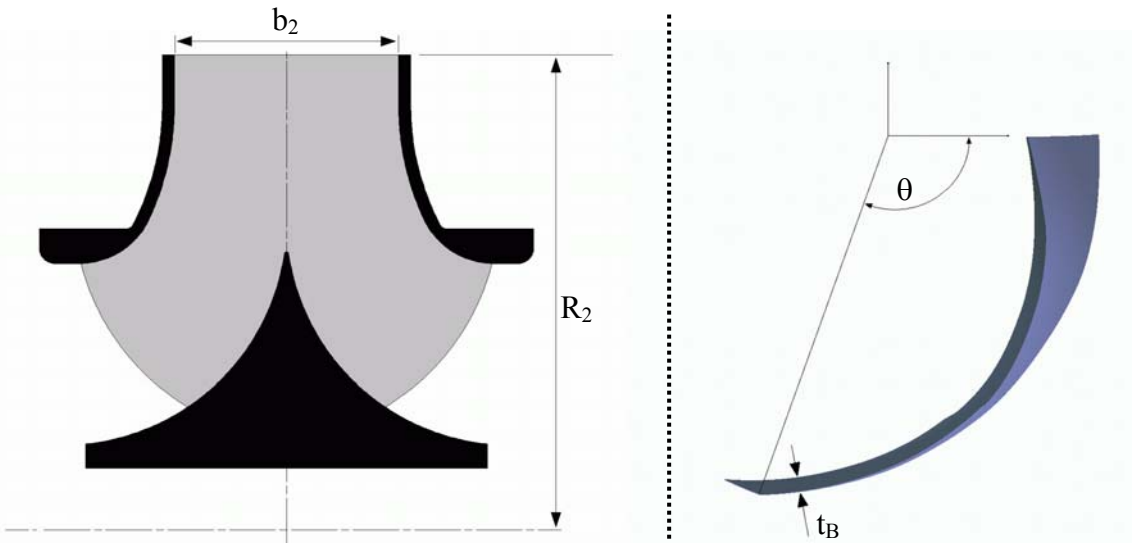

Figure 4.4: Diagram of an inline impeller, meridional and blade views.

Figure 4.5a: Photograph of an inline impeller
(blade B1 and shroud S1 transducer positions labelled)

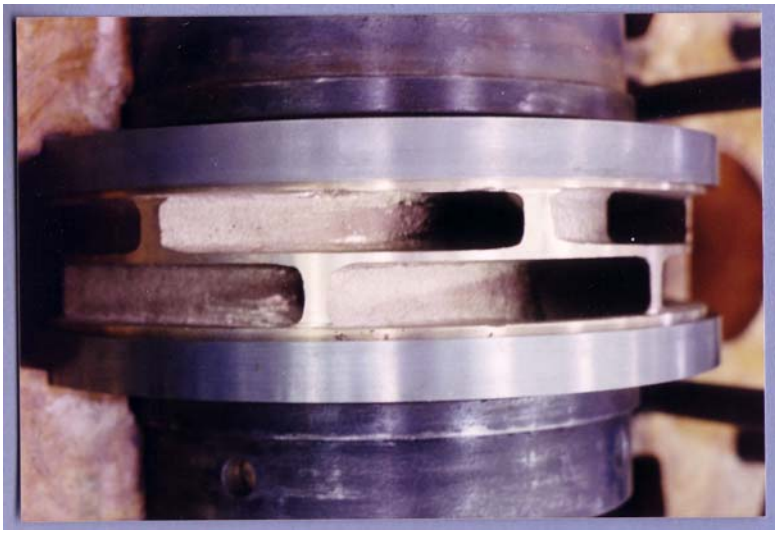

Figure 4.5b: Photograph of a staggered vane impeller

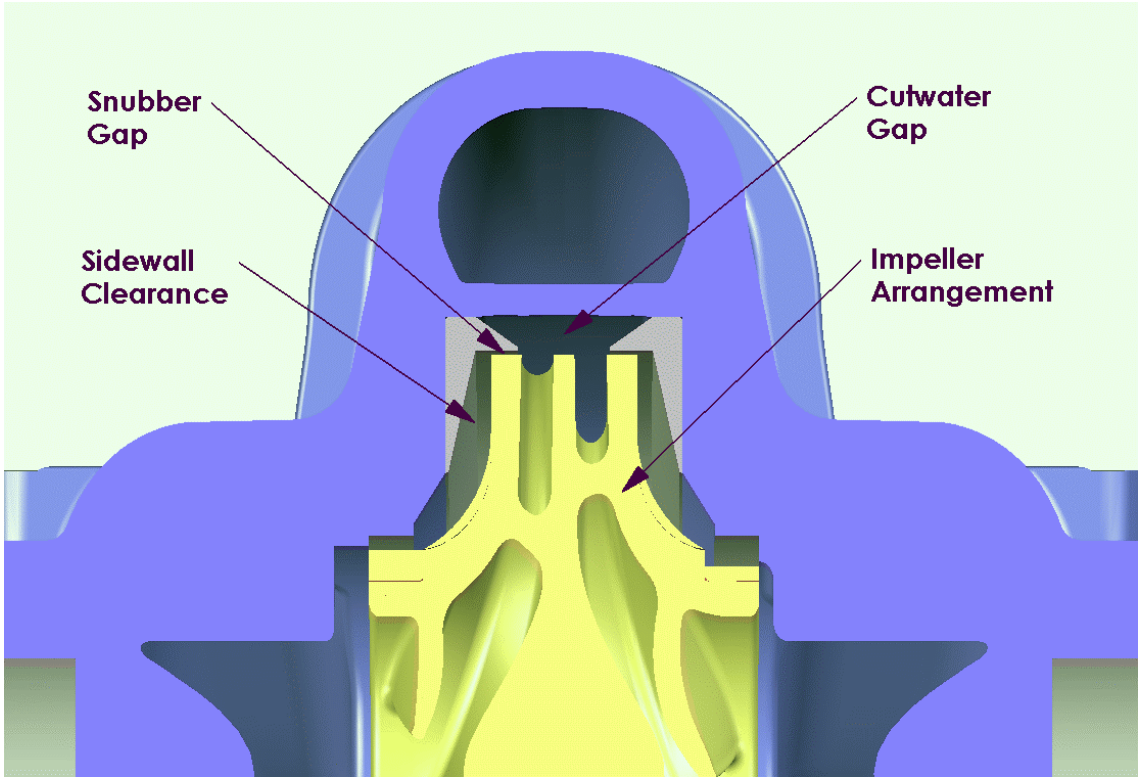

Figure 4.6: Pump section identifying the main geometrical parameters.

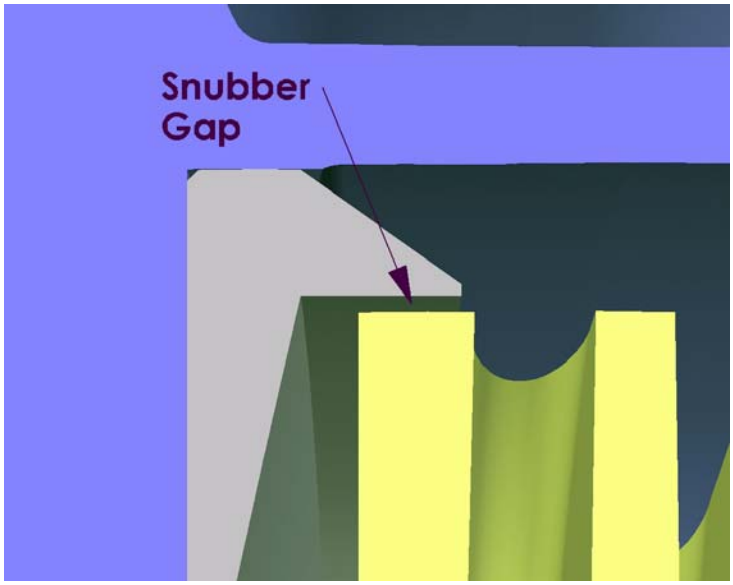

Figure 4.7: Snubber gap clearance location

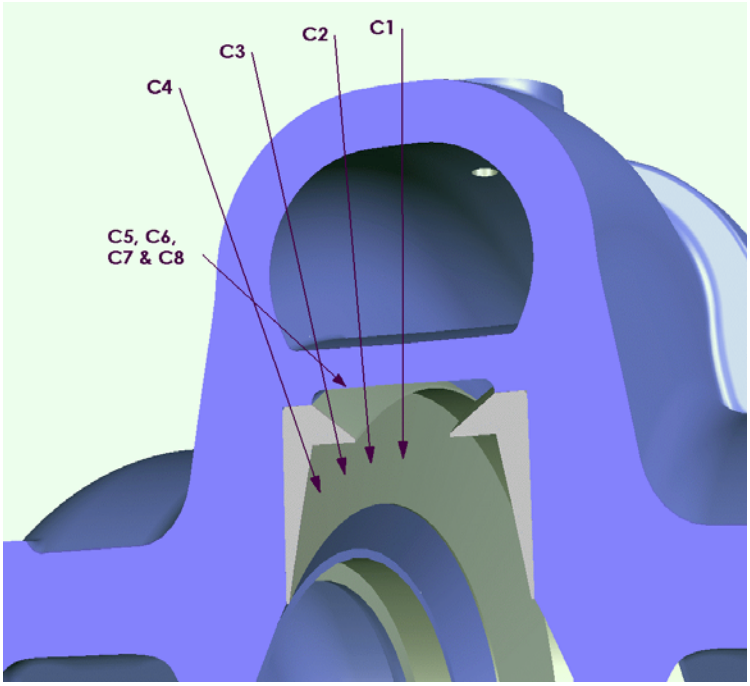

Figure 4.8: Pump section identifying the axial position of the sidewall tapping locations (C1, C2, C3 & C4) and the cutwater tapping locations (C5, C6, C7 & C8)

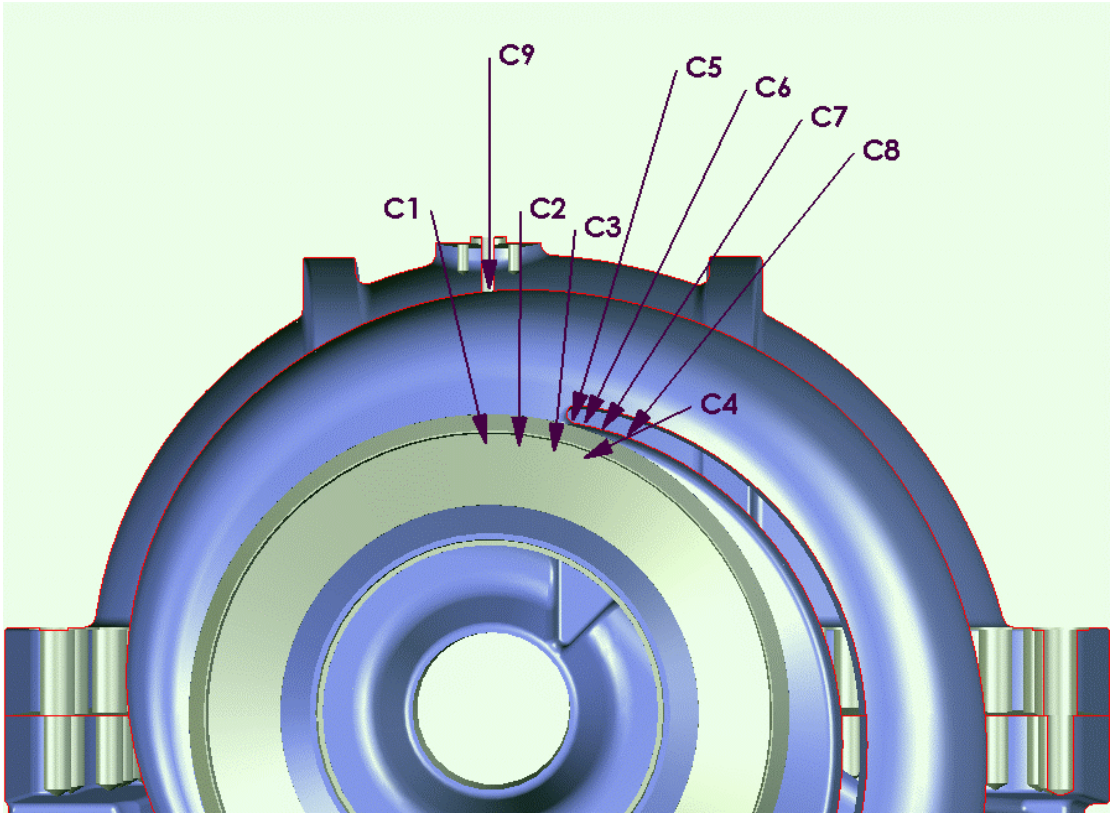

Figure 4.9: Pump section identifying the circumferential position of the sidewall tapping locations (C1, C2, C3 & C4) and the cutwater tapping locations (C5, C6, C7,C8 & C9)

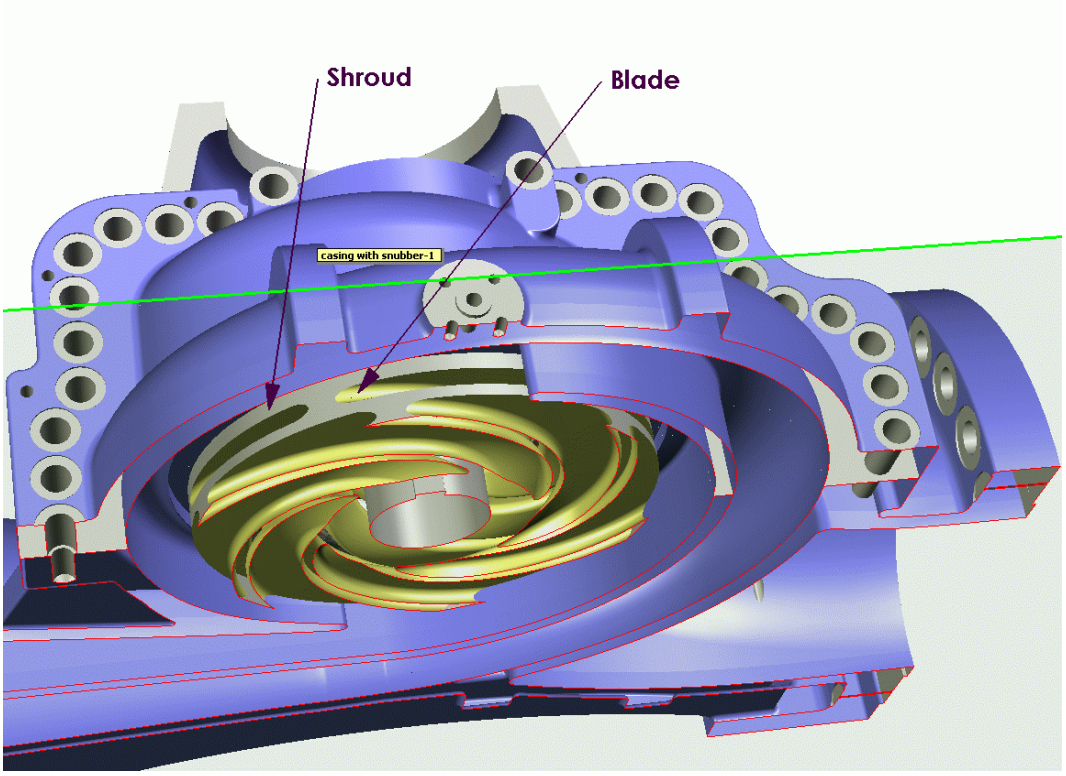

Figure 4.10: Pump section identifying the impeller transducer locations (Blade & Shroud)

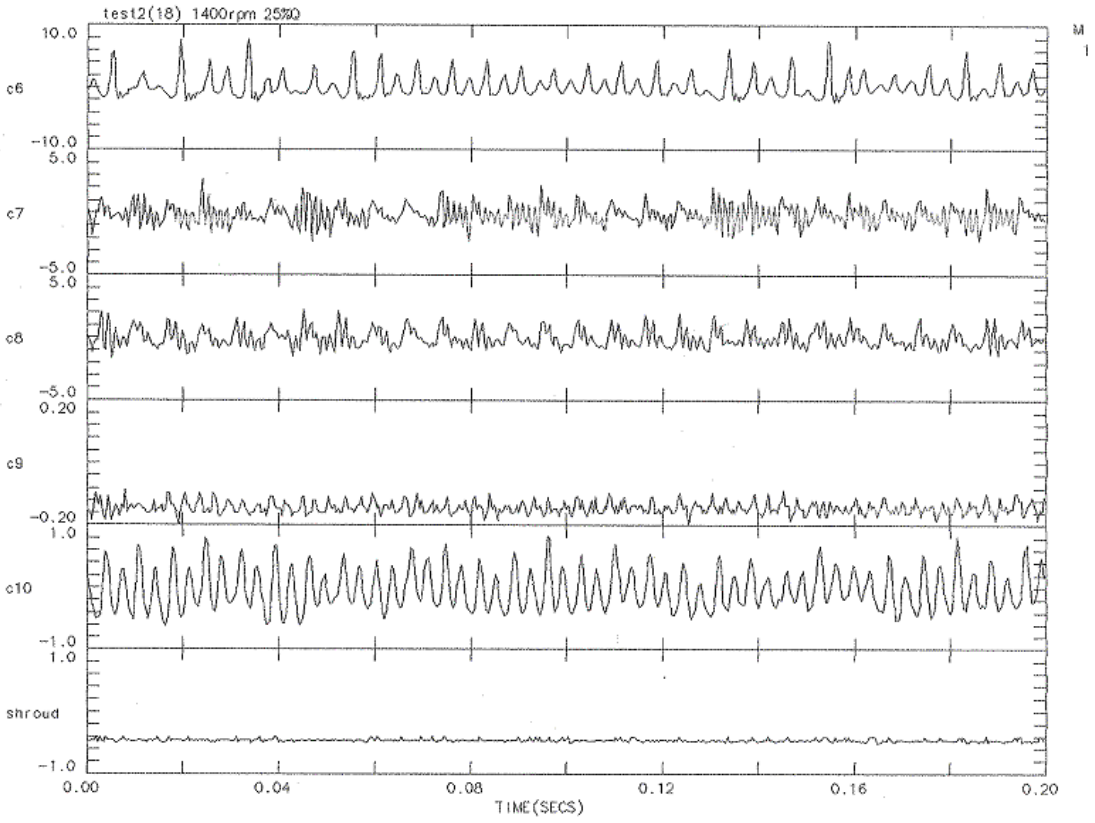

Figure 4.11: Sample time history data output

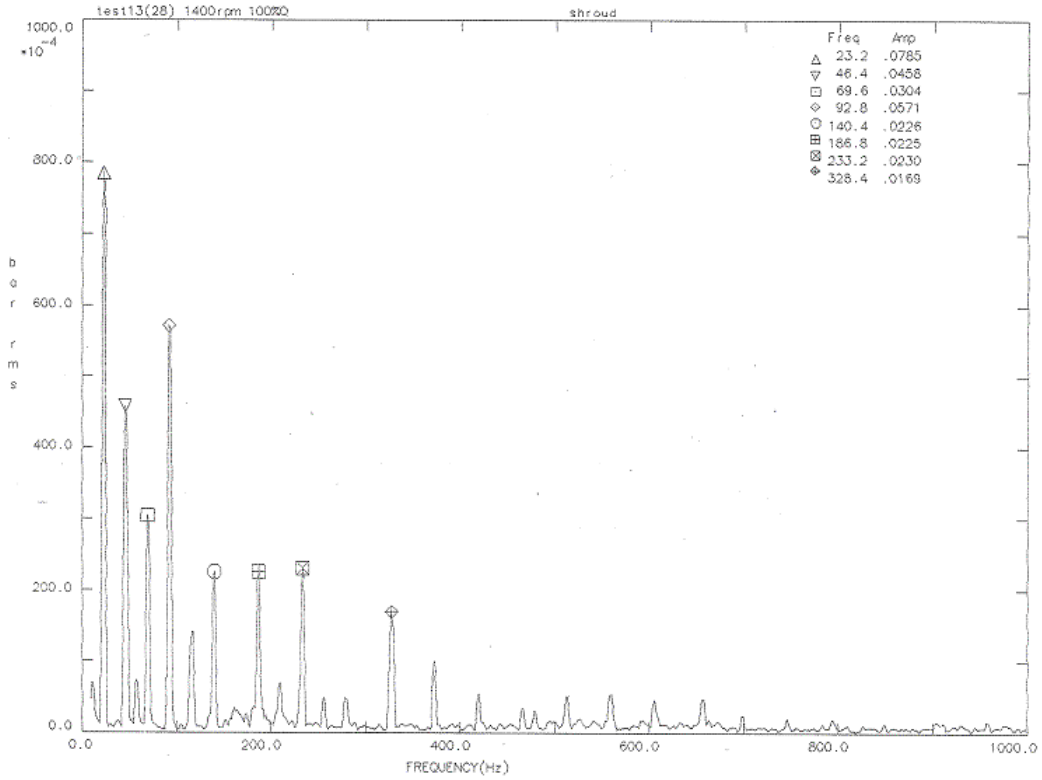

Figure 4.12: Sample frequency spectrum output

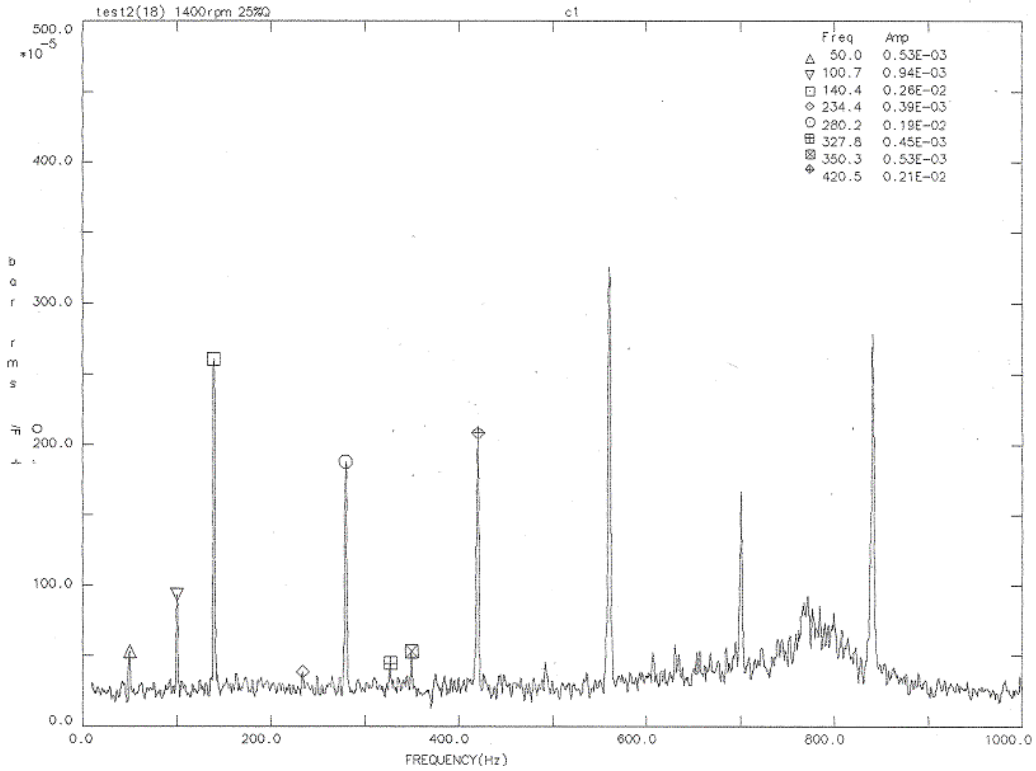

Figure 4.13: Frequency spectrum showing resonance effect

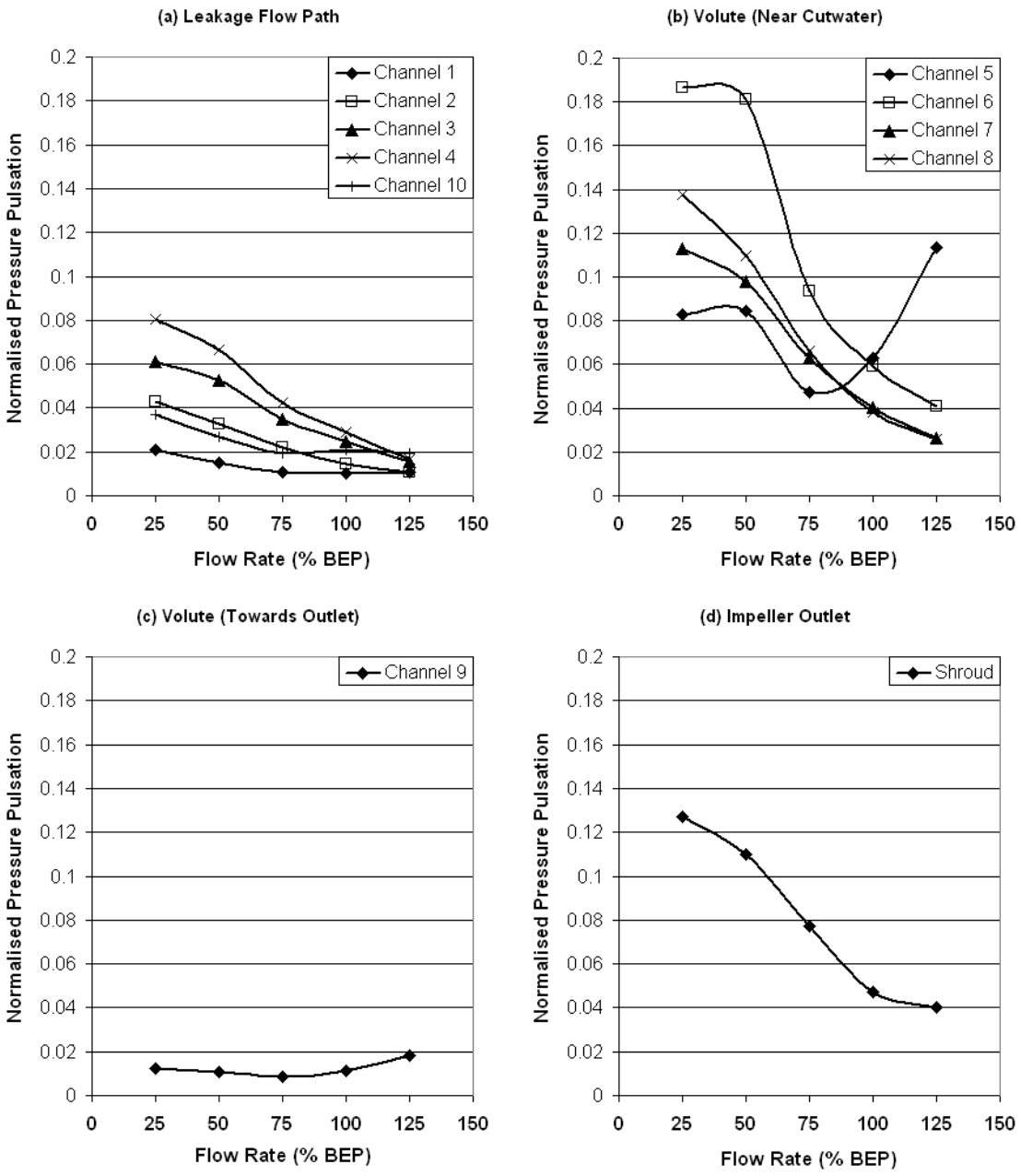

Figure 4.14: Typical results showing the normalised pressure pulsations at various pump locations for experimental test 5

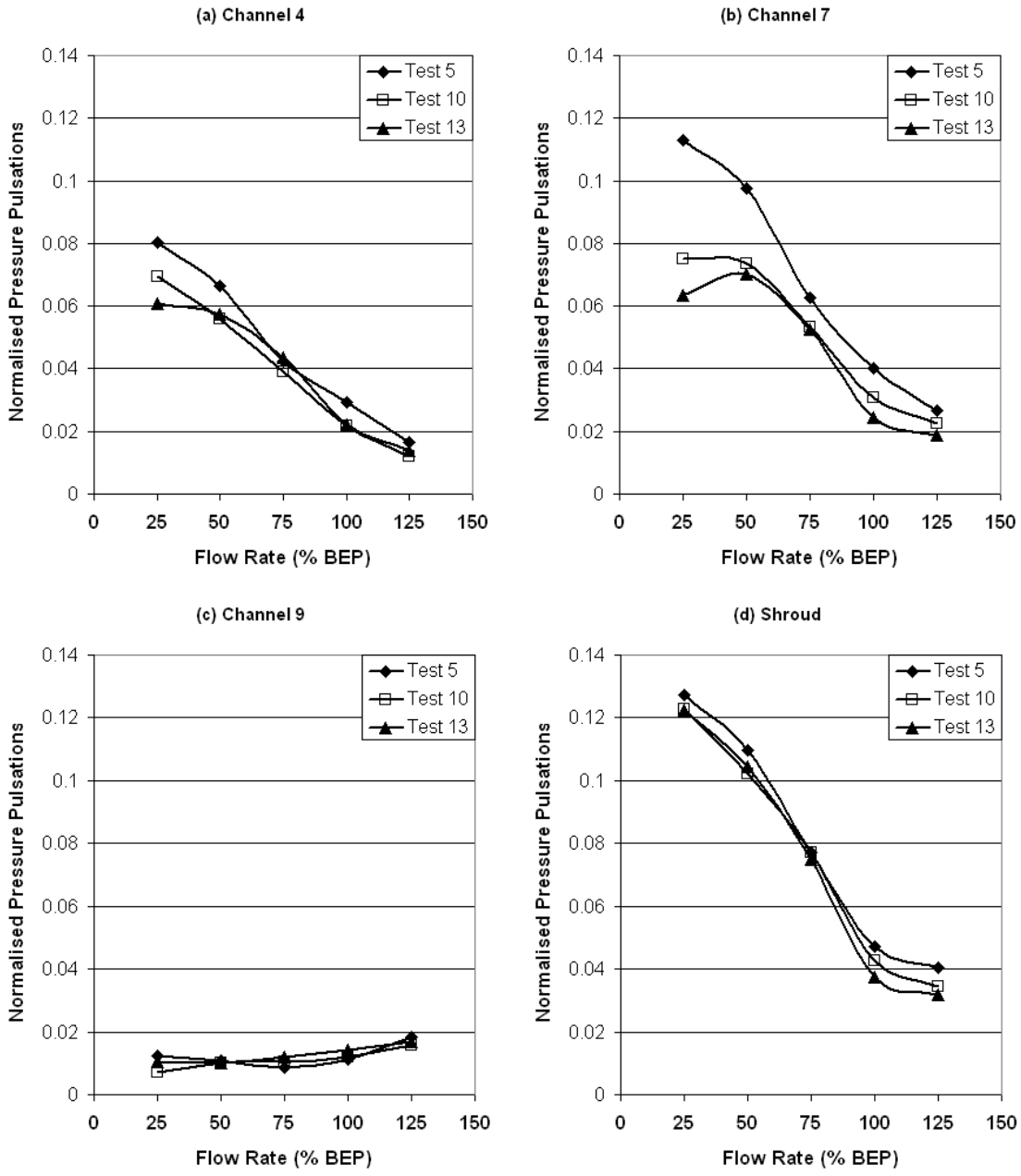

Figure 4.15: Effect of cutwater clearance on the pressure pulsations at various locations around the pump (comparison taken for inline vane arrangement, 1.64% snubber gap and 100% sidewall clearance)

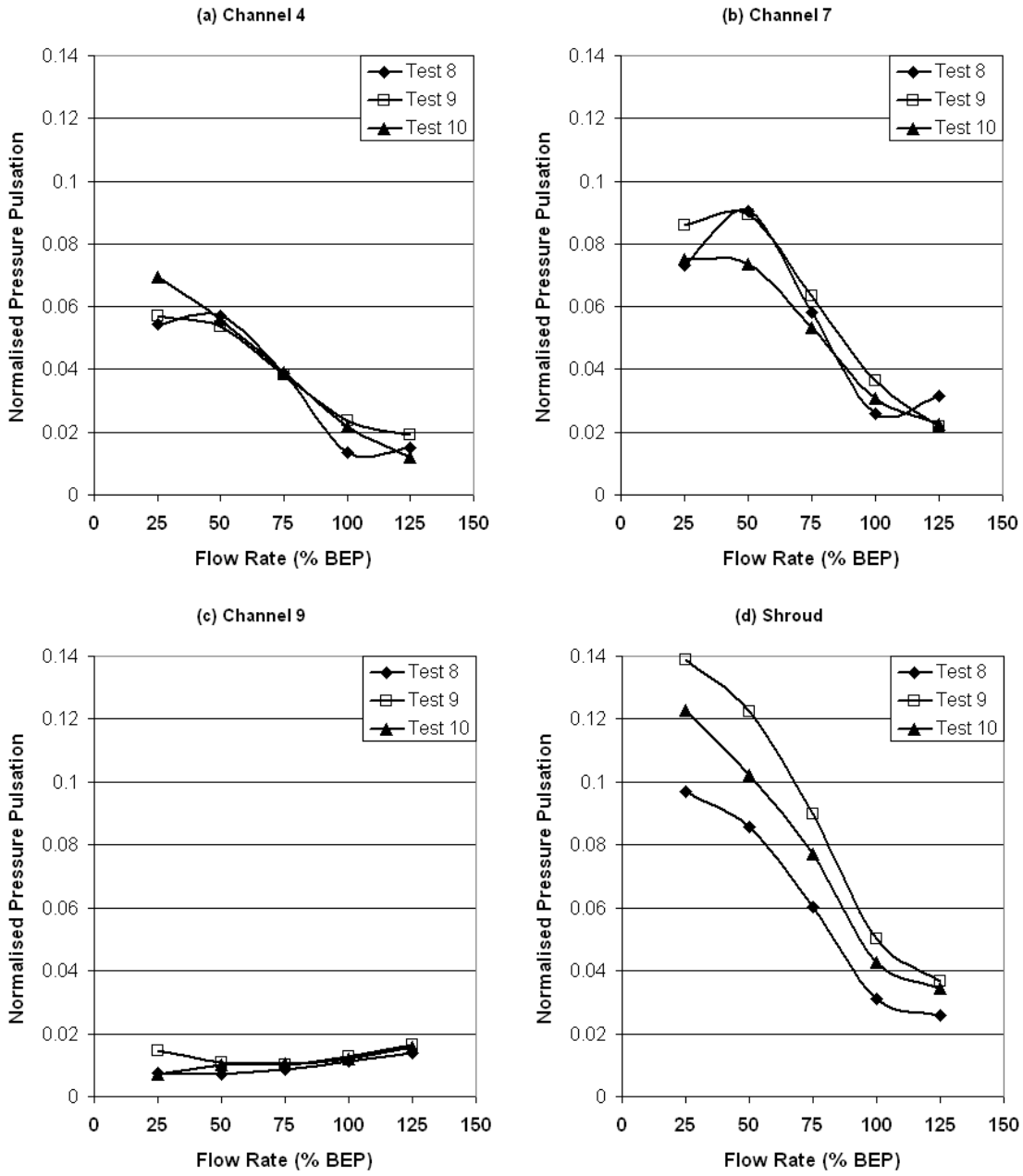

Figure 4.16: Effect of snubber clearance on the pressure pulsations at various locations around the pump (comparison taken 6.00% cutwater clearance, 100% sidewall clearance and for the inline vane arrangement).

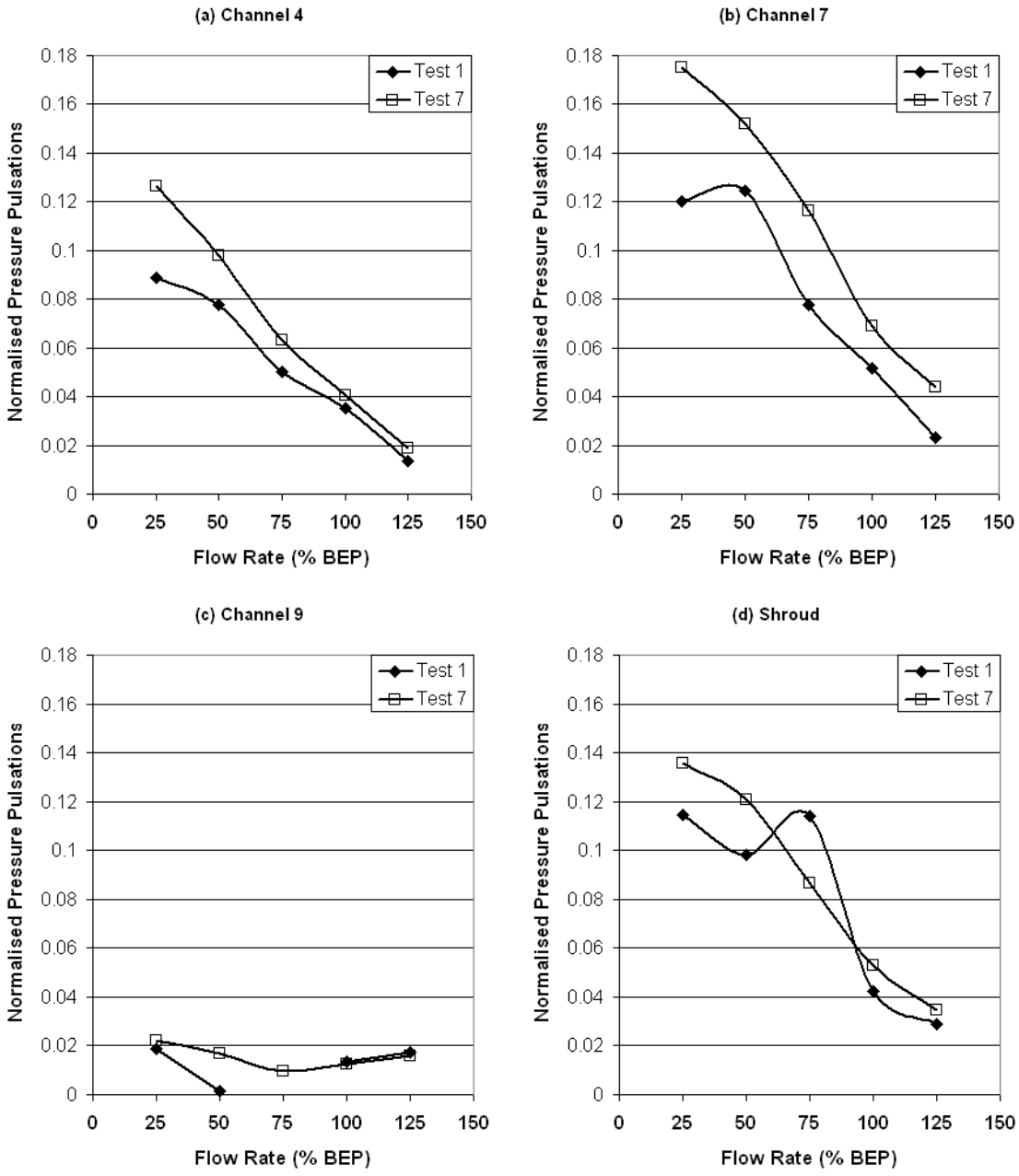

Figure 4.17: Effect of sidewall clearance on the pressure pulsations at various locations around the pump (comparison taken 6.00% cutwater clearance, 6.38% snubber gap and for the inline vane arrangement)

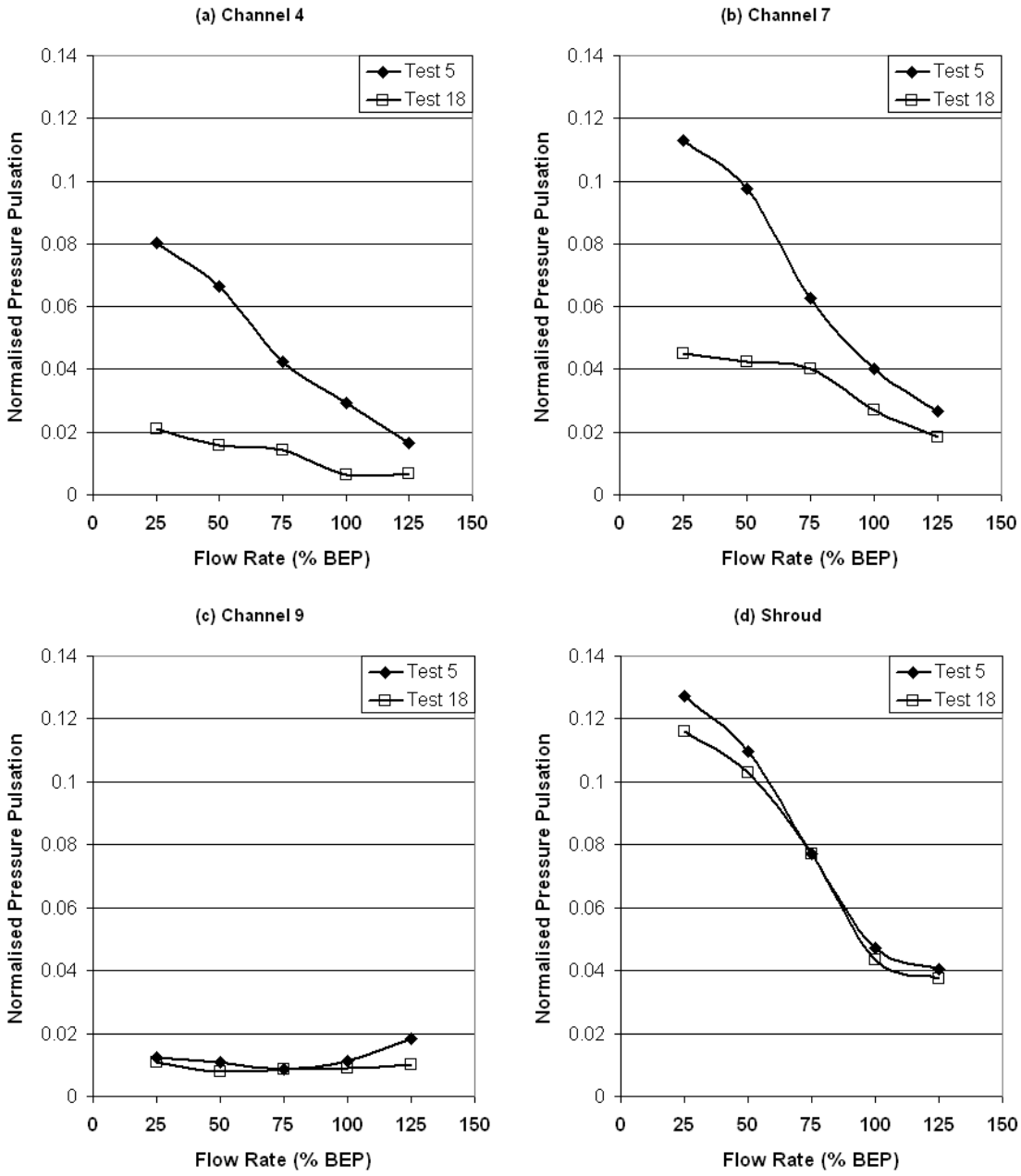

Figure 4.18: Effect of vane arrangement on the pressure pulsations at various locations around the pump (comparison taken 6.00% cutwater clearance, 1.64% snubber gap and 100% sidewall clearance).

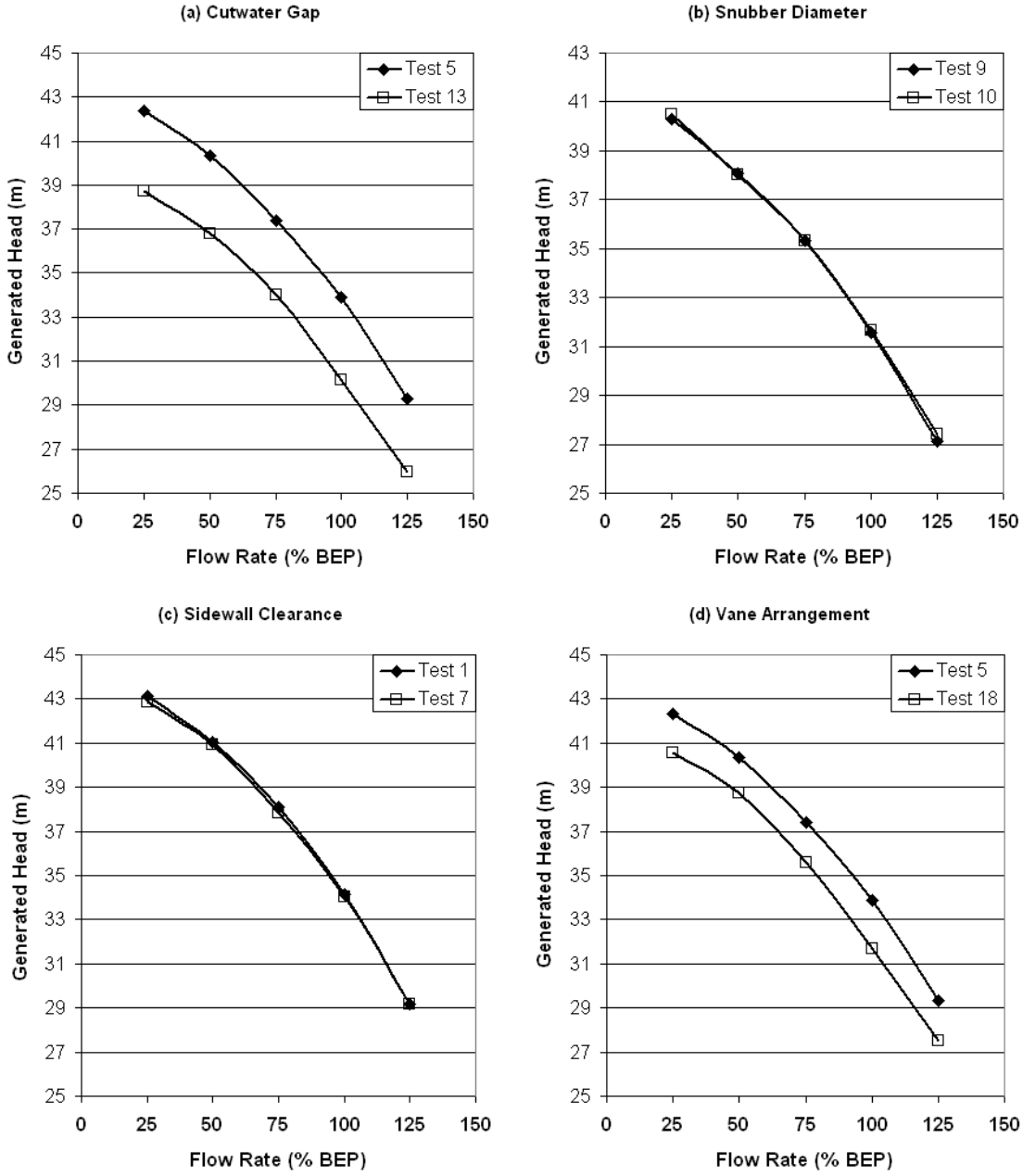

Figure 4.19: Comparison of the pump generated head for each geometrical modification. Comparing (a) 3.83 and 7.95 cutwater gaps, (b) 0.27% and 1.64% snubber gaps, (c) 25% and 100% sidewall clearances and (d) inline and staggered vane arrangements.

Chapter 5

Computational Method and Implementation

5.1 Project Approach

5.1.1 A Complete Pump Model

5.1.2 Pressure Pulsations

5.1.3 Effect of Geometrical Variations

5.1.4 Development of Design Recommendations

5.1.5 Approximation to Transient Pressure Pulsations via Steady State Analyses

5.2 CFD Approach

5.2.1 Grid Generation

5.3 Theoretical Background

5.3.1 CFD Theory Introduction

5.3.1.1 Governing Equations

5.3.1.2 Discretisation

5.3.1.3 Turbulence Modelling

5.3.2 Taguchi Theory Introduction

5.3.2.1 Taguchi Analysis Preparation

5.3.2.2 Analysis of an L_9 Array

5.3.2.3 Analysis of an L_4 Array

5.4 Geometry Definition and Grid Generation

5.4.1 Impeller

5.4.2 Volute

5.4.3 Shroud Leakage Passages

5.4.4 Suction Inlet

5.5 Grid Quality Investigation and Refinement

5.5.1. Double Entry Impeller Passageway

5.5.2 Inclusion of Leakage Passageway

5.5.3 Inclusion of Suction Inlet

5.5.4 Grid Refinement Model

5.6 Analysis Procedure

5.6.1 Pre-Processing

5.6.2 Turbulence Modelling

5.6.3 Numerical Solution Control

5.7 Chapter Summary

5.8 Tables

5.9 Figures

5 Computational Method and Implementation

In this chapter a brief description is given of the process used to generate the computational model employed in the study of pressure pulsations within a reduced scale high energy, double entry pump. Following a short introduction to the commercial CFD package used in the thesis, the chapter provides a brief introduction to the theory appropriate to both CFD and the Taguchi process. Thereafter, details are provided of the numerical model and the measures that were taken to achieve as high a quality grid as possible in each fluid component. Details are given concerning the properties and boundaries involved in each of the analyses involving the assembled model. Finally, the parameters selected for the actual solution are discussed.

5.1 Project Approach

Chapter 1 has detailed the main aims of the project as well as broad processes required to achieve those aims. This section endeavours to provide a brief outline of those processes, before beginning a more detailed description in this and later chapters. Each of the five aims established in Chapter 1 are summarised here for convenience along with a brief outline of the processes required.

5.1.1 A Complete Pump Model

Aim 1: *"To model a complete pump incorporating all of the major flow paths`, i.e. suction inlet, impeller, leakage flow paths and volute casing."*

- The model was split into the pump component parts to in order to generate each mesh individually and tailor it to the flow requirements in that component.
- The grid generation process included
    - careful modelling of components to allow multiple geometric arrangements for a component to be achieved through a single grid.

    - grid independence testing
    - grid refinement.
- A model was assembled by adding one component at a time. An iterative process was used, whereby analyses of the larger model were performed at each stage to check if further refinement of the newly added component was required to model flow interactions between components.

This was a time consuming process, but gives confidence in the large, complex numerical model since each component was capable of modelling not only its internal flow satisfactorily, but had also been generated with consideration of interactive effects with other components.

5.1.2 Pressure Pulsations

Aim 2: *"To fully capture the transient hydraulic flow interactions within the pump in terms of pressure fluctuations at multiple flow rates."*

- Pre-processing was conducted for the numerical model, with consideration of limitations involved with gaining a stable transient analysis while performing the analysis over a wide range of flow conditions.
- A transient analysis was performed of the numerical pump model while monitoring the output to ensure the results have settled.
- The transient analysis was conducted for three flow rates. These are defined as being the duty flow condition, at 50% BEP and at 25% BEP; in this project these flow rates are termed 1.00Qn, 0.50Qn and 0.25Qn respectively. To date no transient analyses had attempted to model a centrifugal pump at a flow rate as low as 0.25Qn as a realistic continuous operating point.
- Information was collected on the pressure pulsation at regular intervals to describe its variation, but with consideration of the limitations of the computational facilities (i.e. computer time and storage).

- The pressure pulsation level was investigated at fifteen locations around the pump. Monitoring locations matched those used in Chapter 4, with additional locations being provided at the impeller outlet and at the pump discharge.

The above process allowed an understanding of how the pressure pulsation varies around the pump, while also indicating how the variation changes as the flow rate changes.

5.1.3 Effect of Geometric Variations

Aim 3: *"To determine how the pressure pulsation across the pump varied depending on the pump geometry. Four key parameters have been identified, namely, cutwater gap, snubber clearance, sidewall clearance and the blade stagger."*

- Firstly the number of variations in the key parameters to be investigated were selected.
- A full factorial comparison was not feasible, therefore the Taguchi method was adopted for planning, set up and post processing of the results.
- A Taguchi array relevant to the number of parameters and variables to be analysed was selected. This reduces the number of analyses required for the comparison considerably.
- The array provided the geometric set up for the arrangements to be modelled.
- The large logistical task of running twenty seven transient analyses in terms of computing resource, time and storage of results files could then be performed.
- The relevant pressure pulsation data from the required fifteen locations was obtained and the performance characteristic information at each transient moment in time evaluated for each arrangement and flow rate.
- Taguchi statistical techniques were used in the post-processing of the information to identify the relative importance of the key parameters and also to generate predictive equations for the pressure pulsations.

- Based on the post-processing information a recommended pump arrangement was deduced that has a lower level of pulsation without significant performance loss.
- Numerical models related to the recommended arrangement were generated and a transient analysis performed at three flow rates. The pulsation and performance data was obtained as above and compared to the data from the initial analyses.

This process generates a great deal of useful information that assists in the understanding of the pressure pulsations in the pump. It also provides a recommended pump arrangement that could be used as the basis for future designs and for which the likely pulsation levels are known.

5.1.4 Development of Design Recommendations

Aim 4: *"To provide pump designers with recommendations that assist in understanding how to control pressure pulsations within the pump and their effect on the design."*

- Pressure pulsations and detailed pressure differentials in the impeller are not usually considered directly in mechanical design or when considering actual stress levels. Two methods of obtaining some relationship were investigated
- Method 1 compared the pressure data from the numerical analyses with the assumed pressure levels used in existing design guidelines that calculated the stress level. The design guidelines were updated to reflect the more realistic pressure assumptions available from the CFD data.
- Method 2 performed a set of limited finite element stress analyses on the impeller shroud using detailed pressure data from the numerical analyses.
- Based on the information provided by both methods and also the output from the Taguchi arrays, a set of general design recommendations were developed relating to pressure pulsations.

The above process correlated the CFD results with both theoretical stress levels gained from design calculations and finite element stresses acting at the impeller shroud. This is aimed at providing the designer with information relating to the mechanical strength of the impeller in light of the CFD pressure data.

5.1.5 Approximation to Transient Pressure Pulsation via Steady State Analyses

Aim 5: *"To assess a methodology for estimating transient pressure pulsation in a shorter time frame using steady state analyses."*

- One of the initial Taguchi transient arrangements was re-modelled as a steady state analysis and run for different impeller positions over two blade passes.
- The steady state analysis was repeated for the other flow rates and compared the pressure pulsation results with those found using the full transient analyses.
- A second, different arrangement was re-modelled and the following comparisons were performed
    - Comparison of pulsations with transient analysis
    - Comparison of pulsation trends between the two steady state analysis arrangements with the trends from the two transient analyses for the same arrangements.

The above process potentially can determine whether steady state analyses can be used to reasonably predict pressure pulsations within a pump, which if successful could avoid the requirement for lengthy transient analyses and large volumes of results files.

5.2 CFD Approach

The task of analysing a turbo-machine using CFD is not straightforward for a number of reasons. For instance the complicated geometry requires careful modelling and large grids as well as the interaction of rotational and stationary components requires a

reliable multiple frame of reference capability to name but two areas. In selecting a CFD package Weir Pumps spent a significant time assessing the commercial packages available. An important factor in the selection of CFX-TASCflow was its proven track record in turbomachinery applications. A wealth of published literature is available that literally numbers hundreds of articles that detail the use of TASCflow with respect to turbomachinery related analyses during a period of over fifteen years. One of the earliest works is a three-dimensional flow analysis of a multistage crossover diffuser by Graf and Sloteman of Ingersoll Rand Corporation as well as others (52) in 1990. Sulzer Pumps' interest and later adoption of CFX-TASCflow in the early to mid nineties can also be followed through a number of published works, Schachenmann et al (96) and Casey et al (97). Weir Pumps' adoption of CFX-TASCflow (61) was in the latter stages of the nineties. CFX-TASCflow has also been used by various institutes and laboratories to investigate turbomachinery fluid flows, e.g. Kaupert et al (98) and Muggli et al (99). Higher learning establishments have also provided a significant contribution to TASCflow being used to study turbomachinery flows, examples from Cranfield University include Michaelides et al (100), Naylor et al (101) and Ganga et al (102). Nevertheless, although CFX-TASCflow's usage with regard to turbomachinery components is well documented, it is worth reviewing some of the fundamental features of TASCflow that enhance its application to turbomachinery applications.

CFX-TASCflow utilises a finite element based finite volume method, which provides the benefit of retaining the geometric flexibility of finite element methods while retaining the conservation properties of the finite volume method, i.e. low numerical error on non-smooth grids. It is a fully-implicit solver, thus it creates no time step limitation and is considered easy to implement. This does not have any bearing on the steady-state solution, but does limit transient calculations to being only first-order accurate in time. Options available in TASCflow for gaining second order accuracy in transient analyses is discussed in section 5.3.1.2. The CFX-TASCflow solver is also a coupled solver meaning that the momentum and continuity equations are solved simultaneously. This approach reduces the number of iterations required to obtain convergence and no pressure correction term is required to retain mass conservation, leading to a more robust and accurate solver. CFX-TASCflow also includes some pre

and post processing capabilities that are specifically geared towards turbomachinery components; these facilitate the set up of the model and the examination of the results. The TASCflow user documentation (103) provides detailed information on the usage of the various features in the program. All of these benefits made CFX-TASCflow appropriate for use in this project. It is also worth noting that the author has had eight years experience in conducting CFD analyses of turbomachinery components with this package.

The analysis procedure is outlined in Figure 5.1 for both turbomachinery and non-turbomachinery specific components. A brief outline of each of the components identified is given here,

CFX-Build4: CFX-Build4 is a general CAD type program that allows the generation of geometry and meshing of 3D models. The program allows both hexahedral and tetrahedral meshing, however only the hexahedral mesh capability is utilised in this project. The CAD style arrangement allows flexibility for creating additional components for analysis that either bolt on to a turbomachinery component (i.e. suction inlet, volute) or complete models (i.e. if modelling sump arrangements).

Bladegen: Bladegen is a geometry creation package that is dedicated to the design of turbomachinery blades and has export links for both CAD and CFD purposes. The program allows the operator to either create or re-create a blade design, view the design in 3D and export the design to other packages.

Turbogrid: Turbogrid generates a 3D computational mesh around an imported blade shape. Templates are provided, catering for most blade shapes, which assist in the creation of a quality computational grid (see Section 5.4). The operator can simply specify the size of grid that is desired and the program will generate a 3D volumetric mesh for that blade passage.

TASCflow: The arrangement of the analysis, the solution and post processing of the results are all performed within TASCflow. Therefore all of the actual analysis

preparation, implementation and analysing of results is performed within the TASCflow program.

5.2.1 Grid Generation

Grid generation is a large topic that cannot be covered in detail as part of this thesis. However the main options available for grid generation will be discussed with brief consideration of the merits and drawbacks of each. For further information on this topic, reference should be made to either an online summary on grid methods (104) or published literature (105).

Methods of grid generation are usually arranged into three main categories: structured, unstructured and multi-block.

Structured Grid: Structured grids are usually created using hexahedral elements (formed with eight nodes and six quadrilateral faces) or blocks and are built with a repeating geometric and topological structure. The block can be shaped to the modelled domain through stretching and twisting of the block. It is therefore important to gain an understanding of the quality of the grid and this is achieved by monitoring the aspect ratio (amount of stretching) and skew angle (amount of twisting) of the grid elements in the model. Advantages for using structured grid include, a high degree of user control, the fact that hexahedral support a high degree of skewness and stretching before a solution is significantly affected and the solvers generally require the lowest amount of memory for a given mesh size. The main drawback of structured grids is the time and expertise required to create a satisfactory grid for an entire model; in general the time to generate a grid is measured in days.

Unstructured Grid: Unstructured grids are usually created using tetrahedral elements arranged in an arbitrary fashion. This method has the ability to be automated to a large extent, making the general time scale for this task to be often measured in minutes and hours. The main advantage of unstructured grid is the ability to generate grids in a short period of time with little user input. This allows the method to be used by

inexperienced users and also allows very large detailed problems to be tackled. Some drawbacks of unstructured grid methods include a lack of user control, a reliance on quality CAD data for ease of meshing and an increased requirement for memory by the solver.

It should be noted that one source of error in CFD simulations, related to the choice of structured or unstructured grid, is numerical diffusion (also termed false diffusion). Numerical diffusion arises from truncation errors that are a consequence of representing the fluid flow equations in the discrete form and is minimised when the flow is aligned with the mesh. Structured mesh can be aligned with the grid, whereas unstructured grid cannot. Therefore when structured grid elements are aligned with the flow, it is possible to gain a better quality solution with fewer cells. The amount of numerical diffusion is inversely related to the resolution of the mesh. However, second order discretisation scheme can assist in reducing the effect of numerical diffusion on the solution.

Multi-Block: Multi-block is simply a collection of grids, of structured or unstructured form, that fill the domain to be modelled. Some multi-block grids are a hybrid of both structured and unstructured grids in an attempt to gain the advantage of both grid methodologies.

CFX-TASCflow can analyse a multi-block arrangement, but the solver can only analyse a structured grid. As the project considered involves reducing the pressure pulsation using a number of parameters, care must be taken at the initial stages to ensure that the computational grid is appropriate to the project task, namely:

- Grid interfaces must be defined with care to allow interchangeability.
- A measure of the quality of the grid must be obtained.
- Nodes should be distributed with care in critical areas of the grid.
- Grid size and distribution between two variant components should be as similar as possible.
- The effect on other parts of the model should be minimised when interchanging components.

In order to generate a numerical model that can analyse such situations with a high degree of consistency and minimal grid modification, significant time had to be spent preparing the basic grid boundaries. The computational model was split into the main pump component parts, i.e. impeller, volute, etc. The modelling of each of these parts will be discussed in detail in section 5.4.

5.3 Theoretical Background

5.3.1 Computational Fluid Dynamics Theory Introduction

The following only provides the briefest of introductions to the basics of CFD theory. It is recommended that for full derivations of the equations and a more detailed introduction to the theory other published works should be consulted, for example, Andersons book (46), "Computational Fluid Dynamics: The Basics with Applications". Additionally, TASCflow theory documentation primer (106) contains detailed information regarding the theory behind the programs numerous features.

5.3.1.1 Governing Equations

In general, all of CFD is based on three fundamental governing principles of fluid dynamics, namely,

Continuity	Mass is conserved
Momentum	Newton's second law (F=ma)
Energy	Energy is conserved

The equations relating to these fundamental laws of physics can be derived through a number of methods. The forms of the equations shown below are as derived from an infinitesimally small element fixed in space and are in a conservation form (i.e. they can be directly obtained from a flow model).

Continuity Equation

$$\frac{\partial \rho}{\partial t} + \nabla \bullet (\rho \vec{V}) = 0 \qquad \text{Equation 5. 1}$$

where ρ is the density

t is the time

∇ is the vector operator and can be described in Cartesian co-ordinates as

$$\nabla = i\frac{\partial}{\partial x} + j\frac{\partial}{\partial y} + k\frac{\partial}{\partial z}$$

$\vec{V}$ is the flow velocity vector.

$\nabla \bullet (\vec{V})$ is termed the convective derivative and is defined as the time rate of change of the volume of a moving fluid element per unit volume.

Momentum Equations

$$\frac{\partial(\rho u)}{\partial t} + \nabla \bullet (\rho u \vec{V}) = -\frac{\partial p}{\partial x} + \underbrace{\frac{\partial \tau_{xx}}{\partial x} + \frac{\partial \tau_{yx}}{\partial y} + \frac{\partial \tau_{zx}}{\partial z}} + f_x \qquad \text{Equation 5. 2}$$

I II III IV V

$$\frac{\partial(\rho v)}{\partial t} + \nabla \bullet (\rho v \vec{V}) = -\frac{\partial p}{\partial y} + \frac{\partial \tau_{xy}}{\partial x} + \frac{\partial \tau_{yy}}{\partial y} + \frac{\partial \tau_{zy}}{\partial z} + f_y \qquad \text{Equation 5. 3}$$

$$\frac{\partial(\rho w)}{\partial t} + \nabla \bullet (\rho w \vec{V}) = -\frac{\partial p}{\partial z} + \frac{\partial \tau_{xz}}{\partial x} + \frac{\partial \tau_{yz}}{\partial y} + \frac{\partial \tau_{zz}}{\partial z} + f_z \qquad \text{Equation 5. 4}$$

where u is the vector component of velocity in the x direction

v is the vector component of velocity in the y direction

w is the vector component of velocity in the z direction

τ_{xx}, τ_{yy} and τ_{zz} are normal stresses

τ_{yx}, τ_{zx}, τ_{xy}, τ_{zy}, τ_{xz} and τ_{yz} are shear stresses

f_x, f_y and f_z are body force acting in the respective directions

The left hand side of the equations contain two terms, the first being the time rate of change (I) and the second the convective term (II). Convection is a physical process in which some property is transported by the ordered motion of the flow. On the right hand side are the pressure gradient term (III) and the diffusion terms (IV); diffusion is a physical process in which the random motion of the molecules of the gas transports some property. Diffusion is related to the stress tensor and to the viscosity of the gas. The final term (V) is the volume force.

The nine normal and shear stress components are termed the stress tensor, where each component in the stress tensor is the secondary derivative of a velocity term. For Newtonian fluids where the stress is proportional to the time rate of strain, the following relations can be used for the normal and shear stresses

$$\tau_{xx} = \lambda(\nabla \bullet \vec{V}) + 2\mu \frac{\partial u}{\partial x}$$

$$\tau_{yy} = \lambda(\nabla \bullet \vec{V}) + 2\mu \frac{\partial v}{\partial y}$$

$$\tau_{zz} = \lambda(\nabla \bullet \vec{V}) + 2\mu \frac{\partial w}{\partial z}$$

$$\tau_{xy} = \tau_{yx} = \mu\left[\frac{\partial v}{dx} + \frac{\partial u}{\partial y}\right]$$

$$\tau_{xz} = \tau_{zx} = \mu\left[\frac{\partial w}{dx} + \frac{\partial u}{\partial z}\right]$$

$$\tau_{yz} = \tau_{zy} = \mu\left[\frac{\partial w}{dy} + \frac{\partial v}{\partial z}\right]$$

Equation 5. 5

where μ is the molecular viscosity and

λ is the second viscosity coefficient given by

$$\lambda = -\frac{2}{3}\mu$$ Equation 5. 6

Energy Equation

$$\underbrace{\frac{\partial}{\partial t}\left[\rho\left(e+\frac{V^2}{2}\right)\right]}_{\text{I}}+\underbrace{\nabla\bullet\left[\rho\left(e+\frac{V^2}{2}\right)\vec{V}\right]}_{\text{II}}=\underbrace{\rho\dot{q}+\frac{\partial}{\partial x}\left(k\frac{\partial T}{\partial x}\right)+\frac{\partial}{\partial y}\left(k\frac{\partial T}{\partial y}\right)+\frac{\partial}{\partial z}\left(k\frac{\partial T}{\partial z}\right)}_{\text{III}}$$

$$\underbrace{-\frac{\partial(up)}{\partial x}-\frac{\partial(vp)}{\partial y}-\frac{\partial(wp)}{\partial z}+\frac{\partial(u\tau_{xx})}{\partial x}}_{\text{IV}}+\underbrace{\frac{\partial(u\tau_{yx})}{\partial y}+\frac{\partial(u\tau_{zx})}{\partial z}+\frac{\partial(v\tau_{xy})}{\partial x}+\frac{\partial(v\tau_{yy})}{\partial y}}_{\text{V}}$$

$$\underbrace{+\frac{\partial(v\tau_{zy})}{\partial z}+\frac{\partial(w\tau_{xz})}{\partial x}+\frac{\partial(w\tau_{yz})}{\partial y}+\frac{\partial(w\tau_{zz})}{\partial z}}_{\text{V (cont.)}}+\underbrace{\rho f\bullet\vec{V}}_{\text{VI}}$$

Equation 5. 7

where $\left(e+\frac{V^2}{2}\right)$ is the total energy (e being the internal energy and $\frac{V^2}{2}$ the kinetic energy

$\dot{q}$ is the rate of volumetric heat addition per unit mass

k is the thermal conductivity

T is the temperature

and equation 5.5 applies to equation 5.7 in addition to 5.2, 5.3 and 5.4.

The first and second terms of the energy equation are the similar to those in the momentum equations in that they are the time rate of change (I) and the convective terms (II). On the right hand side of the equation the third term is the heat flux and consists of the volumetric heating of the element and conduction (III). On the right hand side the fourth terms in the equation (IV) are further convective terms due to the action of body forces on the element. The fifth terms are diffusion terms (V) and are related to the work done on the element by surface forces. This term is the stress tensor and consists of both normal and shear stresses as have been discussed previously for the

momentum equations. The final term (VI) is a source term and is related to the body forces acting on the element.

The governing equations shown above include five equations for six unknowns (i.e. the three velocities, pressure, temperature and the internal energy of the fluid. The ideal gas equation (equation 5.8) is used to provide the additional equation that allows the unknowns in the equations to be solved.

$$p = R\rho T \qquad \text{Equation 5. 8}$$

where R is the real gas constant

The equations above are shown in a general form. As the current work involves incompressible fluid (water) with an absence of heat transfer, the density term does not vary with time or other variables, simplifying the equations significantly. When in their incompressible form the governing equations are often referred to as the Navier-Stokes equations.

5.3.1.2 Discretisation

Discretisation is the process whereby the governing differential equations are transformed into their discrete counterparts, which should correctly approximate the transport properties of the physical processes. The discretisation process identifies the node locations used by CFX-TASCflow to model the physical problem configuration. There are various processes that can be used to achieve this and each has its own advantages and disadvantages. CFX-TASCflow employs advection discretisation schemes called the linear profile (LPS) and the mass weighted skewed (MWS) upstream differencing scheme with physical advection correction (PAC) terms. These schemes are based on the conservative finite volume approach where care has been taken to minimise the errors normally associated with upstream differencing schemes. The numerous discretisation processed provided by CFX-TASCflow largely consist of both first and second order schemes for steady state analyses. In these the first order

schemes are generally considered to be more robust, but are sensitive to numerical diffusion, while the second order scheme is more accurate, but can be less robust and can experience oscillations in the solution. When considering transient analysis, CFX-TASCflow provides a single second order option for the discretisation process. This uses a backwards Euler finite difference scheme, that is discussed in some detail in Section 6.19 of the TASCflow Theory Documentation (106). The documentation notes that when implementing this scheme the error in the transient representation reduces quadratically as the timestep is linearly refined. It is also noted that the method is fully implicit as long as sufficient iterations are employed to resolve all non-linear terms at the new time level.

5.3.1.3 Turbulence Modelling

Turbulence modelling is actually required due to computational inadequacies rather than any requirement for additional flow information. This is because the Navier Stokes equations describe laminar and turbulent flows completely; however at realistic Reynolds numbers, the direct numerical solution (DNS) of these flows would require computation power far in excess of that available at present. To reduce the complexity of the analysis the instantaneous Navier Stokes equations are time averaged, thus describing a mean flow without turbulent fluctuations. The averaging process results in new, unknown turbulence quantities that include additional terms representing the transfer of momentum due to the turbulent fluctuations (these have been previously termed the stress tensor in Section 5.2.1.1). Thus assumptions have to be made relating these unknown quantities to known values in order to obtain a "closed" set of equations, i.e. a sufficient number of equations to solve for all unknowns. Turbulence models are generally classed by the level at which they provide "closure" of the equations (i.e. second moment closure) and the number of equations required to obtain closure (i.e. two-equation models). There are many sources available that discuss in detail the various options available in modelling turbulence, a set of lecture notes by Celik entitled "Introductory Turbulence Modelling" (107), have been found to be helpful by the author. Hwang and Jaw have also published a detailed discussion relating to the general development of turbulence models (108).

As with earlier sections only a brief overview of some of the more common (and appropriate to the application) turbulence models will be discussed briefly with some advantages and disadvantages of each being considered. This work will focus on the two main types of turbulence model that are commonly available in commercial CFD codes, namely eddy-viscosity (EVM) or Reynolds stress models (RSM).

Eddy Viscosity Models

Eddy-Viscosity models use the Boussinesq viscosity concept, which assumes that the turbulent stresses are equal to the product of an eddy-viscosity and a mean strain rate. Two-equation models have been developed to represent the turbulent fluxes through two transport equations for turbulent length and time scales.

The most widely used two-equation model is the k-ε model, where k is the turbulent kinetic energy and ε is the turbulent dissipation rate of k, that is provided in most general-purpose commercial CFD codes. CFX-TASCflow utilises the model developed by Launder and Spalding (109), which solves modelled transport equations for k and ε and then calculates the turbulent viscosity. The k- ε model has proven to be numerically robust and stable, with relatively small computational complexity and expense. It also displays a good performance over a wider range of flows than many of the other models. There are particular flow patterns where the k-epsilon model fares relatively poorly, these include flows with sudden changes in mean strain rate, curved surfaces, secondary motions, rotating and stratified fluids, flows with separation, and three dimensional flows (107)

One specific situation where the k-ε turbulence model performs poorly is when predicting the flow separation from a smooth surface. This is a low turbulence Reynolds number flow that that involves complex damping functions when using the k-ε model. In such situations, a near wall grid resolution of $y+<0.2$ are required and this requirement often reduces numerical stability. In CFX- TASCflow, computing y+ is dependent on the wall function selected (wall functions are discussed later in this section), but in general is based on the distance from the first grid point (at the wall) to the second grid point (y_2-y_1) and is shown in equation 5.9

$$y^+ = \frac{(y_2 - y_1)u^*}{\nu}$$ Equation 5. 9

where u* is an alternative velocity scale used in place of u+ (the near wall tangential velocity) in the logarithmic region of the near wall area and ν is the kinematic viscosity of the fluid.

A second two-equation turbulence model developed to improve the limitations imposed by the derivation of the dissipation rate in the k-ε was the k-ω model. The k-ω model develops a transport equation for the turbulent frequency, ω, as opposed to a transport equation for the dissipation rate, ε. The k-ω model is more accurate when near-wall regions have to be resolved in detail. One of the main drawbacks is that, although an improvement on the k-ε model, the grid resolution at near-wall regions has to satisfy the requirement of y+<2. The initial k-ω was developed by Wilcox (110) and was known to have strong sensitivity to free stream conditions. It also fails to correctly predict the onset and amount of flow separation over smooth surfaces as neither it nor the k-ε model account for the transport of the turbulent shear stress.

Reynolds Stress Models

A Shear Stress Model (SSM) was developed to avoid the over prediction of the eddy-viscosity behaviour experienced by k-ε and the Wilcox k-ω models. This model involves adding a limiter to the formulation of the eddy-viscosity. To avoid the sensitivity to free stream conditions a blending function can be applied to smooth the transition between the k-ω, near-wall turbulence model and the k-ε model. CFX published a technical brief in 2003 explaining the benefits of the SSM model (111)

When the turbulent transport or non-equilibrium effects are important the Boussinesq assumptions that provides the basis for k-ε and k-ω models are no longer valid. Reynolds Stress (or Second Moment Closure – SMC) models are based on transport equations derived for the individual stress components. This results in six partial differential equations that contain unknown correlations between fluctuating velocity

components and pressure (for incompressible flows). The flexibility provided by this approach is coupled with high computational requirements due to the mathematical complexity, which generally rules out their use in complex flows. The model also leads to a reduced numerical stability.

Algebraic Stress Models (ASM) were proposed and assume that the convection minus the diffusion term in the Reynolds stress model is proportional to the convection minus the diffusion term in the turbulent kinetic energy equation. When the anisotropy tensor is assumed constant along the streamline, an implicit algebraic equation is gained. This potentially removes some of the known deficiencies of the eddy-viscosity assumption and extends the range of applicability of the standard 2-equation models. The implicit equation requires an iterative process to solve and is gives rise to convergence difficulties. Current research is ongoing into explicit models; however, no clear improvement has yet been gained (103).

Since no turbulence model is universally applicable for all fluid flows, research continues and the number of turbulence models available is steadily increasing.

Wall Functions

In addition to the choice of the turbulence model, a decision is required concerning the modelling of the turbulent equations close to bounding walls. This determines the accuracy of the wall shear stress and wall heat transfer calculations and has influence on the development of boundary layers and onset of separation. Within many turbomachinery components the free stream turbulence is high, such that the boundary layer is usually transitional or turbulent (112). When modelling, this is often simplified with the flow in the boundary layer being considered fully turbulent (e.g. (113)) and for high Reynolds number applications a wall function is commonly used. The wall function approach employs empirical formulas to provide near-wall boundary conditions for the mean flow and turbulence transport equations. These formulas connect the wall conditions to the near-wall grid node that is assumed to lie within the fully turbulent flow region. This saves computer resource and avoids the need for near wall viscous effects to be present in the turbulence model.

Two main wall functions are available in TASCflow, namely scalable and standard. These wall functions relate the near wall tangential velocity to the wall shear stress by a logarithmic relation. Standard wall functions are limited in that predictions depend on the location of the grid point nearest to the wall and are thus sensitive to near-wall meshing. Scalable wall functions avoid this inconsistency as they allow the user to perform consistent grid refinement independent of the Reynolds number. The basic idea behind he scalable wall function is that it is assumed that the surface coincides with the viscous sub-layer, which is defined to be at a particular Y+ values. This is the intersection between the logarithmic and linear near wall profile. The computer y+ is not allowed to fall below the limiting value. Therefore, all grid points are outside the viscous sub-layer and all fine grid inconsistencies are avoided.

5.3.2 Taguchi Theory Introduction

There are numerous published texts that deal with the Taguchi method's principles either in part or in their entirety. The current work refers to two main texts, "A Primer on the Taguchi Method" by Roy (114) and "Understanding Industrial Designed Experiments" by Schmit and Launsby (115), either of which would provide further detail to that presented here. Both texts provide information on set up of experiments/analyses in a form suited to the Taguchi array, but each has different focus on the investigation of the resulting data. The former text provides excellent information on the ranking of variables to set parameters, while the latter provides helpful information on the generation of predictive equations to determine relationships between the variables and the chosen parameter. This short introduction to the Taguchi Method is split into three sections, the first discusses the selection of a Taguchi array suited to the problem, the second details the calculations required to rank the relative importance of the chosen variables and the final section discusses the method used to generate predictions of both pressure pulsation and performance for arrangements not analysed.

5.3.2.1 Taguchi Analysis Preparation

The historical background to the creation of the Taguchi process is that it was borne out of a desire to design a quality product rather than inspecting a product to determine if it was a quality product. This resulted in Dr Taguchi creating an approach that followed the experimental design process, from laying out experiments through to analysis of the results. Although the process was created for experimental testing its principles are still valid for numerical analysis. The Taguchi methodology assumes that multiple results are available for each test, allowing statistical deviations to be calculated but that aspect is not relevant here.

Taguchi constructed a set of orthogonal arrays to lay out experiments. The terminology used in these arrays is as follows:

> Factor: An item that is to be varied during the simulations
> Level: The number of times a factor is to be varied during the simulations
> Trial Number: The number of simulations that are required to be run to complete the analysis.

For the current work, the geometric variables are the factors and the geometric arrangements to be analysed are the trials. So the cutwater gap is a factor and as three different sizes of cutwater gap are to be investigated, it is a three level factor. In total, the simulations conducted in this work are to investigate four, three level factors (i.e. cutwater gap, snubber gap, sidewall clearance and vane arrangement). There are a large number of Taguchi arrays and the selection of the array is dependent on the number of factors and the levels of the factors to be analysed. The letter L and a subscript number identify the arrays. For instance a common array is the L_8 array (shown in Table 5.1) that can be used to design experiments involving up to seven level two factors. Table 5.1 includes seven factors (A through to G), each of which has two levels (-1 and 1). The eight trials shown, indicate what factor level should be used in that particular trial. Processing through the eight trials would provide information on all combinations of levels. Performing the same investigation using a factorial experiment would involve 2^7 or 128 analyses. A listing of the more common Taguchi orthogonal

arrays is available in the appendices of either of the books listed above; additionally a number of online sources, such as "A Library of Orthogonal Arrays" by Sloane (116) also provide a listing of the arrays. Selecting the array applicable for a specific investigation is determined by the amount of factors and their number of levels. Roy (114) in his appendix provides a table of common orthogonal arrays and their related number of factors and levels; this is reproduced in Table 5.2. This indicates that for the current requirement of four factors having three levels each, the L_9 array is appropriate. The standard Taguchi L_9 array is shown in Table 5.3. Table 5.4 shows the same table but with the current project specific values inserted. Rather than utilise the term "trials" to relate to the varying analyses, the author has chosen to use the term "arrangements", as each row on the table denotes the geometric arrangement to be used in each numerical analysis. Note that to produce a full factorial parameter study of the geometric variables, the number of cases would be 81 (4 factors with 3 levels = 3^4 arrangements) multipled by 3 flow rates, i.e. a total of 243 possible designs. The Taguchi approach reduces this to 9x3, i.e. 27 cases.

It is noted that Schmidt and Launsby (115) provide similar information but with some reservations. They state that due to confounding problems with interactions, the L_9 is not always recommended, and offer the L18 design as an alternative. Confounding means that a factor effect is mixed with an interaction effect preventing them from being evaluated separately. This may be avoided by leaving some columns out of an array (not assigning factors too them). Thus due to the confounding issue Schmidt and Launsby recommend that the L_9 array is only used for two level three factors when evaluating interactions, i.e. leaving two columns blank for interactive effects. However it also noted that the L_9 array is recommended for four factors with three levels when the array is used for screening. Essentially screening is identifying the factors that have a vital effect from those that have an insignificant effect. Thus the choice is to either conduct the analysis using the full factorial array L_{18}, or conduct a screening analysis using the L_9 array. As the current work effectively involves analysing three separate arrays (one for each flow rate, 1.00Qn, 0.50Qn and 0.25Qn), doubling the amount of transient analyses from twenty seven for the L_9 array to fifty four for the L_{18} array is not

practical in terms of time constraints or physical resources. Thus it is decided that an L_9 screening array is to be used to set up the analysis.

The use of an L_9 screening array introduces the added complication that the array will not include any detail concerning the interaction between significant factors. Any additional work depends on the number of significant factors found, but the following work assumes (with some hindsight) that two of the four initial factors are shown to be of primary importance. Rather than constructing a completely new array and conducting additional analyses it was considered that a limited two factor with two level L_4 array could be used to provide additional information for the significant factors. The L_4 array would be as set up in Table 5.5, and would consist of arrangements previously analysed as part of the large L_9 array. The particular arrangements used to form the smaller L_4 array would depend on the geometric arrangements that would be of interest.

In summary, the plan for the analysis of the results was to rank the geometric variables in terms of relative importance to a chosen parameter and then use the data to predict the chosen parameter for an alternate geometric arrangement. It was envisioned that this would be achieved using a single array, but due to peculiarities with particular arrays secondary reduced arrays must be employed to gain the predictive capability for a chosen parameter.

Before analysis techniques can be discussed, a quality characteristic must be determined. The quality characteristic is a measured result that can be obtained from the experiential/numerical results. The aim of this project is to study (and reduce) pressure pulsations; therefore pressure pulsations can be used as the quality characteristic. As the pressure pulsation is unlikely to be consistent at all points in the pump, several sets of data must be selected from various pump locations. The locations where data is obtained will be discussed in a later chapter. As the pump performance is also being considered, the pump generated head can also be used as a quality characteristic. For each set of data the analysis techniques outlined below must be carried out in order to determine the effect of all geometrical factors at each location in the pump. This must be completed for all three flows rates independently to determine

how the change in flow rate affects the variation of the chosen quality characteristic with the geometric parameters. Once that quality characteristic is selected, the criteria of evaluation can be chosen,

- The bigger the better
- The smaller the better
- Nominal is the best

Generally, if the quality characteristic were pressure pulsation, then the criteria of evaluation would be the smaller the better. However, if the generated head were the quality characteristic them the criteria of evaluation would be the larger the better.

5.3.2.2 Analysis of the L_9 Array

The analysis conducted on the L_9 array is essentially an analysis of variance (ANOVA). When used in conjunction with experimental data the analysis of variance generally include an error term that is not appropriate for the numerical simulations investigated in this current work. Full details of the ANOVA process can be found in Ranjit Roy (115), and only a brief summary is presented here.

Relative Performance of Geometric Variables

Ranking the relative importance of the geometric variables selected for this project is, as noted above, effectively a screening operation (in Taguchi terms). Thus the larger L_9 array, as shown in Table 5.4, can be used for this analysis. The definitions presented below use the notation from Table 5.3 along with a set of sample data and detail the calculations required to rank the importance of the geometric variables.

Number of repetitions (rp): Number of times the experiments/ analyses have been repeated. In this case rp=1
Number of arrangements/trials (n): Number of trials in the Taguchi array. For an L_9 array n=9.

Number of level factor arrangements/trials (n_{pj}): Number of trials conducted for a particular factor level, where P is the factor (A to D) and j is the level (-1, 0, 1)

Degrees of freedom (f): The degrees of freedom (DOF) is a measure of the amount of information that can be uniquely determined from a given set of data. The total degrees of freedom (f_T) is defined by the following equation

$$f_T = (n \times r) - 1$$

Factor Degrees of Freedom (f_P): Degrees of freedom related to a particular factor (where subscript P denotes the factor), i.e. for factor A

$$f_A = Number\_of\_levels\_of\_A - 1$$

Total of Results (R_{TOT}): $$R_{TOT} = \sum_{k=1}^{n} Z_k$$ Equation 5.10

Correction Factor (CF): $$CF = \frac{R_{TOT}^{\ 2}}{n}$$ Equation 5.11

Total Variation (S_{TOT}): $$S_{TOT} = \sum_{j=1}^{n} (Z_j)^2 - CF$$ Equation 5.12

Factor Totals (P_j): Summation of the results relating to a particular factor level, where P is the factor (A to D) and j is its level (-1 , 0, 1).

Factor Total Variance (S_P): Summation of the factor totals for each level divided by the number for arrangements for each level minus the correction factor, i.e. for factor A

$$S_A = \frac{A_{-1}^2}{n_{A-1}} + \frac{A_0^2}{n_{A0}} + \frac{A_1^2}{n_{A1}} - CF$$ Equation 5.13

Variance (V_P): The factor total variance divided by the degrees of freedom for the particular factor, i.e. for factor A

$$V_A = \frac{S_A}{f_A}$$ Equation 5.14

Percentage Contribution per factor (P_P): The percentage contribution is the ratio of the factor total the total variation, expressed in percent, i.e. for factor A

$$P_A = \frac{S_A \times 100}{S_{TOT}}$$ Equation 5.15

The calculation of the variance and the percentage contribution per factor effectively provides the same information, however the percentage contribution presents it in a clearer manner. Once the percentage contribution is determined for each factor, the significant factors can be determined.

5.3.2.3 Analysis of the L_4 Array(s)

The L_4 arrays, as used in this project, are a limited data set formed from the large L_9 array. The reduced array allows a number of different operations to be carried out that allows some understanding of the interactions to be formed in addition to predictive equations. Table 5.5 provides the standard L_4 Taguchi array.

Effect and Half Effects

The effect and half effect values are terms that can be used to gain an understanding of the importance the geometric variables. These terms are calculated from the response averages, which are defined as the average of the results for a particular factor level. These values are calculated not only for the factors but also for the interactive effects. A variation of Table 5.5 has been produced including the interactive effects and is presented in Table 5.6. The interactive column is calculated from multiplication of the two interacting components. Using Table 5.5, this response average can be defined as

$$P_j = \sum \frac{Z_j}{k_j} \qquad \text{Equation 5.16}$$

where P is a factor (A to D), Z are items of data at a particular level, j is the level (-1, 0, 1) and k_j is the total number of data items for that level.

These response averages are calculated for all factors and for all factor levels. Thus effect for a factor is simply the difference between the response average at factor level 1 and the response average at factor level –1, i.e.

$$Effect = P_1 - P_{-1} \qquad \text{Equation 5.17}$$

The half effect is simply the effect divided by 2.

The interactive effect of two factors can be determined by plotting factor A values against the half effect, for factor B_{-1} and B_{+1}. If the slopes of the two graphs are approximately parallel then there is no interactive effect, however if the slopes are significantly different then there is likely to be an interactive effect between the two factors.

Prediction Equations

For a simple L_4 array, Schmidt and Launsby provide the general form of the prediction equation as

$$y_P = y_{GM} + \left(\frac{\Delta_A}{2}\right) \times A + \left(\frac{\Delta_B}{2}\right) \times B + \left(\frac{\Delta_{AB}}{2}\right) \times AB \qquad \text{Equation 5.18}$$

where,

y_P = the predicted response

y_{GM} = the grand mean (average of all response values)

$(\Delta_A/2)$ = half effect for factor A

$(\Delta_B/2)$ = half effect for factor B

$(\Delta_{AB}/2)$ = half effect for interaction AB

A, B and AB vary from –1 to 1

5.4 Geometry Definition and Grid Generation

It is generally considered that one of the most important and time consuming tasks in the process of numerical simulation is the generation of a computational grid. This is due to various choices that have to be made during the modelling process, but can also be due to complexity of the geometries being modelled. For this project, where twenty seven transient analyses are to be conducted using the computational model, this is not actually the case. However, as so many analyses are to be conducted using the

computational model, extra time and care had to be spent to ensure that the numerical grid was of as high a quality as possible.

There are additional issues that complicate the modelling process. To the author's knowledge no 3D numerical simulation has attempted to model a complete pump. Blanco-Marigorta et al (39) and González et al (38) have published work involving transient simulations focused on investigating the unsteady impeller/volute interaction. Both reports only model the impeller and volute numerically and are limited to flows greater than 60% of the duty flow condition, although Blanco-Marigorta et al note that "more work has to be made (performed) for lower flow rates". Tamm et al (117) reported results of a steady state analysis of a centrifugal pump that included the impeller, volute and leakage flow passageways. The numerical results for the pump were found to not show good conformity with the experimental results. Thus Tamm concluded that in future work the whole machine should be modelled as a transient analysis, but no further work has yet been published. Therefore, this current body of work extends the boundaries of modelling beyond that published to date. The analyses conducted comprise the complete centrifugal pump consisting of the suction inlet, all impeller passages, volute and leakage flow passageways.

The computing facility available at Weir Pumps limits the total hexahedral grid size of the model to approximately one million elements. The distribution of the grid is complex due to the modelling of the complete pump and also due to the various regions of interest. For example, in order to investigate pulsations at similar locations to those examined by experimental tests in Chapter 4, the computational grid will require refinement in the volute (at the cutwater), the leakage flow path and at the impeller outlet. An initial estimate was made of 500,000 nodes in the impeller related grids (comprising impeller flow passageways and leakage flow paths) and 500,000 for the pump casing (suction inlet, volute and outlet). The method used to generate models of the pump components is described in what follows. Table 5.7 provides details of the component and total grid meshes used for the published works mentioned earlier and also those used for the current projects.

5.4.1 Impeller

The impeller to be modelled is of the double entry radial flow type; a cross section of the impeller is shown in Figure 5.2. To the author's knowledge no published literature exists that models a double entry impeller as part of a computational analysis of a centrifugal pump. At a basic level, the design is essentially two radial impellers back to back. For an inline impeller arrangement the central hub is been terminated in a bull nose instead of extending it to the impeller outlet. For the staggered arrangements the hub is extended to the outlet with the hub thickness being 4mm at the outlet.

The impeller geometry was created using CFX-Bladegen as two mirrored halves, using the maximum diameter of 366mm (Table 4.1 provides the impeller to be used in the analysis). The bull nose aspect of the inline impeller design proved difficult to capture within CFX-Bladegen, as the program is not designed to model double entry impellers and does not allow for hub profiles that terminate in the bull nose arrangement. To avoid this problem, although the true hub effectively finished at the point of symmetry, a fictitious hub was extended from the midpoint of the bull nose to the impeller outlet along the impeller line of symmetry. Therefore with only slight modifications to the meridional hub profile a satisfactory model was produced for the inline impeller. The staggered impellers could be used without any modification as the meridional flow paths for either side of the impeller do not connect.

CFX-Turbogrid was used to generate grid around the two blades. The grid on both sides of the impellers was created identical. For the inline impeller, care was taken to ensure that the grid was radial at the position of the bull nose. This is essential to aid the creation of an interface between the impellers in CFX-TASCflow; however it also limited the quality of the grid. With an initial impeller grid estimate of around 500,000 nodes, it is immediately apparent that splitting this grid between twelve impeller passageways and the leakage flow will result in impeller passageway grids of less than ideal size. Denton and Dawes (45) have observed that 300,000 nodes are required for adequate representation of viscous effects with shock waves and tip leakage, but also note that useful comparisons can be made with 100,000 nodes. The authors own experience and also Miner's published work (62), indicates that relatively coarse

impeller models (20,000 – 40,000 nodes) can be used to predict performance with some accuracy. It is interesting to note that Denton (118) has also observed that the 22,000 grid points per blade row is sufficient for a calculation with approximate allowance for viscous effects. Thus a number of impeller models were analysed for the six grid sizes listed in Table 5.8. Some effort has been made to focus on the lesser grid sizes, while including grids as large as 85,000 nodes. A decision was made to analyse 6 impeller passages within a half pump volute (modelling of the volute is described in section 5.4.2) as the impeller interaction with the volute is extremely important in this project. It is expected that this interaction will cause larger differences to be evident between the grids than is usually displayed in grid independence comparisons due to the increased complexity of the flow patterns. The analyses were run at the duty flow condition with the maximum residual convergence criteria being set to 1e-4 (max).

A comparison of the head generated across the impeller against the various grid sizes is provided in Figure 5.3. This indicates that as the grid size increases there is also a slight increase in the impeller generated head with head starting to plateau at the larger grid sizes. It is important to note that the overall variation in head from the lowest grid size to the largest is small, approximately 1.2%. Examining the pressure, meridional and tangential velocities at various locations in the impeller allows a comparison of the various grids to be performed. These variables are examined at three locations, which are defined below and shown in Figure 5.4

1) an axial line in the middle of the passageway at a radial position equal to the leading edge of the impeller
2) an axial line in the middle of the passageway but near the outlet boundary of the impeller
3) a circumferential line at the outlet of an impeller passageway covering a single blade between two mid passage positions at a mid-axial position between hub and shroud.

Position 1 (towards inlet)**:** Figure 5.5 shows the pressure variation at position 1 (towards inlet). This indicates that the pressure across this region is very similar

between the hub and shroud at all grid sizes. The meridional velocity variation is shown in Figure 5.6 and again indicates that the grid size does not have a significant influence on the meridional velocity at this location.

Position 2 (towards outlet): Figure 5.7 shows the pressure variation at this location for the differing grid sizes. Each of the grid sizes predicts the shape of the pressure variation, but as the grid size increases the overall pressure level decreases slightly. The meridional velocity variation with the grid size is shown in Figure 5.8. Again each of the grids produce similar patterns of velocity variation. It can be observed that the lowest grid size (Grid A [12.6k]) predicts the trough in the velocity at a different axial position than the other grids. Larger grid sizes produce a slightly lower trough at the mid axial position and a higher meridional velocity at the hub and shroud positions.

Position 3 (outlet): The graph of the pressure variation at around the circumferential outlet of an impeller passageway, Figure 5.9, identifies that the shape of the variation is predicted consistently by all grids. There are locations where specific grids differ from the general trend shown by the other analyses, however this tends to be a local effect and does not show any trends that are grid specific. It is notable that the largest grid (Grid E [86.5k]) predicts slightly lower pressures at the mid impeller passage location (0 and 60 degree locations). This agrees with the other results identified for position 2 (Figure 5.7 that is plotted using the same scale), but provides the information in the wider context of the variation in pressure at the impeller outlet rather than at an individual location. The meridional velocity (Figure 5.10) shows the largest discrepancies between the various grids, although again, all grids identify the same general shape of variation of the parameter across the region monitored. The largest grid (Grid E, [86k]) predicts a lower meridional velocity towards the mid passageway location, which is not identified as clearly by any of the lesser grids.

Following the above exercise the grid size selected per impeller passageway for this project was Grid B consisting of 22,200 nodes. This would perhaps appear to be a rather coarse model and it is recognised that this final choice of grid size is influenced

significantly by the limited facilities at Weir Pumps Limited. However the grid independence check has confirmed that at the 22,200 mesh size the impeller model can

- correctly predict the generated head to about 1%
- correctly predict the shape of the pressure variation both circumferentially and axially in the impeller at both inlet and outlet locations.
- predict the pressure level over the majority of the impeller to a satisfactorily degree
- correctly predict the shape of the meridional velocity variation both circumferentially and axially in the impeller at both inlet and outlet locations.

Ultimately it is considered that to gain a significant improvement in the quality of the results via the grid size (in particular the meridional velocity), the grid would need to be double or triple the selected size, which is not feasible for this project. The total mesh size for all twelve impeller passageways is 227,136 hexahedral elements (265,860 nodes). Of course the main purpose of the project is to study pressure pulsations and performance characteristics and these are relatively insensitive to increases in grid size above 22,200 nodes per impeller passageway. A diagram of a single impeller passageway containing the 22,200 nodes is shown in Figure 5.11

Three main impeller grid models were created, one for each of the impeller vane arrangements. These grids contained twelve impeller passageways, six for either side of the impeller. Each model was slightly different, with modifications as detailed below:

- Inline arrangement (Figure 5.12): includes an interface joining the two side of the impeller together. This interface connects the surface from the outer diameter of the hub bull nose moving out radially to the impeller outlet diameter.
- 15 degree stagger arrangement (Figure 5.13): The two sides of the impeller are combined as a single model, with one side of the impeller offset from the other by a rotation of 15 degrees.

- 30 degree stagger arrangement (Figure 5.14): The two sides of the impeller are combined as a single model, with one side of the impeller offset from the other by a rotation of 30 degrees.

Each of these three impeller model arrangements also required three different versions. These versions model the three different impeller diameters for each of the impeller arrangements that allow the three cutwater gaps to be investigated. CFX-Bladegen provides an option termed "Leading Edge/Trailing Edge Cut-Off", allowing the user to introduce a cut at either the leading edge or trailing edge of the blade. This was used to "cut" the impeller diameters to the two smaller sizes, i.e. 358.5mm and 352mm to provide 6.00% and 7.95% cutwater gaps respectively. These new CFX-Bladegen models were meshed using an identical Turbogrid grid configuration file as used for the initial three models. This ensured that the grid was as similar as possible across all models. The models were then assembled as detailed above. It should be noted that while the blades were reduced in diameter the outer shrouds were maintained at the full (366mm) diameter in order to maintain the snubber gap diameter. One small addition was required for the reduced diameter staggered impeller arrangements. As the blades were cut back this also meant that the central hub would also be cut back to the reduced diameter. Thus, two small annular rings, one for each impeller diameter, were modelled. These rings were the thickness of the central hub and extended from the impeller outer diameter to the same diameter as the impeller/volute interface. Figure 5.15 shows a cross section of the ring. The outer surface of the ring (A) became part of the impeller/volute interface, and the side surfaces (B and C) were connected to their respective impeller grids.

Therefore, nine different double entry impeller configurations were modelled in order to provide the three different cutwater gaps and three different vane arrangements.

5.4.2 Volute

The trapezoidal volute design and grid was generated using CFX-Build. The modelling task to create a single continuous grid for the entire volute is extremely complex, especially at the splitter and cutwater regions. This was simplified by splitting the volute into two sections as is shown in Figure 5.16. The first section, volute 'A', contains the interface between the impeller and the volute and the connection between the leakage passage and the volute. The axial grid distribution in the impeller was replicated in the volute to aid the computation of flow across the interface. The second section, volute 'B', contains the flow along the back of the splitter to the outlet and from the cutwater to the outlet.

Even with the split model, the generation of the volute proved complex. Unfortunately the diameter given for the oversized impeller was the same as that of the diameter of the volute cutwater. Sketches of the experimental test rig illustrated that the cutwater diameter had been increased to accommodate the oversized impeller. Discussions were held with the test engineer to understand the process used to enlarge the diameter. Figure 5.17 shows a typical modification to the cutwater as described by the test engineer. Unfortunately, there is no actual record of the modification. The computational model was modified using the procedure shown. Considerable care was taken to reproduce as accurately as possible the geometrical modification.

A number of general grid problems were experienced during the generation of the volute grid. It was noticed that the surface creation tool created a ripple effect at the cutwater and splitter areas and these caused problems when meshing the area. Additional intermediate curves had to be included in order to produce a smooth surface for meshing. Other areas of the grid, also in the region of the cutwater and splitter, were found to have highly skewed elements and negative volumes. Some regions of highly skewed grid were expected due to the geometry and the design of the grid had aimed to focus this poor grid away from regions of complex flow. It was observed that the grid elements containing negative volumes actually appeared internal to solids that

externally showed no fault. Where such effects were observed the solid was deleted and recreated, removing the problem.

Once the volute shape had been modelled using 3D solids the model could be meshed. Grid distributions were specified that concentrated the grid in regions of importance. Two main regions that are of critical importance are at the cutwater and splitter regions, Figure 5.18 provides some detail of the grid at the splitter region. Care was also taken where the volute was to interface with the impeller and leakage grids. As the impeller interface was of prime importance the grid on the volute side of the interface was modelled with the same number and distribution of elements as the impeller flow passage in the axial direction. Figure 5.19 provides a picture of the grid distribution on the volute side of the impeller/volute grid interface

After all these improvements, it was considered that a satisfactory model had been established. In total, the volute model contains 391,848 hexahedral elements (407,248 nodes).

5.4.3 Shroud Leakage Passages

The double entry design of the impeller only includes leakage flow on the shroud sides of the impeller. The initial leakage passage was created using the 12mm sidewall clearance arrangement using CFX-Build and was designed to incorporate the snubber diameter in such a way that it could be easily modified. This model design involved creating the model for the maximum snubber gap size. Then the grid was created in three steps allowing one, two or none of the steps to be blocked off in CFX-TASCflow. With no block off set the snubber gap was the largest (1.64%), with one step blocked off the snubber gap was the middle gap size (1.10%) and with two steps blocked off the snubber gap would be set to the smallest gap (0.27%). A similar method was employed to model the three sidewall clearances. This method of using the same grid to model different geometries reduced the time taken to model these component parts and assemble the required arrangements, as it enabled one grid to be used instead of nine. However the single grid is more expensive in terms of the amount of computational grid

used, than if each geometric option was modelled individually. Figure 5.20 illustrates the connection between the leakage flow and the impeller and volute grids.

Previous experience had highlighted that the region where the leakage flow meets the impeller inlet required careful modelling. Although the amount of grid in the clearance is restricted by the computational facility's capabilities; the grid design was improved by ensuring that grid interfaces, in the complex flow region as the fluid re-enters the impeller inlet, were all one-to-one connections. This is shown in Figure 5.21. The grid size for both mirror image leakage flow passages is 161,760 hexahedral elements (217,800 nodes).

5.4.4 Suction Inlet

The suction inlet geometry was created using CFX-Build. As this model was created after the other three components, a decision was taken to generate a coarse mesh in order to determine whether or not the full pump model could be analysed using the WPL facility. A coarse suction inlet model is acceptable for the pressure pulsation investigation as all of the areas of interest are in the latter sections of the model (between the impeller tip and discharge). Due to the complexity of generating a structured mesh based on the geometry, the suction inlet was modelled in two sections. The first comprised the section incorporating the split into two double entry passages; the second modelled the flow into the impeller eye including the suction guide vane in each suction passage. Figure 5.22 identifies the two sections to this model. The complete coarsely meshed suction inlet model was created with 89,756 hexahedral elements (99,778 nodes).

5.5 Grid Quality Investigation and Refinement

The practice of conducting an investigation into the quality of a computation grid is important and a number of measures were taken to ensure a quality grid; these are as follows:

- Using the author's 8 year CFD experience in modelling and analysing radial flow pumps to distribute the grid adequately
- Conducting a grid independence check on the impeller mesh (see section 5.4.1).
- Ensuring that the grid volume in important grid regions is within that deemed acceptable by published literature
- Ensuring that the minimum grid skew angle is at least twenty degrees. In a few cases this was not possible, but these were located in the volute in regions that contained established flow patterns.
- The grid distribution across multi-frame of reference interfaces is as similar in the axial direction as possible.
- Increasing grid density in regions of interest, i.e. volute cutwater/splitter locations.

Due to the importance of the interactions within the model a procedure was carried out whereby the computational model was built in stages, with an analysis of the model being carried out at each stage along with an assessment and refinement of the grid within the model.

5.5.1 Double Entry Impeller and Volute

An initial steady state analysis was performed, analysing the flow through both sides of the impeller into the volute for the five flow conditions tested in the experimental data, i.e. 25%, 50%, 75%, 100% and 125%. The five flow rates were performed to highlight any grid deficiencies at the lower flow conditions that would not be as obvious at the duty condition.

The analyses detailed some of the local effects at the splitter and cutwater, although the solution did not converge to a satisfactory level (maximum residual of 1e-3). The level of convergence achieved was similar for all flow conditions and had a maximum residual level of around 3e-3. On interrogating the solutions, it was discovered that the convergence problem was within an impeller passage near the cutwater. It is thought that the transient nature of the flow and the fluctuations caused by the presence of the cutwater will prevent a steady state analysis from accurately solving the flow condition. The analysis was useful in that it highlighted regions of poor grid distribution. Lower flow solutions included recirculation that crossed the outlet boundary causing TASCflow to insert walls to preserve the integrity of the boundary condition. The discharge section from the pump was extended downstream so that the outflow boundary would be beyond the recirculation region.

Due to these analyses, modifications were made to both the impeller grid and the volute grid. This involved redistributing grid to locations of importance, for instance additional grid was provided at the outer radii to assist with resolving the complex flows arising from component interaction. The improved grids were used on all further analyses.

5.5.2 Inclusion of Leakage Passageway

The leakage passageway was added to the grids modified from the previous analysis and simulations were again completed for five flow rates. The quality of the solution achieved was similar to that gained in the first analyses, however the problem region was seen to shift to regions located in the leakage section of the model. An examination of the model highlighted two problem areas, the wear ring clearance region and the region as the flow entered the impeller eye area. Grid deficiencies were identified as the cause of the poor solution as the flow entered the impeller eye and these were corrected. However, it was found that no modification to the grid could improve the solution maximum residual level in the wear ring clearance region. A similar phenomenon had been observed when performing an analysis on a multistage impeller (92), where the

problem was thought to exist due to fluctuations in the flow that couldn't be interpreted as accurately using a steady state analysis. In the multistage analysis, it was observed that the maximum residual level was found to no longer be a problem in the leakage area when run as a transient simulation. The current grid was included in the model and the maximum residual in the leakage flow path was monitored during the first transient analysis. It was noted that the maximum residual level was indeed no longer a problem in the leakage flow path during the transient analysis.

.

5.5.3 Inclusion of Suction Inlet

In the previous model the inflow boundary condition assumed a normal, evenly distributed flow. In reality, although the suction inlet would not provide ideal flow into the impeller eye, it was initially considered that the computational facility at Weir Pumps Limited (WPL) would not be adequate to build and solve a model large enough to include the suction branch. Therefore, a revised plan involved investigating the impeller inlet flow bias due to the pump suction using a computation model consisting of only the suction inlet, impeller and a coarse volute. This would allow the flow at the impeller inlet to be observed and enable the bias flow profile to be used as an inlet condition to the more complete pressure pulsation analyses. Experience in conducting transient and steady state analyses had shown, as expected, that the memory required for conducting a steady state analysis was less than that required for the transient analysis even though the model grids were identical. Thus a coarse suction model was combined with the refined grids from previous analyses to form a complete hydraulic pump model and the steady state analysis was run for the duty condition. Before embarking on the investigation into the biased flow profile at impeller inlet, the author attempted a transient analysis for the complete pump. This proved to require less memory that expected and thus could be analysed without resorting to the two stage approach initially envisaged.

This analysis solved to a convergence level comparable with that gained from the model without the suction branch. An examination of the flow at the impeller eye identified

that the flow was indeed biased in this region due to the suction inlet arrangement. Figure 5.23.

5.5.4 Grid Refinement Model

A model comprising all the refined grid components was created and steady state analyses performed at all five flow rates. As stated earlier the static pressure datum for the analysis was reduced substantially in order to investigate the effect on the pressure variation at the cutwater. This produces results with unrealistic pressure levels (i.e. negative in some cases); however as it is the pressure differential that is of prime importance, this is not considered a concern. Where a correct pressure value is required, for example in calculating the axial or radial thrust, the pressure datum can be increased to realistic levels. At the duty flow condition the maximum residual levels reached the required level of 1e-3. However at the off duty condition these maximum residual levels increase to around 3e-3. The total grid for the complete model consists of 870,500 hexahedral elements (990,686 nodes). The final, complete pump model is shown in Figure 5.24

5.6 Analysis Procedure

5.6.1 Pre-Processing

A pump was then constructed using the refined grids obtained as a result of the process described in Section 5.5. This model included the suction inlet, 12 blade passages (six passages back to back), leakage flow paths and the volute. As the analysis involves both steady state and transient arrangements, two sets of boundary conditions and performance parameters are required. The differences in the two sets of boundary conditions are noted in the appropriate sections.

Frames of Reference: As the motion of the impeller blades relative to the stationary volute is central to the investigation, the analysis must involve multiple frames of

reference. Initial arrangements included only the impeller grid component in the rotational frame of reference while all others were in the stationary frame. This proved satisfactory for the steady state analysis, but the analysis failed when a transient analysis was attempted. The solver reported a problem with certain grid interfaces and these are shown in Figure 5.25 where rotor/stator interfaces are in white and stationary interfaces are in light grey. Dark grey illustrates those components that are in the rotational domain and mid grey denotes those in the stationary domain. It was considered that a problem occurred due to two rotor/stator interfaces being perpendicular to one another. The solution to this problem was to extend the rotational frame of reference to include the leakage flow paths in addition to the impeller grids. This modified the interface arrangement to that shown in Figure 5.26, where all of the rotor/stator interfaces are now all in a single plane. In summary,

Rotational Frame of Reference: Double Entry Impeller, Leakage Flow Paths
Stationary Frame of Reference: Suction Inlet, Volute

Grid Interfaces: The grid interfaces used in the project vary depending on the geometrical arrangement being modelled and so typical interface information will be provided rather than information for each specific arrangement.

Internal Component Connection: General grid interface (GGI)
Between Two Stationary Components: General grid interface
Between Two Rotational Components: General grid interface
Between Rotational and
Stationary Components: Frozen rotor interface (Steady State Analysis)
Rotor/Stator interface (Transient Analysis)

For clarification internal component connections refers for example to the situation found in the volute model, where the component had to be split into two separate parts, Section 5.4.2.

For the selection of the interface between rotating and stationary components for the steady state analysis a choice between two interfaces had to be made. These options have been discussed in a number of places, for instance Burt, Purdom and Spence (61), and their description is summarised below.

a) Frozen Rotor Interface: This interface achieves the frame change without relative position change over time and without interfacial averaging. Local flow features are allowed to transport across the interface, thus allowing pressure non-uniformities to propagate. Appropriate use of this interface is when there is thought to be significant interaction between the components; however any result gained from the analysis is dependent on the relative position between the rotating and stationary components.

b) Stage Interface: At the stage interface the pressure field is circumferentially averaged and the circumferential variation in velocity is smoothed, but the spanwise velocity variation is retained. This averaging process prevents any wake effect from progressing across the interface. A benefit from using this interface are that it allows the operator to compute the flow through the entire pump in a single pass steady state solution, therefore the relative blade position is unimportant. The interface is appropriate when there are many blades (or no blades) and in situations where there is thought to be little or no recirculation.

The concept of backflow into the impeller is one that has been widely reported. Lorett and Gopalakrishnan (48) report a "complete flow reversal in the impeller channels as they approach the volute tongue" and results shown by Dong et al (27), reproduced here as Figure 5.27 show the flow in the volute region directed into the impeller outlet. This phenomenon most likely occurs at off-design flow rates, i.e. the reproduced plot from Dong et al is taken at just under 50% flow condition. As the current work focuses on a low flow condition it is highly likely that such flow reversal will occur at the impeller outlet. This suggests that the stage interface is unsuitable and hence a frozen rotor interface was used.

Boundary Conditions

The boundary conditions utilised for the analyses is summarised below,

Inlet: Mass Flow
Outlet: Static Pressure
Rotating Wall: Impeller internal and external surfaces.
Stationary Wall: All other boundary surfaces

The choice of boundary conditions used here is perhaps unusual, as other analyses have chosen to select a static pressure condition at the inlet and the mass flow at the outlet, effectively reversing the set of boundary conditions imposed above. The author conducted analyses using both arrangements and noted that the boundary conditions listed above were significantly more stable and converged faster than the reversed conditions. González et al report similar findings in their paper (38). Their work also reports that the latter set of boundary conditions (the reversed set) produced pressure pulsations closer to their experimental results. However, the reduction in stability seems to have limited their capability to achieve a converged solution at lower flowrates, with their minimum flow rate analysed being around 60% of the duty flow condition. As this present study is focused on investigating pulsations at flows significantly below that reported by González et al (6, 38), the decision was taken to use the boundary conditions that provided greater stability in the results. It is important to note that while this decision may reduce the accuracy of the results when compared to the experimental results, one of the main aims of this work is to provide a comparison of the pressure pulsations for different geometrical arrangements. Thus any inaccuracy introduced from this set of boundary conditions should be consistent through the analysis of each arrangement.

Initially steady state analyses were conducted for three inlet mass flow conditions, 100%, 50% and 25% of the duty flow condition. The outlet static pressure was kept the same for all analyses and a reduced static pressure was used rather than a realistic pump

outlet pressure in order to better capture the variation in pressure within the numerical model as mentioned in section 5.5.2.

5.6.2 Turbulence Modelling: Requirement for Project

As turbulence models become more specific, the process of selecting a model for a particular application is increasingly complex. Several recently published papers have attempted to simply the task for the field of turbomachinery. Yet even focusing on the application of turbomachines, still involves a vast range of complex flows. Papers, such as Menter (119) provide a brief summary relating turbulence models to particular turbomachine types. Han, et al (120) also include an update to the field of turbulence modelling for turbomachinery applications. Other papers, e.g. De Souza et al (121) provide comparisons of a number of turbulence models and relate their accuracy for a specific turbomachine.

The wide range of turbomachinery designs and applications, demand a similarly large range of turbulence models. In applications such as gas turbines a gain of a fraction of a percent is extremely desirable and so to model such small differences accurately demands some of the more complex, recently developed turbulence models. In contrast, pump machinery isn't subject to such intense optimisations and in general pumps are simpler machines. Therefore, turbulence models used in pump applications are not required to capture as much detail, e.g. heat transfer, in their equations. Additionally, as highlighted by Menter (119), pump impellers often have relatively sharp leading edges and are dependant on the flow angle at the blade leading edge. At flows away from the duty condition, the flow will separate due to the misalignment of the inflow angle and the blade angle and this separation is not sensitive to the selection of a turbulence model.

Further, the computational mesh being considered in this project is relatively complex, due to the inclusion of leakage flow paths and the sheer scale of the model. The computational facility available although reasonable is still not sufficient to model the near wall boundary for such a complex model in a practical time scale. Thus, the

demands of the present project indicate that a two-equation model is likely the most appropriate for the analyses as there is much to be gained from the model's strengths and little to lose from its weaknesses. However, some consideration needs to be taken regarding the near wall flow, in case the grid size is too coarse to model it accurately. Of the two wall functions supplied in CFX-TASCflow, CFX advise the use of the scalable wall function (103) and note that the standard wall function is only included for backward code compatibility. Therefore the analyses were conducted using scalable wall functions.

CFX-TASCflow provides two, two-equation turbulence models k-ε and k-ω; however it also provides further options for the k-epsilon model in addition to the default Launder and Spalding model. These options are termed RNG and ASM. The Re-Normalisation Group (RNG) k-ε model is derived using a rigorous statistical technique that includes the effect of swirl on turbulence, enhancing accuracy for swirling flows. The Algebraic Stress Models (ASM) were developed for situations where the eddy-viscosity assumption in normal two equation turbulence models is not valid. This relates to flow patterns where non-equilibrium affects are important, e.g. strongly swirling flow. Although extending the applicable range of the k-ε model the numerical stability of the model is reduced.

Pump design involves imparting energy to the model while minimising loss; highly swirling flow would be considered a detrimental characteristic of the pump. As the pump analysed is a tried and tested design that has not shown any tendency towards producing regions of swirling flow then it is not considered that either of the RNG model or ASM modifications would provide any benefit to modelling the turbulence.

All three of the k-ε models can be modified using the Kato-Launder generation model (122). This model provides a more realistic estimate of the generation of the kinetic energy where the flow stagnates. It is common for pump impellers to have stagnation regions at the leading edge of the impeller blade, especially at lower flow rates. Data relating to the experimental tests detailed in Chapter 4, detailed that the tests were conducted at a suction pressure level such that there would be little or no cavitation

present even at the lower flow rates. Thus it is likely that any low pressure stagnation region will be small in size and therefore will have only a minor effect on any results. Therefore the Kato-Launder modification has not been considered in the comparison of a number of the two-equation turbulence models below.

5.6.2.1 Investigation of Turbulence Models

A number of smaller analyses were conducted to determine the most appropriate turbulence model for the study. It was deemed sensible to conduct the analyses using the two-equation turbulence models following the theoretical discussions and consideration of the grid model. Therefore, six separate analyses were conducted using the impeller and volute grids from the larger analysis model. The first three analyses explored the different options provided for the k-epsilon model, with the final three performing similar comparisons of options for the k-ω model. These assessed how each of the turbulence models simulated the flow within the model. The analyses were initially conducted at the 100% flow rate. The analysis performed together with the results are given below

It was found that the various models had significant differences in terms of stability and convergence.

K-ε (ASM): The Advanced Stress Model failed to converge from the initial condition. It immediately converges and fails from a fatal overflow after less than ten iterations.
K-ε (RNG): The Re-Normalisation Group model converged to a maximum RMS residual of approximately 1e-2.
K-ε (Default): The standard k-epsilon turbulence model converged to a maximum RMS residual level of 1e-3.
K- ω (SST): The Shear Stress Transport turbulence model is the default model for the k- ω option given in TASCflow. It was found that the model converged to a maximum RMS residual level of 1e-3.
K - ω (ASM): The ASM model fails in a similar manner to that experienced by the k-epsilon ASM model, failing from a fatal overflow after less than ten iterations

K – ω (Wilcox): The Wilcox turbulence model has some initial difficulties, however once settled, it converged to a maximum RMS residual level of 1e-3.

Some basic performance macros were used to ascertain the effect of the turbulence model on the final reported performance of the pump. The sample liquid pump macro supplied with TASCflow has been used to generate performance data for all results that solved to the best degree (i.e. maximum RMS residuals of 1e-3). It was found that the head generated varied by less than 1% between the turbulence models and that the power varied by less than 0.5%. This was considered to be very good agreement. Following this, the turbulence models that proved most stable and robust at the duty flow condition (1.00Qn) were rerun at the lowest flowrate to be considered, 0.25Qn. The converged 1.00Qn results were used as the initial conditions for each of the analyses. The convergence of these models is given below.

K-ε (Default): The standard k-epsilon model converged to a maximum RMS residual level close to 2e-3.

K-ω (SST): The SST model converged to a maximum RMS residual level of 6e-3. The turbulence model experiences trouble with some of the flow patterns in the volute.

K-ω (Wilcox): The Wilcox model converged to a maximum RMS residual level of 2e-3. The Wilcox model experienced more trouble initially in converging than the other two models examined. Artificial computational walls were generated by the programme at the outlet to prevent recirculating flow, and although these reduced as the analysis progressed, remnant walls remain present in the converged solution.

Comparing the two best converged solutions (maximum RMS residual of 2e-3) it was found that there was less than 1.5% variation in the head value calculated, although the power difference had risen to just over 5%.

It was considered that the k-epsilon (default) model provided the most consistent, stable and robust performance across the flow range analysed. Although the K-ω Wilcox model also performs well, the initial difficulty in moving towards a converged solution could be problematic with a larger more complex model.

A review of published work indicates that literature containing numerical flow investigations of pumps commonly use the k-ε turbulence model. Investigations by Guleren & Pinarbasi (123), Muggli et al (99), Gonzalez et al (38) and Shi & Tsukamoto (60) all use the same k-ε turbulence model for different commercial CFD codes. Additionally Tamm et al (124) performed a comparison of the standard k-ε model, the RNG modified k-ε model and a higher order RSM (Reynolds Stress model) on a single entry pump (impeller and spiral casing) at a duty flow condition. The study concluded that there was no appreciable improvement in using the RNG k-ε model over the standard k-ε turbulence model. It is also noted that the RSM model shows lower values for efficiency and the parameters used for monitoring convergence fluctuated at the end of the iteration process. Tamm et al opted to use the standard k-ε turbulence model due to its robust convergence and reduced computational requirement.

Thus, both a numerical study of selected turbulence models and a review of published literature indicate that the standard k-ε turbulence model is applicable to the current project of modelling a complete centrifugal pump.

5.6.3 Numerical Solution Control

The calculations described above were conducted on two separate facilities depending on the specific arrangement, on the "Cluster Grid" at Cranfield University and a stand-alone PC Intel Xeo processor at Weir Pumps Limited. The "Cluster Grid" consists of multiple two Intel 3Ghz processors with 6GB of shared memory apiece, whereas the WPL facility consists of a two 2Ghz Intel processors with 4GB memory. The analyses were run serially due to complications in running the TASCflow in parallel on the "Cluster Grid" and there is no parallel capability at WPL. The time taken per iteration is dependent on the arrangement and flowrate analysed, but can usually assumed to be approximately one iteration per hour. Typically periodic unsteady convergence was achieved in four to five impeller revolutions, thus around 1300 iterations/hours are

required to complete a single analysis. A total of thirty three analyses were completed as part of the pressure pulsation investigation (circa. 45,000 hours computing time).

Koumoutsos has conducted a time independence study of a five blade, centrifugal impeller/volute interaction using both 500 and 250 time steps per revolution (125). This corresponds to 100 and 50 time steps per impeller blade passage respectively. The conclusion of the study reported that the solution was not affected by the time step and therefore 250 time steps per revolution (or 50 time steps per passage) were selected for the work. Unfortunately no information is provided regarding the Courant-Friedrich-Levy (CFL) numbers relating to these values. The timestep selected for use in the current analyses was 1.488e-4 seconds, as this provided a blade rotation of 1.25 degrees between iterations or 288 time steps per impeller rotation (i.e. 48 time steps per impeller blade passage). This kept the CFL number around 25 to 30 and is considered to have preserved the accuracy and stability of the analysis. It is perhaps worth noting that pump analysed by Koumoutsos was running with a larger rotational velocity than that used here (i.e. 2066RPM and 1400RPM respectively). Transient results files were created after every second iterative loop.

It should be noted that slight stability problems were experienced on a couple of arrangements at the lowest flow condition (first, third and ninth arrangements), however these instabilities were overcome by making slight adjustments to the analysis time step (required changes were less than 1% of the time step listed above).

5.7 Chapter Summary

This chapter has provided background to the project, both in terms of the planned route to completion and the relevant theory. The main section of the chapter has detailed the process used to generate a computational model of the complex geometry present in a complete centrifugal pump. The important points discussed in the chapter are summarised below:

- The main points of theory behind the commercial CFX-TASCflow code have been discussed.
- The Taguchi process to be used in setting up the arrangements to be simulated and in analysing the results comparatively has been described and discussed.
- A grid independence check has been conducted for the impeller and has concluded that a grid of 22,200 nodes, while being relatively coarse is sufficient for the project. It is also observed that unless the impeller grid size is increased significantly, little improvement will be obtained.
- The process and considerations used in generating each of the other components, i.e. volute, leakage flow path and suction inlet regions has also been provided in detail.
- The process used to build up the complete pump computational model has been given. This involved building up the model piece-by-piece and conducting analyses at each stage before adding in the next component. This allowed grid refinement of each component to be conducted, while the performance of the component was considered in conjunction with the larger model.
- The boundary conditions used in the project have been described. Some discussion is provided on the selection of the boundary conditions and the resulting increase in stability of the analyses at lower flows.
- An investigation regarding the selection of a turbulence models has been conducted. This included both numerical comparisons of selected models and consideration of models used in published literature when modelling pumps. The investigation resulted in the selection of the k-ε turbulence model.

5.8 Tables

Trial Number	Factors						
	A	B	C	D	E	F	G
1	1	1	1	1	1	1	1
2	1	1	1	2	2	2	2
3	1	2	2	1	1	2	2
4	1	2	2	2	2	1	1
5	2	1	2	1	2	1	2
6	2	1	2	2	1	2	1
7	2	2	1	1	2	2	1
8	2	2	1	2	1	1	2

Table 5.1: Orthogonal array L_8

Array	Number of Factors	Number of Levels
L_4	3	2
L_8	7	2
L_{12}	11	2
L_{16}	15	2
L_{32}	31	2
L_9	4	3
L_{18}	1	2
L_{18}	7	3
L_{27}	13	3
L_{16}	5	4
L_{32}	1	2
L_{32}	9	4
L_{64}	21	4

Table 5.2: Common orthogonal arrays (Roy (102))

Arrangement	Factor				Sample Results
	A	B	C	D	
1	-1	-1	-1	-1	Z1
2	-1	0	0	0	Z2
3	-1	+1	+1	+1	Z3
4	0	-1	0	+1	Z4
5	0	0	+1	-1	Z5
6	0	+1	-1	0	Z6
7	+1	-1	+1	0	Z7
8	+1	0	-1	+1	Z8
9	+1	+1	0	-1	Z9

Table 5.3: Orthogonal array L_9

Arrangement	Factor				Sample Results
	A	B	C	D	
1	3.83%	0.27%	100%	Inline	Z1
2	3.83%	1.10%	50%	15 Degrees	Z2
3	3.83%	1.64%	25%	30 Degrees	Z3
4	6.00%	0.27%	50%	30 Degrees	Z4
5	6.00%	1.10%	25%	Inline	Z5
6	6.00%	1.64%	100%	15 Degrees	Z6
7	7.95%	0.27%	25%	15 Degrees	Z7
8	7.95%	1.10%	100%	30 Degrees	Z8
9	7.95%	1.64%	50%	Inline	Z9

Table 5.4: L_9 array for current work

Arrangement	Factor		Sample Results
	A	B	
1	-1	-1	Z1
2	-1	1	Z2
3	1	-1	Z3
4	1	1	Z4

Table 5.5: Orthogonal array L_4

Arrangement	Factor			Sample Results
	A	B	AB Interaction	
1	-1	-1	1	Z1
2	-1	1	-1	Z2
3	1	-1	-1	Z3
4	1	1	1	Z4

Table 5.6: L_4 array with added interaction column

Published Work	Inlet	Impeller	Volute	Leakage Flow	Outlet	Total Grid
Blanco-Margiorta et al (39)	18948 (Tet)	37872 (Tet)	34254 (Tet)	-	-	91074 (Tet)
Gonzalez et al (38)	34883 (Hex)	162974 (Tet)	89721 (Tet)	-	44684 (Hex)	79567 + 252695 (Hex) + (Tet)
Tamm et al (117)	-	420000 (Hex)	280000 (Hex)	≈600000? (Hex)	-	1300000 (Hex)
Current Work	89756 (Hex) (Suction)	227136 (Hex)	391848 (Hex)	161760 (Hex)	Included in volute grid	870500 (Hex

Table 5.7: Comparison of grid size for published work

(Hexahedral and tetrahedral elements indicated by (Hex) and (Tet) respectively)

Characteristics	Number of Nodes per Impeller Passageway
Grid A	12,597
Grid B	22,155
Grid C	23,552
Grid D	35,478
Grid E	46,303
Grid F	86,499

Table 5.8: Details of varying impeller grid sizes

5.9 Figures

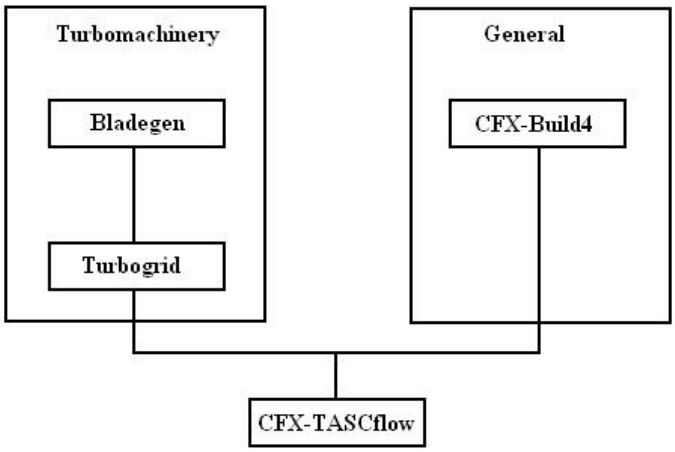

Figure 5.1: Flow diagram of the grid generation methods used for modelling in CFX-TASCflow

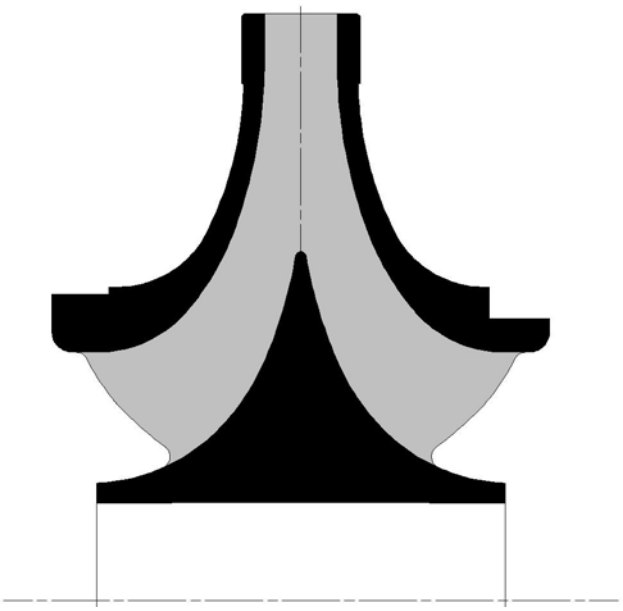

Figure 5.2: Double entry impeller cross-section (inline vane arrangement)

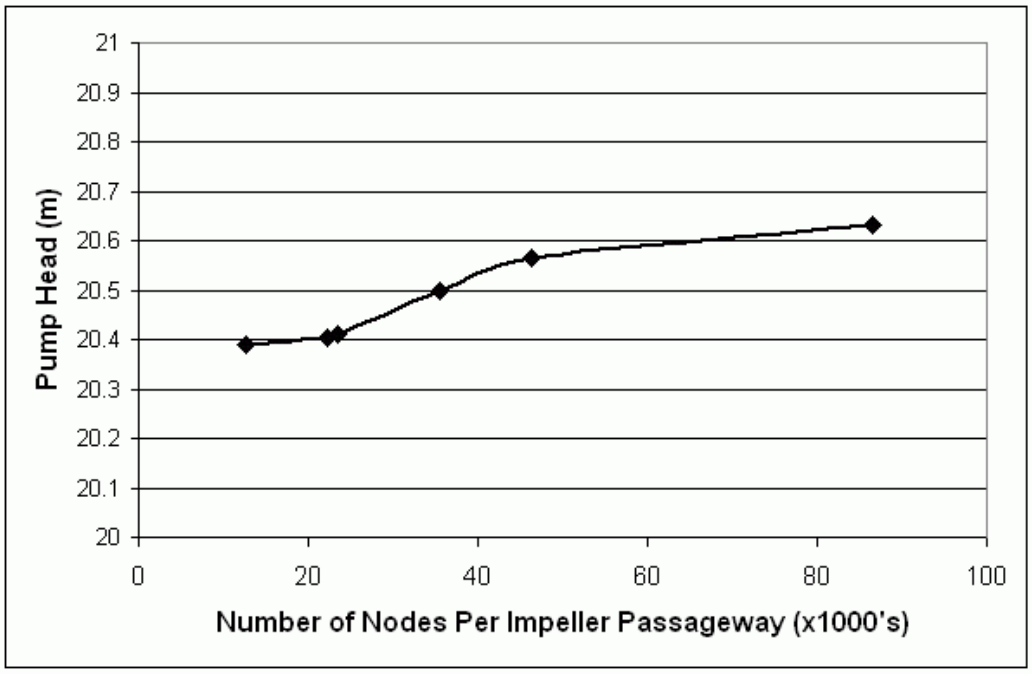

Figure 5.3: Influence of grid size on impeller head

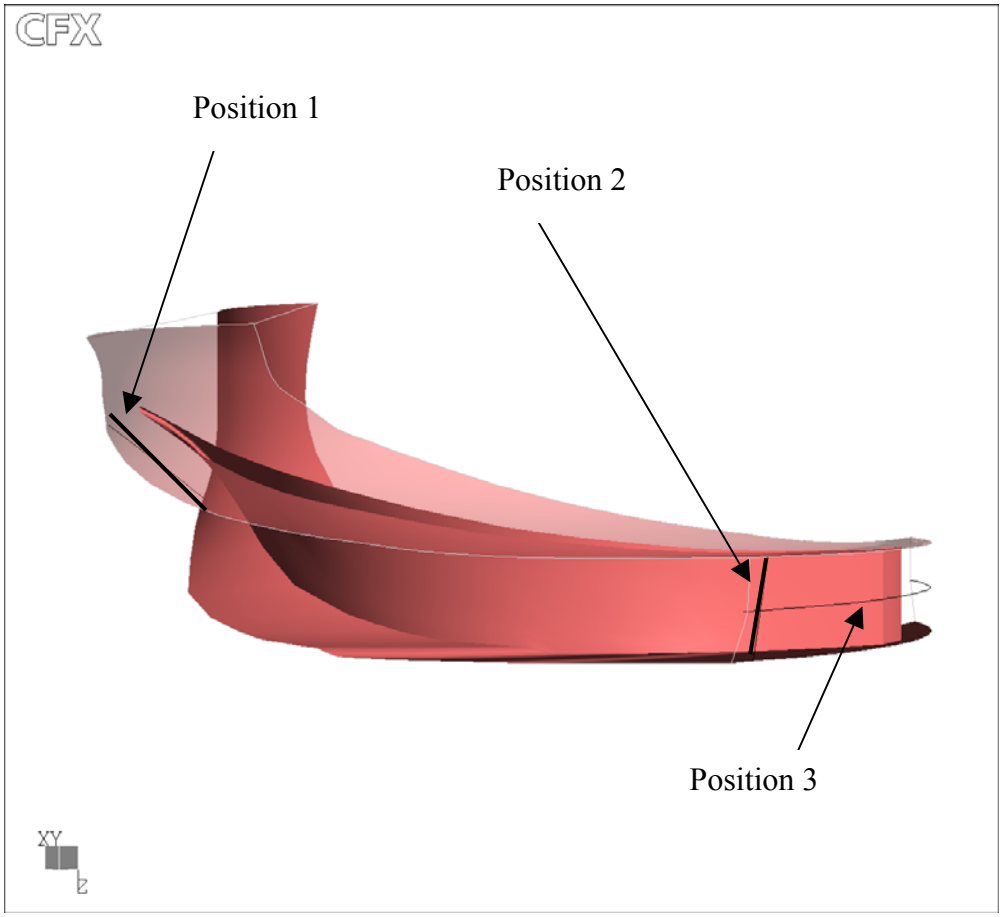

Figure 5.4: Position of monitoring locations within impeller passageway

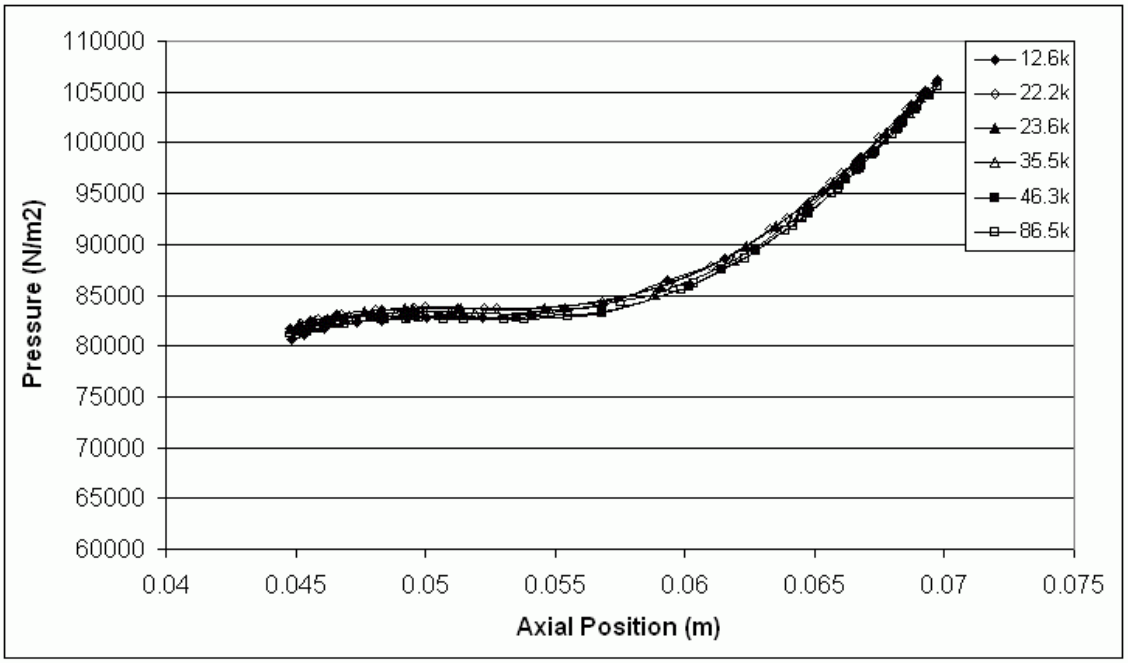

Figure 5.5: Variation of pressure over the axial distance from hub to shroud at a mid-passage position at the blade leading edge diameter for different grid sizes (position 1).

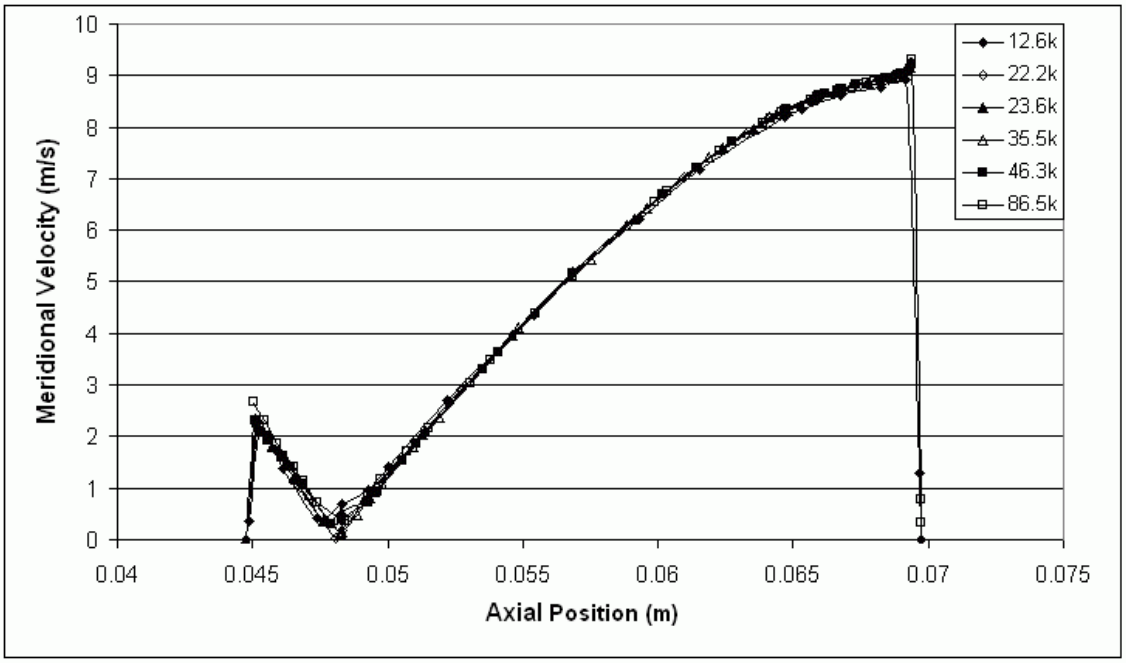

Figure 5.6: Variation of meridional velocity over the axial distance from hub to shroud at a mid-passage position at the blade leading edge diameter for different grid sizes (position 1).

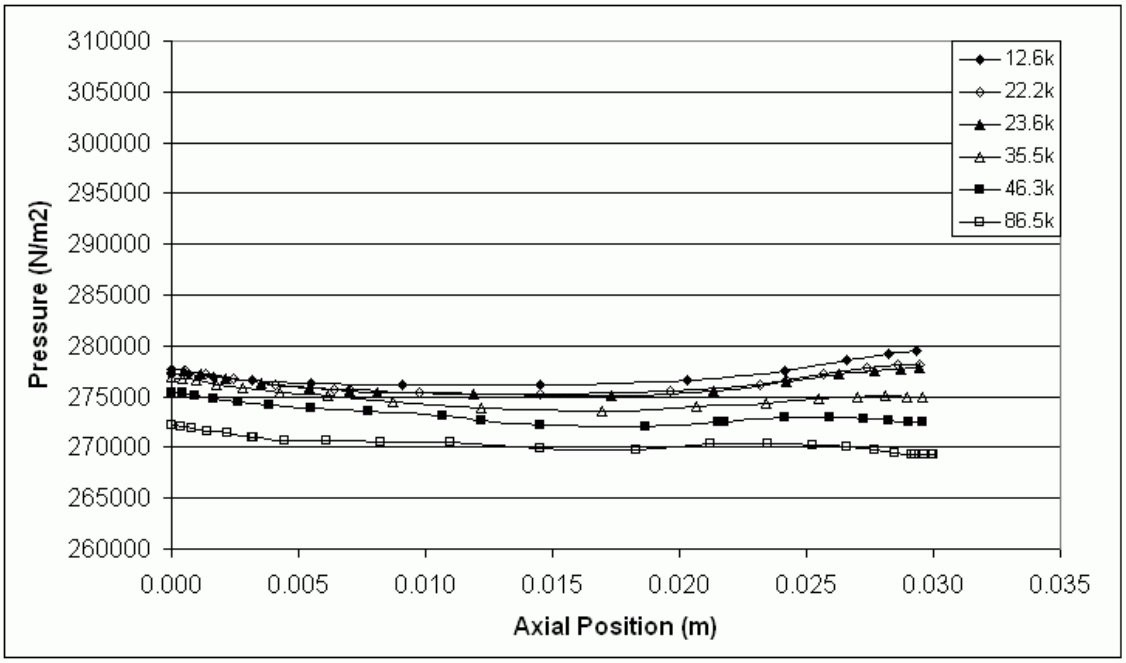

Figure 5.7: Variation of pressure over the axial distance from hub to shroud at a mid-passage position at the blade trailing edge diameter for different grid sizes (position 2).

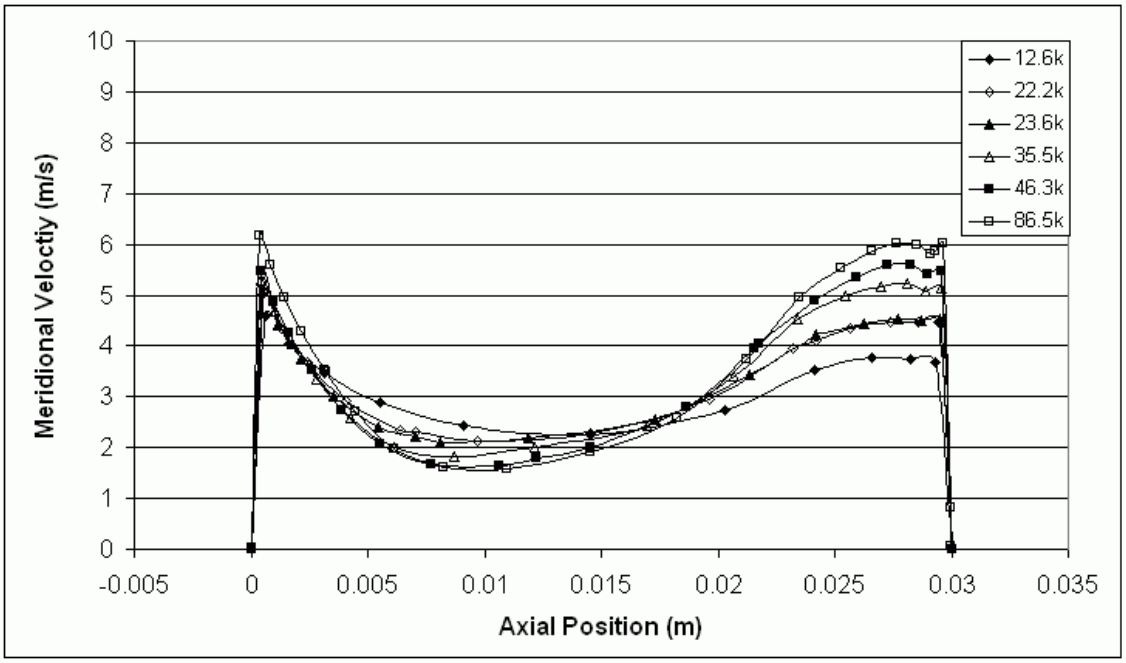

Figure 5.8: Variation of meridional velocity over the axial distance from hub to shroud at a mid-passage position at the blade trailing edge diameter for different grid sizes (position 2).

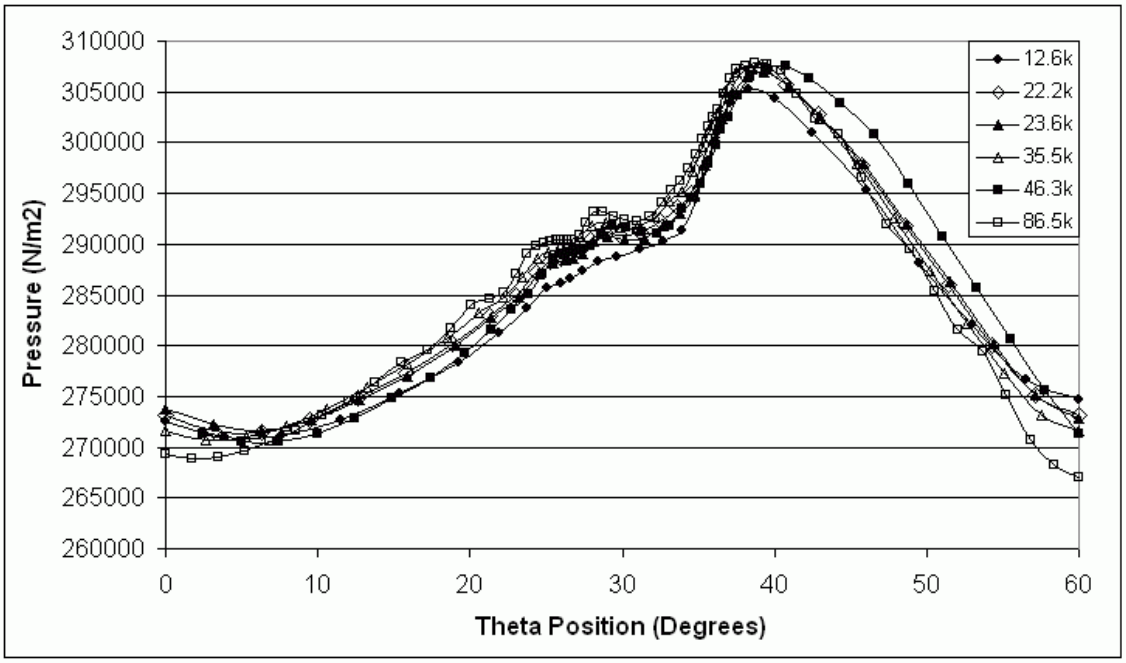

Figure 5.9: Variation of pressure across a single blade passage at the impeller outlet for different grid sizes (position 3).

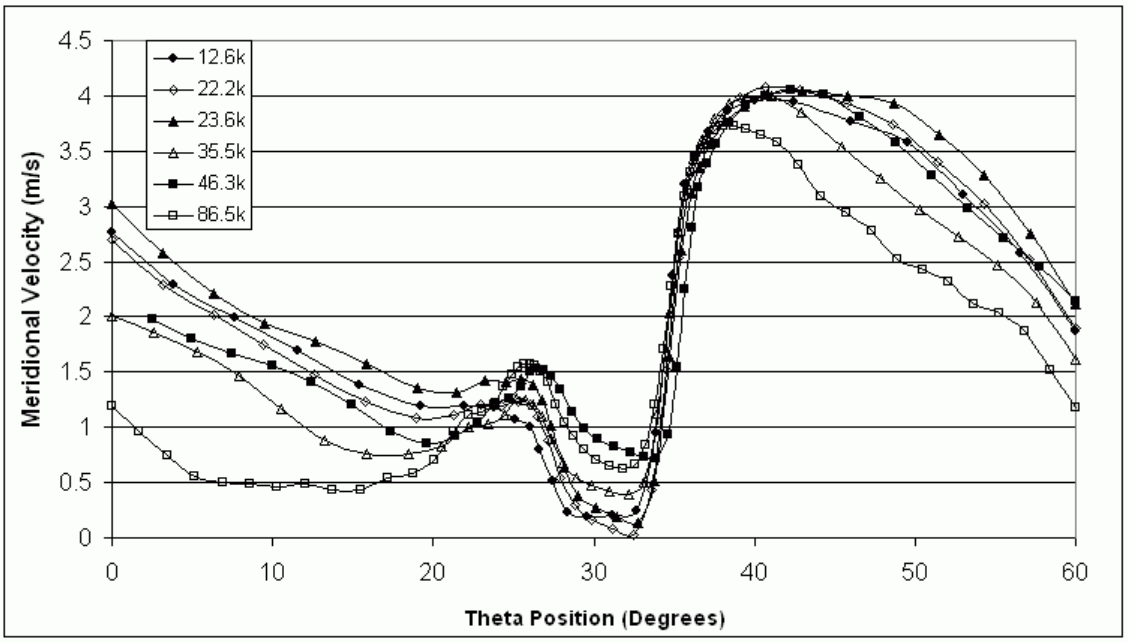

Figure 5.10: Variation of meridional velocity across a single blade passage at the impeller outlet for different grid sizes (position 3).

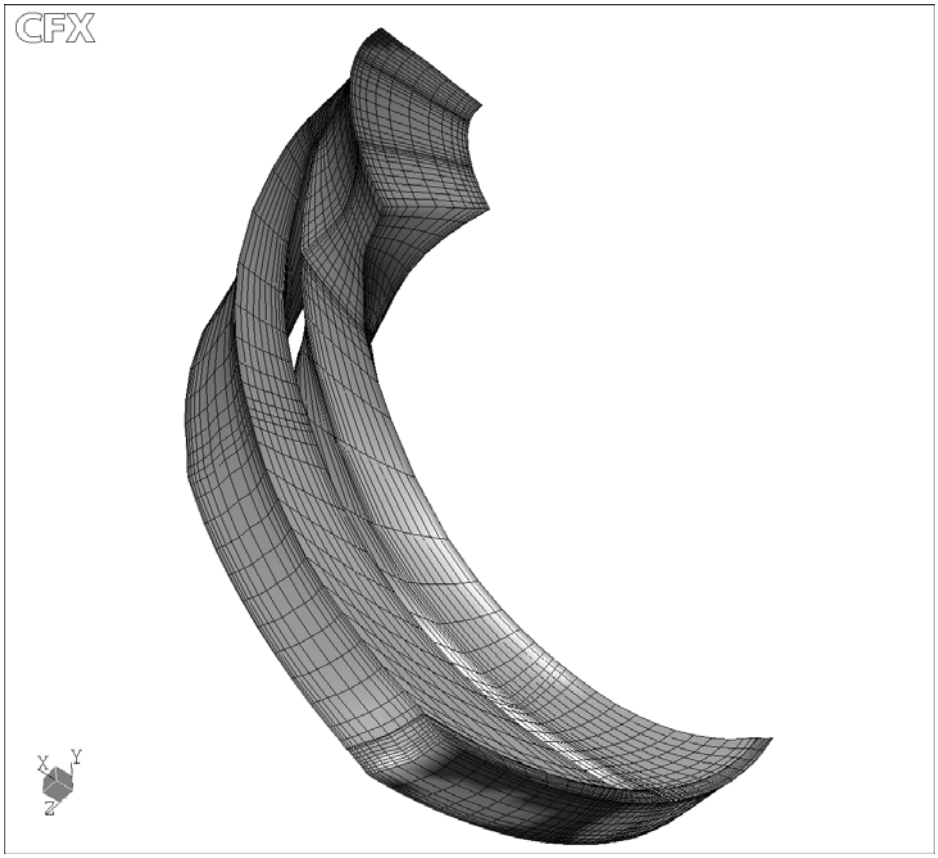

Figure 5.11: Grid in a single impeller passageway

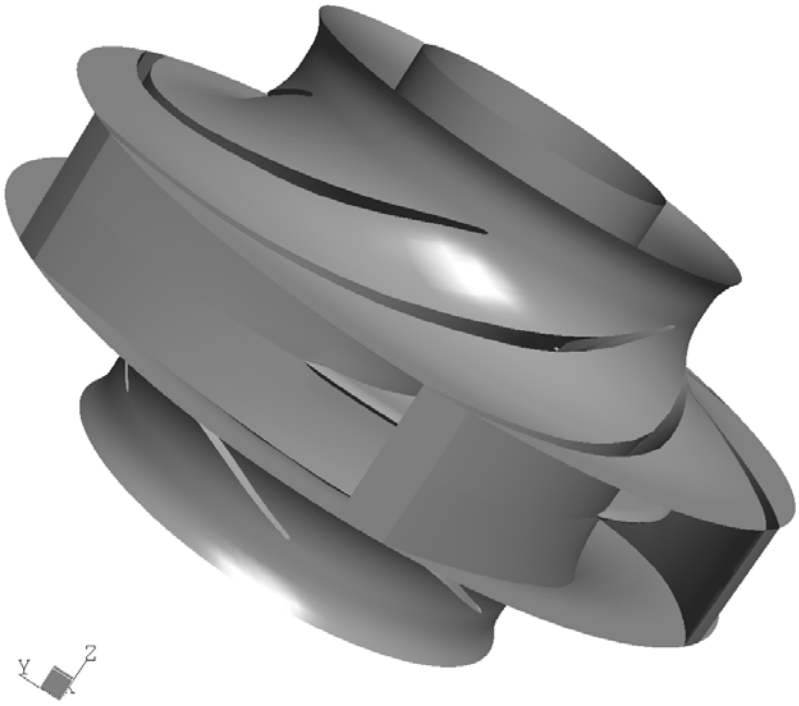

Figure 5.12: Inline impeller arrangement model

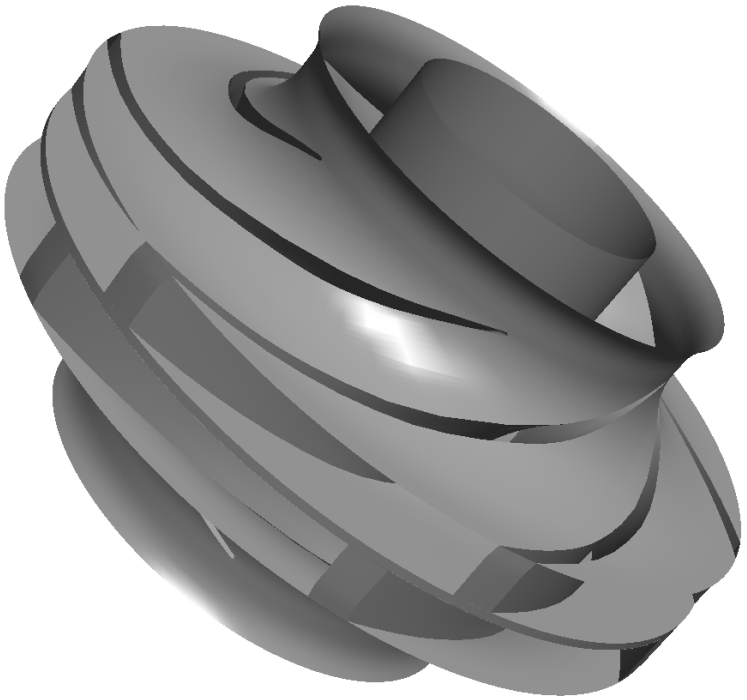

Figure 5.13: 15 degree stagger impeller arrangement model

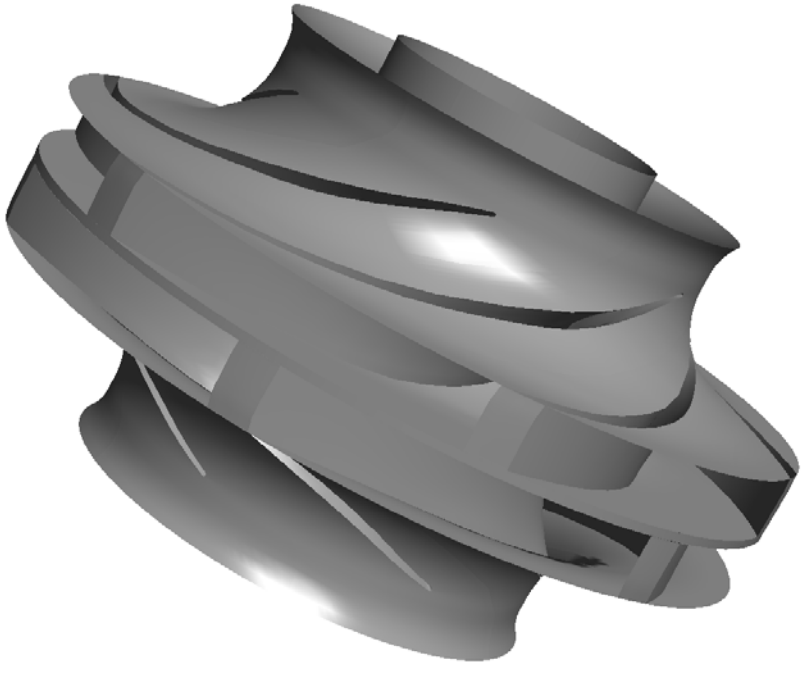

Figure 5.14: 30 degree stagger impeller arrangement model

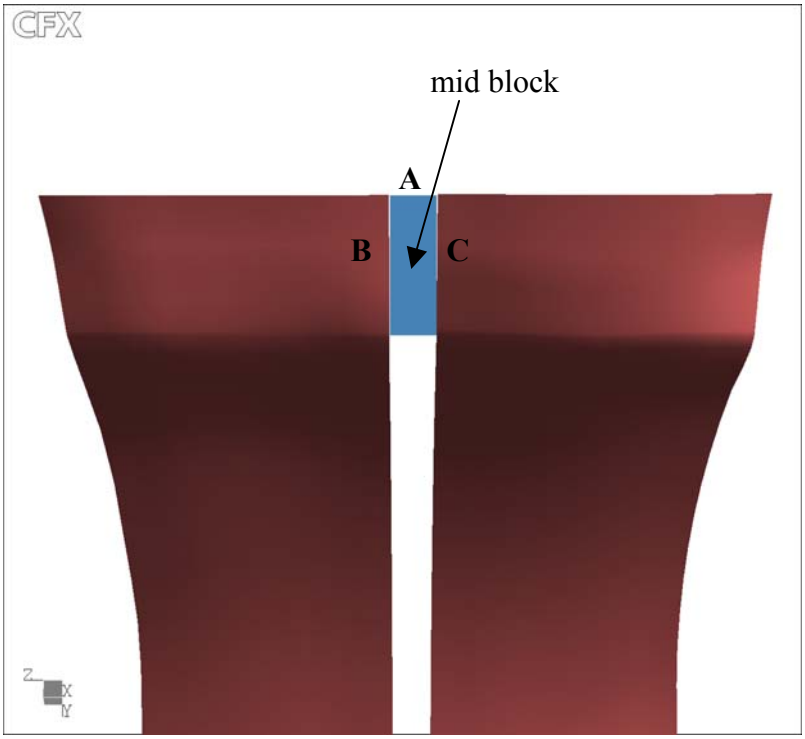

Figure 5.15: Position of mid block at impeller exit

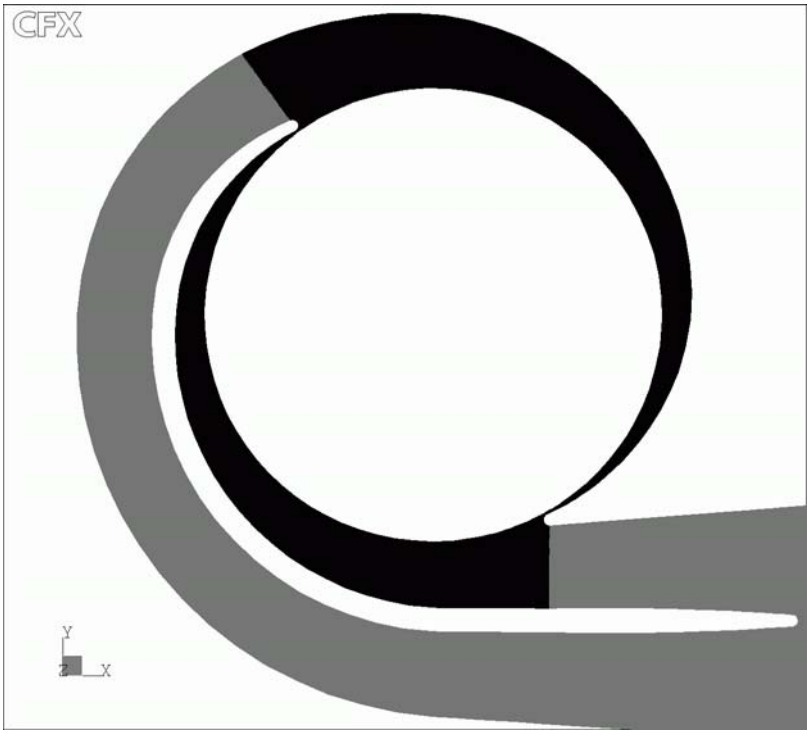

Figure 5.16: The two volute grid sections (Volute 'A' is shown in dark grey and volute 'B' in light grey).

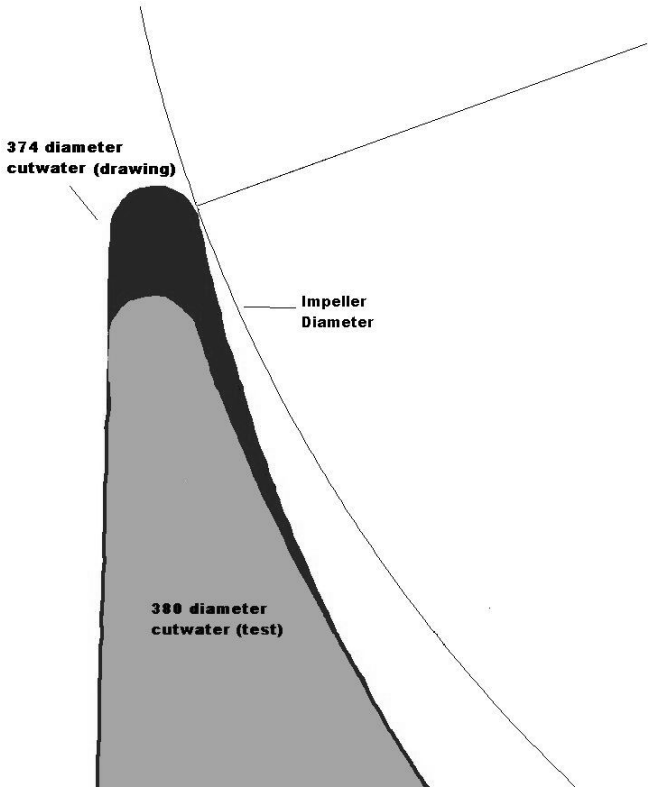

Figure 5.17: Cutwater gap enlargement process

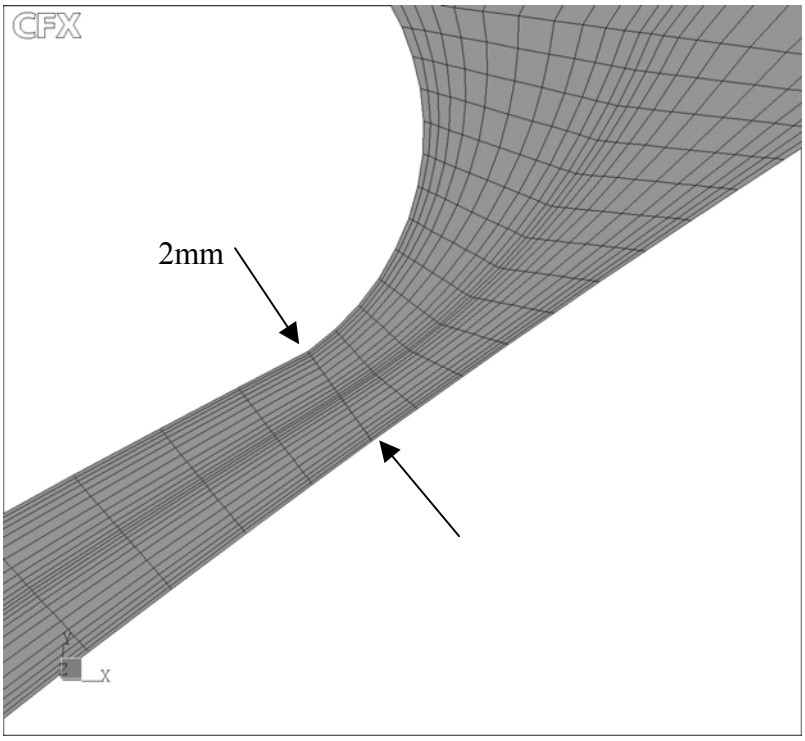

Figure 5.18: Grid distribution local to splitter.

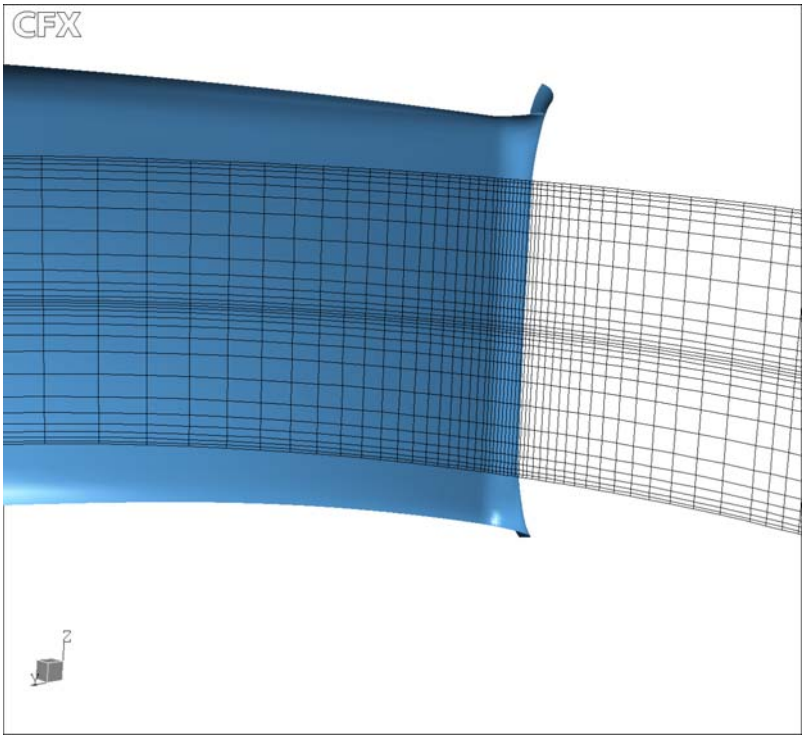

Figure 5.19: Volute interface axial grid distribution for the inline impeller arrangement (close to cutwater position)

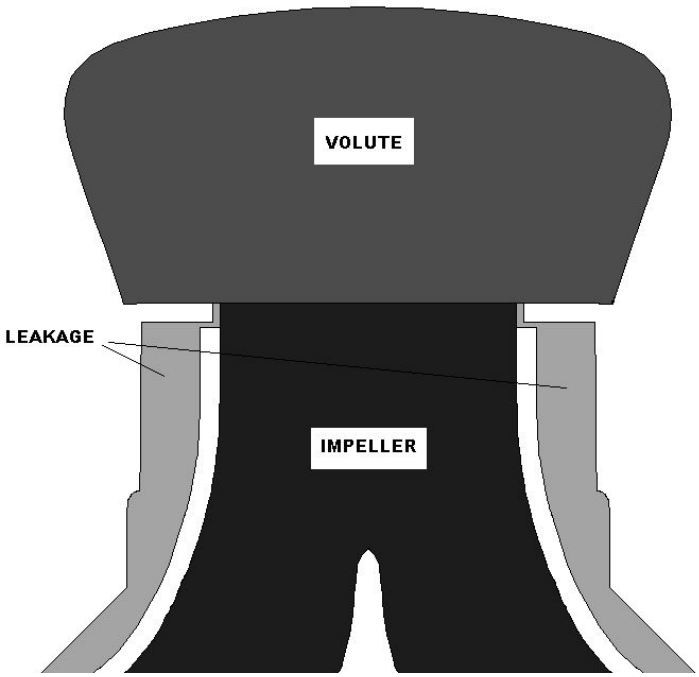

Figure 5.20: Impeller, volute, leakage arrangement at impeller outlet

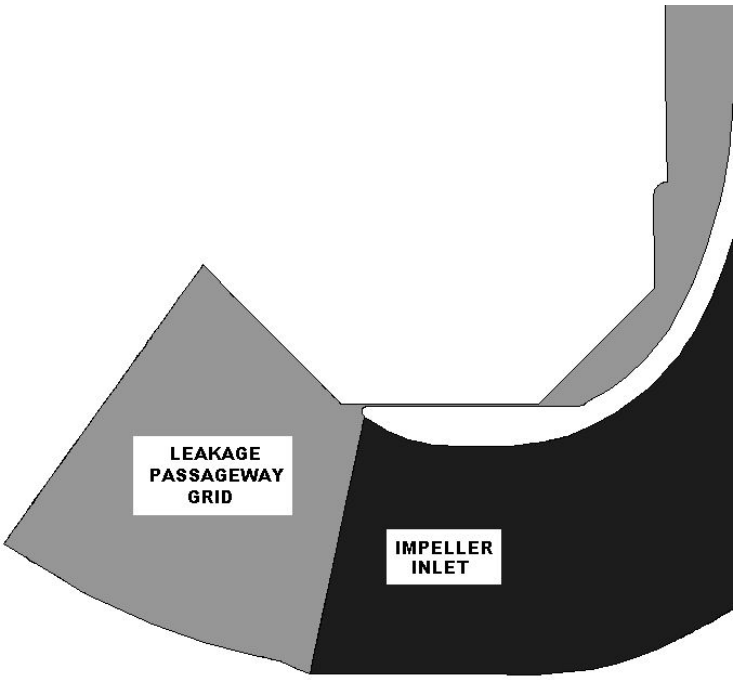

Figure 5.21: Leakage flow model arrangement at impeller inlet

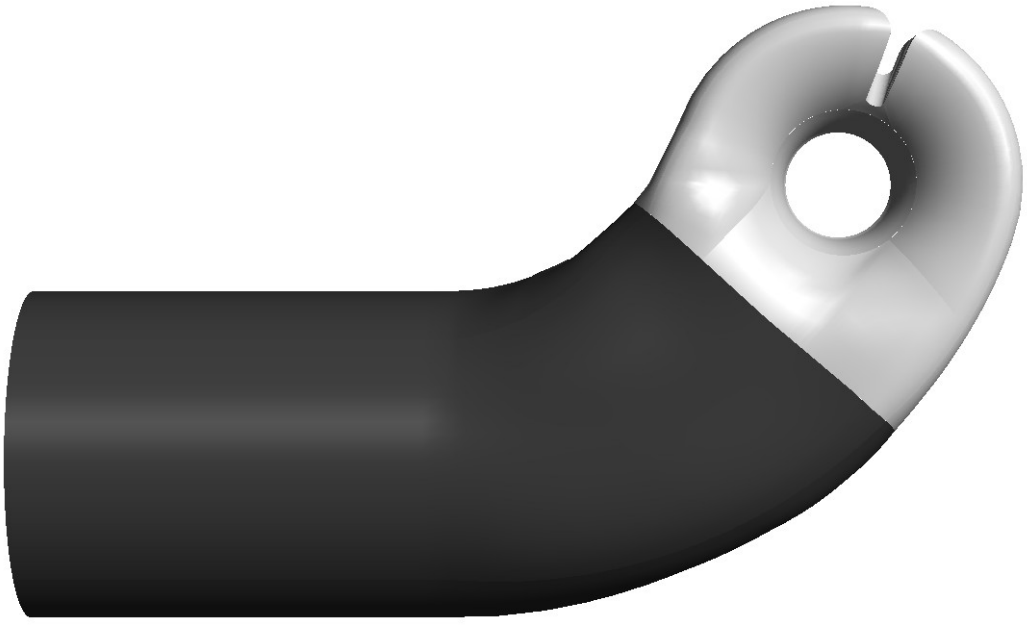

Figure 5.22: The two suction inlet sections

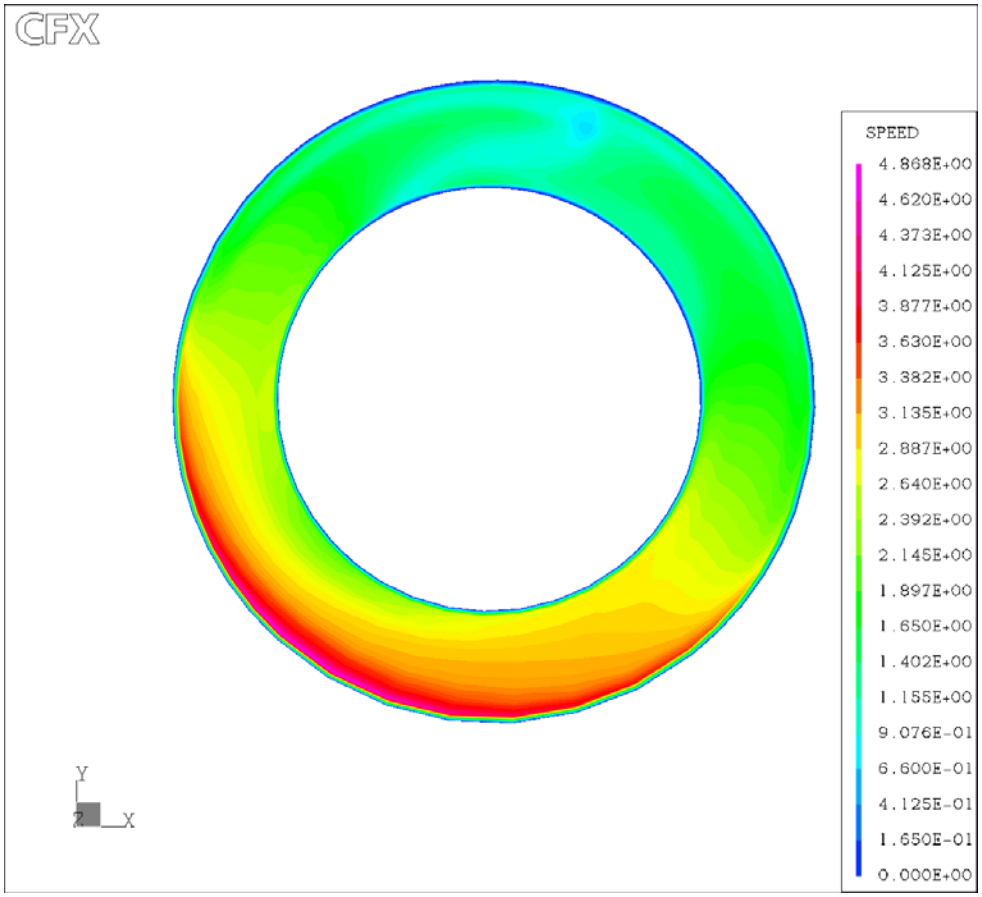

Figure 5.23: Sample flow velocity imbalance at impeller eye for first arrangement at 1.00Qn

Figure 5.24: Full pump analysis model

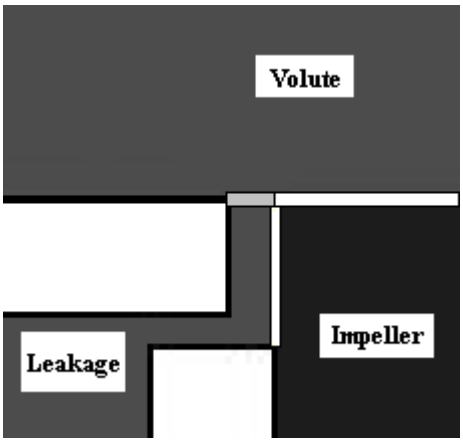

Figure 5.25: Initial interface arrangement at impeller outlet

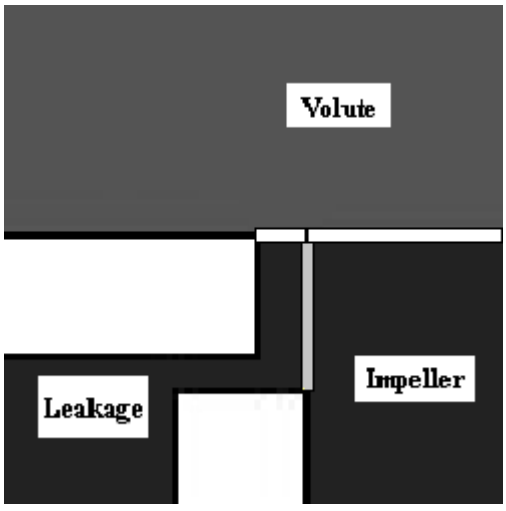

Figure 5.26: Modified interface arrangement at impeller outlet

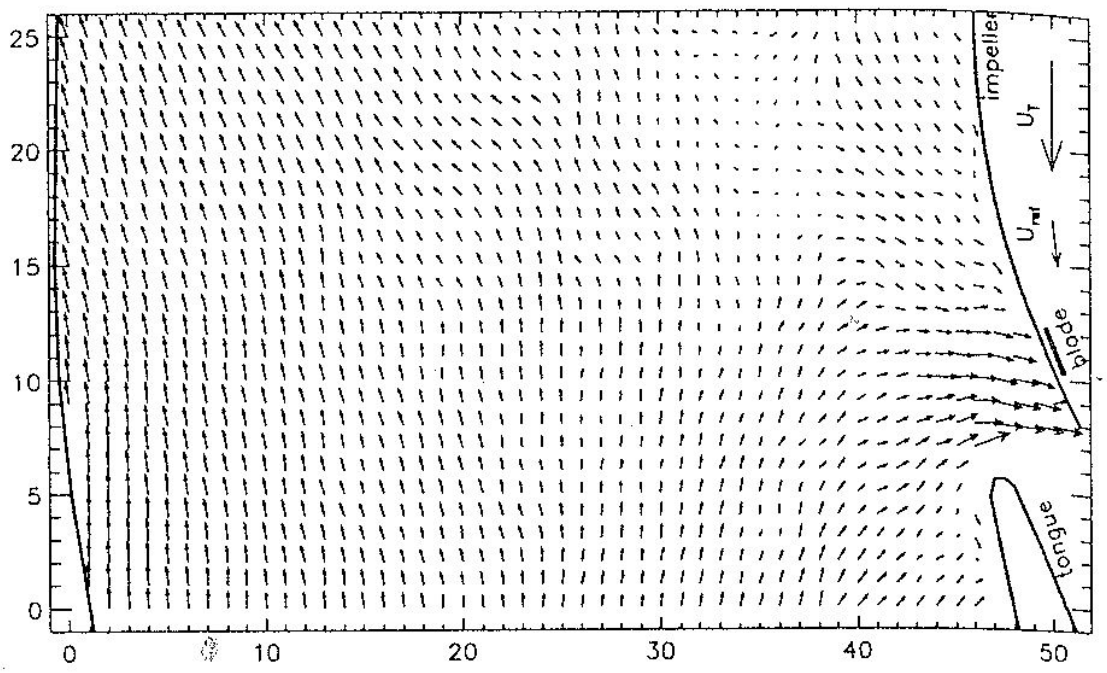

Figure 5.27: Phase averaged velocity distributions near the cutwater at a 45% flow condition (reproduced from Dong et al (27))

Chapter 6

Selected Theoretical/Numerical Flow Results

6.1 Presentational Form of Results

6.1.1 Pressure Pulsation Representation

6.1.2 Monitoring Position for CFD Results

6.1.3 Performance Characteristic Calculation

6.1.4 Flow Animations

6.2 Velocity Flow Results

6.2.1 Suction Inlet

6.2.2 Impeller

6.2.3 Volute

6.2.4 Summary

6.3 Pressure Field Results

6.3.1 Static Pressure Distribution

6.3.2 Unsteady Pressure Distributions

6.3.2.1 Time History Data

6.3.2.2 Frequency Data

6.3.3 Summary

6.4 Comparison with Experimental Results

6.4.1 Comparison A: Experiment 18 with CFD Analysis 5

6.4.2 Comparison B: Experiment 8 with CFD Analysis 3

6.4.3 Summary

6.5 Chapter Summary

6 Selected Theoretical/Numerical Flow Results

A centrifugal pump consists of three main components, each of which has been modelled as part of this study. These components and their task are summarised below

(i) Suction inlet guide: The purpose of the suction inlet guide is to guide the flow into the eye of the impeller.
(ii) Impeller: The impeller comprising the blades and shrouds imparts energy to the fluid in the pump. The shape and number of the blades are important in design.
(iii) Volute: This is a stationary collecting device that directs the flow towards the pump outlet.

This chapter presents a few selected results from the CFD analyses in order to make some comparisons with other sources of published data and some of the experimental work reported in Chapter 4. In Chapter 7 all twenty seven transient analyses are discussed primarily in the context of the Taguchi analysis. These are characterised as nine arrangements at the three different flow rates, 1.00Qn, 0.50Qn and 0.25Qn. In this chapter only three arrangements are used mainly at the duty and lowest flow conditions and the details of these arrangements are given in Table 6.1.

After some necessary preliminaries, the flow patterns are described in terms of velocity components to allow comparison with velocimetry investigations present in published data. Following this, pressure patterns and fluctuations are discussed. Finally two detailed comparisons are made with the experimental data described in Chapter 4.

6.1 Presentational Form of Results

The form in which the results are presented is important as the sheer volume of data generated by a CFD analysis causes difficulty in focusing on important features. The following section clarifies the form that will be used when presenting pressure pulsation

values. It then identifies the locations used in the numerical model to monitor the pressure pulsations and finally details the equations used to calculate the predicted performance of the different pump arrangements.

6.1.1 Pressure Pulsation Representation

There are a number of forms in which pressure pulsations can be presented. Guelich and Bolleter (90) summarise these as follows:

- Peak-to-peak: Δp_{p-p}
- Amplitude: $\Delta p_a = \frac{1}{2}\Delta p_{p-p}$
- RMS amplitudes which, for example, for a sinusoidal pulsation are defined as shown in Equation 6.1

$$\Delta p_{RMS} = \frac{\Delta p_a}{\sqrt{2}} = \frac{\Delta p_{p-p}}{2\sqrt{2}} \qquad \text{Equation 6.1}$$

Guelich and Bolleter note that RMS-values represent the energy content in a defined frequency band and therefore recommend that RMS-values be used when evaluating the effect of pressure pulsations on any component or system.

Others, notably Gonzalez et al in their papers (6)(38), comparing experimental and CFD pulsations opt to compare pulsation amplitudes and not RMS values. The reason for their choice is not stated; it may simply be that for them the pulsation amplitudes provide a more direct comparison. The main output from the experimental work in Chapter 4 has been given as RMS pulsation values. Pulsation amplitude values were not detailed since it was considered that RMS values were more useful, which is consistent with Guelich and Bolleter above.

In order to provide numerical RMS pulsation values for the CFD pressure pulsations for comparison with the experiments the author has taken the mean for the pressure values at each location and set this value as the datum for the RMS-value calculation.

6.1.2 Monitoring Positions for CFD Results

The monitoring positions selected for the experimental tests conducted in Chapter 4 are considered to be appropriate for reporting the CFD results for the pump. The positions used in the experimental tests are detailed in section 4.2.1. Of course the CFD analyses allow a more complete picture of the pulsation pattern to be obtained throughout the pump. For instance, the experimental tests aimed to have 2 monitoring points on the impeller but, due to the failure of the blade transducer, ended up only investigating the pulsations at the shroud. In order to form a more complete picture of the pulsation pattern, an additional three monitoring points have been taken for the CFD results in addition to those used in the experimental tests. Two additional points are placed on the impeller at the suction face of the blade and at the shroud mid way between blades and an additional point is located at the discharge of the pump. The relative positions of the additional pressure monitoring locations at the impeller are shown in Figure 6.1. Thus a total of fifteen CFD monitoring locations were used to investigate the pressure pulsations for each of the twenty seven transient analyses conducted.

In what follows, the results from the CFD analyses are presented using the experimental channel number as a short hand to refer to their position, e.g. the position from the CFD analysis corresponding to Channel 1 is designated C1. The monitoring points are summarised below:

Leakage Flow Path

C1 – On the right hand wall, 60mm ahead of the leading edge cutwater
C2 – On the right hand wall 30mm ahead of the leading edge cutwater
C3 – On the right hand wall at the leading edge cutwater
C4 – On the right hand wall 30mm past the leading edge cutwater
C10 – On the left hand wall, 60mm ahead of the leading edge cutwater

Volute

C5 – Inner face of the leading edge cutwater 5mm back from the leading edge

C6 – Inner face of the leading edge cutwater 15mm back from the leading edge

C7 – Inner face of the leading edge cutwater 30mm back from the leading edge

C8 – Inner face of the leading edge cutwater 50mm back from the leading edge

C9 – Situated in the volute at top dead centre.

Cd – Situated at the discharge of the pump.

Impeller

Shroud B (above blade) – located on the radial tip of the impeller shroud positioned above an impeller blade.

Shroud M (mid passage) – located on the radial tip of the impeller shroud positioned mid way between two impeller blades.

Blade P – located on the pressure face of an impeller blade, adjacent to the shroud.

Blade S – located on the suction face of an impeller blade, adjacent to the shroud.

It has already been shown that the size of the pressure pulsations in the pump is highly variable depending on the location monitored. So far differences have only been discussed in relation to significantly different positions within the pump. However even small differences in location may give rise to substantial differences in pulsations. For example, channel 6's location as detailed by the experimental documentation is given in Figure 6.2. Its exact position was not inline with the pump centreline, but offset axially by 25mm. The difference between the centreline and the offset transducer position may influence the pulsations. Such small differences in location have been investigated by the CFD analysis together with a corresponding symmetrical position at the cutwater on the pump centreline. The results shown in Table 6.2 provide the (normalised) peak-to-peak pulsation over a single rotation over a number of flow rates for the first geometric arrangement.

First Arrangement

Position A: C6's location measured from the cutwater on the pump centreline

Position B: C6's location measured from the splitter on the pump centreline

Position C: C6's location measured from the splitter but axially offset from the pump centreline by 25mm.

It is apparent that there are significant differences in pulsation even for these slight differences in measuring point location. The cutwater/splitter locations have less variation at the best efficiency point, however this increases to around a 20% difference at the 0.25Qn. The axial offset position at the splitter is approximately 10% lower in pulsation that at the pump centreline, with this increasing to 20% at the lowest flow rate. Published literature usually provides clear indication of the circumferential location of measurement points in the pump casing, yet often omits to include the axial position. Some may assume that lack of data indicates a centreline measurement, yet there are often external complications, e.g. lifting points on the centreline of the pump, which force pressure tapping points to be offset axially.

The experimental pressure measurements in the volute were taken at the splitter region but were axially offset from the centreline by 25mm (indicated in the photograph, Figure 6.3). The numerical results have been extracted from these same positions.

6.1.3 Performance Characteristic Calculations

As has been stated, it is important to assess the change in performance caused by the differing geometric arrangements analysed in addition to the pressure pulsations. The current project will estimate this through three typical pump performance characteristics, i.e. head, power and efficiency.

The TASCflow post-processor includes a performance macro that facilitates the calculation of performance characteristics for a number of turbomachines, including pumps. The author has utilised this macro over a number of years to estimate impeller and pump performances and has found it to produce satisfactory results, both during Weir Pumps validatory work and contract work. The author has made slight modifications to the macro, tailoring it to the requirements of the project. This has increased the automation of the macro allowing the performance of the pump to be

estimated at each impeller blade position in a timely manner. The basis of the calculations remains unchanged and are summarised here. Further details concerning the performance macro can be obtained from the TASCflow documentation (103)

Head Calculation

The TASCflow documentation details that the total head calculated by the performance macro is as shown in Equation 6.2

$$Head = \frac{C_t \omega r}{g} \qquad \text{Equation 6.2}$$

Where C_t is the tangential velocity component in the absolute frame
ω is the rotational velocity
r is the outlet radius of the impeller blades
g is the gravitational acceleration.

Within the macro this is actually computed from the mass-averaged differential of the absolute total pressure across the pump as detailed in Equation 6.3

$$Head = \frac{P_{t2} - P_{t1}}{\rho g} \qquad \text{Equation 6.3}$$

Where P_{t1} is the mass-averaged total pressure at the pump inlet
P_{t2} is the mass-averaged total pressure at the pump outlet
ρ is the density
g is the gravitational acceleration.

Torque Calculation

Forces on the impeller blades are computed from pressure, wall shear stress and area information. The tangential force is obtained from this scalar information being

projected in the tangential direction. The torque is then obtained by the sum of the tangential pressure multiplied by the local radius and the viscous forces on each of the blades.

Efficiency Calculation

The efficiency calculated is termed the efficiency from power (η_w) and is effectively the rate of work output to the rate of work input, i.e. the hydraulic head divided by the hydraulic power. This calculation is detailed in Equation 6.4.

$$\eta_w = \frac{\dot{m}}{\rho}\frac{P_{t2} - P_{t1}}{M\omega} \qquad \text{Equation 6.4}$$

Where $\dot{m}$ is the mass flow through the pump

P_{t2} is the mass-averaged total pressure at the pump outlet

P_{t1} is the mass-averaged total pressure at the pump inlet

ρ is the density

M is the torque

ω is the rotational velocity

6.1.4 Flow Animations

A few selected flow animations, from the first arrangement, have been presented for interest on a CD, which is included in Appendix A. This helps to visualise some of the complex flow patterns involved due to the interaction of the impeller blade and volute cutwater. It should be noted that the animation manager does not allow the pressure datum to be corrected; hence the scales on the animation show negative pressures (the use of the reduced pressure datum is discussed briefly in Section 5.5.4). Additionally the animations have been limited to two blade passes and are best viewed on "repeat playback". The animations are as follows:

Animation B1: Pressure local to the cutwater at 1.00Qn - This animation illustrates of the variation in the pressure at the volute and impeller outlet local to the cutwater on a mid position axial plane.

Animation B2: Velocity vectors local to the cutwater at 1.00Qn - This animation illustrates the variation in the magnitude and direction of the velocity at the impeller outlet and cutwater on a mid position axial plane.

Animation B3: Pressure local to the impeller at 1.00Qn - This animation illustrates the pressure variation on the impeller inner and outer surfaces as it passes the cutwater.

Animation B4: Pressure local to the leakage flow path at impeller outlet at 1.00Qn - This animation illustrates the pressure variation at the leakage flow region near the impeller outlet caused by the passing of an impeller blade.

Animation B5: Velocity vectors local to the leakage flow path at impeller outlet at 1.00Qn - This animation illustrates the change in magnitude and direction of the velocity at the leakage flow region near the impeller outlet caused by the passing of an impeller blade.

Animation B6: Pressure local to the cutwater at 0.25Qn - This animation illustrates of the variation in the pressure at the volute and impeller outlet local to the cutwater on a mid position axial plane. It also includes velocity vectors in the impeller in black showing the recirculation at the impeller outlet.

Animation B7: Velocity vectors local to the cutwater at 0.25Qn - This animation illustrates the variation in the magnitude and direction of the velocity at the impeller outlet and cutwater on a mid position axial plane.

Animation B8: Velocity vectors in the impeller at 0.25Qn - This animation illustrates the variation in the magnitude and direction of the velocity on a mid impeller passage plane.

Animation B9: Pressure local to the impeller at 0.25Qn - This animation illustrates the pressure variation on the impeller inner and outer surfaces as it passes the cutwater.

Animation B10: Pressure local to the leakage flow path at impeller outlet at 0.25Qn - This animation illustrates the pressure variation at the leakage flow region near the impeller outlet caused by the passing of an impeller blade. Note: blade is rotating into the screen.

Animation B11: Velocity vectors local to the leakage flow path at impeller outlet at 0.25Qn - This animation illustrates the change in magnitude and direction of the velocity at the leakage flow region near the impeller outlet caused by the passing of an impeller blade. Note: blade is rotating out of the screen.

These are mainly for illustrative purposes and will not be discussed further here.

6.2 Velocity Flow Results

A discussion of the results focusing on velocity distribution will be considered mainly in the impeller, although general comments will also include flow in the volute and in the suction inlet. For brevity the discussion will centre on the duty flow condition (1.00Qn) and the lowest flow condition (0.25Qn).

6.2.1 Suction Inlet

Although the suction inlet is not the focus of the investigation conducted, it has some importance as the effectiveness of the suction inlet design determines the quality of the flow entering the impeller eye. Ideally the flow in the impeller eye should show a constant flow velocity across the inlet area as it is considered that such an even distribution provides the best performance condition for the impeller. In practice there is always some variation in the velocity flow; however the suction inlet should be designed to minimise this. The flow approaching the impeller eye (and continuing into the impeller) can be seen for 1.00Qn in Figure 6.4. This indicates that the fluid is slower in the suction volute, but increases in velocity as it enters the impeller eye. It is important to note that the flow across the impeller eye section shown in Figure 6.4 is more or less constant. Plotting the axial component of the velocity (W) at the impeller eye provides clear indication of the pattern of the variation, Figure 6.5. It can be seen that the axial velocity component is larger on the right side of the inlet as opposed to the left. This is due to the pump inlet being to the right of the picture, with a greater

volume of flow (indicated by the streak lines) flowing directly into the impeller rather than round the suction inlet and in the far side of the impeller inlet. The high velocity values appear at the shroud side of the inlet and follow each of the impeller blades. However the scale in Figure 6.5 has been chosen to illustrate the velocity gradient at the impeller eye and the actual variations are not large. At the lowest flow condition (0.25Qn), the vector flow patterns into the impeller eye show significant differences (Figure 6.6). Most significantly there is a large recirculation region that encompasses half of the passageway width, has its centre in the suction inlet and which is drawn into the impeller eye at the shroud side of the impeller eye. This creates a relatively high velocity flow reversal at the shroud. This flow pattern is fairly typical for off design flow conditions. Makay and Szamody produced a good illustration of the recirculation at off design conditions in a number of their works (85), (87), which is reproduced in Figure 6.7. This clearly indicates the strong recirculation at the impeller inlet and how it is drawn in to the eye of the impeller. Makay and Szamody suggest that the minimum flow of a pump should be above the point at which such recirculations develop. Viewing the axial flow velocity at the impeller eye (Figure 6.8) indicates that the relative pattern is almost radial in nature with the right to left bias indicated at 1.00Qn not being present. The flow reversal is largest near the shroud with localised high regions correspond to the position of the leading edges of the blades at the shroud. It is noted that the reversed flow consistently encompasses 40% to 50% of the inlet area.

6.2.2 Impeller

In this section the relative velocity is examined as a function of the angular position within the impeller passageways. The results given in Figures 6.9 ands 6.10 are taken from a mid passage location using a grid aligned location that is equidistant from hub and shroud surfaces at all impeller radii. The velocity distribution is shown in three impeller passageways for a single moment in time, with the blade between passageways A and B being opposite the cutwater. Thus passageway A is approaching the cutwater, passageway B has just passed the cutwater and passageway C is midway between cutwater and splitter. As the blade to cutwater ratio is effectively 3:1, viewing these three passageways allows the periodic unsteadiness of the flow in the impeller to be

observed. Three radial locations are presented corresponding to r/R_2 = 0.80, 0.87 and 0.96, illustrating the development of the flow through the mid to latter stages of the impeller. The development of the flow is shown in terms of the radial velocity component (C_r), Figure 6.9, and the tangential component (C_t), Figure 6.10, for the duty flow condition (1.00Qn). The values have been shown positive for convenience, but they are actually negative according to the sign convention. The consistency between all three passageways irrespective of their position relative to the volute is apparent although there are some interesting differences. As the radii increases there are larger variations between the plots, yet they are still consistent. As expected the flow velocity is largely tangential with a radial component that is approximately half the tangential component, with the tangential component being more consistent over a larger area of the passage width.

At r/R_2=0.80 the radial velocity gradient increases from the pressure face to the suction face, with the radial component reaching its minimum in the passageway close to the pressure face. As the flow moves towards the outlet the peaks at the blade faces stay consistent, however the minimum moves across the passageway, with it being relatively central at r/R_2=0.87 and closer to the suction face at r/R_2=0.96. This movement of the minimum value changes the radial velocity gradient such that it has reversed from r/R_2=0.8 to r/R_2=0.96. The minimum value also drops as the flow moves towards the outlet, however it drops most significantly between r/R_2=0.87 and r/R_2=0.96 with the radial flow tending to zero or even reversing over a small region in the passageways.

The tangential component at r/R_2=0.80 is relatively constant from the pressure face to mid passage where the tangential velocity increases as it nears the suction face. As with the radial component as the flow moves towards the outlet the gradient changes such that at r/R2=0.96 the gradient is also reversed.

This reversal of radial and tangential velocity components as the flow passes through the impeller, has also been noted by Akhras et al (126) in their experimental tests, reproduced here in Figure 6.11. It should be noted that although the tangential component gradients reported by Akhras et al appear opposite in sign to those presented

here, because of the sign difference in Figure 6.10, they are of course the same. Additionally it should be noted that the impeller investigated by Akhras included seven blades.

The drop in the radial velocity mid passage is caused by the available flow area reduction at the cutwater region due to the tight cutwater clearance. It is interesting that at the duty flow condition this is actually causing the flow to reverse slightly as it nears the outlet. Taking a similar plot from a different arrangement that has a reduced impeller diameter (but with the same vane arrangement), Figure 6.12, this illustrates that the C_r does not drop to as low a level as with the tighter cutwater clearance. It is interesting to note that one feature of the increased cutwater clearance is to reduce the radial component of velocity on the suction side of the blade at all positions, and the radial velocity on the pressure face of the blade is of a similar value to that shown for the initial impeller diameter in Figure 6.9.

Identical radial sections for an identical blade position within the volute are reported for the 0.25Qn flow condition in Figure 6.13 (radial component) and Figure 6.14 (tangential component). The radial component results immediately identify a stall cell present in passage B. Strong flow is present at the suction side of the blade, with the stall cell being attached to the pressure side. At r/R_2=0.80 the actual region of recirculation is small across the passage, however the magnitude of the recirculating vector is strong at around 35% of the maximum outward radial component. The stall cell continues to grow at r/R_2=0.87, with the cell now encompassing a third of the impeller passage and the maximum recirculating radial component now being equal to the maximum outward component. At the outer radial station of r/R_2=0.96 the passage is progressing towards being completely stalled, with the cell now covering around 60% of the passage width and being substantially stronger than the flow in the outward direction. The following passage (passage A) shows a stalled region close to the suction side of the blade, whereas the proceeding passage (passage C) shows a recovery of flow patterns similar to those present at the duty flow condition. This can be confirmed by viewing the relative velocity vectors plotted on a mid plane between hub and shroud from impeller inlet to outlet. The tangential velocity data, Figure 6.14, confirms the presence of the

stall cell within passage B as it shows a reversal of the tangential component at the pressure side of the face. It is interesting to note that passage C also shows a recovery of the flow patterns that are present at 1.00Qn.

Pedersen et al (127 and 128) report a similar progression of stalled flow at low flow in an impeller passage, as part of their research into fluid flow in an impeller passage using both particle image velocimetry (PIV) and laser Dopper velocimetry (LDV). Interestingly, while the recirculation in the current work appears to be influenced by interaction with the volute, Pedersen et al's impeller discharges into a large body of water and so includes no such interaction. It is also interesting to note that Pedersen's leading edge impeller geometry utilises a cut-off design (the present impeller uses a tapered bull nose arrangement) that is likely to be less effective when the flow approaching the blade is not at the optimum angle. Figure 6.15 is a reproduction of the inlet stall cell and reversed flow at outlet discovered by Pedersen et al, while Figure 6.16 presents a velocity vector plot of the flow mid blade passage for the current work showing the similarity between the recirculation patterns. Pedersen et al report that their stalled cell is part of a "two channel" phenomenon consisting of alternate stalled and unstalled passages. This phenomenon is not evident in the current work due to the interaction between the impeller and volute and also due to the asymmetry of the volute; Pedersen et al do not have a volute collector in their experiments and thus no cutwater interactive effects. There does appear to be a consistent stalled and unstalled passage in the current results as the blade passes the cutwater. This is considered to be part of a "three channel" flow pattern caused by the 3:1 impeller to cutwater ratio.

Figure 6.17 presents the summation of the mass flow through a single impeller passage as it rotates through a full revolution for both 1.00Qn and 0.25Qn flow conditions. It can be seen that in the duty flow condition (1.00Qn) there is a pattern that repeats every half revolution that is obviously caused by interaction with the cutwater. It is worthwhile noting that there are slight differences between the two instances of the repeated pattern over the revolution. At the lower flow condition there is a similar repeated pattern but it is of such a low magnitude that it is almost insignificant.

An alternative and interesting presentation of the results can be achieved by following a single impeller passage over a number of impeller positions in order to study the variation in flow patterns, i.e. jet/wake flow effects. However this will not be pursued here.

6.2.3 Volute

A mean plane through the centre line of the pump and normal to the rotational axis is used in Figure 6.18 and 6.20 to illustrate the flow vectors in the volute at flowrates of 1.00Qn and 0.25Qn. The volute is designed to be an efficient collector of the fluid exiting the impeller and redirecting it to the discharge. Figure 6.18 shows that while the flow in the volute appears to guide the flow towards the outlet a strong recirculation zone appears in the discharge branch as it diverges and connects to the downstream pipework. The recirculation zone is present for all positions of the blade within the volute. When the discharge is viewed using streamlines (flow path of a particle of zero mass), Figure 6.19, there are actually two vortices located in line with one another in the rotational axis offset in the discharge branch towards the impeller centreline. The presence of the vortex in the discharge branch is noted by Stepanoff (95) who described the flow at sections past the volute cutwater as being "bent" or deflected by the cutwater from its direction as it leaves the impeller. This deflection causes a reversal of the radial component of flow starting a spiral flow along the volute discharge. The presence of dual vortices is caused by the double entry impeller arrangement. At the 0.25Qn flow condition the flow appears to be discharging without any of the spiral vortices mentioned above, see Figure 6.20, however taking a similar streamline plot, Figure 6.21 reveals that the vortices are actually placed in the middle of the discharge towards the outside wall of the branch.

6.2.4 Summary

A study of the velocity flow within the pump has been conducted to observe and discuss the patterns present in the CFD analysis. The velocity flow patterns in the volute region of the pump (both suction and discharge) are shown in pictorial form at both the duty

and the reduced flow condition. The duty flow condition results contain several features expected at this flow condition, while the reduced flow rate predicts significant recirculations in more than one location that are inline with information available in published data and in pump textbooks. The velocities present in the impeller have been discussed in some detail as this is a key region and the modelling of the flow patterns is of key importance especially at off design conditions. Two separate sources of laser-Doppler-velocimetery are used to compare general velocity trends and patterns in the impeller passageways, with emphasis placed on the impeller outlet. The trends presented by the CFD data compare favourably with the experimental information, with core features of the flow being displayed at both flow conditions. Thus it can be concluded that the flow patterns present in the CFD results are consistent with those found in actual operational pumps, both at the duty condition and at extreme off-design flow conditions.

6.3 Pressure Flow Results

When considering pressure pulsations it is important to understand both the general pressure variation in the pump at a specific moment in time and the variation in the pressure at specific locations over time. The following section attempts to provide information leading to such an understanding. In the first instance the pressure variation within the pump at specific moments in time is provided at multiple flow conditions. The second aspect requires an investigation in greater detail as the time history of the pressure variation of a specific point is complex and will vary dependent on the location in the pump and flow rate. The shape of the pressure variation is important as it can provide information concerning the flow mechanisms present at that pump location, which in turn can assist in understanding the pulsation levels present. To this end a full discussion of the time dependent pressure data for multiple pump locations is presented. The time history data is also converted into frequency spectra to note frequencies dominant in the pulsation and also to identify if any unusual frequencies are present that would be otherwise indistinguishable from the time history data.

6.3.1 Static Pressure Distribution

The static pressure was examined at 120 discrete points at equal intervals around the volute near to the casing wall. Figure 6.22 shows the static pressure distribution for three values of flow rate, with the angular position being set at zero at the cutwater and increasing in an anti-clockwise direction, for the first geometrical arrangement. It can be observed that the static pressure is relatively uniform at the higher flowrates, with the plots becoming less uniform as the flow rate moves away from the duty condition. As the impeller blade passes the cutwater/splitter at zero degrees and 180degrees positions respectively it causes a pressure loss (or shock loss) local to the cutwater/splitter region. This sharp reduction in pressure is caused by a local increase in velocity in the cutwater region of the volute as the impeller blade passes. As the cross sectional area of the volute increases and as the blade progresses, the high velocity fluid decelerates into the slow velocity fluid of the volute causing some recovery of pressure; where pressure recovery refers to the tendency of a decelerating fluid to convert kinetic energy to flow work (defined as pressure times the specific volume). A comparison of the pressure loss at 1.00Qn and 0.50Qn flows indicates that the shock loss increases as the flow rate decreases. The lowest flow also has a larger loss than the 1.00Qn, but not as large a loss as 0.50Qn. It is possible that the behaviour at the lowest flow rate could be less accurate due to inadequacies in the turbulence model when modelling the flow effects in the cutwater region. It is noted that the maximum static pressure increases as it nears the cutwater/splitter regions with the peak becoming higher as the flow rate decreases. Parrondo et al (34) have produced a similar plot for a centrifugal pump over a larger flow range from some experimental tests. This shows similar features to the CFD results relating to the increasing static pressure prior to the cutwater and the increase in the maximum as the flow rate reduces. It is acknowledged that in comparing the CFD graph with the published data there are significant differences, since the centrifugal pump examined by Parrondo et al is different from the CFD model in a number of crucial aspects (i.e. single volute, large cutwater clearance gap, volute cross-sectional shape). One additional issue is that Parrondo et al only monitored the pressure at 12 locations around the volute and so their plot lacks the definition that is shown in the CFD results. In a later paper Parrondo et al (35) increased the monitoring points to 36,

but the graphical information was poorer than shown in Figure 6.23. It is disappointing that they did not have more pressure tapping positions concentrated around the cutwater region to capture the interaction more closely.

Conventional pump design attempts to ensure that a pump is effectively "shockless" for its design condition (1.00Qn), although in practice this is impossible to achieve especially when there is a tight cutwater clearance. In this case, the CFD results in Figure 6.22 for 1.00Qn do show some shock loss as the impeller passes the splitter, albeit significantly less than that present at the lower flow rates. There is an additional complication here in that the "true" design flow for the oversized impeller is larger than the original value, which may contribute somewhat to the shock loss. The experimental tests were conducted at the original value and so this was replicated in the CFD analysis. This was discussed in Section 4.1.2.

General plots of the static pressure field through a mid plane of the impeller and the corresponding slice through the volute are shown in Figure 6.24 and 6.25 at two impeller blade positions but at two different flow rates. At the duty flow condition (Figure 6.24), the pressure distribution in each impeller passage is similar regardless of the position of the impeller blade relative to the cutwater (although only one diagram has been shown). At the lowest flow condition (0.25Qn, shown in Figure 6.25) when the blade is opposite the cutwater there is a marked difference in the pressure distributions in adjacent flow passages. In fact there is a reversal of the normal pressure differential across the blade. This is quite important as was pointed out in Chapter 3 in the context of fatigue failure.

6.3.2 Unsteady Pressure Distributions

The data set created from the twenty-seven transient analyses is significantly large and so to give detailed consideration to each facet of the results is not possible in the limited space available. Time dependent pressure pulsations have been extracted at the fifteen positions described in section 6.1.2, in the pump, eleven in the volute and leakage regions and four in the impeller. This reduces the amount of information to be

presented to a manageable amount, but still comprises a sizable data set (i.e. 405 graphs in total). Thus only selected, typical graphs from the data set will be reported here for discussion.

6.3.2.1 Time History Data

The majority of the data presented in this section will be taken from the first geometrical arrangement. The appropriate locations where the results are extracted have been collected together and reported in four pump regions; i.e. the leakage flow path, the volute, discharge and the impeller. In the figures that follow, a common scale is used across all three regions in order to assess the relative pulsation levels across all three regions. Each plot details a single impeller revolution, except Figure 6.29 where detailed information is provided for two blade passes. Angular position zero corresponds to the impeller blade being opposite the cutwater position.

Leakage Flow Path Region

The pressure fluctuations recorded in the leakage flow region for the 1.00Qn flow rate are presented in Figure 6.26. Data relating to C2 and C4 locations are provided as they are positioned either side of the circumferential cutwater position. The C2 position records a regular pulsation with respect to pulsation amplitude and time, with the pulsation frequency corresponding to blade rate. As the blade approaches the cutwater the pressure increases to its peak, as the blade moves past the pressure decreases to a minimum at the mid blade passage position. The C1 and C10 positions (not shown) are identical to the C2 location in form, which is unsurprising due to the symmetry of the model and the position of these points in advance of the cutwater. The C4 position shows a similar pulsation shape to that at C2, however the peak is reduced in size and an additional element has been added to the wave in the form of a sharp dip in pressure amplitude as the blade moved past the cutwater. This sharp drop in pressure is effectively the shock loss of the blade passing the cutwater being experienced in the leakage passageway. The time history at the C4 location includes this additional dip in pressure as it is situated circumferentially past the cutwater in the flow direction, whereas the C2 position is situated in advance of the cutwater. The C3 position (not

shown and situated at the cutwater) shows similar trends to that at C4, but to a lesser degree, i.e. the peak is not as reduced and the shock loss dip is not a large as at the C4 position.

At the lowest flow condition (0.25Qn, Figure 6.27) the pressure fluctuations are similar to those at 1.00Qn. The pulsation is of similar amplitude for the majority of the impeller revolution, however the last pulsation cycle is slightly larger than the others for both C2 and C4 locations (as the cutwater is approached). Interestingly the trends shown at C2 and C4 are very similar, with the sharp "shock loss" recorded at C4 for 1.00Qn being absent. However this lack of a spike could be due to a slower pressure recovery after the blade passes the cutwater at 0.25Qn than 1.00Qn. It should be noted that at locations C1 and C3 (not shown) the amplitudes and phases of the pulsation is similar to those present at C2 and C4 respectively. The pulsations at C10 (also not shown) are again similar to C2, however they show significantly more deviation than is present at 1.00Qn as the unsteady flow in the pump generates non-symmetrical flow patterns.

Volute Region

The pressure fluctuations at C6 and C8 recorded in the volute for 1.00Qn are presented in Figure 6.28. As with the leakage channels the pulsations are regular in phase and in amplitude, however the amplitudes are generally two or more times those recorded in the leakage region. Each of the volute channels show a peak as the blade passes the cutwater, however each show the sharp "shock loss" caused by the rotor/stator interaction and a rapid initial pressure recovery. The pressure then plateaus until the proceeding blade approaches and the pressure increases again. As C6's position is radially closer to the impeller tip than C8's (as a result of being closer to the cutwater) it experiences larger amplitudes of pulsation. It is interesting to note that the difference in pressure pulsation magnitude from C6 to C8 is largely due to the magnitude of the shock loss at the cutwater. A close inspection of the pulsations reveals that there is a slight phase difference, shown clearly in Figure 6.29, which essentially corresponds to the circumferential distance between C6 and C8.

At the lower flow rate 0.25Qn, Figure 6.30, the shape of the pressure pulsations is simpler than that recorded for the duty flow condition in that it consists mainly of peaks and troughs with no pressure plateau being in evidence. The C6 location experiences a lower average pressure level than the C8 position, however the pulsation amplitudes are around 10-15% higher than those at C8. The slight phase difference between the C6 and C8 locations mentioned above is more evident here. It appears as if the pulsation phase is approximately 20-30 degrees different from that recorded at 1.00Qn. To investigate this apparent phase change, the C6 data is plotted for all three flow rates on a single graph is shown in Figure 6.31. From the plot it is immediately apparent that the peak shown in 0.25Qn corresponds with the "pressure recovery" section of the 1.00Qn graph. This reason for this variation is due to the large stall cell discussed in Section 6.2. As noted in that section the majority of the flow from the impeller into the volute occurs towards the suction side of the blade passage, this causes the pressure in the volute to increase. As the blade progresses the stalled passage pulls fluid from the volute into the cell causing the pressure to drop until the following blade approaches.

Discharge Region

The pressure fluctuations at C9 and at the pump discharge (Cd) are presented in Figures 6.32 & 6.33. It should be noted that the location of C9 is as detailed in Section 4.2.1.1 and as such is not a true discharge position; it is closer to a central volute position. The large vortices in the discharge region, discussed in section 6.2.3, make it difficult to obtain realistic estimates of the pulsations at that region, as the flow in the vortices takes significantly longer to settle than in the rest of the computational model. Fortunately this is not important. The results taken at the discharge have been plotted for both 1.00Qn (Figure 6.32) and 0.25Qn (Figure 6.33)), and illustrate that when plotted at the same scale as other channel location, the pressure variation at the discharge is insignificant for both flow conditions. Therefore in order to estimate the variation of the pulsation as the fluid progresses towards the discharge, it is necessary to consider the pulsation at, at least one other location. Figure 6.32 for 1.00Qn illustrates that the pulsations at C9 are approximately a quarter of those recorded at the cutwater.

However, the graph does successfully record the location of the pulsation peaks, but does not show any "shock loss" being present at this location (as was noted at locations near the cutwater).

At the lower flow condition 0.25Qn (Figure 6.33) the pressure pulsation pattern recorded at C9 resembles that present at the C4 location for the same flow rate. Comparison of the pulsation with the 1.00Qn flow for the same location indicates that the maximum pulsation range over the single revolution has increased somewhat as the flow has been reduced. However, the pulsation values are closer to a third of those recorded at the cutwater for the same flow rate with the appropriate peaks and troughs being present.

An important point to notice is that the true pump discharge location registers little or no pressure pulsation regardless of flow rate. This is perhaps a little surprising as it was anticipated that the large pulsations evident in other locations of the pump would be present to some degree at the discharge. However, if the distance covered from C6 at the cutwater to C9 (top centre of volute) is considered, where the blade is still in close proximity to both C6 and C9 locations, the normalised pressure pulsation variation decreases by a factor of about 4 regardless of the flow rate for this arrangement. Although the distance from the cutwater to the pump discharge is similar in size to the above distance (C6 at cutwater to C9 splitter), the cross-sectional area is significantly larger (i.e. greater than the flow ratios) and the flow at the discharge is not continuing to be influenced by close proximity to the impeller blade. Therefore, it is perhaps less surprising that the pulsation decreases significantly at the pump discharge. Chapter 1 noted that the industry adopted guideline is a guarantee of less than 3% variation in the pump discharge pressure. For the tested pump this equates to a normalised pressure pulsation limit of 0.034 at the discharge. It is obvious that this value is significantly larger than the typical pulsation value recorded by the CFD analyses at the discharge location, which are typically an order of magnitude less than this value.

The negligible pulsation level at the discharge is likely affected to some degree by the selection of steady state boundary conditions during the transient analyses.

Unfortunately, as no pulsation measurement was taken at the discharge during the experimental tests it is not possible to make a direct comparison between the CFD and experimental results at this location. However, regardless, this work indicates that in practice monitoring the pulsation at the pump discharge may be a greater indication of the pulsation in the system rather than the pulsation within the pump. While it is certainly not appropriate to conclude that the pulsation measured at the discharge during experimental tests is due solely to the system and unaffected by the pump, the effect of the system on the pulsation at this location may be significantly larger than is generally anticipated. It is difficult to isolate a pump from the system surrounding it during experimental testing and to investigate the effect of the system on the pulsation would be expensive in terms of time and resource. Guelich and Bolleter (90) provide some indication concerning the important influence that a system can have on pressure pulsations in their discussion on pressure pulsations in centrifugal pumps. They note that the system can have a great influence on the pressure pulsations measured and reference work by Höller (129), which examined the differences in pulsations at the pump inlet due to upstream system components via a simple test arrangement. Figure 6.34 reproduces the diagram by Höller demonstrating the dramatic change in pulsations present at the pump discharge due to upstream system components. Guelich and Bolleter observe that the variation of pulsation at a particular flow rate can exceed 100%. Figure 6.35 reproduces a figure from Guelich and Bolleter that presents the broadband pressure pulsations measured at the discharge of a boiler feed pump in two different systems. These graphs indicate that the magnitude of the pulsation at specific frequencies changes depending on the test loop arrangement. They conclude in their paper that the influence of the system is significantly greater than the influence of temperature and speed, and acts in an unpredictable manner.

Therefore it is worth highlighting that measuring pressure pulsations at the pump discharge may not be indicative of the pulsations within the pump. Additionally any manufacturer quoted pressure pulsation at discharge will certainly not be comparable to a recorded pulsation measured at the discharge at site. As an alternative, it would be a relatively simple matter for manufacturers to provide a pressure tapping at the C9 location to elucidate this matter once the pump is installed in the actual system.

Impeller Region

The pressure fluctuations close to the trailing edge of the impeller are reported in Figures 6.36 and 6.37. These are reported at three locations namely, the pressure side of the blade at the trailing edge (Blade P), on the shroud above the blade in the snubber gap (Shroud B) and mid way between blades on the shroud in the snubber gap (Shroud M). It should be noted that all of these locations are rotating with the impeller.

The blade plot for 1.00Qn, Figure 6.36 shows six peaks corresponding to the six impeller vanes, with two peaks corresponding to the blade passing the splitter (at 180degrees) and the blade passing the cutwater (zero/360degrees). It is interesting to note that although the splitter and cutwater have been designed to be as alike as possible, the pulsation at the splitter is significantly larger due to the shock loss. It is worth noting that, as in the volute cutwater positions, the shock loss contributes significantly to the overall pulsations amplitude over a single impeller revolution. The peaks away from these positions are actually pulsations that are experienced by the impeller as other blades pass the cutwater/splitter. The largest peak occurring as the blade passes the cutwater is approximately double that experienced at the cutwater volute region at the same flow rate. At the lower flow, Figure 6.37 the main features of the pulsation are similar with the largest peaks again appearing at the splitter and cutwater. The amplitude of the peak at the splitter is approximately 1.5 times larger than at the duty flow condition. The additional peaks are less defined and become merged with the pressure build up as the blade approaches the cutwater/splitter.

For the shroud at 1.00Qn, Figure 6.36, the two monitoring points show good correlation, excepting a 60 degree region after the blade passes the cutwater/splitter. This excellent correlation is interesting as the monitoring points are 30 degrees apart circumferentially, indicating that away from the cutwater/splitter the pressure on the shroud is similar across the passage width. In the 60 degree region following the blade passing the splitter it is apparent that the "mid passage" location (Shroud M) is 60 degrees out of phase with the "above blade" position (Shroud B), i.e. when the following blade has moved opposite the cutwater. This is most obvious for the blade passing the splitter (180 degrees), where the trough for the shroud position above the

blade is at 190 degrees, but the corresponding trough appears at 250 degrees for the shroud mid passage position. The phase difference is explicable in terms of the sixty degree passageways, although the location points are 30 degrees apart. The largest peak and trough for the two shroud positions is the same over a single rotation. At the lower flow condition, Figure 6.37 there is little correlation between the pressures at the two monitoring points except over a 60 degree region as the leading blade approaches the cutwater. Again there is a 60 degree phase difference between the "mid passage" and "above blade" positions, with the phase difference being apparent at both cutwater and splitter as the pressure drop is significantly larger than that recorded at 1.00Qn. This large pressure drop is due to the stall cell that dominates the passageway at 0.25Qn when the trailing blade is opposite the cutwater/splitter (discussed in Section 6.2.2).

6.3.2.2 Frequency Data

The time history data for all arrangements can be converted into frequency spectra using fast Fourier transforms (FFT), producing nearly four hundred frequency spectra for investigation. Although all of these have been plotted and examined only the first numerical arrangement is used to illustrate and discuss the spectra, with sample plots showing spectra at important locations in the pump. The analysis reported results for positions of the impeller 2.5 degrees apart for a single impeller rotation; this corresponds to approximately 144 items of information. The frequency spectra produced from the time history data tends to be somewhat coarse, but the major frequency components of the signal are clearly visible. In plotting the frequency spectra, identical scales have been used for all pump locations.

Leakage Flow Path: Figures 6.38 & 6.39 indicate frequency data for positions C2 and C4, for all three flow rates. At location C2, Figure 6.38, indicates that the dominant frequency is at 140Hz, which corresponds to the blade passing frequency (i.e. 1400RPM and 6 blades). Two or three harmonics of this frequency are visible and diminish as the harmonics progress higher in frequency. There is little difference between the amplitude at the blade rate frequency at the various flow rates, however the 0.50Qn condition appears to produce slightly less pulsation amplitude at this frequency than at

1.00Qn or 0.25Qn. At C4, Figure 6.39, shows similar trends to those discussed at C2 although the pulsation amplitudes are slightly larger.

Volute: Figures 6.40, 6.41 and 6.42 provides frequency information for positions C6, C8 and C9 for all three flow rates. At C6, Figure 6.40, there is a strong blade rate frequency of approximately twice the magnitude of that found in the leakage flow location. The lower flows have considerably higher amplitudes at the blade rate; however this is not always the case for subsequent harmonics. Higher harmonics are present and diminish in size as the frequency increases. At C8, Figure 6.41, the blade rate again dominates, with 0.50Qn having the largest amplitude. 0.25Qn has slightly smaller amplitude at both blade rate and the second harmonic. It is noted that C8 shows some low frequency activity at the lowest flow rate. The C9 location, Figure 6.42, shows lower pulsation amplitudes than the other volute monitoring positions, with the pulsation being very similar at blade rate for all flows.

Impeller: The spectra detailing the frequencies present in the pressure fluctuation at the pressure face of the impeller blade is shown in Figure 6.43 for three flow rates. The dominant frequency at all flow rates is at 49Hz, which is approximately twice the running speed (23.33Hz). This corresponds with the blade passing the two stationary cutwaters (cutwater and splitter) during one revolution. The spectra also shows numerous harmonic frequencies with diminishing amplitudes. The lower flow conditions show a significant increase in amplitude at the dominant frequency equal to approximately three times that present at 1.00Qn. Again diminishing harmonics are present. The lack of definition in the frequency plots can make it difficult to determine actual differences in the frequencies, excepting that the lower flows tend to have higher amplitude of harmonics than at 1.00Qn. The shroud spectra, shown in Figure 6.44, illustrates this, where the frequency of the largest amplitude varies depending on the flow rate, i.e. 1.00Qn = 46.4Hz, 0.50Qn = 40.86 and 0.25Qn = 49.28Hz. The shroud spectrum is very similar to the blade spectra in both frequency and amplitude. It can be seen that, for both blade and shroud positions, the 0.50Qn graph shows better definition since a larger amount of data was available for the generation of the spectra.

Low Frequency

When examining the numerous frequency spectra it was observed that in some cases a relatively large, low frequency amplitude was present close to running speed for the lowest flow condition. Figure 6.45 shows the frequency spectra at the impeller for the third arrangement for location C6, where the low frequency component is clearly visible. The third arrangement was selected for investigation as the low frequency amplitude is of a significant size in comparison to the other frequencies present. The data at the C6 location indicate that this frequency is at 19.84Hz, which is less than the rotational frequency of 23.3Hz. Due to the limited number of points available from the Fourier transform for the spectra, it is difficult to confirm the exact position of the low frequency amplitude. In order to extend the data set, it was decided to continue the third arrangement analysis at the low flow condition. This proved difficult due to the instability of the analysis at the original time step, therefore the time step was reduced to a quarter of the original value with transient results files continuing to be produced after every second iteration loop. This increased the number data items for the Fourier transform by a factor of four for a single impeller revolution. The extended simulation took two weeks of continuous analysis to complete and produced 576 transient results files (more than 40Gb). The extended analysis data was taken during the eighth revolution of the impeller. An identical process was used to collect the pressure data for the extended analysis, with the time histories also being transformed into frequency spectra. Monitoring all locations at which the low frequency phenomenon had been identified, it was observed that the position of the low frequency peak had moved slightly to the right and now was positioned at the running speed frequency (23.3Hz). Figure 6.46 shows the change in the spectra at location C6 for the extended analysis. For this location, the strongest frequency continues to be the blade rate frequency with the amplitude being similar for the earlier and the extended analyses. The low frequency pulsation has reduced significantly in magnitude in addition to increasing in frequency. It is concluded that unsteady periodic convergence not being achieved at certain locations around the pump in the original analysis at the 0.25Qn flow rate. This introduced a relatively strong low frequency component equal to the rotational frequency that gradually reduces as the analysis continues.

The time frame for the present work did not allow for the low flow rate to be run for eight revolutions before results could be gained. A comparison of the time histories for locations C6 using the original data and the extended analysis is shown in Figure 6.47. This indicates that there is a great deal of similarity between the actual peak to peak pulsations for the two analyses. Therefore, while the RMS pulsations are used for comparisons with the experimental tests in section 6.4, peak to peak pulsation values will be used in Chapter 7.

6.3.3 Summary

While the overall pressure pulsation magnitude is of prime importance in this project, the actual time variation of the pressure that forms the pulsation is also of interest. The trends in the static pressure variation around the volute have been shown to contain features in agreement with published data, with the significance of the instantaneous pressure differentials within the pump also being highlighted. The pressure pulsations present at various locations around the pump have been compared and the pulsations on the impeller blade have been recorded as being the largest. Other locations of significant pulsation are at the shroud positions and at the volute cutwater. The importance of the shock loss caused by the impeller blade passing the cutwater has been noted because of the influence this can often have on the overall pulsation amplitude. This effect also contributes to the increase in pulsation amplitudes since the shock loss (in addition to the general pressure variation) increases as the flow decreases. The frequency data generated from the time histories confirm the dominance of the blade rate frequency and harmonics. However this has also highlighted a frequency lower than the blade rate that is strongest at the 0.25Qn. Further investigations were conducted and the low frequency was identified as being caused by a delayed convergence in the analyses at specific locations due to the reduced flow level.

6.4 Comparison with Experimental Results

The experimental investigation relating to pressure pulsations in a centrifugal pump performed at Weir Pumps facilities prior to this current work is detailed in Chapter 4. Although there are difficulties in interpreting the experimental measurements collected by the test work, the data available from the experimentation is the closest existing pressure measurements to those being analysed by CFD. Thus it is prudent to attempt to compare the CFD analysis data with this experimental data.

During the set up of the computational analyses a decision was made to set a CFD arrangement geometrically identical to experimental test 1, in order to facilitate the comparison between the experimental data and the CFD results. This arrangement had the tightest clearances and the experimental data suggested that it would produce some of the highest pressure pulsations. Additionally test 1 was believed to have been repeated due to difficulties during the initial test. This would have provided a partial set of data from the initial test and a full set of data for the second test for the comparison. To this end the CFD arrangement was analysed at five flow rates 1.25Qn, 1.00Qn, 0.75Qn, 0.50Qn and 0.25Qn (the same as the experimental tests) instead of the usual three flow rates (1.00Qn, 0.50Qn and 0.25Qn), in order to provide a fuller comparison with the experimental data. As mentioned in Section 4.2.3, it transpired that the repeated experimental test had been mislabelled and in fact repeated a different experimental test arrangement to that indicated in the experimental test documentation. Unfortunately, this was only discovered after the CFD analyses had been completed. Fortunately, there are a number of other arrangements that are geometrically similar (albeit not identical) to the experimental tests. To compensate, two comparisons between the numerical and experimental results are made. Table 6.3 provides details of the experimental and CFD arrangements that are compared; these are termed comparisons A and B respectively. The CFD analyses for these arrangements were conducted for three flow rates as time and facility restraints prevented additional transient analyses from being conducted.

The table indicates where there are geometric differences between the tests compared. This is unavoidable as explained above. Nevertheless, an effort has been made to ensure that the major components (cutwater gap and blade arrangement) are the same. It has not been possible to ensure that the sidewall gap is consistent in either comparison between the experimental tests and the CFD analysis. While it would be possible to conduct further comparisons but the parameters are such that these are unlikely to add much in the way of additional information. This is partly due to a number of the experiments having no snubber gap (not included as part of the scope of this project due to a change in practice at WPL) and partly due to the CFD analyses incorporating a 15 degree vane stagger arrangement. The situation is not assisted by the experimental work only involving a limited number of tests with certain geometrical parameters, i.e. only two tests are performed with tight sidewall clearances and the 30 degree vane stagger is only investigated at a single cutwater gap. Before progressing to the comparison of the experimental tests and CFD analyses there are some factors that require consideration.

Comparisons between the experimental and CFD data will be discussed using three graphs, one for each major monitoring location in the pump, i.e. leakage flow region, volute and impeller. Selected monitoring points are included and are consistent for both comparisons. For each pump area the selected positions are

Leakage Path:	C2, C4 and C10
Volute:	C6, C8 and C9
Impeller:	Shroud

It should also be noted that the CFD analysis number corresponds to the CFD arrangement number mentioned previously.

6.4.1 Comparison A: Experiment 18 with CFD Analysis 5

Leakage Region (Figure 6.48): The first point to note here is that the experimental results for channel 10 are unusual and quite different from the pattern observed in other

tests. Normally channel 10 and channel 2 give similar results, as expected, being at similar positions on either side of the pump leakage flow path region and being in advance of the cutwater circumferential location. Thus it would have been expected that channel 10 results should be close to channel 2. Bearing this in mind, the CFD normalised RMS pressure pulsations are very similar in magnitude and follow the trend of the experiments where the pulsations are low at 1.00Qn and high at 0.25Qn. Results at C2/Channel 2 show best agreement with the results being relatively close at all flows. The experimental results are almost linear but the CFD results are not due to a relatively low pulsation value at the 0.50Qn flow rate. At C4, the CFD results predict larger pulsations relative to C2 and indeed a larger pulsation than the corresponding experimental results, with the largest difference being at 1.00Qn. The experimental results for channel 10 are suspect as discussed above being higher than the channel 2 results with which it would be expected to be comparable. However it should be borne in mind that the pressure pulsation in the leakage area are lower than at other locations of interest in the pump.

Volute Region (Figure 6.49): The CFD results predict a RMS normalised pressure pulsations of a similar magnitude to that found by experiment and are generally greater in magnitude than that present in the leakage flow path. At C6, C8 and C9 the pulsations levels are also correctly rated in relation to the experiments and to one another, with the increasing pulsation trend as the flow rate decreases present. There is remarkable good agreement between channels 8 and 9 and CFD locations C8 and C9, with a slight divergence between C8/channel 8 at the lowest flow. There is a larger difference between C6/channel 6 with the greatest deviation at 0.50Qn. This is likely to be exacerbated due to C6/channel 6's close proximity to the cutwater.

Impeller Region (Figure 6.50): The numerically predicted shroud pulsation follows the experimental test data remarkably well, showing the same levels of pulsation (slightly larger than at the cutwater locations of C6 and C8). Again the CFD results predict the same trend of pulsations increasing as the flow rate decreases. The pulsation appears to be marginally under predicted compared with the experiments at all flows.

6.4.2 Comparison B: Experiment 9 with CFD Analysis 3

Leakage Flow Path (Figure 6.51): The pulsation levels predicted from the CFD analyses are of a similar order to that found by experiment. As for the experiments, the analyses predict that position C4 has larger RMS pulsations than those at C2 and C10 (which are of a similar lesser level). The CFD results for C4 also show an increase in pulsation as the flow rate reduces, although the results at C2 and C10 do not. The C2 and C10 results agree broadly with the experiments for 1.00Qn and 0.25Qn but the experiments show a peak at 0.50Qn whereas the CFD results show a minimum. It is noted that the geometry in the leakage flow and snubber regions differ from those in the experimental test and this undoubtedly contributes to the differences observed. The differences are more noticeable as the pressure pulsation scale is larger, but the pressure pulsation values are relatively small in comparison to other areas of the pump.

Volute Region (Figure 6.52): The CFD results again predict RMS-pulsation values of similar magnitude as the experiments with each location showing similar trends to those found using experimental means. Pulsations at C6/channel 6 are almost identical at 1.00Qn, but the CFD does not show the same rate of increase as the flow rate reduces, with considerable divergence at 0.25Qn. The C8/channel 8 location comparison shows good agreement at all flows, with their being some divergence between the CFD and experimental results as the flow rate reduces. The C9/channel 9 locations are in excellent agreement at all flow rates although the magnitudes are small.

Impeller Region (Figure 6.53): The CFD is in excellent agreement with the experimental normalised RMS pulsations at the impeller shroud at all flow conditions. The pulsations appear to be slightly under predicted compared with the experiments at the higher flow rates.

6.4.3 Summary

At the majority of pump locations the CFD analyses show reasonably good agreement with the experimental data. The magnitude of the RMS normalised pulsations are of similar order at most locations, with the relative pulsation magnitudes at different locations within the pump also being well predicted. Unsurprisingly, the largest deviation between the CFD results and the experimental data tends to occur at the lowest flow level, although even here some are remarkably good particularly the large pulsations at the volute cutwater.

A number of the deviations between the CFD and experimental test may be attributable to the geometrical difference between the two arrangements. This is especially relevant to pulsation differences in the leakage flow region as this region is in close proximity to the geometric differences in both comparisons. At the volute locations, those closest to the cutwater tip (C6) show some deviation, however this settles quickly as C8 shows better agreement while only being 50mm from the cutwater tip. It is noted that the comparison of C6/Channel 6's results is better in comparison A than in comparison B. This is likely to be due to the staggered vane arrangement present in comparison A as this appears to not produce as sharp an increase in pressure pulsations as the flow rate decreases.

It is interesting to note that the pulsation levels at all comparable locations are higher for experimental test 9 (comparison B) relative to test 18 (comparison A). The CFD results agree with this, with the CFD results from analysis 3 being larger than those from analysis 5 at the respective locations. Considering the difficulties in both performing the experiments and analysing them and taking account of the geometric differences between the CFD models and the experiments, it is conclude that the CFD is in reasonably good agreement overall with the experiments and that the analyses may be used with some confidence to capture the overall change in pressure pulsation levels for different geometrical arrangements.

6.5 Chapter Summary

This chapter has provided a detailed investigation of the flow in selected arrangements analysed as part of the project and has compared these results both with published experimental data and with the experimental data discussed in detail in Chapter 4. The salient points emerging are summarised as follows:

- Velocity flow patterns generated by the numerical analysis identify features of the flow that agree with those in published literature. Detailed investigations of the velocity components at the impeller outlet have shown these to be comparable in shape to those published in two independent external experimental tests.
- The shape of the pressure distribution around the volute has been discussed with the loss and recovery features and their contribution to the overall pressure pulsation being highlighted.
- Similarly, the pressure field in the volute has been discussed with the loss and recovery features being identified and their contribution to the pressure pulsation highlighted.
- The regions in the pump experiencing the largest pressure pulsations are located at the impeller outlet, with large pulsations also being present in the volute at positions in close proximity to the cutwater or splitter.
- It has been found that the pressure pulsations at the pump discharge are largely unrelated to pulsations within the pump, but are probably more dependent on the system in which the pump is operating. The C9 location gives a better indication of pulsations present in the pump and so would provide a useful monitoring position for actual pumps installed in real systems.
- The RMS pulsations predicted by the CFD analyses show reasonable agreement with the experimental data. The CFD results predict the relative pulsations at different pump locations reasonably well.
- Comparisons between the CFD and the experiments at the duty flow condition are generally better that those at reduced flows, with the greatest deviation appearing at the lowest flow condition.

6.6 Tables

Arrangement/ Analysis	Cutwater Gap	Snubber Gap	Sidewall Clearance	Vane Arrangement
1	3.83%	0.27%	100%	Inline
3	3.83%	1.64%	25%	30 Degrees
5	6.00%	1.10%	25%	Inline

Table 6.1: Geometrical arrangement of the analyses discussed in this chapter.

C6 Location	1.00Qn	0.50Qn	0.25Qn
Position A	0.295	0.411	0.422
Position B	0.287	0.336	0.348
Position C	0.259	0.263	0.283

Table 6.2: Comparison of peak-to-peak normalised pressure pulsations for the C6 location for the first arrangement from the CFD analyses

	Type	Test No.	Cutwater @Blade	Cutwater @Shroud	Snubber Gap	Sidewall Gap	Blade Arrangement
A	Experimental	18	3.83%	3.83%	1.64%	100%	Stagger (30^o)
	CFD	3	3.83%	3.83%	1.64%	25%	Stagger (30^o)
B	Experimental	9	6.00%	3.83%	0.27%	100%	Inline (0^o)
	CFD	5	6.00%	3.83%	1.10%	25%	Inline (0^o)

Table 6.3: Similar experimental and CFD arrangements to be compared

6.7 Figures

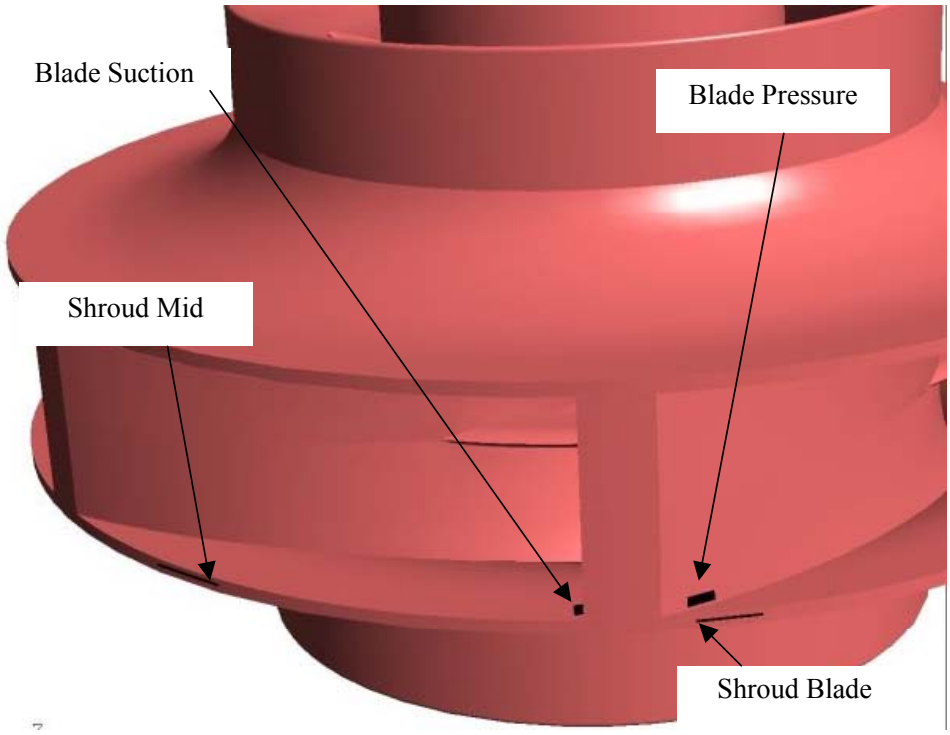

Figure 6.1: Location of blade and shroud monitoring positions

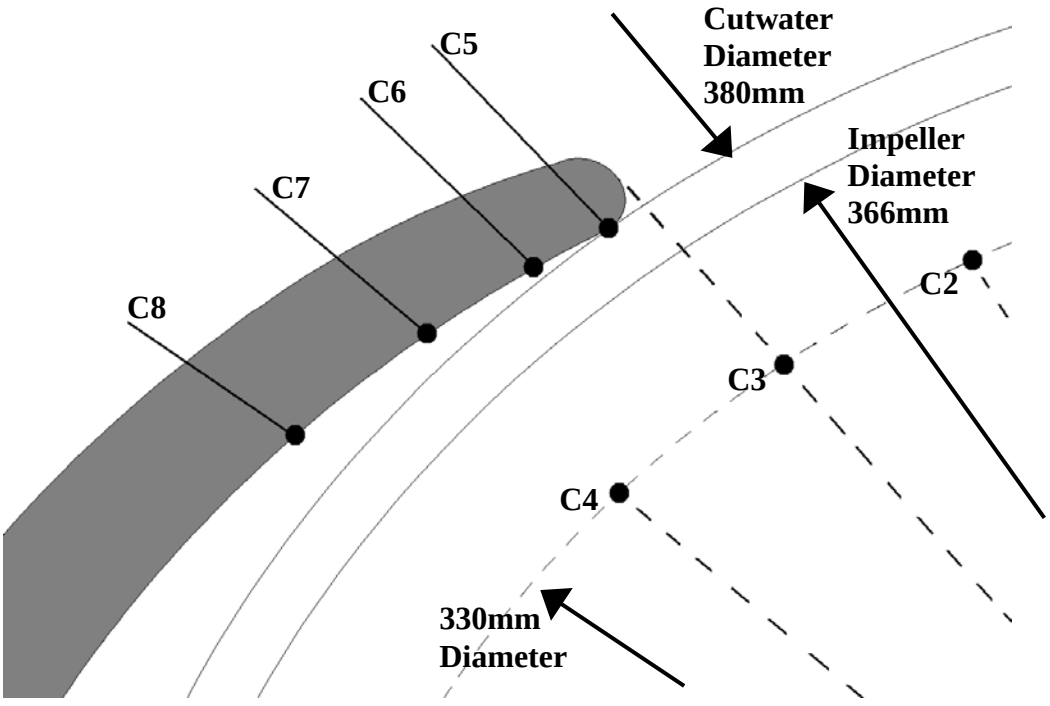

Figure 6.2: Sketch of cutwater test monitoring locations

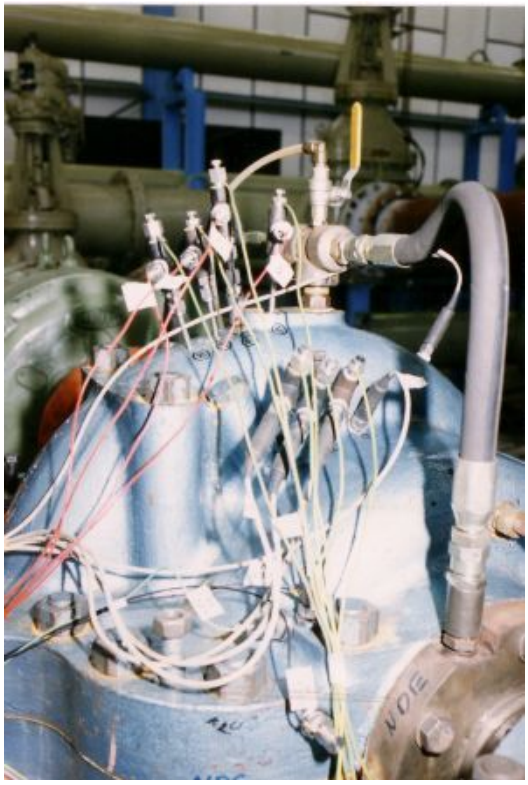

Figure 6.3: Photograph of top casing of test pump showing external location of pressure tapping

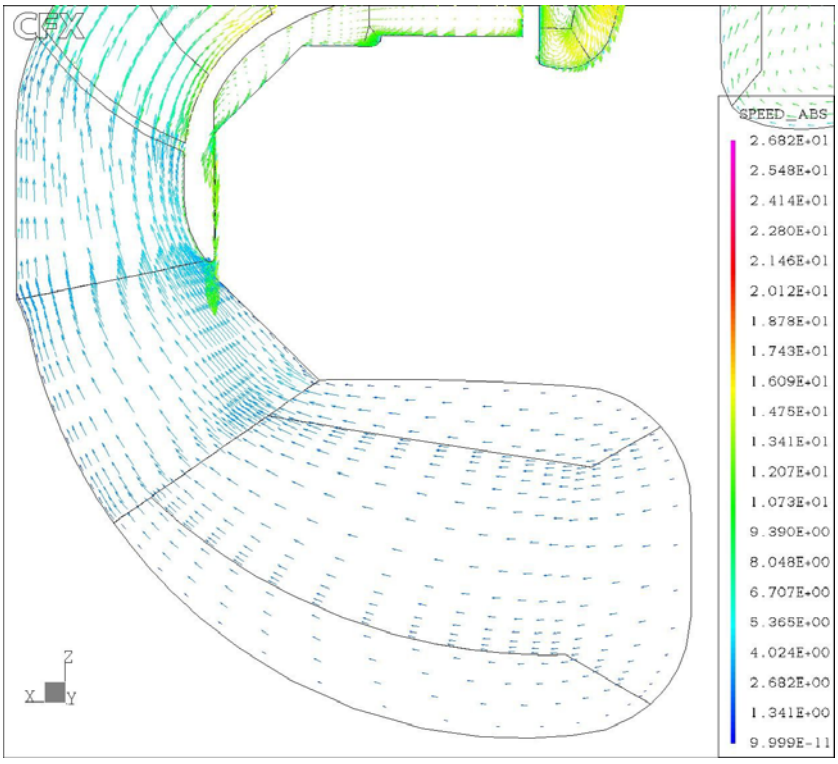

Figure 6.4: Plot of velocity vectors entering impeller eye at 1.00Qn

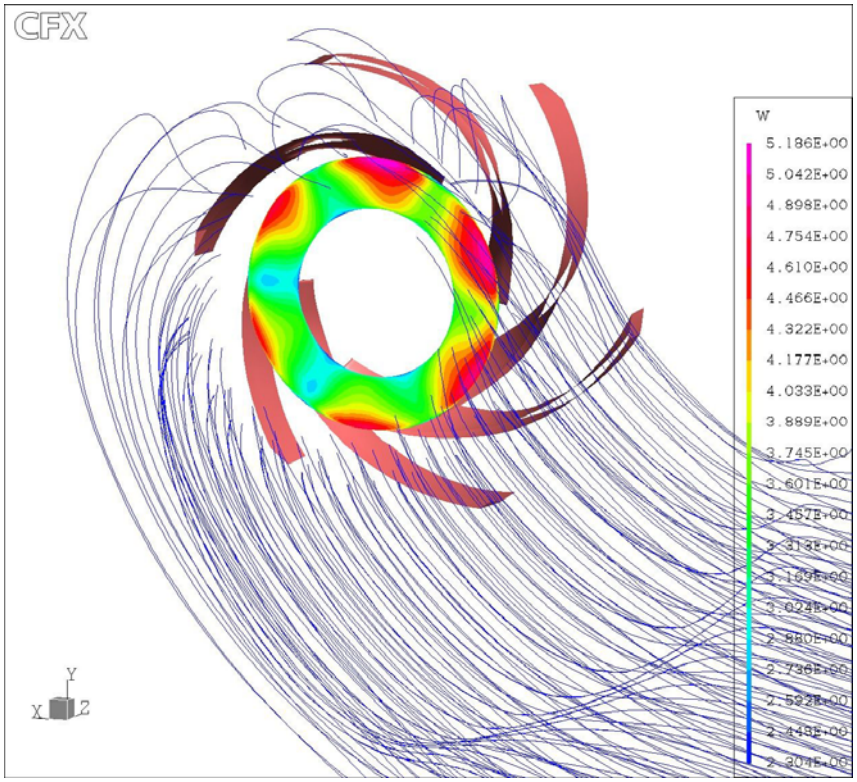

Figure 6.5: Plot of axial velocity component (W) at impeller eye with streak lines entering impeller eye at 1.00Qn

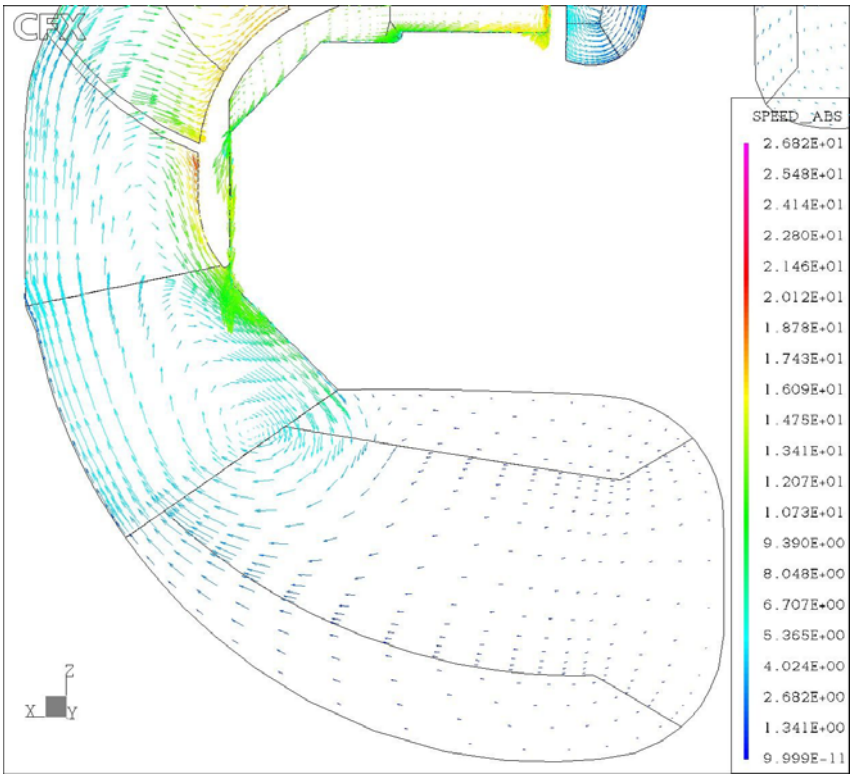

Figure 6.6: Plot of velocity vectors entering impeller eye at 0.25Qn with recirculation in suction inlet

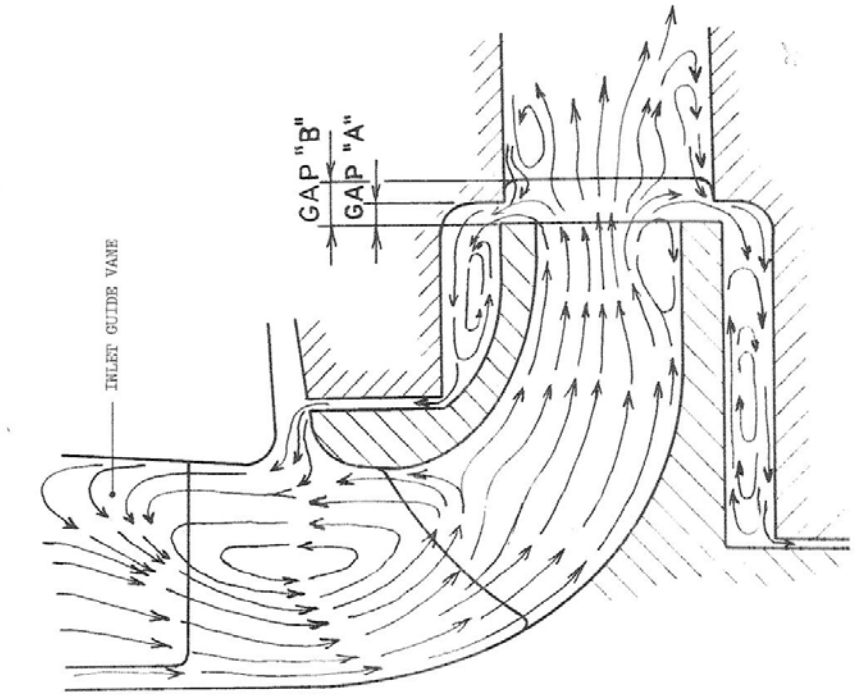

Figure 6.7: Secondary Flow Pattern in and around a pump impeller stage at off-design flow operation (from Makay & Szamody (85))

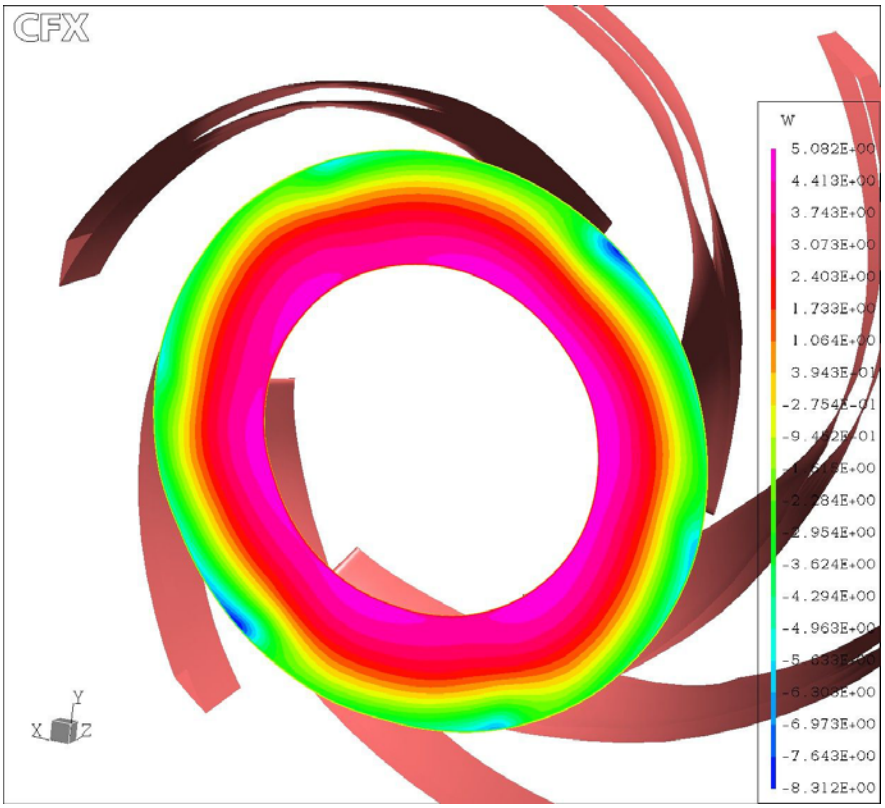

Figure 6.8: Plot of axial velocity component (W) at impeller eye at 0.25Qn

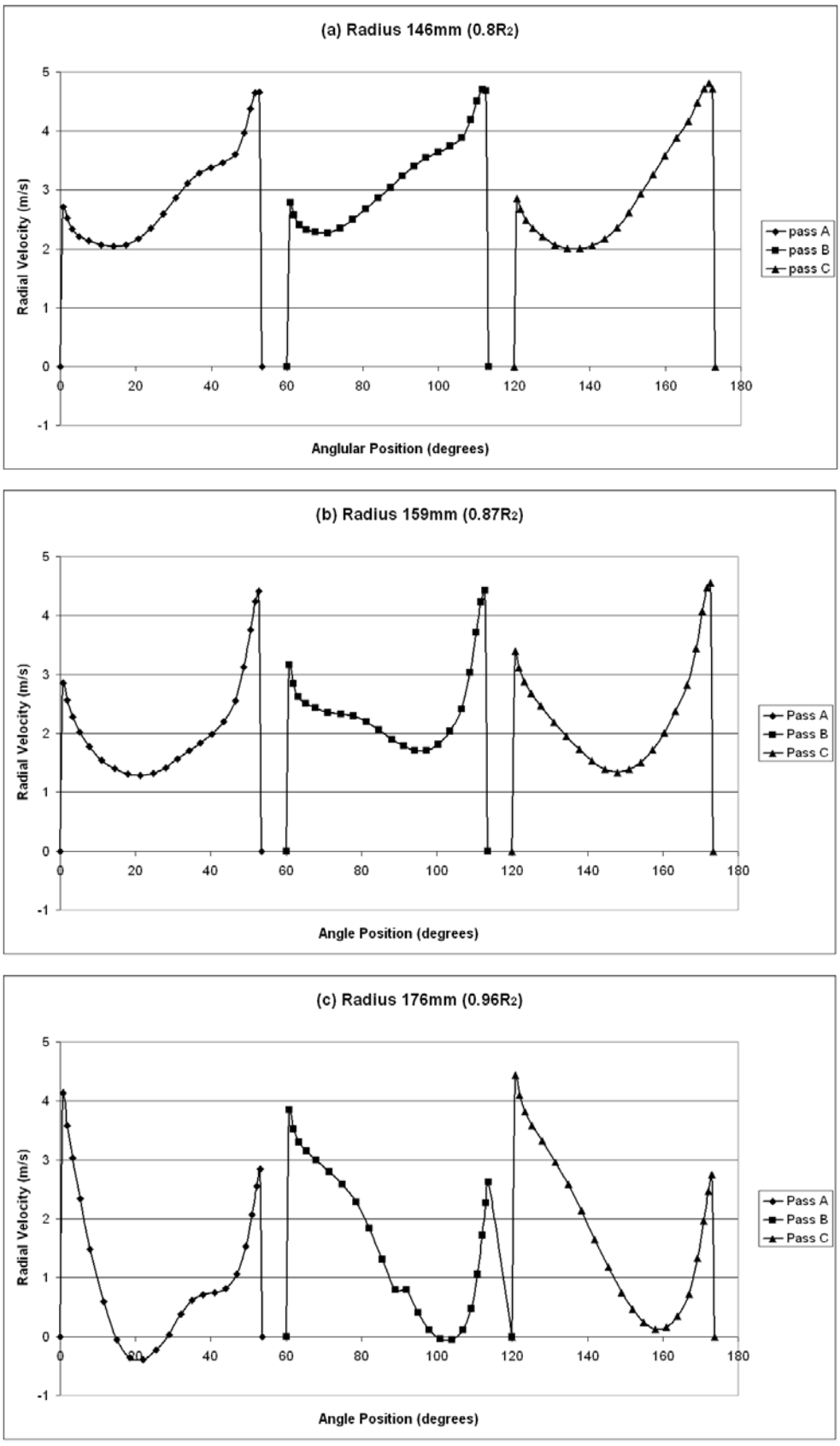

Figure 6.9: Radial Velocity at the mid plane of the impeller through 3 impeller passageways at different radii for the first arrangement at 1.00Qn

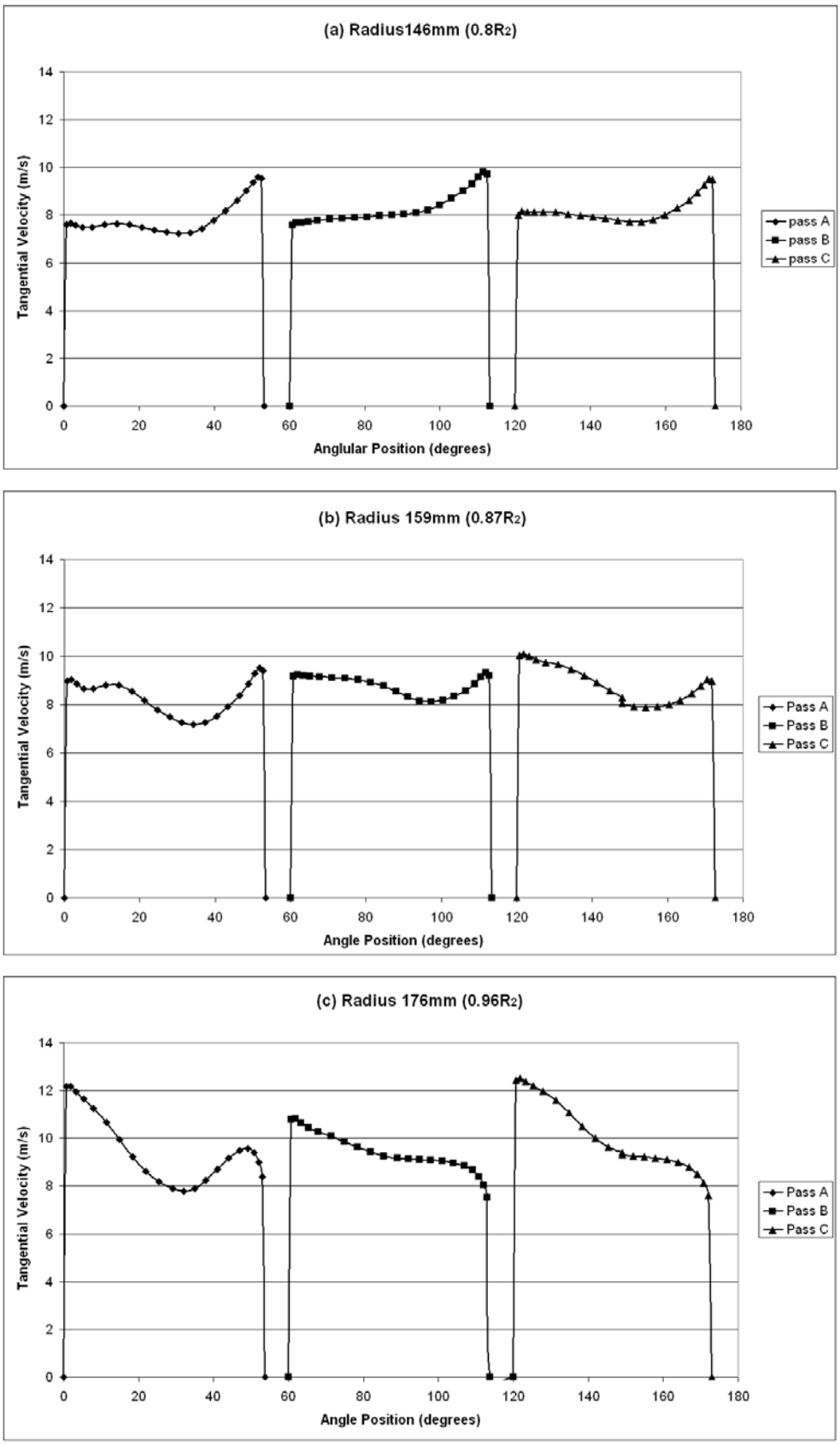

Figure 6.10: Tangential Velocity at the mid plane of the impeller through 3 impeller passageways at different radii for the first arrangement at 1.00Qn

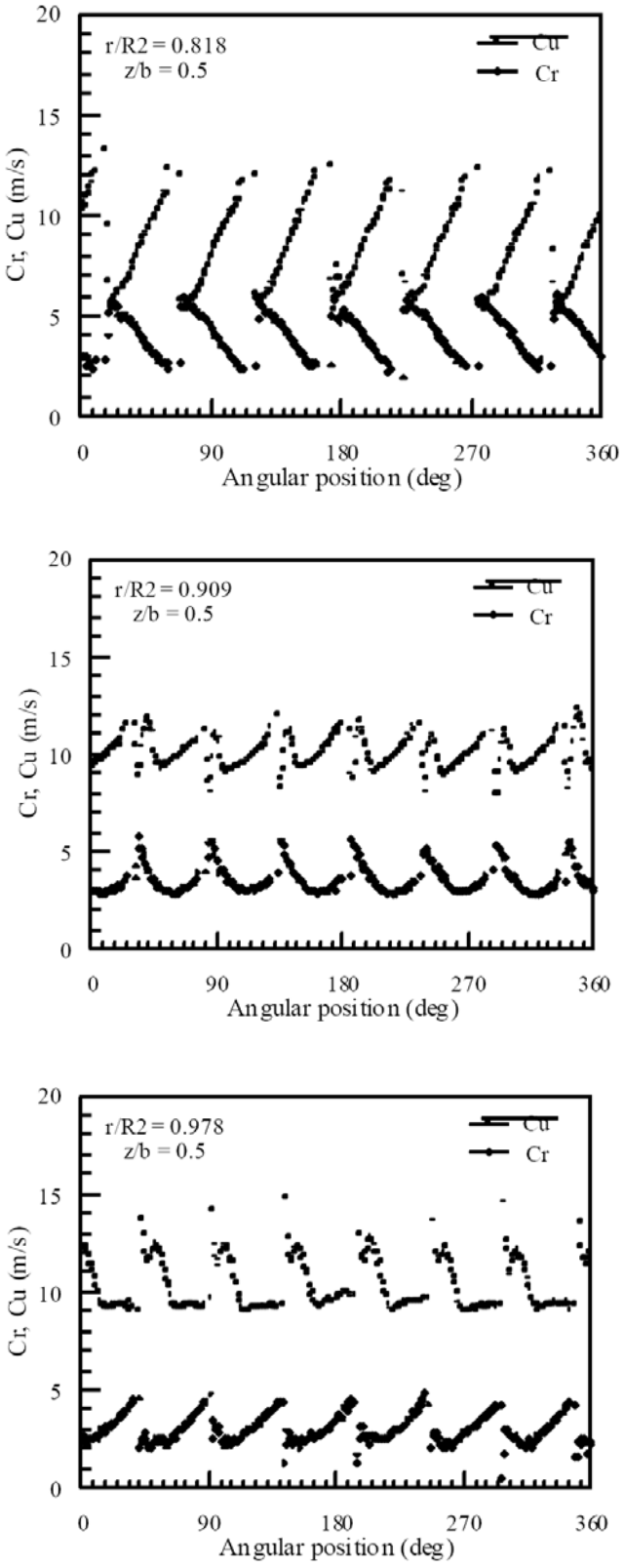

Figure 6.11: Fluctuating Velocity at the impeller channels (copied and re-arranged from Akhras et al (126))

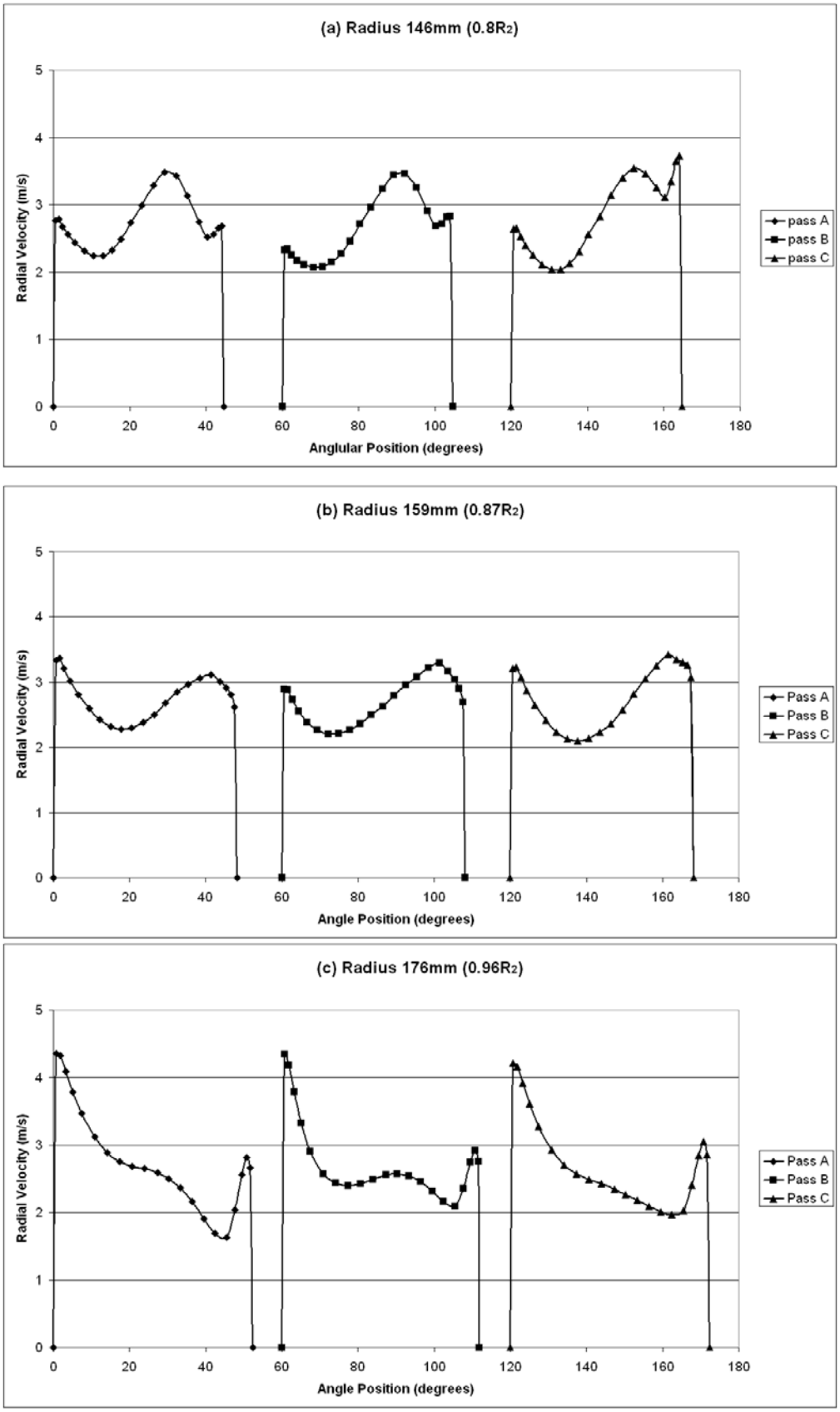

Figure 6.12: Radial Velocity at the mid plane of the impeller through 3 impeller passageways at different radii for the third arrangement at 1.00Qn

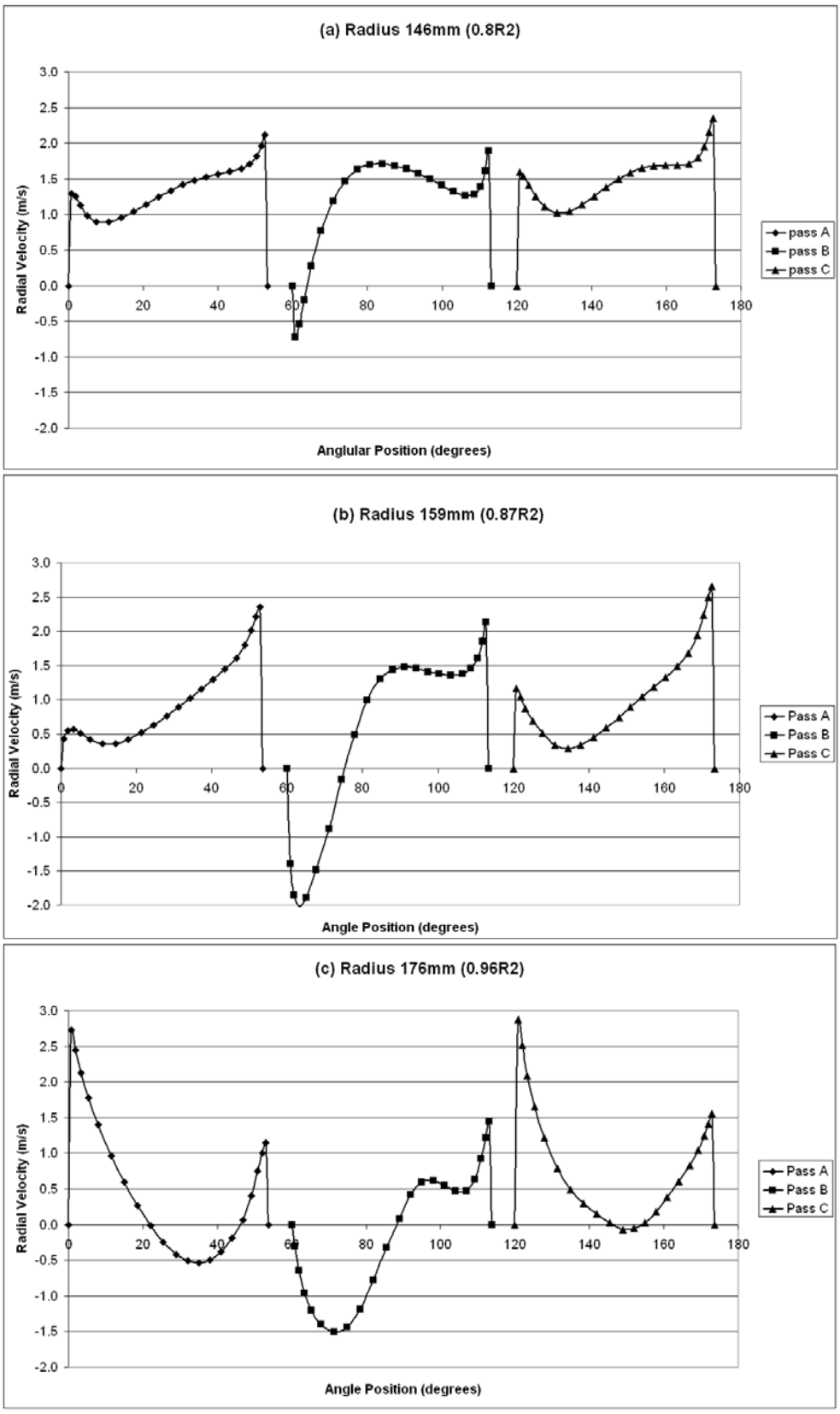

Figure 6.13: Radial Velocity at the mid plane of the impeller through 3 impeller passageways at different radii for the first arrangement at 0.25Qn

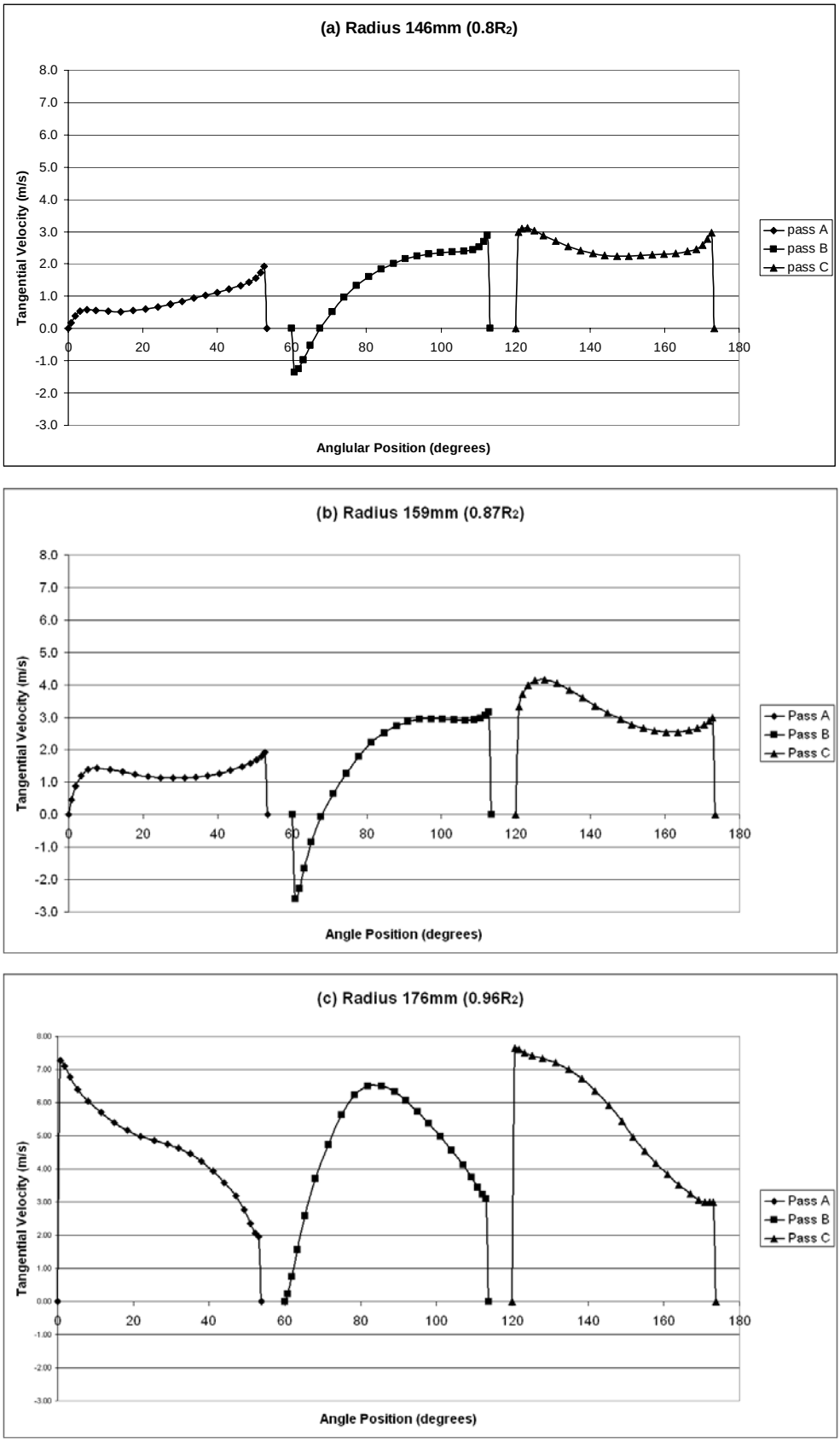

Figure 6.14: **Tangential Velocity at the mid plane of the impeller through 3 impeller passageways at different radii for the first arrangement at 0.25Qn**

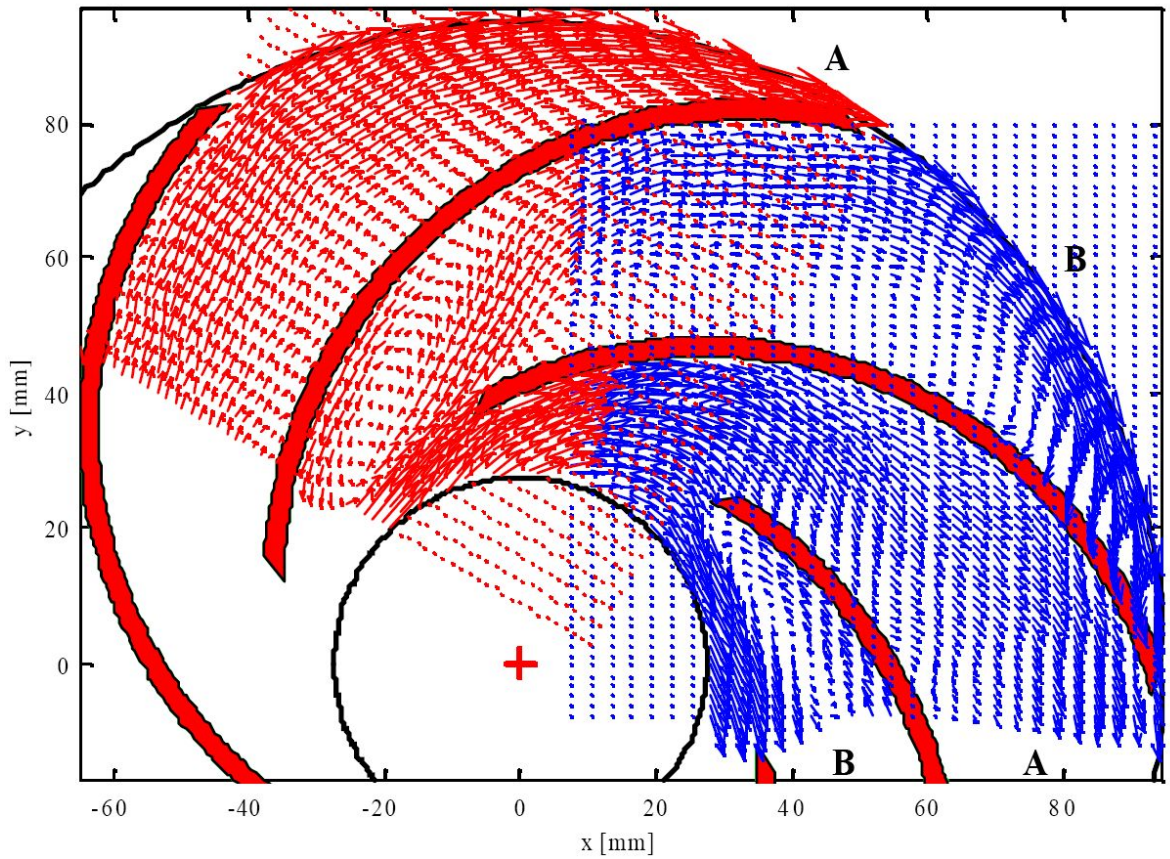

Figure 6.15: Vector maps of the ensemble averaged relative velocity. The well behaved passage is denoted A and the stalled passage is denoted B. (Q/Qd = 0.25), reproduced from Pedersen et al (129)

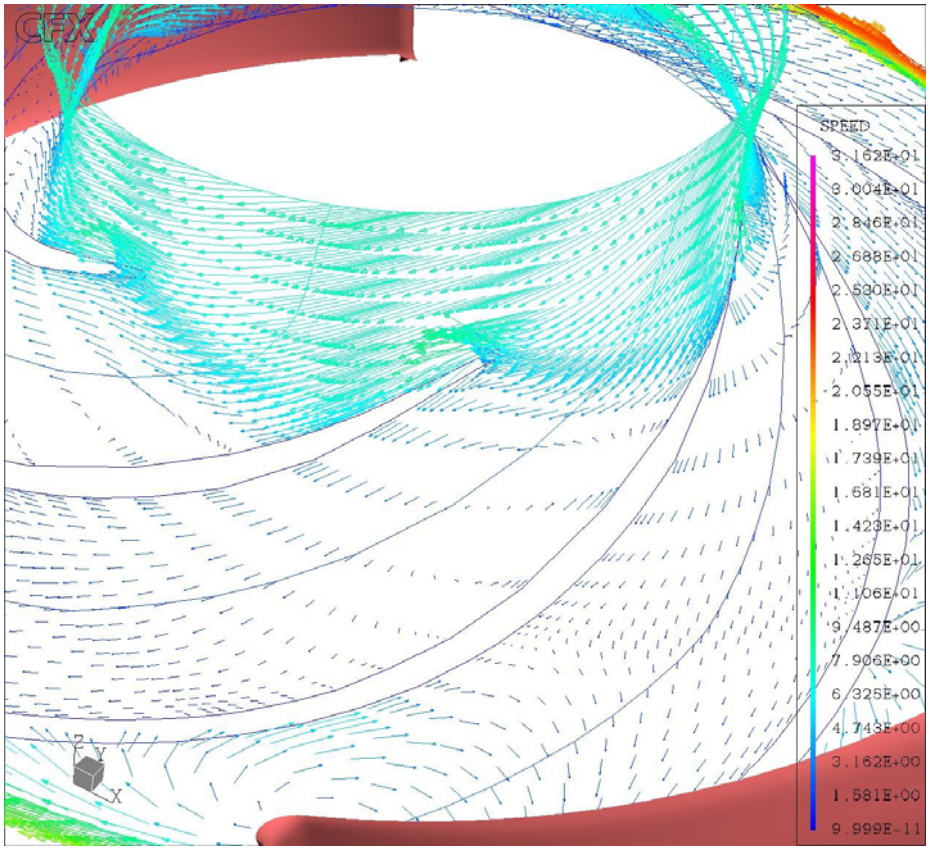

Figure 6.16: Stall cell present for first arrangement at 0.25Qn

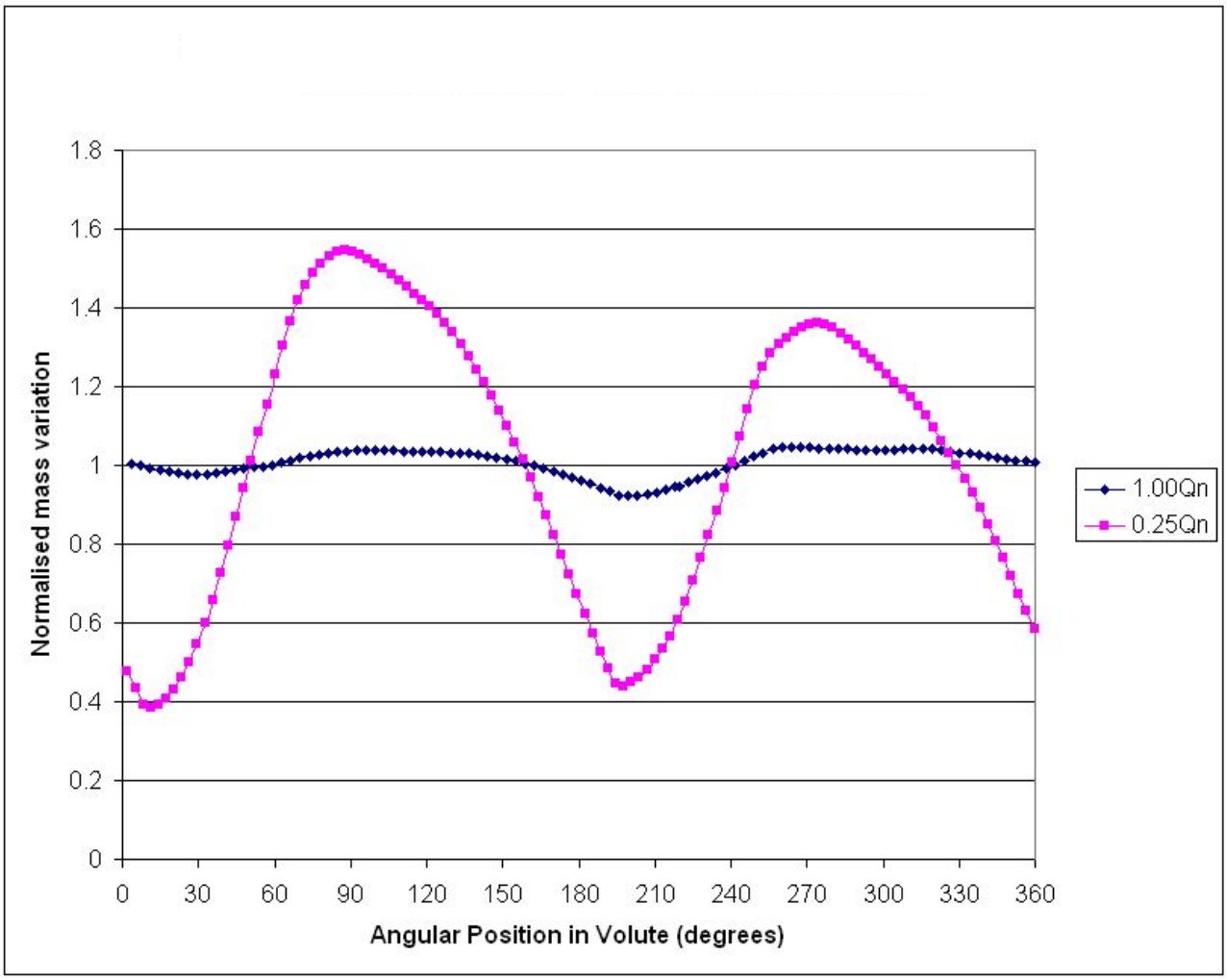

Figure 6.17: Comparison of mass flow variation for a single passage during a single revolution for 1.00Qn and 0.25Qn for the first arrangement. Mass flow normalised by the average mass flow through the passage.

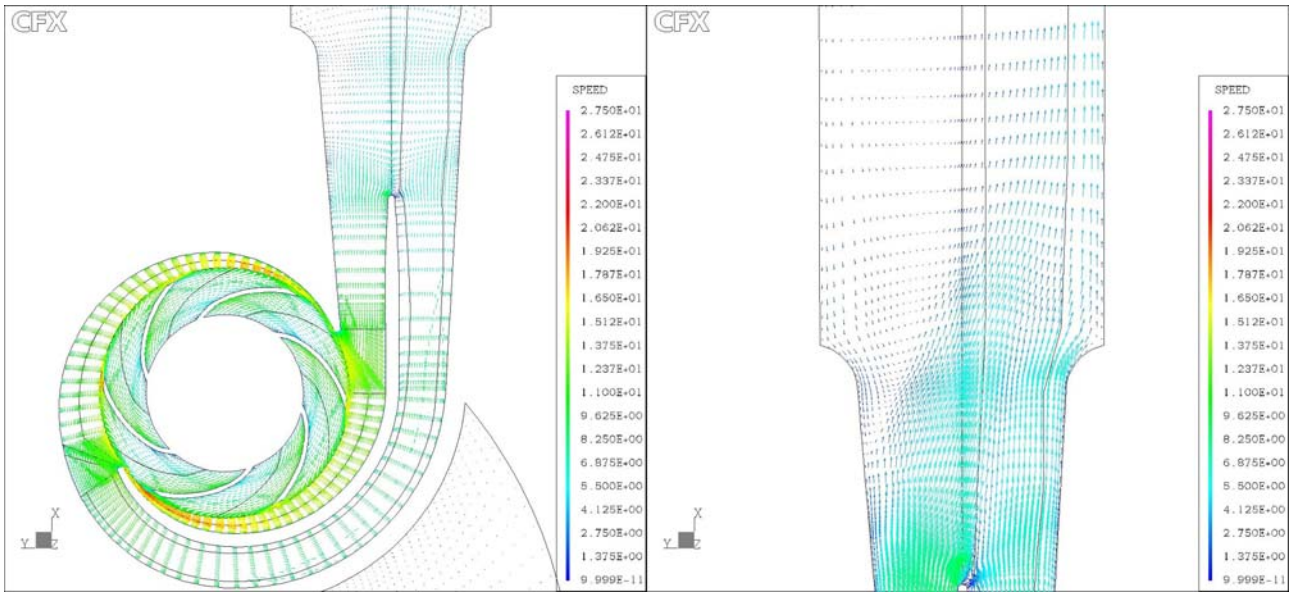

Figure 6.18: Flow vectors in volute/discharge at 1.00Qn

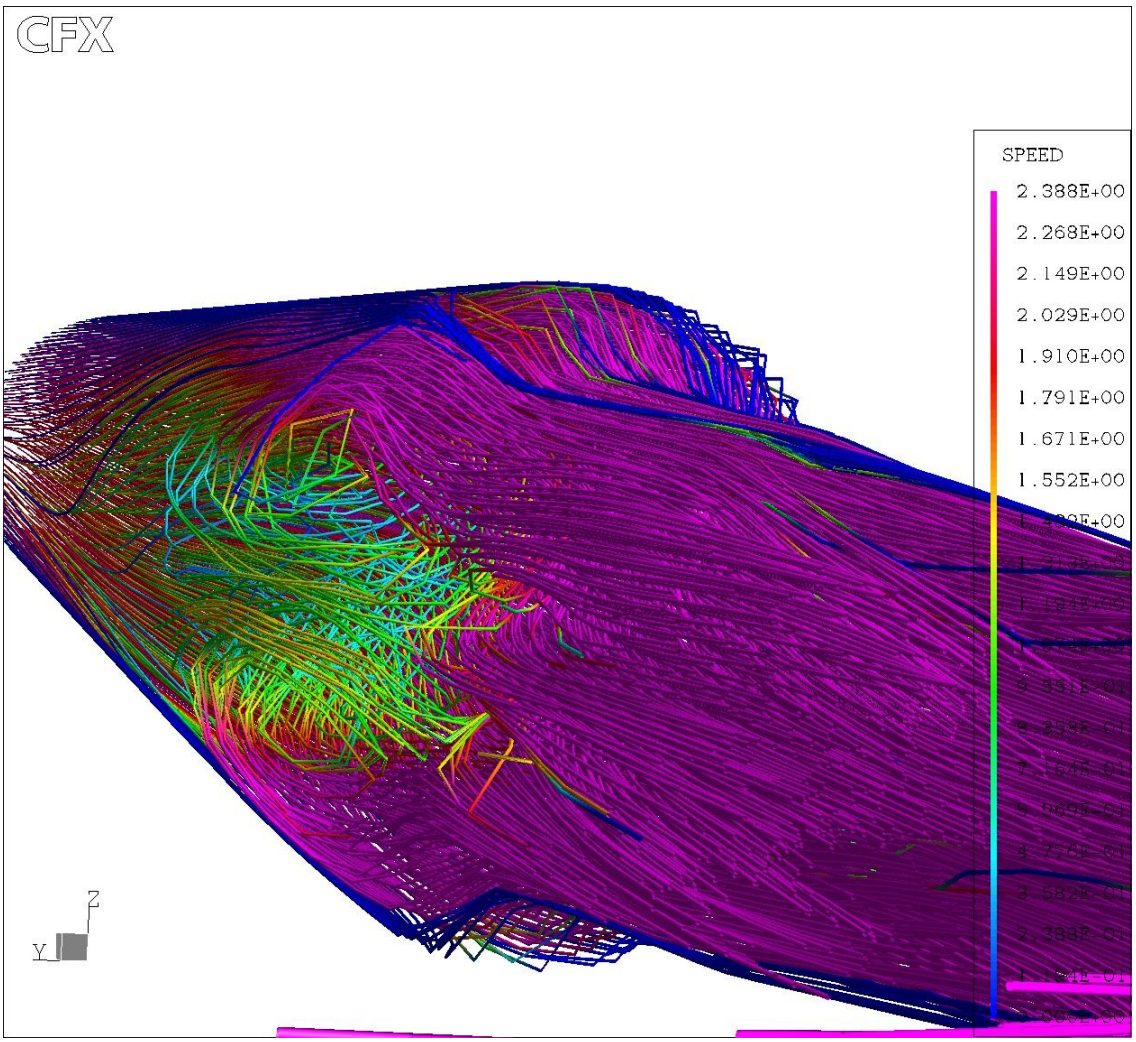

Figure 6. 6.19: Vortices in the pump discharge at 1.00Qn

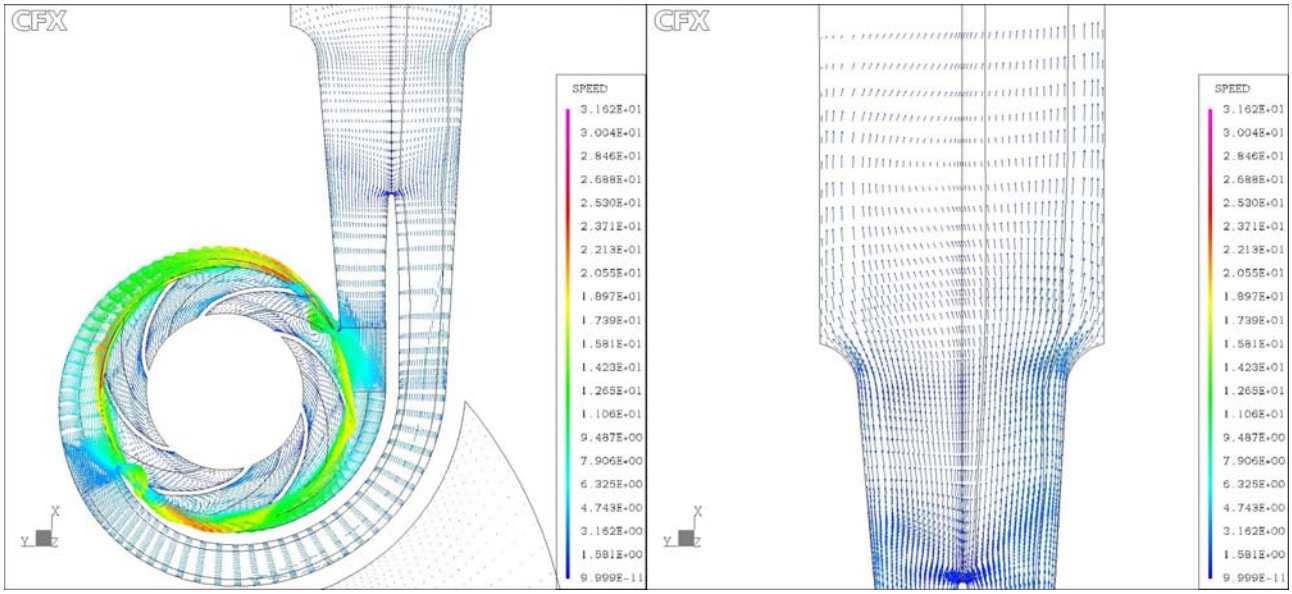

Figure 6.20: Flow vectors in volute/discharge at 0.25Qn

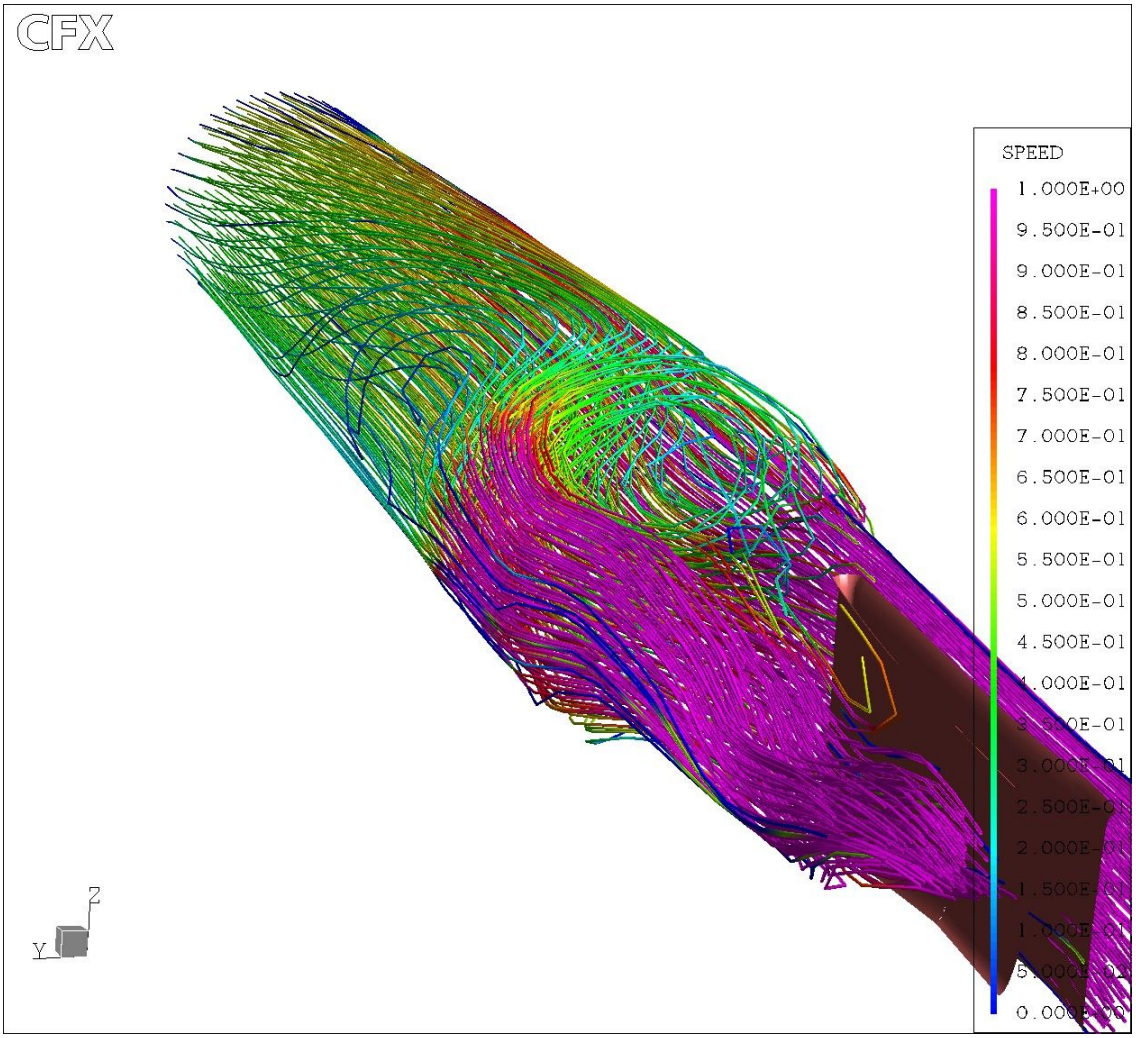

Figure 6. 6.21: Vortices in the pump discharge at 0.25Qn

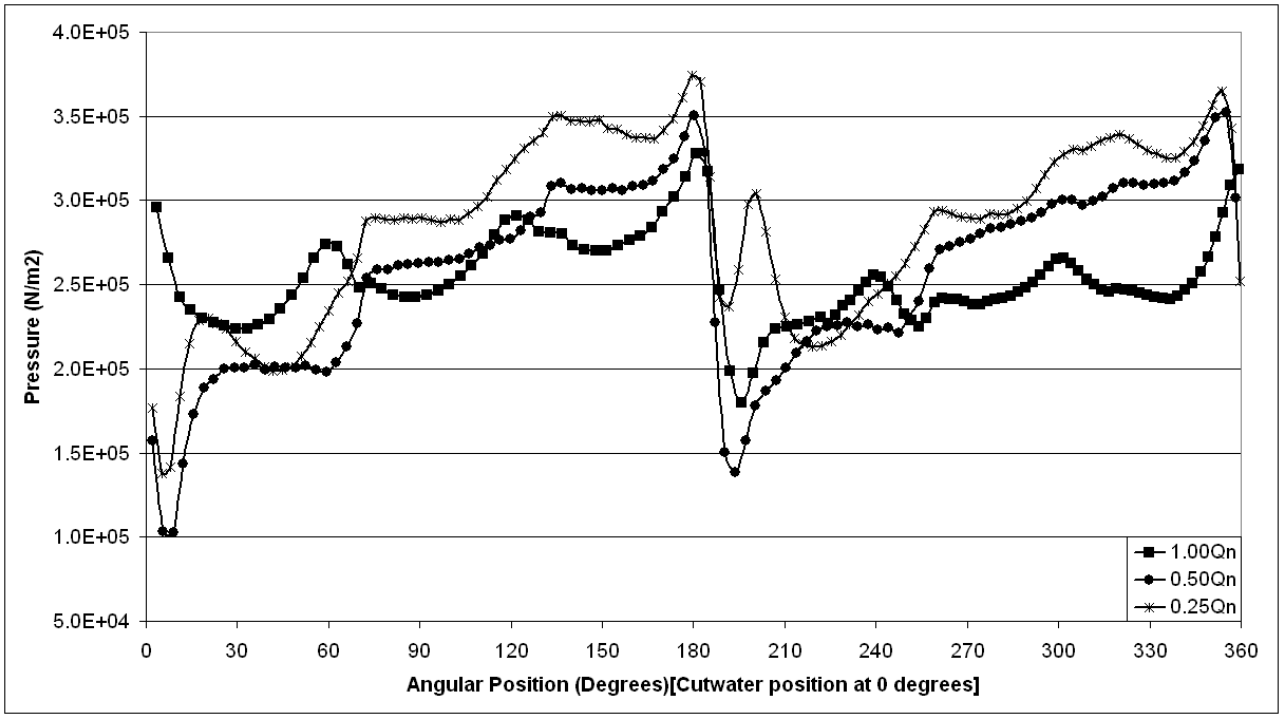

Figure 6.22: Variation in static pressure at impeller exit for differing flowrates. Data taken from blade pressure data position

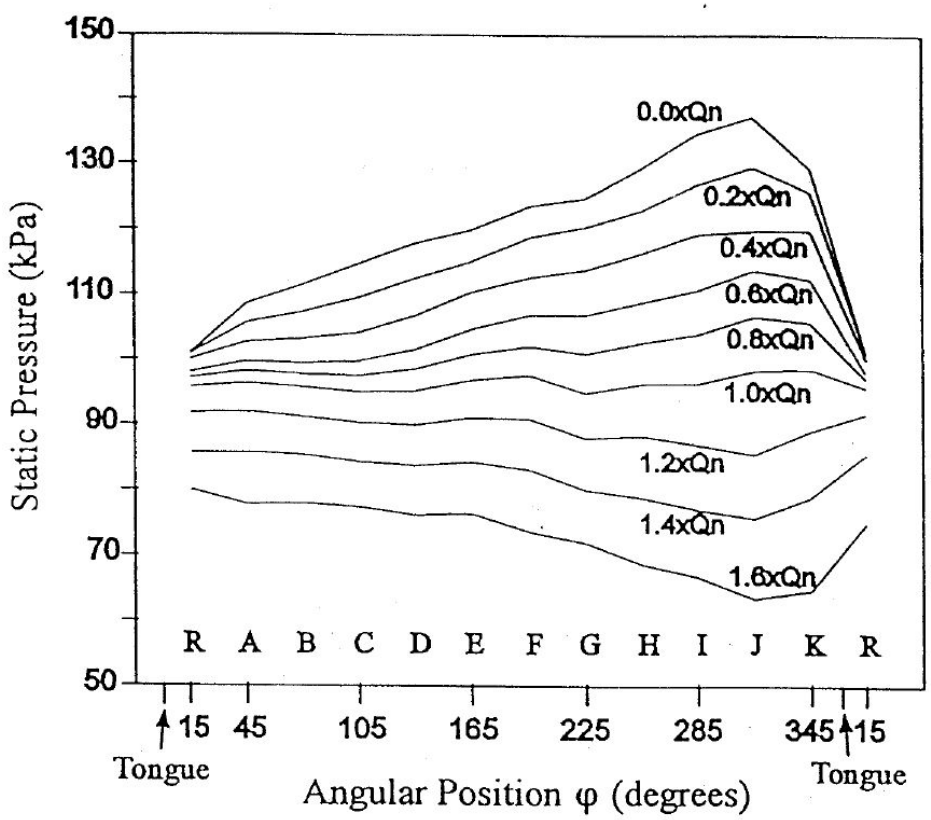

Figure 6.23: Static pressure distribution around the impeller outlet for different flow rates (reproduced from Parrondo et al (34)

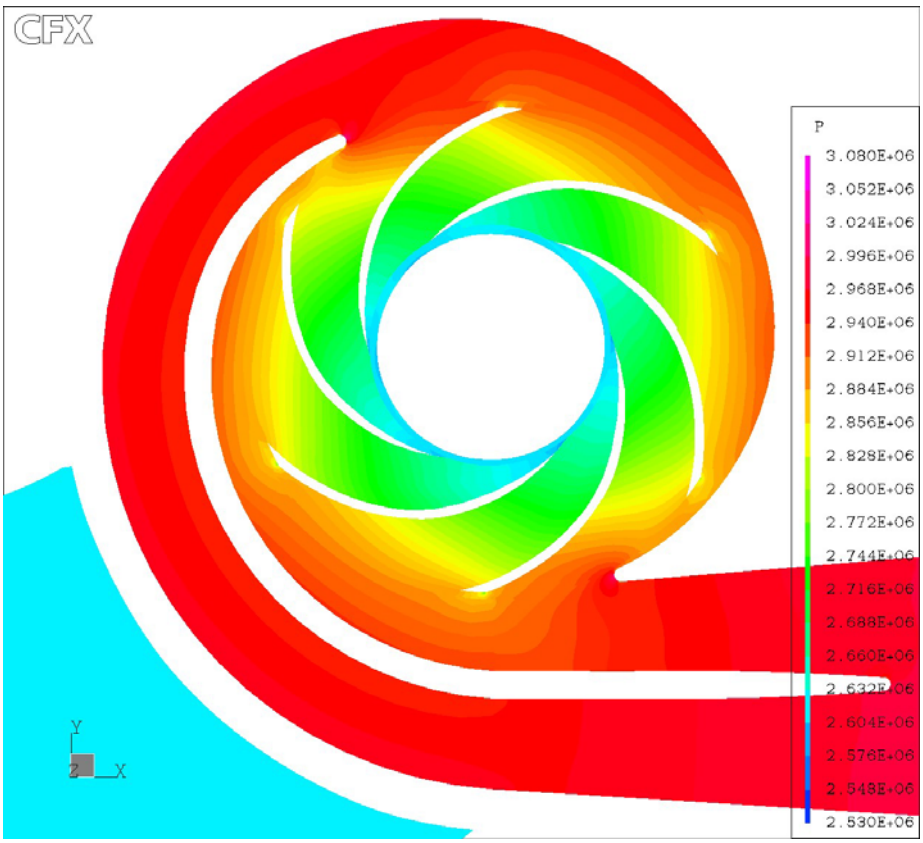

Figure 6.24: Static pressure through mid plane of impeller and into volute at 1.00Qn

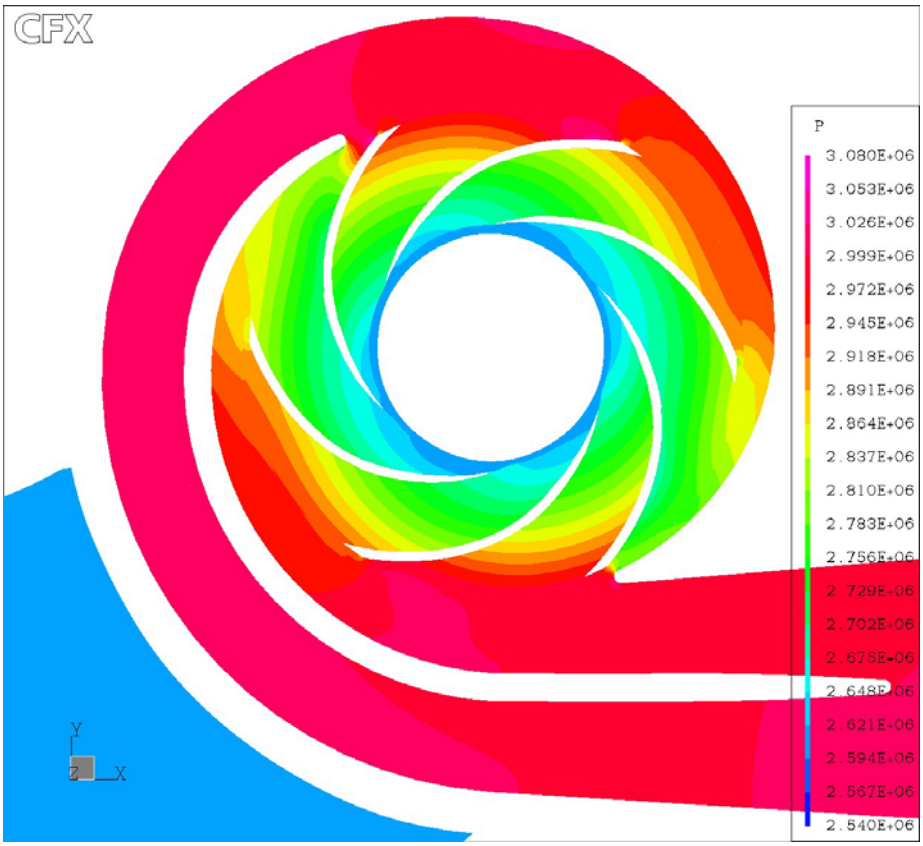

Figure 6.25: Static pressure through mid plane of impeller and into volute at 0.25Qn

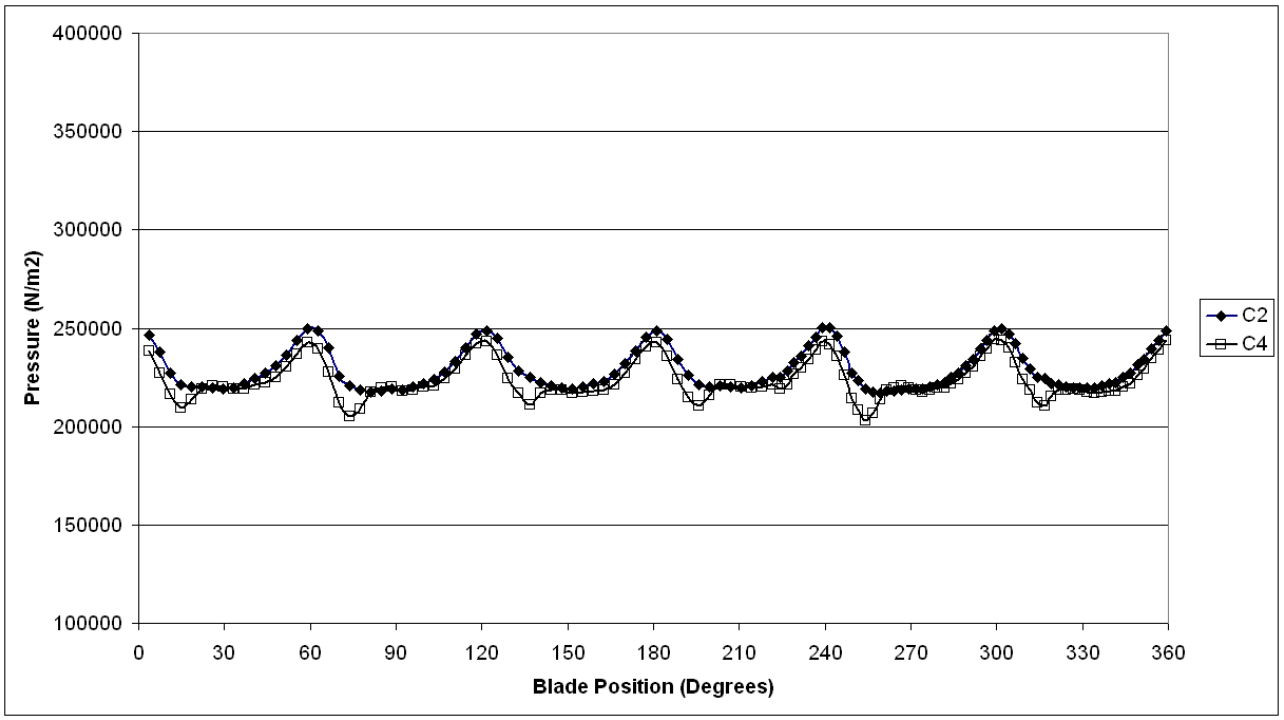

Figure 6.26: Pressure fluctuations at sidewall locations for first arrangement at 1.00Qn

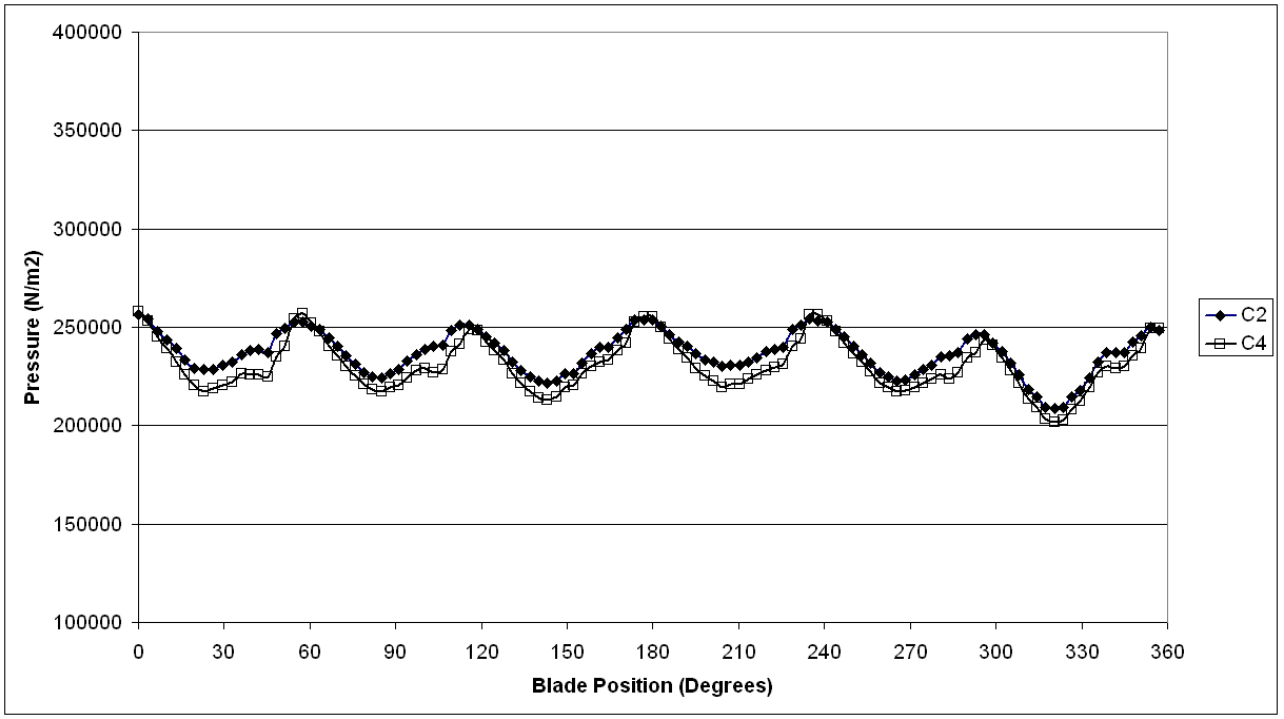

Figure 6.27: Pressure fluctuations at sidewall locations for first arrangement at 0.25Qn

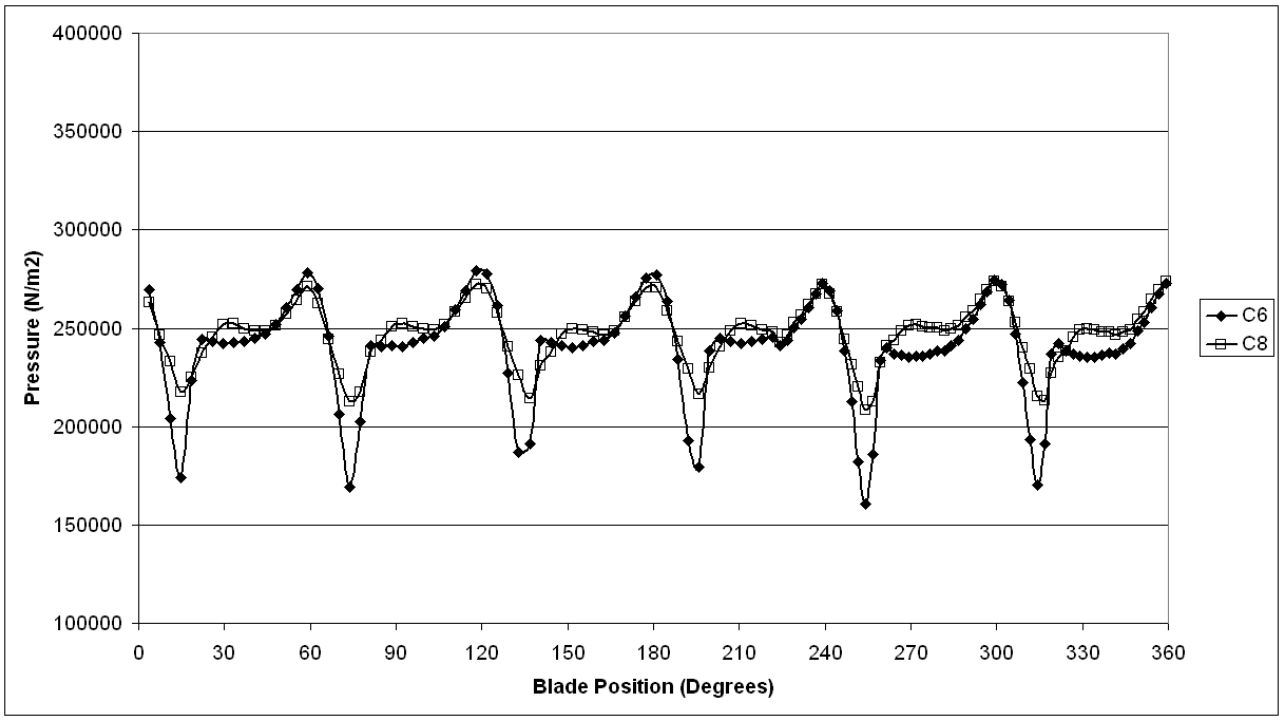

Figure 6.28: Pressure fluctuations at volute locations for first arrangement at 1.00Qn

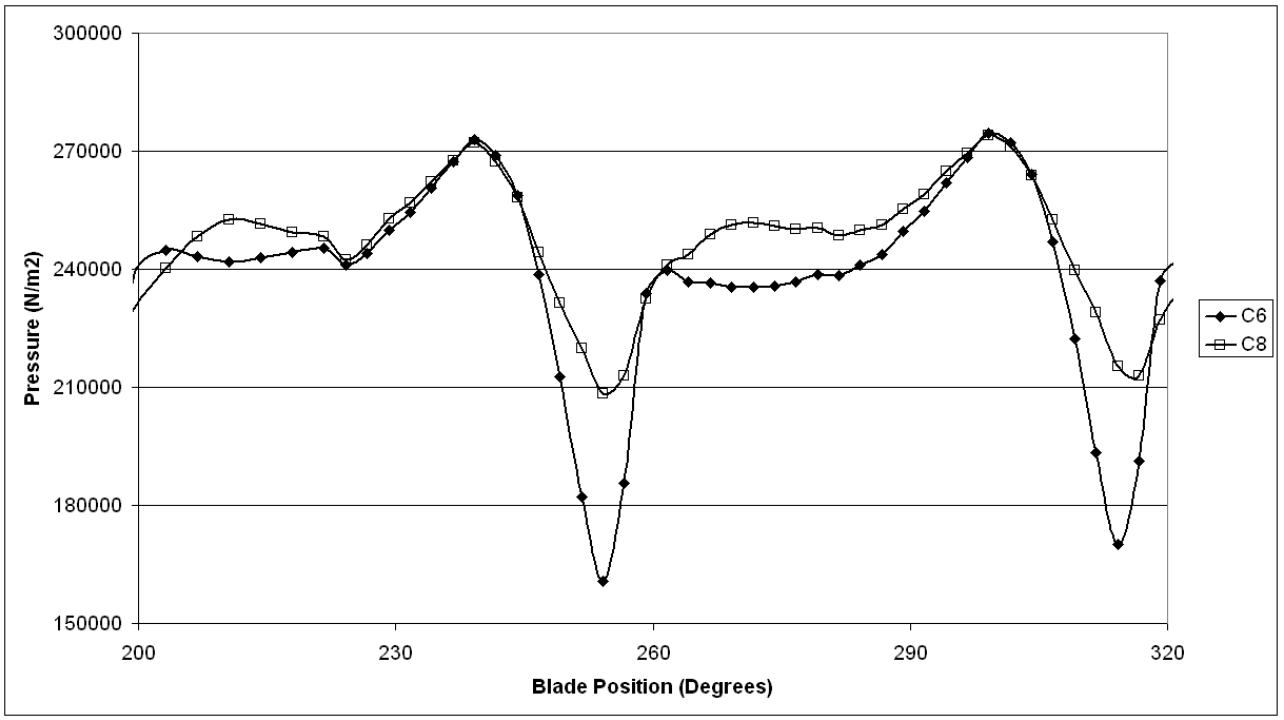

Figure 6.29: Pressure fluctuations at volute locations for first arrangement at 1.00Qn , 120 degree limited range

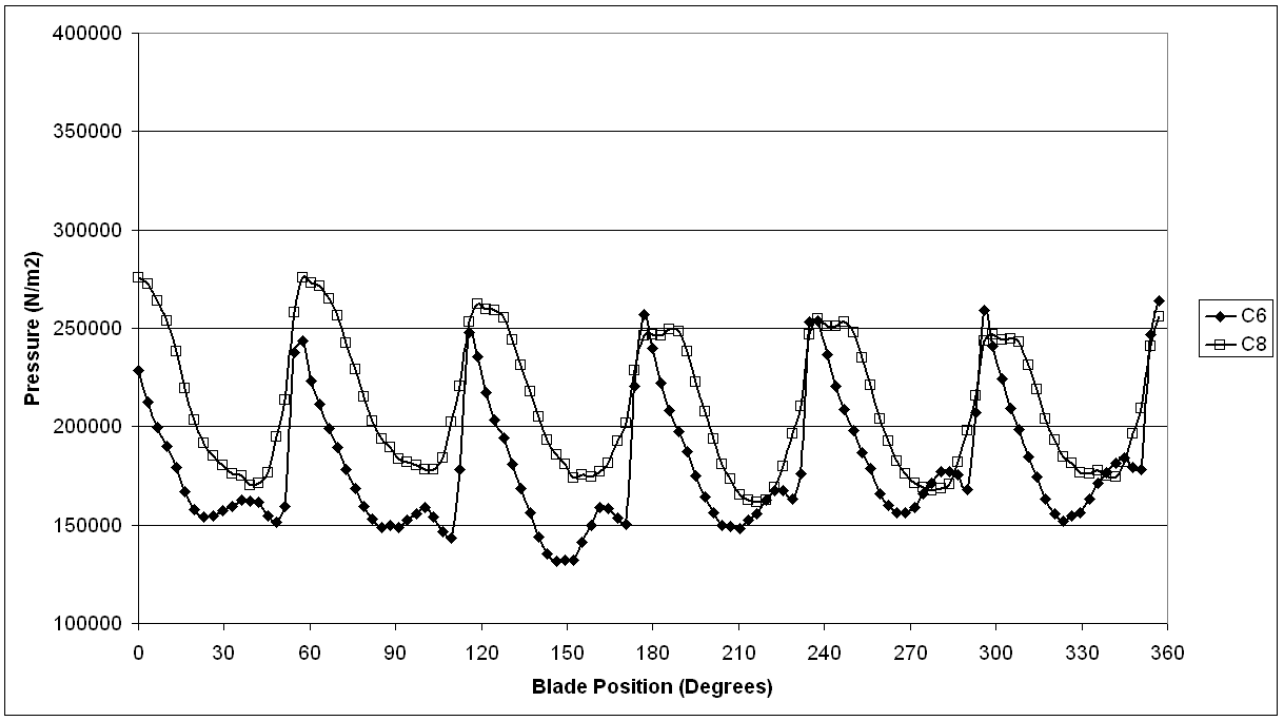

Figure 6.30: Pressure fluctuations at volute locations for first arrangement at 0.25Qn

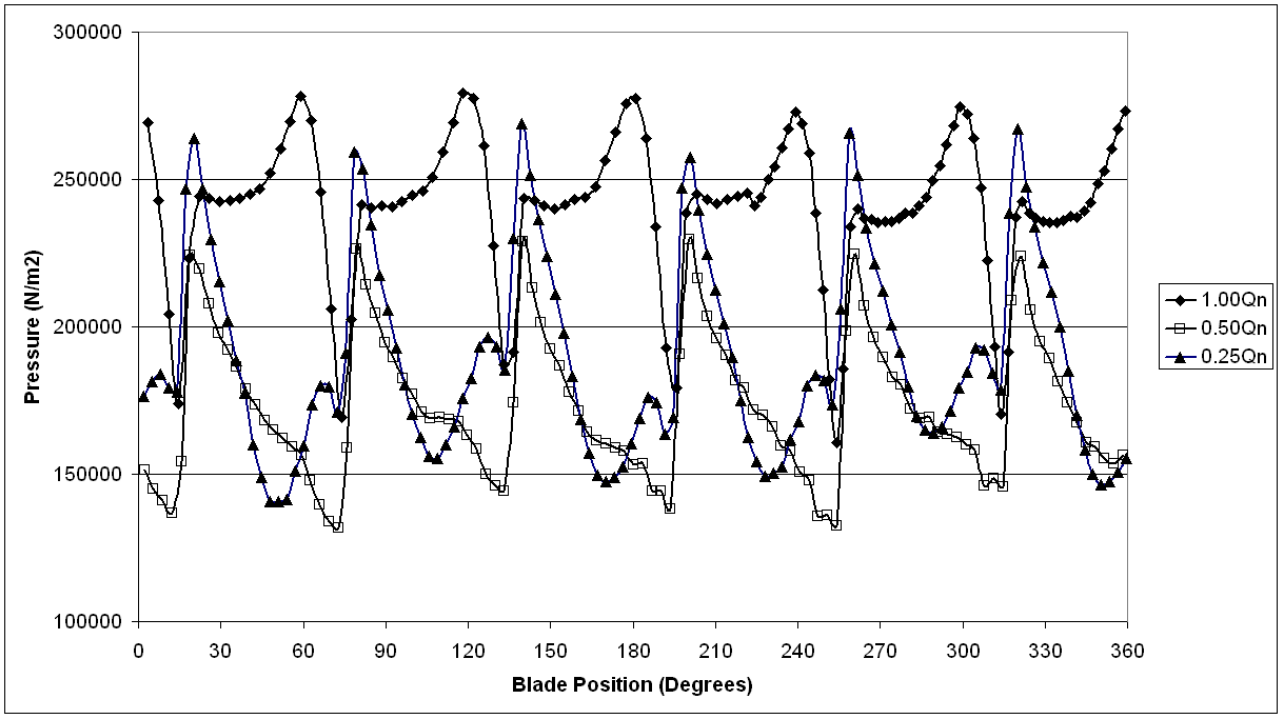

Figure 6.31: Comparison of pressure pulsations at location C6 for three flow rates

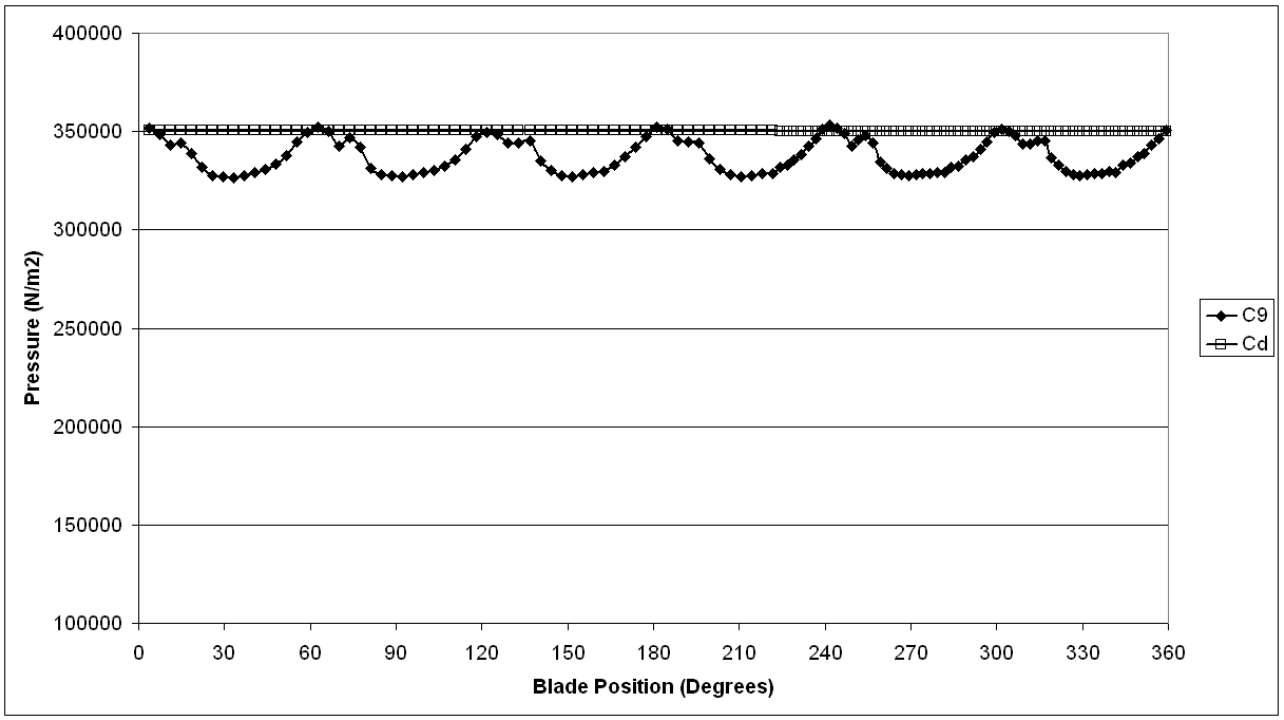

Figure 6.32: Pressure fluctuations at discharge locations for first arrangement at 1.00Qn

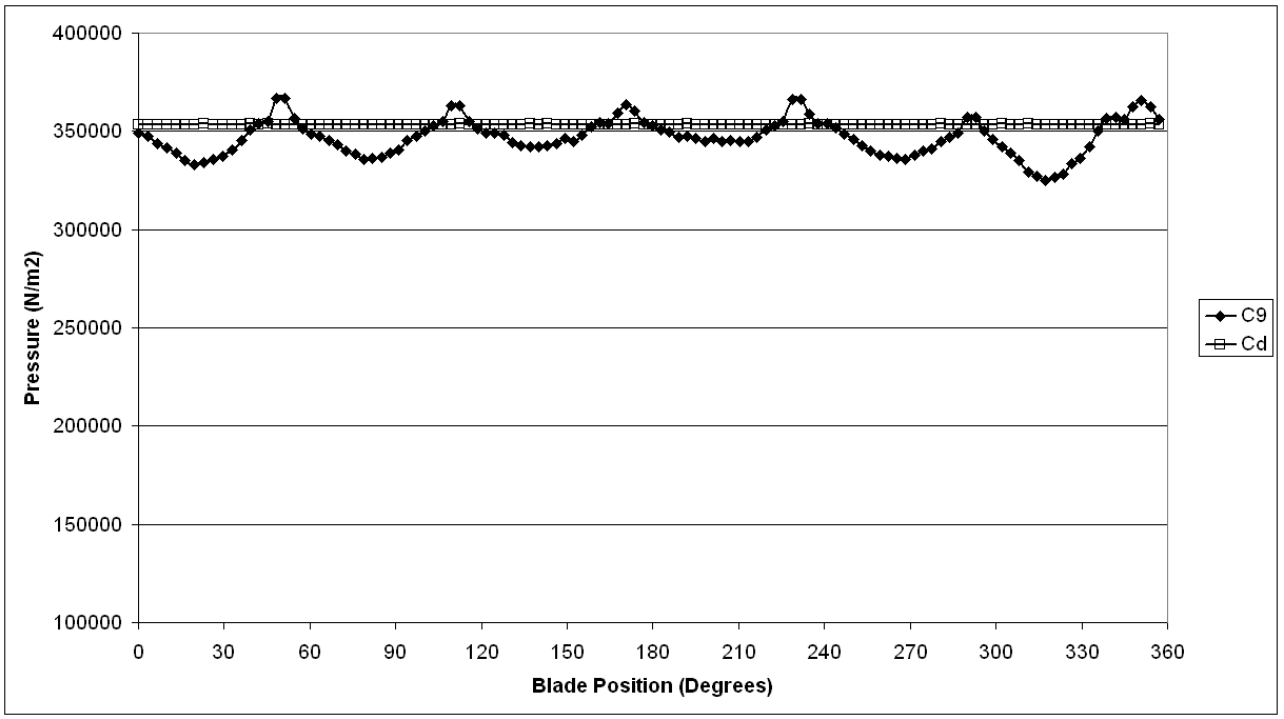

Figure 6.33: Pressure fluctuations at discharge locations for first arrangement at 0.25Qn

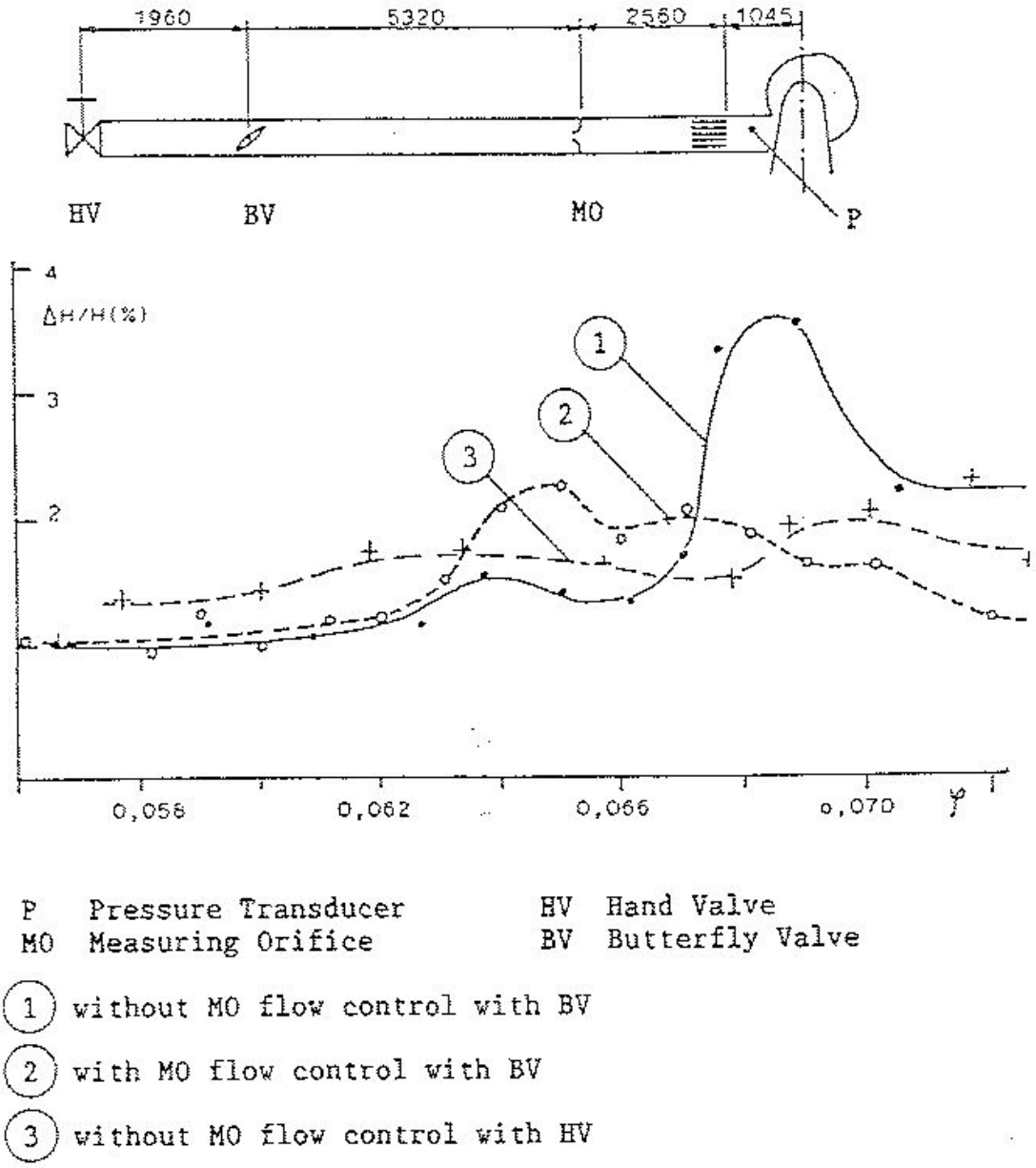

Figure 6.34: Influence of a system on pressure pulsations reproduced from Holler (131)

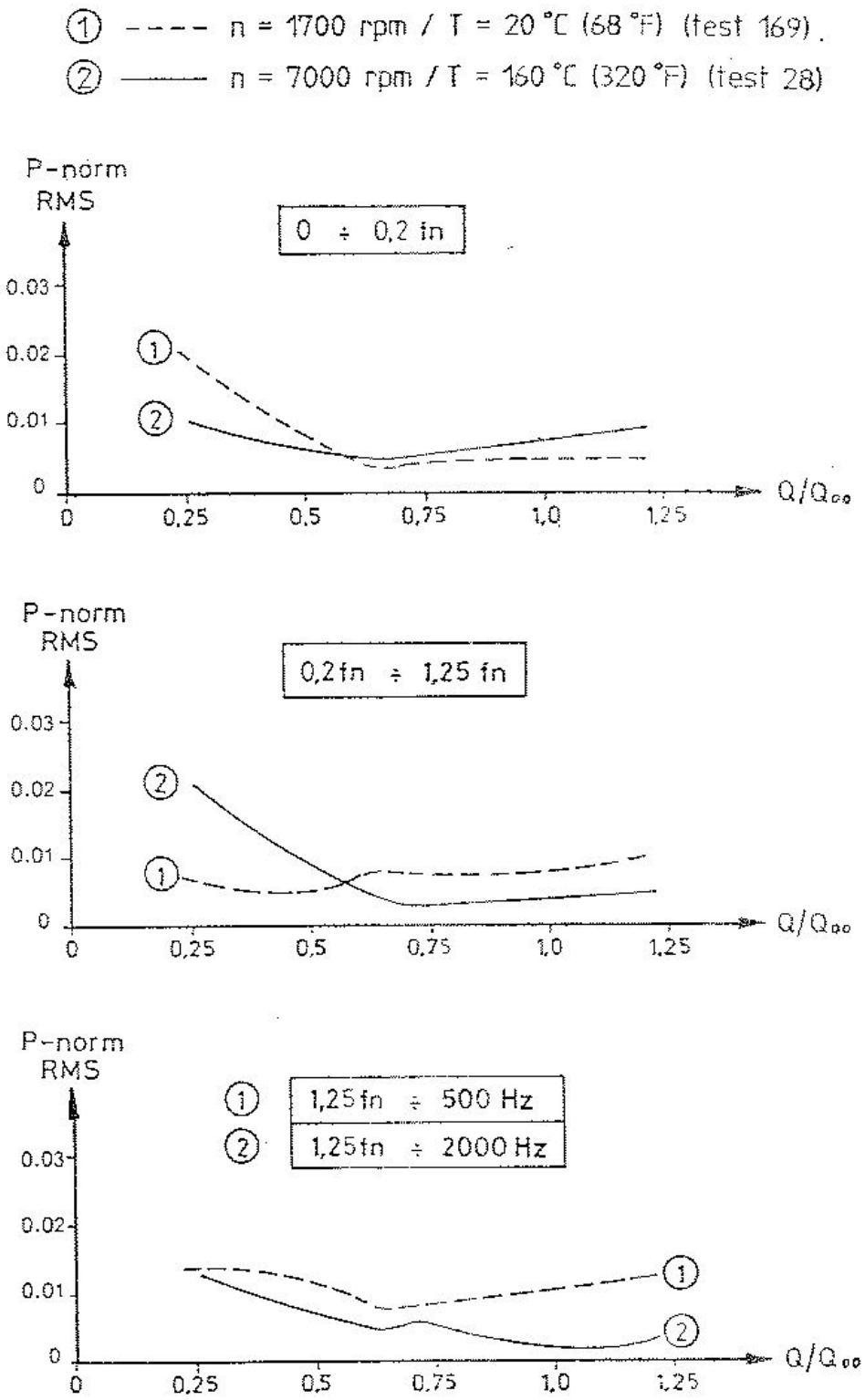

Figure 6.35: Pressure pulsations of a 10,000 kW boiler feed pump measured in two different test loops (reproduced from Guelich & Bolleter (90)).

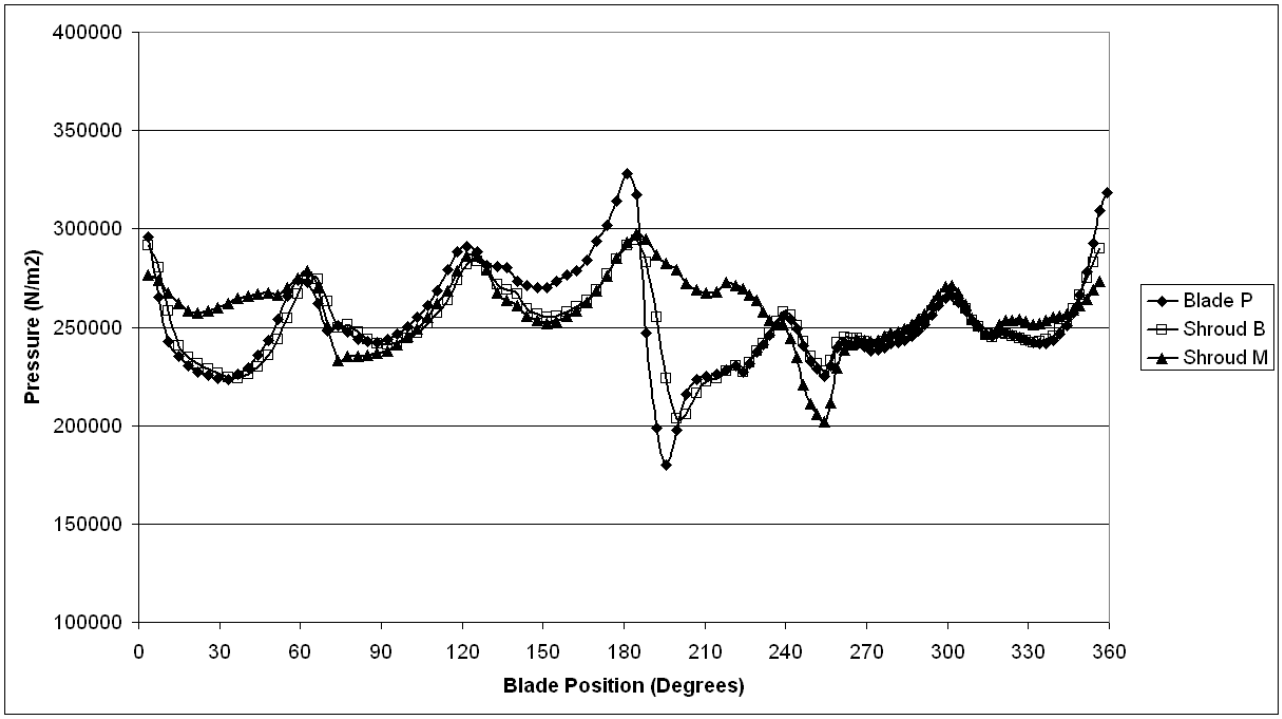

Figure 6.36: Pressure fluctuations at impeller locations for first arrangement at 1.00Qn

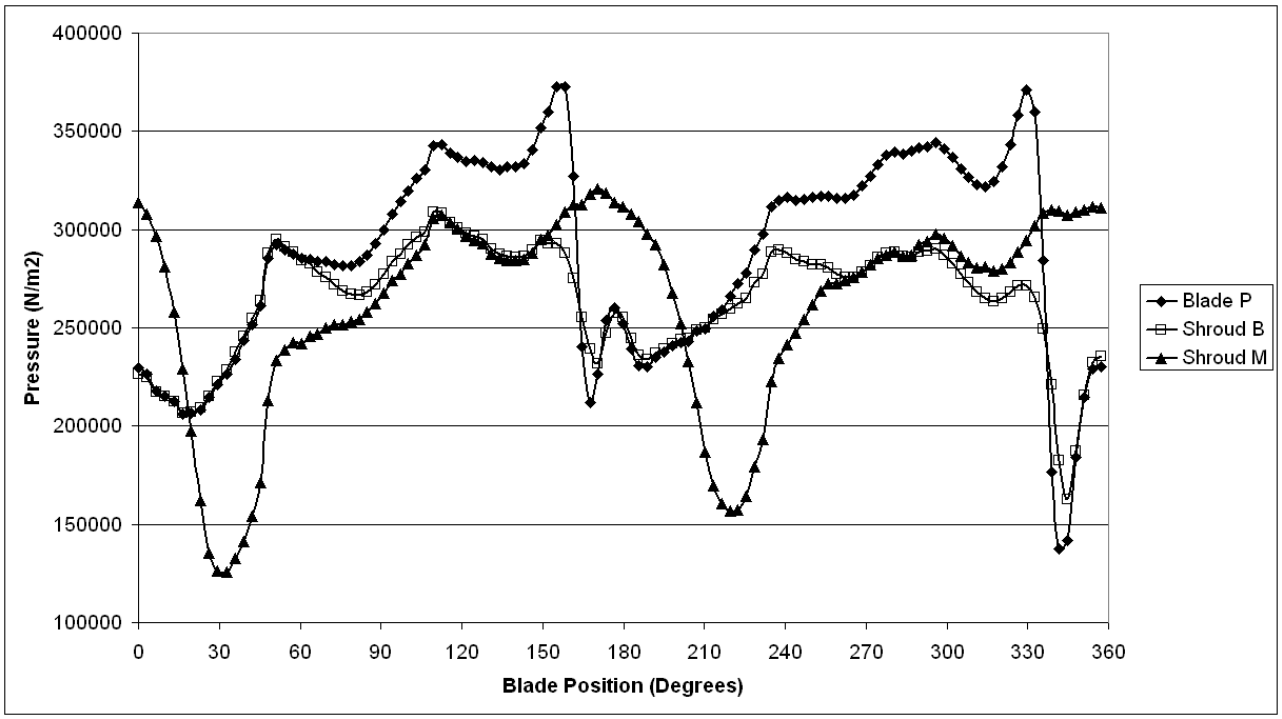

Figure 6.37: Pressure fluctuations at impeller locations for first arrangement at 0.25Qn

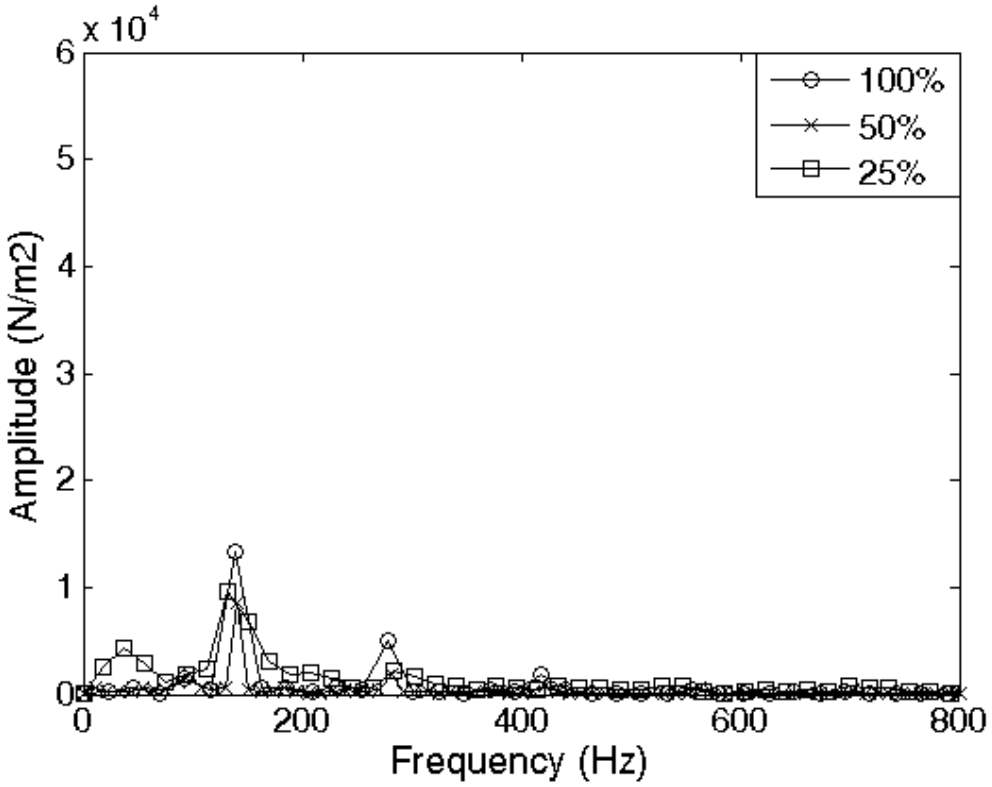

Figure 6.38: Frequency spectra for sidewall location C2, first arrangement at three flow rates

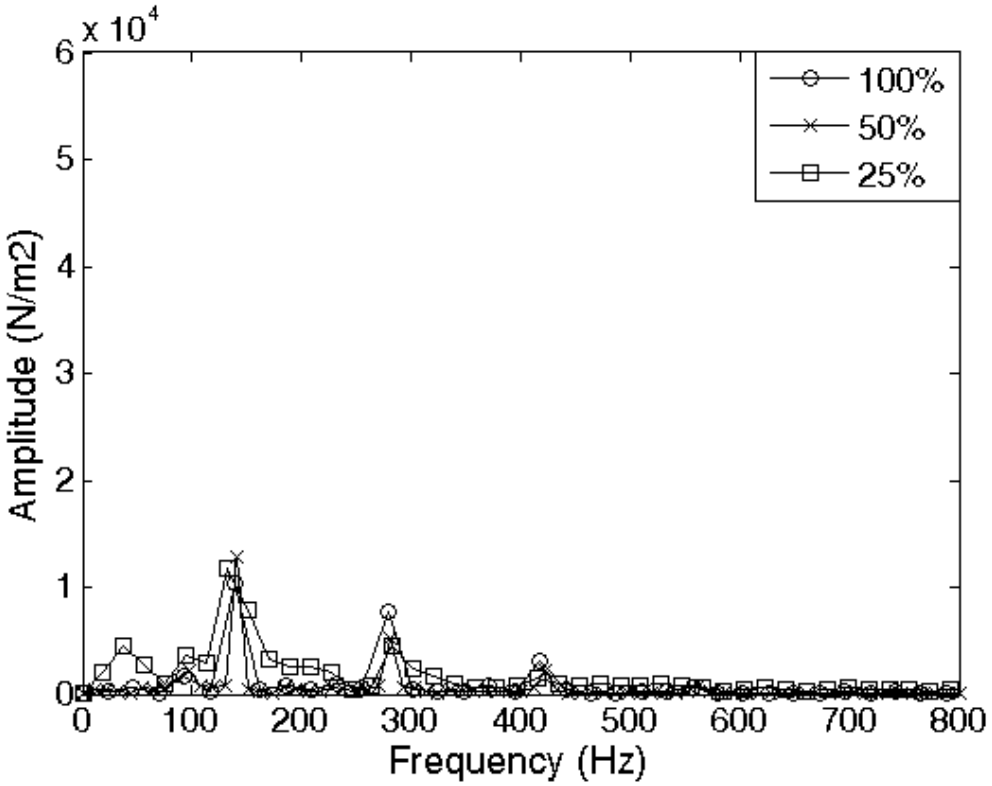

Figure 6.39: Frequency spectra for sidewall location C4, first arrangement at three flow rates

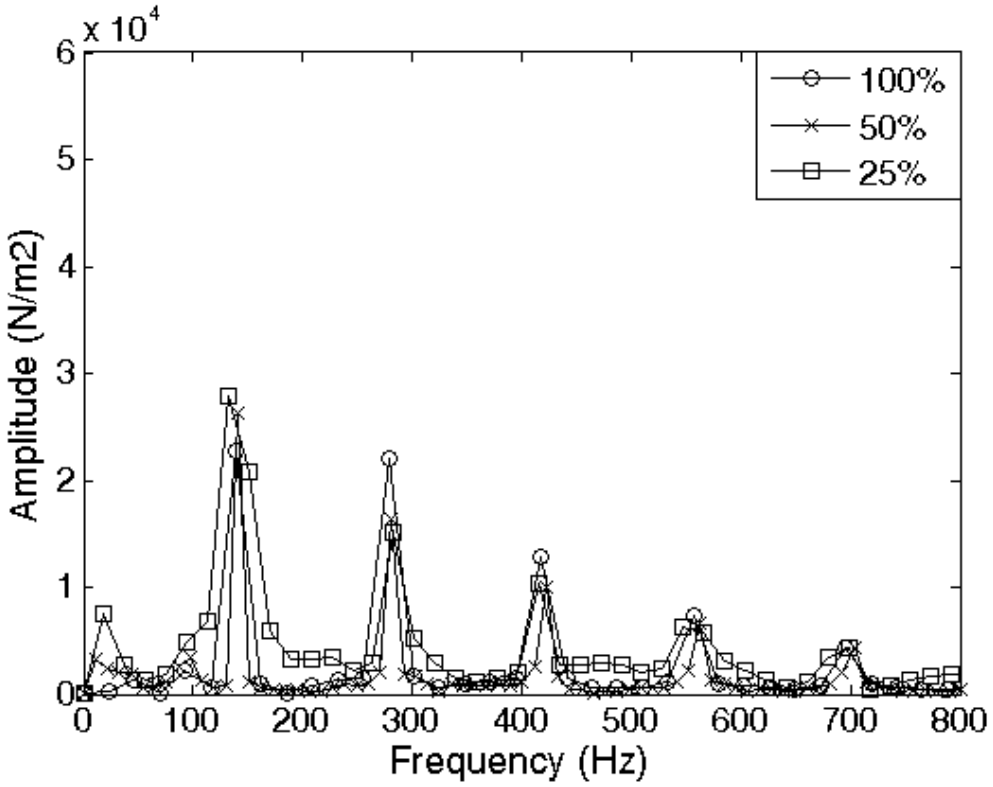

Figure 6.40: Frequency spectra for volute location C6, first arrangement at three flow rates

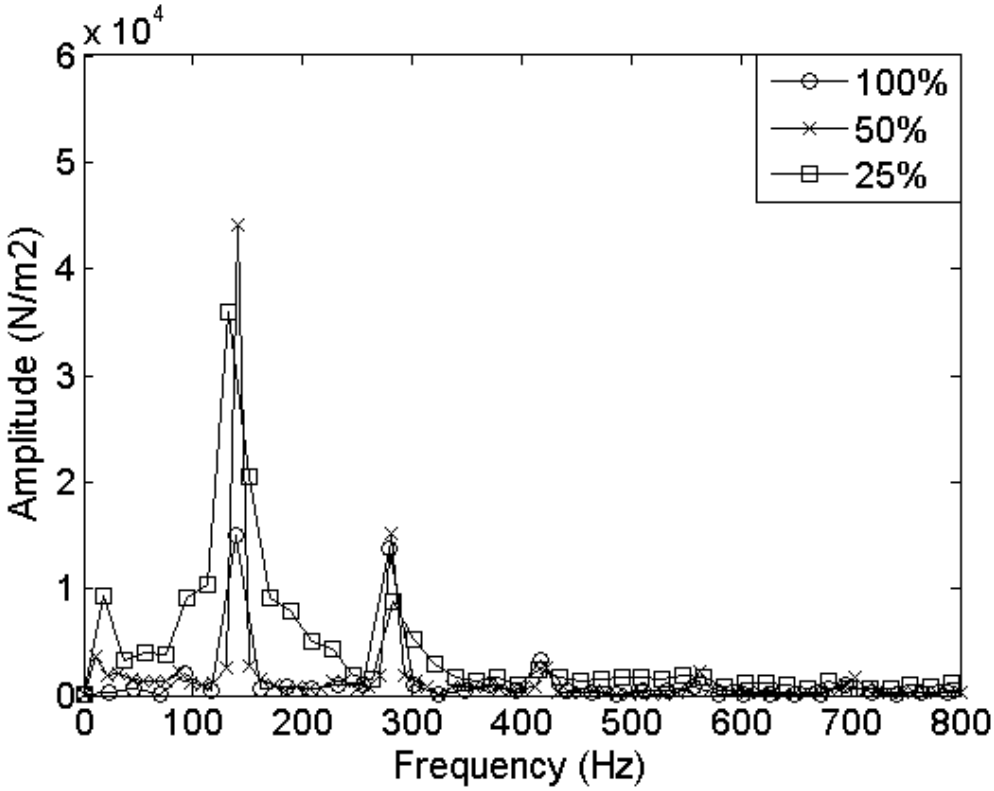

Figure 6.41: : Frequency spectra for volute location C8, first arrangement at three flow rates

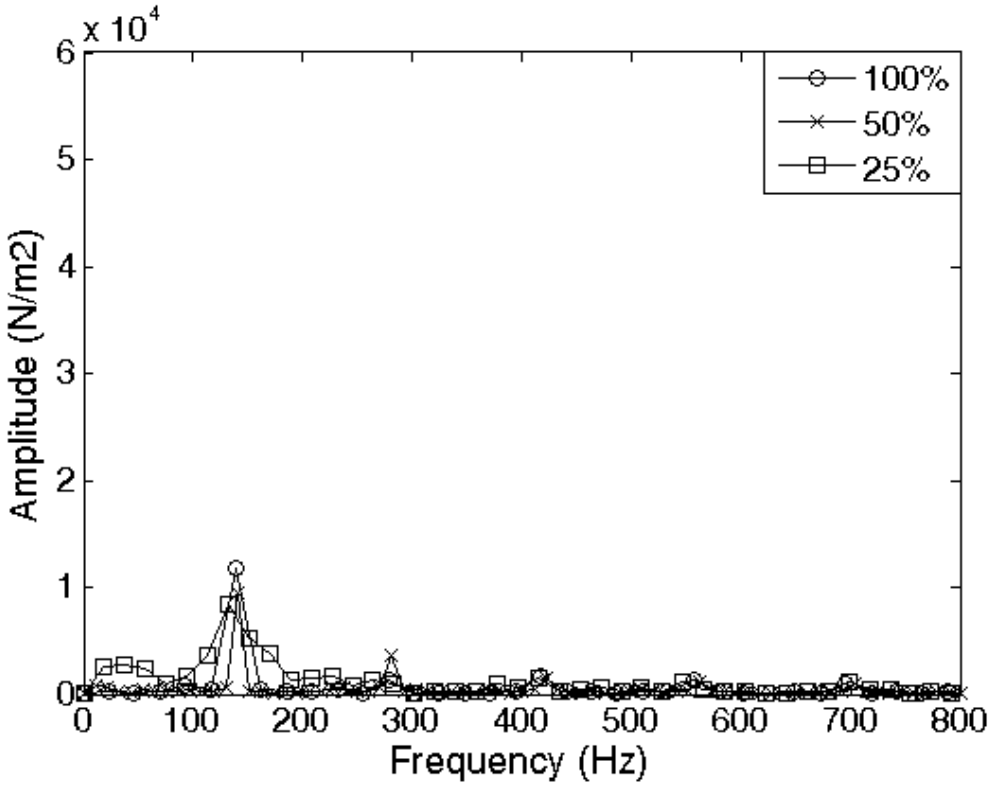

Figure 6.42: Frequency spectra for volute location C9, first arrangement at three flow rates

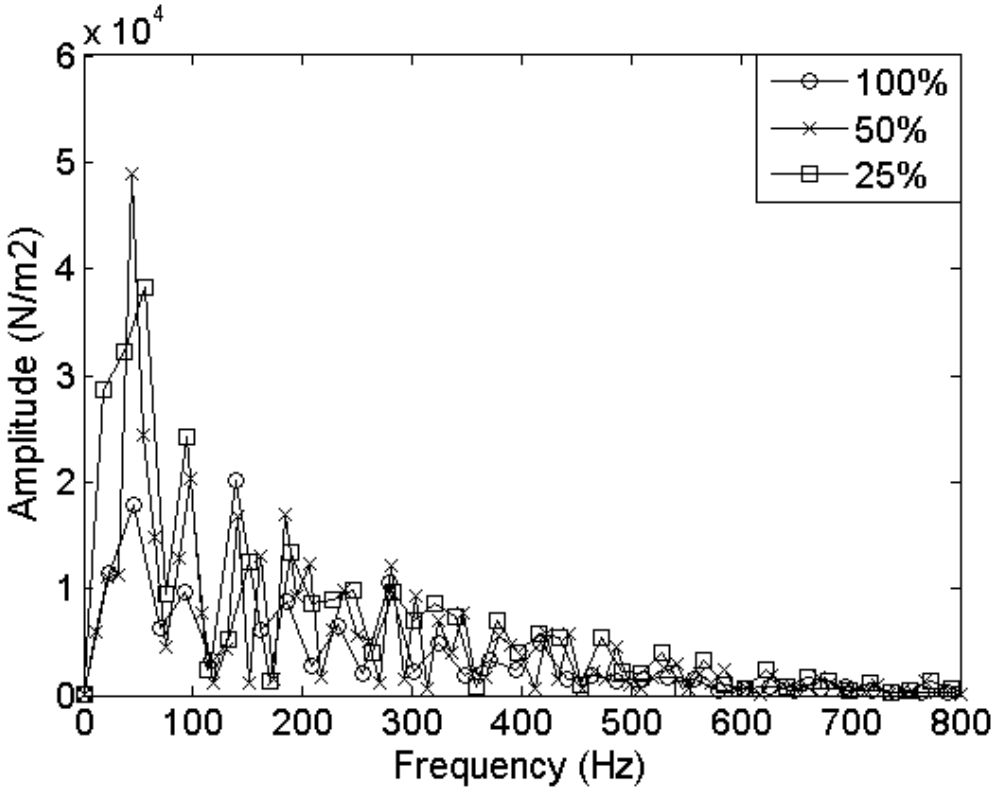

Figure 6.43: Frequency spectra for impeller location, blade pressure Face, first arrangement at three flow rates

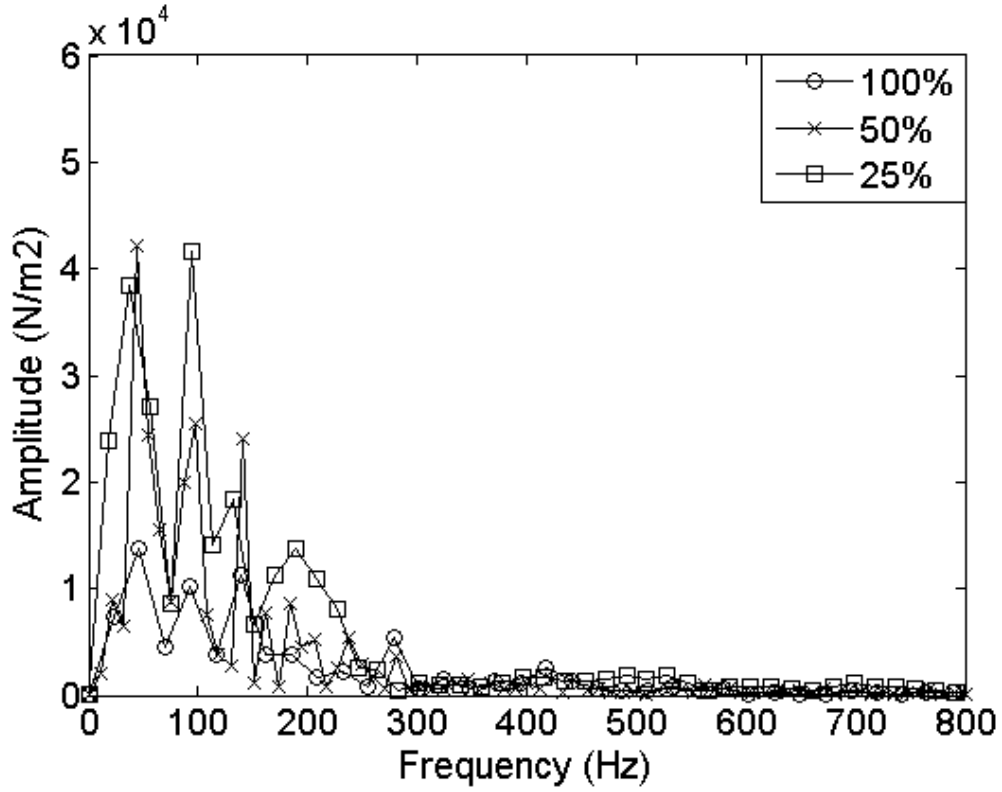

Figure 6.44: Frequency spectra for impeller location shroud mid passage location, first arrangement at three flow rates

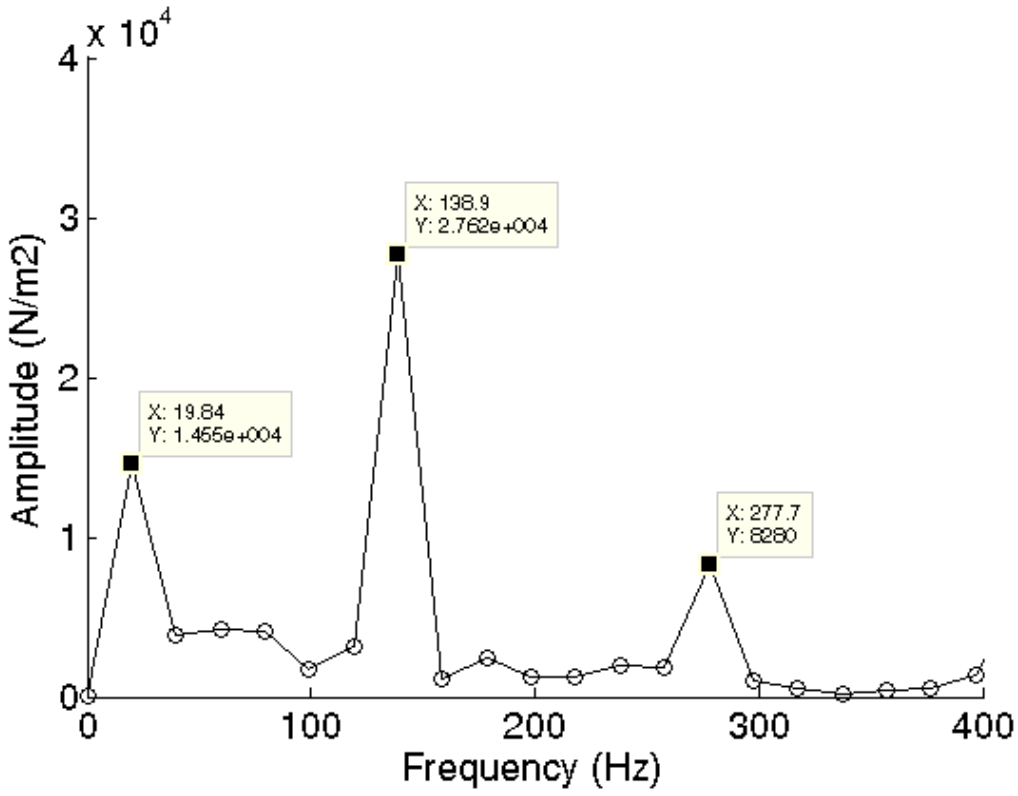

Figure 6.45: Frequency spectra for impeller locationC6, third arrangement at 0.25Qn

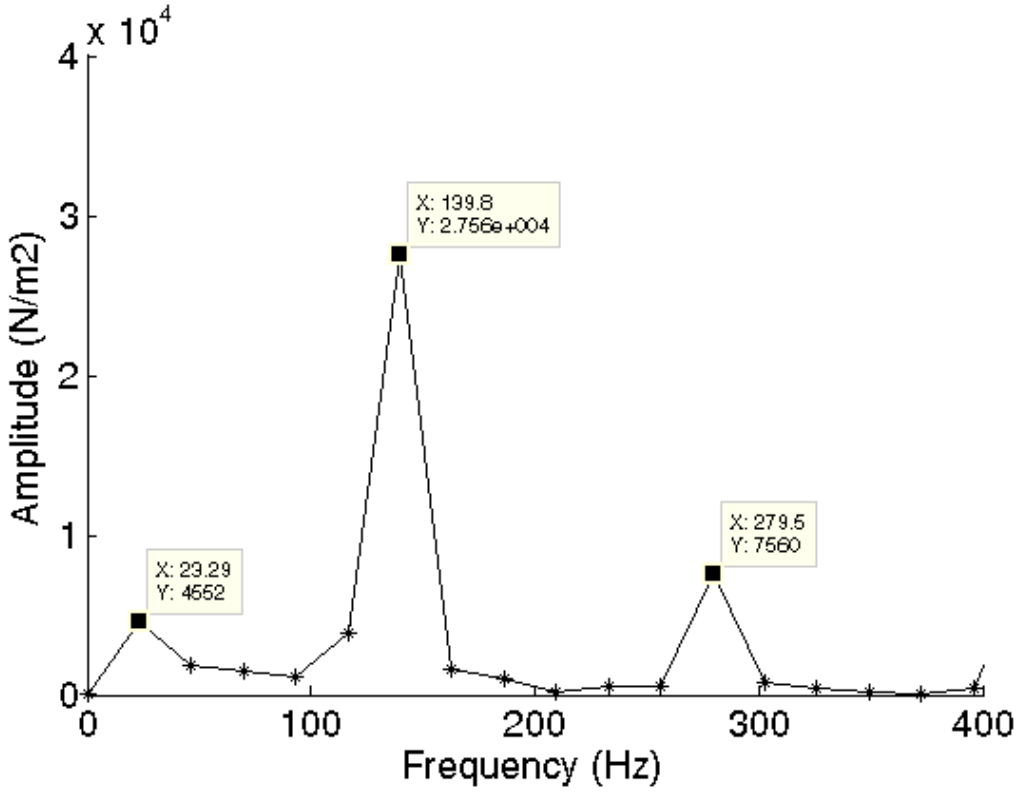

Figure 6.46: Frequency spectra for impeller location C6, third arrangement at 0.25Qn using extended analysis data

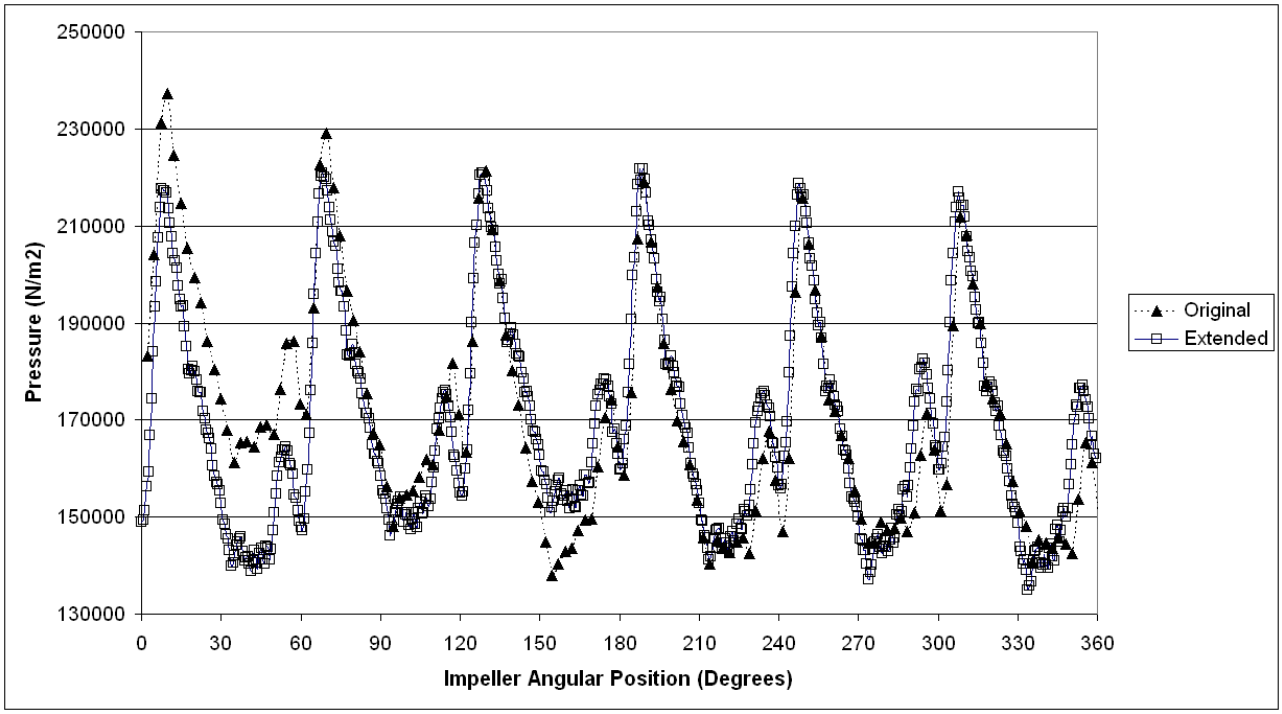

Figure 6.47: Comparison of time histories at location C6 for original and extended analyses

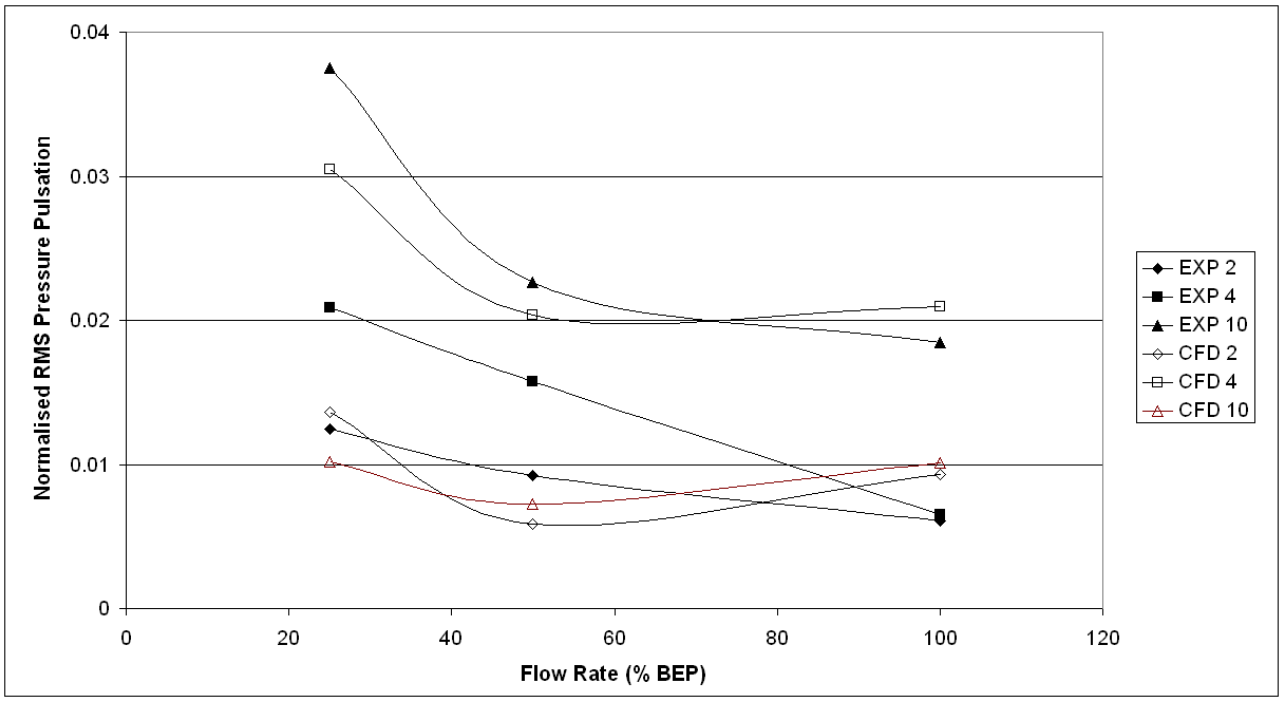

Figure 6.48: Normalised RMS comparison of experimental test 18 and CFD analysis test 5 for leakage region

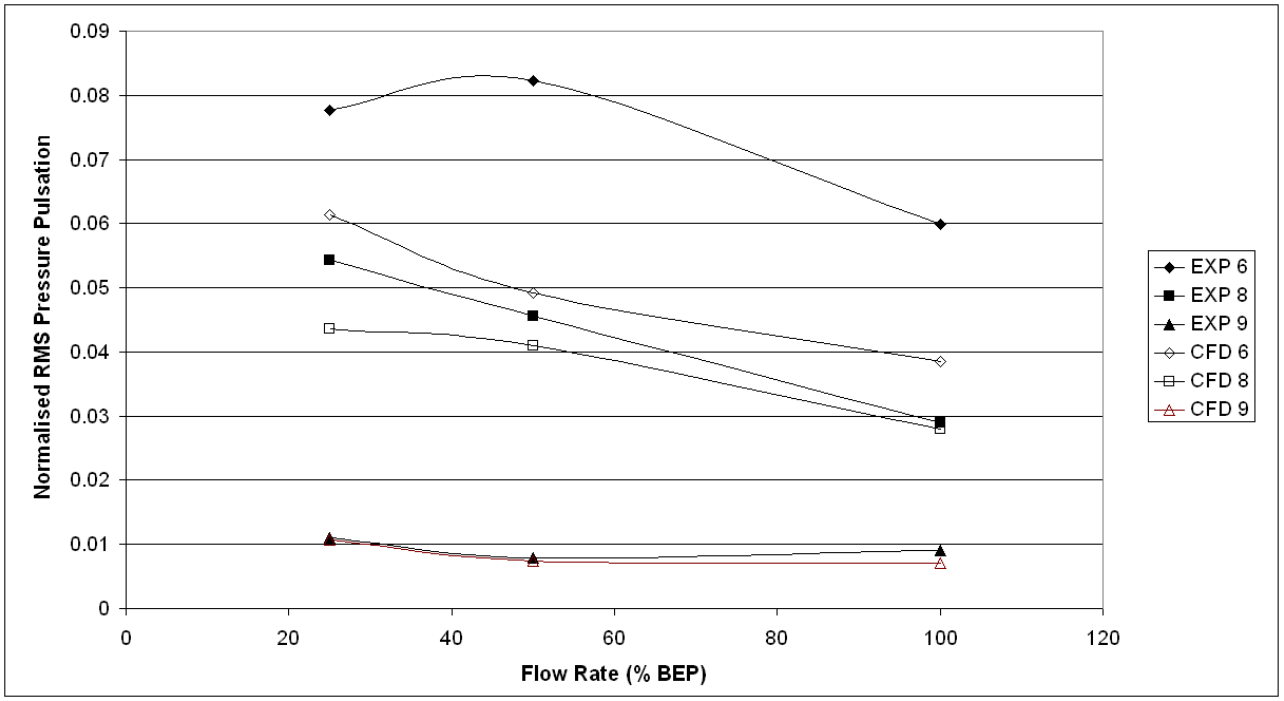

Figure 6.49: Normalised RMS comparison of experimental test 18 and CFD analysis test 5 for volute region

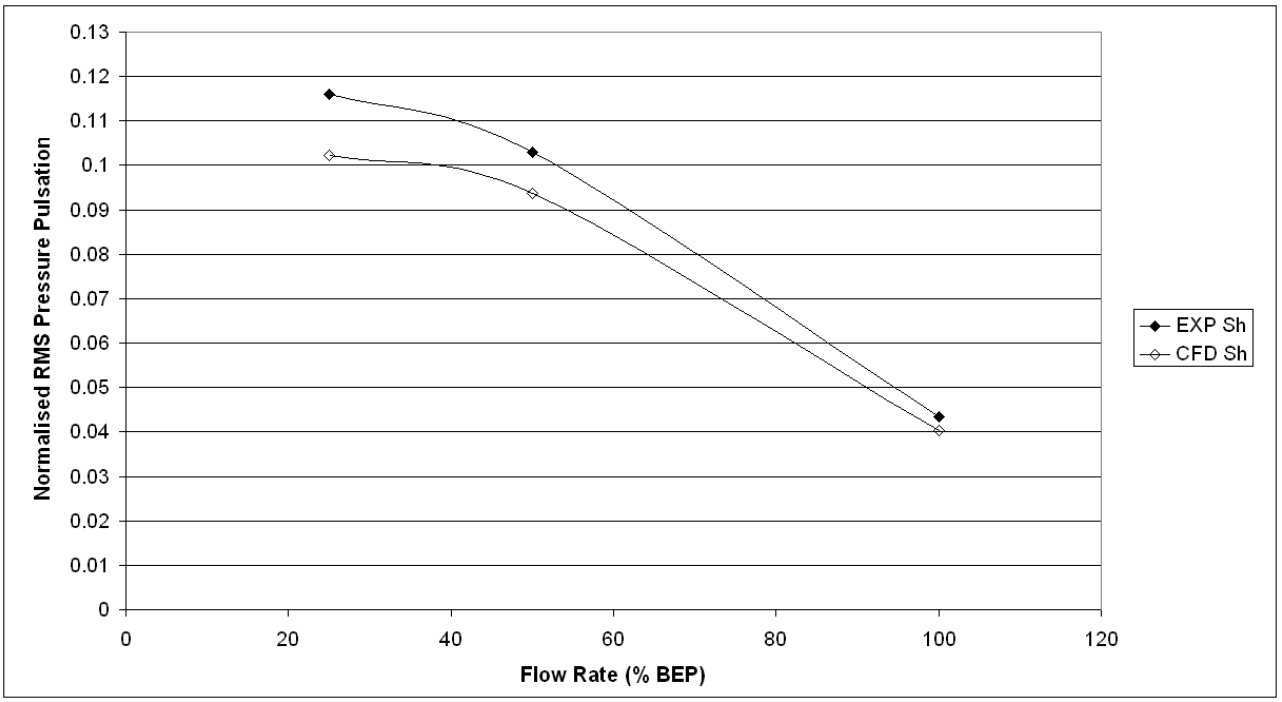

Figure 6.50: Normalised RMS comparison of experimental test 18 and CFD analysis test 5 for impeller region

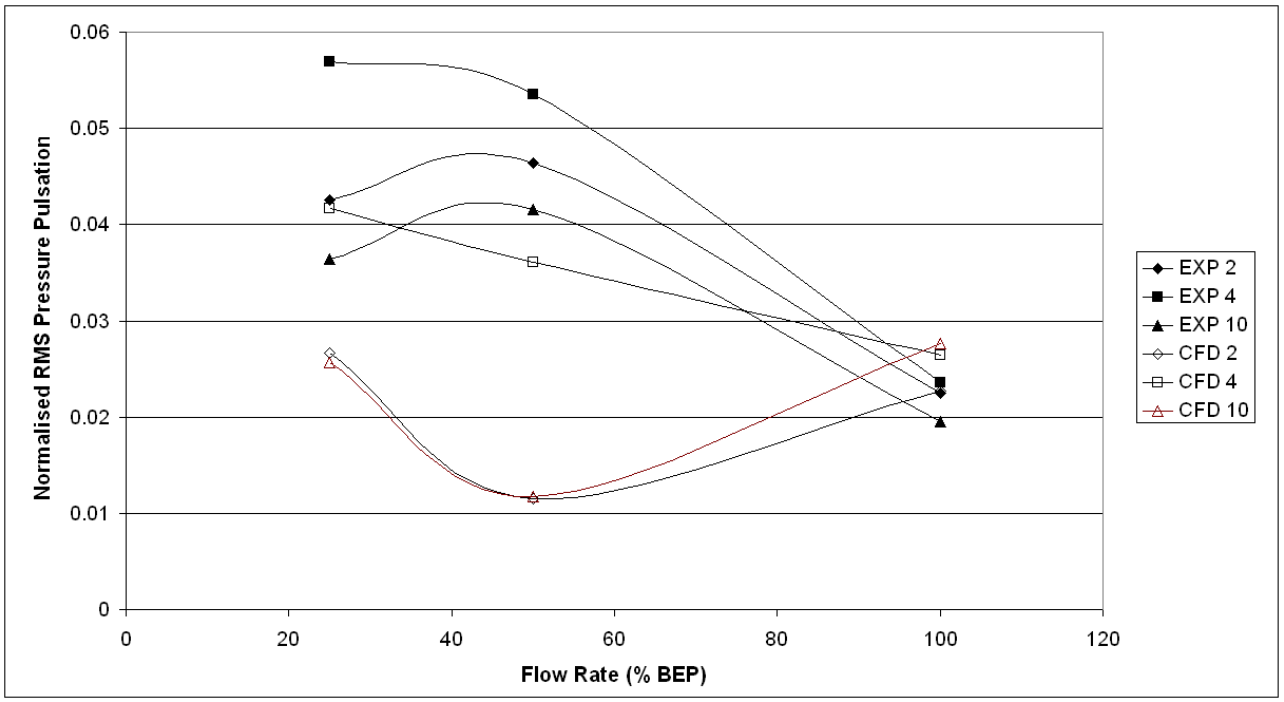

Figure 6.51: Normalised RMS comparison of experimental test 9 and CFD analysis test 3 for leakage region

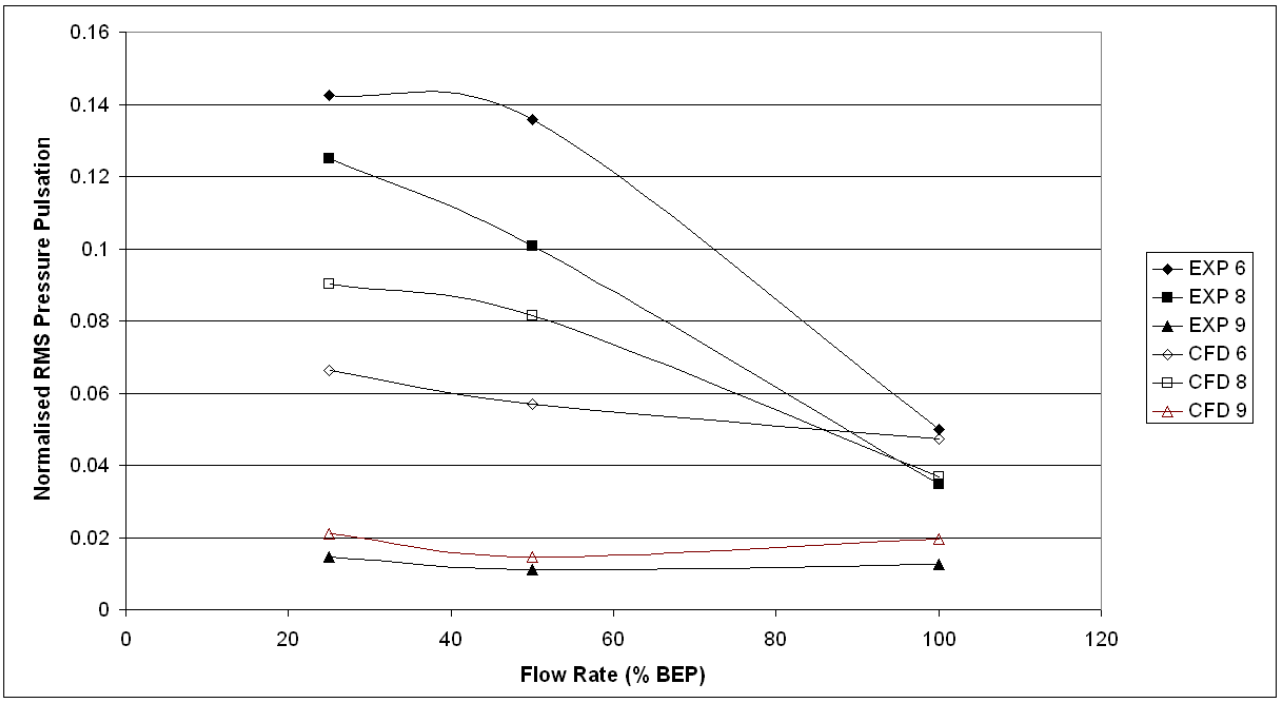

Figure 6.52: Normalised RMS comparison of experimental test 9 and CFD analysis test 3 for volute region

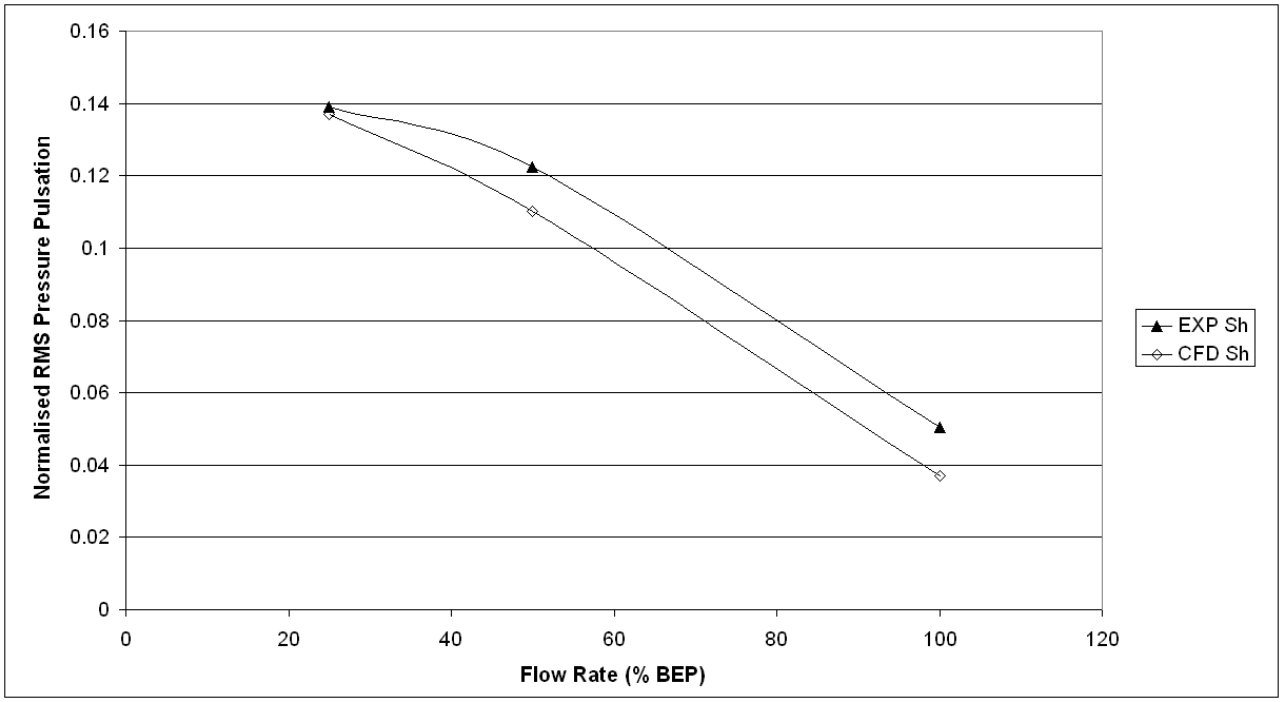

Figure 6.53: Normalised RMS comparison of experimental test 9 and CFD analysis test 3 for impeller region

Chapter 7

Discussion of CFD Results and Optimisation Studies

7.1 Visual Observations

7.1.1 Initial Observations

7.1.2 Geometrical Variations and Effect on Pulsation Levels

7.1.3 Summary

7.2 Taguchi Results

7.2.1 Resolution of the full L_9 Taguchi Array

7.2.2 Interactive Effects and Predictive Equations

7.2.3 Pressure Differentials Across the Impeller Shroud

7.2.4 Summary

7.3 Rationalisation leading to an Optimised Design

7.3.1 Consideration of Component Life

7.3.2 Pump Noise and Vibration Levels

7.3.3 Optimisation Observations and Further Analysis

7.3.4 Additional Analyses

7.3.5 Summary

7 Discussion of CFD Results and Optimisation Studies

The analyses conducted have been arranged so that they can be optimised using a Taguchi process. Thus all results are presented in the Taguchi array format for simplicity and consistency. The core of the CFD analysis results is the output of the twenty-seven transient analyses. Selected results for a few cases have been presented in Chapter 6. To give all of the results in that form would involve many graphs and may be unhelpful. This chapter attempts to summarise key elements of the results, particularly those related to pressure pulsations and performance.

The chapter first provides some discussion relating to initial observations of the results in relation to the geometric variables. Thereafter the results are presented in the context of a Taguchi analysis employing the nine arrangements (each at three flow conditions) in a L_9 array (see section 5.3.2). The geometric details of the nine arrangements are given in Table 7.1. Two smaller L_4 arrays selected from the analysis are also reported which allows additional information to be derived. The results of the Taguchi analyses are used to determine a geometric configuration that produces lower pressure pulsations. A rationalisation process was used to consider two main motivations, firstly reducing pressure pulsations with a view to extending component life and secondly reducing general pump vibration levels resulting from fluid effects. Additional analyses have been conducted based on the results of the rationalisation process and the new results presented and compared with pulsation predictions that can be made from the Taguchi analysis. Also, in section 7.4, transient analysis results are compared with steady state frozen rotor analyses to determine if steady state analyses can provide a simple method of obtaining a measure of the transient effects present in the pump. The chapter concludes with a brief description of an existing industrial impeller design guideline and an explanation of how the current work may enhance it.

7.1 Visual Observations

Performing a visual examination of the CFD results is the simplest analysis that can be conducted. Although limited, simple observation of the results can identify values that appear unusual when compared with the other values and can also indicate the important parameters that effect the pressure pulsation. The CFD results discussed in this section are provided as normalised peak to peak pressure pulsation values at fifteen chosen locations (detailed in section 6.1.2) in addition to performance data for each of the nine arrangements. This data is arranged in the Taguchi array format in Tables 7.2 to 7.4, with each table containing data for one of the three analysed flow conditions, 1.00Qn, 0.50Qn and 0.25Qn respectively.

The Taguchi array format does not assist the examination of the results using visual observation because of the efficient method by which the arrays minimise the number of arrangements to be utilised. Each arrangement only contains a single common geometric parameter with any other arrangement, so that trying to isolate the effect of a parameter visually can be complex; nevertheless certain strong trends can be determined.

7.1.1 Initial Observations

It is important to examine the results critically to determine if they are of a sensible value and to identify whether trends are as anticipated. If values do not appear to be as expected the results can then be investigated further. Chapter 6 has already determined that the pulsations and performance characteristics calculated by the CFD analysis are reasonable when compared to experimental tests, so that the emphasis here will be on values diverting significantly from anticipated trends.

It is simpler to detect deviations from the anticipated trends in the performance characteristics than in the pulsation data. The performance characteristics values are strongly linked to a single geometry parameter and hence trends can be established in a relatively straightforward manner. The general trend for the power characteristic is that

it decreases as the cutwater gap increases. However the power value for arrangement 9 at 0.25Qn does not follow this trend (Table 7.4), where the power value is slightly higher for a cutwater gap of 7.95% than the corresponding vane arrangement (arrangement 5) that has a smaller cutwater gap (6.00%). This seemingly large power value has a corresponding effect on the efficiency, causing the efficiency at arrangement 9 to be lower than expected. This effect could be caused by a number of factors but once highlighted the analysis was checked from pre-processing through to post-processing. These checks eliminated operator error as a factor and consequently the value is assumed to be a valid result.

It is also noted that pressure pulsations at 0.50Qn can be higher in some cases than those found at 0.25Qn, especially for arrangements with the tighter cutwater gaps. The process of determining the peak-to-peak pressure pulsation at all locations was reviewed for these arrangements and the process was found to be identical to those used at the larger cutwater gap arrangements. The difficulties of conducting a robust stable transient analysis at low flow conditions has already been discussed in Chapter 5.

7.1.2 Geometrical Variations and Effect on Pulsation Levels

Each of the four geometrical parameters was examined in turn. Even a brief inspection allows the following conclusions,

- Pressure pulsations increase as the flow decreases.
- The largest pulsations in the pump exist at the trailing edge of the impeller blade.
- Volute pulsations are larger than those in the leakage region

More detailed observations are provided below; these are largely general and are broadly consistent across the three flow rates.

7.1.2.1Cutwater Gap

The size of the cutwater gap exerts a strong influence on the pressure pulsation over a wide range of the locations monitored, with the pressure pulsations reducing as the cutwater gap increases. This influence is strongest at the impeller outlet region (Blade and Shroud positions) and at circumferential locations close to the cutwater/splitter locations in both the volute (C5 and C6) and the leakage flow region (C3 and C4). The influence, although still present, tends to decrease to some degree at regions circumferentially remote from the cutwater/splitter (locations C1, C2, C8, C9). These trends are understandable as the cutwater gap controls the distance between the impeller outlet and the cutwater and it is reasonable that varying the parameter would have the greatest influence in these areas.

The performance characteristic results show that the cutwater gap also has a strong effect on the head and power values, with their values decreasing as the cutwater gap increases. The efficiency shows a slight increase as the cutwater gap increases. The reduction in head and power are as a direct effect of the cutwater gap being modified by changing the impeller outlet diameter. The scaling law discussed in Section 4.3.3 predict that the head will reduce with the square of the impeller diameter. Additionally with the blade being made shorter by the reduction in impeller diameter, the reduction in power is not unexpected.

It is possible to compare the head generated values that the scaling law would predict for the reductions in the impeller diameter used in the project with the values calculated using CFD for similar impeller vane arrangements. For a single flow rate with the 3.83% cutwater diameter head generated value as a datum, the scaling law can be used to calculate what the change in head would be should the impeller diameter be reduced to give cutwater gap of 6.00% and 7.95% respectively. This calculation can be performed for each impeller vane arrangement (to keep the impeller shapes consistent) and the CFD values compared with the results gained from the scaling law for a single flow condition. The results of the calculation at the 1.00Qn flow condition and for the three vane arrangements are shown in tabular form in Table 7.5 and are plotted in Figure 7.1. The graph shows that the predicted head values from the scaling laws are

larger than those calculated from the CFD analyses. It is interesting to note that the relationship between head and the cutwater gap is reasonably linear over the range investigated. This performance loss with increasing cutwater gap is similar to that observed by Goulas and Truscott (77). Using the performance data provided by Goulas and Truscott, reproduced in Figure 2.2, and plotting it using a similar format to Figure 7.1, results in Figure 7.2. There are obvious similarities between the two plots, with Goulas and Truscott's showing a greater non-linearity but over a larger range of cutwater gaps (it is relatively linear over a cutwater range of 4% to 7%). The head scaling law used here is in common use, but is known to lack accuracy, especially for increasing reductions in impeller diameter. This is due to the assumption that the subtractive term in Euler's equation can be omitted; in practice this term is seldom zero and increases as the impeller diameter is reduced, hence the increasing difference between scaled and calculated heads as the cutwater gap increases as shown here. Obviously the scaling law should be used with care.

7.1.2.2Snubber Gap

Visual observations of the results for differing snubber gap clearances produce no clear trends at any of the three flow rates. Thus it is concluded that the snubber gap effect is significantly smaller than that caused by varying the cutwater clearance.

7.1.2.3Sidewall Clearance

Similar to the snubber gap clearance, visual comparisons of the three sidewall clearance sizes show no clear trends at any flow rate. Again it can be concluded that the sidewall clearance effect on pressure pulsations is significantly smaller than that caused by the cutwater clearance.

7.1.2.4Vane Arrangement

The vane arrangement can be seen to have an effect on the pressure pulsations at all pump locations. The inline vane arrangement has the strongest pulsations with the 30 degrees vane stagger typically registering lower pulsations; the 15 degree vane stagger

pressure pulsation values are between those produced at the two extreme vane positions but are not the average of them. Typically, pulsations with the 15 degrees vane arrangement will be closer to the 30 degrees vane results rather than the inline arrangement, however this does change depending on the location in the pump. The vane arrangement has the strongest effect on the pressure pulsations at the leakage flow location (C1 to C4), in the volute remote from the cutwater position (C7 & C8) and at the shroud. Reductions in the pressure pulsations at the cutwater (shown clearly at C6) and blade locations due to the vane arrangement are generally less than reductions due to the cutwater gap.

The vane arrangement has a small but noticeable influence on the performance characteristics, with the head and power reducing slightly when moving from an inline arrangement to a staggered arrangement. It is possible that the reduction in the generated head is caused by additional friction loss present due to the central hub extending to the outlet in the staggered case instead of terminating earlier in the inline arrangement. The efficiency is generally larger for a staggered impeller arrangement than an inline vane arrangement.

7.1.3 Summary

Visual observations conclude that the cutwater gap and vane arrangements have a strong effect on the pressure pulsations at certain locations in the pump, while the snubber gap and sidewall clearance effects are minimal and difficult to identify. As the cutwater gap is increased there is a reduction effect in both the pressure pulsations produced and the head generated. The results indicate that the area of influence of the cutwater gap on the pressure pulsations is strongest at the outlet of the impeller and at circumferential volute locations near the cutwater/splitter.

A comparison of staggered vane arrangements with the inline arrangement indicates that the staggered impellers produce smaller pressure pulsations in both the pump volute and leakage flow regions. The strong effect of the vane arrangement in the volute and leakage regions is rather less at circumferential positions close to the cutwater and splitter. Interestingly, although the staggered impellers generate a slightly lower head

than the inline impeller, the CFD results indicate that they are likely to be slightly more efficient. The above observations appear to be relatively consistent across the three flow rates.

7.2 Taguchi Results

The Taguchi process utilised here has been detailed in section 5.3.2, where the step by step process used to analyse the CFD results has been described. As mentioned, a full analysis of the interaction between all of the components is not readily achievable; however, it was anticipated that utilising the Taguchi method would provide a relative measure of the influence of the four geometry variables at critical pump locations in order to allow an investigation of the pump with regard to pressure pulsations.

The Taguchi method for the L_9 array is shown in detail by considering a single pump location as an example, namely position C8. This demonstrates the process used to determine the changes in the pulsation at this location caused by the geometrical variations and the flow rate and ranks the relative importance of the geometrical variables depending on their contribution to the pressure pulsation at that particular location. The results for all selected locations, calculated using all twenty-seven transient analyses are then presented and discussed.

Thereafter, reduced Taguchi arrays (L_4) are used to formulate simple equations relating the significant geometric variables directly to the pressure pulsation level at specific pump locations. The equations are restricted in form, but allow estimates of the pressure pulsations generated at each of the previously monitored locations for geometrical arrangements different from those analysed. The equations are limited to linear relationships for each of the geometrical variables, with the maximum and minimum levels for the variables set by those used in the analyses. This process generates equations for each location at each of the flow rates analysed.

Although the pressure pulsations are of primary significance in this study it is also important to consider the influence of the geometrical parameters on the pressure differential across the impeller shroud. The process used to investigate the pressure differential is similar to that described for the L_9 array above. However the investigation will not be as detailed as that for the pressure pulsations.

7.2.1 Resolution of the full L_9 Taguchi Table

The L_9 Taguchi array shown in Table 7.1 is reconfigured as illustrated in Table 7.6, where the actual factors have been replaced with +1/0/-1 to signify the minimum, mid and maximum values of the variables. Table 7.7 provides details clarifying the variables contained in Table 7.1 that have been replaced by –1, 0 or 1. Table 7.6 also provides pressure pulsation data for the 1.00Qn flow condition at C8 as an example of the layout of a data set used in the Taguchi method. Response averages can then be calculated from the normalised pressure pulsation values, also termed the variance data, for each of the geometric variables, Table 7.8 provides the response averages for the data set relating to location C8 at 1.00Qn. This table provides the outcome of the calculations is averages (or variance data) for each of the low (-1), mid (0) and high (+1) geometrical variables. A large difference in the variance data indicates a large influence on the pressure pulsations at that location. The data in Table 7.8 may also be reported in graphical form, as shown in Figure 7.3. This indicates that for the C8 location at the 1.00Qn condition, the vane arrangement has a strong effect from –1 to 0, but a lesser effect from 0 to +1, i.e. the strong effect is from an inline vane arrangement (the low –1 condition) to a staggered arrangement (0 and +1 conditions), but a lesser effect from a 15 degree staggered vane (0 mid condition) to a 30 degree staggered vane (+1 high condition). The cutwater gap has a consistent reduction in the pressure pulsation level as the cutwater gap increases in size. The snubber gap and sidewall clearance have lesser influence.

The data presented in this form is useful and the work in calculating and graphing each of the items of information has been performed for the three analysed flow rates. The above approach results in more than forty-five graphs covering fifteen items of

information (pulsation and performance related) for each of the three flow rates, but these have not been presented here. A simpler and potentially more useful format has been used that gives the percentage contribution to the pressure pulsation due to each geometric factor. The percentage contribution format is powerful as it allows the geometric factors to be compared against each other and ranked in order of importance in a single table for each flow rate. The detailed calculations required to calculate the percentage contribution have been provided in section 5.3.2.2, and a sample set of calculations using data at C8 for the 1.00Qn flow condition is shown in Table 7.9. Performing similar calculations for all monitoring points at 1.00Qn produces similar sets of percentage contributions. The process can then be repeated for both lower flows. Tables 7.10, 7.11 and 7.12 provide summaries of the percentage contributions to the pressure pulsation of the various geometrical modifications for 1.00Qn, 0.50Qn and 0.25Qn flow rates respectively.

The information in Table 7.10, 7.11 and 7.12 are complex but fascinating and the trends in the different areas of the pump will be discussed in some detail in what follows. The discussion will normally consider at least two monitoring points in each pump region in order to formulate trends within regions or consistent contributions over a number of points rather than concentrate on specific values.

7.2.1.1Leakage Flow Path

1.00Qn (Table 7.10): The major contributing geometrical factors to the pulsations in the leakage flow region are the cutwater gap and the vane arrangement. Surprisingly the snubber gap shows a negligible effect at all monitored positions and the sidewall clearance only manages a 5-14% contribution for regions in the leakage flow path that are circumferentially close to the cutwater/splitter locations. Away from the cutwater circumferential position the vane arrangement is really the only geometrical variation that has any significant effect of the pulsation. Near the circumferential cutwater position the cutwater gap exerts an increasing influence, but even at its largest values this is still only two-thirds of the influence of the vane arrangement.

0.50Qn (Table 7.11): At the lower flow condition the trends are similar to 1.00Qn, although there are a number of important differences. Firstly the sidewall clearance seems to contribute more towards the general pulsation levels, although this influence decreases sharply near to the cutwater position. The cutwater gap again exerts an increasing influence as the cutwater circumferential position is approached; the increase appears to be more of a "step" increase rather than a gradual change. The vane arrangement is still the dominant geometrical factor, but its effect decreases significantly when the cutwater gap influence is at its peak. The snubber gap shows a larger effect than at 1.00Qn, however this tends to be consistently in the range of 5 to 10%.

0.25Qn (Table 7.12): The lowest flow condition indicates that there are further changes to the trends above. The snubber gap now produces a significant effect on the pulsations close to the circumferential cutwater position. The sidewall clearance shows a consistently small effect regardless of position in the leakage area. Of greatest interest is the change in influence of both the cutwater and vane arrangement factors. In the leakage region away from the cutwater the vane arrangement contributes a large influence of around 65-81%, however this drops sharply once past the cutwater circumferential position. In contrast the cutwater gap exerts a limited, but still significant, influence in the general leakage flow path (C1), but this effect more than doubles close to the cutwater circumferential position (C3). It is also interesting to note that the cutwater gap influence is rather narrow as it reaches its peak at the C3 circumferential position and is already diminishing by the C4 position.

7.2.1.2Volute Regions

1.00Qn (Table 7.10): Close to the cutwater the cutwater gap is, as expected, the dominant influence on the pulsation. This influence diminishes relative to the distance from the cutwater and decreases to 16% at the top dead centre position of the volute immediately prior to the splitter position. The vane arrangement shows the opposite trend with its influence being around 30% close to the cutwater and increasing to 80% prior to the splitter. Both snubber and sidewall clearances have a minor to insignificant influence depending on position.

0.50Qn (Table 7.11): The trends experienced at 1.00Qn are very similar to those found at a lower flow condition. The percentage contributions for the cutwater gap and vane arrangement at either flow rate are generally within 5-10% except for C5, however as this is closest to the cutwater tip, some variation at this location is not unexpected. Snubber contributions are consistently slightly higher than at 1.00Qn but are still small. Sidewall contributions are of a similar level to 1.00Qn.

0.25Qn (Table 7.12): The previous trends continue, but the cutwater gap influence is more dominant at the cutwater gap than at the higher flows. In contrast the vane arrangement influence is much reduced at all locations; it does show an increase away from the cutwater but only reaches a 30% contribution, far less than at 1.00Qn. At the discharge this rises to 70%. The sidewall clearance is consistently small again, typically staying around the 3% value. The snubber gap shows little clear trend, although it is generally at a higher contribution level than the sidewall clearance.

7.2.1.3Impeller Trailing Edge

1.00Qn (Table 7.10): At the mid shroud position the cutwater has the greatest influence (67%), with the vane arrangement being significantly less (11%). For the above blade position on the shroud, the cutwater influence is similar to the vane arrangement at a 40% contribution. The snubber and sidewall clearances are consistent at around 8 to 13% for the shroud positions. At the blade locations, on the pressure face the cutwater is effectively the sole influence with a 95% contribution, and the major contributor at the suction face with 75%. The vane arrangement has no significant influence over the pulsations at the impeller blade. The snubber gap has a small but consistent effect. The sidewall clearance has no influence at the pressure face, but registers an 18% contribution at the suction face.

0.50Qn (Table 7.11): The shroud positions show very similar trends for the cutwater gap and vane arrangements for 0.50Qn and 1.00Qn flow rates. The snubber and sidewall clearances show consistently small contributions of less than 10%. At the blade positions there are some significant changes to the trends observed at 1.00Qn.

The cutwater is still the dominating influence at the pressure side of the blade, but has dropped to a 65% contribution. Both the snubber and vane arrangement register approximately a 15% contribution on the pressure face with the sidewall clearance showing a smaller contribution. At the suction face the snubber gap is the greatest contributor at 60%. The sidewall clearance continues to have a significant contribution of around 18%, while the cutwater gap and vane arrangement contribute around 10% of the pressure pulsation variation.

0.25Qn (Table 7.12): At the lowest flow condition, the contributing factors to the pulsation at the shroud positions change significantly. The vane arrangement effect at the shroud mid position continues to increase as the flow decreases, rising here to around 40%, however its contribution at the "above blade" position decreases. The cutwater gap effect reduces to almost half of its previous contributions at the mid shroud position; however the above blade influence increases to close to 60%. The snubber gap has a consistently strong contribution of just under 20% at both shroud positions, with the sidewall clearance also producing a consistent contribution of around 10%. At the blade pressure face the cutwater gap contributes at a level similar to 0.50Qn and at the suction face the contribution increases. The vane arrangement shows some significant influence of around 30% at both blade faces. The snubber gap continues to show a significant contribution at the suction face. The sidewall gap has no significant contribution at either location.

7.2.1.4Performance Characteristics

The largest influence on the generated head of the pump is the cutwater gap, which has a contribution of around 90% or more depending on the flow rate. The vane arrangement effectively provides the majority of the remainder, with the snubber and sidewall contributions being largely insignificant. The power characteristic is again dominated by the cutwater gap, especially at the higher flow rates, with the vane arrangement providing the most of the remainder. It is interesting to note that while the head and power contributions for the vane arrangement are relatively low, the contribution to the efficiency at 1.00Qn and 0.50Qn is surprisingly large. However at the lowest flow condition the contribution is effectively zero, with the cutwater gap

becoming the dominant influence. It is not clear why this is so but it is possible that the unusual result for arrangement 9 at the 0.25Qn flow for the efficiency may have influenced the percentage contributions to some degree.

7.2.2 Interactive Effects and Predictive Equations

The L_9 array provides useful information in the form of the percentage contributions, but does not provide information on interaction effects between the geometric parameters. The L_9 array is generally not recommended for this purpose (these issues are detailed in section 5.3.2.1), although it can be used to screen the factors to identify those that are the most important. From the discussion above it appears that, of the four factors investigated, the cutwater gap and the vane arrangement are the two most important by a significant degree. An L_4 Taguchi array can now be used to gauge the interactive effect between the strongest two factors. It is important to recognise that the L_4 array can only compare two factors with two levels each, therefore all relationships will automatically be approximated as linear with geometry. It has already been shown that, for some locations, the pressure pulsation change is approximately linear with geometry but this may not be the case for every location. The vane arrangement effect on the pulsation is certainly not linear. The investigation was performed in two stages:

Stage 1: A single array was formed for each flow rate, with the vane arrangement being limited to either being inline or with a 30 degree stagger and the cutwater being variable between 3.83% and 7.95%. This generated equations (using the process detailed in section 5.3.2.3) that can gauge the effect of the cutwater gap for both inline and staggered vanes.

Stage 2: A further array was formed for each flow rate, for cutwater gap values of 3.83% and 7.95% and vane arrangements of 15 and 30 degree stagger. This array generated further equations that can be used to investigate the relationship between the pulsation at specific pump locations and the pump geometry.

Makay and Szamody (86) have suggested that the pressure pulsation relationship with the cutwater gap is exponential over a large range of cutwater gaps. The prediction equations derived from the above are linear and will only be accurate over relatively small ranges. If at a later stage there is more interest in cutwater gaps in the range of 4% to 6% or 6% to 8% rather than from 3.83% to 7.95% then a reduced cutwater gap range could be used to improve the accuracy of the predicted relationships.

The analysis strategy for these reduced arrays is detailed in Section 5.3.2.3 and is a graphical approach with a prediction equation relating the pressure pulsation or head generated to cutwater diameter and vane arrangement. The analysis involves a number of steps, although some of these steps have effectively been conducted as part of earlier examinations of the larger L_9 array.

7.2.2.1 Stage 1 (Vane: Inline & 30^o Stagger, Cutwater Gap Values: 3.83% & 7.95%)

The array used for stage 1 is indicated in Table 7.13, which details those arrangements from the L_9 Taguchi array that have been used to construct the L_4 array; sample information is again provided for location C8. The data resulting from this analysis is shown in full in Table 7.14.

The interaction between the cutwater gap and the vane arrangement can be investigated through plotting the response averages; the interaction plot for 1.00Qn is shown in Figure 7.4 for a selection of locations within the pump. The response averages are plotted for the low (-1, inline) and high (+1, 30 degree stagger) vane arrangements, for the low (-1, 3.83%) and high (+1, 7.95%) cutwater gap conditions for specific locations. Where the lines are parallel, this indicates little or no interaction, whereas lines with very different gradients indicate significant interaction. Figure 7.4 illustrates that interaction does exist between the two factors examined, but not at every location. The interaction appears strongest close to the trailing edge of the impeller and almost non-existent at locations C1 and C6. Figure 7.5 provides a plot of the interaction data for 0.25Qn illustrating that as the flow rate reduces the strength of the interactive effect can

change significantly depending on the location and the majority of the locations in the pump are affected.

Table 7.15 provides a list of the calculated response averages, effects (Δ) and half effects (Δ/2) for a selection of pump locations. As the interaction can be important depending on the location the calculation for the interaction column is included in the tabulated results. It should be noted that the grand mean has also been calculated and reported in the table. There are a number of methods to determine the relative importance of the various factors, including plotting the averages for each factor and comparing the gradients or plotting a Pareto chart. The Pareto chart is a more striking visual representation of the relative importance and so sample Pareto plots are provided in Figure 7.6 for four pump locations at 1.00Qn. Plots at the same locations are provided for the lower flow rate of 0.25Qn in Figure 7.7. This indicates that while the most important factor can switch between the cutwater gap and the vane arrangement (e.g. C3), the interaction effects are never the most important and at positions away from the impeller are generally the least influential factor.

The general prediction equation is of the form shown in equation 5.18. The calculations performed above have obtained all of the information required to form the predictive equation for the pressure pulsation at any of the reported pump locations. The equation is simply formed by inserting the grand mean and the half effect values for each of the factors into the general prediction equation. Equation 7.1 below provides a sample equation for location C8 at 1.00Qn.

$$y = 0.11237 - 0.03091A - 0.02773B - 0.00376AB \qquad \text{Equation 7.1}$$

Where y is the pressure pulsation at location C8 at 1.00Qn

A is the cutwater factor varying between –1 and 1

B is the vane arrangement factor varying between –1 and 1

AB is the interaction factor calculated from the selected A and B factors.

By varying each of the factors between –1 and 1 it is possible to determine what pressure pulsation (or head generation) is likely to be obtained with a certain geometry set, even if it is not one of the arrangements that were analysed. For instance, from Equation 7.1 for the C8 location, it is possible to obtain predictions of the pulsations at this location for a cutwater gap of 5% (a cutwater gap (A) factor of approximately –0.5) and an inline vane arrangement (a vane arrangement (B) factor of -1). Entering this data into the equation produces a normalised pressure pulsation of 0.154 at location C8 for 1.00Qn. This can then be compared with the pulsation for a 30 degree staggered impeller (a vane arrangement factor of +1), i.e. 0.102. Both of these predicted values seem sensible when compared with the analysis data contained in Table 7.2. Due to the marked differences between inline and staggered arrangements the vane arrangement factor is restricted to either –1 or +1, as intermediate increments will not provide realistic predictions. The Stage 2 analysis will provide a better comparison of varying the vane stagger angle.

7.2.2.2Stage 2 (Vane 15degree & 30degree stagger, Cutwater Gap Values: 3.83% & 7.95%)

The array for use in stage 2 is provided in Table 7.16, again including details of the arrangements from the L_9 array that are to be used and sample data for position C8. The results from this analysis are given in Table 7.17. It is not felt that there is a need to present the interaction plots similar to Stage 1, but the interaction effects are included as before.

The calculated response averages, effects and half effects are provided in Table 7.18 for the same pump locations shown in Stage 1. The grand mean has again been calculated and reported in this table for each of the pump locations. Again Pareto charts are provided for four pump locations (position C3, C6, C9 and on the shroud above the blade) at flow conditions 1.00Qn and 0.25Qn in Figures 7.8 and 7.9 respectively. These graphs show that when considering all locations and both flow rates, the cutwater gap has the strongest influence. The vane arrangement (in this instance relating to the amount of stagger only) is strongest at location C9 for 1.00Qn and its effect appears to strengthen at the lower flow, especially at the shroud above blade position. The

interactive effect is again smaller than the other two factors, however it can be seen that at location C3 it can provide a significant contribution.

As in Stage 1, the data in Table 7.18 can be used to generate predictive equations for the pressure pulsation (or generated head) for any of the pump locations. For the geometrical arrangements used in the Stage 2 array, both the cutwater gap and vane arrangement can be varied from –1 to 1 in order to investigate other arrangements. Using the C8 data at 1.00Qn as provided in Tables 7.16 and 7.17 results in the data presented in Table 7.18. This data can then be used to generate Equation 7.2.

$$y = 0.0812 - 0.019A + 0.0035B - 0.0155AB \qquad \text{Equation 7.2}$$

Again we can use this equation to predict other geometrical arrangements. For example, a cutwater gap of 5% (cutwater gap factor of approximately –0.5), and a 25 degree vane stagger angle (vane arrangement factor of around +0.33) results in a normalised pressure pulsation value of 0.087 at position C8. This could be compared, for example, with a 20 degree vane stagger angle (-0.33 vane arrangement factor), which results in a normalised pulsation of 0.094.

7.2.3 Pressure Differentials Across the Impeller Shroud

In the context of design it is useful to have some knowledge of the pressure differential across the shroud since this is the primary loading causing bending stress in the shroud. To find the pressure differential the pressure was monitored at defined radial positions on the inside and outside of the impeller shroud at the mid point in the impeller passage between two impeller blades. The grid in the leakage flow path varies in a straight radial direction, whereas the grid in the impeller follows the blade curvature, so it was not possible to simply read off pressure points from grid locations to obtain the differential. A number of probe points were generated a short distance away from the mid passage line to gain information away from the internal impeller interfaces. These points were then varied in the axial direction so that one set sat along the inside of the shroud, with a second set being included that were arrayed along the outside of the

shroud. This was the only method available to ensure pressure was selected at identical circumferential positions at the inside and outside of the shroud. The points were located radially, at 5mm increments, ranging from the wear ring radius of 111mm out to the impeller outlet (a total of fifteen points for the smallest impeller diameter and seventeen for the largest). The differential calculated is presented both as a pressure value in N/m^2 and relative to the generated head, as this latter format is of benefit when considering design guidelines.

The pressure data at these points was then monitored at three blade/cutwater positions, illustrated in Figure 7.10

1. Leading blade opposite the cutwater.
2. Mid passage position opposite the cutwater
3. Trailing blade opposite the cutwater.

This data was collected at the mid passageway for both 1.00Qn and 0.25Qn flow conditions and for all nine Taguchi arrangements.

At 1.00Qn, Figure 7.11 shows the pressures acting on both the inside and outside of the shroud from the first arrangement, for each of the three impeller positions, described above. It should be noted that the general shape of the graphs at each location and the relative pressures from the inside to the outside of the shroud are remarkably consistent across all nine arrangements at the same flow condition, although only the first arrangement is shown here. It can be seen that the pressure differential from the inside to the outside of the shroud forms a triangular type shape. At the duty condition the pressure differential is reasonably consistent at both the wear ring diameter and at the impeller outlet, varying on average from around $1.2e5N/m^2$ at the wear ring to zero at the impeller outlet. The pressure differential can be related to the head generated using the values shown in Table 7.2, which indicates that $1.2e5N/m^2$ corresponds to 0.34 times the generated head (0.34*H). It is observed that taking the maximum variation increases the value slightly to 0.35*H ($1.23e5N/m^2$). The graphs confirm the consistent

pressure differential at different impeller positions, with the largest deviation tending to occur close to the impeller outlet.

At 0.25Qn, a similar graph, Figure 7.12, can be produced showing the pressures on the inside and outside of the shroud at different impeller positions. Again the general shape of the graphs at the nine different arrangements is relatively consistent, but the three positions show different patterns, i.e. at position 1 there is a reversal of the pressure differential, while at positions 2 and 3 there is a considerable differential across the shroud all the way from the wear ring to the impeller outlet. This change in the pressure differential is caused by a reduction in the pressure in the impeller passage as it passes the cutwater. This reduction in pressure occurs at the lower flow condition due to the strong recirculation described in section 6.2.2. It is obvious from the graphs that there is a significant difference in the shape of the differential at 0.25Qn compared with 1.00Qn and it is therefore less appropriate to use average differential values across the three positions. However, it is important to note that the largest differential at the wear ring is 1.88e5Nm^2 (0.48*H) with the shape of the differential (with radius) being closer to a trapezoid. Also the larger variation in the differential at the impeller outlet is also clearly identified through the difference in values from position 1 to positions 2 and 3 at the impeller outlet (radius 0.183m), which forms a pulse in the differential of 1.8e5 (0.46*H) as the impeller rotates.

For all nine arrangements, values of the average of the three differentials, the maximum differential and the pulse in the differential as the impeller rotates has been provided at both the wear ring diameter and the impeller outlet in Tables 7.19 and 7.20, for flow conditions 1.00Qn and 0.25Qn respectively. The tables provide the differentials in both the pressure format (N/m^2) and relative to the equivalent head (*H) for each specific arrangement and flow condition. At 1.00Qn (Table 7.19) the wear ring average pressure differential values are 0.4*H or lower for all but two arrangements. The average pressure differential values at the impeller outlet are significantly smaller than those at the wear ring diameter, often an order of magnitude or more smaller. The variation in the differential pulse at both the wear ring and the impeller outlet is relatively small (around a quarter or less of the differential at the wear ring). At 0.25Qn (Table 7.20) the

maximum pressure differential at the wear ring is always larger than at 1.00Qn, with the range being between 0.45*H and 0.56*H. The maximum pressure differential at the impeller outlet is also significantly larger than that at 1.00Qn and is certainly non-zero. The variation (or pulse) of the differential also changes significantly as the flow rate decreases. At the impeller outlet the pulse increases by a factor of four or more in all but one arrangement. At the wear ring the pulsations are often half the magnitude of those at the impeller outlet, however arrangements 2,3,5 and 6 show high pulses at the wear ring relative to the pulse at the impeller outlet.

It is important to note that due to the pressure reversal for the 0.25Qn flow condition, the impeller outlet is the main location of the sizable increase in the pulsation of the pressure differential. The CFD results show that there is a complete pressure differential reversal that varies from the pressure differential at the impeller outlet to an approximately equal pressure differential in the opposite direction. This complete pressure differential reversal at the impeller outlet would indicate that fatigue might be a concern due to these actions.

The results presented in the above tables can be used to generate the percentage contributions to the pressure differential at the wear ring and impeller outlet by the four geometry parameters varied in this project. The percentage contributions relating to the maximum pressure differentials and the pulsation of the differentials at the wear ring and impeller outlet for both 1.00Qn and 0.25Qn flow conditions are shown in Table 7.21.

The percentage contributions indicate that the snubber gap is the dominant factor relating to the pressure differential at the wear ring and impeller outlet as well as the pulsation in the differential at the outlet irrespective of the flow rate. This dominance arises due to the restrictive effect that the snubber gap exerts on the flow trying to enter the region at the back of the impeller. Yet it is surprising that the dominance is so strong since the individual pressures (examined in section 6.3) do not show a significant effect relating to the snubber gap. Essentially, the tighter the snubber gap the greater the differential across the shroud and the greater the variation in the pressure differential

at the impeller outlet. Each of these effects is detrimental to the structural integrity of the impeller. The sidewall clearance is also shown to make an important contribution especially in relation to the pulsations in the pressure difference at both the wear ring and impeller outlet. The largest contributions due to the cutwater gap are at the wear ring with the strongest contributions being at the lower flow condition. The vane arrangement contribution is small relative to the other parameters, although it does increase slightly at the lower flow rate.

In a similar manner to that described in Section 7.2 it would be possible to generate predictive equations relating the geometry parameters to the pressure differential. Some changes would have to be made to the process, as the snubber gap parameter was not included in the predictive equations previously. However the results presented in this section are relatively consistent across all arrangements particularly at 1.00Qn and it is considered that deriving the predictive equations would give little further benefit.

7.2.4 Summary

The Taguchi process has provided significantly more detail concerning the influence of the geometric parameters on the pressure pulsation and performance characteristics than can be obtainable from direct observation. In the leakage flow region, the vane arrangement is the dominant influence on the pressure pulsation at all three flow rates, although this influence reduces rapidly as the flowrate reduces and also reduces with circumferential distance from the cutwater and as the flow rate reduces. The cutwater gap has a significant influence at the circumferential positions close to the cutwater, with its significance at both this location and more generally increasing as the flow rate decreases. The snubber gap and sidewall clearance typically have a much smaller influence than the other geometrical parameters.

The results at the volute region shows similar trends to that described above, i.e. the vane arrangement has the strongest effect on the pressure pulsations at locations remote from the cutwater position, while the cutwater gap effect is strongest at the cutwater position. Although the strength of the vane arrangement influence does appear to

reduce with flow rate, the reduction is not as significant as that observed in the leakage region. The effect of the vane arrangement on the pulsations at the impeller outlet is especially complex making trends relating this influence to geometric parameters difficult to describe in a simple manner. In broad terms the cutwater gap has the strongest influence, with the vane arrangement gaining more influence across a number of positions at the lowest flow condition. Both the snubber gap and the sidewall clearance can have a significant influence at the impeller outlet depending on the flow rate and specific location.

The cutwater gap has the most significant influence on the performance characteristics. It is important to note that the vane arrangement can show a significant contribution to the efficiency coupled with a smaller influence on either the head or power characteristics.

Two lesser Taguchi L_4 arrays have been used to generate two typical sets of linear equations that can be used to predict both pressure pulsation and performance characteristics for geometrical configurations other than the nine analysed. These equations could also be utilised to predict pressure pulsations at similar internal pump locations for other double entry volute pumps. Of course one could use the CFD results to develop predictive equations for any location of interest not just the ones discussed here.

An examination of the pressure differentials across the impeller shroud has indicated that at the duty condition the differential is relatively consistent as the impeller rotates, but with the largest differential tending to occur at the wear ring. At the lowest flow condition the pressure differential increases significantly, with there also being a large change in the pressure patterns on the inside and outside of the impeller shroud depending on the position of the impeller in the volute. It has been observed that at the low flow condition there is a reversal in the pressure differential at the impeller outlet as the impeller rotates indicating that fatigue may be a concern. Consideration of the percentage contributions of the various geometrical parameters to the pressure differential has indicated that the snubber gap is the dominant factor.

7.3 Rationalisation Leading to a Recommended Design

Optimised design in the present context is rather complicated, as one cannot easily optimise on "pressure pulsations." The work conducted here has shown that there are complex relationships between geometry and pressure pulsations depending on the location of the monitoring positions. These relationships also change significantly depending on the flow rate at which the pump is operating. Therefore any rationalisation process requires some consideration of exactly where the pulsations are to be reduced. For example a design aimed at reducing the pulsations at the impeller trailing edge would be quite different to one that minimised the pulsations at the cutwater. In the present context, there are two main motivations behind the requirement to reduce pulsations

1) Component Life: Large pulsations may cause fatigue within the pump. The component most likely to be subject to damage due to fatigue is the impeller. A typical fatigue failure pattern was discussed briefly in section 3.1 and shown in Figure 3.1. The aim of the rationalisation process in this case would be to increase component life by reducing both the pressure differentials and the pressure pulsations at the impeller outlet.

2) Pump Vibration Levels: Large pulsations in the pump also cause vibration and noise. Thus the aim of the rationalisation process in this case would be to reduce hydraulically generated noise and vibration by reducing the overall level of pressure pulsations in the pump.

These requirements could exist separately or together depending on the application of the pump. Additionally, regardless of the motivation behind the process, the benefit gained in terms of pulsation reduction must be balanced against any possible loss in pump performance.

7.3.1 Consideration of Component Life

It is recognised that stress concentrations play a large role in fatigue failure and where fatigue is a factor, the usual first step in extending component life is to minimise any stress concentration factors present in the component. However the important stress concentration area between the impeller blades and the shroud has limited potential for improvement since the maximum radii size is limited to half the impeller tip width. Therefore, with the detailed mechanical design constrained by the impeller dimensions, it is important to minimise the hydraulic pressure loadings and fluctuations on the impeller. This will be achieved through focusing on the reduction of:

(1) pulsations at the impeller outlet
(2) the pressure differential across the impeller shroud

Using the work presented in Chapter 6 and earlier in this chapter, where the results are considered in relation to the general effect of geometric variations on the pressure pulsations and the structural integrity of the impeller shroud over the flow range, it is possible by rational argument to arrive at an optimisation. Each geometric factor will be examined in turn and its effect considered relating to the above parameters as well as possible effects on the pump performance.

Cutwater Gap: The cutwater gap has been found to exert one of the strongest influences, if not the strongest influence on the pulsations at the impeller blade and shroud locations. The CFD results agree with published data that increasing the cutwater gap reduces the pressure pulsations. Yet it is difficult to determine an adequate reduction in pressure pulsation while offsetting this against a reduction in performance (due to the impeller diameter reduction) without some relationship between the two. The ideal situation is to achieve as much reduction as possible in pressure pulsation for as small a reduction in the head generated as can be achieved. Figures 7.13, 7.14 and 7.15, plot the response averages for the normalised pressure pulsations at the blade pressure face and shroud mid positions in addition to the generated head for the three cutwater gaps averaged over a single impeller revolution. The change in pulsation at the blade pressure face, Figure 7.13, is reasonably linear at

1.00Qn, but slightly less so at the lower flow rates. At the lower flow rates there is a slight lessening in the pulsation reduction as the cutwater gap increases. The change in pulsation at the shroud mid position, Figure 7.14 again shows reasonable linearity at 1.00Qn, but a significant non-linearity at the lower flows. The lower flow results introduce some confusion as the 0.50Qn result indicates a reducing effect as the cutwater gap increases, while 0.25Qn shows the opposite effect. It is observed that the 6% and 7.95% cutwater gap values for both 0.50Qn and 0.25Qn are reasonably consistent, with the overall shape of the graph being controlled by the 3.83% values. During the initial observations (section 7.1.1), it was noted that the pulsation values for tight clearances at the lowest flow might be under predicted. The relationship between the generated head and the cutwater gap, Figure 7.15 is linear at all flow rates with a slight non-linearity, inverse to that previously shown, being shown at the lowest flow condition.

From the above discussion it can be observed that there is no clear optimised solution relating to the cutwater and reducing the pulsations at the impeller outlet. The linear relationship between both the pulsations at the blade pressure surface and the generated head would perhaps indicate that any increase in the cutwater gap will reduce the pressure pulsation but this must be tempered by the reduction in head. The non-linearity of the shroud pulsations, especially at lower flow conditions, would indicate a lesser reduction in pulsations at this location as the cutwater gap increases. Therefore selecting a cutwater gap of around 6% or slightly larger provides a substantial reduction at both the blade and shroud locations. Increasing the cutwater gap beyond 6% will provide little pulsation reduction at the shroud for a continuing reduction in head.

Vane Arrangement: The vane arrangement has a mixed effect on the pressure pulsations at the impeller outlet. Figures 7.16 and 7.17 indicate the effect of the vane arrangement on the average blade and shroud pulsation values at the three flow rates analysed, with Figure 7.18 detailing the relationship with the head generated. In these figures the points are simply joined by straight lines rather than curves because of the discrete geometry changes involved. The staggered arrangement appears to decrease the pulsations at the impeller blade tip slightly all flow rates (Figure 7.16), with the

exception of the 30 degree stagger at the lowest flow condition. At the shroud (Figure 7.17), both staggered arrangements provide significant pulsation reductions in comparison to the inline blade impeller, with the 30 degree stagger producing a slightly lower pulsation than the 15 degree impeller. Moving from an inline arrangement to a staggered arrangement also causes a reduction in head (Figure 7.18), however at low flow rates the 30 degree staggered impeller generates a higher head than the 15 degree impeller at both 0.50Qn and 0.25Qn.

Thus the decision concerning optimisation of the vane arrangement centres on whether the reduction in pulsation at the shroud and blade locations is worth the reduction in head generation. As stated earlier the failure mechanism for impellers focuses around the stress at the impeller vane/shroud connection caused by pressure across the shroud span at outlet (especially the mid position). Thus it is judged that the reduction of pressure variation at the impeller outlet is of significant importance when considering the life of the impeller. Therefore a staggered impeller appears to be a better option than the inline impeller. However there remains some uncertainty whether the slightly higher pulsations at the blade for the 30 degree stagger is offset by the lower pulsations at the shroud and the higher head generation characteristic in comparison to the 15 degree arrangement.

Snubber Gap: The analyses indicate that the snubber gap can play a significant role in the pulsations across the impeller outlet and will provide a measure of control over the pressure differential across the impeller shrouds. A tight snubber gap will prevent the pulsation from passing into the leakage flow area; this causes the pulsation energy to remain close to the impeller outlet, increasing the pulsation in this area. However at the same time this will maintain a larger differential across the shroud. Conversely, a large snubber gap allows the pulsation to pass into the leakage flow region causing large shifts in pressure, which published literature indicates can cause shuttling of the impeller if the gap is sufficiently large (84). Therefore some mid size gap appears to provide the optimum solution, a snubber gap that is large enough to allow the pulsation to pass away from the impeller tip into the leakage path, yet not enough to cause the shuttling effect. It is considered that this gap should be greater than 1% to reduce the

pressure differential across the shroud, but less than 1.5%. It is noted that in industry a general rule of thumb relating to the snubber gap is that the length of the snubber gap should be six times its height in order to attenuate the pressure pulsations (130). The author has not determined the source of this rule of thumb, but the above recommendation of 1.0% would equate to a radial snubber gap distance of 1.8mm. The rule of thumb would indicate that the snubber gap should be 11mm in length. The shroud thickness for the analysed impeller is 7mm, equating to less than 4 times the radial snubber gap distance. Six times the gap is not practical without increasing the impeller shroud thickness considerably, which is not economically viable. Section 7.2 has indicated that the cutwater gap and vane arrangement are more significant geometric factors that can be used to reduce the pressure pulsation in the leakage flow path. Therefore, it appears likely that when used in conjunction with a geometric arrangement that has relatively low pressure pulsation levels in the leakage flow path a larger snubber gap than that indicated by the rule of thumb could be used.

Sidewall Clearance: The sidewall clearance exhibits only a small effect on the pulsation at the impeller outlet region, and any contribution occurs at the lower flow conditions. Thus, while the sidewall clearance has no apparent effect on the performance of the pump, results indicate that maintaining a 100% clearance gap may provide slight benefits at lower flows. Thus the 100% sidewall clearance is considered the most sensible configuration.

7.3.2 Pump Noise and Vibration Levels

The pump noise and vibration levels due to blade passing frequency directly relates to general pulsation levels within the pump. Published literature by Srivastav et al (131) has noted that the blade passing frequency dominates the vibration spectra and governs the overall vibration level, with the strength of the frequency being dependent on the radial gap. Section 2.2 has reported published work which clearly shows that unsteady rotor/stator interactions can be related to pump acoustics. These unsteady interactions are also related to the radial force due to an imbalance in the pressure field at the impeller outlet, which is a cause of pump vibration. Therefore, both the vibration and

acoustic levels can be related in some manner to the variation in pressure in the pump. This is not related to a specific location in the pump, but rather to general pulsation levels in the pump. This section will follow a similar format to that used in section 7.3.1, where information presented in previous sections is used to arrive at a best compromise.

Cutwater Gap: The percentage contributions presented in Section 7.2.1 indicate that the influence of the cutwater gap is largest close to the cutwater and that its influence reduces significantly over a relatively small distance. Plotting response averages at locations C3 and C7, Figures 7.19 and 7.20 respectively, provides some indication to the relationship between the pressure pulsations in the leakage flow region and the cutwater gap. For C3 (Figure 7.19) the relationship is reasonably linear at the higher flows, but shows a lessening reduction in the pulsation at 0.25Qn. At C7 (Figure 7.20), the relationship is certainly non-linear at 1.00Qn and 0.25Qn, but shows more linearity at 0.50Qn. The non-linear relationship indicates a reducing rate of pulsation reduction as the cutwater gap increases. Therefore the above graphs indicate that a greater reduction in the pulsation within the volute and leakage flow path is obtained for the cutwater range 3.83% to 6% than from 6% to 7.95%, for a similar reduction in head. As a result, a 6% cutwater gap is selected as an optimum solution that gives a substantial pressure pulsation reduction in the pump while limiting the reduction in the generated head.

Vane Arrangement: A staggered impeller provides significant reductions in pulsation at most locations in the volute. The effect of the vane arrangement tends to be strong where the cutwater gap influence is weak and vice-versa. The effect of the vane arrangement on the pressure pulsation response averages is shown for the same two locations as used in section 7.3.1 (C3 and C7) in Figures 7.21 and 7.22 respectively. The averaged pulsations at location C3 (Figure 7.21) indicate that both staggered vane arrangements provide significant benefits over the inline arrangement at 1.00Qn and 0.50Qn. However at the lowest flow the 30 degree staggered arrangement, shows a significant reduction in pulsation over both the inline and 15 degree arrangements whose values are quite similar. At location C7, Figure 7.22, both staggered

arrangements provide a reduction in pulsation over the inline arrangement. There are slight differences between the staggered arrangements at different flowrates as at the highest flow rate the 15 degree staggered impeller has the lowest pulsation, while at the lowest flow rate the 30 degree staggered impeller is the lowest.

The discussion above indicates that there are only slight differences in the pressure pulsation averages to separate the different values of impeller blade stagger. It is interesting that the 30 degree arrangement indicates a higher head. The general opinion in industry (132) is that the mid stagger position should perform slightly worse than other stagger angles. The classic jet-wake flow structure resulting from impeller flow is shown in Figure 7.23. It is usually considered that when staggered at a mid position the jet flow from one side of the impeller, will be mixing with the wake flow on the opposite side and therefore it is considered that the mixing losses due to this interaction will be relatively high in comparison with other blade stagger angles. To identify the amount of mixing between the two halves of the impeller in this current work for the two staggered impeller blade angles, a plot of the axial component of the flow in close proximity to the impeller outlet is examined. Figure 7.24 and 7.25 show this axial exchange of fluid from one side of the impeller towards the other for the 30 degree and 15 degree vane stagger angles respectively. It is immediately apparent that the 30 degree vane stagger arrangement includes an axial mixing of the flow at the impeller outlet over a considerably larger area than the 15 degree stagger. In the current work this larger mixing region does not appear to have had a significant effect on the pump generated head, although for other impeller designs this may not be the case. Therefore, while in this case the higher head may influence the selection of the 30 degree vane arrangement over the 15 degree arrangement, this cannot be a universal recommendation.

Snubber Gap: This has a small effect on the pulsations in the leakage flow region at the lowest flow condition according to percentage contributions. The effect is slight and does not allow clear guidelines to be drawn relating to an optimised design. The obvious conclusion that can therefore be drawn is that for noise and vibration considerations the snubber gap does not contribute significantly for the sizes analysed

Sidewall Clearance: The sidewall clearance has a slight effect on the pulsations in the leakage flow path at the lowest flow condition according to percentage contributions. However, in a similar manner to the snubber gap, this data is not substantial or significant enough to draw optimised design conclusions. Thus the sidewall clearance does not contribute significantly to the blade rate noise and vibration of the pump for the sizes analysed.

7.3.3 Optimisation Observations and Further Analysis

Although the pump geometry has been examined using two different motivations there is likely to be some agreement between the two. Table 7.22 provides a comparison of the results of the two sections discussed above

Consideration of the table allows a final "optimised" or recommended arrangement to be selected,

- The minimum cutwater gap should be 6%.
- The vane arrangement should use a 30-degree stagger (i.e. a mid position stagger).
- The diametral snubber gap should be greater than 1%, but less than 1.5% of the impeller diameter.
- The sidewall clearance should be 100%.

Originally the project had planned for an analysis of the "optimised" arrangement to be performed. As it happens, the above arrangement is very similar to the fourth arrangement analysed, with the cutwater diameter and vane arrangement being the same. It was therefore decided to perform some further analysis based on the recommended arrangement to provide some additional information on one of the two strongest parameters, i.e. the cutwater gap or the vane arrangement. There are two obvious possible courses of action that can be followed, the first considering further

values of the cutwater gap and the second investigating additional vane arrangements; the possible advantages and disadvantages of either course of action is discussed below.

- Cutwater Gap: An additional analysis could be conducted using a different cutwater gap than those analysed previously in this project. The initial analyses have identified that a cutwater gap of 6% provides a reasonable balance relating to pressure pulsation reduction while maintaining reasonable performance levels. Thus any further analysis might be conducted at either 5% or 7% cutwater gaps. The 7% condition is known to produce pulsations less than the 6% value, thus is not likely to provide additional helpful information. The 5% cutwater gap may provide information that would assist in estimating pressure pulsations for current designs that may have tighter cutwater gap clearances.

- Vane Arrangement: The optimisation process has already identified that a staggered vane provides significant benefits in the reduction of pressure pulsations over the inline impeller at almost all locations. It has also been reported that the benefits in the reduction of pressure pulsations are marginal for different values of blade stagger. Thus any further work relating to the blade angle would be focused on analysing a different blade stagger angle, e.g. 7 degrees or 22 degrees. This would assist in fine-tuning the marginal benefits gained from adjusting the angle of blade stagger but is less likely to have practical benefit.

Although, both options have benefits, it was decided to concentrate on the analysis using a cutwater gap of 5%. This additional data may be beneficial for design recommendations relating the geometric arrangement to the expected pressure pulsations.

Additionally it was noted during the literature review that there is some uncertainty relating to the performance reduction experienced through increasing the cutwater gap depending on how the cutwater gap is achieved. This is discussed in Section 2.3.1 and

covers a variety of published work, e.g. (73) and (77). The additional analysis provides an opportunity to investigate this area of ambiguity by performing the analysis with the same basic parameters, but two different geometric set ups. Table 7.23 provides two possible model geometrical arrangements for a nominal 5% cutwater gap.

Thus this additional work will consist of two sets of three transient analyses that have the same cutwater gap, vane arrangement, snubber gap and sidewall clearance, but differing geometrical set ups for the cutwater water gap at the three flow conditions.

7.3.4 Additional Analyses

Although these analyses are related to the recommended arrangement from the rationalisation process they are not strictly an analysis of the recommended condition; they will be termed additional analyses and will be referred to as model A and model B.

7.3.4.1Analysis Set Up

Model A: This model was based on modifications to arrangement 3 in the original analyses. The snubber gap and sidewall clearance was modified using block-off regions to give the recommended arrangement and the 366mm diameter impeller with a 30 degree stagger, already present, was used. A significant amount of modelling work had to be performed to modify the CFX-Build volute model to the larger cutwater diameter. The 4mm diametral increase appears small but CFX-Build has no capacity to allow the 3D solid components that make up the model to be changed simply. Hence any solids that were affected by the diameter change had to be removed and recreated. The new volute was meshed using the same mesh distribution parameters as the original volute.

Model B: The impeller for model B was generated using the same Bladegen file as the other impellers. Bladegen includes a facility that allows reduced diameter impellers to be output from the same file. Thus the 366mm diameter impeller was used to output data for a 362 diameter impeller in a format that could be used in Turbogrid. The Turbogrid configuration file was copied from the earlier models to ensure that the grid

size and distribution would be as close as possible to the earlier models. This process was performed for both halves of the impeller, which were then combined. The relevant existing model components were selected, i.e. 380mm cutwater volute diameter, leakage path with a block-off region being set to restrict the snubber gap to 1% and the sidewall clearance to 100%.

Both models were analysed for three flow conditions, 1.00Qn, 0.50Qn and 0.25Qn to allow direct comparison with the previous analyses. The analysis process used was identical to that described in Section 5.6 and is summarised below

Frames of Reference

Rotational Frame of Reference: Double Entry Impeller, Leakage Flow Paths

Stationary Frame of Reference: Suction Inlet, Volute

Interfaces

GGI between same frame of reference

Rotor/Stator for interfaces across differing frames of reference

Boundary Conditions

Inlet: Mass Flow

Outlet: Static Pressure

Rotating Wall: Impeller internal and external surfaces.

Stationary Wall: All other boundary surfaces

Turbulence Modelling

k-epsilon turbulence model

Result Monitoring

Results taken during fourth and fifth revolutions

7.3.4.2 Additional Analysis Results

The results of the additional analyses are given in the form of the largest normalised pressure pulsation that occurs during a single revolution of the impeller. The results are presented in Table 7.24 for a number of pump locations.

Comparison with Previous Analyses

Comparing the results in the light of the previous transient analyses (Tables 7.2, 7.3 and 7.4) it is observed that the pressure pulsations are either between or even lower than the 30 degrees vane arrangements at 3.83% and 6.00% cutwater gaps (arrangements 3 and 4). In Table 7.24, pulsations that are lower than both the corresponding 3.83% and 6.00% are highlighted, while all other pulsation values are equal to or between those gained for arrangements 3 and 4. Note that a value within 0.002 of the earlier results is taken as being equal. There are a significant number of the lower pulsations at all flow rates, but these appear most common at the 0.50Qn flow rate. It is likely that interactive effects involving the snubber gap and sidewall clearances cause the lower pulsation values. For instances where the results sit between the 6.00% and 3.83% cutwater gap pulsation values, they are usually significantly closer to the 6.00% values.

Additionally the performance characteristics also compare favourably, with model A generating a head larger than an average of the head generated from arrangements 3 and 4 and with model B being slightly less. The power required to generate the head also compares favourably, with model A being above the averaged value from arrangements 3 and 4 and model B being below it. Both models generate efficiency larger than the averaged value.

Therefore it appears from the results generated at a 5.00% cutwater gap show that not only have the pressure pulsations been reduced, in some case to lower than that generated at the larger 6.00% cutwater gap values, the performance characteristics are typically as good or better than expected for that cutwater gap. There may even be a further improvement in the pulsation levels if the additional analyses were repeated with the 6.00% cutwater gap as indicated by Section 7.3.

Comparison of Models A and B

The recorded pulsations are generally consistent for both cases, typically there being less than 10% variation between the arrangements. Model A tends to produce pulsation levels that are similar to or less than those found by Model B at the duty flow condition.

At lower flows there is less consistency, with Model B producing lower pulsations than Model A at some locations, while at other locations the opposite is true. Locations where there are significant differences (larger than 0.01) between the models are generally located in the volute and impeller outlet locations. Location C5 is the only location at which a consistently large difference (minimum of 0.05) is found between the two models for all three flow rates. It is possible that the remodelled volute used for model A may have had minor changes at the cutwater region, due to the modelling process in CFX-Build (i.e. marginally different radius or angle), in relation to that used in model A and that these small changes produce differences in the recorded pressure variations. The larger impeller diameter model (model A), unsurprisingly, provides a superior head generation characteristic at all flow rates. In a similar manner the extra length of blade in model A contributes to this model requiring a larger power. It is interesting to note that while these values combine to produce a larger efficiency for model A at flow rates 1.00Qn and 0.25Qn, the efficiency at 0.50Qn is actually less than that recorded for model B.

It is possible to utilize the generated head values calculated from the additional analyses to provide some information concerning the uncertainty of a possible performance loss dependent on the method used to vary the cutwater gap. Firstly a comparison is made between the head generated by two pump arrangements where the cutwater gap is varied by the volute cutwater (i.e. both arrangements have the same impeller diameter). Then a second comparison is made for two pump arrangements that have the same cutwater gap and two different impeller diameters. In the second comparison the generated head will always be larger for the larger diameter and so to provide a like for like comparison the generated head value for the larger diameter is scaled down to the smaller diameter using the scaling law equation (equation 4.6). This is typically the inverse of how the scaling law is used in industry. In industry if a pump is too high in head at a diameter, the scaling law is used to calculate the reduced diameter that would provide the required head generation value. In this case both diameters are known and so the scaling law is used to calculate the generated head that will be obtained if the larger diameter was reduced to a specific value. The generated head calculated for the smaller diameter can then be compared with actual results from the analyses carried out

at that diameter. Table 7.25 provides details of the various arrangements compared with the generated head details for each of those arrangements. For the first arrangement, model A is compared with arrangement 3 of the original transient analyses. The generated head values indicate that there is no clear trend, with model A having a slightly higher head at the lower flows and vice-versa at the highest flow. It is noted that Uchida (73) has recorded that any loss from increasing the cutwater area would be larger at the duty condition that at lower flow rates. This is attributed to changing shear and shock losses at different flow rates and Uchida provides a detailed explanation in his published work. However it is also important to notice that as the cutwater gap increases the cutwater radius also increases significantly. This geometry change is likely to contribute its own loss separate from the increasing cutwater gap. For the second comparison the model A generated head data (366mm) is scaled the same diameter as model B (362mm). It can be observed that the model B generated head values are consistently less than those predicted by the scaled model A values, with the difference between the values become larger at the lower flows. Thus model B appears to show a reduction in performance that is not present in model A. Therefore, while the above doesn't provide conclusive proof, the results indicate that varying the cutwater gap by changing the volute cutwater (first comparison) does not reduce the expected performance whereas varying the cutwater gap by reducing the impeller diameter (second comparison) results in reduced performance.

This is of extreme importance as it suggests that the cutwater gap can be increased without a significant loss in performance as long as the impeller diameter is maintained. The loss in performance was central to the decision to select a 6% cutwater gap for the optimised arrangement, and so it appears possible that a larger cutwater gap could realistically be considered. Published data (Stanmore (78)) has indicated that "increasing the cutwater gap up to 8.22% showed no loss in the overall pump efficiency when the volute inlet tips were recessed". Therefore an 8% cutwater gap may provide a lower level of pulsation while maintaining the pump performance, but there is no real reason why cutwater gaps greater than 8% should not be considered. This area may benefit from further work with detailed investigations being made for the same impeller

diameter over a larger cutwater gap range (say 4% through to 12%), with each of the localised cutwater dimensions being kept as similar as possible.

Comparison of Additional Results with Prediction Equations

The equations generated in Sections 7.2.2.1 and 7.2.2.2 can be used to determine how close a value they predict for a 5% cutwater gap with a 30degree vane stagger arrangement. As the additional arrangements use a 30 degree stagger the data used by the predictive equations to calculate pulsation values will be weighted towards arrangements in the initial analyses that also have a 30 degree vane stagger. Although the equations derived from Stage 1 and Stage 2 in Section 7.2.2 above are different, when predicting pulsations for a 30 degree vane stagger they actually predict the same value. Thus, only one set of predictions is provided over a range of pump locations. Additionally the Model B arrangement has been used as a comparison with the predicted results as the method used to vary the cutwater gap in that arrangement matches that employed by the arrangements used to generate the predictive equations. Table 7.26 provides the predictive data in addition to the relevant data from Model B analysis results for three flow conditions for comparison. Overall the predicted results compared favourably, typically predicting a pulsation within 5-15% of that recorded during the analysis. The two main regions that deviate significantly (i.e. by more than 30%) from the predicted results are at position C4 and at the shroud mid position. When considering a cutwater gap of 5%, the predictive data will be weighted towards the closest data set, i.e. the 3.83% cutwater gap arrangement values rather than those at the 7.95% arrangement. Thus considering the 3.83% arrangement (arrangement 3), it is observed that this arrangement has a large snubber gap (1.67%) and a tight sidewall clearance (25%), whereas the additional analysis contains a medium snubber gap (≅1%) and large sidewall clearance (100%). Therefore the predictive equations are predicting data based on a larger snubber gap and tighter sidewall clearance, which results in larger pulsation predictions at locations in the leakage flow path region. The shroud mid position is located within the snubber gap region; hence it is likely to experience the same trend as the positions in the leakage flow region. The blade pressure face location

is not similarly affected as this monitoring point is further away from the snubber gap region and the pulsation at this point is strongly dependent on the cutwater gap.

It is also worthwhile to note that in all but one case (location C1 at 0.50Qn), the predicted pulsation is larger than the recorded pulsation from the analysis. This provides some confidence that while the prediction is typically within 15%, it is a conservative prediction. In critical regions, such as the shroud mid position, the prediction is more conservative.

7.3.5 Summary

The results gained from the CFD analyses and processed using the Taguchi method have been used to reconfigure the pump design for two motivations. The first was for component life, and focused on reducing the pulsations at the impeller outlet while attempting to minimise pump performance losses. This procedure examined both the pressure pulsations at the impeller outlet and the pressure differential across the shroud. The pressure differential identified important effects different from those shown by the pressure pulsations. While the pulsation data highlighted the importance of the cutwater gap, the shroud differential identified the importance of the snubber gap on the pressure differential and the variation of this differential at the impeller outlet. The second sought to reduce noise and vibration levels by reducing general pulsations in the pump, while again attempting to minimise losses in the pump performance.

It was observed that without deviating significantly from the recommendations resulting from the two approaches, a single "optimised" arrangement could be produced. This arrangement was found to be similar to the fourth transient analysis. Additional analyses were run for a cutwater gap less than the recommended value and the additional analyses were used to investigate two different methods of varying the cutwater gap. The results of these additional analyses indicated that in the majority of the pump locations, there was little change in the pressure pulsations except close to the cutwater at the impeller blade where both gave a larger difference. The analyses also indicated that modifying the cutwater gap by reducing the impeller diameter causes an

apparent performance loss. Whereas when the cutwater gap is varied by changing the stationary volute cutwater and maintaining the impeller diameter, no such loss is noted.

The predictive equations generated earlier in the chapter were used to provide predictive data for both the pulsations and the performance characteristics for one of the additional analyses. The predictive data was found to compare reasonably with the CFD analysis, with the main regions of divergence being in the leakage flow path close to the cutwater circumferentially and at the impeller outlet. It was noted that the equations over predict the pulsations in the majority of cases possibly providing some useful conservatism if such equations are used in design.

7.4 Transient/Steady State Analysis Comparison

It is considered that multiple steady state analyses offer possible advantages over transient analyses in terms of the amount of file storage space and the time taken for the analyses. These advantages would make the multiple steady state analysis an attractive prospect when assessing pumps that are outside the design parameter ranges used in this project. However, this would only be so if the multiple steady state analyses are able to correctly predict trends in the pulsation magnitudes both within the pump and relative to different geometrical arrangements.

Comparisons within the pump have been studied by conducting steady state analyses for three flow rates (1.00Qn, 0.50Qn and 0.25Qn) using the first arrangement geometry over a 120degree impeller progression, with analyses being conducted at 2 degree intervals. The comparison for a further geometrical arrangement was examined by conducting a steady state analysis using the Model A geometry at 1.00Qn. In total 244 steady state results were analysed, these took approximately 480 hours of analysis time in total, in comparison with around 5500 hours for four complete transient analyses. Therefore the steady state analyses take less than a tenth of the time of the transient analyses. Storage space for a single set of steady state analyses amounted to 15Gb, whereas the space required for a transient analysis was actually less, at around 11Gb.

The large size of storage space for the steady state analyses is due to the large size of the full result (rso) files (220Mb) in comparison to the transient (trn) files (75Mb). The steady state requires an rso file for every analysis, while the transient only requires a single rso file. The transient analysis requires approximately 144 trn files at 2.5 degree increments to describe a full 360 degree rotation, which equates in file size to around 100 degrees of steady state analyses. As each individual steady state analysis only takes just under two hours to run, it would be possible to reduce the final storage size of the steady state analyses by deleting every second rso file. This would reduce the file storage size to 8.4Gb. However the deleted results files would need to be recomputed if the data was required at a later date.

7.4.1 Comparison within the pump at three flow rates

The pressure variation with impeller position is plotted for the first arrangement steady state analyses in Figures 7.26, 7.27 and 7.28 for flow conditions 1.00Qn, 0.50Qn and 0.25Qn respectively. Each figure plots the pressure variation at four distinct pump locations, namely in the leakage flow path (C3), at the cutwater (C6), towards the discharge (C9) and at the impeller outlet (Blade Pressure) and also shows the transient first arrangement data over a similar period. Figure 7.29 provides impeller position dependent data relating to the instantaneous head generated for all three flow rates.

1.00Qn: In general the pulsations recorded by the steady state analyses appear reasonably good in comparison with the transient analyses. Location C3 (Figure 7.26a) appears to have a settling in period over the initial 60 degrees or so, but then models the pulsation in this location fairly well. Position C6 (Figure 7.26b) records the pulsation shape in excellent detail, although the pulsation is significantly smaller and the pressure level is higher. At C9 (Figure 7.26c) a good approximation of the pulsation magnitude is achieved, however this appears to have a phase lag of around 30 degrees. Finally the blade location (Figure 7.26d) picks up the pressure increase, but not the rapid pressure drop as the blade passes the cutwater. In short there are some issues with the capture of the pulsations in the pump. However there is some encouragement that certain aspects of the pulsation features can be modelled using the steady state option.

0.5Qn: The pulsations at the reduced flow rate are considerably poorer than those at the duty condition. The magnitude of the pulsation at position C3 (Figure 7.27a) is of the correct order, although there appears to be a considerable phase lag present. At location C6 (Figure 7.27b) the steady state analyses do pick up some pulsations, however the shape of the pressure variation is not consistent with the transient result. The C9 position (Figure 7.27c) shows a good pulsation magnitude compared with the transient. A similar phase lag to that found at C1 is also present. The blade position (Figure 7.27d) does not record any significant pulsation, whereas the transient records a large pulsation.

0.25Qn: The steady state recorded pressure pulsation results continue to deteriorate in comparison with the transient results as the flow rate decreases. The C3 position (Figure 7.28a) shows some cross over of the results around the 30-40 degree impeller angular position. At the C6 location (Figure 7.28b) there appears to be slight pressure drop at the correct location, but again the overall shape of the two curves is quite different. The C9 position (Figure 7.28c) perhaps provides the best agreement of the pulsation magnitude and shape between the two analysis methods. As with 0.50Qn, the blade location (Figure 7.28d) for the steady state analyses does not predict the large pressure pulsation as the blade passes the cutwater, although the overall shape is similar. Thus it is clear that steady state results deteriorate significantly in comparison with the transient analyses as the flow rate decreases, with the analyses not recording the large pulsation at the impeller outlet and not recording the correct shape of pressure variation in the cutwater region.

Head Generation Variation (Figure 7.29): At all flow rates the head generation is of a similar value to that calculated using transient analysis methods. The variation in the head generated as the impeller rotates is generally less for the steady state analysis than for the transient analysis. The shape of the pulsation has similarities at all flow rates. The similarity in shape is strongest at 1.00Qn with two distinct peaks and poorest at 0.25Qn where multiple peaks are appearing in the steady state case. However the

magnitude comparison is lower at 1.00Qn that at the other flows. The average values of the generated head have been included in Table 7.27.

7.4.2 Comparison Between Steady State/Transient Results of the First Arrangement and Model A at 1.00Qn

Before comparing the steady state results of the first and model A arrangements, a brief comparison of the model A transient and steady state results is given. The impeller position dependent pressure pulsations are shown for both transient and steady state analyses in Figure 7.30 for Model A, plotting the same locations as in Section 7.4.1. Location C3 (Figure 7.30a) shows a significant settling period covering approximately 60degrees, however once settled the steady state analysis does not appear to identify any notable pulsation. At C6 (Figure 7.30b) the steady state analysis appears to identify troughs in the correct locations, but these troughs are not captured to any significant degree to allow any real assessment of the pulsations. The C9 position (Figure 7.30c) shows a smaller settling in period and does appear to record peaks and troughs in the correct places, however the shape of the pulsation is not consistent. The blade location (Figure 7.30d) does record a peak at the correct location, but the shape and magnitude of this peak does not agree with that found using the transient analysis.

Table 7.28 provides a comparison of the 1.00Qn data for both the first arrangement and the model A arrangement for both analysis methods. The steady state/transient comparisons for both arrangements are not good and the table identifies that the pressure pulsations trends predicted between the two arrangements by the steady state analysis do not generally match those predicted by the transient analysis except in a few cases. At the leakage flow locations the steady state analysis predicts an increase in pressure pulsations of 0.035 at both C1 and C3 when changing from arrangement 1 to model A, however the transient analysis predicts substantial reductions of 0.062, and 0.054 at the same locations. In contrast, in the volute, steady state results at location C6 indicate a far larger reduction between the arrangements than is shown by the transient analyses. Yet at location C8 the steady state pulsations register a substantial reduction whereas the transient analyses indicate an increase. At the impeller positions both the

steady state and transient analyses indicate a reduction in the pulsation, but the steady state predicted reduction is significantly smaller than the transient.

The steady state pressure pulsations here are significantly less than those captured using transient analyses. It is likely that the steady state analysis could only capture the pulsations when the pulsations were large (tight cutwater gap and snubber gap). The model A arrangement contained a geometric set up designed to reduce the pulsations, which suggests that the steady state analysis was unable to record the pulsation with any accuracy. Again the average generated head values have been included in Table 7.28. Figure 7.31 provides a comparison of the generated head for the transient and steady state results. At 1.00Qn the steady state head values are less than the transient analysis values and only appear to record significant pulsations in the head after a 60 degree settling period.

7.4.3 Summary

The above analyses show that performing multiple steady state analyses do not necessarily provide a reliable quick route to investigating transient flow features. The initial steady state simulations analysing the first arrangement at three flow rates produced results that indicates that the steady state method could identify the pattern of the pulsations to some degree, it was unable to adequately capture the magnitude and phase of the pressure pulsations at different pump locations especially at lower flows. The results of multiple steady state analyses for two different geometrical arrangements at 1.00Qn were compared with the transient analyses and the results indicate that the pulsation trends shown by the steady state data do not really correspond with the trends from the transient analyses. Nevertheless the multiple steady state analyses does show some features similar to the transient analysis at the duty flow condition albeit the pressure pulsation magnitudes may differ. Overall it is not considered appropriate for multiple steady state analyses to be used to predict transient effects.

This conclusion is important as steady state analyses are already being utilised in literature in an effort to identify transient flow features. Asuaje (133) reports the static

pressure distribution at the impeller periphery for a number of impeller blade conditions using a multiple steady state analysis method. Although the static pressure distribution is only reported for a duty condition, Asuaje performed calculations of the radial thrust at different impeller positions at 0.50Qn and 1.4Qn in addition to the duty condition. The present work raises doubts on the reliability of such work in the absence of further evidence. Further work would allow a better understanding of the limitations of (and possible applications of) using steady state analyses to predict transient flow features

7.5 Relation of CFD Analyses to Impeller Structural Integrity and Design

The above sections are typical of pressure pulsation analyses in that they consider the pulsations at discrete locations around the pump. However in order to make an assessment of the effect of the pressure pulsations on the structural integrity of the pump differential pressures across a critical component must also be considered.

7.5.1 Introduction to Structural Integrity

Indications from published literature and from the author's own experience are that the component most likely to be structurally compromised by hydraulic pressure fluctuation is the impeller. The most likely failure mechanism is fatigue of the shroud at the impeller outlet. Failure usually starts at the outermost edge of the impeller shroud near the suction edge of the blade at the stress concentration that exists where the blade meets the shroud. A crack then propagates along the blade/shroud junction for around a third of its length, before moving across the impeller passageway to the pressure face of the trailing blade. A section of shroud is then only restrained on one side, at the pressure face of the trailing blade. This section is typically removed by the changes in pressure that lead to it breaking away from the impeller.

The actual stress within the impeller is mainly caused by two actions. The first is the hydraulic pressure loading across the impeller that causes a hoop stress, also termed the

circumferential or bending stress. The second is the centrifugal stress caused by the rotating motion of the impeller. The centrifugal stress is largely independent of the impeller geometry variations analysed in this work and so the main focus is placed on the evaluation of the hydraulic pressure loadings that could be used in the calculation of the hoop stress. To gauge the effect of the pressure loadings on a single region of the impeller, i.e. the impeller shroud, is actually an extremely complicated task. It is easy to state that the pressure loading is equal to the pressure differential across each area of the shroud; yet the pressure differential is dependent on a wide range of variables, irrespective of the geometrical arrangements examined here, including:

- circumferential position between blades
- radial location
- position of impeller blade to volute cutwater
- flow rate

Thus a data set embracing the above would require pressure loadings for all circumferential and radial positions on the shroud, for a minimum of 180 degrees blade rotation (3:1 blade to volute splitter ratio) with data produced every 2.5 degrees typically, for three separate flow conditions. Considering the number of points located on the impeller shroud, this equates to approximately two million pressure loadings forming an immense data set. This process would then need to be repeated for each of the nine geometrical arrangements analysed in order to gauge the effect of the arrangements on the shroud's structural integrity. The above is for a single shroud, assuming that a symmetry condition exists across the impeller (i.e. an inline arrangement) and does not include loadings at other impeller locations, i.e. at the impeller blades, which add a further one and a half million pieces of information, approximately. The immensity of this task is outside the scope of the current project and could form a project in its own right. However some useful information can be derived and some observations made on the structural integrity aspects that should be helpful for design. The pressure loading on the impeller has been characterised from the CFD results for two arrangements and a relatively simple finite element analysis conducted to indicate how the problem may be tackled.

7.5.2 Design Guidelines and Comparison of CFD Shroud Pressure Differentials

A description of the WPL Guidelines and their background is given in Appendix B. An important part of the approach is based on stress equations for the centrifugal stress (σ_{cs}) and the bending stress (σ_{bs}), namely

$$\sigma_{cs} = \frac{K\rho_m U_2^{\,2}}{802408} \qquad \text{Equation 7.3}$$

(Equation B.1)

$$\sigma_{bs} = \frac{\rho U_2^{\,2}}{5.4x10^5} \times \frac{D_2^{\,2}}{t_s^{\,2}} \times \left[1 + \frac{D_{wr}}{D_2}\right] \times \frac{\sin^2 \beta_2}{z^2} \qquad \text{Equation 7.4}$$

(Equation B.11)

Perhaps the most significant point to note in this context is that, inherent in the derivation of the bending stress, there is an assumption that the pressure differential across the shroud wall can be approximated by a constant value of 0.3H.

As discussed in Appendix B, the design guidelines assume a triangular variation across an impeller shroud at the duty flow condition (1.00Qn), with the variation reaching a maximum of 0.4 times the generated head. The CFD analyses at 1.00Qn (Figure 7.11) indicate that the assumed triangular variation in pressure differential appears to be an acceptable approximation. For the comparison, arrangement 4 is selected, as it is geometrically similar to the optimised arrangement recommended in section 7.3.3. In the CFD arrangement, the pressure differential variation, while being near zero at the outlet, reaches in the region of 0.90e5 N/m^2 (from Table 7.19) at the wear ring radius. This is equivalent to 0.28*H, which is significantly less than that assumed by the guidelines. This is largely due to the pressure variation on the outside of the impeller shroud being larger than assumed in the guidelines. The guidelines assume a variation of 0.73*H and 0.33*H (Figure B.1) at the wear ring on the outside and inside of the

shroud respectively, whereas the CFD analysis indicates that the variation is closer to 0.53*H and 0.28*H at the wear ring on the outside and inside of the shroud respectively.

At the lowest flow condition (0.25Qn) the CFD analyses indicate that the pressure differential variation may not be triangular but can have a more trapezoidal shape (Figure 7.12). This is perhaps not dissimilar in shape to the uniform loading that is ultimately assumed in the design guide. The actual maximum loading that is noted from the CFD analyses varies from 0.32*H to 0.44*H (Table 7.20, arrangement 4) from the outlet to the wear ring radii respectively. The maximum value for this arrangement at the wear ring is not dissimilar to that assumed by the design guide (0.4*H); however this value is dependent on the actual geometric arrangement and is higher in other cases (i.e. the highest is 0.56*H for arrangement 2). It is the change in shape of the pressure differential from the wear ring to impeller outlet that indicates an overall larger average loading across the shroud. Using the data from arrangement 4 and simplifying it slightly so that it is a trapezoidal shape and varies from 0.32*H to 0.4*H (see Figure 7.32) it is possible to repeat the same process that was used in the design guidelines to gain the uniform 0.3*H loading, but using the CFD data rather than an assumed loading. The design guideline process conservatively takes a uniform value equivalent to 75% of the triangular range, this is shown in Equation 7.5

$$\text{Uniform Loading} = \text{Base Loading} + (\text{Range} * 0.75) \qquad \text{Equation 7.5}$$

For the design guidelines the base loading is zero and the range is between zero and 0.4*H; this results in the uniform loading equal to 0.3*H. The data from arrangement 4 can be viewed as a rectangle of height 0.32*H, plus a triangle varying from 0.32*H to 0.44*H (Figure 7.32). This gives a base loading of 0.32*H and a range from 0.32*H to 0.44*H, which gives an approximated uniform loading of 0.41*H. Due to the conservative approximations in the calculation process it does not seem unreasonable to round this value down to 0.4*H. This value is still significantly higher than that proposed by the design guidelines. This is largely due to the use of single flow condition (duty condition) to determine the pressure differential in the design guidelines.

It is also worth noting that the design guide, when considering fatigue, assumes a "full stress reversal" that it describes as being from the maximum bending stress to zero. At the lowest flow condition the CFD analyses indicate that rather than varying between the design guide loading (0.3*H) and zero, the pressure differential actually varies from +0.21*H to -0.27*H (totalling 0.48*H shown in Table 7.20 for arrangement 4 at 0.25Qn), where positive denotes the pressure inside the impeller being greater than that on the outside. This provides a stress reversal larger than that assumed by the design guide, and shows that a true full stress reversal from positive to negative takes place at the outlet of the impeller.

7.5.3 Stress Analysis Comparison

In section 7.2.3 a process is detailed for collecting pressure data on the inside and outside of an impeller passageway as it passes the volute cutwater. Comment has been made earlier (section 7.5.1) that although conducting finite element stress analyses (FEA) with the CFD pressure data was possible, it was a sizable task that was beyond this project. Nevertheless it was considered that it would be helpful to perform some finite element stress analysis to determine sample stress levels present in the impeller, while also demonstrating a method for transferring the data from the CFD results files for the stress analysis. This finite element analysis necessarily has to be limited in form and a decision was made to focus on the stress levels in the shroud.

7.5.3.1Pressure Loading Transfer and FEA Model

A decision was made to model one half of the double entry impeller rather than a single impeller passageway. This enables different loadings to be applied on each of the six passageways and represents the actual loadings on that side of the impeller at a single moment in time. Consideration of the data obtained in section 7.2.3 led to a plan to generate four sets of pressure loading data for application to this half impeller model. It was recognised that the FEA would have to model the worst and best case pressure loadings for a single arrangement in order to gain a realistic measure of the stress levels

in the shroud as the impeller rotates. The pressure differentials, e.g. Figure 7.11, indicate that the blade opposite the cutwater and the passageway mid position opposite the cutwater are representative of these worst and best loading positions. When considering the arrangement for use in the analysis, it seems reasonable to obtain loadings from an arrangement that is close to the recommended arrangement from section 7.3.3. This narrowed the arrangements down to three, arrangements 4, 5 and 6, as they all have 6% cutwater gaps. Only a single side of the impeller will be modelled. This assumes symmetry with the non-modelled side of the impeller, which would only exist for the inline vane arrangement. It is observed that if analyses were run for both arrangements 4 and 6, then the stress data would be obtained for the maximum and minimum snubber gaps used in the parametric CFD investigation. It is known that the snubber gap is a dominant factor relating to the pressure differential, but it is of interest to know whether this influence extends to the impeller stress levels. Table 7.29 provides a summary of the four data sets selected for investigation using FEA.

The process used to obtain the pressure data from the CFD analyses was similar to that detailed in section 7.2.3. The main difference was that instead of gathering the data on the inside and outside of the shroud at a mid passage position for a single passageway, it was gathered for all six passageways on the same side of the impeller. Additional data was gathered relating to the pressure on the inside of the hub. The pressure data was then plotted against the radius, and a trend line was generated mimicking the pressure data as closely as possible. Figure 7.33 illustrates the pressure data at the inside and outside of a single impeller passageway along with the trend lines. The equations for the pressure variation at the sample passageway shown in Figure 7.33 are shown below:

$$y = -22944341443072.00\varkappa^6 + 20151150804641.30\varkappa^5 - 7339835829004.53\varkappa^4 + 1418845042798.85\varkappa^3 - 153487896644.40\varkappa^2 + 8812082749.08\varkappa - 209676784.37 \quad \text{Equation 7.6 (inside shroud)}$$

$$y = -398676434.63\varkappa^3 + 176612654.84\varkappa^2 - 24396067.73\varkappa + 1396268.50 \quad \text{Equation 7.7 (outside shroud)}$$

where $\varkappa$ is the radii (m) and y is the pressure (N/m^2)

The trend lines generally take the form of a third order equation at the outside of the shroud and a fifth order equation or higher at the inside of the shroud. This was required to adequately replicate the shape of the pressure variation between the shroud inlet and outlet. This work was repeated for the hub pressure data resulting in each data set containing three pressure equations for each of the six impeller passageways; an equation for the inside shroud, outside shroud and the hub pressure variations respectively. When applied as loadings, these pressure variations taken at the mid passage position are assumed to be acting across the whole impeller passage. No load data was taken from the CFD analyses for the blade surface in the stress analysis model. A fifth condition was added to the plan of finite element analyses as none of the above included any centrifugal loading due to the rotation of the impeller. This fifth analysis was conducted using only the centrifugal loading, i.e. no pressure loading on the shroud or hub.

A CAD model was generated in Solidworks from the blade surface profile information provided from the Bladegen impeller model. Hub and shroud geometry were added to produce a solid model of the impeller (shown in Figure 7.34). This geometry was transferred to the Ansys FEA system and meshed to create a model suitable for stress analysis. SOLID187 elements were used, which are higher order 3-D, 10-node tetrahedral elements, having quadratic displacement behaviour and are well suited to modelling irregular meshes (such as those produced from various CAD/CAM systems). SURF154 elements, used for various load and surface effect applications, overlaid the external area faces of the 3-D Solid187 elements, allowing pressure distributions to be applied. A coarse finite element mesh is considered to be adequate to provide representative results; the mesh is shown in Figure 7.35.

The pressure distribution around the impeller and the pressure loadings for the individual passageways were applied to the internal passages and outside shroud surfaces using the equation form as described above. This replicated the pressure distribution of the various geometry configurations and relative impeller/volute

positions. Constraints were specified to represent symmetry of the double inlet impeller and fixing to the shaft. It should be noted that the impeller analysed is a reduced scale, slower rotational velocity version of high head double entry impellers used in industry. Therefore the stress levels, although interesting for comparative purposes, produced will not be representative of the stresses present in the larger diameter, faster running pump impellers.

Analysis was carried out using ANSYS Version 10 FEA system. It should be noted that although the author prepared the loading information and interrogated the results, the Principle Engineer for Stress/FEA at Weir Pumps Limited conducted the actual generation of the solid model, impeller mesh and finite element analyses.

From the interrogation of the stress analysis results, stresses were obtained on the shroud and blade at the outer diameter, and a mid-diameter intersection of the blades and front shroud. It should be noted that the reported stresses are calculated internal to the element at Gaussian points and extrapolated to the nodes as appropriate. The positions of these result locations are detailed in Figures 7.36 and 7.37. Figures 7.38 and 7.39 show the hoop stress on the impeller shroud and the resulting axial displacement for arrangement 4 at the blade position.

7.5.3.2 Finite Element Stress Analysis Results

The results are presented at ten locations in each impeller passage, eight on the outer diameter (a to h) and two on the blade at a reduced diameter (j and k). These locations were selected due to being in close proximity to expected regions of high stress level and being close to the typical shroud breakage zone shown in Chapter 3, Figure 3.1. The ten locations were used for all six impeller passages and for all analyses. The stress information recorded at these locations are in a cylindrical co-ordinate system and so are termed the radial, hoop and axial stresses. Therefore 900 items of stress related data are selected from the finite element analyses. It is not possible to present this volume of data here, therefore the data has been analysed to identify the maximum and minimum stress levels at each monitoring location for each analysis. This information, along with

the difference between these values is presented in Tables 7.30 (radial), 7.31 (hoop) and 7.32 (axial). It should be noted that positive stresses are tensile and negative stresses are compressive. Due to the fact that cracks propagate under tensile stresses rather than compressive stresses, more significance will be placed on tensile stresses in the discussion of the results below.

The radial stress (Table 7.30) at the outlet diameter (locations a to h) is close to zero, with the two locations (j and k) showing significant values. Of course, the radial stress at the outlet tip of the impeller should be zero and it is only due to the limitations of the stress analysis mesh that non-zero values are estimated in this location. If the impeller mesh was refined the radial stresses at the outlet would decrease. The axial stress (Table 7.32) is typically very low at all locations except at positions b and c. This is because the thin shroud cannot develop axial stress, but axial stress can develop at a stiffening ridge, i.e. the impeller blade. It is interesting to note that the axial stress at position b, for arrangement 4 (blade opposite the cutwater) is the highest tensile stress recorded at any of the selected points during the analyses. It should also be noted that position b is actually on the blade rather than on the shroud. The hoop stresses (Table 7.31) show similar trends to the axial stresses, with the tensile stress at positions b and c being larger than at any other position for the majority of the pressure load cases. The highest value occurs at position c and is equal to 4.31N/mm^2. It is of interest to observe that this value is greater than the bending stress value calculated by the existing Weir Pumps design guideline, 3.41N/mm^2 (Equation 7.4, which assumes a uniform pressure loading of 0.3*H across the shroud). Using an increased pressure loading of 0.4*H, as recommended in section 7.5.2 for a different reason, increases this expected bending stress loading to 4.54N/mm^2, which is more consistent with the largest stress level indicated above. It is also important to note that the hoop stresses for arrangement 4 tend to be higher than those found for arrangement 6. This change in stress levels is due to the change from a tight snubber gap (0.27%) at arrangement 4 to a large snubber gap (1.64%) at arrangement 6. This is observed to be especially important at position c, where the hoop stress for arrangement 4 is more than 2.5 times that at arrangement 6. Therefore the snubber gap has an extremely important influence over the stress levels at the outer diameter of the impeller.

It is interesting to revisit the published work by Stanmore (78) that reported alleviating high vibration and noise issues by increasing the cutwater gap from 1% to 9% and by adding snubber gaps of 0.39%. Stanmore reports that six months after the modifications were made a section of the impeller shroud suffered fatigue failure and attributes the failure to prolonged operation of the pump at partial load. In light of the above work it seems likely that the tight snubber gaps introduced by Stanmore made a sizable contribution to the fatigue failure of the shroud.

The centrifugal load case identifies that the rotational movement of the impeller provides a sizable and consistent contribution to the hoop stress at most locations. Positions d, e, g and h are all located on the shroud and the hoop stress values calculated from the centrifugal loading are all consistent with the Roark (134) theoretical stress value of 2.53N/mm^2 (Equation B.3) for a hollow disk. The hoop stress at position f, although also positioned on the shroud, is influenced by the blade and shows a larger hoop stress of 3.21N/mm^2. However, it is interesting to note that the Weir Pumps theoretical calculation, which includes a 25% increase in the theoretical centrifugal stress from Roark to account for the effect of the blades, produces a predicted hoop stress of 3.19N/mm^2 (Equation B.1). This indicates that the theoretical hoop stress equation in Roark for a hollow disk and the amendment to it in the Weir Pump design guidelines show rather good agreement with the stress analysis of the centrifugal load case for an actual shroud.

The difference between the maximum and minimum stress values for the radial, hoop and axial stresses is also shown on each of the tables. This is the difference present at the analysed moment in time and is not strictly the variation experienced by a specific point as the impeller rotates. The true maximum difference is the difference between the maximum and minimum values for a specific point for both impeller position stress analyses for a single arrangement. These values are not shown, as while they do increase the maximum difference it is not by a significant value. For example, the difference for the hoop stress for arrangement 4 at the blade position is 10.45N/mm^2, while the maximum difference for arrangement 4 is 11.78N/mm^2.

7.5.4 Summary

The relevant assumptions made in existing Weir Pumps design guidelines have been compared to the shroud pressure loadings available from the CFD analyses. This comparison observed that the current assumption of a 0.3*H uniform pressure differential acting on the shroud was low and that a value of 0.4*H was more representative of the general pressure differential level across the shroud. The recommendation to increase the assumed loading to 0.4*H was later supported by finite element stress analyses that indicated that stress levels did go above that predicted by the 0.3*H loading, but were lower than those predicted by 0.4*H.

A selected data set of pressure loadings from the CFD analyses have been used to demonstrate a method enabling the transferral of information from CFD analyses for use in a finite element analysis. Five separate stress analyses were conducted using four different CFD sourced pressure loadings and a centrifugal loading to simulate the rotation of the impeller. The centrifugal loading results have been found to be extremely consistent with theoretically predicted stress values. The stress analyses using the CFD pressure loading data, in addition to supporting earlier recommendations as described above, also identified that the snubber gap had a large influence on the stress levels on the impeller outlet. It was observed that reducing the snubber gap significantly could more than double the stress level at particular locations.

7.6 Design Recommendations Summary

A number of recommendations have been made in the various sections of this chapter. These recommendations are tied to individual aspects of the investigation and are therefore likely difficult to locate within the text. This section gathers together these recommendations and endeavours to present them in a succinct manner that will be of benefit to pump designers.

The largest pressure pulsations in a pump are located at the pressure side of the impeller blade at the outlet, with the cutwater gap largely controlling the magnitude of the pulsation. Using a staggered vane arrangement in preference to an inline arrangement will reduce general pulsation levels in the pump. The snubber gap controls the pressure level in the leakage flow region and so exerts a large influence over the shroud pressure differential.

The overall recommended pump design parameters are as follows

Cutwater Gap:	6% minimum diametral distance (of the impeller diameter)
Vane Arrangement:	staggered at the mid position
Snubber Gap:	1.0% minimum diametral distance (of the impeller diameter)
Sidewall Gap:	100%

The results have indicated that a staggered vane arrangement offers significant benefits over an inline arrangement. Therefore while the above recommends a mid position stagger (i.e. 30 degrees in this case) other stagger angles are also likely to provide benefits over the inline arrangement. The selection of a blade stagger angle requires more careful consideration of the flow at the impeller outlet and the size of the axial mixing regions between the two impeller sides may influence this choice. It is noted that if the pump designer is limited to an inline impeller arrangement, then a larger cutwater gap of say 8% (as a minimum) should be considered.

The reason for the inclusion of a snubber gap is largely to reduce the pressure pulsations down the back of the shroud in order to reduce axial forces. While the effect on axial forces has not been studied in this work, the project has indicated that great care is required when utilising snubber gaps as too tight a snubber gap can be detrimental to the life of the impeller.

The sidewall gap uses the largest gap as the recommended value. While it is recognised that a value of 100% is not specific, the effect of any change in pulsations due to the sidewall was marginal. Therefore it is reasonable to assume that current levels of

sidewall clearance are adequate and there is no basis for reducing or increasing them to gain lesser pressure pulsations.

Additionally, this project has provided a recommendation relating to existing, Weir Pumps Limited, design guidelines. This recommendation involves increasing the assumed uniform loading on the shroud when calculating the bending stress to better replicate the level of pressure differential experienced by the impeller shrouds as identified by the CFD results. This involved a substantial increase from 0.3*H to 0.4*H, which has been supported by some simplified finite element analyses.

It is also important to observe that if confirmation is required for the level of pressure pulsations in a pump, then it is suggested that measuring the pulsations at the top dead centre pump volute position will provide a better indication of the overall pulsation levels in the pump than current practice where pulsations are measured at the discharge.

7.7 Chapter Summary

This chapter has conducted an in depth analysis of the results using a number of techniques. These techniques have been used to determine the importance of the various parameters on the pressure pulsations in the existing pump and thereby to make recommendations to pump designers as to how to reduce such pulsations in this pump type. The important points and work conducted are summarised below:

- The results have been inspected visually to confirm data values and to identify the strongest geometrical influences on the pressure pulsation.
- A Taguchi array has been employed to minimise the arrangements to be analysed in order to perform the parameterisation investigation.
- Using Taguchi post-processing techniques, the level of dominance of the cutwater gap and vane arrangement on the pressure pulsation has been determined. This reveals that although the amount of influence the two geometric parameters exert changes depending on location and flow, they are by

far the strongest influences on the pressure pulsation. The snubber gap and sidewall clearance exert significantly lesser influences although each can be of importance under specific circumstances.

- The variation in the pressure differential across the shroud as the impeller rotates has been investigated for the 1.00Qn and 0.25Qn flow conditions. This identified a pulse in the pressure differentials at 0.25Qn and showed that the snubber gap was the dominant geometric influence at all flow rates on the shroud pressure differential.
- A rationalisation/optimisation process has been conducted to reduce the pressure pulsations with a view to extending component life and reducing noise and vibration levels. The process resulted in a single recommended arrangement that is summarised in section 7.3.3.
- Two hundred and forty four steady state simulations have been conducted and the pressure pulsations and generated head results compared with transient analyses. This work has indicated that the steady state analyses do not capture the magnitude and phase of the pressure pulsations to a satisfactory degree, especially at lower flow rates. The steady state analyses are also unable to predict the same pressure pulsation trends for different pump geometries as those from the transient analyses.
- Assumptions relating to the differential pressure across the shroud, made in the Weir Pumps Limited design guidelines, are compared with the pressure differential data obtained from the CFD analyses. This comparison indicates that the current assumption of 0.3*H is insufficient and that a larger value of 0.4*H is more inline with the CFD data
- One possible method for using the CFD data in finite element analyses has been demonstrated. The FEA model used was limited, but could be used to compare the stresses arising due to four different sets of shroud pressure loadings obtained from the CFD. A fifth analysis was conducted using only a centrifugal loading to simulate the stress due to the rotating impeller.
- The centrifugal stress results obtained from the work are shown to compare favourably both with published data and with the Weir design guidelines. The Weir Pumps bending stress calculation, using a 0.3*H assumption, was found to

under predict the hoop stress at the impeller outlet. Increasing the value, as recommended by this work, to 0.4*H was found to compare more favourably. The snubber gap was shown to have a significant influence over the stress levels at the impeller outlet, indicating that the snubber gap might be increased to reduce shroud pressure levels.

- A summary of the final design recommendations resulting from this work has been collected together and is presented in section 7.6.

7.8 Tables

Experimental Arrangement	Cutwater Gap	Snubber Gap	Sidewall Clearance	Vane Arrangement
1	3.83%	0.27%	100%	0 degrees
2	3.83%	1.10%	50%	15 degrees
3	3.83%	1.64%	25%	30 degrees
4	6.00%	0.27%	50%	30 degrees
5	6.00%	1.10%	25%	0 degrees
6	6.00%	1.64%	100%	15 degrees
7	7.95%	0.27%	25%	15 degrees
8	7.95%	1.10%	50%	30 degrees
9	7.95%	1.64%	100%	0 degrees

Table 7.1: Geometric configuration of Taguchi arrangements

	Normalised Pressure Pulsations														Single Rotation Averaged Pump Performance		
	Leakage Flow Path Locations					Volute Locations					Impeller Outlet Locations						
	Circumferentially Distant To Cutwater			Circumferentially Near Cutwater		Distance to Cutwater (mm)				Toward Outlet	Blade		Shroud				
						5	15	30	50								
Arr.	C1	C2	C10	C3	C4	C5	C6	C7	C8	C9	Press. Face	Suct. Face	Blade Pos.	Mid Pos.	Head (m)	Power (kW)	Eff. (%)
1	0.094	0.087	0.094	0.090	0.101	0.253	0.259	0.217	0.167	0.072	0.411	0.185	0.181	0.149	36.05	63.07	85.74
2	0.056	0.043	0.061	0.056	0.067	0.231	0.200	0.134	0.081	0.049	0.332	0.254	0.128	0.115	34.71	59.94	86.72
3	0.038	0.035	0.037	0.063	0.095	0.264	0.208	0.180	0.119	0.025	0.381	0.234	0.178	0.160	35.2	60.35	87.33
4	0.030	0.030	0.033	0.038	0.048	0.172	0.140	0.122	0.094	0.022	0.247	0.189	0.078	0.073	32.72	56.07	87.38
5	0.089	0.075	0.089	0.085	0.109	0.242	0.203	0.185	0.143	0.065	0.327	0.207	0.206	0.137	33.76	58.26	86.84
6	0.056	0.045	0.049	0.040	0.042	0.133	0.108	0.079	0.067	0.040	0.227	0.167	0.122	0.114	32.86	55.74	88.27
7	0.050	0.044	0.045	0.041	0.042	0.118	0.096	0.083	0.074	0.034	0.175	0.131	0.075	0.062	30.89	52.42	88.26
8	0.023	0.019	0.025	0.027	0.036	0.133	0.098	0.083	0.050	0.015	0.148	0.126	0.074	0.068	30.33	51.28	88.57
9	0.072	0.069	0.073	0.073	0.077	0.199	0.153	0.149	0.113	0.044	0.206	0.155	0.129	0.084	31.83	55.02	86.61

Table 7.2: Normalised pressure pulsation and pump performance results for 1.00Qn flow rate

	Normalised Pressure Pulsations														Single Rotation Averaged Pump Performance		
	Leakage Flow Path Locations					Volute Locations					Impeller Outlet Locations						
	Circumferentially Distant To Cutwater			Circumferentially Near Cutwater		Distance to Cutwater (mm)				Toward Outlet	Blade		Shroud				
						5	15	30	50								
Arr.	C1	C2	C10	C3	C4	C5	C6	C7	C8	C9	Press. Face	Suct. Face	Blade Pos.	Mid Pos.	Head (m)	Power (kW)	Eff (%)
1	0.058	0.063	0.056	0.083	0.107	0.233	0.263	0.340	0.316	0.086	0.693	0.443	0.432	0.540	39.31	44.09	68.16
2	0.038	0.051	0.042	0.073	0.094	0.289	0.221	0.218	0.185	0.044	0.628	0.291	0.228	0.355	38.97	42.04	69.90
3	0.025	0.029	0.030	0.063	0.087	0.226	0.226	0.204	0.173	0.036	0.582	0.319	0.295	0.364	38.97	41.96	69.57
4	0.042	0.043	0.042	0.054	0.064	0.260	0.210	0.188	0.159	0.028	0.526	0.373	0.217	0.261	37.26	39.55	70.55
5	0.045	0.050	0.049	0.089	0.132	0.308	0.237	0.287	0.278	0.068	0.578	0.333	0.275	0.359	37.93	41.48	69.69
6	0.033	0.025	0.026	0.035	0.050	0.178	0.136	0.124	0.154	0.032	0.423	0.338	0.197	0.275	37.03	39.52	70.48
7	0.025	0.026	0.027	0.029	0.043	0.159	0.116	0.140	0.163	0.036	0.416	0.347	0.191	0.279	35.66	37.75	71.12
8	0.023	0.030	0.029	0.037	0.045	0.143	0.124	0.111	0.109	0.021	0.421	0.312	0.195	0.214	35.96	37.81	71.22
9	0.060	0.055	0.058	0.068	0.078	0.223	0.163	0.186	0.196	0.049	0.455	0.296	0.260	0.252	36.32	39.28	69.97

Table 7.3: Normalised pressure pulsation and pump performance results for 0.50QnQn flow rate

	Normalised Pressure Pulsations														Single Rotation Averaged Pump Performance		
	Leakage Flow Path Locations					Volute Locations					Impeller Outlet Locations						
	Circumferentially Distant To Cutwater			Circumferentially Near Cutwater		Distance to Cutwater (mm)				Toward Outlet	Blade		Shroud				
						5	15	30	50								
Arr.	C1	C2	C10	C3	C4	C5	C6	C7	C8	C9	Press. Face	Suct. Face	Blade Pos.	Mid Pos.	Head (m)	Power (kW)	Eff. (%)
1	0.113	0.115	0.124	0.123	0.132	0.313	0.283	0.330	0.293	0.113	0.648	0.373	0.355	0.522	39.54	33.13	45.70
2	0.101	0.124	0.077	0.169	0.189	0.315	0.268	0.309	0.330	0.067	0.580	0.291	0.281	0.327	38.19	33.16	43.37
3	0.063	0.059	0.050	0.098	0.111	0.282	0.263	0.303	0.182	0.044	0.714	0.319	0.340	0.388	39.40	32.83	44.97
4	0.049	0.050	0.043	0.061	0.072	0.206	0.216	0.183	0.160	0.034	0.576	0.380	0.270	0.353	37.47	30.42	46.15
5	0.095	0.090	0.090	0.112	0.136	0.209	0.233	0.298	0.294	0.080	0.611	0.379	0.288	0.482	38.38	32.25	45.56
6	0.059	0.077	0.059	0.096	0.102	0.177	0.174	0.174	0.151	0.046	0.430	0.338	0.253	0.367	37.26	30.07	46.85
7	0.042	0.040	0.046	0.045	0.058	0.223	0.171	0.136	0.165	0.043	0.427	0.347	0.201	0.359	35.86	28.25	48.14
8	0.038	0.047	0.045	0.055	0.061	0.231	0.173	0.158	0.124	0.026	0.468	0.312	0.283	0.242	35.84	28.02	47.92
9	0.099	0.082	0.094	0.088	0.087	0.214	0.227	0.227	0.169	0.068	0.473	0.351	0.261	0.388	36.05	32.61	42.25

Table 7.4: Normalised pressure pulsation and pump performance results for 0.25Qn flow rate

Impeller Diameter (mm)	Cutwater Gap (%)	Total Head (m)					
		1.00Qn		0.50Qn		0.25Qn	
		Curve	Scaled	Curve	Scaled	Curve	Scaled
254	2.36	19.65	19.65	21.61	21.61	21.49	21.49
244	6.56	17.34	18.13	19.66	19.94	20.12	19.83
235	10.64	15.87	16.82	17.38	18.50	17.43	18.40

Table 7.5: Performance data comparison of Euler predicted and measured total head for three impeller diameters (measured data taken from Goulas & Truscott (78))

Arrangement	A (Cutwater Clearance)	B (Snubber Clearance)	C (Sidewall Clearance)	D (Vane Arrangement)	C8 (Z)
1	-1	-1	+1	-1	0.167
2	-1	0	0	0	0.081
3	-1	+1	-1	+1	0.119
4	0	-1	0	+1	0.094
5	0	0	-1	-1	0.143
6	0	+1	+1	0	0.067
7	+1	-1	-1	0	0.074
8	+1	0	0	+1	0.050
9	+1	+1	+1	-1	0.113
				Result Total *(Eqn. 5.10)*	0.908

Table 7.6: Reconfigured Taguchi L_9 array with sample data for location C8 at 1.00Qn

Factor	Arrangement	-1	0	+1
A	Cutwater Clearance	3.83%	6.00%	7.95%
B	Snubber Clearance	0.27%	1.10%	1.64%
C	Sidewall Clearance	25%	50%	100%
D	Vane Arrangement	Inline	15 degree stagger	30 degree stagger

Table 7.7: Summary of replacement variables in reconfigured array

Arrangement	Response Average Pressure Pulsation (Normalised)		
	-1	**0**	**+1**
A	0.122	0.101	0.079
B	0.112	0.091	0.100
C	0.112	0.095	0.095
D	0.141	0.074	0.088

Table 7.8: Response averages for location C8 at 1.00Qn

Factor	Low $(A_{-1})^2$	Mid $(A_0)^2$	High $(A_1)^2$	Total Variance *(Eqn. 5.13)*	Degrees of Freedom (DoF)	Variance *(Eqn. 5.14)*	Percentage Contribution *(Eqn 5.15)*
A	0.37	0.30	0.24	2.83E-3	2	1.41E-3	24.44
B	0.34	0.27	0.30	0.64E-3	2	0.32E-3	5.51
C	0.34	0.29	0.28	0.58E-3	2	0.29E-3	4.98
D	0.42	0.22	0.26	7.53E-3	2	3.76E-3	65.07
				Total DoF	8		
				Correction Factor	0.092	*(Eqn 5.11)*	
				Total Variation	0.012	*(Eqn. 5.12)*	

Table 7.9: Sample set of Taguchi calculations for C8 location at 1.00Qn

	Normalised Pressure Pulsations														Single Rotation Averaged Pump Performance		
	Leakage Flow Path Locations					Volute Locations					Impeller Outlet Locations						
	Circumferentially Distant To Cutwater			Circumferentially Near Cutwater		Distance to Cutwater (mm)				Toward Outlet	Blade		Shroud				
						5	15	30	50								
Geometric Parameter	**C1**	**C2**	**C10**	**C3**	**C4**	**C5**	**C6**	**C7**	**C8**	**C9**	**Pres. Face**	**Suct. Face**	**Mid Pos.**	**Blade Pos.**	**Head (m)**	**Power (kW)**	**Eff. (%)**
Cutwater	6.59	4.11	8.32	20.74	31.53	59.61	66.69	40.32	24.44	16.39	94.42	74.75	67.88	37.89	91.10	85.73	34.41
Snubber	0.25	2.43	0.92	0.33	1.62	3.04	0.73	0.40	5.51	2.76	3.45	7.50	8.57	8.40	0.72	0.68	2.10
Sidewall	1.52	0.70	0.09	4.30	13.42	7.84	1.14	4.13	4.98	0.79	0.28	17.71	12.17	13.21	0.26	0.17	10.33
Vane	91.64	92.75	90.67	74.62	53.43	29.51	31.44	55.16	65.07	80.05	1.84	0.04	11.38	40.50	7.91	13.42	53.16

Table 7.10 Percentage contributions for 1.00Qn flow rate at all pump locations

	Normalised Pressure Pulsations														Single Rotation Averaged Pump Performance		
	Leakage Flow Path Locations					Volute Locations					Impeller Outlet Locations						
	Circumferentially Distant To Cutwater			Circumferentially Near Cutwater		Distance to Cutwater (mm)				Toward Outlet	Blade		Shroud				
						5	15	30	50								
Geometric Parameter	**C1**	**C2**	**C10**	**C3**	**C4**	**C5**	**C6**	**C7**	**C8**	**C9**	**Pres. Face**	**Suct. Face**	**Mid Position**	**Above Blade**	**Head (m)**	**Power (kW)**	**Eff. (%)**
Cutwater	1.98	11.76	3.01	32.23	34.17	42.40	67.19	39.02	21.25	17.88	63.30	11.29	61.20	40.07	95.17	80.92	54.53
Snubber	3.97	7.64	1.71	6.43	9.67	9.36	3.55	8.92	6.71	5.08	16.35	61.06	8.74	7.36	0.50	0.22	2.65
Sidewall	22.83	21.12	19.46	7.11	7.97	31.78	3.94	1.22	2.84	2.31	6.18	17.87	6.51	5.09	0.09	0.14	0.98
Vane	71.23	59.48	75.82	54.23	48.18	16.46	25.32	50.84	69.20	74.72	14.17	9.77	23.54	47.48	4.23	18.73	41.83

Table 7.11 Percentage contributions for 0.50Qn flow rate at all pump locations

	Normalised Pressure Pulsations														Single Rotation Averaged Pump Performance		
	Leakage Flow Path Locations					Volute Locations					Impeller Outlet Locations						
	Circumferentially Distant To Cutwater			Circumferentially Near Cutwater		Distance to Cutwater (mm)				Toward Outlet	Blade		Shroud				
						5	15	30	50								
Geometric Parameter	**C1**	**C2**	**C10**	**C3**	**C4**	**C5**	**C6**	**C7**	**C8**	**C9**	**Pres. Face**	**Suct. Face**	**Mid Pos.**	**Blade Pos.**	**Head (m)**	**Power (kW)**	**Eff. (%)**
Cutwater	26.53	40.02	13.52	58.45	40.03	89.57	72.92	68.29	43.90	23.59	66.37	29.70	28.48	57.96	88.91	52.41	81.62
Snubber	2.18	8.29	0.40	16.25	30.90	8.93	0.08	4.84	21.77	3.05	7.73	32.71	17.94	16.97	0.22	6.75	10.06
Sidewall	6.85	11.11	4.87	5.92	5.02	0.75	7.46	2.24	3.45	1.06	2.43	1.38	9.96	8.90	3.84	12.19	7.67
Vane	64.44	40.57	81.21	19.39	24.06	0.75	19.54	24.63	30.88	72.30	23.47	36.20	43.62	16.18	7.04	28.65	0.65

Table 7.12 Percentage contributions for 0.25Qn flow rate at all pump locations

Arrangement	A (Cutwater Clearance)	B (Vane Arrangement)	AB (Interaction)	C8
1 (1)	-1	-1	+1	0.167
3 (5)	-1	+1	-1	0.119
9 (3)	+1	-1	-1	0.113
8 (9)	+1	+1	+1	0.050
			Result Total	0.449
Where Cutwater Clearance –1= 3.83%; +1 = 7.95% Where Vane Arrangement –1= Inline; +1 = Staggered 30 degrees				

Table 7.13: Stage 1 array arrangement with sample data for location C8 at 1.00Qn

	Normalised Pressure Pulsations														Single Rotation Averaged Pump Performance		
	Leakage Flow Path Locations					Volute Locations					Impeller Outlet Locations						
	Circumferentially Distant To Cutwater			Circumferentially Near Cutwater		Distance to Cutwater (mm)				Toward Outlet	Blade		Shroud				
						5	15	30	50								
Arr.	**C1**	**C2**	**C10**	**C3**	**C4**	**C5**	**C6**	**C7**	**C8**	**C9**	**Pres. Face**	**Suct. Face**	**Blade Pos.**	**Mid Pos.**	**Head (m)**	**Power (kW)**	**Eff. (%)**
1.00Qn																	
1	0.094	0.087	0.094	0.090	0.101	0.253	0.259	0.217	0.167	0.072	0.411	0.185	0.181	0.149	36.05	63.07	85.74
3	0.038	0.035	0.037	0.063	0.095	0.264	0.208	0.180	0.119	0.025	0.381	0.234	0.178	0.160	35.2	60.35	87.33
9	0.072	0.069	0.073	0.073	0.077	0.199	0.153	0.149	0.113	0.044	0.206	0.155	0.129	0.084	31.83	59.93	79.53
8	0.023	0.019	0.025	0.027	0.036	0.133	0.098	0.083	0.050	0.015	0.148	0.126	0.074	0.068	30.33	51.28	88.57
0.50Qn																	
1	0.058	0.063	0.056	0.083	0.107	0.233	0.263	0.340	0.316	0.086	0.693	0.443	0.432	0.540	39.31	44.09	68.16
3	0.025	0.029	0.030	0.063	0.087	0.226	0.226	0.204	0.173	0.036	0.582	0.319	0.295	0.364	38.97	41.96	69.57
9	0.060	0.055	0.058	0.068	0.078	0.223	0.163	0.186	0.196	0.049	0.455	0.296	0.260	0.252	36.32	39.28	69.97
8	0.023	0.030	0.029	0.037	0.045	0.143	0.124	0.111	0.109	0.021	0.421	0.312	0.195	0.214	35.96	37.81	71.22
0.25Qn																	
1	0.113	0.115	0.124	0.123	0.132	0.313	0.283	0.330	0.293	0.113	0.648	0.373	0.355	0.522	39.54	33.13	45.70
3	0.063	0.059	0.050	0.098	0.111	0.282	0.263	0.303	0.182	0.044	0.714	0.319	0.340	0.388	39.40	32.83	44.97
9	0.099	0.082	0.094	0.088	0.087	0.214	0.227	0.227	0.169	0.068	0.473	0.351	0.261	0.388	36.05	32.61	40.00
8	0.038	0.047	0.045	0.055	0.061	0.231	0.173	0.158	0.124	0.026	0.468	0.312	0.283	0.242	35.84	28.02	47.92

Table 7.14 Stage 1 array results for 3 flow conditions

Factor	Sym	Locations									Head
		Leakage Flow		Volute			Blade		Shroud		
		C1	C3	C6	C8	C9	Pres. Face	Suct. Face	Blade Pos.	Mid Pos.	
1.00Qn											
Cut-water (A)	-1	0.066	0.076	0.233	0.143	0.048	0.396	0.209	0.179	0.154	35.62
	+1	0.047	0.05	0.125	0.081	0.029	0.177	0.140	0.101	0.076	31.08
	Δ	-0.018	-0.026	-0.108	-0.061	-0.019	-0.219	-0.069	-0.078	-0.078	-4.54
	Δ/2	-0.009	-0.013	-0.054	-0.031	-0.009	-0.109	-0.034	-0.039	-0.039	-2.27
Vane Arr. (B)	-1	0.083	0.081	0.206	0.14	0.058	0.308	0.17	0.155	0.116	33.94
	+1	0.0305	0.045	0.153	0.084	0.02	0.264	0.18	0.126	0.114	32.76
	Δ	-0.052	-0.036	-0.053	-0.055	-0.038	-0.044	0.01	-0.029	-0.002	-1.175
	Δ/2	-0.026	-0.018	-0.026	-0.028	-0.019	-0.022	0.005	-0.014	-0.001	-0.587
Inter-action (AB)	-1	0.055	0.068	0.180	0.116	0.034	0.293	0.194	0.153	0.122	33.51
	+1	0.058	0.058	0.178	0.108	0.043	0.279	0.155	0.127	0.108	33.19
	Δ	0.003	-0.009	-0.002	-0.007	0.009	-0.014	-0.039	-0.026	-0.013	-0.325
	Δ/2	0.002	-0.005	-0.001	-0.004	0.004	-0.007	-0.019	-0.013	-0.007	-0.162
Grand Mean		0.057	0.063	0.180	0.112	0.039	0.287	0.175	0.140	0.115	33.35
0.50Qn											
Cut-water (A)	-1	0.041	0.073	0.244	0.244	0.061	0.637	0.381	0.363	0.452	39.14
	+1	0.041	0.052	0.143	0.152	0.035	0.438	0.304	0.227	0.233	36.14
	Δ	0.000	-0.020	-0.101	-0.092	-0.026	-0.199	-0.077	-0.136	-0.219	-3.00
	Δ/2	0.000	-0.010	-0.050	-0.046	-0.013	-0.100	-0.038	-0.068	-0.109	-1.50
Vane Arr. (B)	-1	0.059	0.075	0.213	0.256	0.067	0.574	0.370	0.346	0.396	37.81
	+1	0.024	0.05	0.175	0.141	0.028	0.501	0.315	0.245	0.289	37.46
	Δ	-0.035	-0.025	-0.038	-0.115	-0.039	-0.072	-0.054	-0.101	-0.107	-0.35
	Δ/2	-0.017	-0.013	-0.019	-0.057	-0.019	-0.036	-0.027	-0.050	-0.053	-0.175
Inter-action (AB)	-1	0.042	0.065	0.194	0.184	0.042	0.518	0.307	0.277	0.308	37.64
	+1	0.040	0.06	0.193	0.212	0.053	0.557	0.377	0.313	0.377	37.63
	Δ	-0.002	-0.005	-0.001	0.028	0.011	0.038	0.07	0.036	0.069	-0.01
	Δ/2	-0.001	-0.003	-0.000	0.014	0.005	0.019	0.035	0.018	0.034	-0.00
Grand Mean		0.042	0.062	0.194	0.198	0.048	0.538	0.343	0.296	0.343	37.64
0.25Qn											
Cut-water (A)	-1	0.088	0.110	0.273	0.237	0.078	0.681	0.346	0.347	0.455	39.47
	+1	0.068	0.071	0.2	0.146	0.047	0.470	0.331	0.272	0.315	35.94
	Δ	-0.019	-0.039	-0.073	-0.091	-0.031	-0.210	-0.014	-0.075	-0.14	-3.52
	Δ/2	-0.010	-0.019	-0.036	-0.045	-0.016	-0.105	-0.007	-0.038	-0.07	-1.76
Vane Arr. (B)	-1	0.106	0.105	0.255	0.231	0.090	0.560	0.362	0.308	0.455	37.79
	+1	0.050	0.076	0.218	0.153	0.035	0.591	0.315	0.311	0.315	37.62
	Δ	-0.055	-0.029	-0.037	-0.078	-0.055	0.0305	-0.046	0.003	-0.14	-0.175
	Δ/2	-0.028	-0.014	-0.018	-0.039	-0.028	0.0152	-0.023	0.002	-0.07	-0.087
Inter-action (AB)	-1	0.081	0.093	0.245	0.175	0.056	0.593	0.335	0.300	0.388	37.72
	+1	0.075	0.089	0.228	0.208	0.069	0.558	0.342	0.319	0.382	37.69
	Δ	-0.005	-0.004	-0.017	0.033	0.013	-0.035	0.007	0.018	-0.006	-0.035
	Δ/2	-0.003	-0.002	-0.008	0.016	0.007	-0.018	0.004	0.009	-0.003	-0.017
Grand Mean		0.078	0.091	0.237	0.192	0.063	0.596	0.338	0.253	0.395	37.70

Table 7.15 Response averages, effects and half effects for stage 1 analysis at three flow rates

Arrangement	A (Cutwater Clearance)	B (Vane Arrangement)	AB (Interaction)	C8
2 (4)	-1	-1	+1	0.081
3 (5)	-1	+1	-1	0.119
7 (7)	+1	-1	-1	0.074
8 (9)	+1	+1	+1	0.050
			Result Total	0.324
Where Cutwater Clearance –1= 3.83%; +1 = 7.95% Where Vane Arrangement –1= Staggered 15 degrees; +1 = Staggered 30 degrees				

Table 7.16: Stage 2 array arrangement with sample data for location C8 at 1.00Qn

	Normalised Pressure Pulsations														Single Rotation Averaged Pump Performance		
	Leakage Flow Path Locations					Volute Locations					Impeller Outlet Locations						
	Circumferentially Distant To Cutwater			Circumferentially Near Cutwater		Distance to Cutwater (mm)				Toward Outlet	Blade		Shroud				
						5	15	30	50								
Arr.	**C1**	**C2**	**C10**	**C3**	**C4**	**C5**	**C6**	**C7**	**C8**	**C9**	**Pres. Face**	**Suct. Face**	**Blade Pos.**	**Mid Pos.**	**Head (m)**	**Power (kW)**	**Eff. (%)**
1.00Qn																	
2	0.056	0.043	0.061	0.056	0.067	0.231	0.200	0.134	0.081	0.049	0.332	0.254	0.128	0.115	34.71	59.94	86.72
3	0.038	0.035	0.037	0.063	0.095	0.264	0.208	0.180	0.119	0.025	0.381	0.234	0.178	0.160	35.2	60.35	87.33
7	0.050	0.044	0.045	0.041	0.042	0.118	0.096	0.083	0.074	0.034	0.175	0.131	0.075	0.062	30.89	52.42	88.26
8	0.023	0.019	0.025	0.027	0.036	0.133	0.098	0.083	0.050	0.015	0.148	0.126	0.074	0.068	30.33	51.28	88.57
0.50Qn																	
2	0.038	0.051	0.042	0.073	0.094	0.289	0.221	0.218	0.185	0.044	0.628	0.291	0.228	0.355	38.97	42.04	69.90
3	0.025	0.029	0.030	0.063	0.087	0.226	0.226	0.204	0.173	0.036	0.582	0.319	0.295	0.364	38.97	41.96	69.57
7	0.025	0.026	0.027	0.029	0.043	0.159	0.116	0.140	0.163	0.036	0.416	0.347	0.191	0.279	35.66	37.75	71.12
8	0.023	0.030	0.029	0.037	0.045	0.143	0.124	0.111	0.109	0.021	0.421	0.312	0.195	0.214	35.96	37.81	71.22
0.25Qn																	
2	0.101	0.124	0.077	0.169	0.189	0.315	0.268	0.309	0.330	0.067	0.580	0.291	0.281	0.327	38.19	33.16	43.37
3	0.063	0.059	0.050	0.098	0.111	0.282	0.263	0.303	0.182	0.044	0.714	0.319	0.340	0.388	39.40	32.83	44.97
7	0.042	0.040	0.046	0.045	0.058	0.223	0.171	0.136	0.165	0.043	0.427	0.347	0.201	0.359	35.86	28.25	48.14
8	0.038	0.047	0.045	0.055	0.061	0.231	0.173	0.158	0.124	0.026	0.468	0.312	0.283	0.242	35.84	28.02	47.92

Table 7.17: Stage 2 array results for 3 flow conditions

Factor	Sym	Locations									Head
		Leakage Flow		Volute			Blade		Shroud		
		C1	C3	C6	C8	C9	Pres. Face	Suct. Face	Blade Pos.	Mid Pos.	
1.00Qn											
Cut-water (A)	-1	0.047	0.059	0.204	0.100	0.037	0.356	0.244	0.153	0.137	34.95
	+1	0.036	0.034	0.097	0.062	0.024	0.161	0.128	0.074	0.065	30.61
	Δ	-0.010	-0.025	-0.107	-0.038	-0.012	-0.195	-0.115	-0.078	-0.072	-4.345
	Δ/2	-0.005	-0.013	-0.053	-0.019	-0.006	-0.097	-0.058	-0.039	-0.036	-2.172
Vane Arr. (B)	-1	0.053	0.048	0.148	0.077	0.041	0.253	0.192	0.101	0.088	32.80
	+1	0.030	0.045	0.153	0.084	0.02	0.264	0.180	0.126	0.114	32.76
	Δ	-0.022	-0.003	0.005	0.007	-0.021	0.011	-0.012	0.024	0.025	-0.035
	Δ/2	-0.011	-0.002	0.002	0.003	-0.011	0.005	-0.006	0.012	0.013	-0.017
Inter-action (AB)	-1	0.044	0.052	0.152	0.096	0.029	0.278	0.182	0.126	0.111	33.04
	+1	0.039	0.041	0.149	0.065	0.032	0.240	0.190	0.101	0.091	32.52
	Δ	-0.004	-0.010	-0.003	-0.031	0.002	-0.038	0.007	-0.025	-0.019	-0.525
	Δ/2	-0.002	-0.005	-0.001	-0.015	0.001	-0.019	0.004	-0.013	-0.010	-0.262
Grand Mean		0.042	0.047	0.150	0.081	0.032	0.259	0.186	0.114	0.101	32.78
0.50Qn											
Cut-water (A)	-1	0.031	0.068	0.223	0.179	0.04	0.605	0.305	0.261	0.359	38.97
	+1	0.024	0.033	0.12	0.136	0.028	0.418	0.329	0.193	0.246	35.81
	Δ	-0.007	-0.035	-0.103	-0.043	-0.011	-0.186	0.024	-0.068	-0.113	-3.160
	Δ/2	-0.004	-0.017	-0.052	-0.021	-0.006	-0.093	0.012	-0.034	-0.056	-1.580
Vane Arr. (B)	-1	0.031	0.051	0.168	0.174	0.04	0.522	0.319	0.209	0.317	37.31
	+1	0.024	0.05	0.175	0.141	0.028	0.501	0.315	0.245	0.289	37.46
	Δ	-0.007	-0.001	0.006	-0.033	-0.011	-0.020	-0.003	0.035	-0.028	0.150
	Δ/2	-0.004	0.000	0.003	-0.016	-0.006	-0.010	-0.002	0.018	-0.014	0.075
Inter-action (AB)	-1	0.025	0.046	0.171	0.168	0.036	0.499	0.333	0.243	0.321	37.31
	+1	0.030	0.055	0.172	0.147	0.032	0.524	0.301	0.211	0.284	37.46
	Δ	0.005	0.009	0.001	-0.021	-0.003	0.025	-0.031	-0.031	-0.037	0.150
	Δ/2	0.003	0.004	0.001	-0.010	-0.002	0.013	-0.016	-0.016	-0.018	0.075
Grand Mean		0.028	0.050	0.171	0.157	0.034	0.511	0.317	0.227	0.303	37.39
0.25Qn											
Cut-water (A)	-1	0.082	0.133	0.265	0.256	0.055	0.647	0.305	0.310	0.357	38.79
	+1	0.040	0.05	0.172	0.144	0.034	0.447	0.329	0.242	0.300	35.85
	Δ	-0.042	-0.083	-0.093	-0.111	-0.021	-0.199	0.024	-0.068	-0.057	-2.94
	Δ/2	-0.021	-0.042	-0.047	-0.056	-0.010	-0.100	0.012	-0.034	-0.028	-1.47
Vane Arr. (B)	-1	0.071	0.107	0.219	0.247	0.055	0.503	0.319	0.241	0.343	37.02
	+1	0.050	0.076	0.218	0.153	0.035	0.591	0.315	0.311	0.315	37.62
	Δ	-0.021	-0.030	-0.001	-0.094	-0.020	0.087	-0.003	0.070	-0.028	0.595
	Δ/2	-0.010	-0.015	-0.001	-0.047	-0.010	0.044	-0.002	0.035	-0.014	0.297
Inter-action (AB)	-1	0.052	0.071	0.217	0.173	0.043	0.570	0.333	0.270	0.373	37.63
	+1	0.069	0.112	0.220	0.227	0.046	0.524	0.301	0.282	0.284	37.01
	Δ	0.017	0.040	0.003	0.053	0.003	-0.046	-0.031	0.011	-0.089	-0.615
	Δ/2	0.008	0.020	0.002	0.027	0.001	-0.023	-0.016	0.006	-0.044	-0.307
Grand Mean		0.061	0.092	0.219	0.200	0.045	0.547	0.317	0.219	0.339	37.32

Table 7.18 Response averages, effects and half effects for stage 2 analysis at three flow rates

Arr.	Tip ($x10^3 N/m^2$)	Wear Ring ($x10^3 N/m^2$)

No.	Average		Maximum		Pulse		Average		Maximum		Pulse	
	10^3 N/m^2	*H	10^3 N/m^2	*H	10^3 N/m^2	*H	10^3 N/m^2	*H	10^3 N/m^2	*H	10^3 N/m^2	*H
1	12.4	0.04	30.5	0.09	30.7	0.09	-119.2	-0.34	122.8	0.35	10.4	0.03
2	6.1	0.02	19.8	0.06	20.7	0.06	-123.9	-0.36	126.5	0.37	5.9	0.02
3	3.9	0.01	15.0	0.04	18.6	0.05	-127.7	-0.37	129.9	0.38	4.4	0.01
4	18.3	0.06	35.6	0.11	32.7	0.10	-89.8	-0.28	90.7	0.28	1.8	0.01
5	6.6	0.02	14.1	0.04	14.3	0.04	-128.2	-0.39	131.1	0.40	8.1	0.02
6	4.2	0.01	15.4	0.05	20.0	0.06	-127.3	-0.40	129.8	0.40	3.8	0.01
7	18.6	0.06	31.8	0.10	24.6	0.08	-97.3	-0.32	101.1	0.33	11.0	0.04
8	4.5	0.02	15.8	0.05	21.3	0.07	-120.6	-0.41	134.9	0.45	26.3	0.09
9	1.5	0.00	11.2	0.04	19.3	0.06	-139.6	-0.45	145.6	0.47	13.6	0.04

Table 7.19: Pressure differentials at 1.00Qn for nine Taguchi arrangements

Arr. No.	Tip ($x10^3 N/m^2$)						Wear Ring ($x10^3 N/m^2$)					
	Average		Maximum		Pulse		Average		Maximum		Pulse	
	10^3 N/m^2	*H	10^3 N/m^2	*H	10^3 N/m^2	*H	10^3 N/m^2	*H	10^3 N/m^2	*H	10^3 N/m^2	*H
1	-30.1	-0.08	105.3	0.27	179.0	0.46	-163.3	-0.42	188.0	0.48	71.7	0.18
2	-39.7	-0.11	62.7	0.17	84.3	0.23	-186.6	-0.50	209.7	0.56	62.1	0.17
3	-2.2	-0.01	43.9	0.11	83.5	0.22	-165.1	-0.43	201.1	0.52	100.4	0.26
4	-37.1	-0.10	115.8	0.32	177.5	0.48	-135.8	-0.37	162.7	0.44	67.4	0.18
5	18.6	0.05	60.3	0.16	116.4	0.31	154.2	0.41	186.7	0.50	96.8	0.26
6	-10.6	-0.03	49.8	0.14	97.9	0.27	-162.1	-0.44	190.8	0.52	85.4	0.23
7	-30.1	-0.09	72.5	0.21	131.4	0.37	-136.2	-0.39	157.8	0.45	52.2	0.15
8	-24.5	-0.07	66.0	0.19	119.3	0.34	-154.8	-0.44	181.7	0.52	67.8	0.19
9	-41.0	-0.12	76.9	0.22	120.3	0.34	-155.9	-0.44	192.6	0.55	20.4	0.06

Table 7.20: Pressure Differentials at 0.25Qn for nine Taguchi arrangements

Geometric Parameter	1.00Qn						0.25Qn					
	Average		Maximum		Pulse		Average		Maximum		Pulse	
	Tip	Wear Ring	Tip	Wear Ring	Tip	Wear Ring	Tip	Wear Ring	Tip	Wear Ring	Tip	Wear Ring
Cutwater	5.44	2.44	1.39	7.92	1.41	60.10	29.50	23.56	0.79	39.81	3.40	49.20
Snubber	70.26	90.54	93.62	68.55	76.27	16.33	19.07	16.04	63.96	53.46	70.73	4.47
Sidewall	2.14	3.20	0.96	5.93	17.55	16.73	27.80	56.27	22.59	3.13	7.83	37.92
Vane	22.16	3.82	4.03	17.60	4.77	6.84	23.63	4.13	12.67	3.60	18.03	8.41

Table 7.21: Percentage contributions for shroud differential pressure

Optimisation Motivation	Cutwater Gap	Vane Arrangement	Snubber Gap (Diametral gap)	Sidewall Clearance
Impeller Life	6% - 8%	Staggered vane impeller	1% -1.5% of impeller diameter	100%
Noise and Vibration	Close to 6%	30 degree stagger	Not influenced	Not influenced

Table 7.22: Comparison of optimised results

Geometric Set Up	Impeller Diameter (mm)	Cutwater Diameter (mm)	Cutwater Gap
A	366	384	4.92%
B	362	380	4.97%

Table 7.23: Two different 5% cutwater gap arrangements

	Normalised Pressure Pulsations														Single Rotation Averaged Pump Performance		
	Leakage Flow Path Locations					Volute Locations					Impeller Outlet Locations						
	Circumferentially Distant To Cutwater			Circumferentially Near Cutwater		Distance to Cutwater (mm)				Toward Outlet	Blade		Shroud				
						5	15	30	50								
Geometric Factor	**C1**	**C2**	**C10**	**C3**	**C4**	**C5**	**C6**	**C7**	**C8**	**C9**	**Pres. Face**	**Suct. Face**	**Blade Pos.**	**Mid Pos.**	**Head (m)**	**Power (kW)**	**Eff. (%)**
1.00Qn																	
Model A	0.032	0.029	0.033	0.036	0.051	0.137	0.147	0.120	0.083	0.018	0.251	0.198	0.107	0.093	34.57	59.21	87.43
Model B	0.032	0.030	0.032	0.041	0.054	0.203	0.159	0.119	0.081	0.018	0.281	0.196	0.120	0.098	33.72	57.11	88.42
0.50Qn																	
Model A	0.026	0.026	0.034	0.044	0.056	0.137	0.194	0.177	0.157	0.017	0.575	0.360	0.248	0.267	39.67	42.07	70.63
Model B	0.028	0.030	0.028	0.041	0.052	0.182	0.188	0.164	0.144	0.029	0.520	0.342	0.238	0.245	37.93	40.52	71.41
0.25Qn																	
Model A	0.051	0.056	0.042	0.067	0.077	0.185	0.224	0.212	0.181	0.019	0.562	0.351	0.301	0.311	39.89	32.03	46.67
Model B	0.047	0.057	0.034	0.078	0.086	0.236	0.211	0.217	0.169	0.037	0.564	0.342	0.264	0.267	38.22	31.21	45.87

Table 7.24: Additional analysis arrangement results

Arrangement	Impeller Diameter (mm)	Cutwater Gap	Vane Arrangement	Generated Head (m)		
				1.00Qn	**0.50Qn**	**0.25Qn**
Model A	366	4.92%	30 degree stagger	34.57	39.67	39.89
Arrangement 3	366	3.83%	30 degree stagger	35.20	38.97	39.40
Comparison of Model A to 3				-1.8%	+1.8%	+1.2%
Model B	362	4.97	30 degree stagger	33.72	37.93	38.22
Euler based on Model A (Euler A)	362	4.92	30 degree stagger	33.82	38.97	39.02
Comparison of Model A to Euler A				-0.3%	-2.7%	-2.1%

Table 7.25: Comparison of generated head data

Comparison	Predicted Normalised Pressure Pulsations							Single Rotation Averaged Pump Performance
	Locations					Blade	Shroud	
	C1	C4	C6	C8	C9	Pressure Face	Mid Position	Head (m)
1.00Qn								
Predict Model B	0.034	0.080	0.180	0.102	0.023	0.323	0.137	33.93
Model B	0.032	0.054	0.159	0.081	0.018	0.281	0.098	33.72
0.50Qn								
Predict Model B	0.025	0.076	0.200	0.157	0.032	0.541	0.326	38.21
Model B	0.028	0.052	0.188	0.144	0.029	0.520	0.245	37.93
0.25Qn								
Predict Model B	0.056	0.098	0.241	0.168	0.039	0.652	0.304	38.51
Model B	0.047	0.086	0.211	0.169	0.037	0.564	0.267	38.22

Table 7.26: Predicted optimised analysis results

Comparison	Locations					Impeller		Performance
	C1	C3	C6	C8	C9	Blade Pres. Face	Mid Shroud Location	Head
1.00Qn								
Steady State	0.047	0.058	0.141	0.158	0.048	0.156	0.098	33.84
Transient	0.094	0.090	0.259	0.167	0.081	0.411	0.149	36.05
0.50Qn								
Steady State	0.110	0.090	0.118	0.108	0.028	0.373	0.193	39.37
Transient	0.058	0.083	0.263	0.316	0.086	0.693	0.540	39.31
0.25Qn								
Steady State	0.105	0.099	0.102	0.138	0.053	0.565	0.174	41.64
Transient	0.114	0.123	0.283	0.293	0.113	0.648	0.522	39.54

Table 7.27: Comparison of steady state analysis and transient analysis normalised pressure pulsations and average head

Arrangement	Analysis Type	Locations					Impeller		Performance
		C1	C3	C6	C8	C9	Blade Pressure Face	Mid Shroud Location	Head
First	Steady State	0.047	0.058	0.141	0.158	0.048	0.156	0.098	33.84
	Transient	0.094	0.090	0.259	0.065	0.072	0.411	0.149	36.05
Model_A	Steady State	0.082	0.093	0.051	0.065	0.015	0.146	0.087	33.52
	Transient	0.032	0.036	0.147	0.083	0.018	0.251	0.093	34.57

Table 7.28: Comparison of steady state analysis and transient analysis normalised pressure pulsations between two arrangements at 1.00Qn

Data Set	Arrangement	Impeller Position at Cutwater	Snubber Gap
1	4	Blade	0.27%
2	4	Mid Position	0.27%
3	6	Blade	1.64%
4	6	Mid Position	1.64%

Table 7.29: Summary of pressure loading data sets supplied for stress analysis

Result	Location	Arrangement 4		Arrangement 6		Centrifugal Loading (N/m^2)
		Blade (N/m^2)	Mid (N/m^2)	Blade (N/m^2)	Mid (N/m^2)	
Maximum	a	-0.157	-0.204	-0.274	-0.274	0.093
	b	0.267	0.333	0.260	0.018	0.021
	c	-0.466	-0.336	-0.666	-0.352	0.226
	d	-0.186	-0.096	-0.264	-0.182	-0.028
	e	-0.270	-0.208	-0.342	-0.221	0.006
	f	-0.098	-0.255	-0.171	-0.197	0.156
	g	-0.321	-0.347	-0.414	-0.383	0.027
	h	-0.357	-0.368	-0.429	-0.374	0.007
	j	2.833	1.373	0.978	-0.306	1.286
	k	2.154	3.017	1.905	1.092	0.395
Minimum	a	-0.607	-0.581	-0.620	-0.568	-0.271
	b	-0.831	-0.466	-0.459	-0.582	-0.472
	c	-1.073	-0.948	-0.962	-0.551	0.030
	d	-0.601	-0.563	-0.519	-0.357	-0.030
	e	-0.503	-0.520	-0.483	-0.364	-0.009
	f	-0.575	-0.743	-0.674	-0.577	-0.080
	g	-0.549	-0.614	-0.561	-0.478	0.024
	h	-0.502	-0.552	-0.521	-0.450	0.004
	j	-3.666	-4.807	-3.379	-1.781	1.241
	k	-2.726	-1.557	-1.133	-0.240	0.101
Difference	a	0.449	0.377	0.347	0.294	0.364
	b	1.098	0.799	0.719	0.601	0.493
	c	0.607	0.612	0.296	0.199	0.197
	d	0.415	0.467	0.255	0.175	0.001
	e	0.233	0.313	0.141	0.143	0.015
	f	0.478	0.488	0.504	0.380	0.236
	g	0.228	0.268	0.147	0.095	0.003
	h	0.145	0.184	0.092	0.076	0.003
	j	6.499	6.180	4.357	1.475	0.046
	k	4.880	4.574	3.038	1.332	0.294

Table 7.30: Radial stress results at all shroud positions for finite element stress analyses

Result	Location	Arrangement 4		Arrangement 6		Centrifugal Loading (N/m^2)
		Blade (N/m^2)	Mid (N/m^2)	Blade (N/m^2)	Mid (N/m^2)	
Maximum	a	-0.148	-0.194	-0.228	-0.427	1.062
	b	3.935	1.990	1.483	-0.200	0.814
	c	4.306	2.316	1.584	0.032	2.684
	d	0.414	0.985	0.279	0.151	2.444
	e	0.087	0.463	-0.046	-0.152	2.610
	f	1.309	2.236	1.127	-0.208	3.211
	g	1.340	0.521	0.236	-0.671	2.280
	h	0.582	0.090	-0.058	-0.404	2.110
	j	0.550	-0.155	-0.501	-1.193	4.099
	k	0.226	0.856	0.135	-0.041	3.360
Minimum	a	-0.749	-0.589	-0.669	-0.697	0.864
	b	-5.404	-7.132	-5.382	-2.802	0.155
	c	-6.148	-7.470	-5.782	-3.055	2.496
	d	-1.976	-1.652	-1.457	-1.028	2.421
	e	-1.759	-1.554	-1.422	-1.195	2.600
	f	-4.069	-3.336	-2.910	-2.057	3.154
	g	-2.878	-3.548	-2.698	-1.910	2.252
	h	-1.847	-2.082	-1.729	-1.300	2.090
	j	-2.612	-3.381	-2.718	-2.232	3.994
	k	-1.873	-1.461	-1.223	-0.868	3.028
Difference	a	0.601	0.395	0.441	0.271	0.198
	b	9.339	9.122	6.865	2.602	0.660
	c	10.454	9.786	7.366	3.088	0.188
	d	2.390	2.637	1.737	1.179	0.023
	e	1.846	2.018	1.376	1.043	0.010
	f	5.378	5.572	4.037	1.850	0.057
	g	4.218	4.068	2.934	1.239	0.028
	h	2.428	2.173	1.670	0.896	0.020
	j	3.162	3.226	2.217	1.039	0.105
	k	2.099	2.317	1.358	0.827	0.331

Table 7.31: Hoop stress results at all shroud positions for finite element stress analyses

Result	Location	Arrangement 4		Arrangement 6		Centrifugal Loading (N/m^2)
		Blade (N/m^2)	Mid (N/m^2)	Blade (N/m^2)	Mid (N/m^2)	
Maximum	a	0.520	1.615	0.744	0.682	2.049
	b	4.694	3.305	2.386	-1.230	-1.220
	c	1.161	1.133	1.043	0.203	0.322
	d	-0.265	-0.304	-0.299	-0.348	0.003
	e	-0.247	-0.284	-0.286	-0.345	0.008
	f	-0.025	-0.162	-0.170	-0.339	0.043
	g	-0.343	-0.378	-0.352	-0.370	0.010
	h	-0.330	-0.378	-0.335	-0.359	0.003
	j	-0.082	-0.151	-0.155	-0.213	0.205
	k	0.029	-0.062	-0.227	-0.320	0.445
Minimum	a	-1.987	-1.704	-1.373	-0.959	1.874
	b	-7.740	-9.559	-6.734	-6.272	-2.141
	c	-1.490	-1.864	-1.309	-0.758	0.177
	d	-0.474	-0.447	-0.451	-0.418	-0.001
	e	-0.468	-0.463	-0.464	-0.423	0.003
	f	-0.517	-0.523	-0.435	-0.444	-0.005
	g	-0.407	-0.410	-0.422	-0.409	0.004
	h	-0.431	-0.412	-0.421	-0.409	0.002
	j	-0.381	-0.482	-0.439	-0.325	0.128
	k	-0.526	-0.844	-0.734	-0.470	0.158
Difference	a	2.506	3.319	2.117	1.641	0.175
	b	12.434	12.863	9.120	5.043	0.921
	c	2.652	2.998	2.353	0.961	0.144
	d	0.209	0.143	0.152	0.070	0.004
	e	0.221	0.179	0.179	0.077	0.004
	f	0.492	0.361	0.265	0.105	0.047
	g	0.064	0.032	0.070	0.039	0.006
	h	0.101	0.033	0.086	0.050	0.001
	j	0.299	0.331	0.284	0.112	0.077
	k	0.556	0.782	0.507	0.150	0.286

Table 7.32: Axial stress results at all shroud positions for finite element stress analyses

7.9 Figures

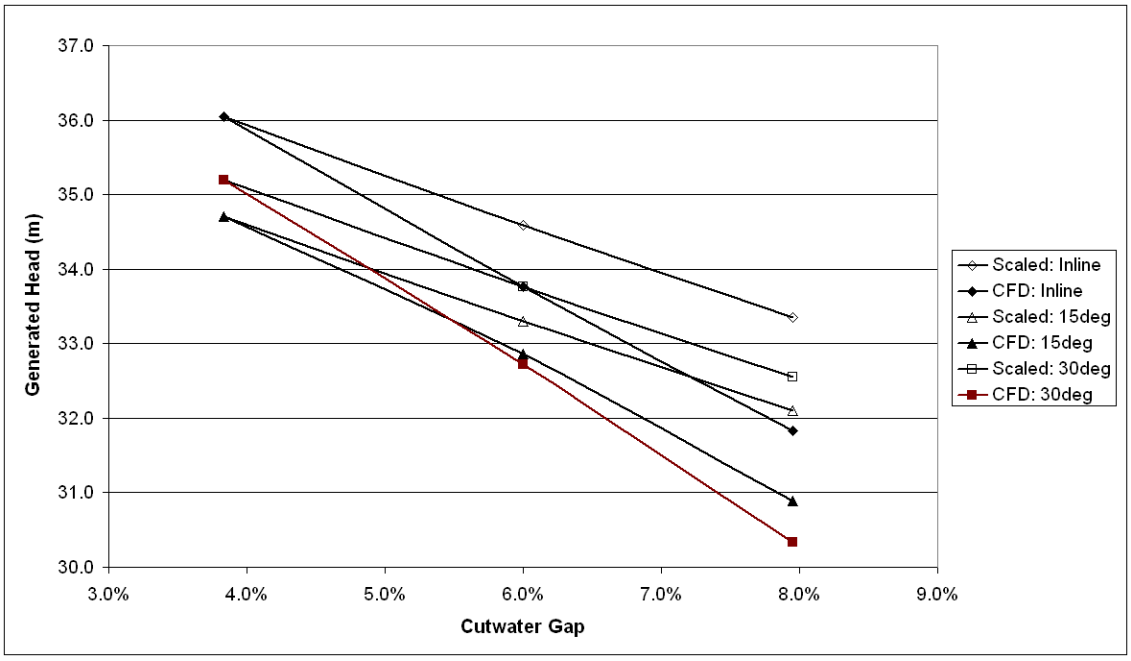

Figure 7.1 Comparison of CFD generated head with Euler predicted values at 1.00Qn for three vane arrangements

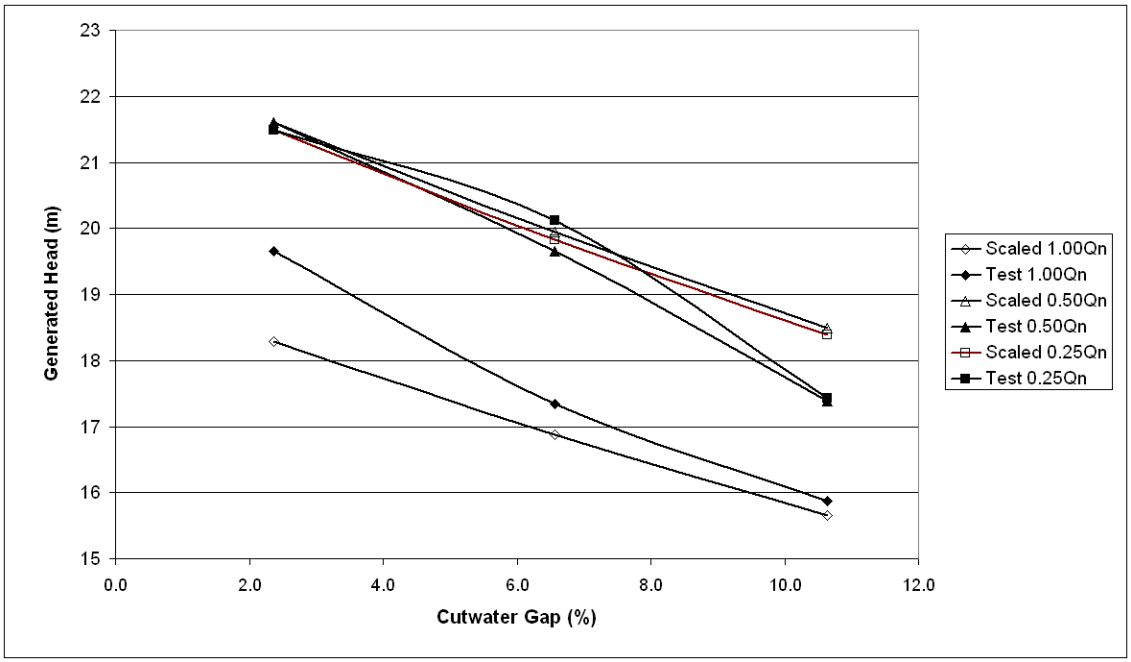

Figure 7.2: Total head comparison with Euler scaled head using Goulas and Truscott data (78)

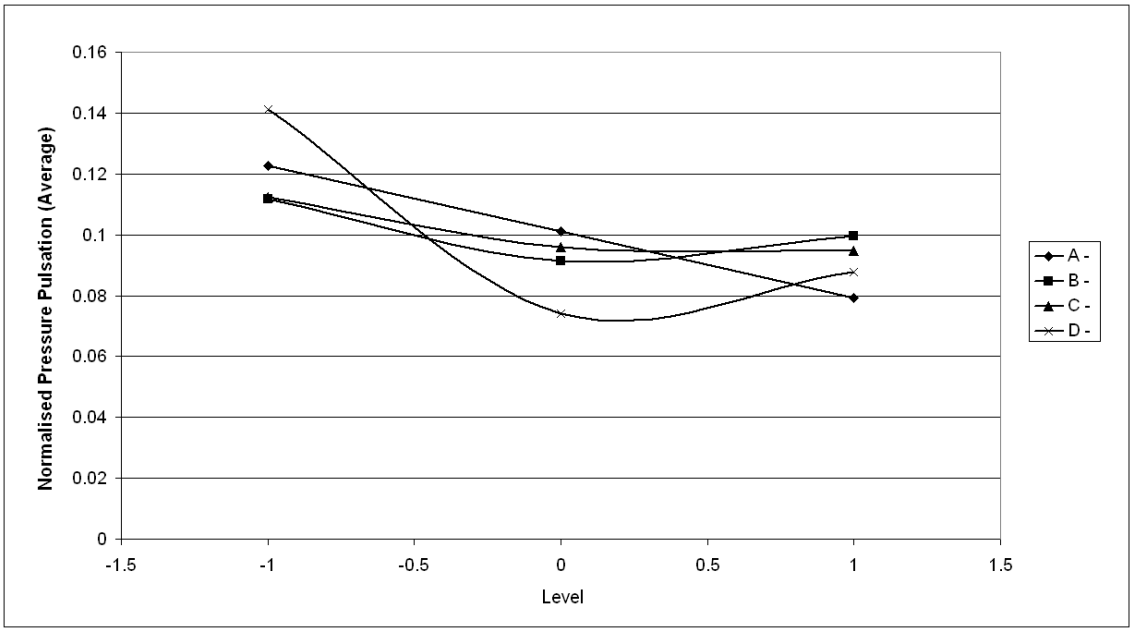

Figure 7.3: Response average (variance) for location C8 for each of the four geometric parameters.

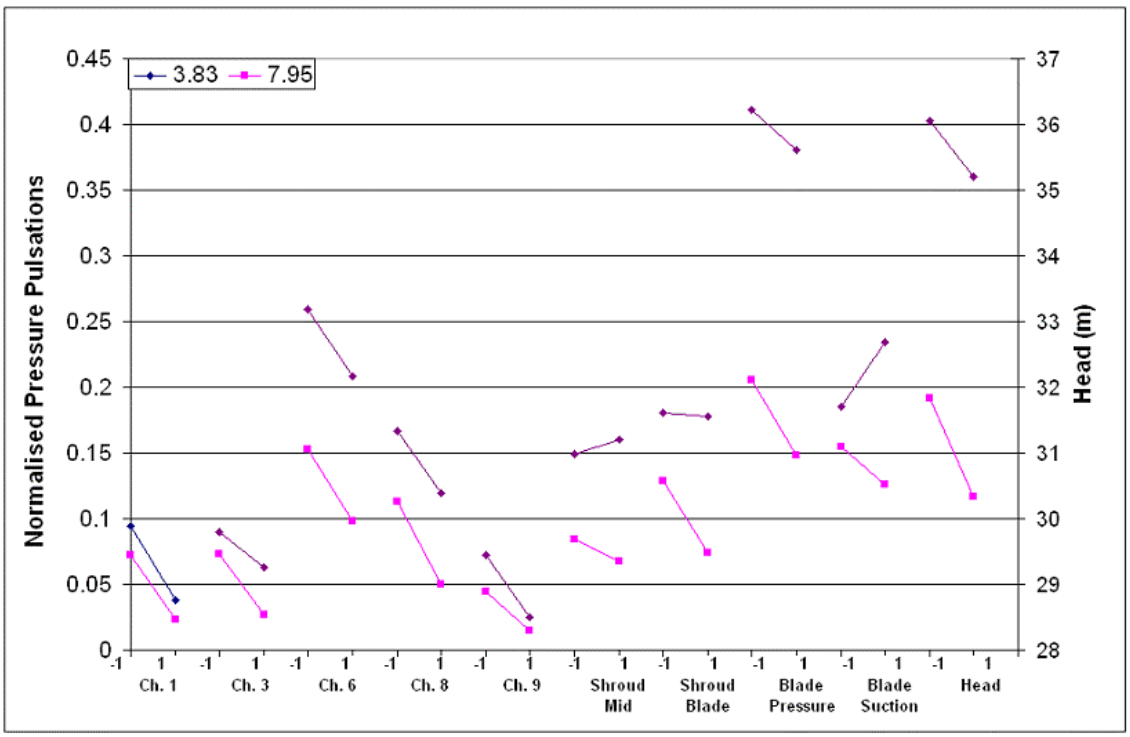

Figure 7.4: Interaction graph for 1.00Qn stage 1 analysis

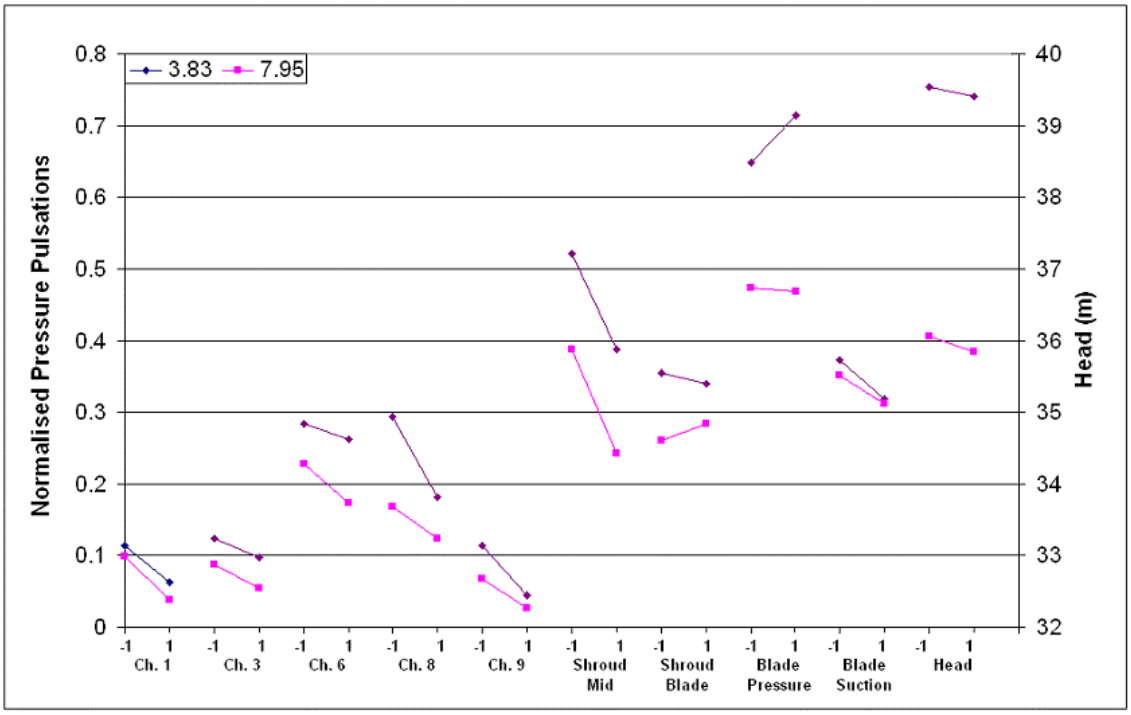

Figure 7.5: Interactions graph for 0.25Qn stage 1 analysis

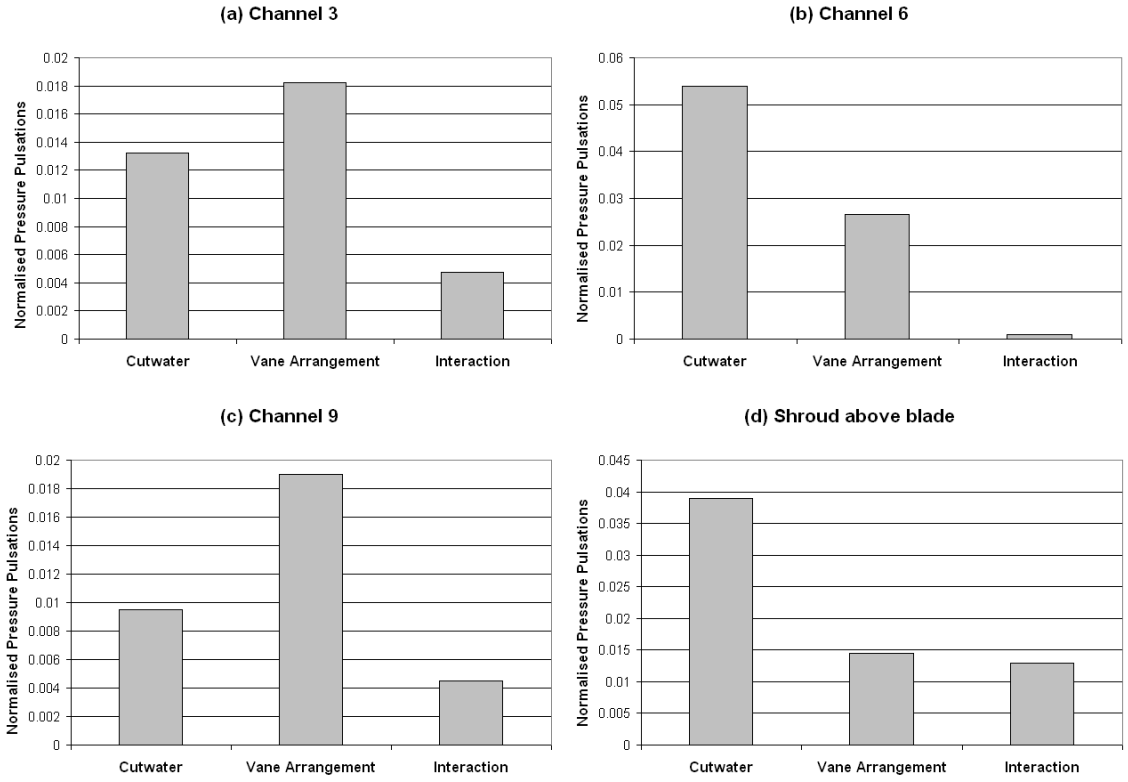

Figure 7.6: Pareto half effect chart for stage 1 at 1.00Qn

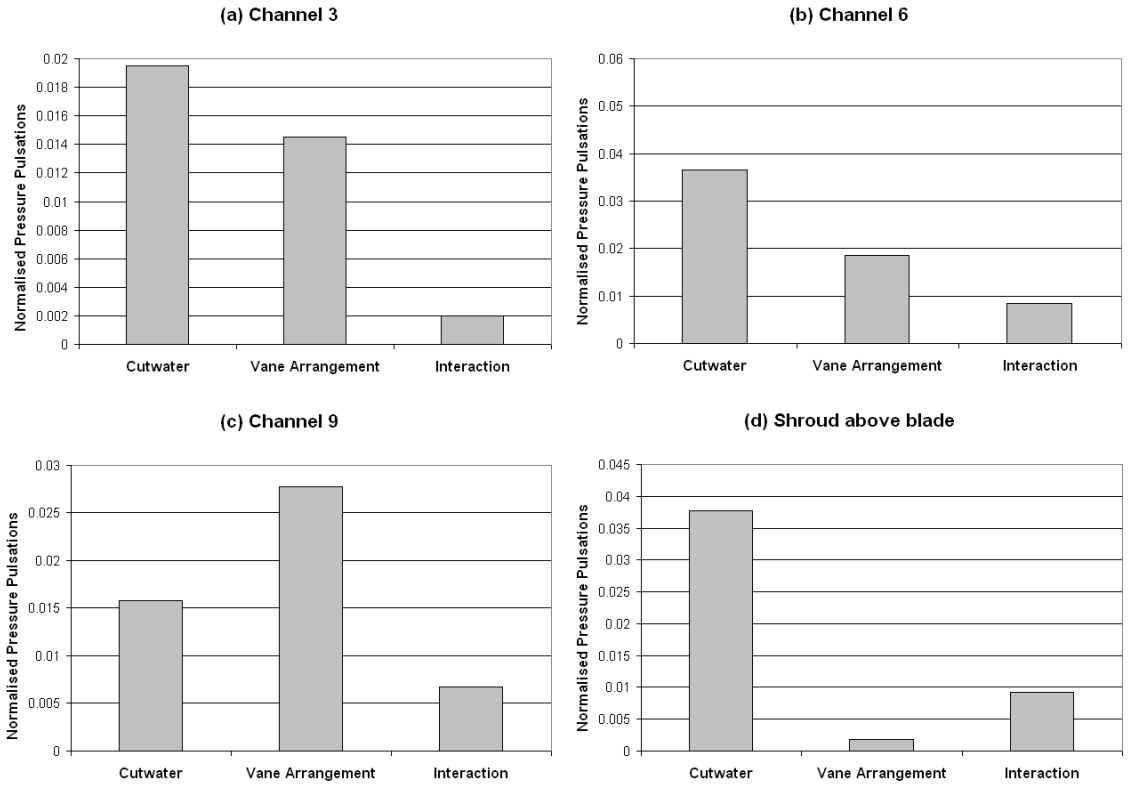

Figure 7.7: Pareto half effect chart for stage1 at 0.25Qn

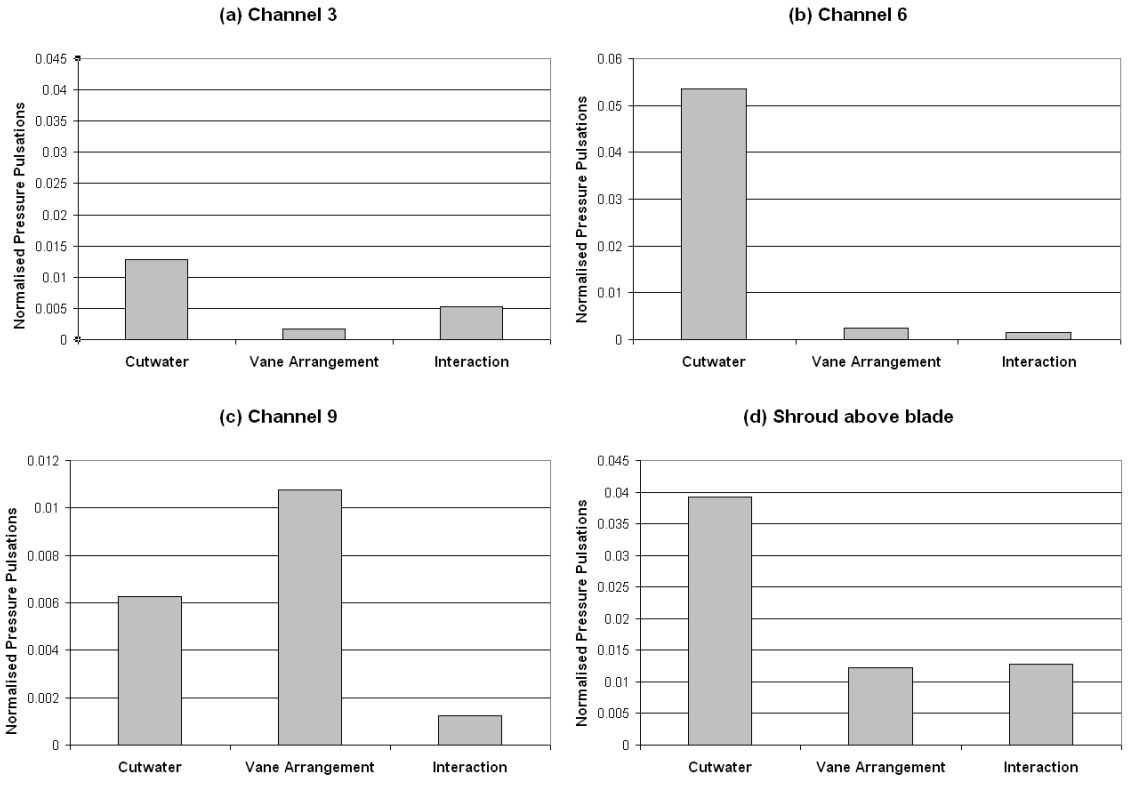

Figure 7.8: Pareto half effect chart for stage 2 at 1.00Qn

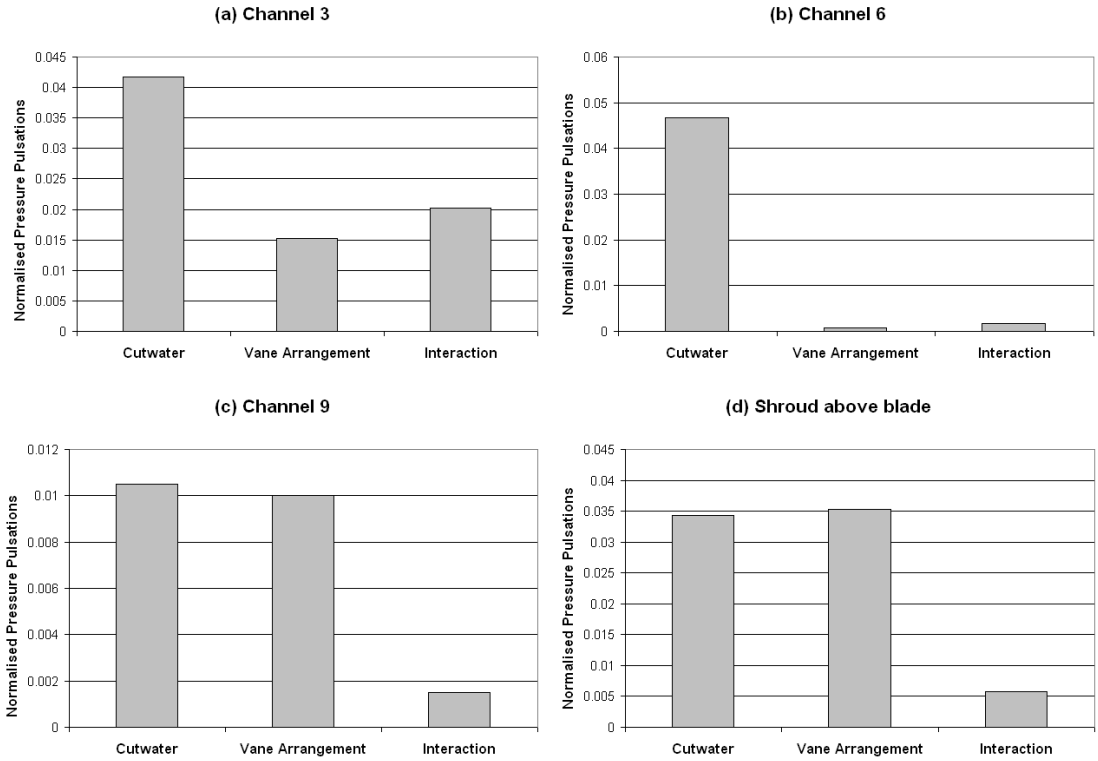

Figure 7.9: Pareto half effect chart for stage 2 at 0.25Qn

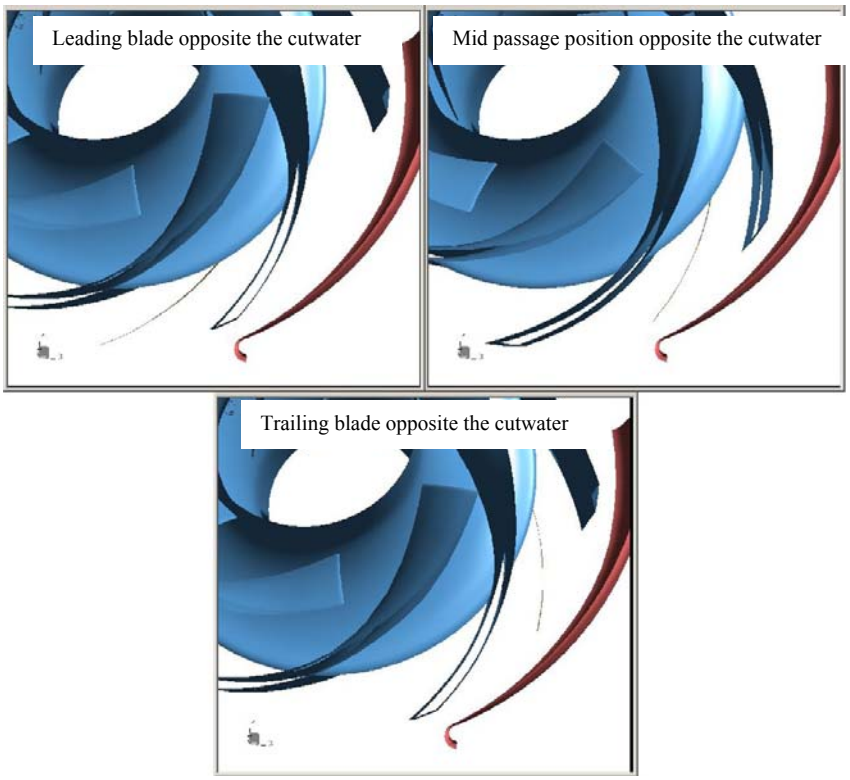

Figure 7.10: Positions of the impeller blade relative to the cutwater used to calculate the pressure across the impeller shroud

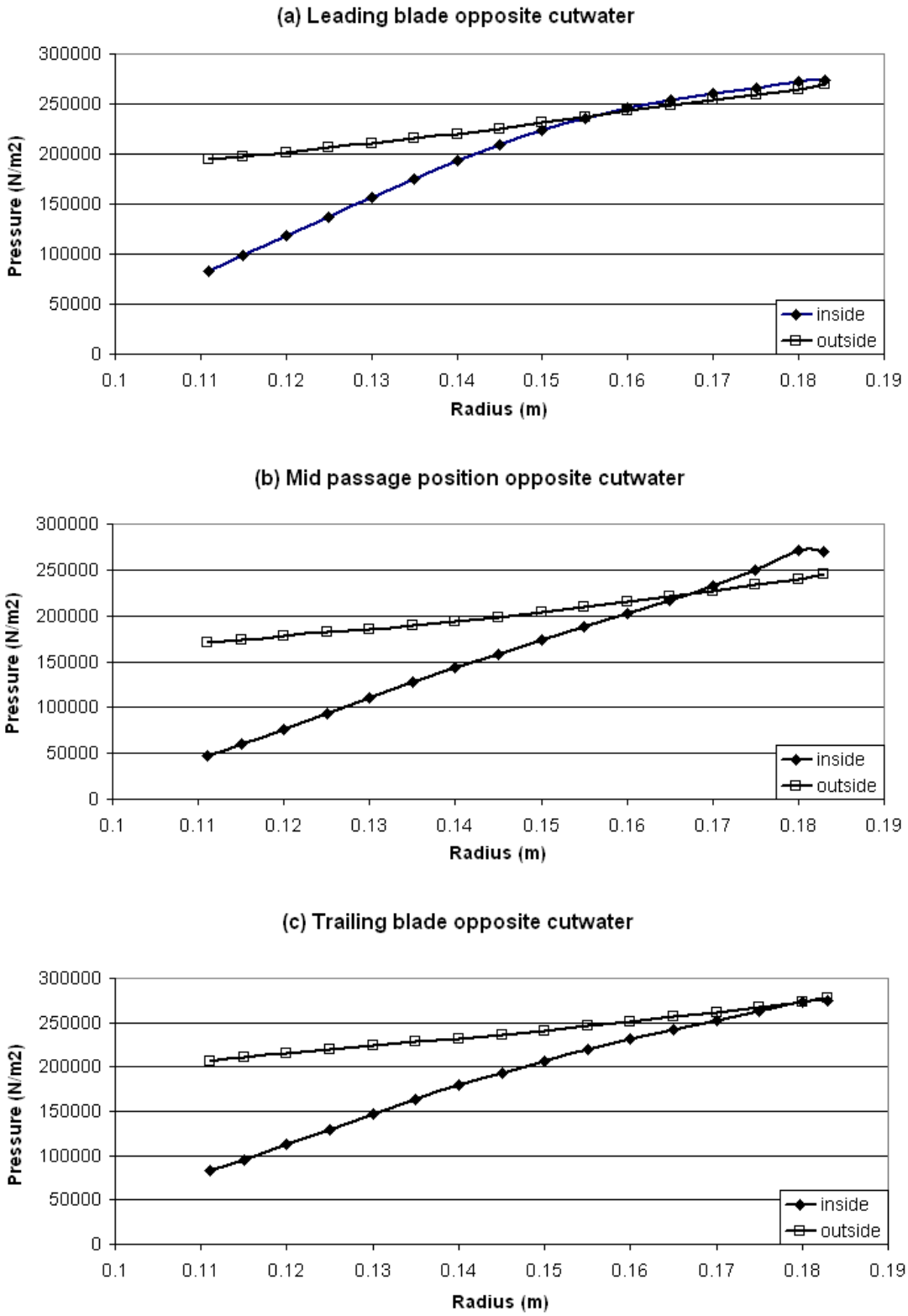

Figure 7.11: Plot of shroud differential pressure variation for three impeller positions at 1.00Qn

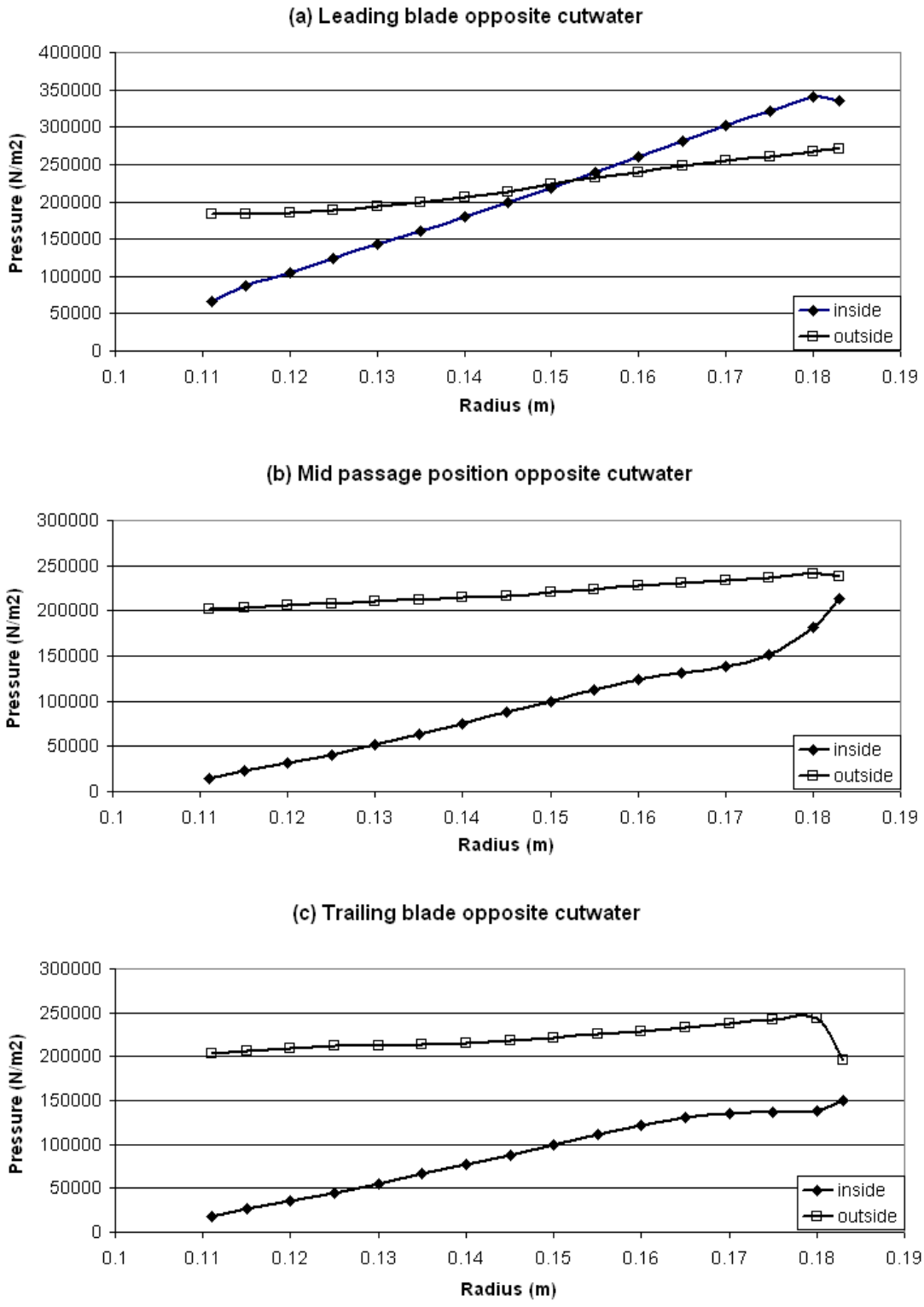

Figure 7.12: Plot of shroud differential pressure variation for three impeller positions at 0.25Qn

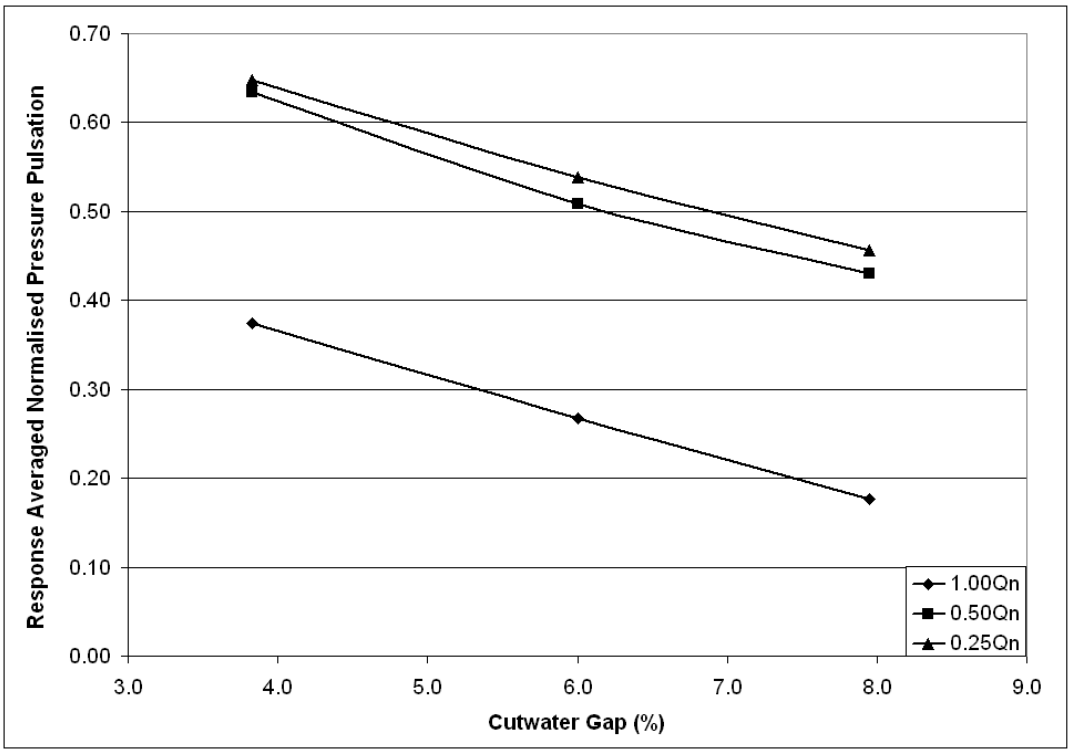

Figure 7.13: Comparison of the effect of the cutwater gap on the pressure pulsations at the pressure face of the blade pressure face location at three flow rates.

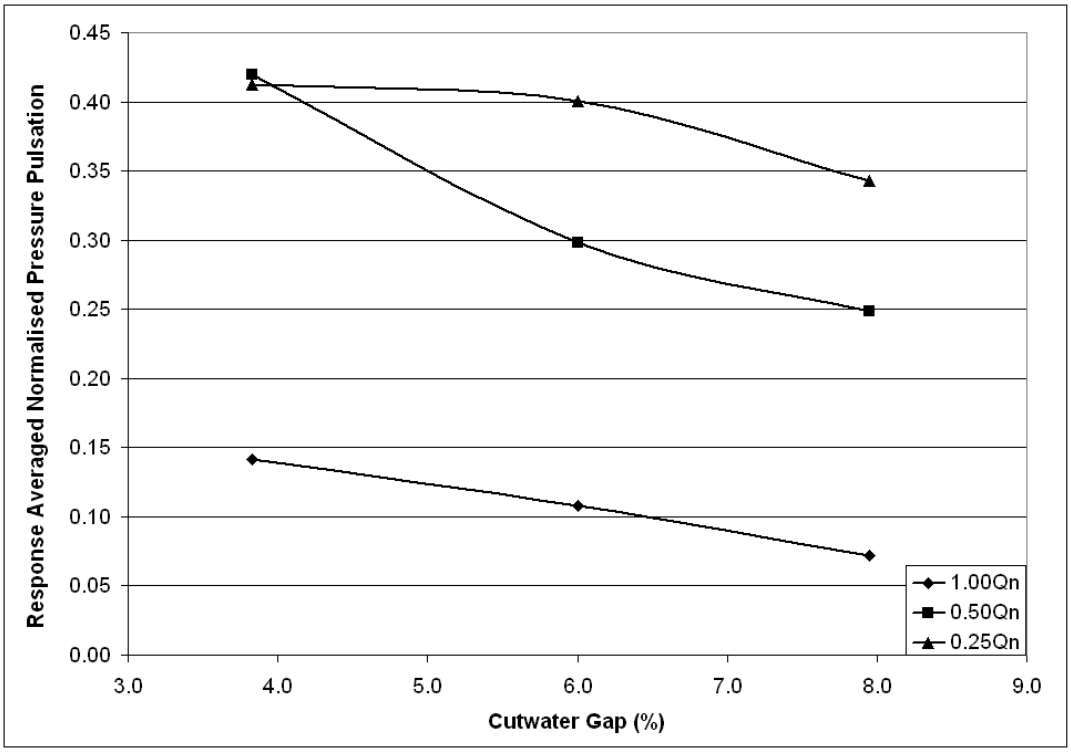

Figure 7.14: Comparison of the effect of the cutwater gap on the pressure pulsations at the mid shroud location at three flow rates.

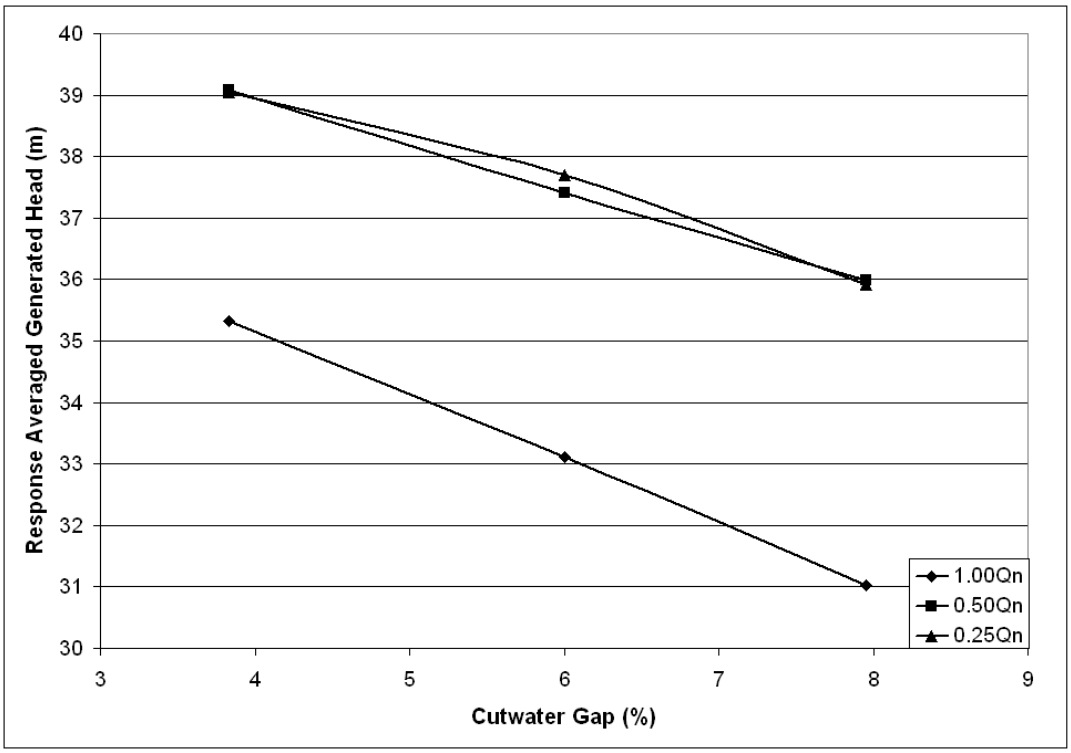

Figure 7.15: Comparison of the effect of the cutwater gap on the generated head at three flow rates.

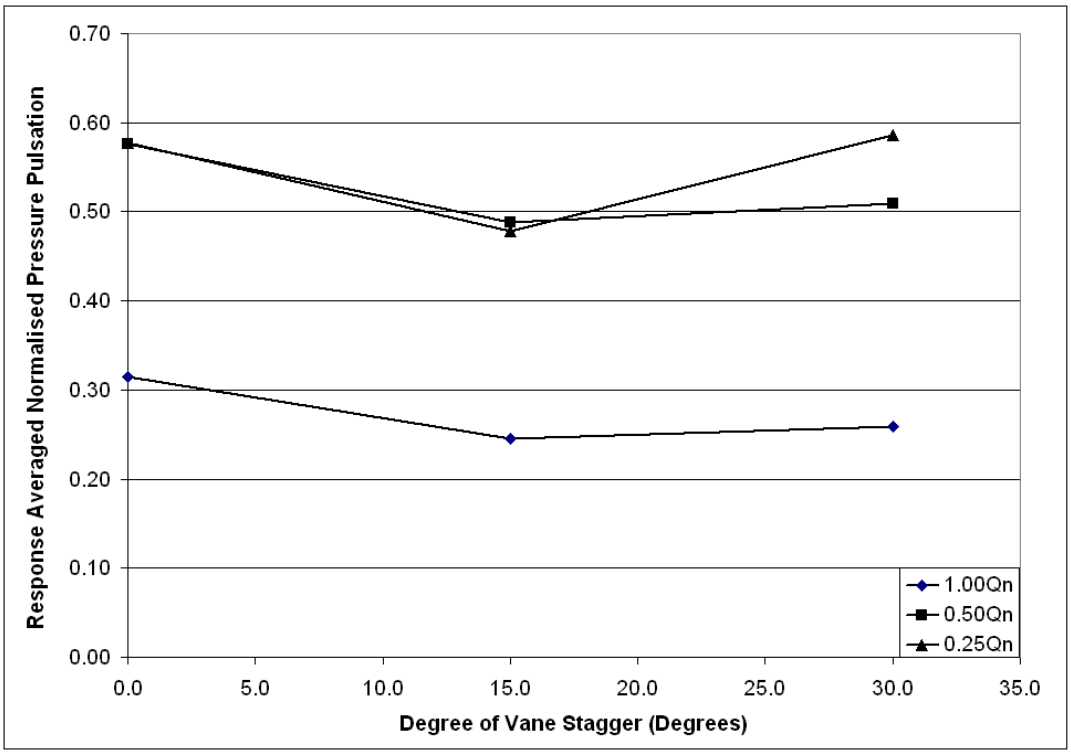

Figure 7.16: Comparison of the effect of the vane arrangement on the pressure pulsations at the pressure face of the blade location at three flow rates.

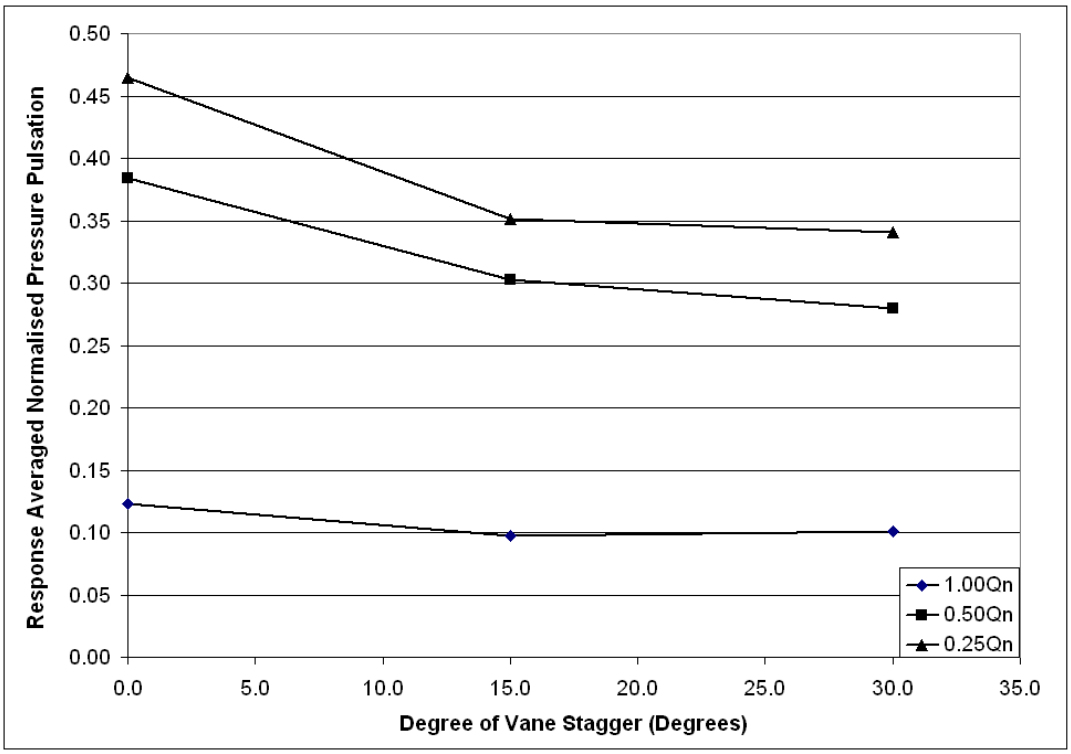

Figure 7.17: Comparison of the effect of the vane arrangement on the pressure pulsations at the shroud mid location at three flow rates.

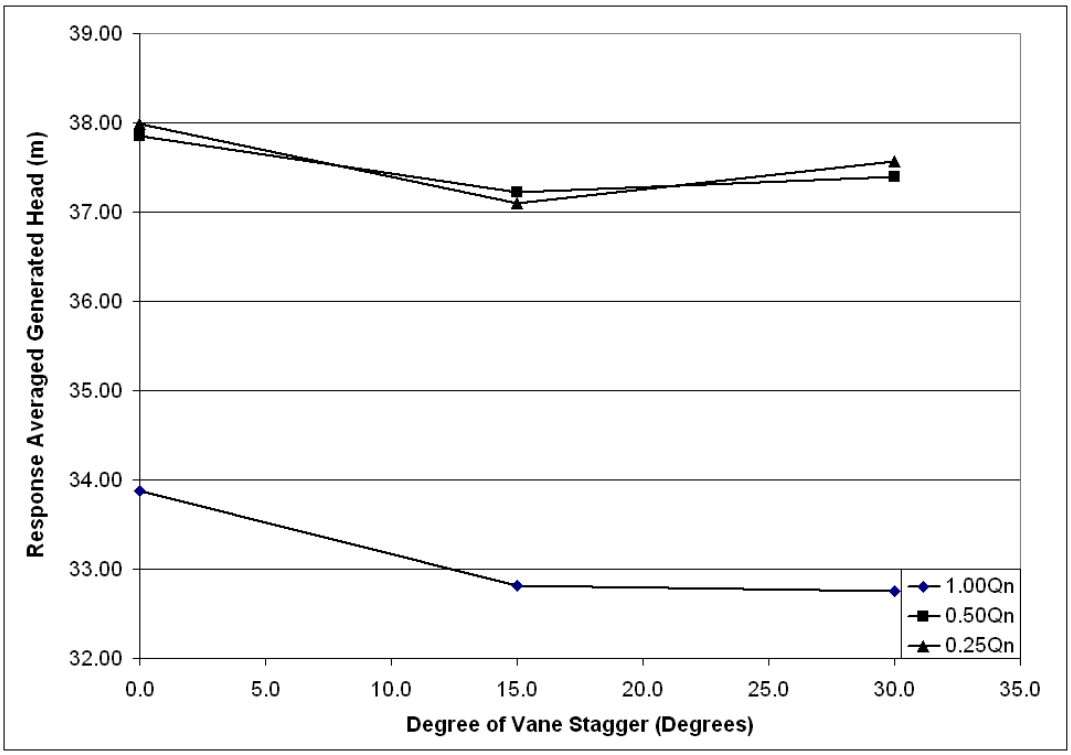

Figure 7.18: Comparison of the effect of the Vane Arrangement on the generated head at three flow rates.

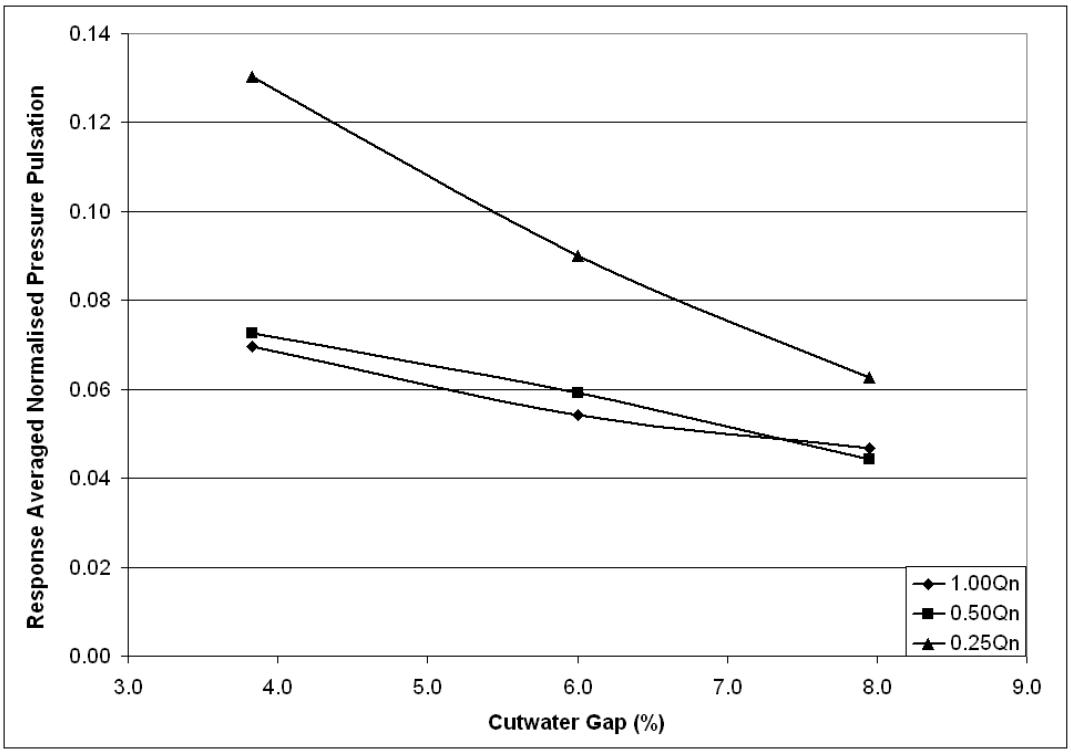

Figure 7.19: Comparison of the effect of the cutwater gap on the pressure pulsations at the C3 location at three flow rates.

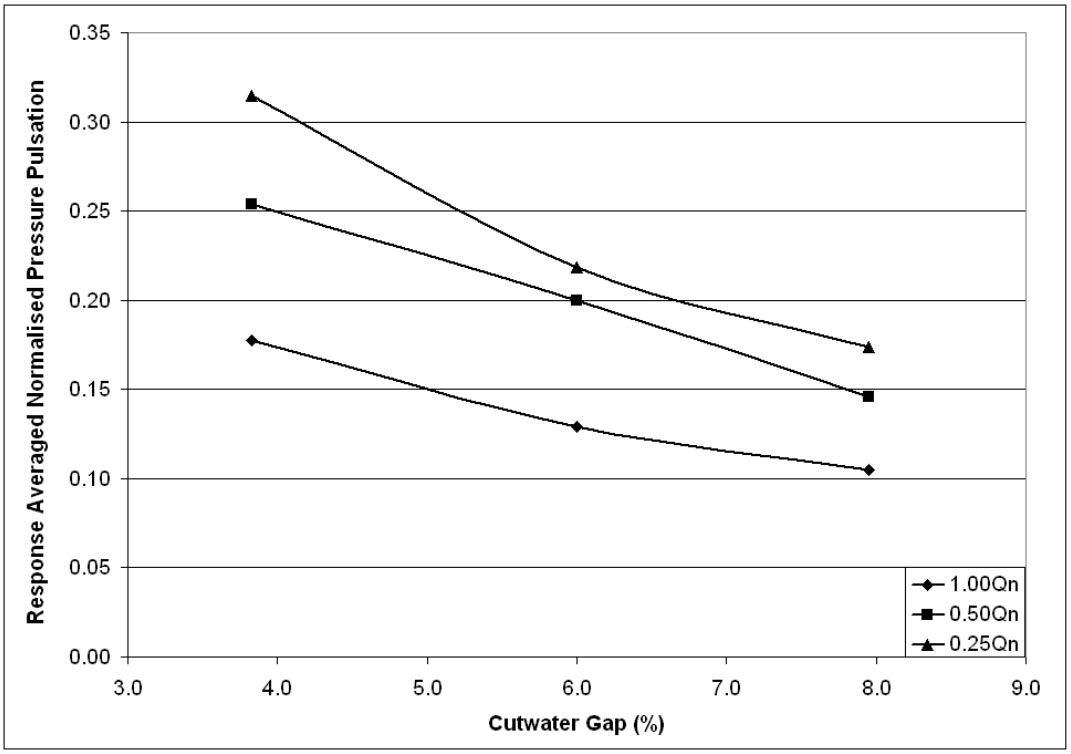

Figure 7.20: Comparison of the effect of the cutwater gap on the pressure pulsations at the C7 location at three flow rates.

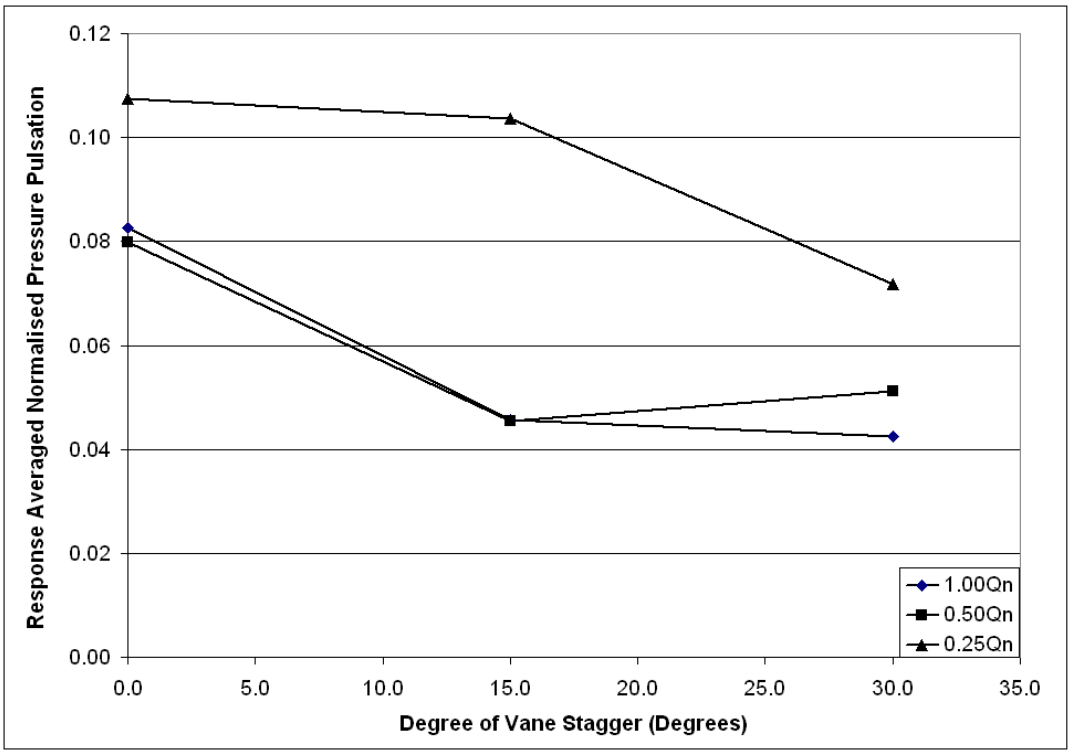

Figure 7.21: Comparison of the effect of the vane arrangement on the pressure pulsations at the C3 location at three flow rates.

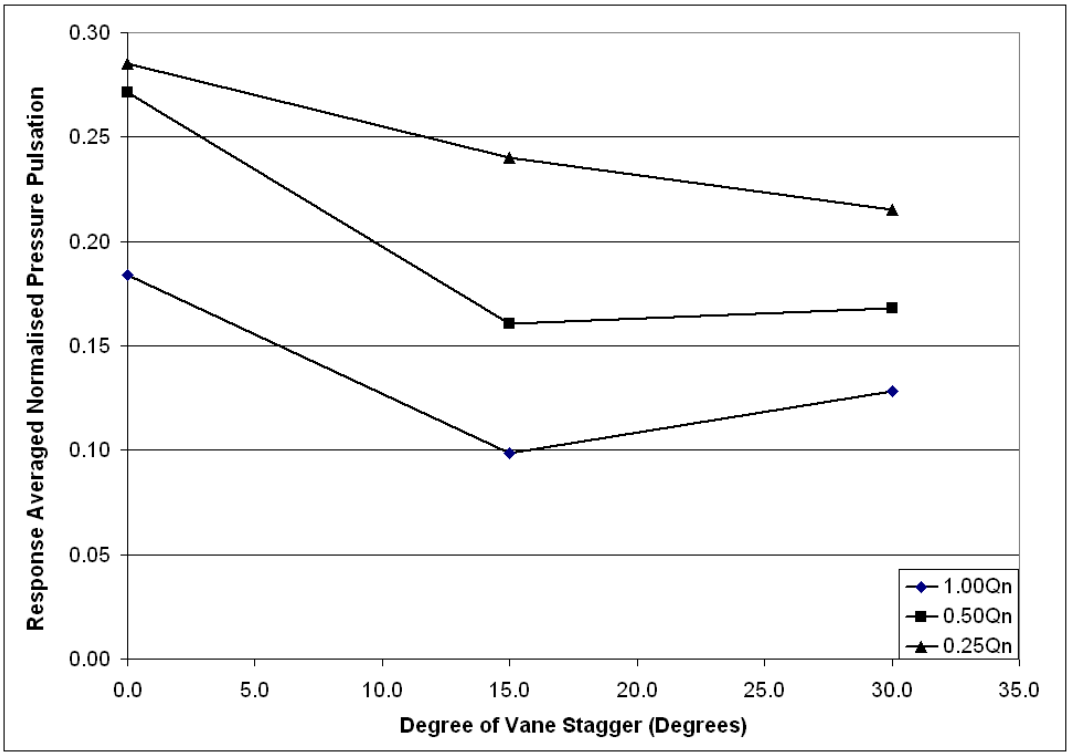

Figure 7.22: Comparison of the effect of the vane arrangement on the pressure pulsations at the C7 at three flow rates.

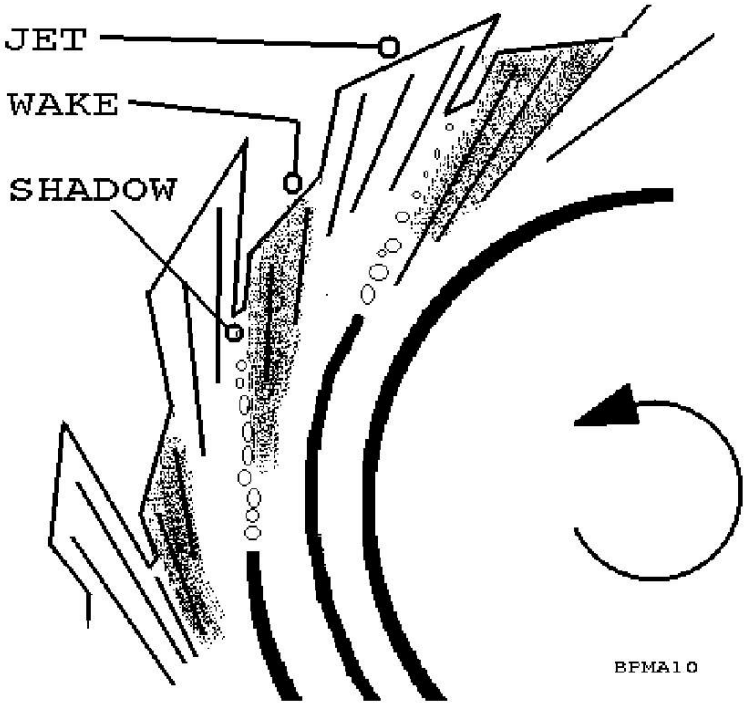

Figure 7.23: Jet/wake flow pattern caused by impeller blades at the impeller outlet

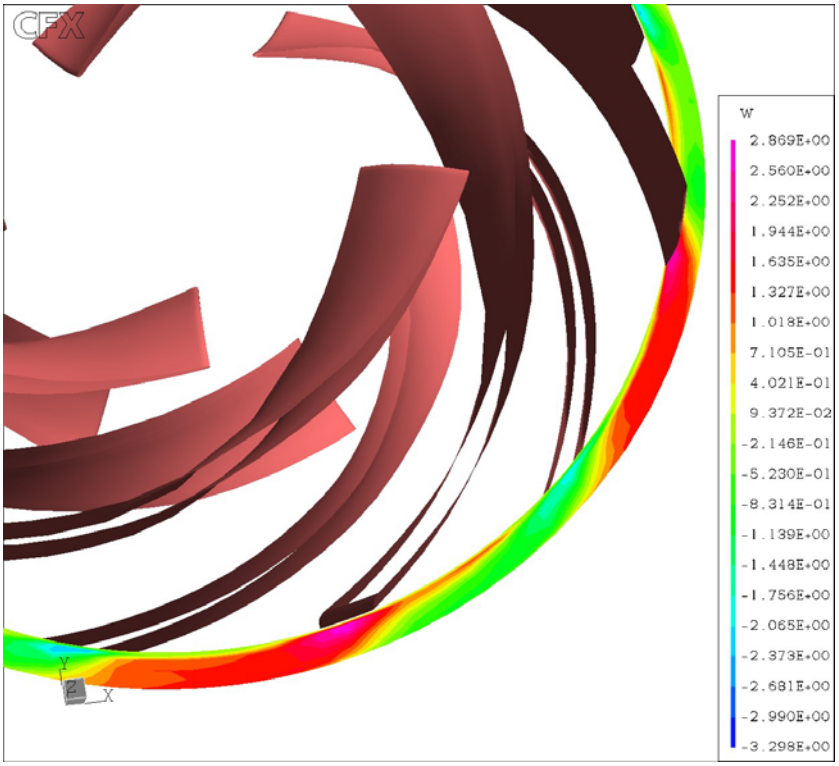

Figure 7.24: Axial velocity at the outside of a 30 degree staggered vane arrangement (illustrating mixing between the two sides of the double entry impeller)

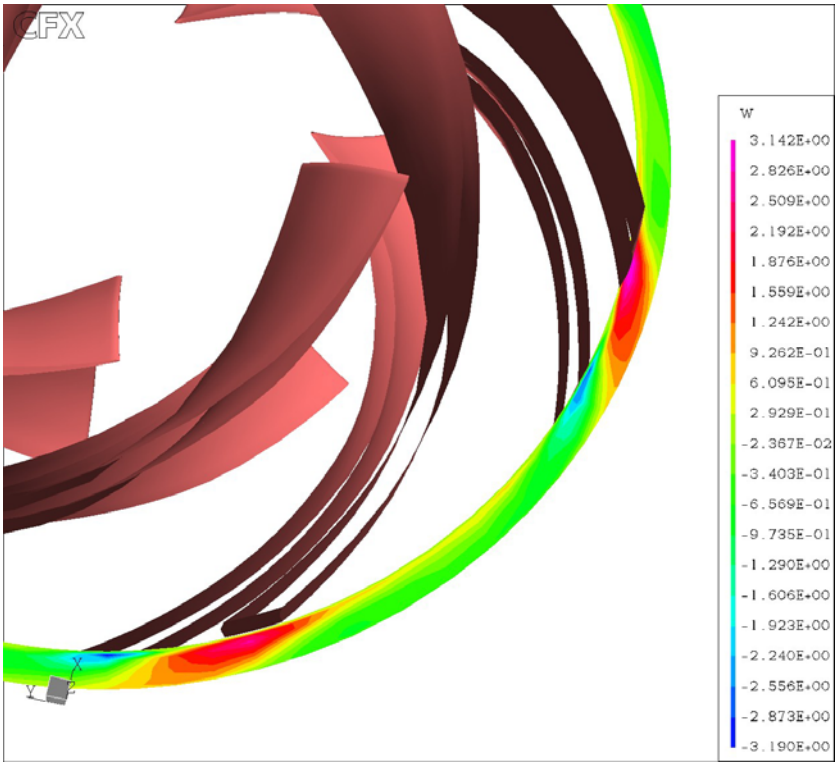

Figure 7.25: Axial velocity at the outside of a 15 degree staggered vane arrangement (illustrating mixing between the two sides of the double entry impeller)

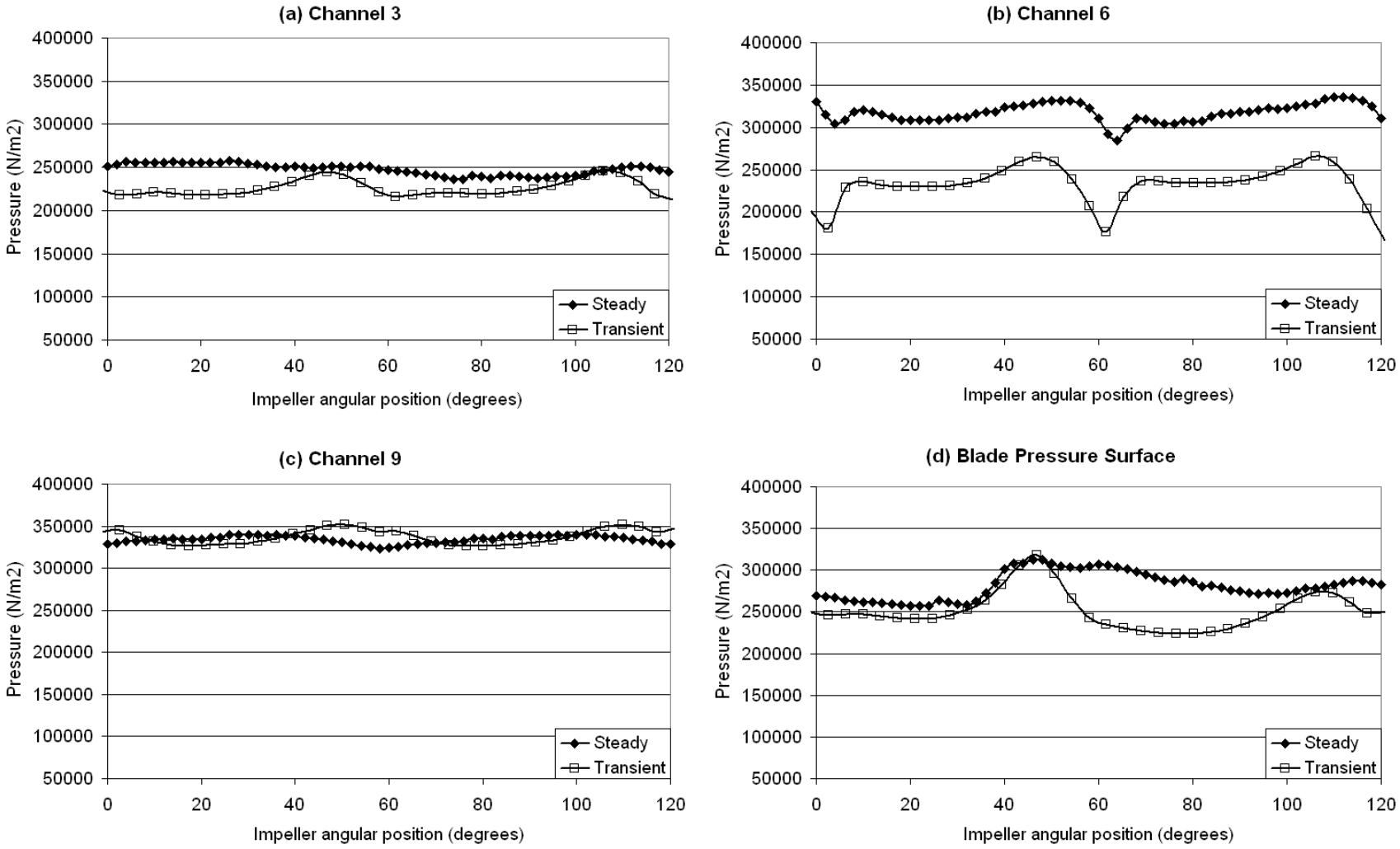

Figure 7.26: Comparison of steady state and transient results for first arrangement at 1.00Qn

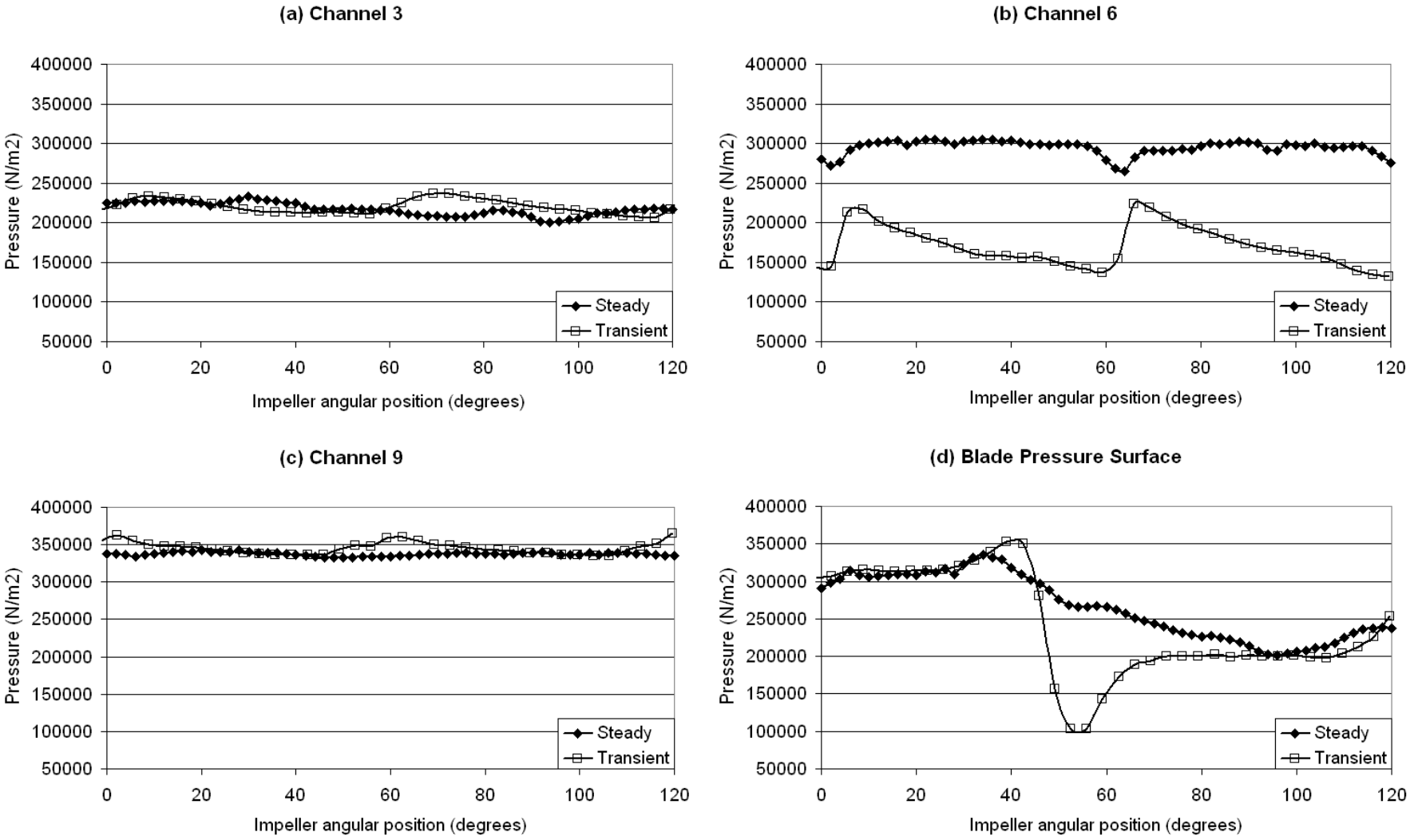

Figure 7.27Comparison of steady state and transient results for first arrangement at 0.50Qn

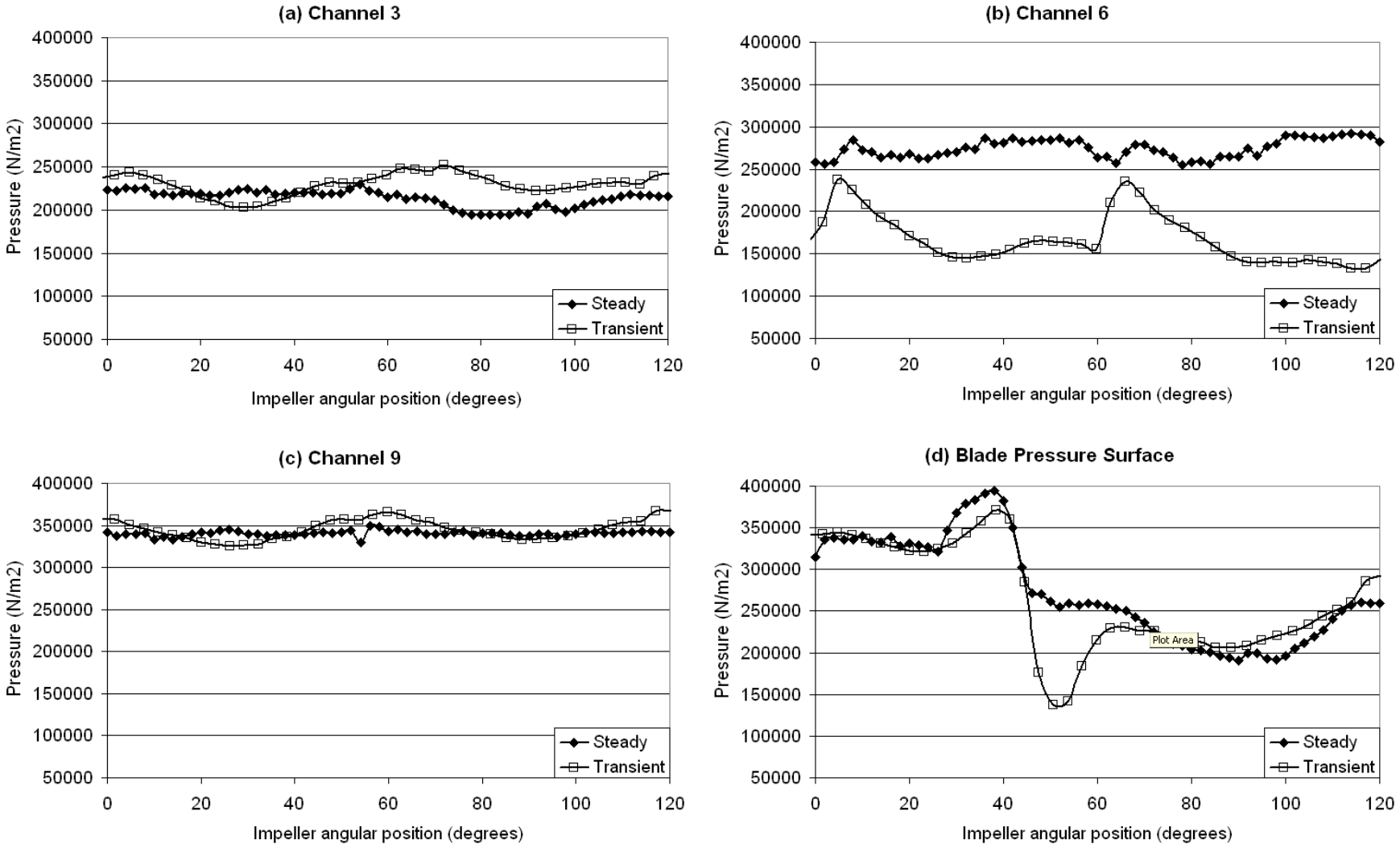

Figure 7.28: Comparison of steady state and transient results for first arrangement at 0.25Qn

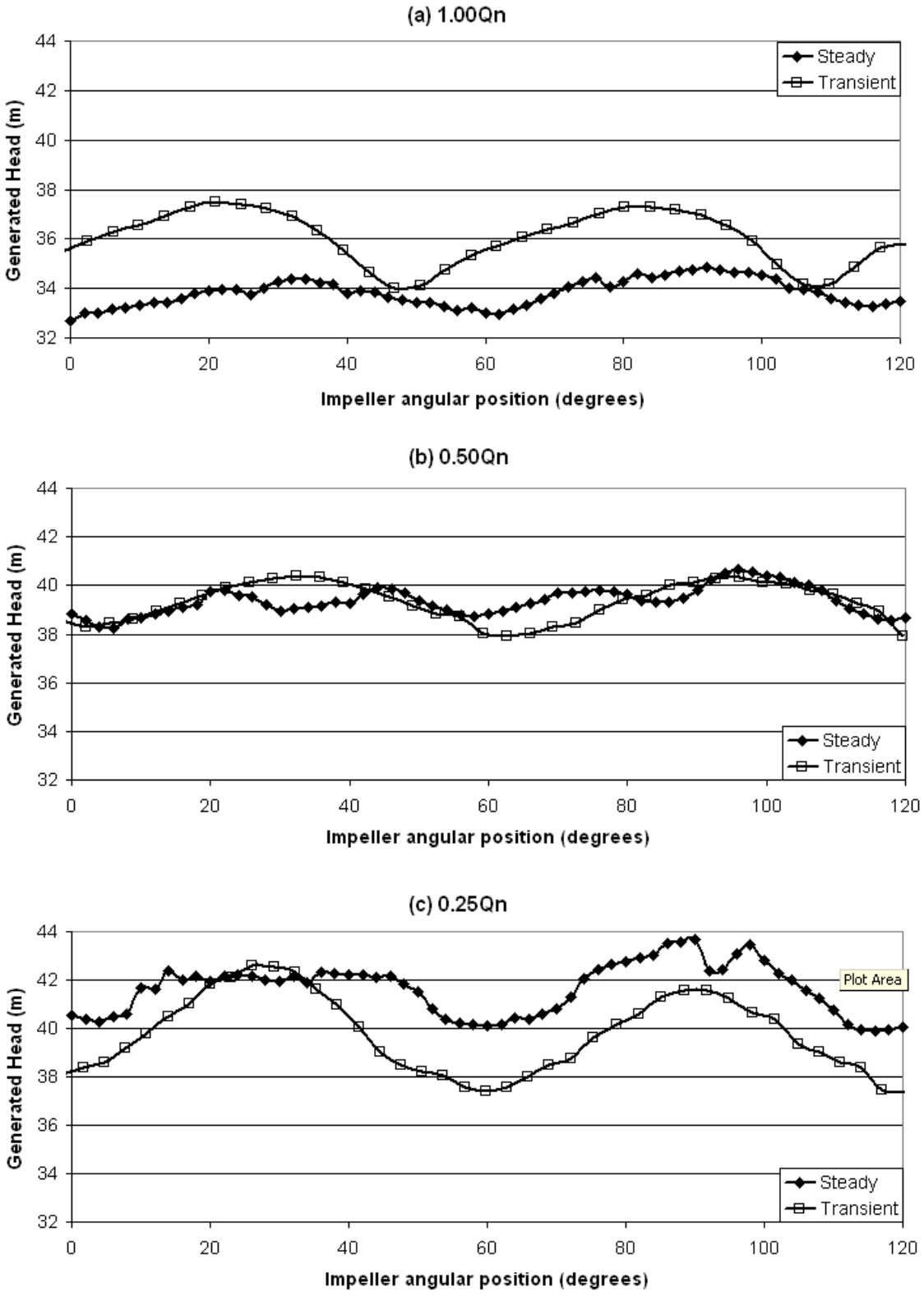

Figure 7.29: Comparison of steady state and transient results for first arrangement at three flow rates for the generated head

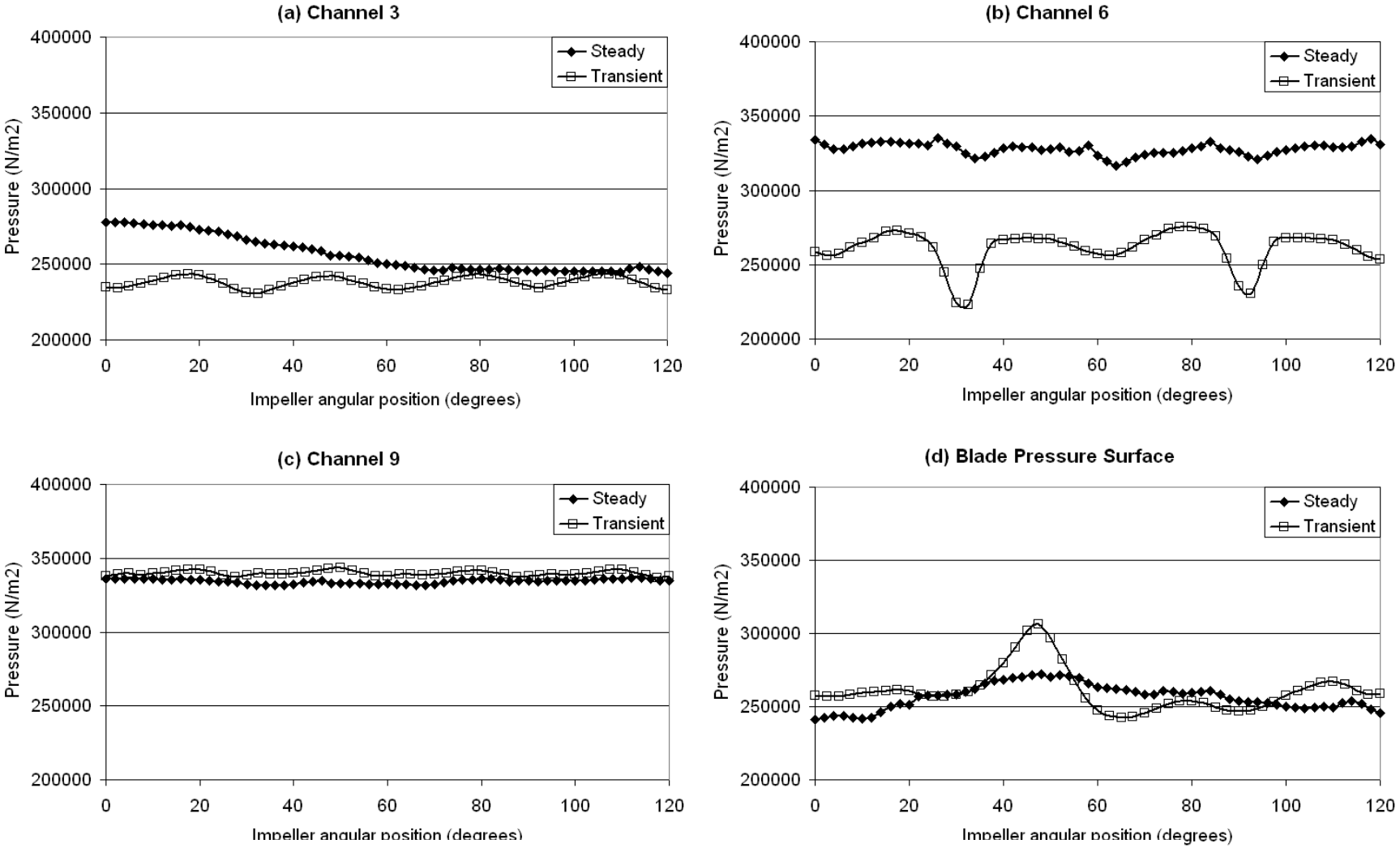

Figure 7.30: Comparison of steady state and transient results for model A arrangement at 1.00Q

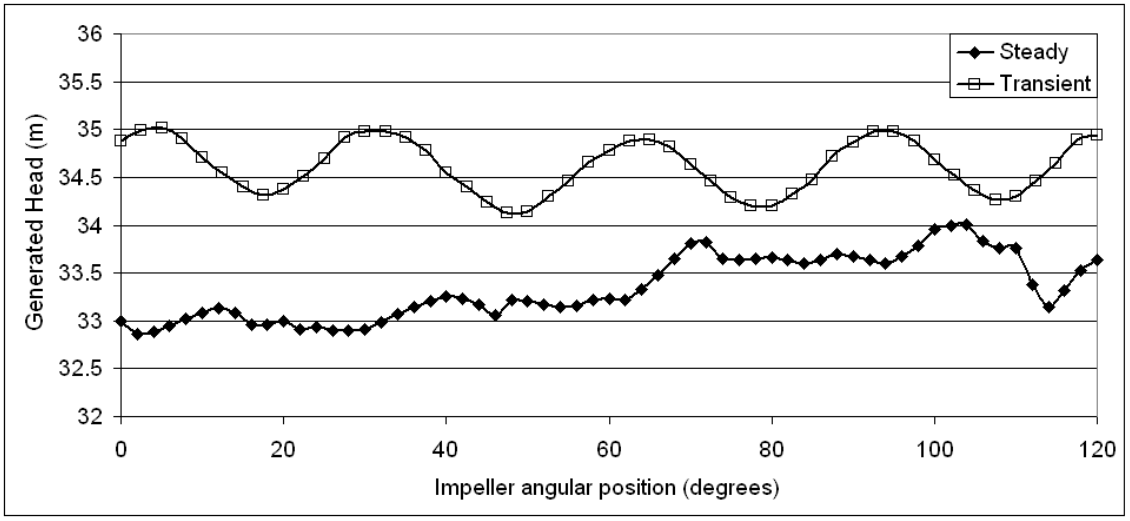

Figure 7.31: Comparison of Steady State and Transient results for the generated head using the model A arrangement at 1.00Qn

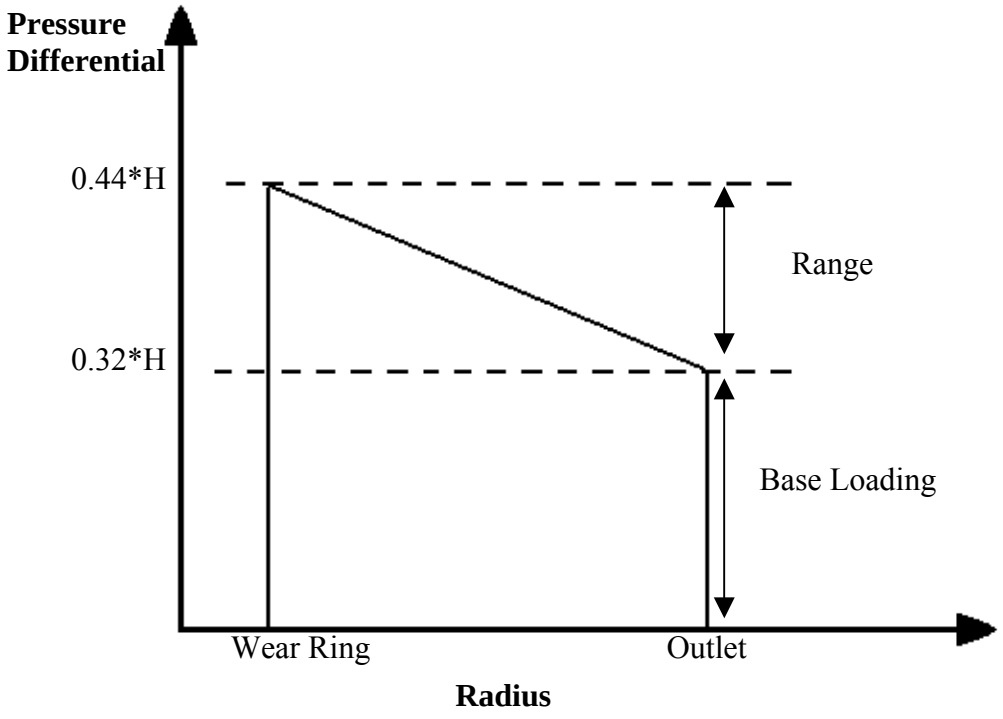

Figure 7.32: Approximate trapezoidal pressure differential from CFD results for arrangement 4 at 0.25Qn

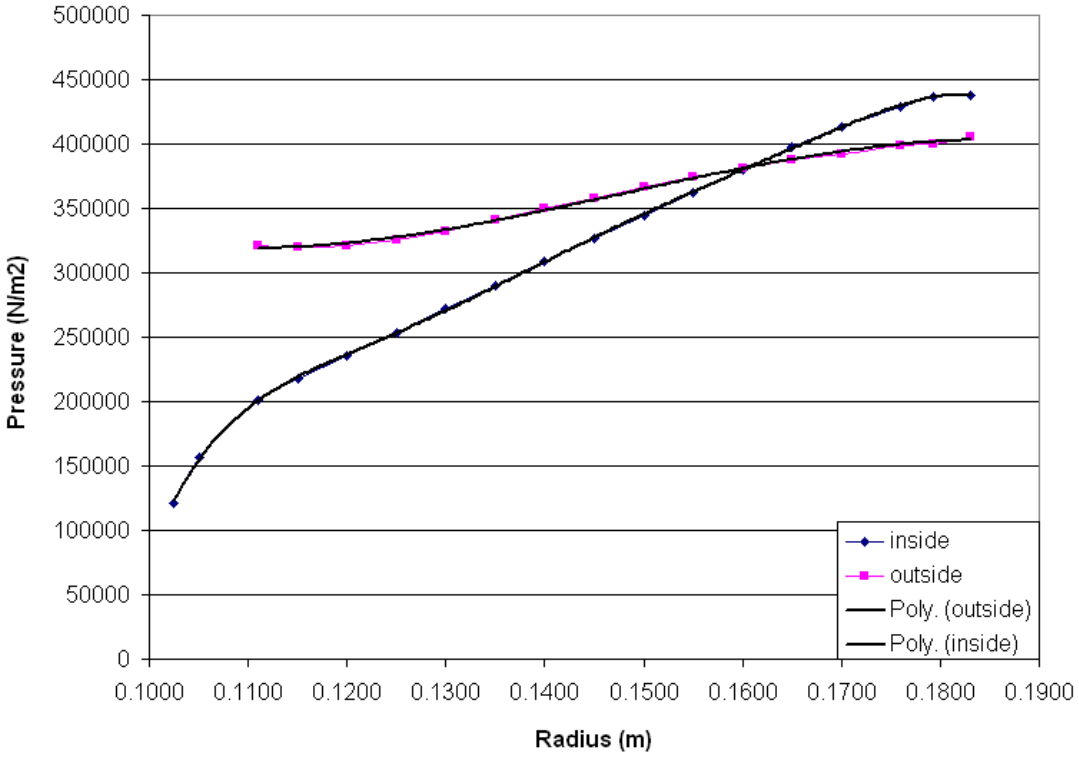

Figure 7.33: Pressure data at the outside and inside of the shroud between the impeller eye and outlet for arrangement 6 at0.25Qn. Trend lines labelled as "Poly."

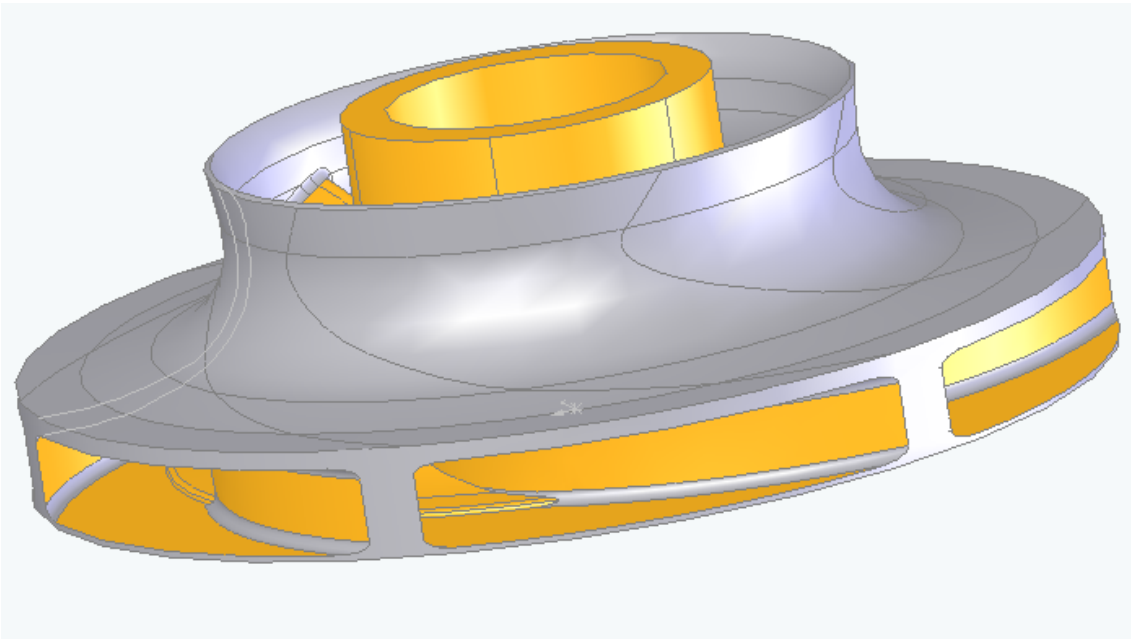

Figure 7.34: Solid model of impeller produced for finite element analysis

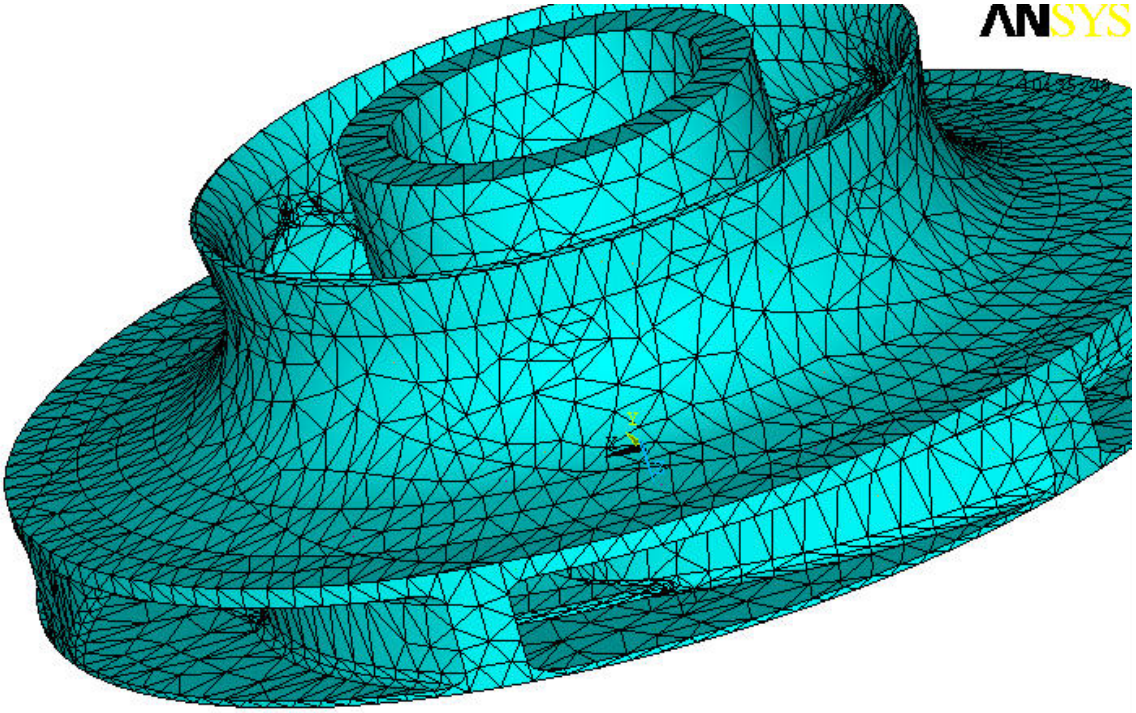

Figure 7.35: Finite element mesh of analysed impeller

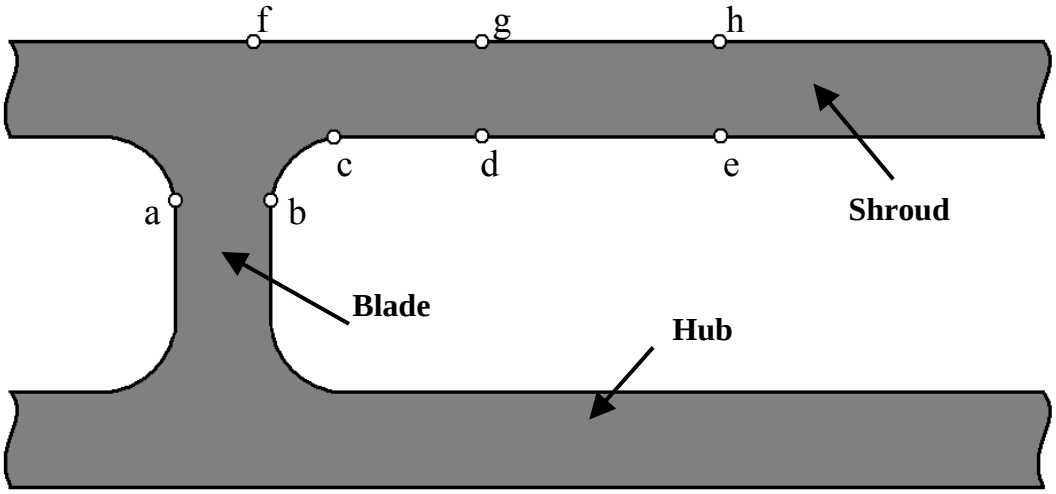

Figure 7.36: Shroud section showing positions of result locations at the impeller outlet (a, b, c, d, e, f, g and h)

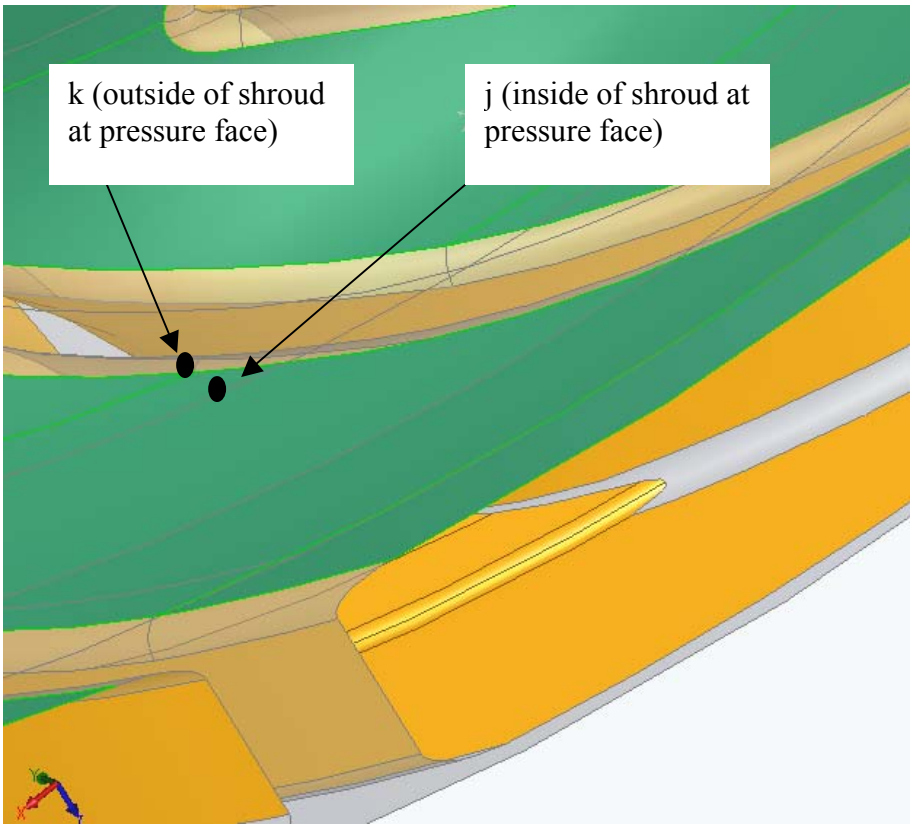

Figure 7.37: Shroud section showing position of result locations on following blade pressure face at inside and outside of the shroud (j and k respectively)

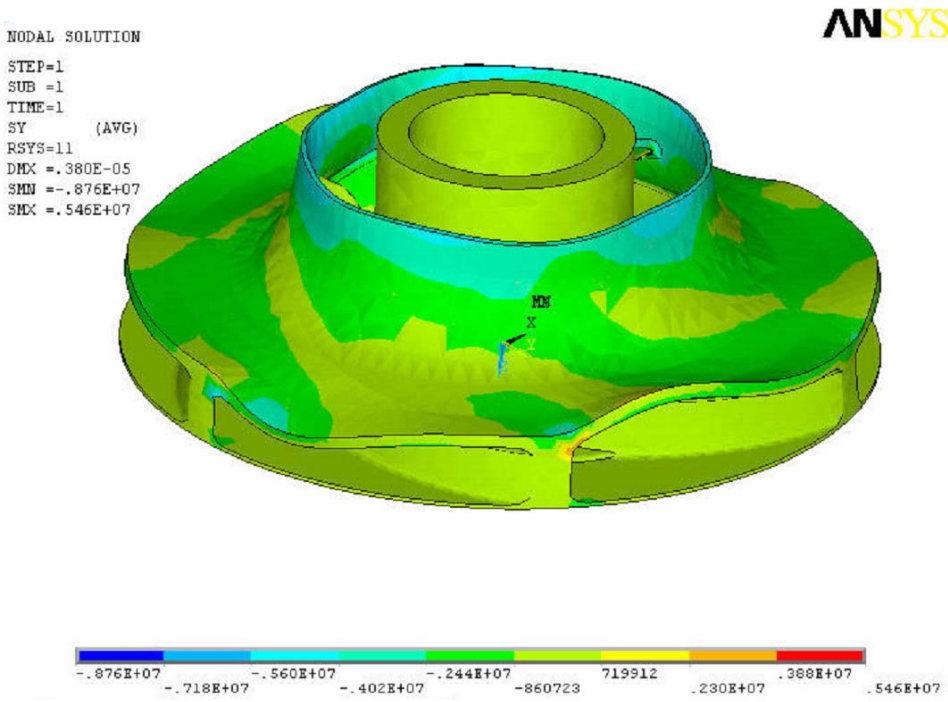

Figure 7.38: Hoop Stress at the impeller shroud for arrangement 4 with the blade opposite the cutwater

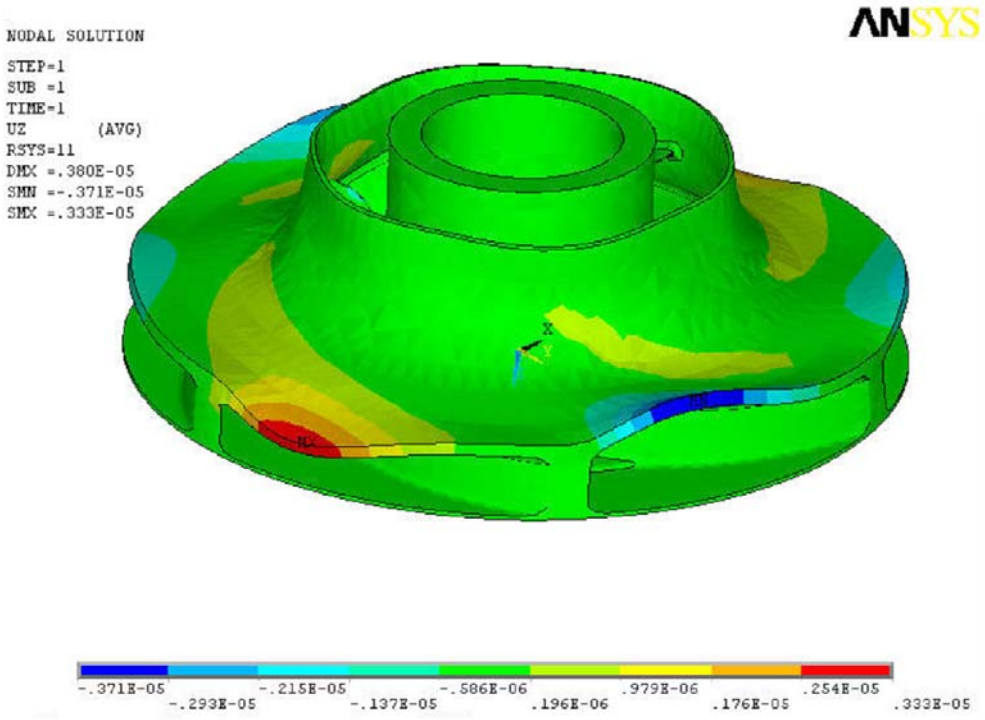

Figure 7.39: Axial displacement of the impeller shroud for arrangement 4 with the blade opposite the cutwater

Chapter 8

Concluding Remarks and Suggestions for Further Work

8.1 Concluding Remarks

8.2 Further Work

8 Concluding Remarks and Suggestions for Further Work

The final remarks on this project are presented in two sections. This chapter provides a brief description of the salient points regarding the work undertaken along with a summary of the important conclusions. A number of possible avenues of further work have been identified that would enhance, extend and/or refine the information presented here.

8.1 Concluding Remarks

An investigation has been undertaken to gain an understanding of the pressure pulsations within a double entry pump and also the variation of these pulsations for a number of pump geometries and flow rates. The planned work centred around five primary aims (see Chapters 1 and 5), with the first three involving the investigation of the pressure levels. The work relating to the fourth aim derived and detailed recommendations from the work that could be applied to a design process. To complete the last aim steady state analyses were run to identify whether these analysis methods would allow this work to be extended in a quick and simple manner. The work presented in this thesis has met each of the aims in full.

The main observations and conclusions to emerge from the investigation of pressure pulsation variation with pump geometry are summarised below. Many of these represent unique contributions.

a) A numerical model of the entire pump has been successfully generated and analysed for the first time. This model consists of a suction inlet, double entry impeller, leakage flow passageways and the volute.

b) The numerical model of the double entry impeller is the first of its type to be successfully modelled for analysis. In total, three different double entry impeller configurations are used in the project. Similarly, the double volute is the first of its type to be successfully modelled for numerical analysis.

c) A total of thirty three transient analyses have been successfully conducted within a parametric analysis, representing 45,000 hours of continual analysis time and consisting of over 550 gigabytes of analysis and result data. This is the first parametric type analysis to be conducted on an entire pump.

d) Velocity flow patterns generated by the numerical analysis identify features of the flow that agree with those identified in published literature. Detailed investigations of the velocity components at the impeller outlet have shown these to be comparable in shape to those published in two independent external experimental tests

e) The pressure levels predicted by the numerical analysis have been successfully generated and give rise to an enormous and interesting data set. The results have been presented by concentrating on fifteen selected locations around the pump. The pressure levels have been converted into RMS pressure pulsations and provide detailed information regarding the pressure pulsation close to the impeller outlet, in the volute and in the leakage flow region.

f) The pressure pulsations predicted by the CFD analyses show reasonable agreement with the experimental data. The CFD results predict the relative pulsations at different pump locations quite well. It is clear that the regions in the pump experiencing the largest pressure pulsations are located at the impeller outlet, with large pulsations also being present in the volute at positions in close proximity to the cutwater or splitter.

Comparisons between the CFD and the experiments at the duty flow condition are generally better that those at reduced flows, with the greatest deviation appearing at the lowest flow condition.

g) It has been found that the pressure pulsations at the pump discharge are largely unrelated to pulsations within the pump, but are probably more dependent on the system in which the pump is operating. Monitoring the pulsations at a top dead centre position on the pump casing (C9 location) gives a better indication of pulsations present in the pump itself and therefore provide a more useful monitoring position for actual pumps installed in real systems.

h) An L_9 Taguchi array has been successfully constructed for all fifteen pressure monitoring locations and three performance characteristics. An analysis of the Taguchi array has been completed that has identified the dominant geometrical influences on the pulsation and the performance of the pump. In general, the cutwater gap and vane arrangement are the two strongest influences on the pressure pulsation, with the snubber gap and sidewall clearance being considerably less important. While the magnitude of these influences vary depending on the location within the pump, the flow rate, the cutwater gap and vane arrangement are still the most significant factors. However, depending on the location and flow rate, the snubber gap and sidewall clearance can also be of some importance in terms of pulsations.

i) Smaller L_4 Taguchi arrays have been employed to determine the importance of the interactive effect between the cutwater gap and vane arrangement. This has determined that the interactive effect can be more important than the parameter of secondary importance, but is never as large as the dominant parameter. The smaller arrays allow sets of predictive equations to be obtained. Predictive equations can identify expected pressure pulsations at the specific pump locations for

arrangements different from those analysed. However the equations are somewhat limited as relationships between known results are assumed linear and the maximum and minimum parameters are set by those used in the analyses.

j) An investigation into the variation in the pressure differential across the shroud has been conducted for all transient analyses. This has identified that while there is consistency in the differential at the duty flow condition, there are significant pulses in the differential at the lowest flow condition. These pulses reveal a reversal of the pressure differential, where as the impeller passes the cutwater there are periods where the pressure on the outside of the shroud is significantly larger than that on the inside of the shroud at the impeller outlet diameter. Importantly, at all flow rates the snubber gap has been found to exert the strongest influence on the pressure distribution variation across the impeller shroud.

k) The L_9 Taguchi array pressure pulsation information has been used in two separate investigations with a view to firstly, increasing the component life and secondly, reduce the noise and vibration. This has been achieved through a rationalisation process and a single recommended arrangement has been realised that satisfies both requirements. The recommended arrangement was found to be similar to the fourth arrangement analysed.

l) Additionally, analyses have been completed which confirm that the recommended arrangement will indeed provide reduced pulsation levels. The additional analyses add to the data set of pressure pulsation variations with geometry and the new pressure pulsation values are found to compare well with those generated from the relevant predictive equations.

m) A series of two hundred and forty steady state simulations have been completed with the resulting pressure pulsation levels being compared with those from the transient analyses. This work has shown that the steady state pressure pulsations do not adequately capture the magnitude and phase of the pressure pulsations especially at lower flow rates. The steady state analyses pulsation results do show some features similar to the transient analysis, but the pressure magnitudes may differ. It has also been demonstrated that the steady state pulsations do not predict the same trend in pulsations for different pump geometry arrangements. This work concluded that it is not appropriate for multiple steady state analyses to be used to predict transient effects.

n) The pressure differential variation predicted by the transient analyses has been compared with pressure values assumed in existing design guidelines. The numerical information has been used to update the guideline information to more accurately reflect the pressure level in the pump.

o) A number of simple finite element stress analyses have been successfully conducted using the pressure loading information from two of the numerical models at two different impeller blade positions within the volute. The results show that the increased pulse in the pressure differential caused by a reduction in the snubber gap increases the stress at the impeller outlet considerably. This indicates that while the snubber gap may not influence the pressure pulsations significantly, the geometric parameter is still of extreme importance when designing the pump. The indicated stress levels also support the adoption of the modified pressure differential in the Weir Pumps Limited design guidelines.

p) A number of pump design recommendations have made as a result of this project. These are presented in a summarised form in section 7.6.

8.2 Suggestions for Further Work

Throughout the preceding chapters, attention has been drawn to areas that require further investigation. These items are collected here and summarised in what follows.

The volume of analysis work conducted for this project is significant. The present project has focused on the pressure pulsations at the impeller outlet and towards the discharge, yet there are a large number of other areas that could be investigated. For instance, in some circumstances the transmission of the pulsations at the impeller inlet and suction inlet may be of interest.

Similarly the pressure data could be used to determine the effect of the various geometry parameters on the pump thrust. Both axial and radial thrusts are calculable from the existing data set. This information could be used in conjunction with existing design methods of determining the thrust levels to improve the assumptions made in the design methods.

The analyses conducted as part of this work have produced a large volume of pressure results that could be used as loading data for the analysis of stresses within the pump. Typical, relatively simple, stress analyses have been presented here to indicate the potential information that is attainable from the pressure loadings. These analyses have been limited to providing a single loading on the inside and outside of an impeller passage. Pressure information exists at all nodes of the impeller passageway inside and out, including the pressure acting on the impeller blade. Of course this pressure information is time dependent so it would be possible to build up a complete picture of the stress variation as the impeller rotates. The stress work conducted in this thesis assumes a symmetry boundary acting at the hub. This is a sensible assumption for an inline vane arrangement where the flow on one side of the impeller is very similar to that on the other. However when using a staggered vane arrangement this is certainly not the case as the impeller passageway on the reverse side of the impeller will be at an angular offset. Therefore a stress analysis model of the full impeller would be required

in order to investigate the effects of the vane arrangement. Such a body of work is sizable especially considering the time dependent analyses, but would provide significant benefit in terms of understanding the mechanical design stresses present in an impeller and how they are affected by the pump geometry.

This project has shown that stable transient low flow analyses can be conducted successfully. Although some accuracy has to be sacrificed in order to obtain stability. Current pump analyses tend to be conducted in the relatively "safe" flow region of flows higher than 0.6Qn, and rarely investigate at flows below this. A number of organisations have produced "best practice guidelines" for turbomachinery applications (QNET (135), ERCOFTAC (136), but the broad range of applications prevents any aspect from being specifically covered in detail. Therefore there is a need for benchmark testing and analysis to investigate the practicalities of analysing pumps at low flows, provide a comparison of the various modelling options available and detail their effect on the numerical results.

In the late nineties it was generally accepted that while the accuracy of CFD was not always reliable, its ability to correctly predict the direction of any changes was reliable (137). Others stated that CFD was particularly adept in aiding understanding of the effect of ranges of parameters (45). Since that time little has been published regarding CFD being used for parametric studies. Published work has centred on comparing numerical model results with experimental data and trying to investigate more complete models. This present work has identified that parametric studies can now be conducted successfully on complete models. It is anticipated that more investigations exploring the flow comparisons of differing designs, leading to a greater understanding of the flows within a pump, will be forthcoming. One obvious area of interest mentioned in this project that readily extends itself to such a study, is the investigation of the possible performance reduction due to the enlarging of the cutwater gap.

9 References

1. Dalley, S. and Oleson J. (2003). "Sennacherib, Archimedes, and the Water Screw: The Context of Invention in the Ancient World". Technology and Culture Volume 44, Number 1, January 2003.
2. Papin, D. (1689). "Rotailis Suctor et Pressor Hassiacus, in Serenissma Aulo Cassellana demonstratus et detectus," Actis Eruditorum, p317. Cited in Van Esch, B. P. M., (1997). "Simulation of three-dimensional unsteady flow in hydraulic pumps." Published thesis, University of Twente, Enschede.
3. Elms, K. "The World of Rotodynamic Pumps, chapter 2: The innovators of rotodynamic devices". (WWW document). http://x-stream.fortunecity.com/laras/63/id20.htm (accessed 28th February 2006)
4. Gülich, J. (1999). "Impact of Three-Dimensional Phenomena on the Design of Rotodynamic Pumps." Journal of Mechanical Engineering Science, Proceedings Part C, 1999 Vol. 213, pp. 59-70.
5. Hergt, P. (1999). "Pump Research and Development: Past, Present and Future." ASME Journal of Fluids Engineering, Vol. 121, pg. 248-253.
6. González, J., Fernandez, J., Blanco, E., and Santolaria, C. (2002). "Unsteady Flow Structure on a Centrifugal Pump: Experimental and Numerical Approaches." In 2002 Joint US-European Fluids Engineering Summer Conference, Montreal Canada, July 14-18, 2002. FEDSM2002-31182.
7. Euler, L. (1750). "Détermination de l'effet d'une machine hydraulique inventée par Mr. Segner, Prof à Gottingue.
8. Abramian, M. and Howard, J. (1994). "Experimental Investigation of the Steady and Unsteady Relative Flow in a Model Centrifugal Impeller Passage." ASME Journal of Turbomachinery, Vol. 116, pp. 269-279
9. Ohashi, H. and Tsujimoto, Y. (1999). "Pump Research and Development: Past, Present and Future – A Japanese Perspective." ASME Journal of Fluids Engineering, Vol. 121, pg. 254-258
10. Durst, F. (2000). "Fluid Mechanics Developments and Advancements in the 20th Century." In 10th International Symposium Applications of Laser Techniques to Fluid Mechanics, Lisbon, Portugal, 10-13 July 2000,
11. Fischer, K. and Thoma, D. (1932). "Investigation of the Flow Conditions in a Centrifugal Pump" Transactions of ASME: Hydraulics HYD-54-8, pp. 141-155
12. Lennemann, E. and Howard J. (1970). "Unsteady Flow Phenomena in Rotating Centrifugal Impeller Passages." ASME Journal of Engineering for Power. Vol. 92, pp. 65-72
13. Eckardt, E. (1976). "Detail Flow Investigation Within a High Speed Centrifugal Compressor Impeller." ASME Journal of Engineering For Power, Vol 98 pp. 390-402.
14. Adler, D. and Levy, Y. (1979), "A Laser-Doppler Investigation of the Flow Inside a Backswept, Closed, Centrifugal Impeller." Journal of Mechanical Engineering Science, IMechE, Vol. 21, pp. 1-6.
15. Krain, H. (1981), "A Study on Centrifugal Impeller and Diffuser Flow." ASME Journal of Engineering for Power Vol. 103, pp. 688-697.
16. Rose, M. (1987), "Flow in the Impeller of a Centrifugal Water Pump with Three-Dimensional Blading." Published by IMechE, C274/87, pp. 81-93.

17. Binder and Knapp (1936), “Experimental determinations of the flow characteristics in the volutes of centrifugal pumps.” Trans ASME Paper No. HYD-58-4
18. Iversen, H., Rolling, R. E., Carlson, J.J. (1960), “Volute Pressure Distribution, Radial Force on the Impeller, and Volute mixing Losses of a Radial Flow Centrifugal Pump.” ASME Journal of Engineering for Power, April, pp. 136-144.
19. Csanady, G. (1962), “Radial Forces in a Pump Impeller Caused by a Volute Casing.” ASME Journal of Engineering for Power, October, pp. 337-340.
20. Colding–Jorgensen, J. (1980), “Effect of Fluid Forces on Rotor Stability in Centrifugal Compressors and Pumps.” NASA CO-2133, pp.249-266.
21. Chamieh, D. S., Acosta, A. J., Brennan, C. E. and Caughey, T. K. (1985), “Experimental Measurements of Hydrodynamic Radial Forces and Stiffness Matrices for a Centrifugal Pump-Impeller.” ASME Journal of Fluids Engineering, Vol. 107 pp. 307-315
22. Adkins, D. and Brennen, C. (1988), “Analyses of Hydrodynamic Radial Forces on Centrifugal Pump Impellers.” ASME Journal of Fluids Engineering, Vol. 110, pp. 20-28.
23. Baun, D., Köster, L. and Flack, R. D. (2000), “Effect of Relative Impeller-to-Volute Position on Hydraulic Efficiency and Static Radial Force Distribution in a Circular Volute Centrifugal Pump.” ASME Journal of Fluids Engineering. Vol. 122, pp. 598-605.
24. Miner, S., Beaudoin, R. J. and Flack, R. D. (1989). “Laser Velocimeter Measurements in a Centrifugal Flow Pump.” ASME Journal of Turbomachinery Vol. 111, pp. 205-212.
25. Arndt, N., Acosta, A. J., Brennan, C. E. and Caughey, T. K. (1990). “Experimental Investigation of Rotor-Stator Interaction in a Centrifugal Pump With Several Vaned Diffusers.” ASME Journal of Turbomachinery Vol. 112, pg. 98-108.
26. Dong, R., Chu, S. and Katz, J. (1992), “Quantitative Visualisation of the Flow Within the Volute of a Centrifugal Pump. Part A: Technique.” ASME Journal of Fluids Engineering, Vol. 114, Pg. 390-395
27. Dong, R., Chu, S. and Katz, J. (1992), “Quantitative Visualisation of the Flow Within the Volute of a Centrifugal Pump. Part B: Results and Analysis.” ASME Journal of Fluids Engineering, Vol. 114, Pg. 396-403.
28. Chu, S., Dong, R. and Katz, J. (1995), “Relationship Between Unsteady Flow, Pressure Fluctuations, and Noise in a Centrifugal Pump – Part A: Use of PDV Data to Compute the Pressure Field.” ASME Journal of Fluids Engineering Vol. 117, Pg. 24-29.
29. Chu, S., Dong, R. and Katz, J. (1995), “Relationship Between Unsteady Flow, Pressure Fluctuations, and Noise in a Centrifugal Pump – Part B: Effects of Blade-Tongue Interactions.” ASME Journal of Fluids Engineering Vol. 117, pp. 30-35.
30. Abramian, M. and Howard J. (1994). “ A Rotating Laser-Doppler Anemometry System for Unsteady Relative Flow Measurements in Model Centrifugal Impellers.” ASME Journal of Turbomachinery, Vol. 116, pp. 260-268.
31. Wo, A. and Bons, J. (1994), “Flow Physics Leading to System Instability in a Centrifugal Pump.” ASME Journal of Turbomachinery, Vol. 116, pg. 612-620.
32. Kaupert, K. and Staubli, T. (1999). “The Unsteady Pressure Field in a High Specific Speed Centrifugal Pump Impeller – Part 1: Influence of the Volute.” ASME Journal of Fluids Engineering, Vol. 121, pp. 621-626.

33. Kaupert, K. and Staubli, T. (1999). "The Unsteady Pressure Field in a High Specific Speed Centrifugal Pump Impeller – Part 2: Transient Hysteresis in the Characteristic." ASME, Journal of Fluids Engineering, Vol. 121, pp. 627-632.
34. Parrondo-Gayo, J. L., Fernandez, J., Santolaria, C. and Gonzalez, J. (1996). "Measurements in the Dynamic Pressure Field of the Volute of a Centrifugal Pump." In: Proceedings of the 18th IAHR Symposium on Hydraulic Machinery and Cavitation, Valencia, Spain, 16-19 September 1996, pp.401-410.
35. Parrondo-Gayo, J. L., Fernandez-Francos, J., Gonzalez-Perez, J., and Fernandez-Arango, J. (2000). "An Experimental Study on the Unsteady Pressure Distribution around the Impeller Outlet of a Centrifugal Pump." ASME FEDSM'00Fluids Eng Division Summer Meeting. June 11-15, 2000. Boston, pp 1-6.
36. Parrondo-Gayo, J. L., Gonzalez-Perez, J., Fernandez-Francos, J. (2002). "The Effect of the Operating Point on the Pressure Fluctuations at the Blade Passage Frequency in the Volute of a Centrifugal Pump." ASME Journal of Fluids Engineering June 2002, Vol. 124. pp. 784-790.
37. Blanco-Marigorta, E., Fernandez-Francos, J., Jorge, L. and Santolaria-Morros, C. (2000), "Numerical Simulation of Centrifugal Pumps." ASME 2000 Fluids Engineering Division Summer Meeting, June 11-15, Boston. FEDSM200-11162.
38. González, J., Fernandez, J. Blanco, E. and Santolaria, C. (2002), "Numerical Simulation of the Dynamic Effects Due to Impeller-Volute Interaction in a Centrifugal Pump." ASME Journal of Fluids Engineering June 2002, Vol. 124, pp. 348-355.
39. Blanco-Marigorta, E., Fernandez-Francos, J., Gonzalez-Perez, J., et al (2000), "Numerical Flow Simulation in a Centrifugal Pump with Impeller-Volute Interaction." FEDSM200-11297. Proceedings of ASME FEDSM'00. ASME 2000 Fluids Engineering Division Summer Meeting Jun 11-15 Boston Massachusetts.
40. Everett, W. (1979). "Predicting Centrifugal Pump Pressure Excursions (Noise)." In: "Performance Prediction of Centrifugal Pump and Compressors", The 25th Annual International Gas Turbine Conference and the 22nd Annual Fluids Engineering Conference, New Orleans, USA, March 9-13, 1980, pp. 287-289
41. Marscher, W. (1986). "The Effect of Fluid Forces at Various Operation Conditions on the Vibrations of Vertical Turbine Pumps." In: Radial Loads and Axial Thrusts on Centrifugal Pumps: Papers Presented at a Seminar Organized by the Fluid Machinery Committee of the Power Industries Division of Mechanical Engineers on 5 February 1986.
42. Corley, J. (1997). "A Pump Instability Theory Using an Acoustic Feedback Mechanism." Journal of Engineering for Gas Turbines and Power. Vol. 119, Pg. 651-657.
43. Jones, H. and Burley, C. (1997). "A Study of The Effects of Blade Shape On Rotor Noise." Presented at the AHS Technical Specialist's Meeting for Rotorcraft Acoustics and Aerodynamics; Williamsburg, USA, October 28-30, 1997.
44. McNally, W. and Sockol, P. (1981). "Computational Methods for Internal Flows With Emphasis on Turbomachinery." Presented at the Symposium on Computer in Flow Predictions and Fluid Dynamics Experiments at the ASME Winter Annual Meeting, Washington, USA, 15-20th November 1981. NASA TM 82764, pp 12-42.

45. Denton, J. and Dawes, W. (1998), " CFD for Turbomachinery Design." Presented at IMechE seminar "The Successful Exploitation of CFD in Turbomachinery Design." on 19th March 1998 London.
46. Anderson, J. (1995). "Computational Fluid Dynamics: The Basics With Applications." McGraw-Hill.
47. Barber, T. (1987). "Computational Fluid Dynamics for Internal Flows." ASME Journal of Propulsion Vol. 3, No. 5, pg. 385-386.
48. Lorett, J. and Gopalakrishnan, S. (1986), "Interaction Between Impeller and Volute of Pumps at Off-Design Conditions." ASME Journal of Fluids Engineering, Vol. 108, pp. 12-18.
49. Giles, M. (1988). "Calculation of Unsteady Wake/Rotor Interaction." ASME Journal of Propulsion Vol. 4, pp. 356-362
50. Weber, K. F., Thoe, D. W., and Delaney, r. A. (1990). "Analysis of Three-Dimensional Turbomachinery Flows on C-Type Grids using an Implicit Euler Solver." ASME Journal of Turbomachinery, Vol. 112, pg. 362-369.
51. Rai, M. and Madavan, N. (1990), "Multi-Airfoil Navier-Stokes Simulations of Turbine Rotor-Stator Interaction." ASME Journal of Turbomachinery, Vol. 112, pg. 377-384.
52. Graf, E., Singh, P., Sloteman, D. and Raw, M. J. (1990). "Three-Dimensional Flow Analysis In a Multistage Pump Crossover Diffuser." Presented at the ASME Winter Meeting, Dallas, November 1990. Also in: ASME Fluids Machinery Components, FED- Vol. 101, pp. 23-28
53. Cooper, P., Graf, E. and Luce, T. (1994). "Computational Fluid Dynamical Analysis of Complex Internal Flows in Centrifugal Pumps." Presented at the 11th International Pump Users Symposium, Houston, Texas, 8-10th March 1994, pp 83-94.
54. Rai, M. (1987), "Navier-Stokes Simulations of Rotor/Stator Interaction Using Patched and Overlaid Grids." ASME Journal of Propulsion Vol. 3, pp. 387-396.
55. Denton (1992), "The Calculation of Three-Dimensional Viscous Flow Through Multistage Turbomachines." ASME Journal of Turbomachinery, Vol. 114, pp. 18-26.
56. F.L. Tsung, Loellback, J., and Hah, C. (1996), "Development of an Unsteady Unstructured Navier-Stokes Solver for Stator-Rotor Interaction." 32nd Joint AIAA/ASME/SAE/ASEE Propulsion Conference, 1-3rd July, Lake Buena Vista, USA. AIAA 96-2668.
57. Hah, C., Tsung, F.L. and Loellbach, J. (1997) "Unsteady Flow Analysis in a High Work Turbine Stage with Two 3-D Navier Stokes Codes." 35th Aerospace Sciences Meeting and Exhibit, 6-10th January 1997, Reno, USA. AIAA 97- 0503.
58. Chen and Liaw (1997), "The Flowfield Calculations of a Centrifugal Pump with Volute." Presented at the International Gas Turbine and Aeroengine Congress & Exhibition, Orlando, Florida, USA, 2-5th June 1997.
59. Badie, R., Jonker, J. B. and Van den Braembussche, R. A. (1998), "Finite Element Calculations and Experimental Verification of the Unsteady Potential Flow in a Centrifugal Volute Pump." International Journal for Numerical Methods in Fluids, Vol. 19, 1994, pp 1083-1102.
60. Shi, F. and Tsukamoto, H. (2001) "Numerical Study of Pressure Fluctuations Caused by Impeller-Diffuser Interaction in a Diffuser Pump Stage." ASME Journal of Fluids Engineering Volume 123, September 2001. Pg 466-474
61. Burt, D., Purdom, T. R. and Spence, R (1998), "Prediction of the Three Dimensional Flow Field in a Vertical Mixed-Flow Pump with Vaned Diffuser."

Presented at IMechE Seminar, CFD in Fluid Machinery Design, 15th October 1998, IMechE, London, pp 59-70.
62. Miner, S. M. (2000), "Evaluation of Blade Passage Analysis Using Coarse Grids." Journal of Fluids Engineering. ASME Vol. 122, pp. 345-348.
63. Williams, R. W., Skelley, S. E., Marshall, E.T., and Prueger, G. H. (2000), "High Head Unshrouded Impeller Pump Stage Technology." 36th AIAA/ASME/ SAE/ASEE Joint Propulsion Conference, 17-19th July, Huntsville, USA. AIAA 2000/3243.
64. Dyson, G. (2001), "Recommendations to Designers for CFD Pump Impeller and Diffuser Simulations." Presented at IMechE conference "Advances of CFD in Fluid Machinery Design" on 13th June 2001.
65. Pembroke, J (1998), Sabini, G., and Littlefield, D. E. "Computational Fluid Dynamics Analysis Solves Pump Noise Problem." Chemical Processing, April Issue pg. 51.
66. Cailleau, J., Madec, A, Berge, D. and Dumas, M. (2000), "Low Noise Fan Design Using Rotor to Stator Unsteady 3D-CFD Method." 36th AIAA/ASME/SAE/ASEE Joint Propulsion Conference, 17-19th July, Huntsville, USA. AIAA 2000/3193.
67. Biedron, R., Rumsey, C., Podboy, G. and Dunn M. H. (2001), "Predicting the Rotor-Stator Interaction Acoustics of a Ducted Fan Engine." 39th Aerospace Sciences Meeting and Exhibit, 8-11th January 1997, Reno, USA. AIAA 2001 – 0664.
68. Scheuerer, G. (2001), "Coupling of CFD and Optimization Methods for Turbomachinery Applications." (Oral Only) Presented at IMechE seminar "Advances of CFD in Fluid Machinery Design" on 13th June 2001.
69. Zangeneh, M., Goto, A. and Takemura, T. (1996). "Suppression of Secondary Flows in a Mixed-Flow Pump Impeller by Application of Three-Dimensional Inverse Design Method: Part 1 – Design and Numerical Validation." ASME Journal of Turbomachinery Vol. 118 pp. 536-
70. Goto, A., Takemura, T. and Zangeneh, M. (1996). "Suppression of Secondary Flows in a Mixed-Flow Pump Impeller by Application of Three-Dimensional Inverse Design Method: Part 2: Experimental Validation." ASME Journal of Turbomachinery Vol. 118 pp. 544-
71. Zangeneh, M., Goto, A and Takemura, T. (1998). "On the Role of 3D Inverse Design Methods in Turbomachinery Shape Optimisation." Presented at IMechE seminar "The successful Exploitation of CFD in Turbomachinery Design." On 19th March 1998.
72. Zangeneh, M. and Tiow, W. (2001), "A Three-Dimensional Inverse Method Based on Pressure Loading for the Design of Turbomachinery Blades." Presented at IMechE seminar "Advances of CFD in Fluid Machinery Design" on 13th June, 2001.
73. Uchida, N., Inaichi, K and Shirai, T. (1971). "Radial Force on the Impeller of a Centrifugal Pump." Bulletin of the Japan Society of Mechanical Engineers, 1971,Vol. 14, pp.1106-1117.
74. Milne, A. (1986). "A Comparison of Pressure Distribution and Radial Loads on Centrifugal Pumps." In: Radial Loads and Axial Thrusts on Centrifugal Pumps: Papers Presented at a Seminar Organized by the Fluid Machinery Committee of the Power Industries Division of Mechanical Engineers on 5 February 1986.
75. Guelich, J., Jud, W. and Hughes, S. F. (1986). "Review of Parameters Influencing Hydraulic Forces on Centrifugal Impellers." In: Radial Loads and Axial Thrusts

on Centrifugal Pumps: Papers Presented at a Seminar Organized by the Fluid Machinery Committee of the Power Industries Division of Mechanical Engineers on 5 February 1986.
76. Konno, D. and Ohno, T. (1986). "Experimental Research on Axial Thrust Loads of Double Suction Centrifugal Pumps." In: Radial Loads and Axial Thrusts on Centrifugal Pumps: Papers Presented at a Seminar Organized by the Fluid Machinery Committee of the Power Industries Division of Mechanical Engineers on 5 February 1986.
77. Goulas, A. and Trusott, G. (1986). "Dynamic Hydraulic Loading on a Centrifugal Pump Impeller." In: Radial Loads and Axial Thrusts on Centrifugal Pumps: Papers Presented at a Seminar Organized by the Fluid Machinery Committee of the Power Industries Division of Mechanical Engineers on 5 February 1986.
78. Stanmore, L. (1988). "Field Problems Relating to High-Energy Centrifugal Pumps operating at Part-Load." In IMechE Conference C343/88 Pumps in Part Load.
79. Hsu, C. and Brennan, E. (2002). "Fluid Flow Equations for Rotordynamic Flows in Seals and Leakage Paths." ASME Journal of Fluids Engineering, Vol. 124 pp.176-181.
80. Baun, D. and Flack, R. (2003). "Effects of Volute Design and Number of Impeller Blades on Lateral Impeller Forces and Hydraulic Performance." International Journal of Rotating Machinery, Vol. 9, pp. 145-152.
81. Worster, R. (1958). "The Effects of Fitting Guide Vanes in a Centrifugal Pump." British Hydromechanics Research Association, Report Number RR 586.
82. Worster, R. (1958). "The Effect of Reducing Impeller Width on the Performance of a Centrifugal Pump." British Hydromechanics Research Association, Report Number RR 607.
83. Rashed, M. (1951). "Pressure Fluctuations in a Centrifugal Pump and the Calculation of Pump." British Hydromechanics Research Association, Report Number T (translation) 415.
84. Makay, E. and Nass, D. (1982). "Gap-Narrowing Rings Make Booster Pumps quiet at Low Flow." Power, September, pp. 87-88.
85. Makay, E. and Szamody O. (1978). "Survey of Feed Pump Outages." Prepared for Electric Power Research Institute Research, Project 641. Report: FR-754.
86. Makay, E. (1976). "How to Avoid Problems with… Boiler Feed Pumps." Hydrocarbon Processing, December Pg 79-84.
87. Makay, E. and Szamody, O. (1980). "Recommended Design Guidelines for Feedwater Pump in Large Power Generating Units" (1980), Prepared for Electric Power Research Institute Research, Project 1266-18, Report: CS-1512.
88. Sudo, S., Komatsu, T., and Kondo, M. (1980). "Pumping Plant Noise Reduction: Reduction of Pressure Pulsation in Pump Discharge Pipe Systems." Hitachi Review vol. 29 (1930), No. 5.
89. Haldeman, C., Krumanaker, M. L. and Dunn, M.D. (2003). "Influence of Clocking and Vane/Blade Spacing on the Unsteady Surface Pressure Loading for a Modern Stage and One Half Transonic Turbine." ASME Journal Turbomachinery, Vol. 125, pp. 743-753.
90. Guelich, J. and Bolleter, U. (1992). "Pressure Pulsations in Centrifugal Pumps." ASME Journal of Vibration and Acoustics, Vol. 114, pp. 272-279.
91. Spence, R. and Purdom, T. (1999), "Prediction of Impeller Loadings using CFD Analysis Techniques". Presented at IMechE Seminar, Up and Coming in Fluid Machinery, 17th November 1999 IMechE, London.

92. Spence, R. and Purdom, T. (2003), "Numerical Prediction of Transient Loadings on Multistage Pump Impellers." Presented at IMechE Seminar, "Advances of CFD in Fluid Machinery Design.", 18th November 2003, IMechE, London.
93. Weir Pumps Internal Documentation (1980). Hydraulic Engineering Department, Alloa. "Impeller Vane Design." P0084A.
94. Makay, E. (1979). "Better Understanding of Sources of Feedpump Damage Boosts Performance, Reliability." Power, June.
95. Stepanoff, A.J. (1957). "Centrifugal and Axial Flow Pumps". John Wiley and Sons, fifth printing 1967.
96. Schachenmann, A., Muggli, F. and Guelich, J. F. (1993). "Comparison of Three Navier-Stokes Codes with LDA-Measurements on an Industrial Radial Pump Impeller. FED. Vol.154, Pumping Machinery, ASME 1993.
97. Casey, M., Eisele, K., Muggli, F., Gülich, J. and Schachenmann, A. (1995). "Flow Analysis in a Pump Diffuser: Part 2 Validation of a CFD Code for Steady Flow." FED- Vol. 227 Numerical Simulations in Turbomachinery ASME 1995.
98. Kaupert, K. A., Holbein, P. and Staubli, T. (1996). "A First Analysis of Flow Field Hysteresis in a Pump Impeller." ASME Journal of Fluids Engineering Vol. 118. Pg.685-691.
99. Muggli, F. A., Holbein, P. and P. Dupont (2002). "CFD Calculation of a Mixed Flow Pump Characteristic From Shutoff to Maximum Flow." ASME Journal of Fluids Engineering Vol. 124, pp:798-802.
100. Michaelides, K. V., Tourlidakis, A. and Elder, R. L. (2001). "Use of CFD for the three-dimensional hydrodynamic design of vertical diffuser pumps." Presented at IMechE conference "Advances of CFD in Fluid Machinery Design" on 13th June 2001 at One Birdcage Walk, London.
101. Naylor, E., Freeman, C., Herring, S., Ivey, P. (2003). "Application of the TASCflow CFD package to the Simulation of Embedded Compressor Stages." Presented at IMechE seminar "Advances of CFD in Fluid Machinery Design" on 18th November 2003 at One Birdcage Walk, London.
102. Ganga, D. P., Ivey, P. C., Govender, S. (2003). "A Three Dimensional Flow Simulation in an Axial Flow Turbine using a Commercial CFD Code." Presented at IMechE seminar "Advances of CFD in Fluid Machinery Design" on 18th November 2003 at One Birdcage Walk, London.
103. CFX TASCflow User Documentation version 2.12.
104. CFD Review article – posted by nwyman. "State of the Art in Grid Generation." (2001). Citing Internet Resources (WWW document). http://www.cfdreview.com/article.pl?sid=01/04/28/2131215&mode=thread. (accessed 28th February 2006).
105. Thompson, J. Soni, B and Weatherrill, N. (1999), "Handbook of Grid Generation." CRC Press. ISBN 0849326877
106. CFX TASCflow Theory Primer Documentation version 2.12.
107. Celik, I. (1999). "Introductory Turbulence Modelling" Citing Internet resources (WWW document). http://files.asme.org/asmeorg/Jobs/Resources/CareerSeries/9673.pdf (accessed 12/9/2006).
108. Hwang, R. and Jaw, S. (1998). "Second-Order Closure Turbulence Models: Their Achievements and Limitations." Proceedings of the National Science Council, Republic of China, Vol. 22, 1998, pp. 703-722.

109. Launder, B and Spalding, D. (1974). "The Numerical Computation of Turbulent Flows." Computer Methods in Applied Mechanics and Engineering, Vol. 3, pp. 269–289.
110. Wilcox, D. (1986). "Multiscale model for turbulent flows." In AIAA 24th Aerospace Sciences Meeting. Cited in: Chapter 4.1.3:k-ω Turbulence Model, CFX TASCflow Theory Documentation.
111. "CFX5: The CFX approach to Turbulence Modeling: Accurate and Effective Turbulent Flow Simulations." CFX Technical Brief PDF0072, 07/03.
112. Casey, M. (2004). "Thematic Area 6: Best Practice Advice for Turbomachinery Internal Flows." QNET-CFD Network Newsletter, Volume 2, No. 4 – July 2004. Citing Internet resources (WWW document). http://www.qnet-cfd.net/newsletter/8th/n8_40-46.pdf (accessed 12/9/2006).
113. Marx, Y. P. (1997) "Unsteady Simulations of Impeller – Diffuser Interactions in a Centrifugal Pump." EPFL Supercomputing Review No. 9 November 1997. Citing Internet resources (WWW document). http://sawww.epfl.ch/SIC/SA/publications/SCR97/scr9-page24.html (accessed 12/9/2006).
114. Roy, Ranjit (1990). "A Primer on the Taguchi Method.", Van Nostrand Reinhold, New York.
115. Schmidt, Stephen and Launsby, Robert (2005). "Understanding Industrial Designed Experiments" 4th Edition, Air Academy Press, Colorado Springs.
116. Sloane, N. J. A. "A Library of Orthogonal Arrays" Citing Internet resources (WWW document). http://www.research.att.com/~njas/oadir/index.html. (accessed 12/9/2006).
117. Tamm, A., Gugau, M. and Stoffel, B. (2002). "Experimental and 3-D Numerical Analyses of the Flow Field in Turbomachines Part II." QUANSE 2002, International Quality Assessment of Numerical Simulations in Engineering April 9-12 2002, University of Concepción, Chile.
118. Denton, J. (1994). "Turbomachinery Design Using CFD." AGARD Lecture Series 195. Cited in: Tsuei, H. et al (1999). "The Validation of Rapid CFD modelling for Turbomachinery." Presented at CFD Technical Developments and Future Trends, IMechE, London, 13-14th December 1999.
119. Menter, F. (2003). "Turbulence Modelling for Turbomachinery." QNET-CFD Netweork Newsletter, Vol. 2, No. 3 December 2003. Citing Internet Resources (WWW document). http://www.qnet-cfd.net/newsletter/7th/n7_10.pdf (accessed 28th February 2006).
120. Han, H., Yokoyama, Y. and Konno, M. B. (2002), "Recent Developments and Applications for CFD in Turbomachinery." The 4th International Conference on Pumps and Fans (4th ICPF) August 26-29, 2002 Tsinghua University, Beijing.
121. De Souza, L., de Moura, M. D. and Brasil, A. C. P. (2003), "Assessment of Turbulence Modelling for CFD simulations into Hydroturbines: Spiral Casings." 17th International Mechanical Engineering Congress (COBEM 2003) at São Paulo (Brazil).
122. Kato, M. and Launder, B. (1993), "The Modeling of Turbulent Flow Around Stationary and Vibrating Square Cylinders", Proceedings of the 9th Symposium on Turbulent Shear Flows, Kyoto, August 1993, pp. 10.4.1-10.4.6.
123. Guleren, K. M., Pinarbasi, A. (2004). "Numerical Simulation of the Stalled Flow within a Vaned Centrifugal Pump." Proceedings of the Institution of Mecanical Engineers, Journal of Mechanical Engineering Science, Vol. 218, part C pp:425-435.

124. Tamm, A., Ludwig, G. and Stoffel, B. (2001). "Numerical, Experimental and Theoretical Analysis of the Individual Efficiencies of a Centrifugal Pump." Proceedings of ASME FEDSM'01. 2001 ASME Fluids Engineering Division Summer Meeting. New Orleans, Louisiana, May 29-June 1, 2001.
125. Koumoutsos, A. (1999), "Unsteady Flow Interactions in Centrifugal Turbomachinery Configurations." (Unpublished PhD Thesis) Cranfield University, Cranfield.
126. Ahkras, A., El Hajem, B. M., Morel, R., Champagne, J. Y. (2000), "The Internal Flow Investigation of a Centrifugal Pump." 10th International Symposium on Applications of Laser Techniques to Fluid Mechanics, Lisbon, 10-13th July. Session 28: Turbomachinery, Paper 28.5.
127. Pedersen, N., Jacobsen, C. B. (2000). "PIV Investigation of the Internal Flow Structure in a Centrifugal Pump Impeller." 10th International Symposium on Applications of Laser Techniques to Fluid Mechanics, Lisbon, 10-13th July. Session 28: Turbomachinery, Paper 28.3.
128. Pedersen, N., Larsen, P. S. and Jacobsen, C. B. (2003). "Flow in a Centrifugal Pump Impeller at Design and Off-Design Conditions – Part 1: Particle Image Velocimetry (PIV) and Laser Doppler Velocimetry (LDV) Measurements". ASME Journal of Fluids Engineering, Vol. 125 January 2003, pp 61-72.
129. Höller, H. K., (1979). "Beispiele für Schwierigkeiten bei der Uebertragung von Modellmessungen auf Wasserturbinen- und Pumpengrossausführungen," 25 Jahre ASTRÖ, pp. 71-78. Cited in: Guelich, J. and Bolleter, U. (1992). "Pressure Pulsations in Centrifugal Pumps." ASME Journal of Vibration and Acoustics, Vol. 114, pp. 272-279.
130. Palgrave, Ron (2006) Hydraulic Manager Weir Pumps Limited. Private Communication (26/9/06) regarding current industry practices.
131. Srivastav, O. P., Pandu, K. R. M. Gupta, K. (2003). "Effect of Radial Gap between Impeller and Diffuser on Vibration and Noise in a Centrifugal Pump." Institute of Mechanical Engineers (India). Technical journal – Mechanical Engineering, MC1 – April 2003, Vol. 84, pp. 36-39. Presented at the Annual Paper Meeting held concurrently with the National Seminar on 'Emerging Trends in Mechatronics for Automation' at Rourkela on November 2002.
132. Palgrave, Ron (2006) Hydraulic Manager Weir Pumps Limited. Private Communication (26/9/06) regarding current industry opinion relating to staggered vane impellers.
133. Asuaje, M., Bakir, F, Kouidri, S., Kenyery, F and Rey, R. (2004) "Numerical Modelisation of the Flow in Centrifugal Pump, Volute Influence in Velocity and Pressure Fields. 10th International Symposium of Transport Phenomena and Dynamics of Rotating Machinery, Honolulu, Hawaii. March 07-11, 2004 Paper ID No. 99.
134. Roark, J.R. and Young, W.C. (1975). Formulas for Stress and Strain (5th Edition). McGraw-Hill.
135. QNET-CFD. A thematic network on quality and trust for the industrial application of Computational Fluid Dynamcis. (WWW document). http://qnet-cfd.net/ (accessed: 21st September 2006)
136. European Research Community on Flow, Turbulence and Combustion. (WWW document). http://www.ercortac.org/ (accessed: 21st September 2006)
137. Gallimore, S. (1998). "Axial Flow Compressor Design" Presented at "The Successful Exploitation of CFD in Turbomachinery Design." At IMechE, 1 Birdcage Walk, London on the 19th March 1998.

Appendices

Appendix A: Flow Animations (on CD)

Appendix B: Design Guidelines

Appendix B: Design Guidelines

Industrial design guidelines are notoriously difficult to decipher. This may be partly due to commercial confidentiality but more often due to the fact that they have been developed over many years and the original basis is uncertain or has been totally lost. Usually there is some rudimentary theoretical background coupled with a great deal of empirical knowledge, which together have shaped the final guidelines.

The WPL guidelines are no different in this respect. The most commonly used guide (B1) relies heavily on commercially sensitive empirical data from past impeller failures. The guide allows the basic scantlings such as the shroud thickness and the cutwater gap to be established and via a graphical method determines a safe zone for the impeller design. This general method is not applicable to high energy double entry type pumps and will not be discussed further here.

There are also two older WPL guidelines (B2, B3) that can be used to check the design acceptability and susceptibility to fatigue. Broadly these assume that the stress in the impeller shroud is due to two actions, namely a centrifugal stress caused by the rotating action of the impeller and a bending (hoop) stress across the shroud wall due to the hydraulic pressure loading.

It should be observed that the notation presented for equations in this section is as per the WPL design guides and will be provided as required.

The centrifugal stress is derived from the stress in a thin rotating ring and modified by a factor K to give the result for a hollow spinning disc. The WPL version of the centrifugal stress equation includes a factor of 1.25 to account for the effect of the blades.

$$\sigma_{cs} = \frac{K\rho_m U_2^{\,2}}{802408} \qquad \text{Equation B.1}$$

where σ_{cs} is the centrifugal stress (N/mm^2)

ρ_m is the density of the material (Kg/m^3)

U_2 is the impeller tip velocity (m/s)

K is a function of the radius ratio of the disc, $\frac{R_2}{R_1}$, and $\frac{r}{R_2}$, where r is the general radius, R_1 is the shroud eye radius and R_2 is the impeller outlet radius.

Values of K can be found from Roark & Young (B4) but are also available in a simple spreadsheet calculation within WPL. However the general equations for the hollow disc are,

$$\sigma_r = \frac{3+\nu^*}{8}\frac{\rho\omega^2}{386.4}\left(R^2 + R_1^2 - \frac{R^2R_1^2}{r^2} - r^2\right) \qquad \text{Equation B.2}$$

$$\sigma_t = \frac{1}{8}\frac{\rho\omega^2}{386.4}\left[\left(3+\nu^*\right)\left(R^2 + R_1^2 + \frac{R^2R_1^2}{r^2}\right) - \left(1+3\nu^*\right)r^2\right] \qquad \text{Equation B.3}$$

where σ_r is the radial stress (lb/in^2)

σ_t is the tangential stress (lb/in^2)

ρ is the density (lb/in^3)

ω is the rotating speed (rad/s)

ν* is Poisson's ratio

R is the outer radius of the disk (in) (equivalent to $R = \frac{D_2}{2}$)

R_1 is the radius of the central hole in the disk (in) (equivalent to the radius of the impeller shroud inlet diameter)

r is the radius at any point from the centre where there is a radial tensile inertia stress (in)

For particular values of R, R_1 and r the stresses can be evaluated directly if required. In general the hoop stress is larger than the radial stress and its maximum value is at the bore of the disc. Here two values of the hoop stress are of interest, namely the maximum

value and the value at the periphery of the disc. Inserting the appropriate parameters the two values are 2.75e6N/mm^2 and 5.52e6N/mm^2 respectively.

The calculation of the shroud bending stress is an approximation based on a fixed beam analogy. Figure B.1 provides a simple diagram of the estimated pressure distribution over an impeller for best efficiency point at positions both inside and outside the shroud. This is approximated to a triangular pressure differential across the impeller shroud, varying from zero pressure differential at the impeller outlet to 0.4H at wear ring diameter. This varying pressure differential is then assumed (conservatively) to be equivalent to an average pressure differential action over the shroud of 0.3H. Ignoring the stiffening effect at the wear ring, the shroud is assumed to be a fixed beam (Figure B.2). The span of this beam between "supports" will depend on the impeller radius and blade angle. Assuming an average length at a point midway between the outside diameter and the wear ring diameter and letting the vane angle equal the outlet angle for simplicity we have,

$$MaxBendingMoment = \frac{WL}{12} \text{ at the blade-shroud junction,} \qquad \text{Equation B.4}$$

$$W = \text{Pressure x Width x Length} \qquad \text{Equation B.5}$$

$$\text{Pressure} = \frac{0.3H}{2.31} \text{ (lbs/inch}^2\text{)} \qquad \text{Equation B.6}$$

where $H = \frac{U_2{}^2}{2g}$

and where U_2 is in ft/sec and g is in ft/sec^2

The average length L is

$$Length = \frac{\Pi}{v} \times D_m \times \sin\theta \qquad \text{Equation B.7}$$

where $D_m = \left(\frac{D_2 + D_{wr}}{2} \right)$, D_{wr} is the wear ring diameter and is in mm

$$Section\_Modulus = \frac{1}{6} \times Width \times (thickness)^2 \qquad \text{Equation B.8}$$

$$\sigma_{bs} = \frac{MaxBendingMoment}{Section\_Modulus} \qquad \text{Equation B.9}$$

Substituting: Equations B.5, B.6 and B.7 into equation B.4 and Equation B.4 and B.8 into B.9 results in

$$\sigma_{bs} = \frac{U_2{}^2}{401} \times \frac{D_2{}^2}{t_s{}^2} \times \left(1 + \frac{D_{wr}}{D_2}\right)^2 \times \frac{\sin^2 \beta_2}{z^2} \qquad \text{Equation B.10}$$

As can be seen from the derivation the equation is not ideal, as it has mixed imperial and metric units. Thus Equation B.10, has been converted completely to metric units giving Equation B.11

The final version of the bending stress is

$$\sigma_{bs} = \frac{\rho U_2{}^2}{5.4x10^5} \times \frac{D_2{}^2}{t_s{}^2} \times \left[1 + \frac{D_{wr}}{D_2}\right] \times \frac{\sin^2 \beta_2}{z^2} \qquad \text{Equation B.11}$$

where σ_{bs} is the bending stress (N/mm^2)

ρ is the density of the pumped fluid (Kg/m^3)

U_2 is the impeller tip velocity (m/s)

D_2 is the tip diameter (mm)

t_s is the impeller shroud thickness (mm)

β_2 is the impeller blade outlet angle (degrees)

z is the number of impeller blades

Inserting the appropriate values for the various parameters gives a bending stress of $3.41N/m^2$

Once calculated, the values for the bending stress and the centrifugal stress are normally compared with a fraction of the material UTS value or yield to ascertain their acceptability (a factor of safety is included in the values used).

References

B1: Weir Pump Internal Design Guide DES/DGM/1800, “Tip Geometry For High Performance Impellers”, D. Cree.
B2: Weir Pumps Internal Design Guide BH6, “Design Method for Fixing Impeller Vane and Shroud Thicknesses”, J Richardson.
B3: Weir Pumps Internal Design Guide, “Pump Impeller Design Checks”, S. Bradshaw.
B4: Roark, J.R. and Young, W.C. (1975). Formulas for Stress and Strain (5th Edition). McGraw-Hill.

Figures

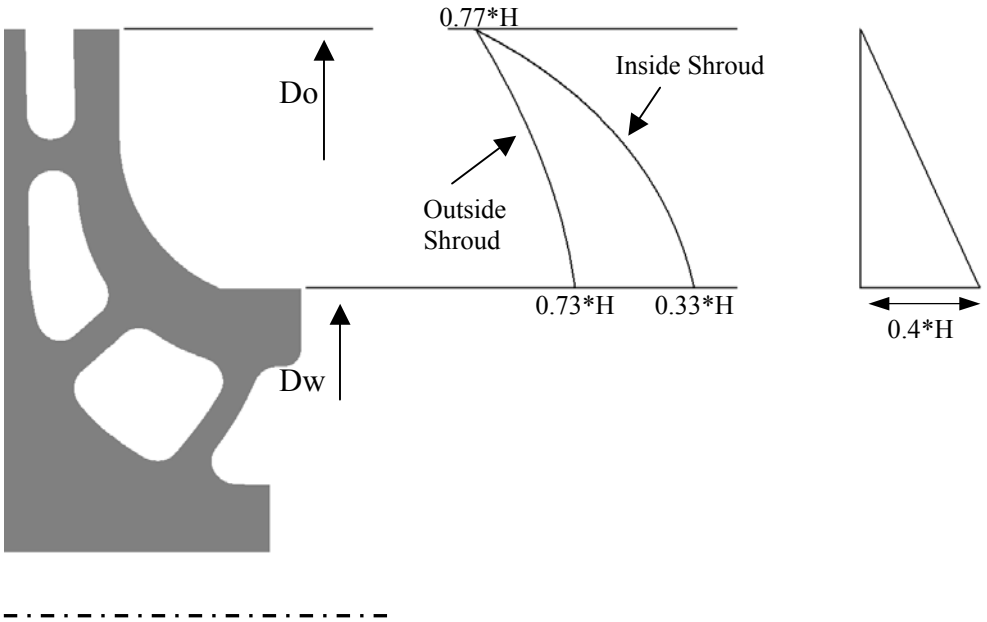

Figure B.1: Estimated pressure distribution over an impeller shroud at best efficiency

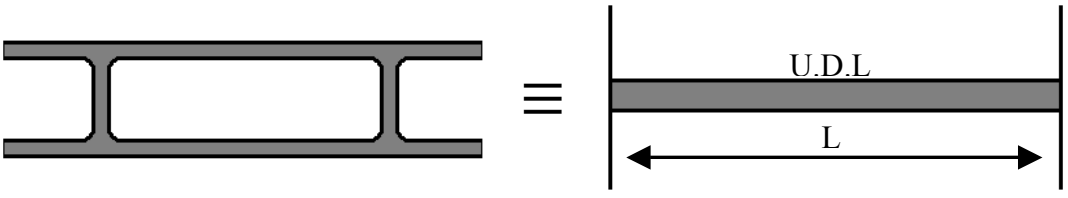

Figure B.2: Shroud assumed to be a continuous beam, with loading as a uniform distributed load (UDL)